IAEA-TECDOC-345

NEUTRON PHYSICS AND NUCLEAR DATA MEASUREMENTS WITH ACCELERATORS AND RESEARCH REACTORS

LECTURES PRESENTED AT THE
INTERNATIONAL ATOMIC ENERGY AGENCY
INTERREGIONAL TRAINING COURSE
HELD AT TASHKENT, USSR, 4–30 SEPTEMBER 1983

A TECHNICAL DOCUMENT ISSUED BY THE
INTERNATIONAL ATOMIC ENERGY AGENCY, VIENNA, 1985

NEUTRON PHYSICS AND NUCLEAR DATA MEASUREMENTS
WITH ACCELERATORS AND RESEARCH REACTORS
IAEA, VIENNA, 1985
IAEA-TECDOC-345

Printed by the IAEA in Austria
August 1985

PLEASE BE AWARE THAT
ALL OF THE MISSING PAGES IN THIS DOCUMENT
WERE ORIGINALLY BLANK

PREFACE

This report contains the lectures delivered at the Institute of Nuclear Physics of the Academy of Sciences of the Uzbek SSR, Tashkent, from 4-18 September 1983 during the first part of the IAEA TC Interregional Training Course and Study Tour on Neutron Physics and Nuclear Data Measurements with Accelerators and Research Reactors which was jointly organized by the IAEA and the USSR State Committee on the Utilization of Atomic Energy, on the recommendation of the Agency's International Nuclear Data Committee.

The main reason for organizing this course was that neutron measurement techniques are used in many laboratories in developing countries both for research and for technological applications. Different sources of neutrons are used for these measurements. Among the most common are neutron generators, research reactors, charged-particle accelerators of various types and for various energies, and isotopic neutron sources. The number of such facilities in laboratories in developing countries is constantly growing, partly with the support by the Agency's Technical Co-operation Programme. It is a continuous responsibility of the IAEA to assist these laboratories in the profitable utilization of these devices in technological research and educational applications.

The whole programme of the course and the lectures presented in this report in particular gave an opportunity to the participants to become acquainted with the latest developments in the field of fast neutron measurements, in the studies of neutron interactions with nuclei, and in related technological applications of immediate benefit to their countries.

CONTENTS

SOME ASPECTS OF THE PRODUCTION AND APPLICATION OF RADIOACTIVE ISOTOPES

E.S. GUREEV
INP AS Uzbek SSR,
Tashkent, Union of Soviet Socialist Republics

Abstract

Methods of the production of radioactive isotopes using charged particle accelerators, neutron irradiation in reactors, and extraction from the fission products of heavy elements are described.

The discovery of natural and then artificial radioactivities has led in a relatively short period of time to the creation of powerful nuclear energetics and, at the same time, to the wide use of radioactive isotopes in industry, science, engineering, and particularly in medicine.

The useful radioactive isotopes are prepared by means of charged particle accelerators, by neutron irradiation in nuclear reactors and by recovery from the fission products of heavy elements.

At present the short-lived isotopes are produced on a mass scale in neutron fluxes of ($2\ 10^{12}$-4.10^{13}) n/(cm^2.s) with exposures of 1.4-2, 5, 21, 42, 63, 100 hours and longer, 40 items of such isotopes being produced regularly.

The relatively short-lived isotopes required in large amounts (^{32}P, ^{131}I, etc.), as well as the long-lived isotopes, are produced in special reactors with high neutron flux densities.

In addition to the most common (n,γ) reaction the (n,p) and (n,α) nuclear reactions and the secondary nuclear reactions with tritons and protons are employed to prepare a number of isotopes in a reactor. The advantage of these reactions lies in possibility of preparing carrier-free sources. Three of those reactions proceeding with thermal neutrons have been used for a long time to prepare such important isotopes as tritium, ^{16}C and ^{35}S. They are $^{6}Li(n,\alpha)^{3}H$, $^{14}N(n,p)^{16}C$ and $^{35}Cl(n,p)^{35}S$.

A semi-automatic separating plant recently developed for catching the radioactive carbon produced in the irradiation of nitrogen and for separating it in the form of barium carbonate permits approximately 100 Ci/yr of ^{14}C with a specific activity up to 250mCi/g to be produced.

The threshold (n,p) reactions have been employed to prepare a number of carrier-free isotopes, in particular, ^{32}P from sulfur, ^{58}Co from nickel, ^{54}Mn from iron, etc.

In all these cases the elements are chemically separated after irradiation to isolate the isotope of interest from the target material and the radioactive impurities.

Some isotopes are prepared on the basis of the secondary reactions occuring in composite targets. Thus, tritium nuclei are produced in a target containing lithium and oxygen (lithium carbonate) by the $^{6}Li(n,\alpha)^{3}H$ reaction. The produced tritium nuclei have, in turn, a sufficient energy to induce the $^{16}O(t,n)^{18}F$ reaction. The identical method has been developed for preparing ^{28}Mg by the $^{26}Mg(t,p)^{28}Mg$ reaction in a target containing magnesium and lithium.

The use of isotope-rich targets in one of the ways for producing radioisotopes with high specific activity and high radioisotopic purity. This method has been recently used moreand more widely to produce ^{42}K, ^{51}Cr, ^{55}Fe, ^{59}Fe, ^{69m}Zn and other isotopes, in particular, for medical injection purposes. At present about 90% of regularly produced radioactive isotopes are prepared by neutron irradiation in reactors.

Using charged-particle accelerators it is possible to prepare the majority of radioisotopes now in use, but it is simpler to prepare most of them in nuclear reactors where they are produced on a large scale.

However, some radioactive isotopes either cannot be prepared in nuclear reactors or their production in reactors is inefficient. These are neutron-deficient isotopes produced by reactions with charged particles usually in cyclotrons which represent the most high-current accelerators of particles with a required energy. Owing to this the above isotopes are named cyclotron isotopes. Thus, the reactor and cyclotron methods of isotope production make a pair, but with some exceptions compete with each other. The important fe-

ature and advantage of both the cyclotron isotopes and those prepared in a reactor by the threshold and secondary reactions are that they have in most cases a chemical nature differing from that of irradiated target material. Therefore, they can be isolated from the target with no carrier, i.e. in such a form when all atoms of the given isotope are radioactive. This makes it possible to prepare the required sources with a high specific activity.

The intensive investigations directed to development of the cyclotron methods for producing radioisotopes, to selection of optimal cyclotron operating conditions for producing different isotopes, to development of mechanized targets, etc. allowed in a short time the isotope nomenclature to be increased up to 60 and their regular production to be organized. 22-MeV proton and deuteron beams as well as 44-MeV alpha-particles are used in the cyclotron production of radioisotopes.

The method of processing materials irradiated in a reactor or cyclotron, of recovering high-activity isotopes free from a carrier and radioisotope impurities and preparing labelled compounds and special sources has been developed and improved. If at first simple, mainly inorganic, compounds were produced, later on the methods of preparing hundreds of complex labelled organic compounds, pharmaceutical, biologically-active and therapeutic-diagnostic preparations including sterile and apyrogenic injection solutions were developed.

Practically all the up-to-date techniques of radiochemistry and organic chemistry are applied to isolation of labelled compounds and various special radioactive sources from targets, to their production and purification. For this purpose the Soviet scientists have intensively developed the theoretical problems of adsorption, cocrystallization, solvent extraction, chromatography, isotopic exchange and other special methods as applied to the isotope separation and isolation, and to the production of radioactive sources.

The simple and reliable precipitation technique was conventionally used in the technology of radioactive source preparation. After the mathematical theory of equilibrium solvent extraction systems and the methods of calculation of extraction apparatus design have been developed and the mechanism of solvent extracting microquantities of a substance from aqueous solutions has been studied, it became possible to apply widely and efficiently the extraction method to separation of many isotopes from targets irradiated in a reactor or a cyclotron.

Recently a certain attention has been drawn to developing "generators" of short-lived isotopes. The delivery of short-lived isotopes to users, especially long-distance transportation, leads to a great loss in activity and, therefore, makes no sense in many cases. These difficulties can be overcome using isotopic generators, i.e. systems containing two isotopes: a long-lived, parent isotope and a short-lived, daughter one; the latter can be repeatedly separated in situ as it is accumulated. The task involved selection of suitable pairs of the isotopes, development of a fast and simple method of separating the required isotope and designing of the generator. The generators of ^{132}I, ^{99m}Tc, ^{90}Y, ^{87m}Sc, ^{68}Ga have been developed and development of other short-lived isotopes generators is in progress.

The systematic investigations of the physical-chemical properties, of industrial separation methods and development of the flow sheet for separation and preparation of pure ^{106}Ru ^{95}Zr, ^{131}I, ^{144}Ce, ^{147}Pm, ^{90}Y, ^{90}Sr, ^{137}Cs, ^{99}Te and other radioisotopes were initiated in the fifties.

The waste solution of nuclear industry amounts of which are large enough to provide the continuous production and the required output of the above isotopes for their wide use in national economy is the basic material, a supplier of fission fragment elements.

Taking into account the composition of solutions contaminated by impurity cations of corrosion nature the technology of producing the fragment elements provides for a stage of their concentration through coprecipitation with such a carrier, as ferric hydroxide, with a subsequent conversion of the concentrate into nitric acid solution containing strontium, cerium, promethium, yttrium, zirconium, niobium, ruthenium. At this stage the radioactive isotopes of caesium and technetium are converted in alcaline decantate from where they are recovered by adsorption with inorganic sorbents or ione change resins: nickel ferrocyanide in case of caesium and organic resins in case of technetium.

The nitrate concentrate containing elements of the second and third groups as well as zirconium, niobium and ruthenium is treated by use of the precipitation-extraction flow sheet. The most promising long-lived elements, cerium, promethium and strontium, are separated from the bulk of the impurities either by precipitation with a carrier (calcium) in the form of oxalates with a subsequent isolation of the strontium in the form of anhydrous nitrate or by solvent extraction. The use of efficient extractants makes it possible to extract practically the whole of strontium and rare-earth elements from the nitrate mixture of isotope.

The further separation of rare-earth elements is carried out by the solvent extraction with tributyl phosphate-nitric acid system. The strontium and the calcium are separated, the calcium being purified from barium impurities, lead and other elements also by solvent extraction technique. The purity of prepared sources of long-lived fragment elements is rather high. The purification factor of strontium from cerium is 10^4-10^5, that from promethium and other trivalent rare-earth elements being 10^2-10^3. At the final processing stages the promethium enrichment is 10^6 relative to cerium and 10^4 with respect to other rare-earth elements, in particular, to samarium and neodymium. The yields of above elements amount to 95-98%.

The numerous investigations on development of radioisotope ionizing radiation sources of different types, sizes and ratings have been performed.

High-power beta- and gamma-sources based on ^{60}Co, ^{137}Cs and ^{90}Sr are used in irradiation apparatus for investigation of radiation chemistry processes, irradiation sterilization, and in experimental irradiators. Kilocurie isotopic thermal units of different types and purposes have been recently developed on the basis of alpha- and beta - active isotopes, some units being produced in lots.

Isotopic X-ray sources have been developed; sources for removal of electrostatic charges, a variety of sources for radioisotopic instrumentation designed for process monitoring, inspection and calibration of radiometric and dosimetric apparatus, including reference sources, have been developed and are in production; the production of "Mossbauer" sources has started.

Neutron-deficient, or cyclotron, isotopes are produced mainly in nuclear reactions with charged particles. These isotopes can be separated from a target without carrier. High specific activity and a high radioisotopic purity is a feature of the sources of cyclotron isotopes.

There are a number of specific requirements to a cyclotron designed for industrial production of radioisotopes. These requirements are reduced, in general, to necessity of developing high-efficient methods of isotope production with using mechanization and automatization of radiation hazardous works.

The amount of radioactive isotope produced in an irradiated target is defined by the relationship

$$A = \varepsilon B I t \qquad (1)$$

where A is the activity, ε is the coefficient determining a loss of the isotope in the course of the target irradiation ($\varepsilon \leq 1$), B is the yield of the isotope for a thick target, I is the beam current, t is the time of irradiation, $t \ll T_{1/2}$

The coefficient ε depends on properties of irradiated material, cooling method, design of the target, and power of particle beam.

An important requirement to the cyclotron is a possibility of attaining high currents of accelerated particles to ensure a high efficiency of the cyclotron. This is provided mainly by minimizing the loss of particles in the course of their acceleration at the cost of eliminating the vertical instability of the beam.

Preparation of ^{195}Au and its use in activation analysis

The radioactive tracers: gold-195 and gold-199 separated and concentrated mainly by solvent extraction methods are widely used in chemical and radiochemical investigations, in particular in works of analytical type. The problem of extracting and concentrating gold from solutions of hydrochloric and nitric acids is met in practice.

The technique of extraction-chromatographic concentration, purification and separation of radioisotopes has been developed and possibility of preparing the carrier-free radioactive gold-195 in a

radiochemically pure form, from platinum irradiated by neutron flux in a nuclear reactor has been investigated in our laboratory taking into account the above problem.

In so doing, we aimed to develop a simple flow sheet of separating the isotope of interest comparatively quickly and with a high yield. The separated isotope is subsequently used for quantitative neutron-activation high-sensitive analysis of gold in individual samples of ore-bearing rock.

This task has been solved with success. The radiochemical separation of gold-195 and gold-199 from the irradiated platinum matrix was made by extraction-chromatographic method in columns filled with fine polytetrafluoroethylene (PIFE) powder coated with tri-n-octylamine as a fixed organic phase. The technique of coating an inert carrier by organic phase was developed in the laboratory.

The irradiated targets were dissolved in aqua regia with heating. The solution was transferred into the column and passed through the working layer with a certain flow rate. The choice of eluents for purification of gold in the column depends on composition of microimpurities in the initial material. 1M solution of thiourea was used for the gold elution.

The produced carrier-free sources of gold were then applied in developing the neutron-activation method of analysis for gold content of ore.

The comparison between results of assay and activation analysys shows a sufficient reliability of the suggested method of gold content determination.

Preparation of cobalt-57

The favourable nuclear-physical properties of the radioactive cobalt-57 underlie its wide use in X-ray radiometric and X-ray spectral equipment.

Rigid requirements are laid to purity of radionuclide, especially in using it as a "Mössbauer" source. The most advantageous reactions of its preparation are the following.

Separation of cobalt-57 from irradiated nickel matrices is reduced to separation of the trace amounts of the required isitope produced in irradiating a starting target from the gram amounts of nickel (matrix material), radioactive impurities produced both from the target material and from inactive impurities in nickel, as well as to purification of cobalt-57 from the associated reagent microimpurities.

An extraction-chromatographic express method for separation, concentration and purification of cobalt-57 produced by proton irradiation of nickel matrices has been developed in the laboratory.

The method is based on extractability of cobalt into organic phase (tri-n-octylamine) from solutions concentrated with nickel and hydrochloric acid.

In consequence of investigating the solvent extraction and extraction-chromatographic behaviour of cobalt and such microimpurities, as copper, iron, zink, nickel, which are controllable in evaluating the purity of cobalt-57 sources in the system: tri-n-octylamine-hydrochloric acid, optimal conditions of sorption and elution of cobalt-57 on extraction-chromatographic columns with tri-n-octylamine as an organic phase have been established.

The concentration of the isotope is performed in the course of sorption; its purification from microimpurities and contaminating salts is conducted by washing the column with solutions of hydrochloric acid of different concentrations.

The cobalt-57 is eluted from the column with 3M hydrochloric acid.

In developing the technique the purification of starting materials from controllable microimpurities and inactive cobalt was specified to ensure a high specific activity of the separated isotope and its radiochemical purity.

Radioisotope generator of indium-113m

Indium-113m as a short-lived isotope of the generator type is used not only in medical-biological investigations, but it also serves as a good standard for measuring activity of some short-lived radionuclides.

The static and dynamic mechanisms of solvent extraction and extraction-chromatographic behaviour of indium, antimonium and tin in the system of tri-n-octylamine-mineral acids have been studied by using radiotracers.

An optimal regime for sorption of tin under dynamic conditions, maximum capacity of extractant to sorbed element, conditions of indium and antimonium elution, optimal parameters and operating conditions of the working column have been determined.

The natural mixture of tin isotopes as well as tin enriched with tin-112 were used as targets.

The qualitative and quantitative compositions of impurity elements in the used targets were determined in advance by neutron activation method with the help of extraction chromatography.

The radiochemical flow sheet of indium separation from antimonium and tin was developed and tested with imitating mixtures and taken as a basis for indium-113 radioisotope generator.

The purification of the matrix material from associated controllable microimpurities was envisaged at the state of the generator preparation and charging.

The indium-113m extracted from the generator has high specific and volume activities, high radiochemical, isotopic and chemical purity quite corresponding to the requirements imposed on the isotope.

The generator is characterized by stability of operating parameters during long-term use.

THE EXPERIMENTAL INVESTIGATION OF REACTIONS WITH FORMATION OF NEUTRONS ON THE IAE CYCLOTRON

E.A. KUZ'MIN
I.V. Kurchatov Institute of Atomic Energy,
Moscow, Union of Soviet Socialist Republics

Abstract

The fast neutron time-of-flight spectrometer used at the IAE cyclotron is described. The procedure of data processing and the method of the error propagation are explained. The spectrometer was used for investigation of the neutron formation in (alpha, ^{6}Li), (alpha, ^{7}Li) reactions at energies of 8.6 and 11.2 MeV. The results obtained and their comparison with published data are presented.

I. INTRODUCTION

For the past 50 years from the moment of discovery of neutron paramount changes have taken place both in the understanding of mechanisms of nuclear reactions with neutron participations and in the method of such a reaction research. In the recent years the interest has appeared in the study of complex nucleus interactions of energies of several tenth's of megaelectronvolts per nucleon, which is connected with appearance of new accelerators making it possible to carry out fundamental investigations of nuclear reactions within a wider range of projectile nucleus energies and masses. On the other hand, in connection with the studying of various models of controlled thermonuclear reactors the sphere of demands for nuclear data is being widened and requirements for their accuracy are being increased. This has resulted in creation of complicated multiparametric neutron recording systems, brought into being on the basis of accelerators or reactors and up-to-date systems of data storage and processing.

2. FAST NEUTRON SPECTROMETER ON THE BASIS OF IAE CYCLOTRON

To obtain a complete experimental information on a reaction with the neutron yield one needs to measure the energy spectra at different angles about the incident particles beam. The most perfect method of measurement of fast neutron energy spectra is the time-of-flight method, in which an energy is determined by the time of a neutron flight of the distance from a target or a scattering sample to a detector. In practice it is accomplished by measuring the time interval between the pair of pulses, one of which corresponds to the moment of particles escape from the target (a base pulse), the second one, to the moment of neutron registration by a detector. Therefore, it is clear, that in using the time-of-flight method the pulsed accelerators (cyclotrons or pulsed electrostatic accelerators) have more advantages, which make it possible to do without creation of a complicated system for determining the moment of the particle escape from the target.

The IAE one and a half-meter cyclotron has been put into operation in 1947 [1] . For the past years it has been modernized repeatedly and at the present time it represents an isochronous cyclotron enabling ions with mass up to 20 to be accelerated. The use of modified ion source worked out to obtain multiple-charged lithium and beryllium ions, with a powerful pulse power supply system, together with minimizing the ion losses in accelerating and escape made it possible to obtain multiple-charged ion beams or high intensity. The wide range of ion energies of all stable isotopes from hydrogen through neon (from 1 to 15 MeV/nucleon),high intensities of the multiple-charged ions external beam, the pulse character of the accelrated particle beam (the pulses time duration is 2 - 10 ns), all these allow the given IAE cyclotron to be used for researches of a wide range of reactions with the neutron yield.

When creating a time-of-flight fast neutron spectrometer one needs to solve problems of measurement of low time intervals with a high accuracy, stability of the installation operation, shielding from a background radiation, etc. Usually such a spectrometer consists of a fast scintillation detector with a shielding and electronic system of the signals processing and measurement results storage.

The basis of measuring-computing complex of the IAE cyclotron is two computers EC-1010 and CAMAC standard equipment [2] . Each of the computers has the 64 kilobyte main memory, units on magnetic disks and tapes, input-output devices. The CAMAC multiple system interface unit is a part of the computer to connect with an experimental equipment. The complex consists of two parallel-operating measuring systems with possible connection of peripheral measuring stations to them as well as processing of data obtained in the off-line regime. To lessen a dead-time of the system in performing operations of collection, sorting and storage these functions are divided due to a buffer memory accomplishing data acquisition and accumulation. This permitted the recording efficiency to be increased by approximately 4 times. In the worked out system the dead time, when measuring three-parametric events, amounts to 23 μs.

The described IAE fast neutron spectrometer was designed on the basis of the IAE isochronous cyclotron and the measuring-computing complex. It is designed for experimental investigations of a wide class of nuclear reactions with the neutron yield within the energy range of 1-100 MeV.

2.1. Neutron Detector

In the IAE spectrometer the detector of particles is a scintillation counter on the basis of a photomultiplier and an organic scintillator. When selecting the scintillation for a time-of-flight spectrometer its main parameter is a low de-excitation time needed for obtaining a high resolution time. This confines the circle of scintillators practicable for employment to several types of organic and plastic scintillators. On the other hand the necessity of neutrons identification in conditions of intense gamma-background existing practically in all measurements limits even more the selection of scintillators potential for use. For fast neutron spectrometers with identification of particles use is made of stilbene crystals and certain types of liquid organic scintillators NE-213, NE-218, NE-230 being more convenient for fabrication of scintillators of a more complicated shape or larger size. The stilbene crystal of a cylindrical form of the size of 50x50 mm^2 is employed in the IAE spectrometer.

Fast photomultipliers are used for scintillation counters recording the time of particles hit with the accuracy up to tenth parts of nanosecond. At the optimal selection of the detector design the multiplier photocathode diameter should be close to the scintillation diameter, which improves the collection of light from scintillations and decreases its losses. In the detector under consideration the fast photomultiplier FEU-30 is placed with the photocathode diameter of 50 mm.

2.2. Scintillation Detector Efficiency

When determining the true neutron flux one needs the knowledge of a detector's efficiency, i.e. the ratio of amount of recorded neutrons to amount of neutrons hiting the detector. The accurate knowledge of efficiency can be obtained by means of special measurements. However, taking into account great experimental difficulties in making such measurements with a high accuracy, in the majority of cases use is made of the calculated efficiency value. At the energy up to 10 MeV the main process of neutron registration is an elastic scattering on hydrogen nuclei with subsequent detection of recoil protons. At higher energies the reactions on carbon nuclei being a part of organic scintillators begin to affect the neutron efficiency value.

For the IAE spectrometer the calculation of neutron efficiency with energy from 0.1 to 50 MeV was carried out by the Monte-Carlo method with the BESM-6 computer according to the special FORTRAN-program [3,4] . The allowance for various channels of neutron interactions with hydrogen and carbon was performed with the aid of evaluated data of reaction cross-sections, taken from nuclear data libraries. For certain reactions the new evaluation of cross-sections was carried out according to results of experimental works published recently. The feature of efficiency calculations for the detector with a stilbene crystal is the necessity of accounting for dependence of light output on the direction of recoil protons. In the calculations use was made of the empiric dependence of light output $P(E,\theta)$ for the recoil proton with energy E , moving at an angle θ relative to the crystal axis [4,5] $P(E,\theta) = B(\theta) \cdot E^{3/2} \exp(0.016E^{-3/2} - 0.021E^{0.9})$ where $B(\theta) = 0.176 \cdot (1 - 0.311 \sin^2\theta)^{-1/2}$.

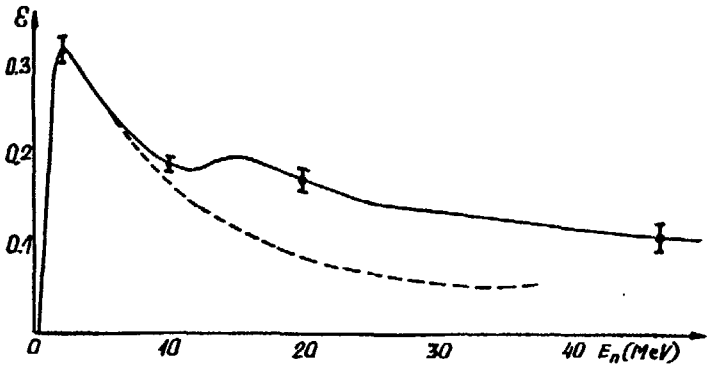

Fig.1. The scintillation detector efficiency ε with the 50x50mm^2 stilbene crystal depending on the neutron energy. The recording threshold is 800 keV.

Fig. 1 presents the results of calculation of neutron efficiency by the detector with cylindrical stilbene crystal with the size of 50x50 mm^2 when its axis was installed along the lines of incidence of the neutron beam. The dotted line marks the contribution due to processes of n-p scattering. It is well seen that at the increase in neutron energy the contribution of processes with participation of carbon nuclei becomes predominant. The analysis of calculation results made it possible to single out reactions giving a certain contribution to different ranges of neutron energies. At the neutron energies from 8 to 14 MeV this is the reaction $^{12}C(n,\alpha)^{9}Be$, from 14 to 22 MeV, the reaction $^{12}C(n,n')3\alpha$, and from 22 to 50 MeV, the reactions $^{12}C\ (n,n')3\alpha$ and $^{12}C\ (n,n'p)^{11}B$.

To calculate errors of measurement results one needs to know the accuracy of the used detector efficiency. When taking measurements of absolute values of reaction cross-sections the error due to the efficiency uncertainty markedly exceeds quite often the error due to inaccuracy of all other parameters. If the calculated efficiency is used then its error depends on the statistical accuracy of Monte-Carlo calculations and nuclear data employed. In our conditions the statistical accuracy of calculations amounted to ~3%. The nuclear data inaccuracy contribution was determi-

ned by the used reactions cross-section variation method within the limits of experimental errors and possible evaluation variants. The obtained errors of efficiency are also given in Fig.1 at several neutron energies. At the neutron energy below 10 MeV the error does not exceed 5%. With the increase of energy up to 50 MeV the error value rises to 20% which is explained by a low accuracy of nuclear data available in this energy region.

2.3. Calibration of Detector Threshold

The detector's efficiency value depends upon the registration threshold, i.e. the minimum energy of recoil protons recorded. To determine this threshold the calibration of measuring equipment should be performed in energy units of the recorded particles. The absence of simple monoenergetic neutron sources forces us to employ indirect calibration methods based on recording of other sort particles obtained by means of accessible sources, and on scaling of the obtained threshold value with the aid of ratio of light outputs for these particles and protons.

The calibration of the IAE spectrometer is accomplished according to spectra of Compton electrons, obtained in irradiating the scintillation detector by sources of γ-radiation of the known energy (^{22}Na, ^{60}Co, ^{137}Cs). As a calibration point use was made of the middle of Compton spectrum decay, of the maximum energy of which Ee_{max}, connected with the incident gamma-radiation energy E_γ by the ratio $Ee_{max}=2E_\gamma^2/(mc^2+2E_\gamma)$, where m is the electron mass. The threshold value obtained is recalculated into units of recoil proton energy by means of the ratio between the light output in the stilbene for electrons and protons.

The other method can determine the threshold of recording system directly according to the time spectrum of neutrons, where defining the maximum time-of-flight of recorded neutrons one can assess their minimum energy.

The threshold value in measurements on the IAE cyclotron amounted to 0.5-1.5 MeV depending on experimental conditions and the problem under solution. The uncertainty of the energy threshold value was estimated by means of the results disagreement obtained by both methods and came up to ~10%.

2.4. The detector Shielding

To reduce a detector sensitivity to a background induced by scattering of a neutron beam on measuring hall walls the scintillation detector was placed into a shield [6]. At highly changing background depending on the reaction under investigation or an unknown background distribution in the hall the optimal is a spherical shape shielding at which the value of background weakening does not depend on the direction of the particle incidence on the shield. It is such a shape that has been chosen to shield the scintillation detector of the fast neutron spectrometer. When choosing the shield material it was borne in mind that with the increasing of neutron energy the shield efficiency based on hydrogen-containing materials drops due to decrease in the $n-p$ scattering cross-section. Therefore, the multilayer shield has been chosen (Fig.2), the external layer of which was made of iron. In this layer of the 150-mm thickness the absorption of fast neutrons or the decrease in their energy takes place, mainly

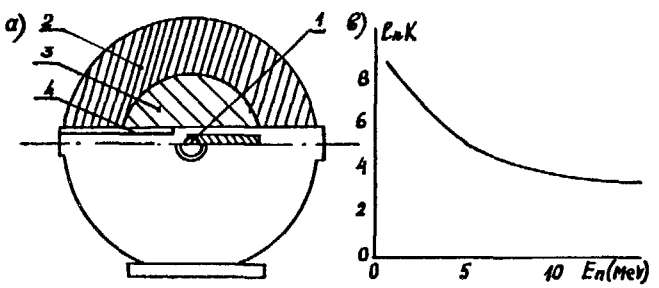

Fig.2. a) Spherical protection.
1 - detector; 2 - (Fe) shielding layer, 3 - shielding layer (borated polyethylene), 4 - collimator.

b) Dependence of attenuation factor K of the neutron flux for the spherical shielding on energy.

due to inelastic interaction processes. The 250-mm borated polyethylene layer is the following. The third iron shield layer is an additional shield against gamma-rays originating in the first layer. The cylindrical shape of this layer has been chosen to ensure the detector installation and an input collimator. The ex-

ternal diameter of the entire spherical shield is 950 mm. The internal diameter of the cylindrical channel is 110 mm, defining the maximum possible diameter of the scintillation detector.

The dependence of neutrons attenuation coefficient of the worked-out multilayer shield upon energy was calculated by means of neutron absorption macroscopic factors. Fig.2 shows the calculation results. With the increase of neutron energy the attenuation coefficient decreases smoothly from $6x10^3$ at 1 MeV to 42 at 10 MeV. At neutron energies being less than 5 MeV, where the main part of background neutron spectrum is located, the attenuation coefficient exceeds $1.5x10^2$.

2.5. Measuring Neutron Hall

It should be noted that the shield design and shape in every concrete case, are determined, basing on a wide variety of conditions. Main among them are the energy range of neutrons under investigation, the required attenuation value and the background radiation intensity. In measuring neutron spectra by the time-of-flight method the detector is removed from the target at a considerable distance and the background near the detector is determined by scattered on the walls neutrons and gamma-quanta as well as by radiation from the charged particle beam transportation system. Therefore, the optimum design and the shield shape depends strongly on measuring hall sizes and location of the detector in it. Shield shapes being most highly distinguished from the spherical one are used in studying the neutron scattering, where the main is shielding of the detector from the primary beam of neutrons bombarding a sample.

The measurement of neutron spectra on the IAE cyclotron by the time-of-flight method is accomplished in the measuring hall of $13x10x4m^3$ in size (Fig.3). The spherical shield with the detector is placed on a movable base which can move relative to the target center located nearby. The control of the shield's movement with the detector is accomplished remotely. The range of potential measurements of angles comes up to $0 - 160^\circ$, and the flight path can vary from 2 through 6 m. The height of detector location above the floor level is 1.7 m.

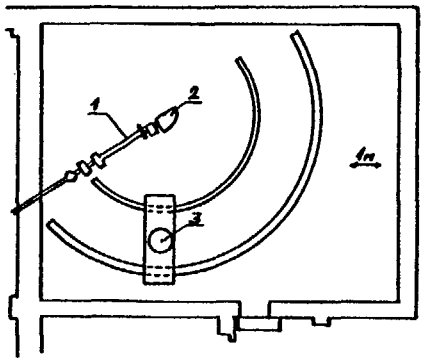

Fig.3. Measuring neutron hall.
1 - the system of transportation of accelerated particle beam; 2 - target; 3 - detector with shielding.

2.6. Data Recording System

In Fig.4 presented is the simplified circuit of the fast neutron spectrometer used at the IAE. The spectrometer consists of a pulse-shape discriminator (PSD) with time discriminators, a charge-digital converter (CDC), two time-digital converters (TDC) and a discriminator of reference pulses from HF of the cyclotron. All the units were made in the CAMAC standard and connected through a buffer memory with the computer EC-1010 in which data sorting and storage are performed.

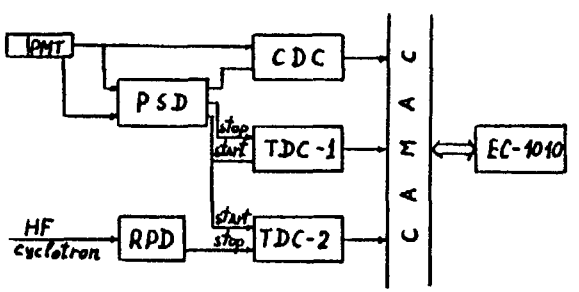

Fig.4. Block diagram of the time-of-flight neutron spectrometer.

To separate pulses from neutrons and gamma-quanta use is made of the pulse shape discrimination method based on the fact that in interacting the recoil-proton with the scintillator substance the relative contribution of a slow component to the scintillation intensity is higher than for electrons generated at the record of background gamma-radiation. Time diagrams explaining the principle of shape discrimination and the discriminator operation, are presented in Fig.5. In the PSD an active differentiation of the PMT dynode pulse is accomplished with the time constant of 0.5 μs, corresponding to the maximu difference of t_p and t_e intervals (Fig.5), and the pulse is generated, corresponding to the moment of intersection of a zero line by a bipolar signal [13].

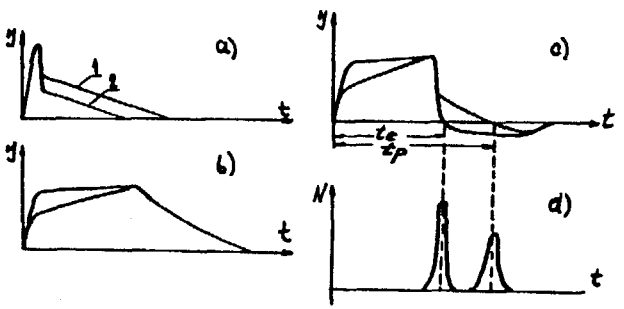

Fig.5. Time diagrams of a discriminator operation according to a pulse shape.
a) The pulse form of PMT current at irradiation of stilbene crystal by neutrons (1) and gamma-quanta (2).
b) Integrated pulses.
c) Differentiated pulses.
d) The density of probability of time interval distributions of the t_e and t_p responding to signals from electrons and recoil protons.

To obtain the signal on the time of particle recording by the detector the discriminator with the leading edge is installed in the PSD, at the input of discriminator fast signals arrive from the PMT anode. This discriminator's threshold determines the spectrometer's recording threshold.

Pulse pairs corresponding to momenta of particle recording and to the moment of intersection of zero line by the bipolar signal, arrive in the TDC "start" and "stop" inputs. The distributions obtained from this converter have the form presented in Fig.5d. A simple differential discriminator generating logic signals corresponding to the chosen kind of particles is often used to separate neutrons and gamma-quanta. In the IAE spectrometer the separation is accomplished according to two-dimensional spectrum formed from TDC-1 signals and CDC signals, giving an amplitude spectrum of radiation recorded. The analogous procedure is employed in identifying charged particles by the ΔE-E method. In the case of neutron separation from background gamma-quanta by means of the described two-dimensional spectrum, more optimum neutron discrimination is successfully accomplished with allowance for both the amplitude dependence of the n-γ discrimination parameter and the character of the spectrum recorded.

The recording of time-of-flight spectra is performed by means of the TDC-2, at whose input pulses corresponding to the moment of particle incidence to the detector, and reference pulses arrive. The dimension of the time-of-flight spectra stored is 512 or 1024 channels.

The reference pulses needed for the spectrometer operation, are generated with the help of a single reference pulse discriminator (RPD) to whose input a high-frequency voltage is applied from a capacity divider, connected with the cyclotron. The time inaccuracy of RPD measured within the entire working range of the HF cyclotron did not exceed ±0.25 ns.

The main technical parameters of the IAE spectrometer recording system:

- the own resolving time within the dynamic range of 1-50 MeV neutron energies — 1 ns;
- the background γ-quanta suppression coefficient — 10^4;
- the load capability — 10^4 puls/s.

2.7. Experimental Data Processing

For experimental data processing the second computer EC-1010 of the measuring-computing complex is used, operating in the "off-

line" regime. The processing consists in substraction of the background spectrum (determined by the neutron yield from the target substrate and the Faraday cylinder) from the measured spectrum, recalculation of the spectrum from the time-of-flight scale into the neutron energy scale and calculation of neutron yield absolute cross-sections.

As it was shown above, in the IAE spectrometer several methods were employed for the background radiation discrimination. The natural modulation of the cyclotron beam enables the record of radiation not correlated by the bombarding particle beam to be avoided. The application of n-γ discrimination circuit has ruled out practically completely the record of background gamma-radiation. The worked out multi-layer shielding has reduced significantly the efficiency of scattered neutron radiation recording. The measures taken made it possible to decrease essentially the background radiation contribution to the neutron spectra measured. For the majority of reaction with neutron yield studied at the IAE cyclotron the value of the background under computation did not exceed 10-20%.

The calculation of neutron kinetic energy E for the time spectrum channel K was performed by means of ratio:

$$\beta = L/[Z\cdot(K_\gamma - K)\cdot c - L]$$
$$E = m_0c^2\,(1/(1-\beta^2)^{1/2} - 1)$$

where: L is the flight path;
Z is the time width spectrometer channel;
K_γ is the channel's number of γ-peak position in the spectrum;
m_0 is the neutron mass.

While processing continuous neutron distributions from many-particle partial channels the double differentiation cross-sections were calculated by means of the expression:

$$\frac{d^2\sigma}{d\Omega\cdot dE} = \frac{N\cdot\alpha_1\cdot\alpha_2}{d\Omega\cdot\Delta E\cdot\varepsilon(E)\cdot n\cdot\bar{I}\cdot\alpha_3(E)}$$

where N is the number of counts in spectrum within the interval ΔE;
α_1 is the coefficient accounting for dead-time losses;
α_2 is the one accounting for neutron losses in the discrimination circuit;
$d\Omega$ is the detector solid angle;
ΔE is the neutron energies interval;
$\varepsilon(E)$ is the neutron detector efficiency;
n is the number of target nuclei per square unit;
$\bar{I}$ is the bombarding particles flux;
$\alpha_3(E)$ is the coefficient accounting for neutron attenuation in the air and the target chamber.

For presentation of spectra the selection of neutron energy intervals ΔE plays a significant part. The optimum is selection of ΔE being equal to the energy resolution in the spectrum. The energy resolution obtained with the time-of-flight method is determined by the energy and time uncertainty of incident particles, the target thickness and the recording instrument resolution. In measurements on the IAE cyclotron the main contribution was made by the time uncertainty of the incident particle beam and the target thickness influence, and in this case, due to the non-linear coupling of neutron energy with time-of-flight the contribution of the former value is the most significant at high neutron energies, and the latter one , at low ones. Therefore, the value ΔE in the low energy spectrum part is chosen to be equal to the target energy thickness half; in the high energy spectrum part the averaging is carried out according to the number of channels, being equal to the half of width of micropulses of the accelerated particle beam. Such a presentation makes it possible to show the measured spectrum in enough details with insignificant losses of the spectroscopic information.

In calculating two-particle channel cross-sections $d\sigma/d\Omega$ according to the area of peaks in spectra the problem is simplified, since there is no need to choose the value ΔE. The value $d\sigma/d\Omega$ is calculated by means of an expression analogous to the given above.

3. MEASUREMENT ERRORS

While determining errors of indirect multiparametric measurements of the value $Y = f(x_1, x_2, \ldots x_n)$ use is made of the relation

$$\Delta Y = \sqrt{\sum_{i=1}^{n} (\partial f/\partial x_i \cdot \Delta x_i)^2} \qquad (1)$$

where ΔX_i is the error value of parameter X_i. With the aid of this expression the errors due to inaccuracies in measurements of $\alpha_1, \alpha_2, \alpha_3(E)$, n, $\bar{I}$, $\varepsilon(E)$ and $d\Omega$ are calculated. If should be noted that the expression (1) was obtained at expansion of the function $f(X_1, X_2, \ldots X_n)$ in Fourier series and is accurate only in the case when $f(X_1, X_2 \ldots X_n)$ represents the linear function of parameters. For other cases one can apply the relation

$$\Delta Y = \sqrt{\sum_{i=1}^{k} (\Delta Y_i)^2} \qquad (2)$$

where ΔY_i is the deviation of Y from its value at the change in parameter X_i by the value of error ΔX_i. The validity conditions of expression (2) is less rigid, here, enough is the constancy of the value $\partial f / \partial X_i$ on the interval $\bar{X}_i - \Delta X_i < X_i < \bar{X}_i + \Delta X_i$. These features can exert an essential influence on the result of calculation of the error value at the complicated dependence of the function $f(X_1, X_2 \ldots X_n)$ upon parameters. While processing the time-of-flight neutron spectra such parameters are L and τ the variation of which results in recalibration of spectra, i.e. in their non-linear shift in an energy scale.

In processing the neutron spectra obtained at the IAE cyclotron the total error due to parameters α_1, α_2, $\alpha_3(E)$, $\bar{I}$ and $d\Omega$ does not exceed 2%. The error due to the inaccuracy in $\varepsilon(E)$ depends on the neutron energy and amounts to 3-10%. The accuracy in determining the target thickness comes usually up to 5-7%. The total error of $d^2\sigma / d\Omega \cdot dE$ due to L and τ in accuracies depends upon the spectrum character and for its different parts amounts usually to 1-5%. The statistic error is determined by the duration of exposure, which is chosen in such a way that the statistic error value does not exceed 10%.

4. EXPERIMENTAL INVESTIGATIONS OF NEUTRON CHANNELS OF ALPHA-PARTICLE INTERACTIONS WITH LITHIUM NUCLEI

The research of neutron channels of interaction of alpha-particles with lithium nuclei was initiated starting from need for knowledge of this interaction parameters for practical purposes. ^{6}Li is considered as a probable fuel in certain models of controlled fusion reactors. The advantage of such models is a lack in the cycle of tritium, the radioactivity of which leads to a significant complication in reactor based on the D-T reaction. In this connection we need knowledge on processes of lithium nuclei interaction with fast alpha-particles, the amount of which in plasma is usually essential.

Up to now, few data published are available on the experimental research of neutron channels of interactions of alpha-particles with ^{6}Li nuclei as well as ^{7}Li. In paper [8] the neutron yield was measured with the aid of long counters at the angle of 0° in relative units within the energy range of the threshold to 15 MeV. The paper [9] concerns the search of the ^{9}B excited state with the 1.7-MeV excited energy at the alpha-particle energy of 14 MeV in the ^{6}Li (α, n) reaction; in this paper neutron spectra are presented within the range of angles of 15-75° and their cross-sections are estimated. In the paper [10], the spectrum and angular distributions of neutrons from the ^{7}Li (α, n) reaction were studied for alpha-particle energies from the threshold to 8 MeV with the aid of the time-of-flight spectrometer. Neutron yield data, while bombarding thick lithium targets by alpha particles, are contained in the paper [11], which makes it possible to use them only for rough assessments of the cross-section values.

The main information in the papers under consideration is concerned with low-excited states of boron or with the whole neutron spectrum without separation of partial channels. The data on the contribution of multi-particle channels in the ^{6}Li (α, n) reaction and, total cross-sections of neutron formations in this reaction are practically not available. The performed short review of data published showed the necessity of the detailed investigation of neutron partial channels of the ^{6}Li+α and ^{7}Li+α reactions at the alpha-particle energies up to 10-11 MeV.

5. MEASUREMENT PROCEDURE

Measurements of cross-sections and angular distributions for neutron partial channels of alpha-particles and ^{6}Li and ^{7}Li nucleus interactions have been taken at the IAE cyclotron by means of the above-described neutron spectrometer. In the experiments

use was made of ^{6}Li and ^{7}Li self-supporting targets with the 1.5 mg/cm^2 thickness. Neutron spectra were measured within the angle range from 10 to 140° for alpha-particle energies of 8.6 MeV and 11.2 MeV at the time-of-flight spectrometer path of 4.5 m and the neutron threshold of 800 keV.

6. $^{6}Li(\alpha, n)$ REACTION

The neutron generation at the interaction of alpha-particles with ^{6}Li nuclei can proceed at alpha-particles energies of above 6.62 MeV, which is explained by the negative energy of the reaction (-3,975 MeV) for a channel with ^{9}B formation in the ground state.

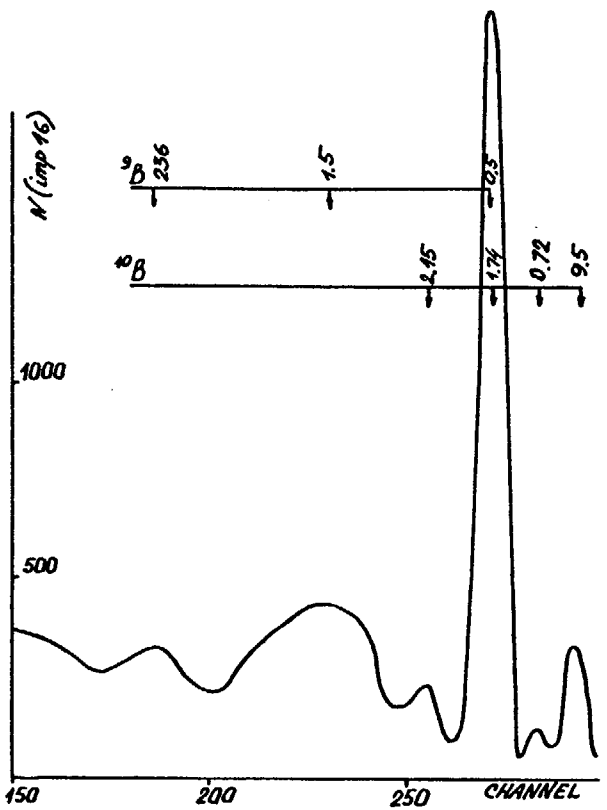

Fig.6. The energy spectrum of neutrons from the $^{6}Li(\alpha, n)$ reaction at the angle of 20° at the α-particle energy of 11.2 MeV. Arrows mark peak's positions, corresponding to various states of ^{9}B and ^{10}B, formed in the $^{7}Li(\alpha, n)$ reaction due to ^{7}Li impurity in the ^{6}Li target.

Fig.6 shows the neutron energy spectrum measured at the angle of 20° at the energy of 11.2 MeV. On the spectrum well-seen are the peaks formed at the excitation of various states of the ^{9}B residual nucleus as well as the continuous spectrum of neutrons generated in the four-particle channel of the $^{6}Li+\alpha \rightarrow 2\alpha+n+p$ reaction (Q =-3.7 MeV). In the spectrum also seen are the neutron peaks from the $^{7}Li(\alpha, n)$ reaction proceeding on the ^{7}Li impurity in the ^{6}Li target. Energy positions of the peaks are indicated with arrows. The data on cross-sections and angular distributions of neutrons from two-particle channels of $^{6}Li(\alpha, n)^{9}B$ for ground and excited (1.6 MeV and 2.36 MeV) states of the ^{9}B residual nucleus were obtained from the results of peaks treatment from such spectra.

These data are presented in Fig.7 for alpha-particle energies of 8.6 MeV and 11.2 MeV. The angular distribution for the ^{9}B gro-

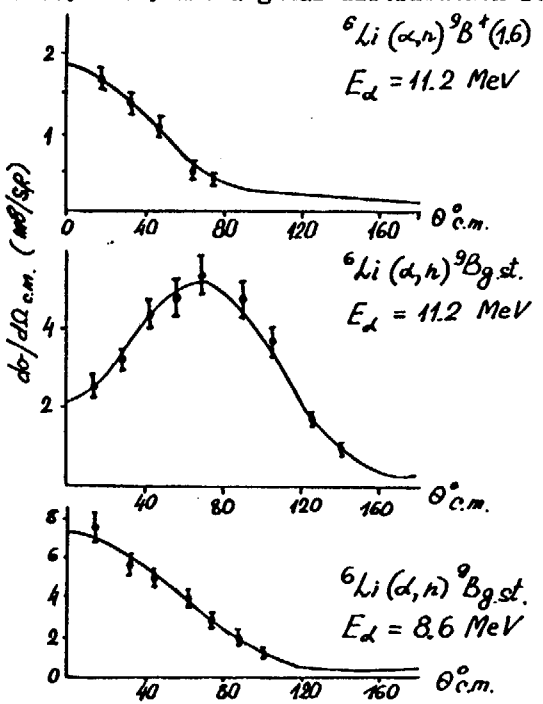

Fig.7. Neutron angular distributions from the $^{6}Li(\alpha, n)$ reaction in the centre-of-mass system. The smooth curves are approximation with the aid of Legendre polynomial expansion.

und state at a lesser alpha-particle energy is significantly anisotropic and shows the priority neutron yield at low angles. Such a shape of an angular distribution can indicate the appreciable contribution of the reaction direct mechanism. Note that such conclusions have been drawn by the authors of paper [8], based upon the lack of resonances in the excitation function at 0° within the alpha-particles energy range from the threshold to 15 MeV.

At the higher energy of alpha-particles the angular distribution for the ^{9}B ground state has maximum at the angle of about 90° and changes smoothly, which does not permit any mechanism of the considered channel to be pointed out unequivocally. Data on the same channel are contained in the work [9], where it is shown that at the 14.4-MeV alpha-particle energy the neutron yield cross-sections in the $^{6}Li(\alpha, n)^{9}B$ g.st reaction amount to 1.0 ± 0.25 mb/sr within the angle range of 15 -60° and to 0.6 mb/sr for the 15° angle in a laboratory system. When changing these data into the mass center system the angular distribution shape will be close to that obtained on the IAE cyclotron, but the cross-section value is considerably lower, which can be explained by the decrease in the channel contribution with formation of the ^{9}B ground state at the increase of the interaction energy.

Data for the $^{6}Li(\alpha, n)^{9}B^{*}$ (1.6MeV) channel were obtained within the angle range of 15 -75° in the centre-of-mass system and are also presented in Fig.7. The angular distribution for this channel neutrons has maximum at low angles and drops with the increase of an angle. The existence of ^{9}B state with the excitation energy of 1.6 MeV was first reported in the paper [12]. There, with the help of $^{10}B(^{3}He, \alpha)^{9}B$ reaction, the energy of this state and its width (~700 keV) have been measured. The estimation of the 1.6-MeV state width according to spectra, obtained at the IAE, gives the value ~500 keV, which is in agreement with data of the paper [12]. The search of this state is attempted in the work [9], where the upper limit of cross-section of the $^{6}Li(\alpha, n)^{9}B^{*}$(1.6 MeV) reaction of 0.1 mb/sr has been gained at the alpha-particle energy of 14.4 MeV. The disagreement of this paper data with results obtained at the IAE can be explained by the strong dependence of the channel cross-section upon energy; on the other hand, measurements of the work [9] were taken in conditions of an intensive background from the target substrate, which could affect the obtained data accuracy.

For the $^{6}Li(\alpha, n)^{9}B^{*}$ (2.36MeV) reaction the cross-section is obtained only for laboratory angles of 10 and 20° (that corresponds to angles of 21 and 43° in the centre-of-mass system); at less values of the laboratory angle, neutrons from this channel have an energy below the recording threshold. In the centre-of-mass system the neutron formation cross-section with excitation of the ^{9}B 2.36 MeV state came up to 0.8 ± 0.1 mb/sr for angles of 21 and 43°. On the assumption of isotropy of neutron yield for this channel the total cross-section calculation gives the value of 10 mb, however, the small number of experimental points of the angular distribution makes it impossible to indicate the accuracy of the estimation carried out.

The measured angular distributions were approximated by means of the Legendre polynomial expansion by the least-square method:

$$d\sigma/d\Omega = \sum_{0}^{n} X_n \cdot P_n(\cos\theta) \quad (mb/sr)$$

The expansion results are presented in Table 1.

Table 1

Coefficients of $P_n(\cos\theta)$ Legendre polynomial expansion of neutron angular distributions from $^{6}Li(\alpha, n)^{9}B$ and $^{7}Li(\alpha, n)^{10}B$ reactions

Reaction channel	Alpha-particle energy (MeV)	Coefficients				
		X_0	X_1	X_2	X_3	X_4
$^{6}Li(\alpha,n)^{9}B$ g.st.	8.6	30±3	44±8	17±9	–	–
$^{6}Li(\alpha,n)^{9}B$ g.st.	11.2	43±4	25±2	-27±3	-13±3	–
$^{6}Li(\alpha,n)^{9}B^{*}(1.6)$	11.2	6.6±0.6	7.7±1.1	5.8±1.4	3.4±1.7	–
$^{7}Li(\alpha,n)^{10}B$ g.st.	8.6	190±20	120±10	-90±15	-56±20	-40±20
$^{7}Li(\alpha,n)^{10}B^{*}(0.72)$	8.6	42±4	30±4	-15±5	–	–
$^{7}Li(\alpha,n)^{10}B$ g.st	11.2	140±15	-4±5	-57±10	–	–
$^{7}Li(\alpha,n)^{10}B^{*}(0.72)$	11.2	46±4	-7±4	-19±7	-9±8	–
$^{7}Li(\alpha,n)^{10}B^{*}(1.74)$	11.2	8.0±0.8	0±0.7	-6±1	–	–

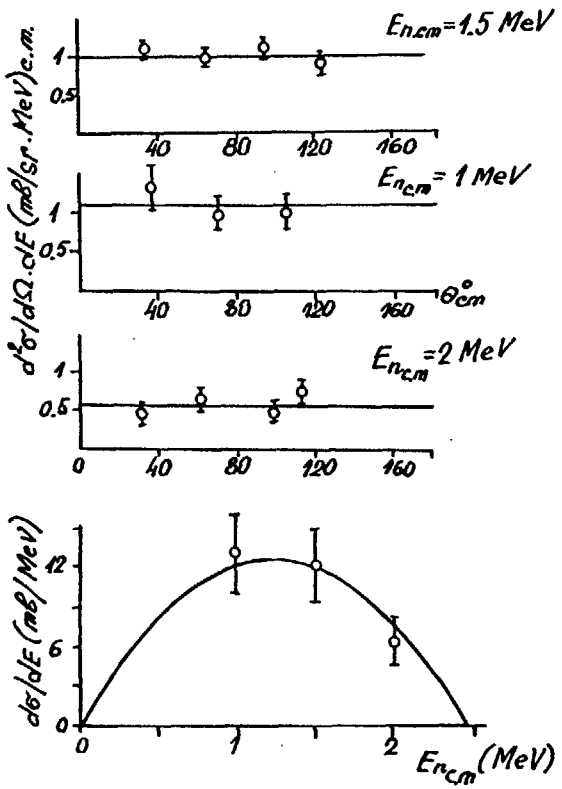

Fig.8. Angular distributions and the energy spectrum of neutrons from the $^6Li(\alpha,n)p2\alpha$ reaction at the α -particle energy of 11.2 MeV.

The neutron formation in interacting alpha-particles with ^6Li is also accomplished in the four-particle channel $n+p+2\alpha$ which leads to a continuous spectrum of neutrons. The cross-section and angular distribution data of these neutrons were obtained within the energy range of 1-2.5 MeV and within the range of angles of 35-110° in the centre-of-mass system. Results are shown in Fig.8. It is seen that angular distributions can be approximated with good accuracy by a horizontal straight line. On the assumption of isotropy, the neutron energy spectrum was obtained within the energy range of 1-2.5 MeV for the whole interval of angles. Extrapolation of this spectrum to zero energy of neutrons with the aid of a smooth curve makes it possible to determine a neutron formation cross-section in the four-particle channel 1.6 mb/sr, which agrees with the estimation available in the work [9] , where this cross-section amounts to about 4 mb/sr at the alpha-particle energy of 14.4 MeV.

The total neutron formation cross-section in the four-particle channel is obtained by integrating the isotropic angular distributions with allowance for the carried out extrapolation accuracy, which is 50%. For the entire spectrum this cross-section amounted to (20±10) mb.

In Table 2 given are total cross-sections of the studied partial channels of the $^6Li(\alpha,n\ )$ reaction. It is seen that with the growth of energy the total neutron formation cross-section increases, which agrees qualitatively with the shape of excitation function at 0°, measured in the paper [8] .

Table 2

Total cross-sections $^6Li(\alpha,n\ )$ and $^7Li(\alpha,n\ )$ reactions

Reaction channel	Alpha-particle energy (MeV)	Total cross-section (mbarn)
$^6Li(\alpha,n)^9B$ q.st.	8.6	30±3
$^6Li(\alpha,n)^9B$ q.st.	11.2	43±4
$^6Li(\alpha,n)^9B^*(1.6)$	11.2	6.6±0.6
$^6Li(\alpha,n)^9B^*(2.36)$	11.2	10 (evaluation)
$^6Li(\alpha,n)p,2\alpha$	11.2	20±10
$^7Li(\alpha,n)^{10}B$ q.st.	8.6	190±20
$^7Li(\alpha,n)^{10}B^*(0.72)$	8.6	42±4
$^7Li(\alpha,n)^{10}B^*(1.74)$	8.6	10
$^7Li(\alpha,n)^{10}B$ q.st	11.2	140±15
$^7Li(\alpha,n)^{10}B^*(0.72)$	11.2	46±4
$^7Li(\alpha,n)^{10}B^*(1.74)$	11.2	8±0.8
$^7Li(\alpha,n)^{10}B^*(2.15)$	11.2	35±15.
$^7Li(\alpha,n)^{10}B^*(3.59)$	11.2	28±14

7. $^{7}Li(\alpha, n)$ REACTION

The formation of neutrons in interacting alpha-particles with ^{7}Li can proceed at the energy of α-particles above 4.38MeV ($Q = -2.79$ MeV). In the measurements only two-particle channels of $^{7}Li(\alpha,n)^{10}B$ reaction were feasible energetically. Data for 3 states were obtained at the energy of α-particles of 8.6 MeV, and for 5 states at the energy of 11.2 MeV.

Fig.9 shows the obtained angular distributions for neutrons from the $^{7}Li(\alpha,n)^{10}B$ reaction with formation of ^{10}B in the ground and the first excited (0.72MeV) states. The angular distributions have the shape close to the symmetric one about 90°, which is in

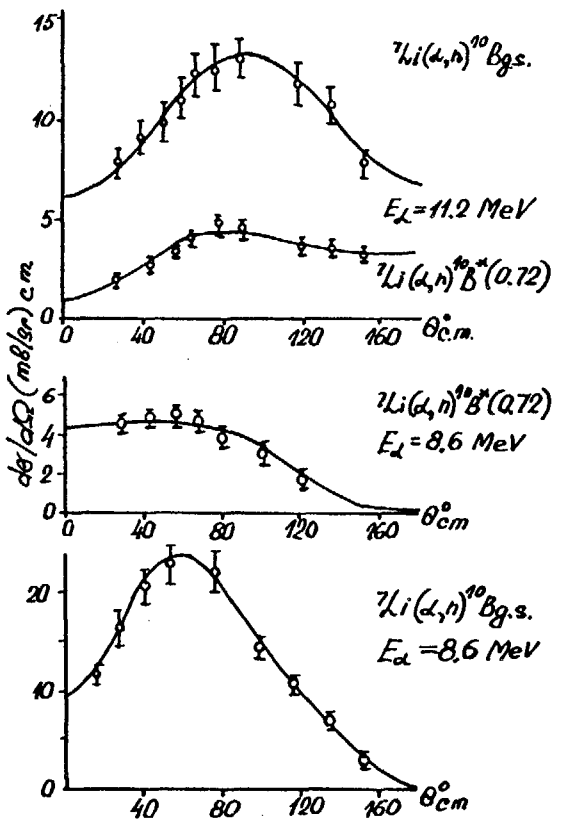

Fig.9. Angular distributions of neutrons from the $^{7}Li(\alpha,n)^{10}B$ reaction in the centre-of-mass system. Smooth curves are the approximation with the aid of Legendere polynomial expansion.

agreement with results of the work [8], indicating the significant contribution of the reaction mechanism with formation of a compound nucleus. Expansion coefficients of the angular distributions measured are presented in Table 1.

For higher energies of ^{10}B excitations the neutron yield was obtained at the energy of 11.2 MeV not in the whole range of angles, therefore, the total cross-section value for these channels was evaluated from results available. For the $^{7}Li(\alpha,n)^{10}B^*$ (2.15MeV) channel the cross-section within the angle range of 25 -85° changes weakly and amounts to 2.7 ± 0.3 mb/sr, which makes it possible to assume isotropy of the angular distribution and to estimate the total cross-section being equal to 35 ± 15 mb. For the $^{7}Li(\alpha,n)^{10}B^*$ (3.59MeV) channel in the angle range of 35-65° the cross-section comes up to 2.2 ± 0.2 mb/sr and the total cross-section was evaluated as 28±14 mb. The cross section and angular distributions for the $^{7}Li(\alpha,n)^{10}B$(1.74 MeV) reaction were obtained at the energy of 11.2 MeV; for the energy of 8.6 MeV the assessment of only the upper limit of the total cross-section was performed.

In Table 2 presented are the obtained data on total cross-sections of the investigated channels of α-particle interactions with ^{7}Li nuclei.

Besides, data on the total cross-sections of this reaction are available in the paper [8] for first two states of ^{10}B at the α-particle energy up to 8 MeV. The total cross-section of the $^{7}Li(\alpha,n)^{10}B$ reaction has the maximum value of 150 mb at the energy of 7.2MeV and then decreases down to 100 mb. The lack of data on further course of the total cross-section dependence upon energy does not permit us to judge the accuracy of agreement of these results with data obtained in IAE. For the $^{7}Li(\alpha,n)^{10}B^*$(0.72 MeV) reaction the total cross-section at the energy up to 8 MeV does not exceed 50 mb, which does not contradict the results presented.

REFERENCES

1. N.N.Venikov, A.G.Volkovich, A.N.Gushchin et al. Isochronous Cyclotron. Preprint IAE-2942, 1978.

2. A.A.Vinogradov, V.V.Paramonov, V.A.Solovjov, et al. The measuring-computing complex for experiment on a Cyclotron. Preprint IAE-3640/15, 1982.

3. E.A.Kuz'min, N.I.Sidorov, L.VChulkov, G.B.Yan'kov. The stilbene crystal efficiency for neutrons with energy of 1-20 MeV. Neytronnaya fizika (Neutron physics), p.4, Obninsk, 1974, p.292.

4. L.V.Chulkov. The scintillation detector efficiency. Preprint IAE-2594, 1975.

5. L.A.Trykov, M.D.Tyufyakov, Yu.V.Fadeev. One-crystal scintillation spectrometer. PTE, No.1, 1973, p.51.

6. O.V.Bochkaryev, E.A.Kuz'min, S.A.Petushkov, A.A.Tsvetkov. The fast neutron spectrometer at the IAE Cyclotron. Proceedings of 4-th All-Union Conf. on the neutron physics, Kiev, 1977, part 4, Moscow, 1977, p.232.

7. Glasgow D.W., Velkley D.E. Brandenberger J.D. et al. Nuclear Instruments and Methods, 1974, v.114, p.521.

8. M.K.Metha, W.E.Hunt, H.S.Plendl, R.H.Davis, Nucl.Phys., 1963, v.48, p.90.

9. R.W.Bauer, J.D.Anderson, C.Wong. Nucl.Phys., 1964, v.56, p.117.

10. L.Van der Zwan, K.W.Geiger. Nucl.Phys., 1972, v.A180, p.615.

11. J.K.Bair, J.Gones del Campo. Nucl.Sci.Eng., 1979, v.71, p. 18.

12. A.Kroepfl and J.Browne. Nucl.Phys., 1968, v.A108, p.289.

13. An investigation of capabilities of a wide-range identification of neutrons through the shape of scintillation detector signals. Collected articles. Ed. by A.A.Kurashov. Preprint IAE-2337, 1973.

NON-EQUILIBRIUM NEUTRON EMISSION IN REACTIONS INDUCED BY LIGHT AND HEAVY IONS

L.V. CHULKOV
I.V. Kurchatov Institute of Atomic Energy,
Moscow, Union of Soviet Socialist Republics

Abstract

The processes occuring in nuclei are reflected in the characteristics of particles produced in nuclear reactions. The mechanism of deexcitation and level densities of compound nuclei are determined from spectra of the evaporation light particles. The nonequilibrium emission of nucleons can be an instrument of studying both the processes of dissipation of energy in collisions of heavy ions and the properties of the nuclear matter in its nonequilibrium phase. Neutrons have some advantages in these investigations.

The rich experimental and theoretical data on nonequilibrium emission have been accumulated to date. The theoretical ideas concerning the mechanisms of preequilibrium processes are rather various. In a number of works the total process is reduced to the successive two-nucleon interactions. The formation of a localized hot zone in a nucleus is believed by some investigators to play a determinative role. There are some works where the intranuclear motion of nucleons is assumed to manifest itself in the spectra of nonequilibrium particles.

In the present report a review of theoretical ideas is presented; the level of conformity of models to the available experimental data and the degree of criticality of the experimental characteristics to the basic predictions of the models are discussed. The model-independent consequences of experimental investigations are also considered.

INTRODUCTION

As early as in a period of developing the theory of equilibrium evaporation from a preformed compound nucleus /1/ a variety of hypotheses appeared about the possible mechanisms leading to discrepancies in the emitted particle spectra from the behaviour predicted

by the evaporation model /2/. But for several decades it was assumed to divide nuclear reactions into two extreme categories: direct reactions and reactions proceeding through a compound nucleus formation. Such a division is based on degree of loss of information about the entrance channel in the course of the reaction. The direct reactions are single-step processes in which the exit channels are directly connected with the entrance one. The processes of this type are usually described by microscopic methods. The compound nucleus formation represents another extreme case. The information about the way and in reactions with which particles the compound nucleus formation has taken place is completely lost during the reaction. In this case the statistical methods are applicable for calculations.

The drastic difference between the direct interactions and the processes proceeding through a compound nucleus formation means, in practice, that there are many types of reactions going on for different time and in which the information on the entrance channel is transferred, to a different degree, to the characteristics of reaction products. One of these processes is a light particle emission and the present review is devoted to the problems of studying its mechanism.

Fig.1 shows an example of the experimentally observed difference from the mechanism of compound nucleus formation and disintegration /3/. The forward direction and high yield of high-energy particles are characteristic of nonequilibrium emission. The shapes of energy spectra are wonderfully similar for all targets (from cobalt to platinum) studied in /3/. There is no abrupt dependence of nonequilibrium proton yield on reaction energy (116 and 89 mbarn for the ^{58}Ni and ^{62}Ni targets, respectively). The nonequilibrium particle yield changes weakly with Z of the target. In case of substituting the nickel-58 target by the platinum one the nonequilibrium nucleon yield decreases a little more than by a factor of two, whereas the equilibrium component of spectra reduces almost by a factor of 10^3 /3/. The measurements have indicated that the excitation functions for ^{142}Ce (p, n) and ^{139}La(α, n) reactions /4/ with formation of the same compound nucleus versus excitation energy practically coincide (Fig.2), although at high energies the difference from the mechanism of compound nucleus formation is considerable. This behaviour of excitation function for different entrance channels cannot be explained by the breakup or knockout processes.

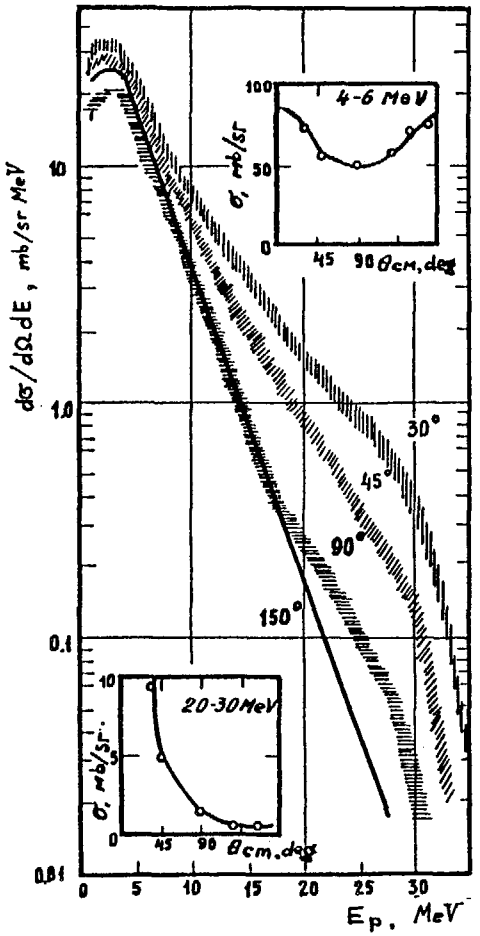

Fig.1. Spectra of protons from ^{58}Ni+α reaction at an energy of 42 MeV. Inserts show angular distributions for groups of particles corresponding to nonequilibrium processes (lower insert) and to a compound nucleus (upper insert). The cross-section of proton emission in the channels with compound nucleus formation is about 2000 mbarn, the cross-section of nonequilibrium processes being about 100 mbarn /3/.

The above data show that the nucleon spectral distributions and cross-sections for their yield are not described by the statistical model of formation and disintegration of a compound nucleus, but at the same time the information about the entrance channel is slightly lost.

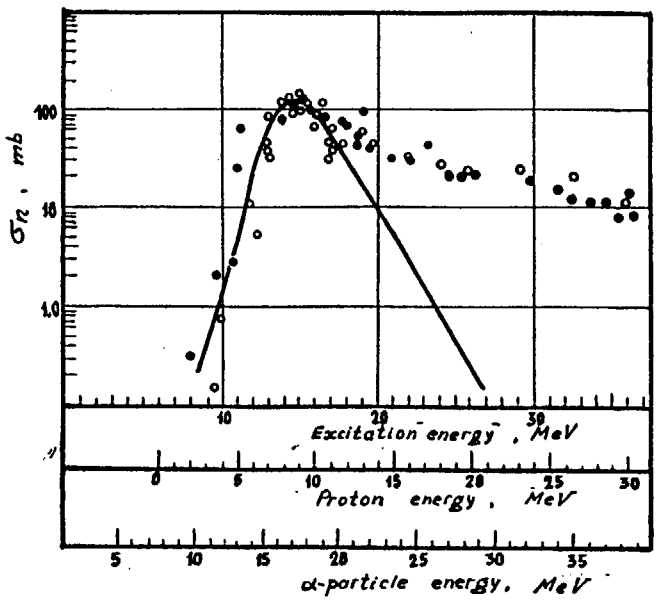

Fig.2. Excitation function for α -particle and proton induced reactions:(solid points) $^{139}La(\alpha,n)$;(open points) ^{142}Ce (p,n). Solid line gives the calculation of excitation function for $^{139}La(\alpha,n)$ reaction with assumption about statistical mechanism of reaction /4/.

The first realization of ideas about the intermediate reactions was made in calculations of intranuclear cascades by the Monte-Carlo method /5/ which is suitable for analyzing high-energy reactions. To describe medium-energy processes an exciton model has been developed /6/. A number of other phenomenological models has appeared more recently /7-13/. The hypothesis about the possible formation of a localized hot zone in a nucleus due to collision with a high-energy particle was suggested by Bethe in 1938 /2/ and has been developed in refs/14-24/. A number of models describes specific properties of high-energy particle emission in interaction between heavy ions. These are the promptly emitted particle model /25-26/, the piston model and the sum rule model /27-30/. A microscopic approach based on theories of multistep direct reactions is also developed /31-33/.

The reactions with production of neutrons will be the focus of attention in the review. It is caused not only by a great deal of experimental data on reactions of this class, but also by the certain advantages of investigating the neutron emission. The angular distributions of neutrons are not affected by the Coulomb field of the nucleus, which could lead to focusing or shadowing effects in reactions with charged particle emission. Moreover, the part of the Fermi motion of nucleons should be reflected more clearly in the emission of nucleons than in that of complex fragments.

We shall assign the processes connected with establishment of equilibrium in a forming compound nucleus to preequilibrium ones. The nonequilibrium processes of this class are separated because the preequilibrium light particle emission can give an information on properties of nuclear matter in its nonequilibrium phase, on mechanisms and time characteristics of the relaxation processes in nuclear matter. Only the phenomena that occur for the time preceding the disintegration of the double nuclear system will be assigned to the preequilibrium light particle emission in deep inelastic or quasielastic collisions. In this case the light particle emission reflects the initial stages of a great loss of energy and angular momentum taking place in reactions with heavy ions.

Spectra and angular distributions of the secondary particles in reactions with nucleons are treated well by microscopic theories of direct nuclear reactions in terms of one- and two-step processes /31-33/. So the reactions of interaction between complex ions, wherein the one-step processes of neutron emission proceed with relatively small probability, are preferable for studying the equilibration in nuclear matter.

The given review is devoted to analysis of the model ideas and experimental data on neutron emission in reactions induced by complex light and heavy ions at energies of 10-20 MeV/nucleon.

I. MODELS FOR NONEQUILIBRIUM MECHANISMS OF HIGH-ENERGY LIGHT PARTICLE EMISSION

1. Fermi-gas equilibration model /7-8/

The Fermi-gas equilibration model is, by its ideology, close to the intranuclear cascade model, but the spatial distributions of nucleons are not considered and by means of calculations it is possible to obtain only the angle-integrated energy spectra. The division of the spectra into the equilibrium and preequilibrium parts

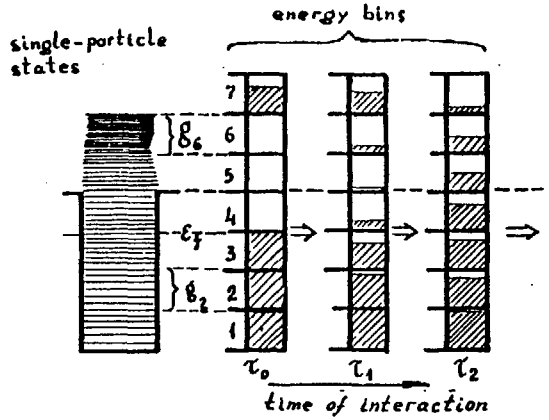

Fig.3. Scheme illustrating the Fermi-gas equilibration model /7,8/.

is not expected. The physical principles of the model are shown in Fig.3. The whole range of excitation energies under consideration is divided into energy bins ΔE. Each bin corresponds to the number of possible single-particle states (g_i). This number of states is calculated on the basis of the Fermi-gas model; it is also possible to use the Nilsson level scheme. The number of single-particle states in the energy interval in the Fermi-gas model is connected with the bin energy (ε_i) by the relationship:

$$g_i = \frac{8}{3}\pi V (2M/h^2)^{3/2}\left[(\varepsilon_i + \tfrac{1}{2}\Delta E)^{3/2} - (\varepsilon_i - \tfrac{1}{2}\Delta E)^{3/2}\right] \qquad (1)$$

$$g_{i'} = \frac{8}{3}\pi \Omega (2M/h^2)^{3/2}\left[(\varepsilon_i + \tfrac{1}{2}\Delta E)^{3/2} - (\varepsilon_i - \tfrac{1}{2}\Delta E)^{3/2}\right] . \qquad (2)$$

Here the primed subscripts refer to particles emitted from a nucleus; V and Ω, the nuclear and lab volumes, respectively, are parameters that do not enter into equations describing the system evolution. The system evolution can begin either from a prescribed distribution of particles in energy intervals or with a nucleus in its ground state, as shown in Fig.3. The transitions in the nucleus are assumed to result from processes of nucleon-nucleon scattering, thus two nucleons are always involved, going from two initial states to two final ones. The transition probability $\omega_{ij\to kl}$ depends only on particle energy (ε_i) and cross-section of nucleon-nucleon scattering (σ_{NN}):

$$\omega_{ij\to kl} = \frac{\sigma_{NN}(\varepsilon_i+\varepsilon_j)\,[2(\varepsilon_i+\varepsilon_j)/M]^{1/2}}{V\sum' g_m g_n\,\delta(\varepsilon_i+\varepsilon_j-\varepsilon_m-\varepsilon_n)} \qquad (3)$$

$$\omega_{i\to i'} = \sigma_{inv}(\varepsilon_{i'})\,[2\varepsilon_i/M]^{1/2}/\Omega\, g_{i'} \qquad (4)$$

The composite system evolution with time is described by a system of coupled equations (master equations):

$$\frac{dN_i}{dt} = \sum_{k,l,j} g_i\Big[\omega_{kl\to ij}\, g_k g_l g_j\, n_k n_l (1-n_i)(1-n_j) - \omega_{ij\to kl}\, g_j g_k g_l\, n_i n_j (1-n_k)(1-n_l)\,\delta(\varepsilon_i+\varepsilon_j-\varepsilon_l-\varepsilon_k) - \omega_{i\to i'}\, g_{i'} n_i\,\delta(\varepsilon_{i'}-\varepsilon_i+\varepsilon_f+BE)\Big], \qquad (5)$$

$$\frac{dN_{i'}}{dt} = \omega_{i\to i'}\, n_i\, g_{i'}\,\delta(\varepsilon_{i'}-\varepsilon_i+\varepsilon_f+BE). \qquad (6)$$

where $N_i = n_i g_i$ is the number of occupied states of the i-th group, $N_{i'} = n_{i'} g_{i'}$ is the number of emitted nucleons, BE is the binding energy of a particle.

2. Exciton and hybrid models /13,9/

The physical conceptions of the models are presented in Fig.4 A nucleon is shown to enter the nuclear potential. The nucleus is in its ground state. A series of two-body interactions is assumed to take place. The first interaction yields a 2p1h state (two particles and one hole) and any configuration is assumed to be equally probable for this state. The next interaction leads to a more complex 3p2h state, to other configurations of the 2p1h state, the recovery of the initial state being possible.

A concept of density of intermediate, or exciton, states is introduced and it means the number of ways by means of which the total energy (E) can be distributed between n excitons. In the model with equally spaced single-particle states the density of exciton states for the definite numbers of particles (p) and holes (h) has the form /33/ (the Ericson formula):

$$\rho_n^{ph}(E) = \frac{g\,(gE)^{n-1}}{p!\,h!\,(n-1)!}\ , \qquad (7)$$

where g is the density of single-particle states. For a small number

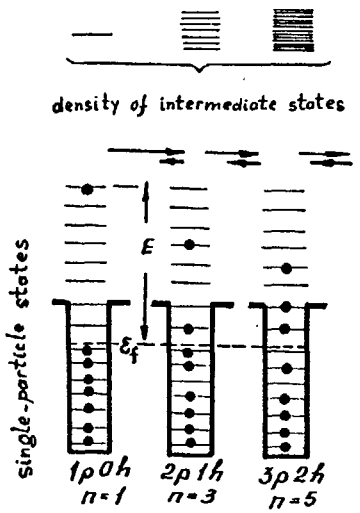

Fig.4. Scheme illustrating the exciton model /6/.

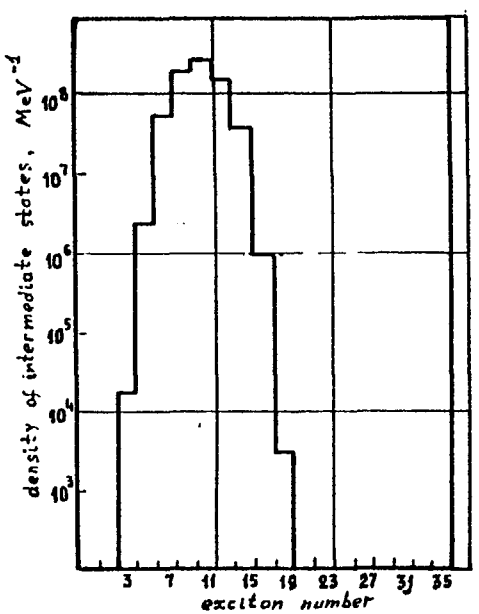

Fig.5. Density of intermediate states versus number of excitons. The calculation was made from the Ericson formula (Eq.(7)) for a compound nucleus with a mass of 130 at an excitation energy of 10 MeV and at a single-particle state density of 10 MeV^{-1}/34/.

of excitons the density of intermediate states is an abrupt function (Fig.5), therefore transitions leading to decrease in the number of excitons can be ignored. For a given state the energy distribution of particle (P(e,E)) or holes (H(e,E)), in the composite system is determined as a fraction of the n-exciton configurations in which one particle, or one hole, has an energy e:

$$P_n(e,E) = g\,\rho_{n-1}^{p-1,h}(E-e)/\rho_n^{p,h}(E), \qquad (8)$$

$$H_n(e,E) = g\,\rho_{n-1}^{p,h-1}(E-e)/\rho_n^{p,h}(E), \qquad (9)$$

The expression for the differential cross-section of preequilibrium emission has the rather simple form:

$$\frac{d\sigma}{d\varepsilon} = \sigma_R \sum_{n=n_0}^{\bar{n}} D_n\, P_n(\varepsilon+B\varepsilon,\varepsilon)\,\lambda_c(\varepsilon)\,t_n(\varepsilon,E), \qquad (10)$$

where σ_R is the total cross-section of the compound nucleus formation. $\varepsilon = E - B\varepsilon$, λ_c is the rate of transitions with emission of a nucleon (its value being obtained from reciprocity principle), D_n is the parameter allowing for decrease in probability of the n-exciton configuration formation due to emission of particles from the previous states.

Taking into account the transitions into states with smaller number of excitons it is possible, like in the Fermi-gas-equilibration model, to obtain a system of master equations describing the particle emission probability versus time /12/. In this case the model will also describe the emission during the equilibrium stage. The division of spectra into the equilibrium and preequilibrium parts has a conditional, model nature. A number of works /35-37/ divide the preequilibrium emission processes into multistage direct ones in which the nucleons escape mainly at small angles and multistage compound ones leading to distribution symmetrical about an angle of 90°.

The basic difference between the exciton and hybrid model versions consists in definition of lifetime t_n /38/ (see Eq.(10)). In the exciton model t_n is defined as a mean lifetime of the exciton state. It is obtained by averaging the decay rate of single-partic-

le states by energy distributions of particles and holes:

$$t_n^{-1}(E) = \int_0^E \lambda_c(\varepsilon) P_n(\varepsilon, E) d\varepsilon + \int_0^E \left(\lambda^p_{n,n+2} P_n + \lambda^h_{n,n+2} H_h\right) d\varepsilon, \qquad (11)$$

where $\lambda^{p(h)}_{n,n+2}$ is the intranuclear decay rate of single-particle states for particles (holes) whose determination can be based on free path of a nucleon in the nuclear matter /13/.

The single particle notion is accepted in the hybrid model, as in the Fermi-gas-equilibration model, and, therefore, the lifetime is /33/:

$$t_n^{-1}(e) = \lambda^p_{n,n+2}(e) + \lambda_c(e - BE), \qquad (12)$$

Here t_n is interpreted as a lifetime of a single particle state with an energy e which decays either through intranuclear transition or with emission of a particle. This time does not depend on concrete exciton state.

In analyzing the same experimental data these models are obviously able to come to contradictory conclusions about the initial exciton number (n_o) or the decay rate ($\lambda_{n,\,n+2}$). Indeed, in analyzing the experimental data in terms of the exciton model the nucleon free path obtained, for example, from optical potentials must be increased by a factor of 4, which can evidence for a predominant contribution of peripheral processes /38/. But in the hybrid model the agreement with the experiment was obtained at calculated values for nucleon free paths /40/.

3. Geometry dependent hybrid model /10/

Change in density of nucleons near the nuclear boundary can affect the preequilibrium decay. First, the mean free path should be greater in the diffuse surface; second, the Fermi energy in this region is considerably lower. The latter of these effects limits the degree of freedom in energy distribution of a given exciton configuration because of a finite depth of hole energy position. Allowance for these effects could act on the preequilibrium emission as well as on the shape of the emitted particle spectrum. In the geometry dependent hybrid model the calculation is performed separately for every impact parameter:

$$\frac{d\sigma}{d\varepsilon} = \pi \lambda^2 \sum (2\ell+1) T_\ell \frac{dP_\ell(\varepsilon)}{d\varepsilon}, \qquad (13)$$

where T_ℓ is the transmission coefficient and $\frac{dP_\ell}{d\varepsilon}$ is the preequilibrium emission probability for a given impact parameter. Allowance for the restrictions in the hole energy depth is made only in the first stage of the preequilibrium decay /10/ when this effect is greatest. The fraction of the preequilibrium emission as a function of impact parameter is shown in Fig.6. It is seen that allowance for the diffuse nuclear boundary caused an increase in non-equilibrium nucleon yield in the peripheral region.

Appearance of the geometry dependent hybrid model made it possible to describe successfully the experimental data on the (p, n) reactions which could not be explained in terms of the exciton and hybrid models /4/.

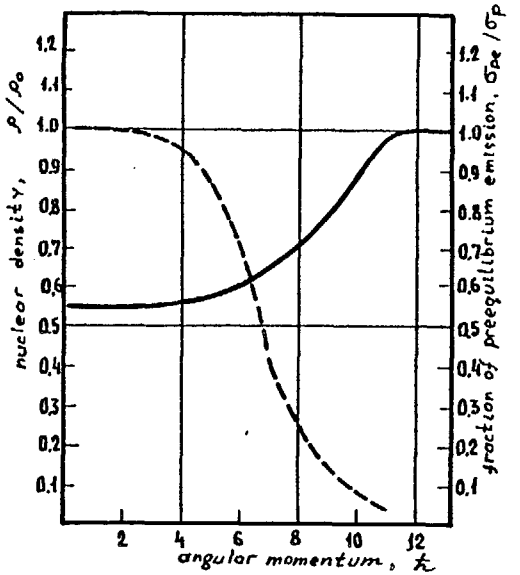

Fig.6. A fraction of preequilibrium emission as a function of orbital momentum in the entrance channel (solid line). The calculation was made for $^{54}Fe(p, p')$ reaction at 62 MeV. Dashed line presents the variation of nuclear density /34/.

4. Description of angular distributions in models of exciton type

The detailed description of different models for mechanisms responsible for the angular dependence of preequilibrium particle yield on angle of detecting is presented in a survey /ref. 42/.

In one of the first works /48,44/ the angular distributions are described on the basis of the generalized master equations of the exciton model. The angular distribution of emitted particles is assumed to be determined only by direction of a leading particle motion. Information about initial direction of the leading particle is gradually lost in two-body interaction between this particle and nucleons of the nucleus. Development of this model was made in /45/.

Description of the angular distributions was developed also on the basis of the hybrid model /46/. A kind of hybrid of the exciton model and the Born plane-wave approximation is presented in /47/.

All calculations of angular distributions of nonequilibrium particles were carried out mostly for reactions with nucleons.

5. Hot spot in central collisions

Assumption of possible formation of a localized hot zone in a nucleus was made in 1938 /2/. A particle of sufficiently high energy loses its energy in the surface layer of a target nucleus and this process leads to an intensive local heating. The "heat" will be gradually distributed over the whole nucleus. Concepts of local equilibrium and local temperature can be introduced only when the number of transitions in the hot spot zone exceeds considerably the number of nucleon collisions at its boundary. But then the hot zone radius should exceed the nucleon free path by a factor of 3, if the relaxation process is based on rescattering of the nucleons. However, it is not workable as in such a case the hot spot size would be comparable with nuclear one ($R \gg 6\sigma$). In order that the local equilibrium existsit is necessary to assume that either the free path in the hot spot zone is considerably less than in the cold nuclear matter /24/ or the relaxation process is determined by other than two-body mechanism. As the accessible local temperature is high enough, evaporation of the particles from the hot spot seems to be possible. These particles can have much higher energies than those calculated by assuming isotropic nuclear temperature. For central collisions the priority emission of nonequilibrium particles is expected to occur at backward angles.

The effect of such a mechanism was possibly found in work /48/ where the proton energy spectra were studied at angles more than 90° in reactions induced by protons and high-energy α - particles. The temperatures obtained by analyzing the high-energy part of spectra ($E_p \geq 20$ MeV) are twice as high as values of equilibrium temperature and do not depend on both proton exit angle and mass number of the target. There are attempts to explain the cumulative effect by formation of the localized hot zone /22/.

6. Hot zone and refraction on nuclear boundary

It is of interest to analyze whether the hot spot model is able to explain the nonequilibrium emission in the region of forward angles. Such a model is developed in works /18-20/. It is assumed that a projectile coalesces with a nucleus to form a compressed hot zone in it. The model parameters are the degree of compression (η) and the relative size of the hot zone (β):

$$\eta = \rho_s / \rho_0 \quad , \qquad \beta = R_s / R \, . \tag{14}$$

It is assumed that there is a local equilibrium in the zone and there is no energy exchange with the cold nuclear matter. Then the zone temperature (T_s) is connected with a projectile energy (E) by the relationship:

$$T_s = \frac{2}{\pi} E_F^{1/2}(\rho) \Big/ (A_p + A_t) \Big[A_t E - \frac{3}{5} (A_p + A_t)^2 \big(E_F(\rho_s) - E_F(\rho) \big) \Big]^{1/2} , \tag{15}$$

where A_p is the number of nucleons in the projectile, A_t is the number of target nucleons involved in the hot zone, $E_F(\rho)$ is the Fermi energy.

When a nucleon emitted from the hot zone reaches the nuclear surface, it can leave nucleus if its kinetic energy in the direction perpendicular to the surface is more than the potential well depth (V_0). The differential multiplicity of emitted particles is determined by the expression:

$$\frac{d^2 N}{p_s^2 \, dp_s \, d\Omega_s} = \frac{4\pi g R_s^2 (R - R_s)}{h^3 \langle V_s \rangle} V_s \, F(E_s) \, \varepsilon \Big(p_s - \frac{(2mV_0)^{1/2}}{\cos\alpha} \Big) , \tag{16}$$

Here F(E) is the nucleon energy distribution in the hot zone which is accepted to be the Fermi distribution at temperature T_s, ε is the Heaviside step function, α is the angle determined in Fig.7, E_s, p_s and V_t are the energy of the emitted particle, its momentum and intranuclear velocity, respectively. When a nucleon crosses the nuclear surface, its energy decreases, the tangential component of the momentum being unchanged (Fig.7). This leads to collimation of the outgoing nucleons. Moving the hot zone close by the focus of the nuclear lens, it is possible to achieve the desired focusing.

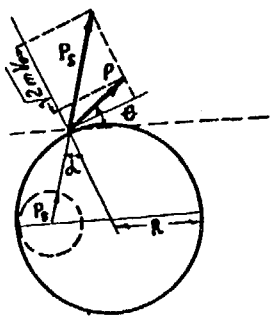

Fig.7. Isolated statistical hot spot model with refraction at nuclear surface /18,19/.

7. Peripheral hot spot /14-17, 23, 54/

The model describes the hot spot formation and decay in reactions of deep inelastic scattering. The hot zone is developed in the overlapping region of colliding nuclei at orbital momenta close to the momentum of grazing collision and becomes apparent after the breakup, of the intermediate complex via particle emission. A large transferred angular momentum causes the rotation of the nucleus with a period comparable with hot zone internal decay time, therefore, the emitted particle spectra reflect the rotational motion of the fragment. The probability of nucleon emission $P(\varepsilon, \theta, t)$ is connected with surface temperature $T(R, \theta, t)$ by the relationship:

$$P(\varepsilon, \theta, t) \sim \varepsilon \exp\left[-\frac{\varepsilon + BE}{T(R, \theta, t)}\right], \qquad (17)$$

where BE is the binding energy of the emitted particle, t is the time from the moment of separation of the fragments. The angle θ in Eq.(15) is the polar angle of emission in the intrinsic coordinate of the emitting nucleus. The time-dependent nuclear temperature field $T(R,\theta,t)$ is calculated on the basis of a diffusion equation with a delta-like initial distribution. The known value of equilibrium temperature permits an unambiguous calculation of temperature field. A light particle is emitted in a time moment t in a direction θ (Fig.8) by an excited nucleus with a probability $P(\varepsilon, \theta, t)$. Then three particles are considered as point charges and their trajectories are calculated by numerical integration of the Newton equations. When the trajectory of the particle under investigation crosses the residual nuclei, the particle is considered absorbed.

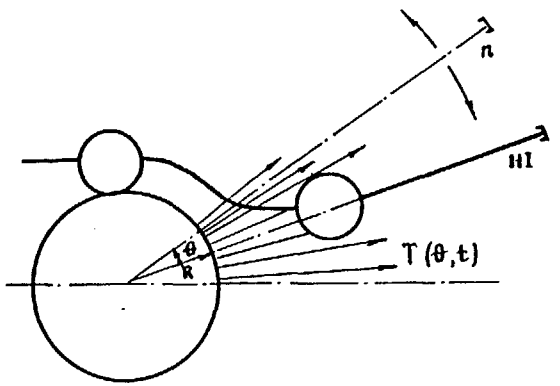

Fig.8. Surface hot spot model in deep inelastic collisions of heavy ions /16,17/.

The angular distributions calculated in /17/ for the $^{58}Ni(^{16}O, ^{16}O'n)$ reaction at 96 MeV are shown in Fig.9. The angle is counted off from the oxygen direction. The positive angles correspond to the particle emission at angles larger than the ^{16}O scattering angle. The model predicts the characteristic picture of angular correlation with a "shadow" minimum shift in the positive angle region. Up to date the calculations have not been compared with experimental data.

The hot zone on the nuclear surface was also considered in /23/. It was suggested to bring an effective temperature to conformity with every angle of particle emission. The authors of /23/ believe that

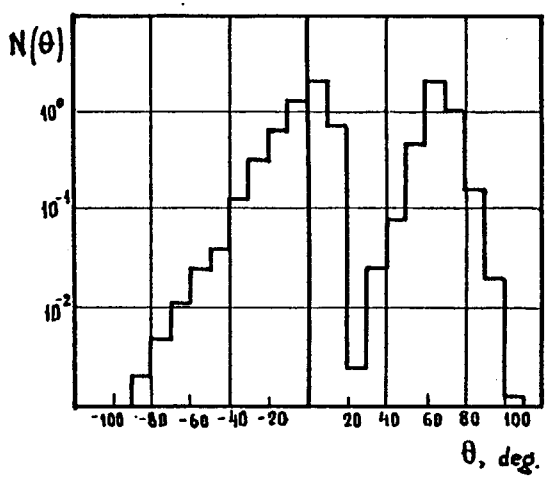

Fig.9. Angular distributions of neutrons in the peripheral hot spot model for ^{58}Ni (^{16}O, $^{16}O'n$) reaction at 96 MeV /17/. Angle θ is counted off from the direction of heavy ion emission.

the particle emission occurs on an average in the direction of velocity of the rotating nuclear surface. Then a definite angle of emission can be brought to conformity with an angle of system rotation and, hence, with a definite time of reaction. However, the assumption on the preferred direction of emission is not substantiated at all.

The decaying hot zone on the nuclear surface was considered in the classical orbiting model /54/. The model comes formally to a fast nucleon source moving at some angle with the beam. The value of this angle is determined by an average time of nucleon emission and an angular velocity of the hot zone. Two extreme cases are usually considered. The composite system of two nuclei either rotates as a single whole (sticking) or one nucleus rolls on the surface of the other one in the rotating composite system (rolling). The law of conservation of momentum allows in these cases the source velocity to be determined unambiguously. The emitted particle distribution in the source system is considered isotropic /54/.

8. Driffing intranuclear hot zone /21,24/

It is assumed that the preformed area of localized excitation energy is expanded and retarded for some time and the system reaches a thermal equilibrium. The excitation in every time moment is localized in some volume where a fraction of the projectile ion nucleons ($A_p(t)$) and a fraction of the target nucleons ($A_t(t)$) is available. The hot zone velocity as a function of time is determined by the expression:

$$v(t) = v_0 A_p / (A_p + A_t). \qquad (18)$$

Here v_0 is the projectile ion velocity. The temperature as a function of time is calculated from Eq.(15). The model does not take into account the particle absorption in the nucleus as well as the refraction in crossing the nuclear surface. The authors of model /21/ assume that although the excitation energy and the longitudinal component of velocity are localized in a small volume, it is attained owing to the phase consistency and the definite dependence of the nucleon density matrix elements on momentum, i.e. owing to the definite momentum distribution of nucleons. The fraction of nucleons whose momenta are large enough to leave the nucleus seems to be proportional to the volume where the excitation energy is concentrated while the nucleons fill the whole volume of the nucleus. Evaporation occurs from surface. The calculations are made with definite assumptions about dynamics of the process (for example, uniform expansion or uniform retardation).

More successive thermodynamic approach in the framework of the similar model has been developed in /24/. The idea of drifting hot zone has also been realized in the so-called two-phase deexcitation model /49/.

9. Promptly emitted particles model /25-26/

The promptly emitted particles or Fermi-jet model /25,26/ describes one of possible mechanisms of fast nucleon formation in reactions with heavy ions. It is assumed in this model that a window forms between the strongly interacting nuclei through which nucleon exchange takes place. The nucleons which are transferred from a donor nucleus to a recipient one have their intrinsic Fermi velocities in the donor system, the same nucleons having different veloci-

ties in the recipient system. The change in velocities results from the relative motion of the nuclei, the high-energy nucleon formation being possible due to summation of velocities. As the intranuclear velocity distribution is connected with nuclear density, the Fermi-jet neutrons could be used to determine the density variations in the course of collision between nuclei.

A model which combines the ideas of promptly emitted particles and hot spot has been developed in /20/.

10. Incomplete fusion sum rule model /27-29/

The fast particles emitted in the initial stage of the interaction take away a fraction of the projectile momentum to facilitate the fusion process. The sum rule model postulates that probabilities P(i) of different processes going through the stage of nonequilibrium system formation, including the fusion process, are proportional to the exponential expression:

$$P(i) \sim \exp\left\{ (Q_{gg} - \Delta Q_c(i))/T \right\}, \quad (19)$$

where Q_{gg} is the energy of the reaction with formation of the ground-state products; ΔQ_c is the change in the Coulomb interaction energy due to charge transfer in the reaction. T can be considered as an effective temperature characteristic of the composite system level density or simply as a model parameter. This empirical relationship is usually used to describe the charge and mass distributions of fragments in deep inelastic reactions.

Restrictions on entrance angular momentum $\ell_{lim}(i)$ reduce the probabilities of the reactions. The limiting angular momentum for each channel is equal to:

$$\ell_{lim}(i) = \frac{m_p}{m_c}\, \ell_{cr}(i) \quad (20)$$

Here m_p and m_c are the masses of the projectile and the captured fragment, respectively. The sum of probabilities of various reaction channels is also assumed to be equal 1 for every orbital momentum of the incident particles. Then the cross-sections for various reaction channels are determined by the relationship:

$$\sigma(i) = \pi\lambda^2 \sum_{\ell=0}^{\ell_{max}} (2\ell+1)\, \frac{T_\ell(i) \exp\left\{(Q_{gg} - \Delta Q_c)/T\right\}}{\sum_m T_\ell(m) \exp\left\{(Q_{gg}(m) - \Delta Q_c(m))/T\right\}} \quad (21)$$

The model uses the following parametrization for the transmission coefficient (T_ℓ):

$$T_\ell = 1./\left(1 + \exp\left(\frac{\ell - \ell_{lim}(i)}{\Delta}\right)\right). \quad (22)$$

The model links the cross-sections of nonequilibrium particle production for different reaction channels without specifying the mechanism of their production.

The authors /30/ suggested also an explanation for the mechanism of fast particle escape. The particle excape in peripheral collisions can occur under the action of radial friction forces which are decisive in the reactions of deep inelastic scattering. In the case of central collisions a hard retardation of a particle in the target-nucleus field can lead to light-particle escape from the nucleus side opposite to the collision (the piston model). However, these ideas have not been developed to the model level when the comparison with experimental data becomes possible.

11. Parametrization of experimental data in moving sources model

Parametrization in the moving sources model has been recently used in most the experimental works devoted to analyzing energy spectra and angular distributions of fast light particles. A source moving with some velocity, as a rule, along the beam direction is suggested to be responsible for the nonequilibrium part of the spectrum. The angular distribution of the decay particles in the source system is isotropic and their momentum distribution is approximated by the Gaussian:

$$\frac{d^2\sigma}{dE\,d\Omega} = A E^{1/2} \exp\left\{ - \frac{(P - P_0)^2}{2B^2} \right\}. \quad (23)$$

Here p and E are the momentum and energy of the fast particle in the laboratory coordinate system, respectively; A,B,P_0 are the model parameters. This source can also be presented as a moving hot area:

$$\frac{d^2\sigma}{dE\,d\Omega} = A E^{1/2} \exp\left\{ - \frac{E + E_0 - 2(EE_0)^{1/2}\cos\theta}{T} \right\} \quad (24)$$

The connection between the parameters of temperature (T) and the dispersion of momentum distribution in Eqs (21) and (22) is given by the expression:

$$T = mB^2. \quad (25)$$

The formulas similar to Eqs (23) and (24) can be obtained in the bombarding light particle breakup model /50/ as well as in the heavy ion prompted fragmentation model /51/, in the framework of both the Fermi-jet model /26/ and the moving hot spot model /21/. The idea of a moving source does not contradict either the exciton models or the incomplete fusion sum rule model. Therefore, such a parametrization can be considered, in a way, as a model-independent approach which makes it possible to speak about a definite mechanism on the basis of the obtained parameters comparing these parameters with predictions of different models.

12. Common features of different models

In dynamics of development of models (Fig.10), as in evolution of life on the Earth (Fig.11), we see the similar picture. Time has led to death of a number of models. The peripheral hot spot was never supported by experimental data /17/; the Fermi-gas equilibration model /7/ is not used because of complex mathematics and for lack of fitting parameters. The present status of development of the models may be called the epoch of pangolins. In some cases the physical meaning of the parameters in use is not clear /6,27/; some models /19,23/ surprise us by naivety of ideas laid in their basis; applicability of almost all models to the described phenomena is poorly substantiated; the energy and mass ranges, wherein the approximations used are valid, are not determined. The degree of experimental data description has become a main criterion of applicability. The surprising variety of models and approaches can be evidently explained just by this fact. We shall try here to establish a degree of relationship for different models and a possibility of comparing the conclusions made in analyzing the experimental data with the help of these models.

The exciton models, as the intranuclear cascade models, reduce the whole process of equalibration in the composite system to two-body interactions. The convincing evidence of difference between the model predictions and experimental data is of physical interest here rather than the successful description. A show of specific properties of the nuclear matter can be expected just in such differences.

The hypothesis on the localized hot zone appearance and decay is based on other ideas. The action of multibody forces actively involved in energy transfer in the nuclear matter is permitted here.

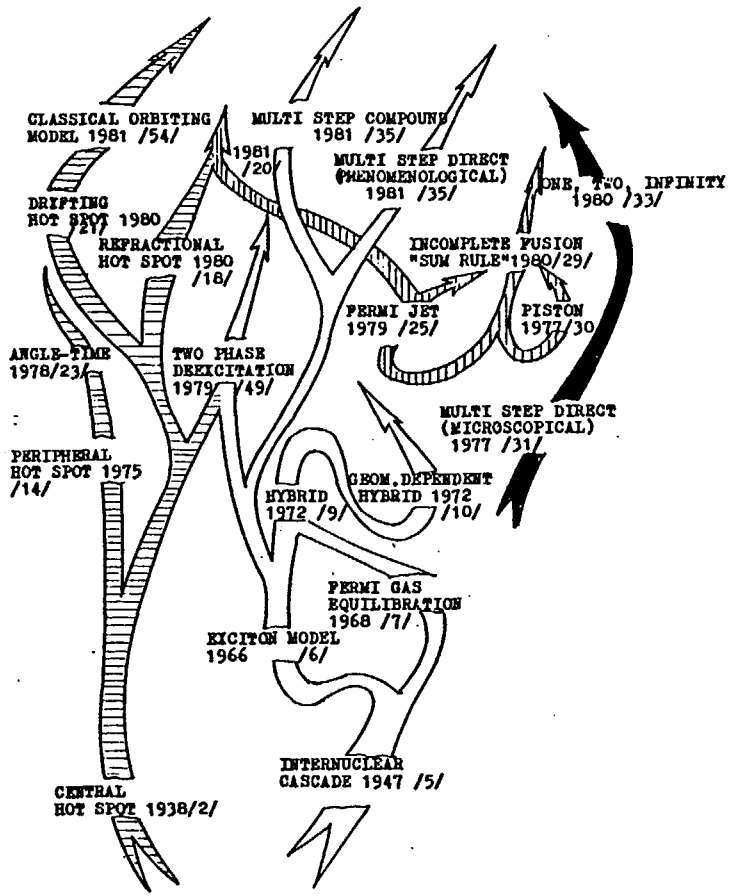

Fig.10. Evolution of nonequilibrium process models
- hot spot models;
- exciton models;
- models in which high-energy particle emission is determined by intranuclear Fermi motion of nucleons;
- microscopic models.

The parameters of the two groups of models cannot be compared. The dependence of hot zone temperature on energy per nucleon above the nucleon barrier of the incident ion is shown in Fig.12 with full circles. The data was taken from the experimental works where the parametrization of spectra in the moving sources model was carried out. At energies up to 20MeV/nucleon only the works where the fusion

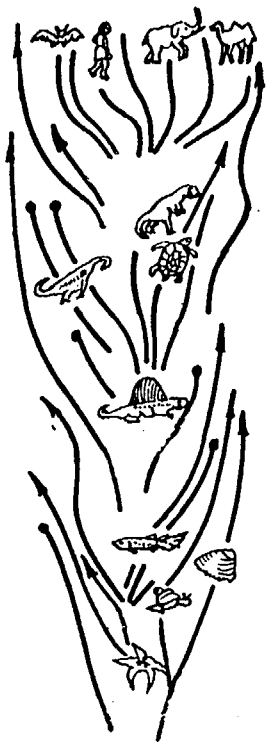

Fig.11. Evolution of life on the Earth.

channel was distinguished /52-54/ and at higher energies the works where the analysis was made for the particle emission at large angles /55/ were taken. Fig.12 shows also the calculation (solid line) of temperatures in the hot spot model (Eq.(15)) with the assumption that the number of target nucleons involved in the hot zone is equal to the number of projectile ion nucleons. It is seen that the energy dependence is repeated rather well.

The parameter which is often compared with the nonequilibrium system temperature figures in the expression for probability of separate reaction channel (Eq.(19)) in the sum rule model /27/. The open circles in Fig.12 present the temperatures obtained in the reactions of fragmentation and the reactions of deep inelastic scattering in constructing the Q_{gg} systematics. The data was taken from review /55/. The emission of the fast fragments may be represented to be

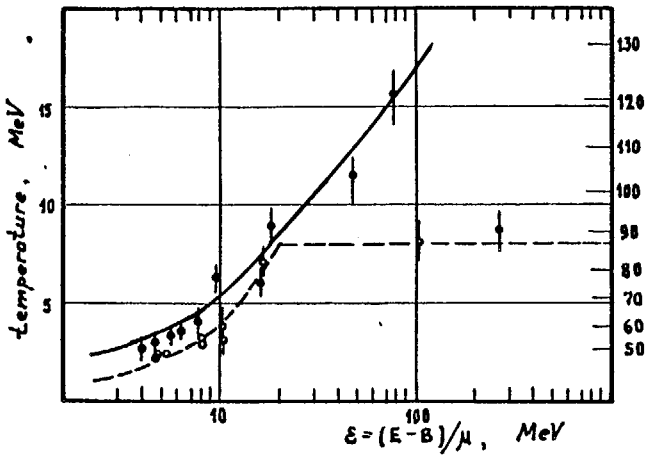

Fig.12. Parameter of temperature versus energy per nucleon in the fragmentation reactions and deep inelastic processes (open circles) as well as in nucleon spectra in the channels of reaction leading to fusion (solid circles). Solid and dashed lines show the results of calculations (see text).

determined by the nucleon flux from one nucleus to another. When the nuclei approach the potential barrier between them in the contact zone decreases down to the Fermi energy and the intensive nucleon exchange is initiated. The dispersion of momentum distribution in such a flux will depend on relative velocities of the nuclei and at incident ion velocities less than the Fermi velocity the dispersion is equal to

$$B = P_o/\sqrt{5}\,, \qquad (26)$$

where $P_o = m v_o$ is the momentum of the nucleon moving with a velocity equal to the incident ion one. At large velocities the dispersion reaches a constant value determined by the Fermi momentum (P_F) /51/:

$$B = P_F/\sqrt{5}\,. \qquad (27)$$

This dependence of dispersion on energy (dotted line in Fig.12) reproduces well the data on the parameter T of deep inelastic processes, predicts both the exsistance of a limiting value of T and the energy

at which this value is reached. Thus, there is a great deal in common between the Fermi-jet and sum rule models, the temperature parameters in the sum rule and hot spot models being distinctly different. Here there are evidently no crossings with the parameters of the exciton models.

II. WHAT CAN ANALYSIS OF INCLUSIVE SPECTRA YIELD?

1. Nonequilibrium processes and inclusive spectra of neutrons

The discrepancies in neutron spectra obtained in interaction of composite nuclei from predictions of the compound nucleus formation model were observed for the first time back in 1961 /57/ when absurd values for parameters of level density of the compound nuclei were obtained in the analysis of neutron evaporation spectra. Then it was suggested that a strongly nonequilibrium process of "localized heating" manifests itself at a sufficiently high energy of projectile ions /57/.

Comparatively few works are devoted to investigation of the neutron spectra because of the definite experimental difficulties in detecting neutrons. In work /58-60/ the dependence of nonequilibrium neutron emission on atomic number of a target nucleus was studied in reactions with light ions: ^{3}He and ^{4}He. The neutron spectra from reactions initiated by different ions were systematically studied in works /61-65/. In these investigations the energy and angular distributions of neutrons were measured in the reactions with ions ^{3}He (E=40.9MeV), ^{4}He(E=52.6MeV), ^{6}Li(E=39.7MeV) and ^{12}C(E=53.0MeV). Targets were chosen so as to obtain the same compound nucleus ^{65}Zn. The incident ion energies corresponded to the excitation energy of the compound nucleus ^{65}Zn, being about 54MeV. Such a choice of energies and targets gives rise to about similar characteristics for the energy and angular distributions of neutrons the production mechanism of which corresponds to evaporation from the compound nucleus. Some discrepancies are possible due to different orbital moments in the entrance channel (see Table 1).

Table 1.

Reaction	Energy, MeV	Y_n, mbarn	l_{cr} $\hbar$	n_o	σ_{ne}, mbarn
^{3}He+^{62}Ni	40.9	1660±40	12.8	5	340
^{4}He+^{61}Ni	52.0	1590±40	16.8	4	361
^{6}Li+^{59}Co	39.7	2160±50	19.5	6	301
^{3}He+^{61}Ni	59.0	2090±50	16.0	5	514
^{6}Li+^{59}Co	90.0	3490±60	29.3	6	700

The additional measurements at high energies were performed for ions ^{3}He(E=59MeV) and ^{6}Li(E=90MeV).

The features characteristic of nonequilibrium processes, the significant yield of high-energy neutrons and the growth of the yield in the small angle area, manifest themselves in the energy spectra and angular distributions of neutrons for the reactions with ions ^{3}He, ^{4}He and ^{6}Li. The angular distributions of neutron yield in these reactions for different energies of neutrons are compared in Fig.13. The contribution of the evaporation from the compound nucleus is more significant for the reactions with the lithium ions than for those with the helium isotopes. The angular distributions for high-energy neutrons weakly change with incident ion energy, as seen in Fig.14, where the distributions of the 15 and 25MeV neutrons are presented for the reaction with the ^{3}He ions at two different energies. In the case of the reactions with the ^{3}He and ^{6}Li high-energy ions in the experimental spectra obtained in the small angle range one can see an intensive peak whose position coincides with the incident ion velocity. This picture is characteristic of the breakup and knockout reactions (Fig.15). On the one hand, the weak dependence of neutron spectral characteristics on type of the incident ion is observed, on the other hand, there are signs of the direct processes of breakup and knockout.

The reaction with the carbon ions shows quite another picture of neutron distributions (Fig.16). All characteristics of the angular and energy distributions agree with the concept of evaporation from the preformed compound nucleus.

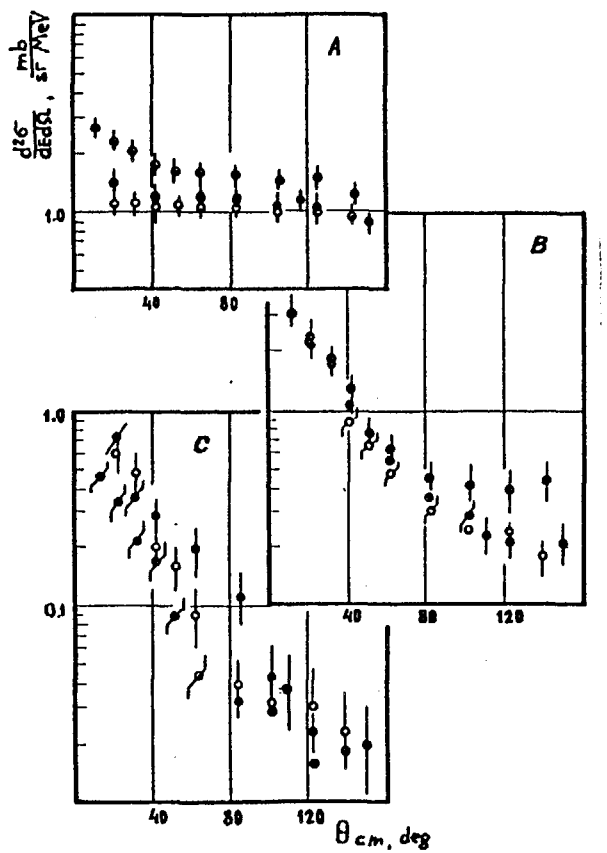

Fig.13. Angular distributions of neutron yield in $^{3}He+^{62}Ni$ (open circles), $^{4}He+^{61}Ni$ (solid circles) and $^{6}Li+^{59}Co$ (dotted circles) reactions for neutron energies of 5, 15 and 25 MeV (A,B and C, respectively).

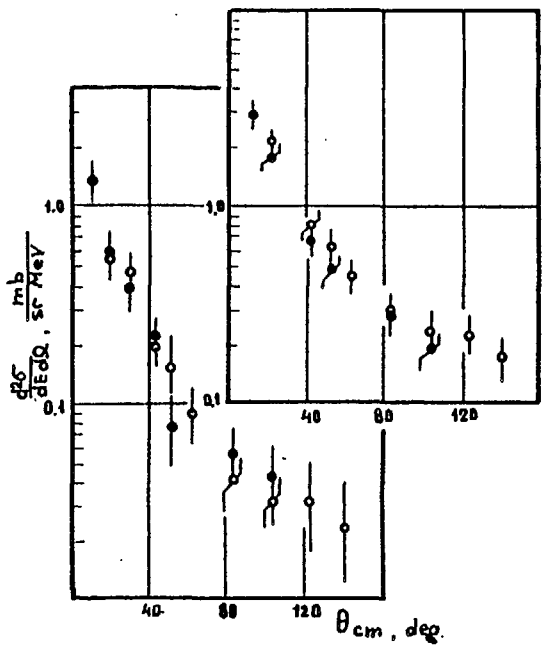

Fig.14. Angular distributions of neutron yield in $^{3}He+^{62}Ni$ reaction at an incident ion energy of 40.9 (open circles) and 59 (solid circles) MeV (the cross-section of reaction at 59 MeV is multiplied by a factor of 0.4) for neutron energies of 25 and 15 MeV (A and B, respectively).

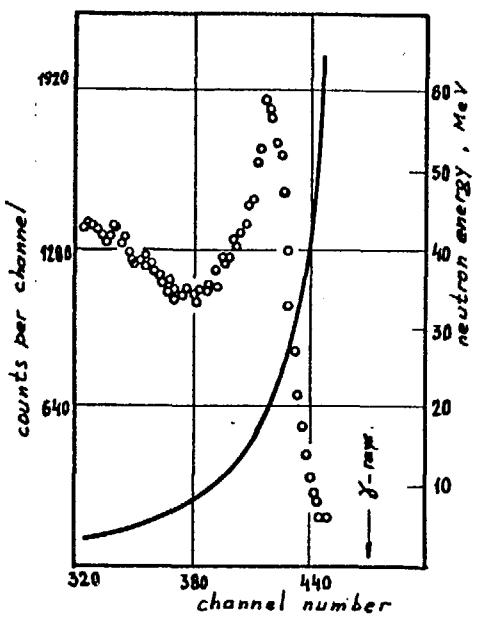

Fig.15. Experimental spectrum of neutrons from $^{3}He+^{62}Ni$ reaction at 59 MeV measured at an angle of 10°. Solid line is the calibration curve (right-hand scale).

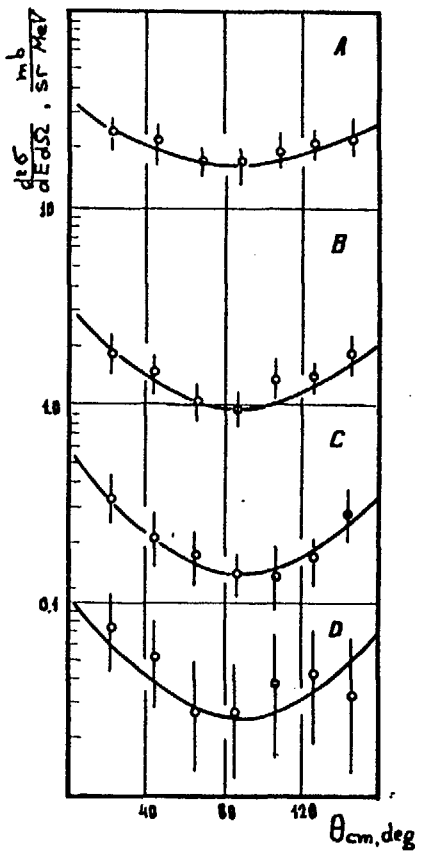

Fig.16. Angular distributions of neutrons from $^{12}C+^{53}Cr$ (E=53MeV) reaction for neutron energies of 5,10,15 and 20 MeV (A,B,C and D, respectively).

Later on we shall analyze the neutron spectra of the reactions where disagreement with mechanism of evaporation from the compound nucleus manifests itself distinctly. The analysis will be made with the use of the basic model concepts which are most frequently applied in studying mechanism of the high-energy light particle formation.

2. Hybrid model of preequilibrium processes

The ALICE program was used to calculate the neutron spectra of reaction under study /66/. The evaporation cascade of the equilibrium part of the neutron spectra was calculated on the basis of the statistical model /67/ with allowance for the competiting channels with proton and α-particle emission. The calculation was made in the S-wave approximation, i.e. it was assumed that the part of energy which is connected with rotation of the nucleus does not take part in the process of particle evaporation and, therefore, in the formula of level density the excitation energy was counted off from the mean energy of nuclear rotation.

Only a part of angular momentum available in the entrance channel leads to nuclear fusion. The necessary condition of the fusion is possibility of approaching of the interacting nuclei to distances shorter than a critical one /68,69/. Alternatively, the restrictions on the limiting momentum for the fusion reactions arise from instability of the composite system /70/. The strong centrifugal forces lead to disintegration of the system before the equilibrium is established. The least values of the critical momenta (ℓ_{cr}) from those obtained in the two representations were used in the calculations, the parameters being taken from /71/.

The hybrid model was used to calculate the nonequilibrium parts of the spectra.

Table 1 summarises data used in the calculations: the parameters of ℓ_{cr}, the initial number of excitons (n_0), the cross-section of preequilibrium emission (σ_{ne}) and the total yield of equilibrium neutrons obtained experimentally (Y_n). The statistical errors are only given for experimental data, the total error for the absolute value of cross-section being about 15%. The preequilibrium emission (σ_{ne}) yields 15-20% of the total yield of the evaporation neutrons. The importance of the nonequilibrium processes grows with increasing the incident particle energy. There is no strong dependence on the projectile ion type. The cross-sections of preequilibrium emission for the reactions with the strongly-coupled α-particle and the "loose"nucleus of ^6Li are close.

Figs 17 and 18 give the experimental energy distributions of neutrons from the reactions under study and their comparison with the calculated data. In all cases the hybrid model reproduces adequately the shape of neutron spectra and the absolute value of cross-section. A decrease in high-energy neutron yield is observed at low energies of incident ions, which is especially noticeable for the reaction in-

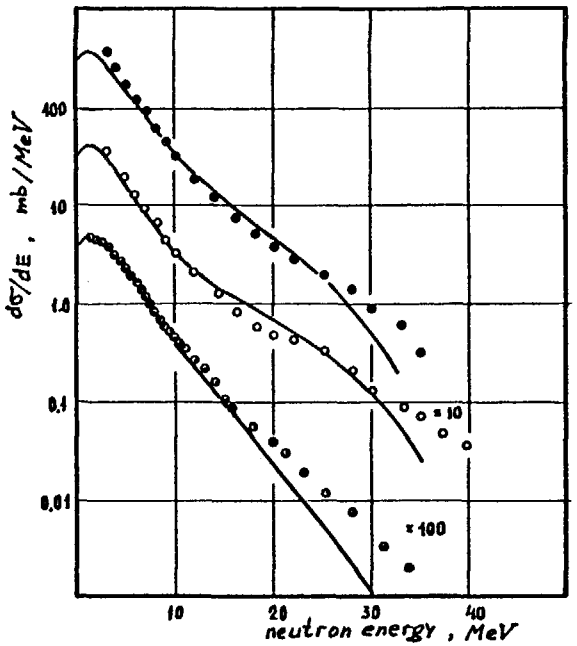

Fig.17. Energy spectra of neutrons from the helium and lithium ion induced reactions: $^{3}He+^{62}Ni$(E=40.9MeV) (solid circles); $^{4}He+^{61}Ni$(E=52.6 MeV) (open circles); $^{6}Li+^{59}Co$(E=39.7MeV) (dotted circles). Solid lines are the hybrid model calculations.

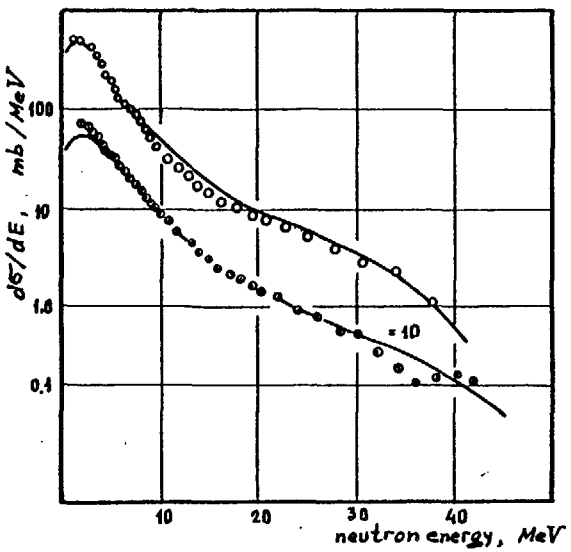

Fig.18. Energy spectra of neutrons from $^{3}He+^{62}Ni$ (E=59MeV; solid circles) and $^{6}Li+^{59}Co$ (E=90MeV; dotted circles) reactions. Solid lines are the hybrid model calculations.

duced by lithium ion. It can be connected with the peripheral processes the geometry dependent version of the hybrid model takes into account. The relative contribution of such processes decreases with increasing the incident energy.

3. Parametrization of spectra in the moving sources model

Here our purpose is to draw definite conclusions about the mechanism of fast neutron emission basing on the obtained values for source velocity and for dispersion of momentum distribution. The neutron spectrum for each detecting angle was presented as a sum of two components. The first one corresponded to evaporation neutrons and was written in the form obtained in calculating the equilibrium parts of neutron spectra with the ALICE program /66/. The formalism used in the program does not permit the angular distributions to be calculated, so to take into account the angular anisotropy the calculated spectrum was multiplied by a coefficient dependent on detecting angle:

$$A(\theta) = 1 + \beta \cos^2\theta, \qquad (28)$$

where β is the fitting parameter. The second component corresponded to the nonequilibrium neutron source moving along the beam direction and had the form presented by Eq.(21). The source velocity (v), the dispersion of momentum distribution (B) and the cross-section of nonequilibrium neutron yield served as parameters here. By fitting

the parameters we succeeded in describing adequately the energy and angular distributions of neutrons only in the range of forward angles (Fig.19). The obtained values of parameters are given in Table 2.

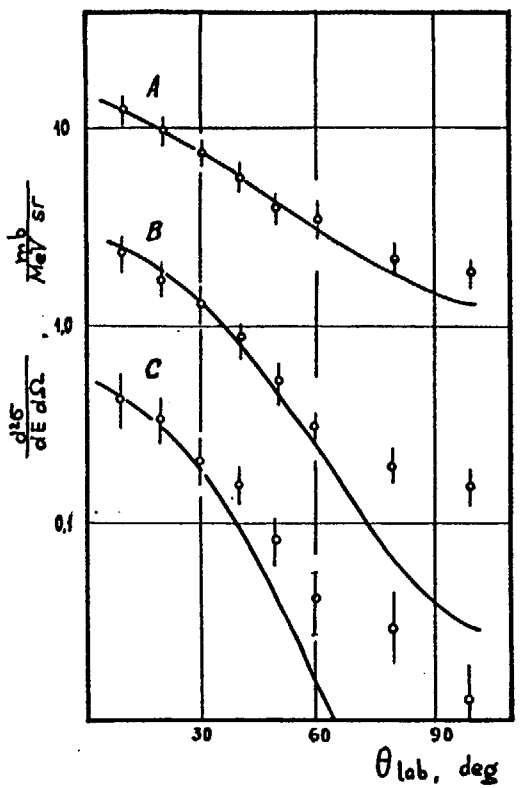

Fig.19. Description of angular distributions of neutrons from $^{6}Li+^{59}Co$ reaction (E=39.7MeV) in the moving sources model for neutron energies of 10,20 and 30 MeV (A,B and C,respectively).

Table 2.

Reaction	$^{3}He+^{62}Ni$	$^{4}He+^{61}Ni$	$^{6}Li+^{59}Co$	$^{3}He+^{62}Ni$	$^{6}Li+^{59}Co$
E, MeV	40.9	52.6	39.7	59.0	90.0
$\bar{n}$	1.6	1.6	1.6	1.9	2.6
Y_n, mbarn	1660±40	1590±40	2160±50	2090±50	3490±60
σ_f, mbarn	1037	994	1350	1100	1342
β	0.09±0.06	0.20±0.08	0.15±0.05	0.11±0.04	0.27±0.06
β^*	0.096	0.161	0.176	0.11	0.34
V, cm/ns	3.96±0.18	3.45±0.28	2.86±0.51	4.99±0.38	5.01± 0.28
V_c^*, cm/ns	4.31	4.42	2.69	5.52	4.81
U_{oc}^* cm/ns	3.68	3.09	2.60	5.07	4.79
T, MeV	3.16±0.37	3.91±0.41	2.72±0.77	2.78±0.52	2.76±0.34
B, MeV/C	54.3± 3.2	60.4±3.2	50.3±7.1	50.9±4.7	50.7±3.2
B^*, MeV/C	48	79	36	48	36

For the adequate description of the spectra in the whole range of angles it is necessary to introduce one more source which has a wider momentum distribution and moves at a smaller velocity. The reproducibility of experimental data will be essentially improved if the neutron sources are assumed to be distributed along directions of their motion. The angular distribution dispersion in this case will be about 10°. With allowance for the angular distribution of the sources the values of fitting parameters (source velocities and momentum distribution dispersions) do not change considerably /65/.

From the total yield of evaporation neutrons (Y_n) obtained by approximation of the equilibrium part of the spectra it is possible to determine the cross-section of fusion (σ_f) dividing the yield into the calculated average number of neutrons ($\bar{n}$). The absolute values of fusion cross-section agree well with the calculated values critical momentum for fusion reactions (see Table 1):

$$\sigma_f = \pi \lambda^2 (l_{cr} + 1/2)^2. \qquad (29)$$

The value of anisotropy parameter can be evaluated, with the following relationship used:

$$\beta^* = \left(\frac{m_n R^2}{\mathcal{J}}\right)\left(\frac{E_{rot}}{2T}\right), \qquad (30)$$

where R, $\mathcal{J}$ and T are the radius, moment of inertia and temperature of the compound nucleus, respectively, and E_{rot} is the rotational energy. As seen from Table 2, the coincidence of the calculated anisotropy parameter β^* with that obtained by fitting, β, is quite satisfactory. Thus, the characteristics of the soft part of neutron spectra completely correspond to the concept of statistic mechanism of neutron emission from the nucleus in thermodynamic equilibrium.

The velocity of the nonequilibrium neutron source is correlated with the projectile ion velocity, being smaller than the latter. For comparison Table 2 gives the incident ion velocities on the peak of the Coulomb barrier (V_c^*) and the ion velocities also on the peak of this barrier but on the assumption that the part of the kinetic energy of motion required to separate a neutron has turned into excitation energy (V_{Qc}^*). As seen from the table, the values of source velocities are close to the velocities V_c^* and V_{Qc}^*. It indicates that the processes of projectile ion breakup are possibly important, but then the momentum distribution dispersion B should be independent of ion energy and proportional to the square root of the binding energy (BE) of the neutron in the projectile nucleus. Indeed, B does not depend on incident ion energy, but in the reactions initiated by α - particles (BE=20.5MeV) and by ions of lithium-6 (BE=3.7MeV) these parameters are close. Table 2 presents the momentum distribution dispersions (B^*) calculated on the basis of the simple breakup model /49/. The good agreement with the fitting parameter B takes place for the reactions with ^{3}He ions, the discrepancies being observed in the case of the reactions with lithium and helium-4. The breakup process can be accompanied also by the processes of neutron knockout from the target nucleus. Then the distribution widths will be determined by form of the neutron wave function in the target nucleus. It is impossible to draw any definite conclusion about the process nature on the basis of the obtained parameters. Possibly we deal with a set of different mechanisms of fast neutron production and the contributions of all the mechanisms are comparable. The obtained parameters do not contradict the preequilibrium exciton models where the incident ion is assumed to dissociate into the definite number of excitons at the initial stage of the reaction and the nucleon emission is determined by the statistic mechanism. There is no contradiction either with the Fermi-jet model /25,26/ or with the sum rule model /27,29/. The latter does not permit one to describe the angular and energy distributions. However, it is seen from the concepts laid in the model that the spectrum of emitted fragments can be parametrized in the form of a fast-moving source. The sum rule model makes it possible to reproduce the cross-section of nonequilibrium neutron yield for the reactions under study at reasonable values of parameters.

4. Hot spot model

The high velocity of the nonequilibrium neutron source does not permit the drifting hot spot model /21,24/ to be used, at least, to describe the fast neutron yield at small angles. A local equilibrium is assumed in the model to exist in a zone embracing the projectile nucleons and a fraction of the target nucleons, so the hot zone velocity should be considerably less than the projectile ion velocity.

Data on calculating the neutron energy spectra with the help of the isolated statistical hot spot model /18,19/ for reactions initiated by ions of helium-4 (E=52.6MeV) and lithium-6 (E=39.7 and 90MeV) are shown in Fig.20 and compared there with the experimental data. It is assumed that there is no change in nuclear density in the hot zone, the model parameter $\frac{3}{3}$ being equal to 0.58 and 0.51 for reactions initiated by ions of lithium-6 and α -particles, respectively. These values correspond to the number of hot zone nucleons, being double the number of projectile ion nucleons. The hot zone temperatures (Eq.(15)) corresponding to the above parameters were 4.0 and 7.0MeV for the reactions induced by 39.7 and 90 MeV lithium ions, respectively, and 6.5MeV for α -particles induced reactions. The calculations with the model reproduce adequately both the form of the high-energy portion of neutron distributions and the change in the form with projectile energy. The angular distributions of neutrons according to the model are determined by refractive effects of nuclear surface. In the framework of the model the reproduction of the experimentally observed angular distributions of neutron failed.

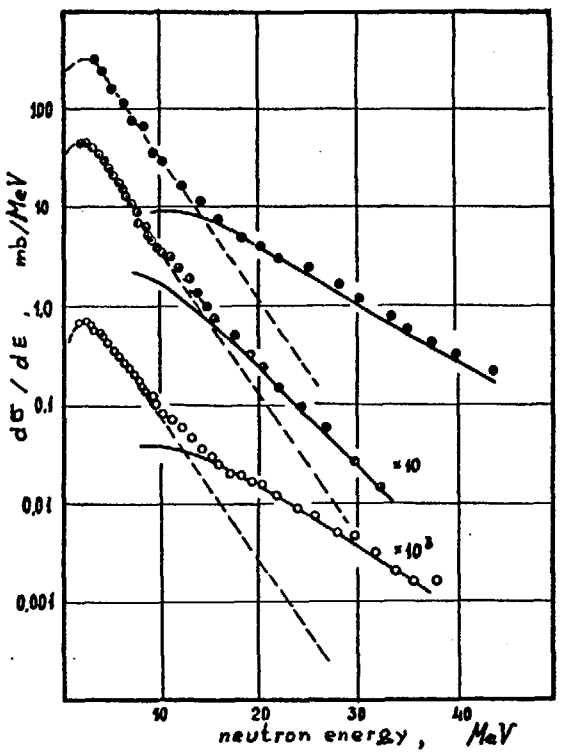

Fig.20. Energy spectra of neutrons from $^{4}He+^{61}Ni$(E=52.6MeV; solid circles), $^{6}Li+^{59}Co$(E=39.7 MeV; dotted circles) and $^{6}Li+^{59}Co$ (E=90MeV; open circles). Solid lines are the calculations by using the isolated statistical hot spot model with refraction at nuclear surface /18,19/. The contribution of neutron evaporation from a compound nucleus is shown by dashed curves.

The yield anisotropy decreases as the emitted neutron energy grows, which is the model consequence contradictory to experimental data.

The agreement of the model predictions with some characteristics of experimental data does not serve as convincing evidence for the fact that we deal just with the given mechanism of neutron emission. The shape of the neutron spectra has no specific singularities and in order to describe it a single parameter is enough.

It is of interest to analyze the large angle region in terms of the hot spot. In this region the contribution of the direct pro-

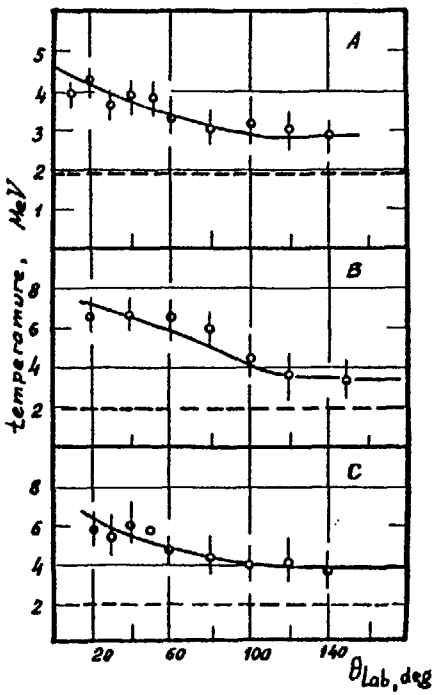

Fig.21. Temperature determined from the slope of the high-energy portion of neutron spectra (E≥15MeV) versus detection angle: (A) $^{6}LI+^{59}Co$(E=39.7MeV);(B) $^{4}He+^{61}Ni$ (E=52.6 MeV);(C) $^{3}He+^{62}Ni$ (E=40.9MeV).

cesses of all kinds is small. Fig.21 shows the dependence of temperature determined from the slope of the high energy portion of the spectra (E ⩾ 15 MeV) on detection angle. The temperature determined in such a way varies with the angle and at angles more than 90° reaches a constant value. But the value of temperature in the large angle region differs from the equilibrium value equal to 1.9 MeV in the given case. At the obtuse angles the variation of temperature with projectile mass agrees qualitatively with the predictions of the central hot spot model /2/. The higher temperatures are observed in reactions induced by ions of smaller mass. The values of temperature at the large angles are equal to 2.8, 3.5 and 4.0 MeV for bombarding ions: ^{6}Li, ^{4}He and ^{3}He, respectively. For reactions initiated by lithium-6 ions the α-particle and deuteron spectra were also

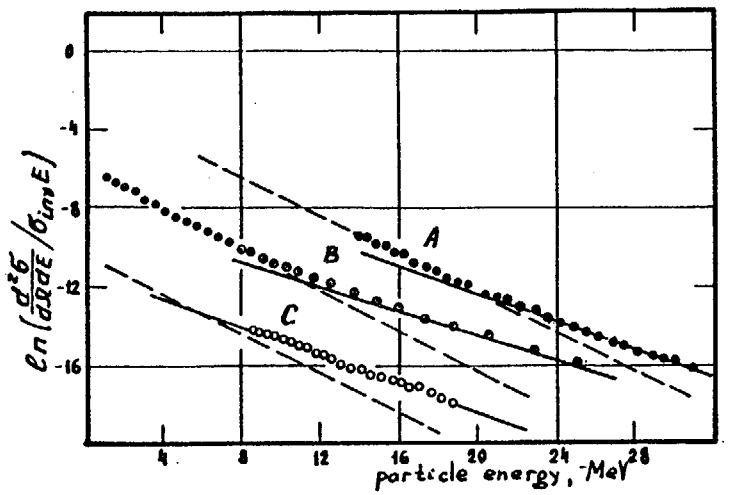

Fig.22. Temperature dependences in spectra of neutrons (B), deuterons (C) and α-particles (A) in $^{6}Li+^{59}Co$(E=39.7MeV) reaction. Dashed lines correspond to the equilibrium temperature (T=1.9MeV), solid lines, to the nonequilibrium component (T=2.8MeV). The spectra are obtained at detection angles of 120-140°.

measured /72/. Fig.22 presents the spectra of α-particles, deuterons and neutrons emitted in interaction of lithium-6 ion incident on a cobalt-59 target which were obtained at detection angles of 120-140°. Two components with different temperatures 1.9 and 2.8 MeV are observed in the α-particle spectra, as in the neutron spectra. The deuteron spectra can be approximated by the Maxwell distribution with a temperature of 2.8 MeV. The disintegration of the hot zone arising due to central collisions with the target nucleus may manifest itself at large angles. The coincidence of "nonequilibrium" temperatures for α-particles, deuterons and neutrons can evidence the establishment of local equilibrium in this hot zone.

5. Brief conclusions

(1) The hybrid model adequately reproduces both the absolute values of cross-sections and the shape of exit angle integrated neutron spectra.

(2) The breakup and knockout processes or the mechanism of the promptly emitted particles type may manifest themselves at small angles. The contribution of such processes into the exit angle integrated cross-section can be small and then the nonequilibrium neutron yield is determined by more complex processes. No definite conclusion on the part played by direct processes can be drawn from the analysis of inclusive spectra.

(3)The fact that neutron energy spectra are reproduced by the hot spot model with refraction on nuclear surface seems to reflect simply the fact that the nonequilibrium neutron spectrum has an inexpressive shape and in order to reproduce it a single parameter is enough. The neutron angular distributions cannot be described in terms of this model.

(4) The nonequilibrium component of the α-particle, deuteron and neutron spectra remains also at angles close to 180°. The parameters of energy and angular distributions agree here with the central hot spot model. However, the nonequilibrium component may well be described also in terms of multistage compound processes leading to a distribution symmetric about 90°.

III. NEUTRON SPECTRA IN CORRELATION MEASUREMENTS

1. Neutron emission in quasielastic and deep inelastic processes

(a) Reactions at incident ion energy up to 10MeV/nucleon

The angular distributions of neutron energy spectra and multiplicity were measured in a wide range of projectile ion masses from oxygen to krypton /73-81/. The neutrons were usually detected in coincidence with light and heavy fragments. Such measurements made it possible to obtain information about the time scale of energy equilibration, distribution of excitation energy between fragments and processes of fragment deexcitation.

As the light fragment velocity is much higher than the basic mass velocity, the neutrons are strongly focused in the direction of fragment emission (Fig.23,/77/). It makes it possible to separate neutrons emitted by each fragment. Data obtained in /73,76-79,81/ correspond to the assumption that all neutrons are produced due to emission from the fragments having left the nuclear and Coulomb field zone and being in statistical equilibrium. The authors of /78,79,81/ revised

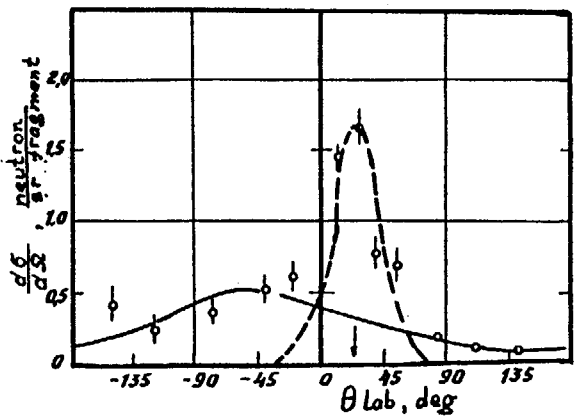

Fig.23. Angular distributions of neutrons from $^{56}Fe+^{165}Ho$ (E=476 MeV) reaction /77/. Arrow points the angle of light fragment emission. Solid line is the calculation for neutrons evaporating from heavy fragment, dashed line, from light one.

the previous reports about discovery of the nonequilibrium processes of neutron emission in reactions of the similar type /74,75,80/. No high-energy particles which would fall out of evaporation spectra, even for small angles of neutron emission, were detected in any experiment /73,76,79,81/.

For reactions with sufficiently heavy ions the temperature determined from the slope of the high-energy portion of the spectrum in the frame of the emitter-nucleus has the same value for the light and heavy fragments. It evidences that the excitation energy is shared between the fragments in proportion to their mass, i.e. the composite system reaches thermal equilibrium. Fig.24 shows the values of temperatures for the light and heavy fragments and the neutron multiplicity ratio as a function of kinetic energy loss for the $^{56}Fe(E=476MeV)+^{165}Ho$ reaction /77/. The values of temperatures and mean neutron multiplicity agree with the calculations (solid lines in Fig.24) made assuming that statistical equilibrium exsists within a wide range of variation of process inelasticity. There is a definite relationship between time of nuclear interaction and kinetic energy loss in collision.

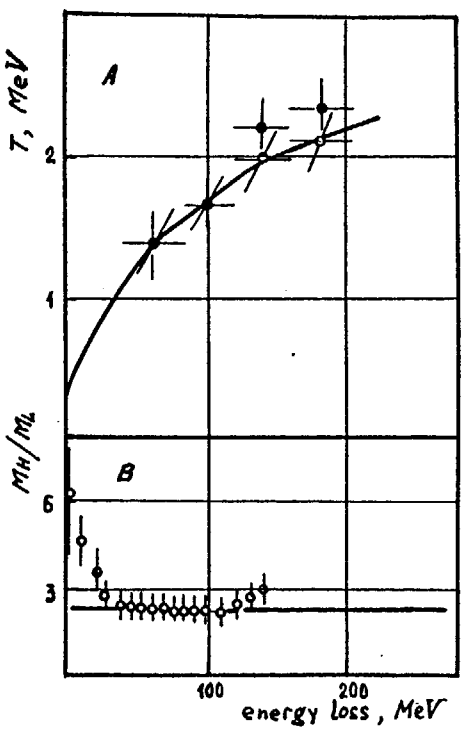

Fig.24. Parameter of temperature (A) for light (solid circles) and heavy (open circles) fragments and ratio of average numbers of neutrons emitted by heavy and light fragments (B) versus kinetic energy loss in $^{54}Fe+^{165}Ho$ reaction at an iron ion energy of 476 MeV /77/. Solid lines show the results of calculations with the assumption about establishment of thermal equilibrium in the double nuclear system

On these grounds the conclusion was made that the equilibrium distribution of thermal excitation energy in the system is established for a time less than $5 \cdot 10^{-22}$s.

For reactions with lighter ions, e.g. with oxygen /81/, the temperature for the light fragment is 50% higher than that for the heavy ones, i.e. in this case the energy is not shared between the fragments in proportion to their mass. It is no wonder, since the level density of such a light nucleus cannot be described in the framework of the degenerated Fermi-gas model and the pointed effect does not evidence the absence of equilibrium in the system /81/. An uncer-

tainty in temperature for light fragments makes it difficult to detect the nonequilibrium effects.

(b) Reactions at incident ion energy higher than 10MeV/nucleon

As seen from the above, the detection of nonequilibrium neutrons in quasielastic and deep inelastic processes is a complicated problem. The neutron spectrum having a highly inexpressive shape consists of two components: evaporation from the moving light and heavy fragments. The components have different energy and angular distributions and represent a background for the nonequilibrium neutrons. Under such conditions errors in interpretating the experimental data are quite possible.

One of the first reports about discovery of preequilibrium neutrons was published in /82/. The reaction of oxygen-16 interaction with niobium-93 at an energy of 204 MeV was investigated. The measured angular and energy distributions of neutrons cannot be explained by evaporation from excited fragments. To describe the experimental data the authors assumed the exsistance of a third source (T=1.5MeV) moving along the beam direction with a velocity nearly equal to half an incident ion velocity. The phenomenon of preequilibrium emission was studied in considerable detail in collisions of ^{86}Kr on ^{166}Er at 11.9 MeV/nucleon /83,84/. The experimental data analysis showed the presence of nonequilibrium neutrons emitted close to the light fragment direction in the case of quasielastic reactions and along the heavy fragment direction for deep inelastic reactions. The behaviour of the obtained experimental data is reproduced in terms of a simple model which assumes that about 10% of neutrons (independent of inelasticity of process) are emitted at an early stage of reaction along the bombarding ion direction. The process is formally reduced to neutron sources having a distribution in velocity (dispersion being 1.7cm/ns) and in direction of motion (dispersion being 15^{o}). The parametrization used resembles the classical orbiting model /54/.

The works carried out so far do not claim to study the mechanism for nonequilibrium neutron emission and only state that such a phenomenon takes place. The detailed and systematical investigations of the nonequilibrium emission behaviour depending on kinetic energy loss during the reaction and on type of projectile ion are required now.

2. Nonequilibrium neutron emission in fusion reactions

(a) Nonequilibrium emission effect and model descriptions

There are two basic methods of distinguishing the channels of reactions resulting in fusion. The residual heavy nuclei moving with velocities close to the center-of-mass velocity of the projectile and target nuclei are detected by the first method /52,53/. The other method is based on identification of concrete isotopes by γ-rays of rotation band and separation of the events characteristic of fusion processes only /54,85-94/. The excitation functions of neutron emission channels /85-87,90-93/ as well as the energy and angular distributions of neutrons /52-54, 88, 89, 94/ were measured in the experimental works.

The hybrid model of preequilibrium emission reproduces the excitation functions in α-particle induced reactions /87/. In the lithium-6 induced reactions the agreement is achieved assuming that the lithium breakup in the nuclear field with subsequent capture of one of its fragments is an analog of incomplete fusion reaction /85,86/. The description of the excitation function in neutron channels can also be made on the basis of the simple model which assumes that the neutron emission is a random process and that probabilities of emission of a definite number of neutrons obey the Poisson distribution /95/. In the framework of the preequilibrium disintegration model of excitonic type it is possible to describe the neutron energy spectra in heavy ion induced reactions /54/. In this case the initial number of excitons considered as a free parameter can exceed the number of projectile nucleons.

The comparison with the promptly emitted particles model was made in /54/. The model reproduces qualitatively the behaviour of neutron spectra at small angles, but gives more abrupt angular dependence. The model predicts that high-energy neutron emission occurs only at forward angles, but a considerable number of high-energy neutrons is experimentally observed at backward angles /52,54,91/.

The hot spot models have not been analyzed thoroughly. Comparison of some characteristics of experimental distributions indicates that the hot zone concept as such does not contradict the experiment /94/.

A low velocity of the source amounting to 0.2-0.4 of the ion one on the peak of the Coulomb barrier was obtained in all works /52-

54/ in the parametrization of neutron distributions in the moving sources model. The low velocity can be explained in terms of the classical orbiting model /52,54/ in which the tangential component of ion velocity plays a decisive part in grazing collision. The calculation of this velocity in the ion motion along the Rutherford trajectories yields nearly doubled values and with the assumption about sticking the value of velocity is somewhat lower than that obtained in parametrization. It evidences a possible influence of friction forces on preequilibrium emission /54/.

Analysis of neutron distributions for α-particle induced reactions in the two-phase deexcitation model leads to the average number of excitons equal to 10 at the preequilibrium stage and the average velocity of the excited complex amounting to 0.4 of the incident ion velocity /89/. Comparison of these parameters with those of other models is hindered.

It is seen from the foregoing that most of the models can give more or less complete description of experimental data, pointing to noncriticality of general rough features of the measured distributions to the model prediction. A more delicate and detailed analysis is required here.

(b) Bombarding nucleus structure and preequilibrium processes

It is experimentally established that the nonequilibrium neutron emission accompanies the fusion process between ^{12}C(E=152MeC) and ^{158}Gd /94/, manifests itself to a lesser degree in the interaction of ^{16}O(E=152MeV) with ^{154}Sm /54/ and is absent in the fusion of ^{20}Ne(E=175MeV) with ^{150}Nd /94/. It indicates a possible effect of projectile structure, as the same compound nucleus ^{170}Yb forms in the reactions at comparable excitation energies. The observed difference was explained in /90/ within the framework of the modified sum rule model /29/. The authors of /91/ substituted Q_{gg} in the model by the reaction energy for two-particle fragmentation, thus introducting the ion structure in the model. The adequate description of a fraction of preequilibrium emission has been obtainedin all the three reactions.

However, the observed difference in the fusion processes can be connected also with the difference in energy per nucleon (at the Coulomb barrier) for bombarding ions. Investigations of fusion process in reactions with nuclei similar in mass but different in structure are decisive experiments in this case. The preequilibrium neutron emission was studied in the fusion reactions of ^{12}C and ^{13}C (neutron separation energies equal to 18.7 and 4.9 MeV, respectively) with ^{158}Gd and ^{157}Gd nuclei. The measurements showed no essential changes in behaviour and fraction of preequilibrium emission in the reactions /52/. The sum rule model (without any modifications) reproduces the ratio of cross-sections in the reactions. The model involves the parameter T (Eq.(19)) the sense of which is not quite clear, thus giving carte blanche for speculations. It is possible that the "discovery" of the projectile nuclear structure effect is explained by this fact /91/.

The projectile ion velocity rather than the nuclear structure or the total incident energy seems to be a determinant in the preequilibrium emission.

(c) Is the preequilibrium neutron emission a peripheral process?

The possibility of distinguishing the peripheral reaction is based on the following concepts. The excitation of a compound nucleus is removed at an early stage by evaporation of light particles, mainly neutrons. The light particles take away only a small fraction of nuclear angular momentum. Then the nucleus changes in the ground state producing a cascade of γ-rays due to transitions between different states of the rotation band. If the reaction proceeds in the sufficuently narrow range of momenta, intensity of γ-transitions is independent of state spin, because the side feedings are absent. In the reactions going at different momenta the intensity of γ-transitions increases with decreasing the state spin.

Such a method was first used in /96/ to study the fusion reactions of ^{14}N with ^{159}Tb at 95 MeV. The intensity of γ-transitions as a function of state spin is shown in Fig.25. The measurements were made both in coincidence with high-energy α-particles (A) and without coincidence selection (B). It is seen that the states of rotation band with momenta 10-14 $\hbar$ are occupied first of all. The data obtained distinctly indicate that production of nonequilibrium α-partucles is a peripheral process.

The similar measurements were carried out in /88/, where the channels of neutron emission in interaction of α-particles with ^{194}Dy at 120 MeV were investigated. The measurement showed that for all the reaction channels there was no notable difference between the

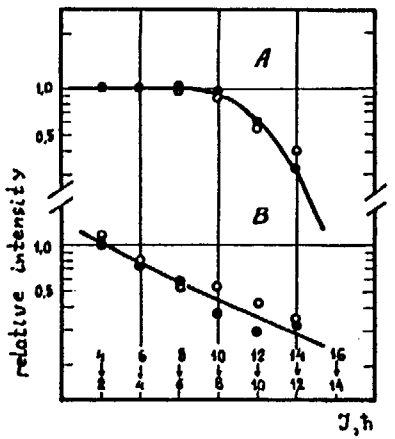

Fig.25. Intensity of γ-transitions versus state spin for isotopes ^{166}Yb and ^{165}Yb produced in fusion of ^{14}N with ^{159}Tb at 95 MeV /96/.(A) measurements in coincidence with high-energy α-particles; (B) measurements without coinddidence selection.

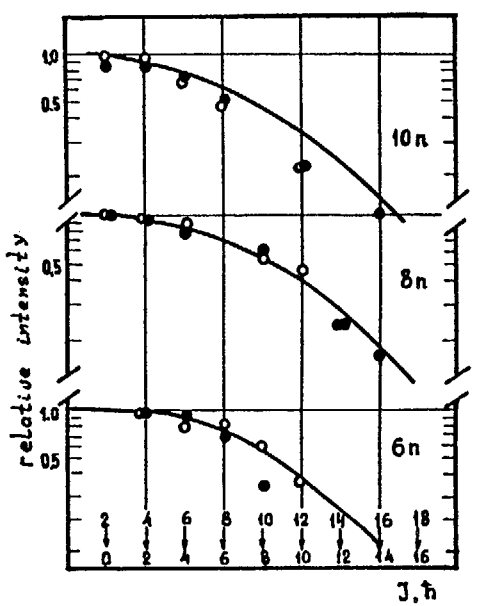

Fig.26. Intensity of γ-transitions versus state spin for ^{165}Dy (α, $x_n\gamma$) reactions at x=10, 8 and 6 /88/. Energy of α-particles was 120 MeV. Solid circles are measurements in coincidence with neutrons ($E_n \geq 2.5$ MeV) emitted at an angle of 145°; open circles, measurements in coincidence with neutrons ($E_n \geq 6.8$ MeV) emitted at an angle of 35°.

intensities of γ-transitions in coincidence with high-energy ($E \geq 6.8$ MeV) neutrons emitted at small angles as well as with neutrons ($E \geq 2.5$ MeV) emitted at forward angles and those obtained without coincidence selection (Fig.26). For heavy ion induced reactions the difference between the dependences of γ-transition intensity on state spin in the channels with high-energy α-particle and neutron emission was pointed out in /97/. It proves that in the nonequilibrium neutron emission there is no preferred area of momenta and that the emission is not a peripheral process.

The conclusion of /91/ about the peripheral nature of nonequilibrium emission is based only on the fact that the experimental dependencies of γ-rays multiplicity on both incident energy and number of emitted neutrons do not contradict the sum rule model. This conclusion rests only on the model and raises doubts. The γ-rays multiplicity reaches a saturation value with increasing the incident ion energy, thus evidencing the exsistance of a critical angular momentum for fusion /70/, but having no direct relations with preequilibrium emission. The maxima of γ-ray multiplicity in light /89/ and heavy /90/ ion induced reactions correspond to the calculated values of critical angular momenta /71/. A decrease in multiplicity with the incident ion energy can be due to both growth of the average number of evaporation neutrons and increase in a fraction of nonequilibrium processes.The turn to assumption about the peripheral nature of the preequilibrium emission in order to explain the obtained behaviour /91-93/ is not required.

BRIEF CONCLUSIONS

(a) The incident ion velocity rather than the total incident energy is a determinative parameter of the preequilibrium emission processes. The nonequilibrium neutron emission manifests itself at energies above ~10MeV/nucleon both in deep inelastic reactions and in fusion reactions.

(b) The experimental works on preequilibrium emission in deep inelastic reactions are at the stage of discovery of the effect. At this point the detailed and systematic investigations with a higher accuracy and for a wider range of reactions are required.

(c) The neutron spectra in fusion reactions are not characterized by any specific shape and, therefore, the description of some of their features can be made within the framework of many rather simple models. Here one cannot limit oneself to the description of the general characteristics, a more detailed analysis of distributions being required.

(d) The structure of interacting nuclei does not affect significantly the preequilibrium emission process. There is no preferred region of angular momenta in this process and the preequilibrium emission takes place also at small impact parameters. These model-independent experimental facts permit one to regard the model description of the process more critically.

CONCLUSION

The field of physics concerned with studying the mechanisms of light particle nonequilibrium emission and, ultimately, the dissipation of energy in nuclear collisions and the processes of equilibration in nuclear matter is now far from a harmonic system of experimental facts and theoretical generalizations. Here there are, so far, only outlines and contours of possible effects and theories. The extensive search leads to a great deal of various models and ideas. On the one hand, it indicates an interest to the problem, on the other hand, makes the comparison of experimental data difficult. A noncriticality to validity of the basic model assumptions also affects the situation.

A wide range of processes from direct reaction to reactions going through compound nucleus formation manifest themselves in inclusive neutron spectra, espesially at small emission angles. Analysis of such spectra is complicated and ambiguous in many cases. A more unambiguous information about the preequilibrium emission can be expected to be obtained from spectra of nucleons emitted at backward angles. And analysis of data on correlation measurements with distinguishing the certain channels of reaction is, of course, simpler and less dependent of the model predictions. But a more detailed, not superficial, analysis of pecularities of experimental distributions is also required at this point.

It is of interest to follow the change in behaviour of the preequilibrium emission in passing to high energies of bombarding ions, to follow how the ideas developed to describe reactions at 10-20 MeV/nucleon transform in those used to interpret data at energies of several hundred MeV per nucleon and above.

REFERENCES

1. V.Weisskopf, Statistics and nuclear reactions, - Phys. Rev. 52 (1937) 295 - 303.
2. H.A.Bethe, Possible deviations from the evaporation model of nuclear reactions, - Phys. Rev. 53 (1938) 675 - 675.
3. R.W.West, Proton emission in 42-MeV alpha-particle bombardments of several elements, - Phys. Rev. 141 (1966) 1033- 1052.
4. E.V.Verdieck, J.M.Miller, Radiative capture and neutron emission in $^{139}La + \alpha$ and $^{142}Ce + p$, - Phys. Rev. 153 (1967) 1253 - 1261.
5. R.Serber, Nuclear reactions at high energies, - Phys. Rev. 72 (1947) 1114 - 1115.
6. J.J.Griffin, Statistical model of intermediate structure, - Phys. Rev. Lett. 17 (1966) 478 - 481.
7. G.D.Harp, J.M.Miller, B.J.Berne, Attainment of statistical equilibrium in excited nuclei, - Phys. Rev. 165 (1968) 1166-1169.
8. G.D.Harp, J.M.Miller, Precompound decay from a time-dependent point of view, - Phys. Rev. C3 (1971) 1847 - 1855.
9. M.Blann, A.Mignerey, Preequilibrium decay at moderate excitations and the hybrid model, - Nucl. Phys. A186 (1972) 245 - 256.
10. M.Blann, Importance of the nuclear density distribution on preequilibrium decay, Phys. Rev. Lett. 28 (1972) 757 - 759.
11. M.Blann, Precompound decay in heavy-ion reactions, Phys. Rev. C23 (1981) 205 - 212.

12. C.K.Cline, M.Blann, The pre-equilibrium statistical model: description of the nuclear equilibration process and parametrization of the model, - Nucl. Phys. A172 (1971) 225 - 259.

13. E.Gadioli, E.Gadioli-Erba, P.G.Sona, Intermediate state decay rates in the exciton model, - Nucl. Phys. A217 (1973) 589 - 610.

14. R.Weiner, M.Westrom, Preequilibrium and heat condition in nuclear matter, - Phys. Rev. Lett. 34 (1975) 1523- 1527.

15. R.Weiner, M.Westrom, Diffusion of heat in nuclear matter and preequilibrium phenomena, - Nucl. Phys. A286 (1977) 282 - 296.

16. P.A.Gottschalk, M.Westrom, Light-particle heavy-ion correlations in deep inelastic processes: a theoretical study of hot-spot particle emission, - Nucl. Phys. A314 (1979)232 - 252.

17. P.A.Gottschalk, M.Westrom, Hot-spot particle emission in deep-inelastic $^{16}O + ^{58}Ni$ collisions, - Phys. Rev. Lett. 93 (1977) 1250 - 1253.

18. S.I.A.Garpman, D.Sperber, M.Zielinska-Pfabe, Nucleon emission from a hot zone in heavy ion reactions, - Phys. Lett. 90B (1980) 53 - 56.

19. S.I.A.Garpman, D.Sperber, M.Zielinska-Pfabe, Nucleon emission from a hot compressed zone at intermediate energy heavy ion reactions, - Nucleonika 25 (1980) 995 - 998.

20. P.Mooney, W.W.Morison, S.K.Samaddar, D.Sperber, M.Zielinska-Pfabe, Nucleon spectra in heavy ion collision prior to equilibrium, - Phys. Lett. 98B (1981) 240 - 243.

21. R.V.Jolos, V.G.Kartavenko, Preequilibrium emission of light particles in reactions with heavy ions, - Preprint JINR P4-80-37, 1980.

22. N.Stelte, R.Weiner, Cumulative effects and hot spots, - Phys. Lett. 103B (1981) 275 - 280.

23. T.Nomura, H.Utsunomiya, T.Motobayashi, T.Inamura, M.Yanokura, Statistical analysis of preequilibrium -particle spectra and possible local heating, - Phys. Rev. Lett. 40 (1978) 694 - 697.

24. N.Stelte, M.Westrom, R.M.Weiner, Drifting hot spots, - Nucl. Phys. A384 (1982) 190 - 210.

25. J.P.Bondorf, J.N.De, A.O.T.Karvinen, G.Fai, B.Jakobsson, Prompt emission of nucleons in heavy-ion collisions, Phys. Lett. 84B (1979) 162 - 165.

26. J.P.Bondorf, J.N.De, A.O.T.Karvinen, G.Fai, B.Jakobsson, J.Randrup, Promptly emitted particles in nuclear collisions,- Nucl. Phys. A333 (1980) 285 - 301.

27. J.Wilczynski, K.Siwek-Wilczynska, E.H.du Marchie Van Voorthuysen, J.Van Popta, R.H.Siemssen, Incomplete fusion in $^{12}C + ^{160}Gd$ collisions, - Nucl. Phys. A330 (1979) 150 - 172.

28. K.Siwek-Wilczynska, J.Wilczynski, E.H. du Marchie van Voorthuysen, J. van Popta, R.H.Siemssen, Incomplete fusion in $^{12}C + ^{160}Gd$ collisions interms of generalized concept of critical angular momentum, - Phys. Rev. Lett. 42 (1979) 1599 - 1602.

29. J.Wilczynski, K.Siwek-Wilczynska, Incomplete fusion reactions in the $^{14}N + ^{159}Tb$ system and a "Sum Rule Model" for fusion and incomplete fusion reactions, - Phys. Rev. Lett. 45 (1980) 606 - 609.

30. D.H.E.Gross, J.Wilczynski, Does radial friction cause emission of fast -particles?, - Phys. Lett. 67B (1977) 1 - 4.

31. T.Tamura, T.Udagawa, D.H.Feng, K.K.Kan, Deep inelastic reactions treated as multi-step direct reaction processes. Application to (p, p') reaction. - Phys. Lett. 66B (1977) 109 - 112.

32. T.Tamura, T.Udagawa, H.Lenske, Multistep direct reaction analysis of continuum spectra in reactions induced by light ions, - Phys. Rev. C26 (1982) 379 - 404.

33. H.C.Chiang, J.Hufner, One, two, infinity: a progmatic approach to nuclear precompound reactions, - Nucl. Phys. A349 (1980) 466 - 482.

34. M.Blann, Preequilibrium models for nuclear reactions, - Proceedings of the International School on Nuclear Physics, Predeal, September, 1974, Buchurest, 1976, pp 249 - 314.

35. C.Kalbach, F.M.Mann, Phenomenology of continuum angular distributions. I. Systematics and parametrization, - Phys. Rev. C23 (1981) 112 - 123.

36. C.Kalbach, Phenomenology of continuum angular distributions. II. Griffin preequilibrium model, - Phys. Rev. C23 (1981) 124 - 135.

37. C.Kalbach, Erratum: Phenomenology of continuum angular distributions. II. Griffin preequilibrium model, - Phys. Rev. C23 (1981) 2798 - 2798.

38. J.Ernst, J.Rama Rao, A unified model of preequilibrium decay, - Z. Physik A281 (1977) 129 - 135.

39. E.Gadioli, E.Gadioli-Erba, G.Tagliaferri, J.J.Hogan, Nucleon mean free path in nuclear matter, - Phys. Lett. 65B (1976) 311 - 315.

40. M.Blann, Comments on nucleon mean free paths in nuclear matter, - Phys. Lett. 67B (1977) 145 - 147.

41. M.Blann, R.B.Deering, A.Galonsky, D.M.Patterson, F.E.Serr, Preequilibrium analysis of (p, n) spectra on various targets at proton energies of 25 to 45 MeV, - Nucl. Phys. A257 (1976) 15 - 28.

42. D.Zeliger, S.Sasopov, Theoretical models of description of angular distributions of preequilibrium nuclear reactions products, - Fizika elementarnykh chastits y atomnogo yadra (Physics of Elementory Particles and Nucleus - Sov. Phys.) v. 11, issue 4, pp 967 - 990, 1980.

43. G.Mantzouranis, D.Agassi, H.A.Weidenmuller, Angular distributions of nucleons in nucleon-induced preequilibrium reactions, - Phys. Lett. 57B (1975) 220 - 222.

44. G.Mautzouranis, D.Agassi, H.A.Weidenmuller, Generalized exciton model for the description of preequilibrium angular distributions, - Z. Physik 276 (1976) 145 - 154.

45. S.Ziyang, W.Shunuan, Z.Jingshang, Z.Yizhong, Angular distribution calculation based on the exciton model taking account of the influence of the Fermi motion and the Pauli principle, - Z. Physik A305 (1982) 61 - 68.

46. G.Mantzouranis, Hybrid model and angular distributions in preequilibrium reactions, - Phys. Lett. 63B (1976) 25 - 26.

47. Y.Irie, M.Hyakutake, M.Matoba, M.Sonoda, Angular distribution of neutrons from precompound decay in inelastic scattering, - Phys. Lett. 62B (1976) 9 - 11.

48. N.S.Wall, J.R.Wu, C.C.Chang, H.D.Holmgren, Medium energy reactions: "Quasi-two-body scaling" and "hot spot", - Phys. Rev. C20 (1979) 1079.

49. H.Ejiri, Y.Nagai, H.Sakai, T.Itahashi, T.Schibata, M.Hoshi, S.Nakayama, T.Kishimoto, K.Maeda, Preequilibrium and equilibrium D_y (α, xnγ) Er reactions induced by 90 MeV alpha particles, - J. Phys. Soc. Japan 44 (1978) 655, Suppl. 1.

50. R.Serber, The production of high energy neutrons by stripping - Phys. Rev. 72 (1947) 1008 - 1016.

51. A.S.Goldhaber, Statistical models of fragmentation processes, - Phys. Lett. 53B (1974) 306 - 308.

52. A.Gavrou, J.R.Beene, R.L.Ferguson, F.E.Obenshain, F.Plasil, G.R.Young, G.A.Petitt, K.G.Young, M.Jaaskelainen, D.G.Sarantites, C.F.Maguire, Neutron emission in ^{12}C + ^{158}Gd and ^{13}C + + ^{157}Gd reactions between 8 and 12 MeV/nucleon, - Phys. Rev. C24 (1981) 2048 - 2069.

53. D.Hilscher, E.Holub, U.Jahnke, H.Orf, H.Rossner, Neutron emission in heavy ion collisions at energies below 15 MeV/ , - Dynamics of heavy-ion collisions, North-Holland Publishing Company, 1981, pp 225 - 239.

54. K.G.Young, D.G.Sarantites, J.R.Beene, M.L.Halbert, D.C.Hensley, R.A.Dayras, Nonequilibrium emission of neutrons from fusion-like reactions of 152 MeV ^{16}O with ^{154}Sm, - Phys. Rev. C23 (1981) 2479 - 2491.

55. B.Jakobsson, L.Carlen, P.Kristiansson, J.Krumlinde, A.Oskarsson, I.Otterlund, B.Schroder, H.A.Gustafsson, T.Johansson, H.Ryde, G.Tibell, J.P.Bondorf, G.Fai, A.O.T.Karvinen, O.B.Nielsen, M.Buenerd, J.Cole, B.Lebrun, J.M.Loiseaux, P.Martin, R.Ost, P. de Saintignon, C.Guet, E.Monnand, J.Mougey, H.Nifenecker, P.Perrin, J.Pinston, C.Ristori, F.Schussler, Proton emission in 58A and 86A MeV ^{12}C-induced heavy-ion reactions, - Phys. Lett. 102B (1981) 121 - 126.

56. D.K.Scott, Nuclear collisions at intermediate energy, - Nucl. Phys. A354 (1981) 375 - 394.

57. V.A.Sidorov, Spectra of evaporation neutrons, Preprint IAE-253, 1961.

58. A.Alevra, R.Dumitrescu, I.R.Lukas, M.T.Magda, D.Plostinaru, E.T.Rutia, N.Chevarier, A.Chevarier, A.Demeyer, Trau Minh Due, Precompound processes in (d, n) reactions, - Nucl. Phys. A209 (1973) 557 - 571.

59. A.Chevarier, N.Chevarier, A.Demeyer, A.Alevra, R.Dumitrescu, I.R.Lukas, M.T.Magda, M.E.Nistor, Neutron, proton and -particle emission from ^{3}He induced reactions, - Nucl. Phys. A231 (1974) 64 - 76.

60. R.Scherwinski, A.Alevra, J.Friese, R.Longhau, W.Scobel, Entrance channel effects in nucleon and -particle preequilibrium decay of ^{63}Cu and ^{64}Zn, - Phys. Rev. C26 (1982) 113 - 128.

61. O.V.Bochkarev, E.A.Kuzmin, A.A.Ogloblin, A.V.Chulkov, G.B. Yankov, Preequilibrium processes of neutron formation in reactions with ions of He and C, - Izv. Acad. Nauk SSSR, ser. Fiz. (Sov. Phys.) v. 43, 1979, pp 2192 - 2200.

62. O.V.Bochkarev, E.A.Kuzmin, A.A.Ogloblin, L.V.Chulkov, G.B. Yankov, The investigation of encrgy spectra of neutrons from reactions with ions of Li, - Voprocy Atomnoy Nauki i Tekhniki, ser. : Yadernye Konstanty (Sov. Phys.) issue 1 (40), 1981, pp 28 - 30.

63. O.V.Bochkarev, A.A.Korsheninnikov, E.A.Kuzmin, L.V.Chulkov, G.B.Yankov, The investigation of neutron formation from the $^{3}He + ^{62}Ni$ reaction at the energy of He ions of 59 MeV, - Theses of reports at XXXI Conf. on Nuclear Spectroscopy and Structure of Atomic Nucleus, Samarkand, April 14 - 16, 1981, Nauka (Sov. Phys.), Leningrad, p. 391.

64. O.V.Bochkarev, A.A.Korsheninnikov, E.A.Kuzmin, L.V.Chulkov, G.B.Yankov, The investigation of energy spectra of neutrons from reactions with ions of He, ^{6}Li and C at the energies from 4 to 20 MeV/nucleon, forming a composition system ZINK-65, - Experimental data. Preprint IAE-3755, 1983.

65. O.V.Bochkarev, A.A.Korsheninnikov, Nonequilibrium processes in the emission of neutrons from reactions with ions of He, ^{6}Li and C. The analysis of experimental data, - Preprint IAE-3756, 1983.

66. M.Blann, Overlaid Alice. A statistical model computer code including fission and preequilibrium models, - US ERDA report, COO-3494-29, 1976.

67. V.F.Weisskopf, D.H.Ewing, On the yield of nuclear reactions with heavy elements, - Phys. Rev. 57 (1940) 472 - 485.

68. D.Glass, U.Mősel, Microscopic description of nuclear friction in heavy ion collisions, - Nucl. Phys. A264 (1976) 268 - 290.

69. D.Glass, U.Mősel, On the critical distance in fusion reactions, - Nucl. Phys. A237 (1975) 429 - 440.

70. J.Wilczynski, Calculations of the critical angular momentum in the entrance reaction channel, - Nucl. Phys. A216 (1973) 386 - 394.

71. W.W.Wilcke, J.R.Birkelund, H.J.Wollersheim, A.D.Hoover, J.R. Huizenga, W.U.Schroder, L.E.Tubbs, Reaction parameters for heavy-ion collisions, - Atomic Data and Nuclear Data Tables 25 (1980) 389 - 619.

72. O.V.Bochkarev, A.A.Korsheninnikov, E.A.Kuzmin, I.G.Mukha, L.V. Chulkov, G.B.Yankov, The investigation of scattering of ^{6}Li on ^{59}Co with the excitation of the 2.18 (3^{+}) MeV state, Theses of reports at XXXII Conf. on Nuclear Spectroscopy and Structure of Atomic Nucleus, Kiev, March 16 - 18, 1982 (Sov. Phys.), Nauka, 1982, Leningrad, p. 363.

73. W.G.Simon, S.T.Ahres, Neutron emitted after heavy-ion bombardment: effects of transfer reactions on particle spectra,- Phys. Rev. C2 (1970) 1292 - 1304.

74. C.R.Gould, R.Bass, J.Crarnecki, V.Hartmann, K.Stelzer, R.Zitzmann, Y.Eyal, Neutron multiplicities in inelastic collisions of ^{132}Xe with ^{197}Au,- Z. Physik A284 (1978) 353 - 354.

75. J.Peter, M.Berlanger, C.Ngo, B.Tamain, B.Lucas, C.Mazur, M.Ribrag, C.Signarbieux, Neutron multiplicity in deep inelastic collisions 365 MeV Cu + Au system, - Z. Physik A283 (1977) 413 - 414.

76. Y.Eyal, A.Gavron, I.Tserruya, Z.Fraenkel, Y.Eisen, S.Wald, R.Bass, C.R.Gould, G.Kreyling, R.Renford, K.Stelzer, R.Zitzmann, A.Gobbi, U.Lyner, H.Stelzer, I.Rode, R.Bock, Neutron emission in strongly damped collisions of ^{86}Kr on ^{166}Er at 602 MeV, - Phys. Rev. Lett. 41 (1978) 625 - 628.

77. D.Hilscher, J.R.Birkelund, A.D.Hoover, W.U.Schroder, W.W.Wilcke, J.R.Huizenga, A.C.Mignerey, K.L.Wolf, H.F.Breuer, V.E. Viola, Jr., Neutron emission in the reaction $^{165}Ho + ^{56}Fe$ at $E_{lab} = 8.5$ MeV/u, - Phys. Rev. C20 (1979) 576 - 591.

78. B.Tamain, R.Chechik, U.Fuchs, F.Hanappe, M.Morjean, C.Ngo, J.Peter, M.Dakowski, B.Lucas, C.Mazur, M.Ribrag, C.Signarbieux, Neutron multiplicity in deep inelastic collisions: 400 MeV Cu + Au system, - Nucl. Phys. A330 (1979) 253 - 268.

79. Y.Eyal, A.Gavron, I.Tserruya, Z.Fraenkel, Y.Eiseu, S.Wald, R.Bass, G.R.Gould, G.Kreyling, R.Renfordt, K.Stelzer, R.Zitzmann, A.Gobbi, U.Lynen, H.Stelzer, I.Rode, R.Bock, Neutron emission in deep-inelastic collisions induced by ^{86}Kr on ^{166}Re at 5.7, 7.0 and 7.9 MeV/nucleon, - Phys. Rev. C21 (1980) 1377 - 1386.

80. H.Gemmeke, P.Netter, Ax. Richter, L.Lassen, S.Lewandowski, W.Lucking, R.Schreck, Emission of fast neutrons in deep-inelastic collisions of ^{16}O on Ni, - Phys. Lett. 97B (1980) 213 - 216.

81. S.Wald, I.Tserruya, Z.Fraenkel, G.Doukellis, H.Gemmeke, H.L. Harney, Neutron, proton, and alpha emission in deep inelastic collisions of ^{16}O on ^{48}Ca at 142 MeV, - Phys. Rev. C25 (1982) 1118 - 1121.

82. A.Gavron, R.L.Ferguson, F.E.Obenshain, F.Plasil, G.R.Young, G.A.Pettit, K.G.Young, D.G.Sarantity, C.F.Majurre, Neutron emission in deep-inelastic collisions of ^{16}O on ^{93}Nb at 204 MeV, - Phys. Rev. Lett. 46 (1981) 8 - 11.

83. I.Tserruya, A.Breskin, R.Chechik, Z.Fraenkel, S.Wald, H. Zwang, R.Bock, M.Dakowski, A.Gobbi, H.Sann, R.Bass, G.Kreyling, R.Renfordt, K.Stelzer, U.Arlt, Nonequilibrium neutron emission in deep-inelastic collisions of ^{86}Kr on ^{166}Er at 1.02 GeV, - Phys. Rev. Lett. 47 (1981) 16 - 19.

84. I.Tserruya, A.Breskin, R.Chechik, Z.Fraenkel, S.Wald, H.Zwang R.Bock, M.Dakowski, A.Gobbi, H.Sann, R.Bass, G.Kreyling, R. Renfordt, K.Stelzer, U.Arlt, Preequilibrium neutron emission in deep-inelastic collisions of ^{86}Kr on ^{166}Er at 11.9 MeV/nucleon, - Phys. Rev. C26 (1982) 2509 - 2524.

85. B.Neumann, J.Buschmann, H.Klewe-Nebenius, H.Rebel, H.J.Gils,- Transfer of ^{6}Li break-up fragments at ^{6}Li projectile energies far above the Coulomb barrier, - Nucl. Phys. A329 (1979) 259-270.

86. J.Kropp, H.Klewe-Nebenius, H.Faust, J.Buschmann, H.Rebel, H.J.Gils, K.Wisshak, Excitation function of $^{191 + 193}Ir$, ^{197}Au (^{6}Li, xn + yp) compound nuclear reactions at E_{Li} = 48 - - 156 MeV, - Z. Physik, A280 (1977) 61 - 72.

87. A.Djoloeis, P.Jahn, H.J.Probst, Investigation of multinucleon emission induced by -particles on ^{197}Au in the energy range 20 - 170 MeV, - Nucl. Phys. A250 (1975) 149 - 162.

88. H.Sakai, H.Ejiri, T.Shibota, Y.Nagai, K.Okada, Preequilibrium neutron emission for the ^{164}Dy (α, xnγ) $^{168 - x}Er$ reaction studied by n-γ coincidence measurements, - Phys. Rev. C20 (1979) 464 - 477.

89. H.Ejiri, Y.Nagai, H.Sakai, T.Sibata, T.Kishimoto, K.Maeda, Preequilibrium deexcitation process for ^{164}Dy (α, xnγ) reaction and angular momentum transfer, - J.Phys. Soc. Japan 49 (1980) 2103 - 2113.

90. Y.Nagai, T.Shibata, H.Sakai, T.Kishimoto, H.Ejiri, Angular momentum transfers in equilibrium and preequilibrium Dy (α, xn, γ) reactions, - J. Phys. Soc. Japan 46 (1979) 1025 - 1026.

91. J.R.Beene, M.L.Halbert, D.C.Hensley, R.A.Dayras, Fusion-like reactions of ^{16}O with ^{154}Sm: ray multiplicity versus bombarding energy, - Phys. Rev. C23 (1981) 2463 - 2478.

92. D.G.Sarantites, L.Westerberg, R.A.Dayras, M.L.Halbert, D.C. Hensley, J.H.Barker, Angular-momentum effects in preequilibrium processes, - Phys. Rev. C17 (1978) 601 - 621.

93. D.G.Sarantites, L.Westerberg, R.A.Dayras, M.L.Halbert, D.C. Hensley, J.H.Barker, Preequilibrium effects in fusion of ^{12}C and ^{158}Cd, - Phys. Rev. C18 (1978) 774 - 795.

94. L.Westerberg, D.G.Sarantites, D.C.Hensley, R.A.Dayras, M.L. Halbert, J.H.Barker, Preequilibrium particle emission from fusion of ^{12}C + ^{158}Gd and ^{20}Ne + ^{150}Nd, - Phys. Rev. C18 (1978) 796 - 814.

95. M.H.Simbel, Is neutron evaporation from highly excited nuclei a Poisson random process?, - Z. Physik A307 (1982) 141 - 147.

96. T.Inamura, M.Ishihara, T.Fukuda, T.Shimoda, H.Hiruta, Gamma-rays from an incomplete fusion reaction induced by 95 MeV ^{14}N, - Phys. Lett. 68B (1977) 51 - 54.

97. R.R.Zolnowski, H.Yamada, S.E.Cala, A.C.Kohler, T.T.Sugihara, Evidence for "massive transfer" in heavy ion reactions on rare-earth targets, - Phys. Rev. Lett. 41 (1978) 92 - 95.

PARTIAL NEUTRON CROSS SECTIONS. EXPERIMENT AND ANALYSIS

Yu.P. POPOV
Joint Institute for Nuclear Research,
Dubna, Union of Soviet Socialist Republics

Abstract

The peculiarities of interaction of resonance neutrons with nuclei are discussed. The methods of high-intensity neutron spectrometry and the results of studying different decay channels of neutron resonances are reported briefly. Special emphasis is put on the latest data on the study of neutron reactions with charged particle emission and gamma-ray spectra of decay. The regularities of the compound nuclei decay are discussed.

I. INTRODUCTION

During the half a century, which passed since the discovery of a neutron by Chadwick in 1932, many basic experimental and theoretical investigations were performed. They led to the development of neutron physics as a highly important branch of nuclear physics and laid the scientific basis of modern nuclear power.

Since a neutron has no electric charge and, consequently, no Coulomb barrier opposing its penetration into a nucleus, it can be used widely for exciting essentially all nuclei in the β -stability valley, in particular, for inducing fission of heavy nuclei. The emission of new neutrons in the process of fission allowed us to realize the chain nuclear reaction and then acquire tremendous amounts of nuclear power. In order to fulfil this most complicated from the scientific and technological point of view task a lot of special physical experiments had been carried out. They gave necessary information about the mechanism of neutron-nucleus interaction and on the structure of high-excited states of nuclei being constituent parts of structural and fission materials employed in nuclear reactors. At present more nuclear data are still required.

The regularly published by the IAEA collections of requests WRENDA are the evidence for that. These requirements can be satisfied by direct measurements of certain physical parameters. But the present status of modern experimental engineering does not always make it possible. Therefore, some of them are calculated within the frame of modern theoretical models of a nucleus and nuclear reactions. However, each model allows us to make estimates within a limited accuracy, which does not always satisfy the needs of the industry. Thus, there arises the need for new experimental data used to develop the existing nuclear models.

The neutron spectrometry plays the most important role in providing organizations dealing with calculations and design of nuclear reactors with nuclear data. Below we shall discuss the latest advances in neutron spectroscopy and some regularities of neutron resonance decay.

2. NEUTRON RESONANCES AND COMPOUND STATES OF NUCLEI

In slow neutron capture specific highly excited states of nuclei (compound states) with a width of about 1 eV are formed near the neutron binding energy ($B_n \sim 7 \div 10$ MeV). The capture probability of a neutron with the energy corresponding to these compound states exceeds that in the neighbouring energy regions by several orders of magnitude. That is the neutron resonance. The compound states live rather long and decay following the exponential law with a half-life of about $10^{-14} - 10^{-16}$ s. By detecting the emission of various particles which are the reaction products and their spectra, it is possible to draw conclusions regarding the partial probabilities for the decay of the compound states through various channels. The diagram in Fig. 1 shows the various channels for the decay of neutron resonances and the relationship between the cross sections and the positions of the excited nuclear states. In this example the capture of a s-wave neutron by the target nucleus A (with the spin and parity $I^{\pi} = 7/2^-$) gives rise to the excitation in the A + 1 nucleus of compound states with spins $J^{\pi} = 3^-, 4^-$ above B_n. These levels may decay through the emission of a neutron (the inverse process), through that of γ-rays, and of α-particles. For each process x there is a corresponding cross section σ_x.

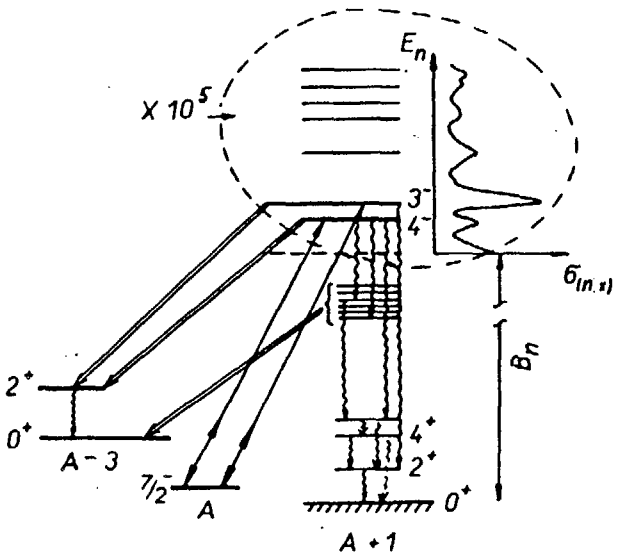

Fig. 1. Production and decay of compound states.

The effective neutron-nucleus cross section σ_t is a measure of the interaction probability, given by

$$dN = N\sigma_t \cdot dn \qquad (1)$$

where dN is the number of neutrons which have interacted in a layer dn (nuclei per square centimeter) of matter, and N is the number of neutrons incident on this layer. Long life time of compound states makes it possible to treat the nuclear reaction as a process which occurs in two independent steps (the Bohr's hypothesis) when the mechanism of decay does not depend on the manner in which the state was formed, i.e. the reaction cross section can be written as

$$\sigma_x = \sigma_c \cdot W_x \qquad (2)$$

where σ_c is the cross section for the production of the compound nucleus, and $W_x = \Gamma_x/\Gamma_t$ is the relative probability of decay through emission of the particle x.

The total neutron cross section σ_t is the sum

$$\sigma_t = \sigma_s + \sigma_\gamma + \sigma_f + \sigma_\alpha + \sigma_p + \ldots \qquad (3)$$

of the partial cross sections corresponding to scattering, capture, fission and reactions involving the emission of α-particles, protons, etc.

For most nuclei in the case of slow neutrons the cross sections σ_s and σ_γ are predominant. The cross sections σ_p are characteristic of light nuclei, and the fission cross sections σ_f so important for nuclear energetics are characteristic of heavy nuclei (actinides). The cross sections σ_α are usually small but at present are known for many nuclei (see below). They are important from the point of view of helium storage in the construction materials of the reactors, which reduces their reliability.

To describe the energy dependence of neutron cross sections in the vicinity of the resonance the Breit-Wigner formula is usually used

$$\sigma_x(E) = \pi \lambda_0^2 g_J \frac{\Gamma_n(E_0)\cdot\Gamma_x}{(E - E_0)^2 + \Gamma^2/4} \qquad (4)$$

Here E_0 is the resonance energy, λ_0 is the neutron wavelength divided by 2π at $E = E_0$, $\Gamma_n(E_0)$ is the neutron width at $E = E_0$, Γ_x is the width of the corresponding reaction, $\Gamma = \sum_x \Gamma_x$ is the total width of the resonance, g_J is the statistical factor dependent on spins of the initial (I) and final (J) states.

The shape of the resonance is noticeably affected by the type of chemical combination and by the thermal motion of atoms in a sample. The shape of the resonance in the reaction cross section is not symmetric because of the factor $\lambda \sim 1/v$ which gives rise to the "$1/v$ law" in the limit $E \to 0$, which is well known for the absorption of slow neutrons.

The theory as it exists today cannot predict the parameters Γ_n, Γ_x, E_0 for individual resonances. These parameters are determined experimentally, and their values have been compiled in an atlas of neutron cross sections by the Brookhaven National Laboratory /1/. At the same time, it is the complex, many-particle nature of compound states which leads to the definite behaviour established by the statistical theory. The behaviour described by this theory deals with the average values of the decay widths for decay by the various channels, the distribution of the partial and total widths, and the distributions of intervals between resonances.

However, before discussing the achievements in the study of partial neutron cross sections and comparing them with those predicted by modern theoretical models, let us review in short the problems of the high-intensity neutron spectrometry. We are considering the high-intensity spectrometry because it allows us to study a greater number of the resonance parameters with the help of the rare reaction measurements, as well as to measure the spectra of secondary particles emitted after the neutron capture. It is very important for the correct description of such complex states as the compound ones of heavy nuclei.

3. GENERAL QUESTIONS OF HIGH-INTENSITY NEUTRON SPECTROMETRY /2/

Modern neutron spectrometry is capable of resolving individual states of nuclei which are separated by a fraction of an electron-volt at a total excitation energy of the order of 7 - 10 MeV. This unique in nuclear physics resolution is achieved by comparatively simple means. The fact is that the excitation energy of a compound nucleus $E^* = B_n + E_n$, where $B_n \sim 10^7$ eV is the constant part, $E_n \leq 10^4$ is the kinetic energy of the captured neutron, while the spectrometry (usually, the time-of-flight one) is realized at the energies of the order of this small addition.

This relationship between the components of the excitation energy ($E_n \ll B_n$) which is possible only in the case of neutron capture, allows us to study in its pure form a distinct class of nuclear reactions which go through a compound-nucleus stage and to study the nature of these complex quasistationary states.

Over the past three decades experimental neutron spectrometry has been improving continuously. It has passed a long way from a simple chopper selectors in the first nuclear reactors to the modern spectrometers installed at powerful pulsed accelerators of electrons, protons and deutrons, pulsed reactors, high-flux steady-state reactors, etc.

Neutron spectrometry is developing along the directions of increasing resolution and intensity. The variety of research programs is forcing improvements in both these major characteristics of neutron spectrometers. However, the experimental general-purpose spectrometers usually cannot claim record-high characteristics, therefore, many interesting and pioneering studies are being carried out

at specialized apparatus. It should also be emphasized that a successful experiment requires matching the basic characteristics of a neutron spectrometer with those of particle detectors, those of the system which detects the event and those of the computer facilities. Otherwise, the record-high characteristics may turn out to be useless.

The modern status of the neutron source problem is considered in detail in the recently published under the editorship of Dr. S. Cirjacks review "Neutron Sources for Basic Physics and Applications" /3/.

There are several ways to raise the intensity of neutron spectrometers.

(1) To increase directly the neutron flux density without changing other characteristics of the spectrometer (raising the current or energy of the accelerated particles or using targets of fissionable materials).

(2) To alter the characteristics of the spectrometer. In the time-of-flight method this would mean increasing the length of the neutron pulse or moving closer to the neutron source. In the latter case it must be kept in mind that a limitation is imposed by the dimensions of the accelerator target (or of the moderator) and by those of the sample (or of the detector).

(3) To use (in the time-of-flight method) a neutron booster-breeder. This booster can be either a steady-state device (like that in Harwell, England) or a pulsed one (like that used with the IBR (FNR)-30 fast neutron reactor in Dubna). At neutron pulse lengths of a few microseconds this approach can raise the neutron flux density by one or two orders of magnitude.

(4) To employ slowdown-time neutron spectrometry.

The Time-of-Flight Method

Neutron sources generally provide neutrons with a continuous energy distribution, and special methods are required to single out neutrons of a particular energy or to measure their energy. The most universal of these methods is the time-of-flight method. Pulsed operation of a neutron source is convenient for this method. We denote by L the distance (in meters) traversed by a neutron moving from the source to the detector, by t (in microseconds), the time of flight, and by Δt, the uncertainty of this time which results from the finite length of a neutron pulse and other factors. Then, from the nonrelativistic equations $E = \frac{mv^2}{2}$ and $t = \frac{L}{v}$ we can derive the basic equations of the method:

$$E_n = 5228 \left(\frac{L}{t}\right)^2; \quad \frac{\Delta E_n}{E_n} = 0.028 E_n^{1/2} \frac{\Delta t}{L} \qquad (5)$$

The total cross section is usually determined as a function of the energy $\sigma_t (E_n)$ by measuring the transmission of neutrons by the sample for various times of flight. The transmission T and the cross section σ_t are related by the simple equation

$$T = \exp(-n\sigma_t) \qquad (6)$$

The IBR-30 fast-neutron reactor has been in operation for many years by now at the Laboratory of Neutron Physics of the Joint Institute for Nuclear Research. The average power of this reactor is 25 kW in all, and at five pulses per second it generates a pulsed power of 60 MW matching that of the best steady-state research reactors. For experiments with resonance neutrons the reactor is operated in a booster mode in combination with an electron injector-accelerator. The accelerator target is placed in the active zone of the reactor, and the neutron pulses produced at the target as a result of a photonuclear reaction are multiplied by the subcritical reactor by a factor of 200. In this mode the source has an average intensity of 3×10^{14} neutron/s at a neutron pulse length of 4.5 μs. By way of comparison, note that the intensity of the operating electron accelerators usually does not exceed 10^{14} neutron/s. A pulsed reactor with an injector is, therefore, one of the best choices for high-intensity neutron spectrometry at a modest resolution.

Recently, in Dubna the experiments were started at a new more powerful pulsed reactor IBR-2 with a peak power of about 2×10^9 W /5/.

The Slowdown-Time Neutron Spectrometry

This is an interesting method due to its physical nature, as well as due to the opportunities it presents and the simplicity of its realization. The concept of the method arose in discussions of a particular feature of the moderation process which results from

the elastic scattering of neutrons in a heavy medium: the bunching of the neutron velocities in a comparatively narrow interval around an average value /6/. A crude explanation is that since the range of the neutron between collisions depends only slightly on the neutron velocity, the faster neutrons collide more frequently with the moderator and lose energy more rapidly.

If a brief pulse of fast neutrons at a velocity v_0 is injected into a large volume of a moderator consisting of nuclei with $A \gg 1$, the neutrons will collide elastically with the moderator nuclei, losing an average fraction of $\sim 2/A$ of their energy in each collision and will, accordingly, accumulate in a comparatively narrow velocity interval. As the moderation time increases, this interval shifts downward along the velocity scale. By operating the neutron detector (or devices which detect particles accompanying the capture of a neutron by a nucleus of the test sample) for a narrow time interval Δt shifted by a time t with respect to the time of the neutron injection, it becomes possible to select approximately monoenergetic neutrons. The average velocity of these neutrons is related to the moderation time t by

$$t = A \lambda (1/v - 1/v_0) \qquad (7)$$

where λ is the neutron mean free path with respect to scattering, and v_0 is the initial velocity of the neutrons. The product $A\lambda$, which is $\sim$ 6 m for lead, is an effective "flight distance", by analogy with the time-of-flight method.

This idea was realized in a slowdown-time spectrometer by a group led by Shapiro at the Lebedev Physics Institute in Moscow /7/. The neutron source with an average intensity of about 10^9 n/s was a tritium target exposed to a pulsed beam of 300-keV deuterons. The target was placed at the centre of a lead prism with dimensions 2x2x2.3 m, in which the neutrons were moderated (Fig. 2). The detector was inserted into a narrow channel in the prism. This method admitted disadvantage is its low resolution ($\sim$ 30%), but it has an undisputed advantage of high intensity. This method was widely used to measure capture and fission cross sections over the energy range from 1 eV to 30 keV. Recently this method was revived at the Ronseller Polytechnic Institute /8/, where a neutron source (a target of an electron accelerator) with an intensity 1000 times higher was inserted into a lead cube. In this case the sensitivity to the measured cross sections for subbarrier fission and the (n, α) and (n, p) reactions amounted to a fraction of a microbarn.

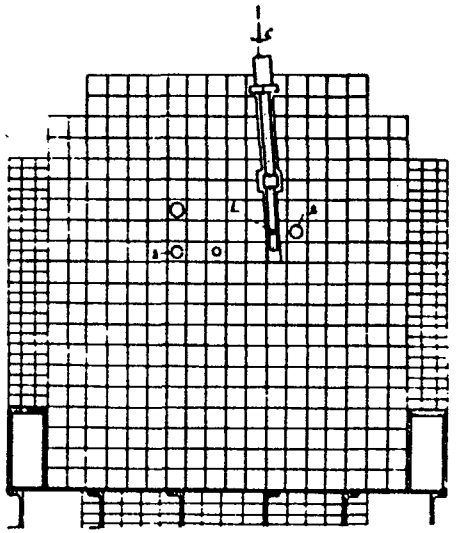

Fig. 2. A layout of slowdown-time spectrometer of neutrons: 1 is a tritium target; 2 and 3 are channels for samples and detectors.

Progress in High-Efficiency Detection Apparatus

The increase in the intensity of the neutron sources have been accompanied by refinements in the apparatus used to detect the products of neutron-nuclei reactions. Ref. /9/ presents a comprehensive review of modern methods for detecting neutrons by means of scintillators. Semiconductor detectors and spectrometers are being used more widely /10/. They are particularly promising in the spectrometry of γ-rays from the radiative capture of neutrons. The good energy resolution and high efficiency of γ-detection of germanium semiconductor spectrometers, combined with the time-of-flight procedure, have finally made it possible to study the properties of the partial γ-transitions for a broad range of individual neut-

ron resonances, as well as to investigate some interesting aspects of the neutron radiative capture mechanism /11/.

Semiconductor charged-particle spectrometers are widely used in measurements with thermal neutrons, which are available in extremely high flux desities in advenced research reactors. In studies of the charged particles produced in reactions with resonance neutrons (where the flux densities are orders of magnitude lower than those of thermal neutrons) semiconductor detectors and spectrometers with a sensitive area no greater than 10 cm^2 run into rough competition with modern ionization and proportional chambers. Although ionization spectrometers have a resolution which is poorer by a factor of several units, their sensitive area (or their efficiency) is larger by two or three orders of magnitude. Studies of the α -spectra for individual resonances and studies of the average partial cross sections in the (n, α) and (n, $\gamma\alpha$) reactions have become possible only by combining special ionization chambers having a large sensitive area with a high-intensity neutron spectrometer on the basis of a linear electron accelerator with a pulsed booster-breeder in the form of an IBR fast neutron pulsed reactor (see below).

Figure 3 is a schematic diagram of such an ionization chamber /12/, with a target area of $\sim 3\times10^3$ cm^2. The collimation system of the neutron beam and the shape of the target (sample) are chosen

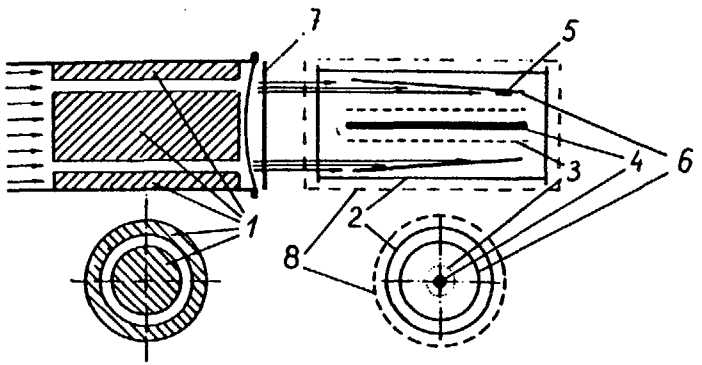

Fig. 3. A schematic diagram of the high-efficiency ionization chamber (2) and neutron collimator (1). 3 is a grid; 4, a collector; 5, a sample.

so as to minimize the bombardment of the sensitive volume of the ionization chamber with neutrons and γ -rays from the source, while the entire target is being exposed. This approach has made it possible to raise the resolution of the spectrometer by a factor of several units and to extend the working range over the time of flight in operation with an intense neutron source and comparatively short flight paths.

At present the study of the regularities of γ -cascades formed as a result of capture of thermal and resonance neutrons arouses much interest. An apparatus for γ -multiplicity spectrometry developed at the Kurchatov Institute of Atomic Energy in Moscow opens up new possibilities in this field. This is a 4π high-efficiency γ -detector consisting of a great number of NaI (Tl) crystals and the corresponding electronic system for recording two-dimentional information (the time of flight end average multiplicity of γ -quanta per cascade of a given resonance) /13/.

New information about the regularities of the two-quanta decay of compound nuclei (the (n, 2γ) reaction) can be obtained now with the help of the spectrometer of summary amplitudes of coincident γ -quanta emitted in one cascade, which has recently been put into operation in the Laboratory of Neutron Physics in Dubna. The spectrometer consists of two Ge (Li) detectors with a volume of ~ 50 cm^3 and equipped with electronics on the basis of a mini-computer. With the help of the latter the times of flight, the amplitudes of pulses in each detector and the code of their coincidence are recorded on magnetic tape /14/.

4. MEASUREMENT AND ANALYSIS OF NEUTRON REACTION CROSS SECTIONS

Having considered some peculiarities of modern studies of neutrons we shall direct our attention to the results of measurements of characteristics of neutron resonances obtained mainly with the help of the high-intensity methods developed by neutron spectroscopy of nuclei.

The neutron cross sections are mainly measured with the time-of-flight method. Figure 4 gives a schematic diagram of the apparatus for the measurement of (a) total cross sections, (b) partial cross sections: (n, γ), (n, p), (n, f), (n, α), etc., depending

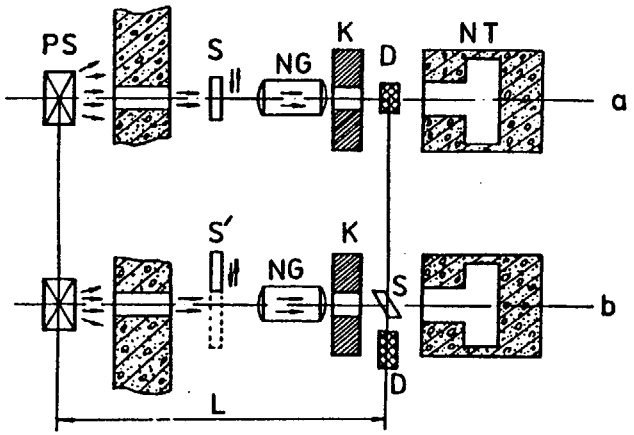

Fig. 4. A scheme of neutron capture cross section measurements by the time-of-flight method: (a) transmission cross sections; (b) reaction cross sections with compound-state decay product detection.

on the type of the detector D. Here PS is the pulsed neutron source; S ans S' are the investigated samples; NG is the neutron guide, usually evacuated; K is the collimator; D is the detector which detects either (a) the neutrons, or (b) the products of the reaction induced by neutrons; NT is the neutron trap. The use of the second sample S' makes it possible to study the self-absorption cross sections thus giving additional information about the neutron resonance parameters /15/.

The measurement of the number of detector counts vs the time of flight allows us to determine the positions of neutron resonances along the energy scale of absorbed neutrons (E_o in expression (4)). The relationship of various neutron capture product yields (with account for the efficiency of their detection, etc.) makes it possible to judge the relationship of the respective widths of the reaction. More detailed information on the characteristics of neutron resonances one may derive from the analysis of spectra of the reaction products for each neutron resonance. But this requires powerful neutron sources and high-efficiency spectrometers.

The main channels of the decay of neutron resonances of medium and heavy nuclei are the neutron emission (scattering through a compound nucleus) or γ-quanta emission, while for the transuranium elements it may also be the fission into two fragments of close masses. At the same time many nuclei may remove excitation by emitting protons, alpha-particles or even ^{8}Be nuclei. But the Coulomb barrier significantly prevents the charged particles from emission reducing the cross section by many orders of magnitude. As a consequence, additional experimental difficulties arise limiting the volume and quality of the information obtained. At the same time, the cross sections of these "rare" channels of decay are of much interest both for the nuclear physics and reactor engineering. For example, the (n, p) and (n, α) reactions are the source of hydrogen and helium nuclei storage in the construction materials of the reactors and thus should be accounted for while selecting those materials.

The time of the lecture does not allow me to consider all the types of reactions with neutrons. Therefore, I shall confine myself to the measurement of the cross sections of the rarest "nonclassical" reactions. These studies have been commenced only recently and, therefore, no information about them has entered the reviews /15 - 17/ (see also ref./1/) containing a detailed consideration of neutron scattering reactions, radiation capture and fission.

Rich experimental information acquired with the help of neutron spectroscopy has showed that the general regularities of neutron reactions are described correctly in the frame of the modern statistical theory. According to the theory, the width of various decay channels may be written in the form:

$$\Gamma_x = 2\gamma_x^2 P_x \qquad (8)$$

where γ_x^2 is the independent of energy reduced width, P_x is the penetrability factor determined by the probability of transmission through the Coulomb and centrifugal barriers of the nucleus in the channel x. The widths Γ_x experience strong fluctuations from resonance to resonance according to the Porter-Thomas distribution, i.e. the χ^2-distribution with one degree of freedom ($\nu = 1$).

The total width being the sum of independently fluctuating partial widths experiences much weaker fluctuations. Therefore, in the decay of the compound nucleus through the channel x to various states of the final nucleus (f) the distribution of widths can be presented /18/ in the form of the χ^2-distribution with the effective number of the degrees of freedom

$$\nu_{eff} = \left(\sum_f P x_f\right)^2 \left(\sum_f P_{x_f}^2\right)^{-1} \qquad (9)$$

According to the statistical theory in the frame of the Blatt and Weisskopf /19/ approach the mean widths of various decay channels may be estimated using the following formula:

$$\langle \Gamma_x \rangle = \frac{D^{J\pi}}{2\pi} \cdot \sum_x P_x (E, l) \qquad (10)$$

where $D^{J\pi}$ is the average spacing between the resonances with spin J and parity π, which amounts to several eV for heavy nuclei; l is either the emitted particle orbital momentum or the γ-quantum multipolarity. This simple expression for the estimation of the order of magnitude of the mean width was proposed 30 years ago. However, a comparison with the most recent experimental data shows that the mean widths can be described considerably more accurately by expression (10) and the like. But it is important to correctly calculate the penetrability of the emitted particle taking into account the effects absent from the statistical model, for example, to account for the semitransparency of the nucleus for neutrons with the help of the optical model.

In the experiment the average widths are determined from the results of measurements of widths of individual resonances. However, the accuracy of such an averaging is not always high due to large random fluctuations. Since the number of reliably studied resonances for each isotope is limited by several dozens, the average width fluctuating according to the Porter-Thomas distribution is determined with an uncertainty of 20%. More exact data on average widths can be obtained from the analysis of mean cross sections averaged over hundred or thousand resonances.

A concept which proved extremely fruitful in neutron physics is the strength function, i.e. the quantity changing little from nucleus to nucleus (from the point of view of the statistical theory), which is defined by

$$S_x = \frac{\langle \Gamma_x \rangle}{D \cdot P_x} \qquad (11)$$

But in the case of neutron widths (here the quantity $S_n^o = \left\langle \frac{\Gamma_n}{\sqrt{E}} \right\rangle^o \cdot \frac{1}{D}$, which differs by a constant factor from that given by exp.(11) is used more often) the experimental data /1/ revealed the giant "dimention resonances" in the dependence of the strength function on the atomic weight of the nucleus (Fig. 5). This effect initiated the development of the optical model of the nucleus.

Now, let us transfer to the results of measurements of the comparatively rare neutron reactions.

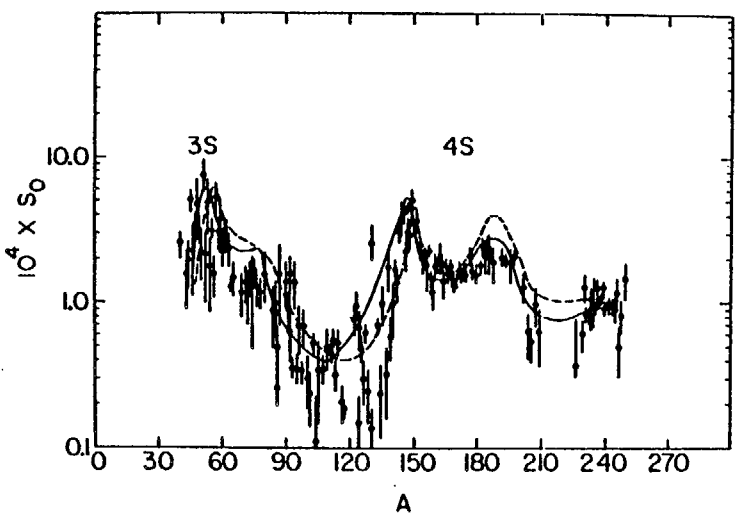

Fig. 5. The neutron strength function as a function of the mass number.

The (n, α) Reaction

Such aspects of the (n, α) reaction as small cross sections, large background from the competing (n, γ) reaction, and short range of α-particles in the target material impose specific requirements on the method for studying this reaction. It is important that the neutron spectrometer has a high intensity and that the bombardment target has a large area. These considerations are particu-

larly important in experiments with resonance neutrons, whose flux densities are several orders of magnitude lower than those of thermal neutrons in modern research reactors. As a result, while semiconductor detectors with an area of ~ 1 cm^2 are commonly used to measure the α-spectra in the (n, α) reaction with thermal neutrons, for measurements with resonance neutrons it has proved extremely useful to combine a "slow" (microsecond range) but high-intensity time-of-flight neutron spectrometer, used with a fast-neutron pulsed reactor, with the highly efficient α-detectors and spectrometers (see, for example, Fig. 3).

The first step was to search for the (n, α) reaction among the resonances of various nuclei. The time-of-flight method and high-efficiency detectors were used to determine the α-yield and total α-widths of the neutron resonances /20/. The second step was to carry out two-dimensional measurements for the nuclei and resonances having the maximum α-yield, i.e. the time of flight and the spectrum of the detected α-particles were determined for each time channel. Thus, the partial α-widths were determined for each resonance /21/.

In addition to the researches on α-decay of individual neutron resonances, recently advances have been made in the measurements of the characteristics of the (n, α) reaction, averaged over many resonances, with the use of "quasimonoenergetic" neutron beams passed through nuclear filters /22/, as well as of the time-of-flight method. These methods are employed when the energy resolution of the neutron spectrometer is inadequate to resolve the individual resonances /23, 12/.

Now, we shall proceed to the analysis of the experimental data available.

Average α-widths. Fig. 6 shows ratios of the experimentally-obtained average total α-widths to those calculated from eq. (10) with the penetrability factor taken from the Kadmensky-Furman cluster model /24/. The errors result primarily from a limited number of resonances over which the experimental α-widths are averaged. We can conclude from Fig. 6 that the statistical theory satisfactorily reproduces the average total α-widths for a broad range of spherical nuclei with $58 < A < 150$. Since the theoretical value of

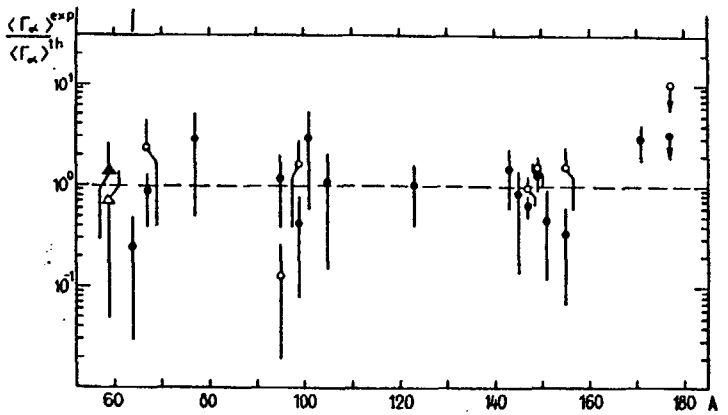

Fig. 6. A ratio of the experimental and theoretical values of the average α-widths, plotted against the mass number of nuclei.

$\langle\Gamma_\alpha\rangle^{cc}$ was calculated from (10), the ratio $\langle\Gamma_\alpha\rangle^{exp}/\langle\Gamma_\alpha\rangle^{cc}$ in Fig. 6 is, within a factor, the strength function for α-particles (see expression (11)). The fact that the strength function S_α remains constant for spherical nuclei, as we see from this figure, may be interpreted as an evidence of strong absorption of α-particles in the nucleus (in other words, the correct model would be that of a "black" nucleus, rather than that of a semitransparent one, as in the case of neutrons). If this is the case, then it follows that the α-cluster states are highly fragmented (distributed) among the levels of a compound nucleus at nuclear excitation energies of ~ 10 MeV.

Distribution of α-widths. Fig. 7 shows the integral distribution of partial α-widths for transitions to the ground state in the ^{123}Te $(n, \alpha)^{120}$Sn reaction. The experimental errors were accounted for in the determination of $\Gamma_{\alpha 0}$ by taking values of these errors from a Gaussian distribution with a half-width equal to the measurement error. The experimental curve (the solid one) turns out to agree well with the Porter-Thomas distribution (the dashed curve). A similar agreement can be demonstrated for other nuclei.

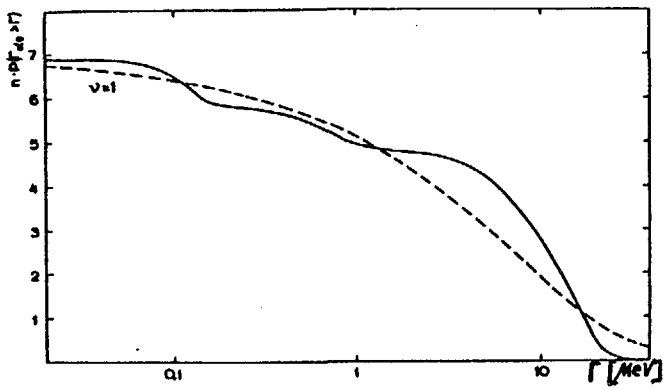

Fig. 7. Integrated distributions of the partial α -widths for the ^{123}Te (n, α) reaction. The dashed curve is for theoretical data, the solid one, for experimental data.

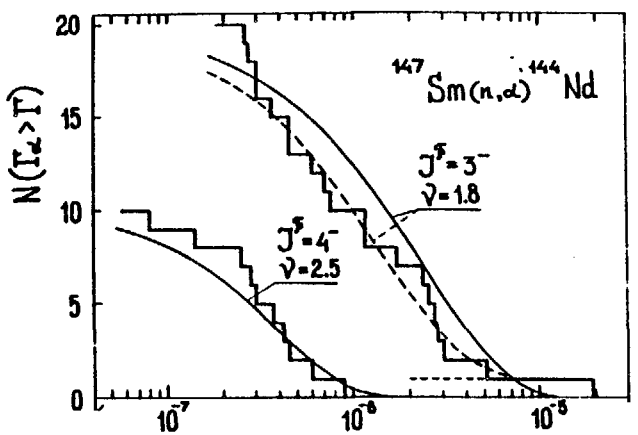

Fig. 8. Distribution of the total α -widths.

We can also study the distributions of the total α -widths by comparing them with a χ^2-distribution with the value of ν_{eff} calculated from (9). Fig. 8 taken from the paper by Balabanov et al. /25/ shows that the experimental distributions of the total α -widths (the hystograms) agree well with the theoretical ones (the solid curves) for resonances of both spins in the case of the ^{148}Sm compound nucleus. The agreement is particularly good if we discard the anomalous resonance at E_0 = 184 eV (the dashed curve).

Measurements with thermal neutrons. Emsallem /26/ has recently reported a detailed analysis of measurements of the (n, α) reaction with thermal neutrons. Comparison of the thermal cross sections with the results of calculating the contribution of the known resonances to the thermal region showed that the calculations and measured results for most nuclei were either in agreement or differed in a way which could be ascribed to bound states of "negative" resonances with plausible α - and γ-widths. In three cases there are discrepancies which require further investigation.

A dramatic situation has developed in a study of the (n, α) reaction in the actinide region. The thermal cross section for the ^{238}U (n, α) reaction found by a group of physicists (Asghar et al. /27/) in Grenoble yields a value for Γ_α which is six orders of magnitude larger than that calculated from the statistical theory although the corresponding calculations in the region $59 \leq A \leq 177$ agree well with experiment (Fig. 6).

Wagemans et al. /28/ recently undertook a new attempt to search for the (n, α) reaction in the various isotopes of uranium. They obtained negative results for the ^{233}U and ^{235}U targets. For ^{238}U (n, α) they reported a cross section of 1.5 $\pm$0.5 μbn with thermal neutrons. This cross section agrees well with that reported by Asghar et al. /27/ but the energies of the α -particles attributed to this reaction by the two groups differ by 0.5 MeV, which goes far beyond the experimental errors. Some new experiments on this problem are required. If such a high value of Γ_α was confirmed, it would substantially change our understanding of the α -decay of heavy compound nuclei.

The (n, p) Reaction

The emission of protons in the reaction with slow neutrons is a rather rare event. This is due to closeness of the neutron binding energy and the proton binding one in stable nuclei, and the energy of the reaction Q (n, p) $\lesssim$ 1 MeV, i.e. the proton decay of neutron resonances, is essentially suppressed by the Coulomb barrier. Therefore, rather poor information about the proton channel of the compound nuclei decay is available.

However, this information is of great interest, even if one simply proceeds on the analogy with the neutron channel of decay. Though, actually, the proton channel is much reacher in information than the neutron one, since one may detect the transitions not only to the ground state, but also to the excited ones with various orbital momenta l. This information is needed by the reactor engineering in order to estimate the storage of hydrogen in the reactor materials and to take into account the distortions of the crystal lattice by the emitted protons.

In principle, to estimate the proton widths, one might use the hypothesis proposed by Bethe in 1937 that the mean reduced widths of various channels of decay with particle emission should be about the same /29/, i.e. the compound nucleus was assumed to be insensitive to the kind of particle emitted, if the nuclear barrier transparency is accounted for. Unfortunately, the lack of the corresponding experimental data does not allow us to verify that. For example, only five resonances /30/ are measured for the "most investigated" ^{35}Cl (n, p) reaction. This gives $\langle \gamma_n^2 \rangle / \langle \gamma_p^2 \rangle \gtrsim 1.5$. Wider studies are needed to make definite conclusions. The similar analysis of data on the (n, α) reaction has shown /31/ that $\langle \gamma_n^2 \rangle / \langle \gamma_\alpha^2 \rangle = 4.5 \pm 2.5$, even with the correction made for the optical effects in the neutron channel for a dozen and a half of spherical nuclei. Yet, it is not clear whether this is due the specific character of the α-channel or due to the rough approximations made by Bethe.

The most advantageous way of studying the proton decay of compound nuclei is the use of radioactive neutron-deficient target nuclei. It results in a considerable difference between the neutron and proton binding energies, so that Q (n, p) is several MeV for a wide number of target nuclei and, consequently, the penetrability amounts to $10^{-1} - 10^{-3}$, which is within the tolerance of the high-efficiency neutron apparatus. A group of scientists of the Laue-Langevin Institute (Grenoble) in collaboration with the ISOLDA group (CERN) /32/ and Nuclear Centre in Belgium /33/ is now carrying out the program of such studies with thermal neutrons.

The study of the (n, p) reaction with resonance neutrons for the radioactive target nuclei is initiated in the Laboratory of Neutron Physics of the Joint Institute for Nuclear Research. The first investigated reaction was ^{22}Na (n, p)^{22}Ne in the energy range up to 1 keV /34/. As a result, the first neutron resonance was observed in the ^{23}Na compound nucleus at a neutron energy of 150 eV. This resonance is responsible for a large value of the thermal cross section σ_{th} (n, p) = $3 \cdot 10^4$ bn (see Fig. 9).

The (n, p) reaction may appear a convenient tool for the study of and the search for the neutron resonances in the radioactive (neutron-deficient) nuclei, since the detection of protons reduces the background conditions due to the gamma- and beta-radiation of the target.

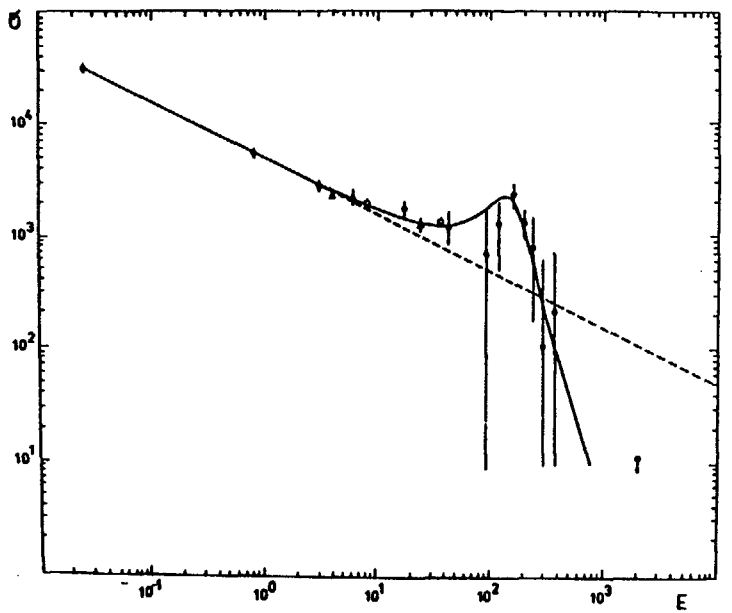

Fig. 9. The ^{22}Na (n, p)^{22}Ne reaction cross section. The solid curve is a fitting of the cross section according to the Breit-Wigner formula.

The (n, γ) Reaction

This reaction is the best studied channel of the decay of neutron resonances, which gave rich information about the structure of the excited nuclear states.

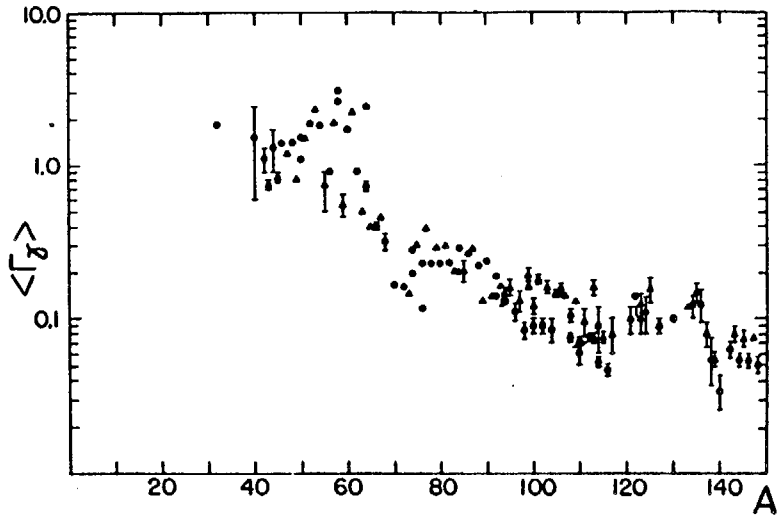

Fig.10. Total radiative widths as a function of the mass number.

Total γ-widths and capture cross sections. The γ-decay of the compound nucleus goes through a large number (about a hundred) intermediate states (see Fig. 1). Therefore, the total radiation width Γ_γ^{tot} is well averaged ($\nu_{eff} \sim 100$) and fluctuates little from resonance to resonance /1/ and changes smoothly from nucleus to nucleus (Fig. 10).

It makes it easier to estimate and describe theoretically the cross sections of the (n, γ) reaction. The neutron radiative capture cross sections averaged over many resonances in the range of dozens and hundreds of keV are of undoubtful interest for the nuclear energetics, in particular, for the design of fast neutron reactors, as well as for the check of the hypothesis of nucleosynthesis and determination of the time of life of the Universe /35/. Besides, the analysis of the dependences of averaged cross sections on the neutron energy allows us to find the average parameters of the interaction of neutrons with nuclei, i.e. the neutron strength functions for the s-, p- and d-neutrons (the capture of neutrons with orbital momenta $l = 0, 1, 2$) and total radiative strength functions /36/. Ref. /37/ gives a detailed systematics of averaged cross sections using, as an example, the radiative capture of the 30-keV neutrons. The dependences of the cross section vs the number of neutrons in the target nucleus (Fig. 11), the neutron binding energy and parameters of the level density are analyzed. The possibility to predict the cross sections for new, for example, radioactive nuclei is also considered. The curve in Fig. 11 illustrates clearly the influence on the averaged cross sections of the even-odd effect of the number of neutrons and protons, as well as that of the magic numbers of neutron shells (the influence of the proton ones is weaker).

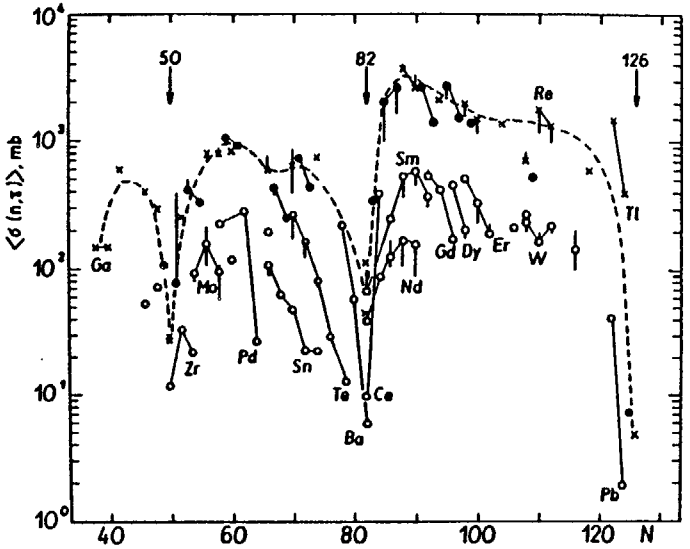

Fig.11. Averaged radiative neutron capture cross sections at 30 keV (in mbn) as a function of the neutron number of the target nucleus N. The circles stand for even-even isotopes; the dots, for even-odd ones; the triangles, for odd-even ones. The solid curves connect the isotopes of one element. The dashed curve is fitted through the circles and triangles.

Partial γ-widths. The partial radiative widths of neutron resonances in medium and heavy nuclei are well described in the first approximation by the statistical theory. They fluctuate according

to the Porter-Thomas distribution and their strength functions

$$S_\gamma = \left\langle \frac{\Gamma_{\gamma i}}{E_{\gamma i}^{2l_\gamma+1}} \right\rangle_i \cdot \frac{1}{D} \qquad (12)$$

are independent of the nature of final states. Here $E_{\gamma i}$ is the energy of γ-transition into the i-th state, D is the average spacing between neutron resonances, l_γ is the multipolarity of the γ-transition. In the case of hard γ-transitions ($E_\gamma \lesssim B_n$) from the compound state into a comparatively simple one (the CS transitions) the E1 multipolarity transitions prevail

$$S_\gamma^{CS}(E1) \simeq 7\, S_\gamma^{CS}(M1)$$

For the initial soft transitions in the γ-decay of neutron resonances into complicate highly excited states (the CC' transitions) the part played by the M1 transitions increases considerably

$$S_\gamma^{CC'}(E1) \simeq S_\gamma^{CC'}(M1)$$

This result was recently obtained in Dubna /38/ in the experiment on the study of secondary α-particle spectra from the ^{143}Nd (n, $\gamma\alpha$)^{140}Ce reaction (see Fig. 1). This exotic to a certain extent method, which was chosen because the analysis of spectra of secondary α-particles, allows us to reproduce unambiguously the spectrum of primary γ-transitions of the CC'-type excluding totally the background from γ-quanta of different nature (see, for details, ref. /39/).

The energy dependence S_γ (E1) was traced /40/ for the ^{144}Nd compound nucleus in the wide range of energies $0.2 \leq E_\gamma \leq 20$ MeV, which included the giant dipole resonance (GDR). In Fig. 12 the experimental points are obtained by analyzing cross sections of the following reactions: ^{144}Nd (γ, n) at E_γ = 8 - 20 MeV, ^{143}Nd ($\bar{n}$, γ) with quasimonochromatic filtered neutrons at E_γ = 5 - 7 MeV and ^{143}Nd (n, $\gamma\alpha$) at E_γ = 0.2 - 1.6 MeV. The Lorenz and Breit-Wigner theoretical dependences describing well only the maximum of the GDR are denoted by 1 and 2, respectively. A more accurate account for the polarization operator properties, as well as the dependence of the GDR width vs temperature of the final state at $E_\gamma < B_n$ allowed the authors of ref. /41/ to derive a different dependence S_γ (E1) on E_γ fitting the experimental data (curve 3) better. The

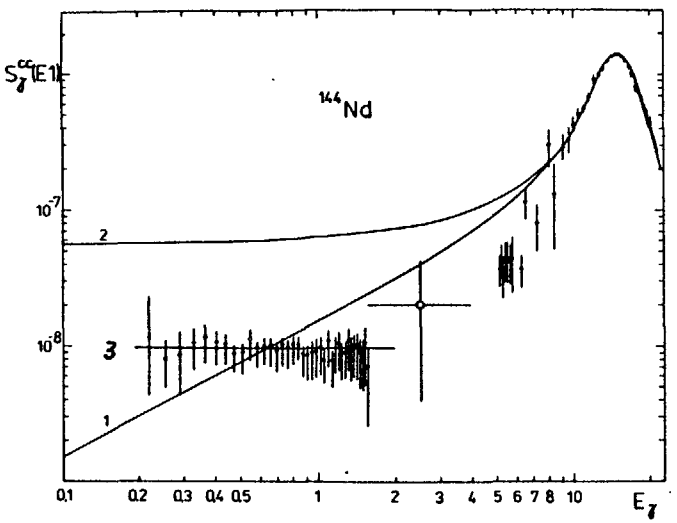

Fig.12. Experimental data on the radiative strength function for the multipolarity E1 for ^{144}Nd and attempts at their theoretical description: 1 is the Lorenz curve; 2, the Breit-Wigner one; 3, the Kadmensky-Furman one.

curve 3, being normalized for the sum rule, i.e. over the total area of the GDR, correctly describes not only the constancy of $S_\gamma^{CC'}$ (E1) but also its absolute value.

In the case of the M1 γ-transitions the new data on the strength function for the CC' γ-transitions in the ^{144}Nd nucleus have shown that

$$S_\gamma^{CC'}(M1) \simeq S_\gamma^{CS}(M1) \simeq 10^{-8}\ \text{MeV}^{-3}$$

if the experimental data on the CS transitions for the nuclei in the vicinity of A ~ 140 were averaged.

The above-described peculiarities of the behaviour of the radiative strength functions S_γ (E1) and S_γ (M1) are derived mainly from the experimental data obtained in the study of the ^{144}Nd nucleus, only. This is explained both by the difficulty in obtaining the experimental information of this kind and by a small number of suitable nuclei. Therefore, the predictability of the new regularities was studied in ref. /42/ by calculating the average total ra-

diative widths of neutron resonances for a wide range of spherical compound nuclei and comparing them with the experimental values often obtained within an accuracy of ~ 10%. It was assumed that $\Gamma_\gamma^{tot} = \Gamma_\gamma$ (E1) + Γ_γ (M1) . So far as the absolute values of Γ_γ^{tot} for the nonmagic nuclei are determined mainly by the CC' γ -transitions, a good agreement of the experimental and theoretical values (see Table 1) means that the proposed mechanism for the description of compound-compound γ -transitions yields both the qualitative and quantitative results. Besides, the high degree of agreement allows us to hope for the validity of the new description in the wide range of spherical nuclei.

Table 1.

Compound nucleus	^{78}Se	^{106}Pd	^{124}Te	^{143}Nd	^{144}Nd	^{145}Nd	^{146}Nd	^{196}Pt	^{200}Hg
$\langle\Gamma_\gamma^{exp}\rangle$, MeV	390 ±33	145 ±8	124 ±20	64 ±8	80 ±9	54 ±5	75 ±9	120 ±15	295 ±20
$\langle\Gamma_\gamma^{theor}\rangle$, MeV	428	140	129	55	81	45	68	115	310
$\frac{\langle\Gamma_\gamma^{theor\ (M1)}\rangle}{\langle\Gamma_\gamma^{theor}\rangle}$	0.47	0.54	0.46	0.49	0.44	0.44	0.40	0.41	0.27

Nonstatistical effects. The general features of the radiative capture of slow neutrons are adequately described by the statistical theory. But in a number of nuclear regions the statistical regularities are distorted by more simple mechanisms of neutron radiative capture which start to play a noticeable part. They are: the direct neutron capture (the capture by a hard sphere), the channel capture (the valent neutron model), the semidirect capture (the formation of a doorway states). More often these phenomena are observed for comparatively light (or near-magic) nuclei and in the vicinity of neutron strength functions maxima where the single-particle components of the wave functions play an important part. Fig. 13 shows the intervals of atomic weights where this or that mechanism of radiative capture prevails. The values of the n-parameter characterizing the energy dependence of the average partial radiative width for a given mechanism $\langle\Gamma_{\gamma i}\rangle \sim E_\gamma^n$, are also presented in the figure.

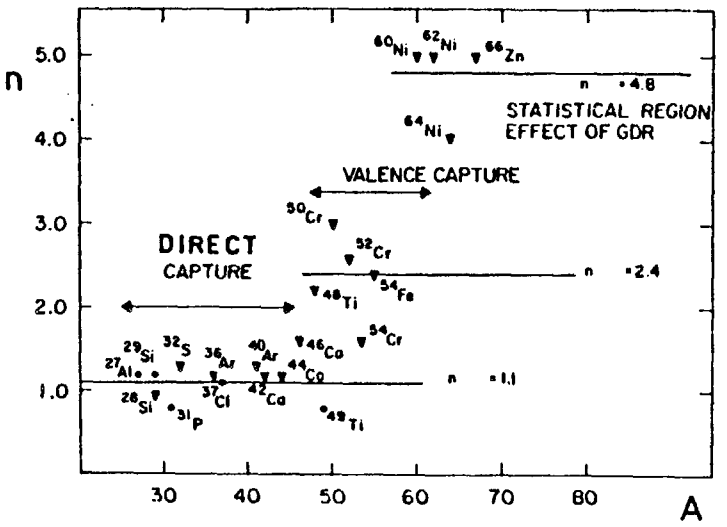

Fig.13. Nonstatistical effects in certain atomic weight regions. n is the power of the gamma-ray energy: $\langle\Gamma_{\gamma i}\rangle \sim E_\gamma^n$.

One may find the review of experimental and theoretical studies on nonstatistical effects in the (n, γ) reaction in ref. /43/ and in the Proceedings of the International Symposia on Neutron Capture Gamma-Ray Spectroscopy and Related Topics /11, 35/.

Gamma-cascades. In the region of medium and heavy nuclei the neutron radiative capture is accompanied by the emission of the γ - quanta cascades. The mean number of γ -quanta per cascade may amount to 6 - 8. While the probability of the emission of the first γ -quantum in the cascade is investigated with the help of Ge (Li) and magnetic gamma-spectrometers (hard γ -transitions at $0.5\ B_n \leq E_\gamma \leq B_n$) or by studying the (n, $\gamma\alpha$) reaction (soft γ -transitions, $E_\gamma \leq 1.5$ MeV), the probability of the emission of the subsequent γ -quanta in the cascade has not been practically studied in the experiment.

It is assumed that γ -cascades in heavy nuclei must be treated in the frame of the statistical theory as it is in the case of primary γ -transitions. However, one does not know to what extent that description agrees with reality. Indirect data indicate the possibi-

lity of a considerable deviation from theoretical predictions. For example, the analysis of fluctuations (from resonance to resonance) of the population of low-lying states formed as a result of γ-cascades made in the Laboratory of Neutron Physics has shown /44/ that in the heavy nuclei region (A > 150) the experimentally observed fluctuations are regularly higher than those predicted by the statistical theory. According to these results, it seems that the de-excitation of compound nuclei in this region does not go through all the intermediate states allowed by the statistical theory, but mostly through some special ones, for example, through those having a large component of the single-particle 4S-state /44/ The presence of enhanced two-quanta cascade going through the special states was confirmed by the first measurements of the ^{164}Dy (n, $^{2}\gamma$) reaction by the method of summary amplitude spectrometry of coincident pulses /14/ (see above). As an illustration, Fig. 14 presents the energy spectrum of intensity distribution of two-quanta γ-transitions (I) with the total energy of 5607 keV, i.e. of those populating the excited state at E_{ex} = 108.2 keV. The calculation in the frame

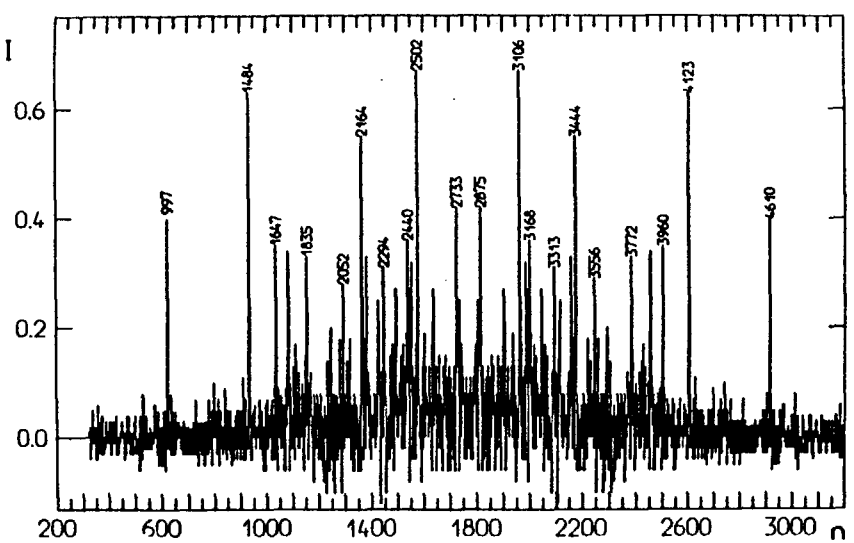

Fig.14. A spectrum of two-quanta γ-transition intensity distribution for ^{165}Dy populating the level E_{ex} = 108.2 keV.

of the statistical theory of the probability of such γ-transitions averaged over the interval of 500 keV gives a smooth curve with the maximum in the middle of the spectrum and $I^{max} \approx 0.05$. Thus, one may conclude that the statistical theory fails to describe even quantitavely the average parameters of the two-quanta γ-cascades of the decay of neutron resonances in heavy nuclei.

5. CONCLUSIONS

We have considered some aspects of the modern experimental neutron spectroscopy , methods for measuring and analysing various neutron cross sections and compared the experimental data with those calculated according to the theoretical models. This comparison indicates that the modern statistical theory can at first approximation describe and predict averaged neutron cross sections and mean parameters of neutron interaction with medium and heavy nuclei, in case these theoretical model parameters are up-dated and normalized to a large set of experimental data.

For example, the optical potential parameters of neutron interaction with nuclei are chosen on the basis of comparing the calculated neutron strength functions with the available experimental values (see Fig. 5). Theoretical penetrability coefficients of nuclear barrier for alpha-particles are up-dated by comparing the predicted and experimental values of average α-particle widths /31, 45/(see Fig. 6). The same holds true in the case of theoretical description of the radiative widths. The experimental up-dating of the energetic dependence of radiative strength functions for γ-transitions of the multipolarity E1 (as well as the new theoretical description of the GDR forms) and normalizing of S_{γ} (M1) to the experimental data make it possible to increase the precision of calculation of Γ_{γ}^{tot} several times.

At the same time it should be noted that in the region of rather light and near-magic nuclei, in addition to the statistical behaviour, one must take into account simpler mechanisms of neutron interaction with nuclei (see Fig. 13). The capabilities of the statistical models are also limited when describing γ-decay of neutron resonances in heavy nuclei (e.g., when one-particle 4S-state is located close to the neutron binding energy). It appears to take place

in the processes where not only initial compound states but also intermediate ones with a considerable admixture of simple components of the wave function play an essential part, as it has been indicated when analysing intensities of two-quanta gamma-cascades in ^{165}Dy.

We hope that these examples and notes might render help by analyzing possibilities of the neutron spectroscopy and statistical theory in describing average parameters of neutron resonances, partial neutron cross sections and obtaining evaluated nuclear data.

REFERENCES

1. Mughabghab S.F., Garber D.I. - Neutron Cross Sections. III ed., BNL-325, 1973. Mughabghab S.F. et al. - Neutron Cross Sections, v. I, part A, Academic, N.Y., 1981.
2. Pikel'ner L.B., Popov Yu.P., Sharapov E.I. Sov. Phys. Usp., 1982, v. 25, No. 5, p. 298.
3. Cierjacks S. (editor). - Neutron Sources for Basic Physics and Applications. Pergamon, Oxford, 1983.
4. Frank I.M.-Fiz. Elem. Chastits At. Yadra. 1972, v. 2, p. 807.
5. Frank I.M., Shabalin E.P. In: IV International School on Neutron Physics. JINR D3, 4-82-704, Dubna, 1982, p. 272.
6. Lazareva L.E., Feinberg E.L., Shapiro F.L.-Zh. Eksp. Teor. Fiz., v. 29, p. 381, 1955 (Sov. Phys. JETP 2, 351, 1956).
7. Shapiro F.L. In: Trudy FIAN SSSR, v. 24, Nauka, Moscow, 1964, p. 3. Popov Yu.P. ibid., p. 111. Bergman A.A. ibid., p. 169.
8. Slovacek R.E., Block R.C. - Nucl. Sci. Eng., 1977, v. 62, p. 455.
9. Harvey J.A., Hill N.W. - Nucl. Instr. & Meth., 1979, v. 162, p.507.
10. Vylov Ts., Osipenko B.P., Chumin V.G. - Fiz. Elem. Chastits At. Yadra, 1978, v. 9, p. 1350.
11. Chrien R.E., Kane W.R. (editors). - Neutron Capture Gamma-Ray Spectroscopy. Pergamon, 1979.
12. Andzheevsky Yu. et al. - Yad. Fiz., 1980, v. 32, p. 1496 (Sov. J. Nucl. Phys., 1980, v. 32, p. 774).
13. Muradyan G.V. In: Neitronnaya Fizika, TsNIIAtominform, Moscow, 1980, v. 2, p. 94.
14. Bogdzel A.A. et al. - Preprint JINR P15-82-706, Dubna, 1982.
15. Hughes D.J. - Neutron Cross Sections, Pergamon, N.Y., 1957.
16. Harvey J.A. (editor). - Experimental Neutron Resonance Spectroscopy, Academic, N.Y., 1970.
17. Michaudon A. (editor). - Nuclear Fission. Neutron Induced Fission Cross Sections. Pergamon, N.Y., 1981.
18. Popov Yu.P., Przytula M., Rumi R.F., Stempinski M.-Acta Phys. Polonica, 1973, B4, p. 275.
19. Blatt J., Weisskopf V. - Theoretical Nuclear Physics. J. Willey, N.Y., 1952.
20. Antonov et al. - Yad. Fiz., 1978, v. 27, p. 18 (Sov. J. Nucl. Phys., 1978, v. 27, p. 9).
21. Popov Yu.P.-Fiz. Elem. Chastits At. Yadra, 1972, v. 2, p. 925 (Sov. J. Part. Nucl., 1972, v. 2, p. 69).
22. Vertebny V.P. et al. - Report JINR P3-11392, Dubna, 1978.
23. Vo Kim Tkhan' et al. - Reports JINR P3-12756, Dubna, 1979.
24. Kadmensky S.G., Furman W.I. - Fiz. Elem. Chastits At. Yadra, 1975, v. 6, p. 469 (Sov. J. Part. Nucl., v. 6, p. 189, 1975).
25. Balabanov N.P. et al. - Nucl. Phys., 1976, v. A261, p. 35.
26. Emsallem A. - These University, Lyon, 1979.
27. Asghar M. et al. - Nucl. Phys., 1976, v. A259, p. 429.
28. Wagemans C. et al. - Nucl. Phys., 1981, v. A362, p. 1.
29. Bethe H.A. - Rev. Mod. Phys., 1937, v. 9, p. 69.
30. Popov Yu.P., Shapiro F.L. - Zh. Eksp. Teor. Fiz., 1961, v. 40, p. 1610.
31. Popov Yu.P., Furman W.I. In: III Intern. School on Neutron Physics. JINR, D3-11787, Dubna, p. 390.
32. Hagberg E. et al. III Intern. Congr. on Nucl. far from Stability. Report CERN/76-13, 1976.
33. Wagemans C. et al. In: Nucl. Data for Science and Technology. (ed. K.H.Bokhoff), Brussel, 1983, pp 148 - 149.
34. Gledenov Yu.M. et al. ibid., pp 150 - 151.
35. Audouze J. In: Neutron Capture Gamma-Ray Spectroscopy and Related Topics, 1981(ed. T.von Egidy et al.) Confer. Ser. No. 62, Bristol, 1982, p. 551.
36. Kononov V.N. In: III Int. Sch. on Neutr. Phys. JINR D3-11787, Dubna, 1978, 1978, p. 415.
37. Niedzwiedzuk K., Popov Yu.P. - Acta Phys. Polonica, 1982, B13, p.51.

38. Vo Kim Thanh, Vtiurin V.A., Popov Yu.P. In: Neutron Capture Gamma-Ray Spectroscopy and Related Topics, 1981 (ed. T. von Egidy et al.) Confer. Ser. No. 62, Bristol, 1982, p. 431.
39. Popov Yu.P. - Fiz. Elem. Chastits At. Yadra, 1982, v. 13, p.1165.
40. Vtiurin V.A., Popov Yu.P.-Report JINR P3-82-309, Dubna, 1982.
41. Kadmensky S.G.,Markushev V.P.,Furman W.I.-Yad.Fiz.,1983,v.37,p.277.
42. Kadmensky S.G. et al. In: Tezisy Dokl. na XXXIII Soveshchanii po Yadern. Spektrosk. i Strukt. Yad. Leningrad,Nauka, 1983, p. 404.
43. Mughabghab S.F. In: III Intern. Sch. on Neutron Physics. JINR D3-11787, Dubna, 1978, p. 328.
44. Popov Yu.P. et al. In: Neitr. Fiz. TsNIIAtominform,Moscow, 1980, v. 2, p. 209. Khitrov V.A. et al. In: Neutron Capture Gamma-Ray Spectroscopy (ed. R.Chrien, W.Kane) Pergamon, N.Y., 1978, p. 655.
45. Kadmensky S.G. et al. - Yad. Fiz., 1981, v. 33, p. 537.

MASS-SPECTROMETRIC STUDY OF THE NEUTRON FISSION OF HEAVY NUCLEI

A.I. MUMINOV
INP AS Uzbek SSR,
Tashkent, Union of Soviet Socialist Republics

Abstract

The mass separator of unmoderated nuclear fission products installed on the horizontal channel of the VVR-SM reactor at the Institute of Nuclear Physics of the UZSSR Academy of Sciences is described. Possibilities of the mass separator for investigation of fission fragment yields, beta-decay of the fission products, gamma-spectrometry of the fission fragments, and radiation damage phenomena are discussed.

Development of the world society is directly dependent on the sources of power supply. The current methods for electricity production have been based on our knowledge in the field of physics. But while application of the nuclear fusion reaction for energy production is a problem to be solved in the future, practical utilization of the energy from the fission of heavy nuclei began as far back as June 27, 1954 after the 5000 kW-nuclear power plant (NPP) had been put into operation in Obninsk.

Later NPPs with higher power outputs, such as Sibirskaya, Beloyarskaya, Novo-Voronezhskaya, Melekeskaya, were constructed in the USSR. The industrial complex for production of nuclear reactors for NPP was put into operation. In 1960 there were 20 NPPs in the world, with a power output of 1 mln kW, in 1975, 130 NPPs with a total power output of 80 mln kW, which was about 5% of all electricity production. In 1980 the NPP power output reached 200 mln kW. By the year 2000 NPPs will produce about half of all world electric power.

The experimental and theoretical basis of the reactor building is the reactor physics. This branch of science covers the processes of nuclear fission, diffusion, neutron moderation and absorption, and γ-radiation.

Though a great number of experimental and theoretical works on nuclear fission have been carried out there exists no unified theory of this nuclear process. Improvement of the technique of experimental investigations, particularly during the last years, made it possible to obtain important data which permit the relation between all stages of the fission process to be determined.

Distribution of nuclear fission fragments and products by nuclear masses, charges and kinetic energies are among the important nuclear data and are of great importance for development of the nuclear fission theory and modern nuclear energy industry.

In the nuclear physics the mass, energy and charge distributions of fission fragments make it possible to estimate the reliability of different models explaining the fission process.

In the nuclear technology the data on the mass yields of fission products (FP) are among the main constants used in designing and operation of the reactors. Using the data on FP yield in the thermal and resonance neutron one can estimate the contributions of individual nuclides to pollution of the environment and to poisoning of the fuel elements.

The analysis of the literature data on low-energy fission of uranium-235 and plutonium-239 shows that the features of the mass distributions of FP have not been described accurately enough, particularly in the resonance neutron fission, the structure features are not fully clarified. This is due to the fact that direct measurement of the experimental data on FP is a rather complicated work.

The recently developed method of deflection of unmoderated FP in the successive homogeneous electric and magnetic fields permits the mass number of FP to be unambiguously determined and detailed measurements of the mass, energy and charge distributions to be made, thus essentially widening the information necessary for studying the fission process.

The investigations of the fission process characteristics were carried out by the radiochemical, instrumental and mass-spectrometry methods. The best attained accuracy of measurement of the fission fragment masses, using these methods was 2-3 amu, the best accuracy of determination of the mass yields was about 5%. These accuracies are not sufficient for determination of relatively small factors affecting the fission process. Therefore, the works on improvement of the existing methods and development of new ones for studying the characteristics of the fission process become very actual.

In the BDR Evald et al. have built the mass separator with the successive electric and magnetic fields . This separator was provided with double focusing (by angles and velocities). They obtained a resolution $M/\Delta M=150$ instead of the rated one, $M/\Delta M=1800$, which limited the application of this instrument.

Armbruster et al. designed the parabolic mass-spectrometer "Loengrin" for separation of fission products, which was installed in the high-flux reactor in Grenoble. This apparatus permits a resolution $M/\Delta M=1200$ for fission products to be reached.

In the USA the mass-spectrometer "Hayawata" for fission products was designed and put into operation. Its mass resolution is 0.5 amu. This apparatus uses the combination of the time-of-flight method and deflections of fission products in the homogeneous magnetic field.

We designed and manufactured the mass-spectrometer of unmoderated nuclear fission products, consisting of the successive electric and magnetic fields. The apparatus has been set on the horizontal channel of the reactor at the Institute of Nuclear Physics (INP) of the UzSSR Academy of Sciences.

In all the works on measurements of the mass yields by the radiochemical, instrumental and mass-spectrometric methods the main attention was given to obtaining better measurement accuracy, search for new isotopes with low yields and interpretation of odd-even and shell effects. An extensive experimental material on these matters was systematized by Amiel and Feldstein. On the mass-separator "Loengrin" which was put into operation in 1974 mass, energy and charge distributions of products from fission of ^{235}U nuclei by thermal neutrons were measured. The measurements showed a good agreement with Amiel's systematics nearly for all mass numbers of fission products of the light group. The nuclear charges of primary fission products of the light group have been determined and odd-even proton (22%) and neutron (8%) effects been found. For the

first time the influence of the coupling effect on the fission product yields at low kinetic energies has been observed.

On the mass-separator "Hyawata" the yields of products from ^{235}U fission by thermal neutrons were measured with an error of about 1%. The fission product yield data obtained by the present are thought to be the most reliable.

One more direction of experimental activity was determined from the theoretical assumption made by Willer, according to which the relative probability of the asymmetric and symmetric fission depends on the spin state of the compound nucleus. The experiment confirmed such a difference for the cases of the low-energy fission of ^{233}U, ^{235}U and ^{239}Pu in spite of the difficulties associated with low intensity of the monochromatic sources of neutrons.

The radiochemical measurements of the relative ^{99}Mo and ^{115}Cd yields carried out by Riger et al. in ^{233}U fission by thermal and resonance neutrons showed that the asymmetric-symmetric fission ratio is higher for the resonance neutron fission case. In another work the similar measurements were made for ^{239}Pu and ^{241}Pu fission and the ratios of asymmetric fission yields to symmetric ones were compared. The authors of this work assume that in the nuclear fission by slow neutrons the compound nucleus in the 0^+ and 1^+ states is formed since the ^{239}Pu nucleus spin is $I=1/2^+$. It is assumed that in the thermal neutron fission the compound nucleus is formed predominantly in the 0^+ state while in the 0.297 eV neutron fission the compound nucleus is in the 1^+ state.

Therefore, the dependence of some characteristics of the fission process (mass yields, total kinetic energies, neutron and γ - quantum yields) on the spin state of the fissioning nucleus can be considered to be experimentally proved. It should be noted that the accuracy of the mass number determination was of several atomic units. This accuracy is insufficient for determining the causes affecting the characteristics of the fission process from the spin states depending on the mass number.

In the present-day form the theory of the nuclear fission at low exoitation energies considers the fission process as consisting of three, coupled, nucleus states separated in time:

I - prefission or compound states;

II-region of the second minimum in the potential surface of the nucleus;

III-state at the point of the nucleus collapse.

The available data on different distributions in the fission are well described by the model of equilibrium at the collapse point.

The following distributions have been obtained in terms of this model, which are in good agreement with the experiment:

a) asymmetry trend depending on the mass of the fissioning nucleus;

b) distribution of the excitation energy between the pair of fragments and, hence, the neutron yield in the dependence of the fragment mass;

c) mass distributions of the fragments from fission of the nuclei from ^{212}Po to ^{258}Fm;

d) kinetic energies of fragments for various fissioning systems;

e) distributions of the widths of the mass and energy distributions;

f) fine structure in the fission fragment mass yields;

g) charge distribution of the fission fragments;

h) odd-even effects in the mass yields.

This indicates that the main features of the fission process are described correctly by this model.

The model, however, does not take into account the influence of the total angular moment of the fissioning nucleus though it is this moment that is the only mechanical quantity that is involved in the three stages of the fission process. This allowance might be made by the dependence of the potential energy of contacting fragments on the total spin.

1. The Mass Separator of Unmoderated Nuclear Fission Products

To enable a wide range of works on fission of nuclei to be carriod out the mass-separator of unmoderated nuclear fission products was designed and constructed. It has been installed on the horizontal channel of the VVR-SM at INP of the USSR Academy of Sciences. This apparatus permits separation of nuclear fission prodcts to be made with the help of the electrostatic field by

the ratio of the kinetic energy E to the ion charge e and then, using the magnetic field, by the ratio of the mass M to the ion charge e. In the apparatus the double (by angle and velocity) focusing of the fission fragment beam is provided. The ion optics of the mass separator permits the resolution at the half of the peak height $(M/e)/(\Delta M/e)=1300$ to be reached.

Fig.1 shows the block diagram of the mass separator. Target 1 of fissioning matter is focused in the mass separator. Fission fragments pass through diaphragm 4 collimating the beam and arrive at electrostatic analyzer 12 whose real field is formed by plates 13 of the cylindric condenser. Fission product separation in the electric field of the cylindric condenser with a definite ratio of the kinetic energy to the ion charge, E/e, occurs in accordance with the formula

$$E/e = \frac{1}{2\ln(r_2/r_1)} V,$$

where r_2 and r_1 are the radii of the curvature of the working surface of the condenser's inner and outer plates, respectively, V is the voltage on the condenser's plates. The high voltage V is applied from a stabilized two-polar source which permits the voltage to be continuously adjusted from 5 to 70 kV of each polarity at a stability of $\pm 0.01\%$. The high voltage is measured via the precision voltage divider by means of the P348 dc bridge of class 0.002.

Behind diaphragm 9 which has an adjustable width of the slit for transmitting a desired range of the value $\Delta(E/e)$ a semiconductor detector is set, this permits the spectrum of kinetic energies and ion charges to be obtained. The fission products with separated values E/e pass then through chamber 15 installed in the gap of the electromagnet which establishes the sector homogeneous magnetic field. There the fission products are separated relative to the mass M and to the ion charge e according to the formula

$$M/e = r_m^2 \ln(r_2/r_1) B^2/V$$

where r_m is the radius of ion deflection in the magnetic field, B is the magnetic inductance. The electromagnet is supplied with power from the current source permitting to provide a long-term current stability of $\pm 0.02\%$. The magnetic inductance is measured by the nuclear magnetic resonance on hydrogen by means of the MI-1-1 magnetic inductance meter having a measurement accuracy of $\pm 0.01\%$ and 43-34 frequency meter with a measurement accuracy of 0.001%.

After they have passed the homogeneous magnetic field, the fission products with the equal ratio M/e are focused in the mass separator where detection chamber 11 is set.

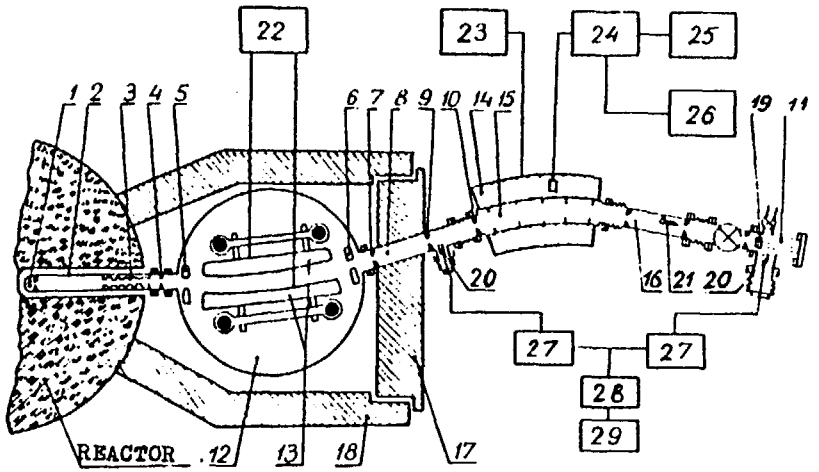

Fig.1. Block-diagram of the mass separator of unmoderated nuclear fission products

1 - ion source; 2 - inlet arm; 3 - neutron beam collimator; 4 - beam collimating diaphragm; 5,6 - screen diaphragms; 7 - diaphragm preventing ion scattering on the walls; 8-ion guide; 9,10-diaphragms determining ion velocity spread; 11-detection chamber; 12-electrostatic analyzer; 13-deflecting plates; 14-electromagnetic poles; 15-magnetic deflection chamber; 16-outlet arm; 17-movable part of the shield; 18-fixed part of the shield; 19-track detector; 20-semiconductor detectors; 21-beam shutter; 22-high-voltage stabilized rectifier; 23-electromagnet power supply; 24-magnetic inductance meter; 25-oscillograph; 26-frequency meter; 27-preamplifier; 28-spectrometric amplifier; 29-amplitude analyzer AI-4096.

Main parameters of the mass separator

	Electrostatic analyzer	Magnetic analyzer
Mean deflection radius	274.2 cm	173.4 cm
deflection angle	$19^{o}7'$	40^{o}
distance between the poles	3.0 cm	7.0 cm

The total length of the fission fragments travel from the target to the detection plane is 11.4 m, flight time is about 1 μs, energy dispersion is 103.2 cm, mass dispersion is 86-88 cm. The mass resolution at the 0.5 peak height, 800-900 for $\Delta E/E=2.56$ and 1100-1300 for $\Delta E/E=1.0\%$. The error of the measurement of masses is $\pm 0.06\%$, of energies $\pm 0.02\%$, of yields $\pm(2-3)\%$. The vacuum in the system, in two hours after beginning of evacuation, is $(2-3).10^{6}$ mmHg.

2. Detection of the Primary Nuclear Fission Products in the Mass Separator

Since the time of fission fragments flight from the target to the detection chamber is about 1μs the fission fragments are recorded before β-decays. In the focal plane of the mass separator the semiconductor detectors may be set and by diaphragming a spectrum line with a definite ratio M/e may be separated. A system consisting of a charge-sensitive preamplifier and AM-4096 amplitude analyzer was provided for recording and spectrometric analysis of the amplitudes of pulses from the semiconductor detectors. A pulse from the pulse generator with a precise amplitude is applied to the common input, which ensures a reliable control of the electron instrumentation stability. The system operation is checked with the help of the spectrometric α-source with half-widths of individual lines of 15 keV and the number of lines is 5. Selection of the semiconductor detectors and their energy calibration were carried out by the method proposed by Schmitt.

Fig.2 shows the amplitude spectrum of the fission products from ^{235}U nuclei, measured after the electrostatic analyzer, and Fig.3 presents the amplitude spectrum of the fission products of one line M/e after the magnet.

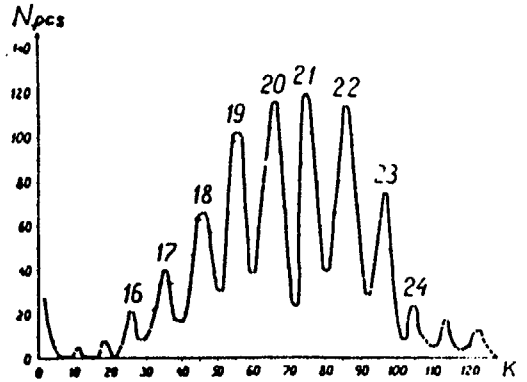

Fig.2. The amplitude spectrum of the products of the ^{235}U nuclei fission, measured by the semiconductor detector after the electrostatic analyzer. The figures at the peaks are the ion charge values. E/e = 3.268 MeV/eo.

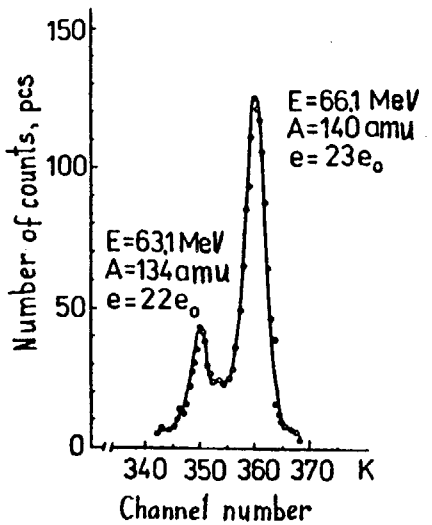

Fig.3. The amplitude spectrum of the fission products of one line M/e, measured by the semiconductor detector after the magnet.

If the mass separator is used in the mode of the mass spectrograph then in the focal plane of the instrument the glass track detectors are installed, which permit 6-7 lines of the spectrum of fission products of the heavy group (Fig.4) or 10-12 lines of that of light group (Fig.5) to be recorded simultaneously. The detection chamber is connected with the mass separator via the vacuum valve which permits the glass detectors inserted into cassettes to be replaced without breaking the vacuum.

For calibration of the mass separator and determination of spatial position of the M/e lines, in the focal plane a photoplate with the size equal to that of the glass track detector was set instead of this detector for recording heavy charged particles.

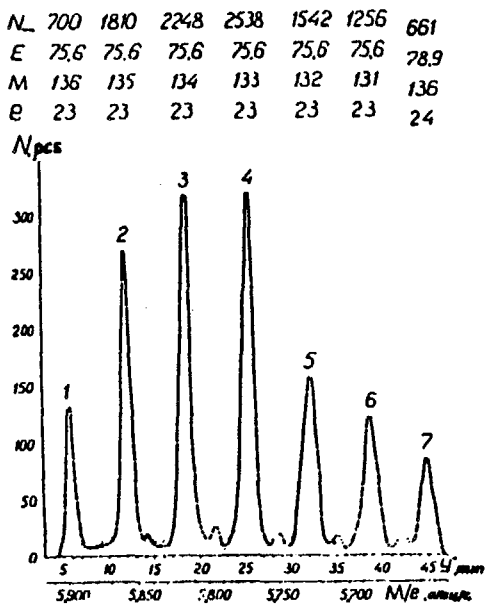

Fig.4. A section of the M/e spectrum of the fission products of the heavy group, measured by one glass detector.

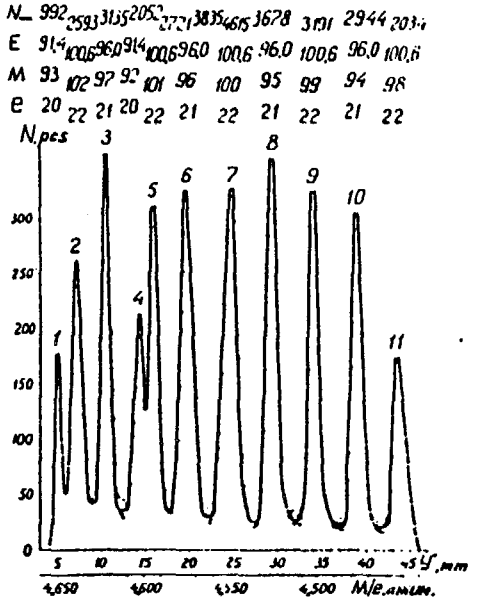

Fig.5. A section of the M/e spectrum of the fission products of the light group measured by one glass detector.

The mass separator was calibrated and the main characteristics were checked by α-particles from ^{238}Pu. The α-particle source was set instead of the target. At the constant deflecting voltage V=59.53 kV on the electrostatic condenser and at several values of the magnetic field the M/e lines of α-particles were obtained in different parts of the photoplate. After developing the photoplate was examined through the microscope. Fig.6 presents the spectrum of α-particles recorded by one of the photoplates. Then, using these data, the calibration curve was built, which further was used for determination of the M/e lines of the fission products.

For the energy calibration of the mass separator the spectrum of α-particles from ^{238}Pu was recorded after the electrostatic analyzer.

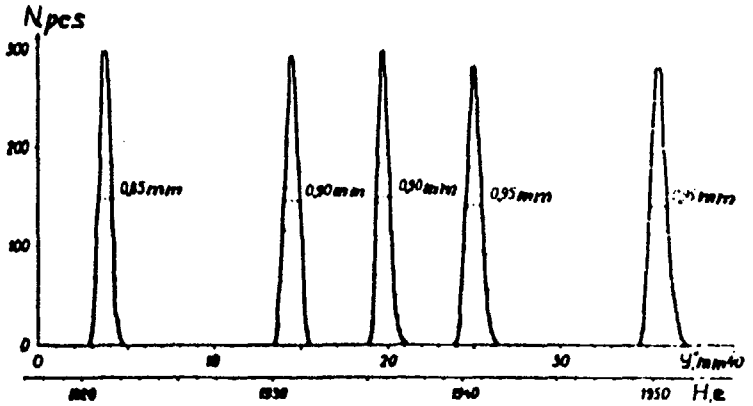

Fig.6. The spectrum of α-particles from ^{238}Pu recorded by nuclear photoemulsion at various magnetic inductances.

After exposure the glass track detectors were treated with the 5% solution of the hydrofluoric acid at room temperature for 45 min. The traces from the fission fragment impacts have a truncated cone form, with a depth of 15-20 μm and a diameter of 10-15 μm on the glass surface. They are easily seen at the microscope magnification by 100-150 times and are well distinguished against the background. To reduce the background defects, the glass was preliminary treated with the 5% solution of the hydrofluoric acid before exposure. In post-irradiation treatment with the acid the background defects had diameters significantly larger and were easily distinguished from the fission fragment traces.

Application of the track technique permits the prolonged measurements to be performed avoiding the danger of overlapping of the background from other types of radiation. A great set of particles may be passed to one line for reduction of the statistic error. The track detectors keep the information for practically infinite time.

3. Mass Distributions of Products from Fission of ^{239}Pu and ^{235}U Nuclei by Thermal Neutrons at Fixed Values of the Kinetic Energy of the Heavy Fragment

The characteristics of the process of ^{239}Pu nuclei fission by neutrons were studied in less detail as compared to the ^{235}U case and no studies were carried out in the mass-spectrometers with the

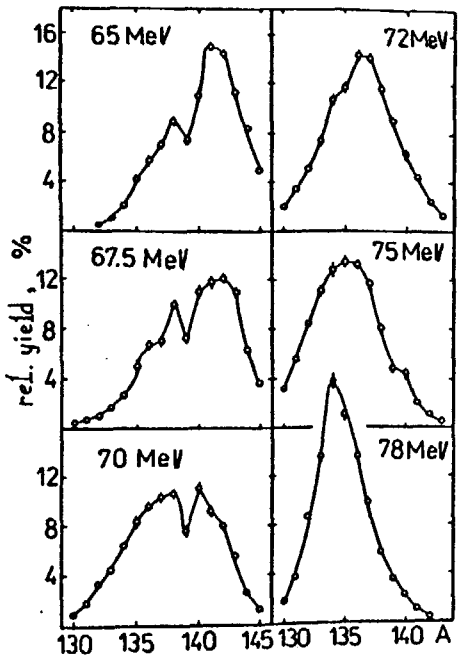

Fig.7. The relative mass yields of the products from the ^{239}Pu nuclei fission by thermal neutrons at the fixed values of the kinetic energy of the heavy fragment.

successive electric and magnetic fields. Therefore, for a more detailed study of the fine structure in the mass distributions we measured the mass distributions of the heavy group of fission products from ^{239}Pu at fixed kinetic energies 65.5 , 67.5 , 70.0 , 72 , 75.0 and 78.0 MeV which are close to the most probable ones for the mass numbers A=130-145. The similar measurements were also made for ^{235}U. Figs 7 and 8 present the individual mass yields of ^{239}Pu and ^{235}U nuclei fission by thermal neutrons at six kinetic energy values. It is clearly seen that the yield of the fission products with A=139 is anomalously low with increase in the excitation energy (for E_k < 70 MeV) in the ^{239}Pu fission case. A low yield for A=136 is observed in the case of ^{235}U fission when E_k < 72.5MeV.

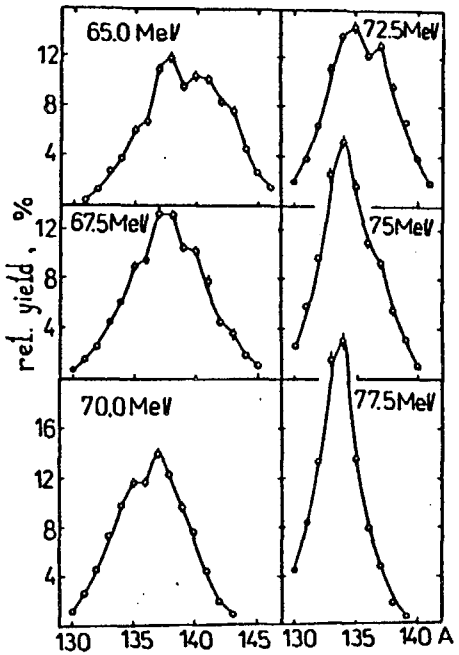

Fig.8. The relative mass yields of the products from the ^{235}U nuclei fission by thermal neutrons at the fixed values of the kinetic energy of the heavy fragment.

It follows from the mass distributions of the fission products that the fine structure cannot be accounted for by only odd-even effects. Its origin is more complicated. Smooth change of fission fragments results in sharp changes in the trend of the curve showing dependence of the relative yields on the mass number.

4. Mass Distributions of Products from Fission ^{235}U and ^{239}Pu Nuclei by Thermal Neutrons at Fixed Values of the Total Kinetic Energy

Fig.9 shows the mass distributions of the fission products of the heavy group at fixed values of the total kinetic energy (TKE) in the case of ^{235}U and ^{239}Pu nuclei fission by the thermal neutrons. These mass distributions have a fine structure, too.

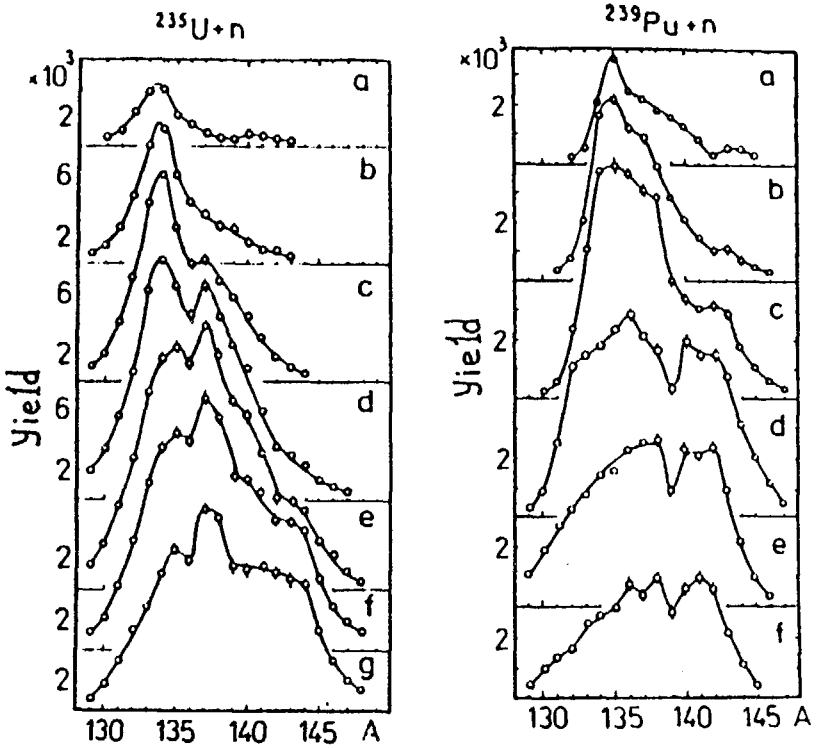

Fig.9. The mass distributions of the products from ^{235}U and ^{239}Pu fission by thermal neutrons at the fixed values of the total kinetic energy (TKE)(a) 190 MeV;(b)185MeV;(c)180MeV;(d)175MeV; (e)170MeV;(f)165MeV;(g) 160MeV.

The existence of the structure in the mass distributions obtained at the fixed values of TKE indicates that formation of some fragment pairs is less beneficial energetically. With allowance for the neutron emission in the ^{235}U fission case such a pair is A=136 and A=100. Attention should be paid to onset of the small peaks in the region of the mass numbers A=140 in the ^{235}U fission and A=143 in the ^{239}Pu case at high TKE values (Fig.9). The reason for this may be that the fissioning system has an oblate ellipsoid form at the discontinuity point.

5. The Method for Comparative Study of the Yields of the Products from the ^{239}Pu Nuclei Fission by Thermal and Resonance Neutrons

For measuring the yields of the products from the ^{239}Pu nuclei fission a target was installed on the inlet arm. The target was prepared of 50 g/cm^2 of 98% enriched ^{239}Pu evaporated in the 1 mm thick aliminium backing. Two subsequent sectors of the spectrum were measured with overlapping equal M,E and e by the lines. At the end of the inlet arm of mass separator 1 (Fig.10) cadmium cup 3 with a thickness of 1 mm was set for absorption of scattered neutrons. In the cup bottom there was a (15x40)-mm^2 rectangular hole opening in front of ^{239}Pu target 2. The flux passing through the hole in the cadmium cup induced fission of ^{239}Pu nuclei. The fission products passed through the electric and magnetic fields of the mass separator by the vacuum line and were recorded by the glass track detectors. When the fragments from the ^{239}Pu nuclei fission by resonance neutrons were measured the rectangular hole was closed by 0.3-mm thick samarium filter 4 through which neutrons with energies higher than 0.29 eV passed. To obtain a set of approximately equal number of counts the time of measurement of one spectrum sector must be increased by 12 times as compared with the time of measurement without the filter.

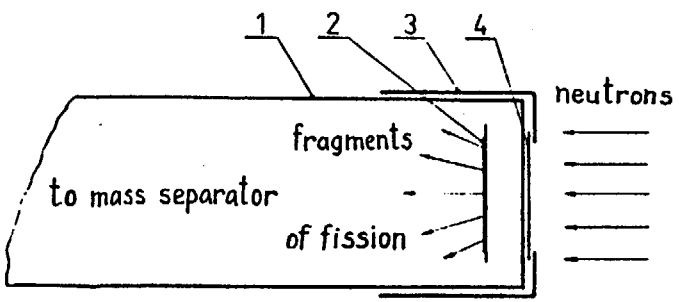

Fig.10. The experimental setup for measurement of the mass distributions of the products from the nuclear fission by thermal and resonance neutrons.

The same sector of the spectrum was measured four times at different times. After interpretation and treatment of each sector the equal ones were summed and the total errors of the yields of fission products with A=138-174 were calculated.

In determination of the cadmium ratio the rectangular hole was closed with the 1-mm thick cadmium filter. The comparison of the measured spectra with and without the filter showed that the cadmium ratio is equal to 75.

6. Mass Distributions of the Products from the ^{239}Pu Nuclei Fission by Thermal and Resonance Neutrons

The effect of the dependence of the nuclear fission products yields on the spin state of the compound nucleus was expected for more deformed nuclei. For determination of the character of this dependence the sector of the spectrum M,E and e in the range of the mass numbers A=138-148 was chosen at the fixed values of the kinetic energy E_k=66.0 , 68.5 , 71.5 , 75.5 MeV (Fig.11).

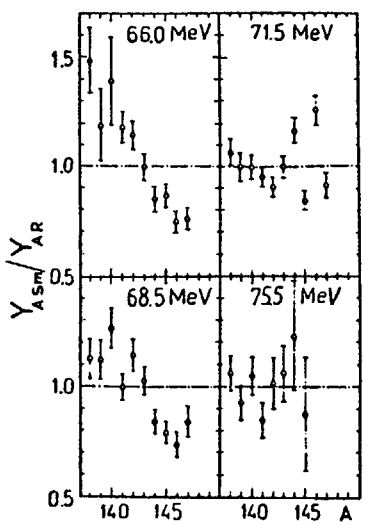

Fig.11. The relative yield of the ^{239}Pu nuclei fission products, normalized by the total yield at the fixed values of the kinetic energy of the heavy fragment.

At high values of the kinetic energy no change in the relative yields from thermal and resonance neutron fission is observed. With a decrease in the kinetic energy the difference between the relative yields begins to increase. When E_k=68.5 MeV a great difference is observed for A=142,144 and 146, which decreases when E_k=66.0 MeV. The observed change in the relative yields of the thermal and resonance fission products may be explained taking into account the shell corrections. For this purpose it is necessary to calculate the parameters of the fission fragment deformation at various kinetic energies. The deformation of the fragments at the above kinetic energies is β =0.5-0.8. From the map of the shell corrections (Fig.2) it is seen that for the above ranges the corrections to the potential energy change significantly with changing deformation parameter. The contour lines in Fig.12 are shown with an energy difference of 1 MeV. The region of neutron-shell correlation variations is to the right of the region H. There the contour lines are rather dense so that any small change in the deformation parameter leads to change in the shell corrections either to higher or lower values.

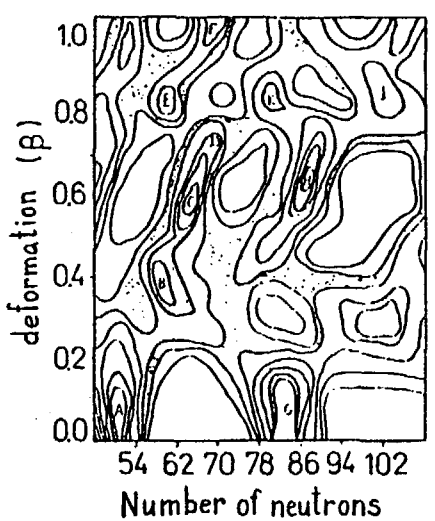

Fig.12. The shell corrections calculated depending on the deformation β and the number of neutrons of the fission fragments

The corrections assotiated with the spin state of the compound nucleus play the similar role. At a kinetic energy of 75 MeV the deformation parameter is β =0.5. In this case the spin correction is not of an essential importance and, therefore, no difference in the yields for two spin states is observed.

Thus, the measurements of the relative yields of products from the ^{239}Pu nuclear fission by thermal and oversamarium neutrons showed that the rotation correction must be introduced into the formula of the potential energy of the fissioning system.

CONCLUSION

The mass separator described above represents a many-purpose instrument which permits investigations of an extensive range of problems in the nuclear physics and interaction of fast multicharged ions with the substance to be carried out. The resolution and intensity obtained are sufficient for these investigations in most cases.

1. Investigation of the fission fragment yields at definite values of M, E_k and Z^*.

The mass separator makes it possible to measure distribution of fragments over M/Z^* and simultaneously determine ($< 0.5\%$) E_{K/Z^*} with a high precision within a time of the order of 1μs after the fission act. Making use of the semiconductor surface-barrier detectors and carrying out the analysis of pulse amplitudes obtained from these detectors, we find the values of mass M, effective charge Z^* and kinetic energy E_K for the fragments separated by the mass spectrometer. Since after the fission act some fragments are formed in the stable state (screened fission fragments) and have known values of M and Z, the coupling of the charge of the nucleus Z and Z^* (at given M and E_K) can be determined and, thus, Z of the rest of the fragments found, i.e. the complete identification of the fission fragments can be accomplished before the beginning of the β-decay and emission of delayed neutrons. Therefore, one can find correspondence in pairs between additional fragments ($Z_1 + Z_2$ =92) and, using the conservation laws, determine the rest of the characteristics of the fissioning system (fragment masses

prior to prompt neutron emission, number of prompt neutrons, total fission and excitation energies in separation of the compound nucleus into an appropriate pair of fragments), which must be known for determination of the behavior of the deformed compound nucleus at the saddle and discontinuity points.

No other instrument being applied at the present for studying fission (ion chambers, time-of-flight, semiconductor detectors, radiochemical technique) allows so many data simultaneously and with such a precision to be obtained at the early stages of the fission process as the mass separator of the given type.

Being important theoretically, these data are also of great interest for construction of reactors and other nuclear devices.

2. β- decay of the fission fragments.

Study of the nuclear β -decay yields much important information on the processes occuring in the nuclei and is of fundamental importance in nuclear physics. Investigation of the β -decay of such anomalous nuclei (with a large neutron excess as compared to the stable nuclei of the same Z) located far from the stability valley will undoubtedly give a great deal of new data on intranuclear processes and regularities of these processes.

In addition, the data on chains of the β -decay of fission fragments, providing information about intermediate fission products and their lifetimes, are necessary in reactor designing and in radiochemistry.

3. γ-spectrometry of the fission fragments.

The γ -spectrometry of the fission fragments permits us to obtain the data on the energy levels of the nuclei containing a larger number of neutrons as compared with the stable nuclei of the same Z. Comparison of these data with the systems of levels of the stable nuclei allows us to get the data on change in the nuclei levels with change in the number of neutrons at a constant Z and, therefore, to obtain new data on nuclear forces. Of great interest is the presence of nuclear isomers among the fragments.

These data are also essential in view of extensive application of the radioisotope technique with use of fission products and in precision calculations of protection against nuclear radiation.

4. Emission of delayed neutrons.

After emission of prompt neutrons from the fission fragments, in the cases when the β -decay is hindered but the neutron emission is energetically feasible, some fragments emit neutrons which are called "delayed neutrons". These neutrons play a great part in controlling the chain reaction in the reactors. But at the present far from all isotopes-fission fragments emitting delayed neutrons with the short life-times are known.

5. Investigation of energy losses of the fission fragments with known M,Z^* and E_K and change in their charges in passing through the substance.

This problem is of a greatest interest both from the viewpoint of practice and theory, since a far greater portion of the nuclear fission energy which can be used in the nuclear devices is determined by the kinetic energy of the fragments and by mechanism of energy transfer to the surrounding substances. The theoretical interpretations of this process, developed so far do not cover the variety of phenomena associated with this process. To a significant degree such a situation is due to unsufficient amount and accuracy of the experimental results. The separator offers the unique possibilities for a detailed and versatile investigation of this process.

6. Investigation of radiation damages of substances, caused by fission fragments.

At the present investigations of the character of damage in the substances from the fission fragments are carried out using the electron microscopy of fragment tracks in these substances. Preliminary separation of bombarding fragments with definite values of mass, charge and energy permits us to clarify the mechanism of these damages, which is very important for all nuclear devices, since

these damages are mostly responsible for the lifetimes of the main structural components in the core.

As the solid-state track detectors are widely applied in various fields of science and technlogy, investigation of their properties are of great importance. The mass separator was used for investigating the recording efficiency and spectrometric characteristics of some plastic detectors and potash mica. A new effect of dependence of the track linear dimensions in the mica on the mica crystal orientation relative to the fragment beam has been found. The recording efficiency of the crystal track detectors depends essentially on this orientation. As a result of the investigations performed a new mechanism of smoothing radiation damages in the crystals, induced by fission fragments, was developed.

7. Investigation of substance sputtering and secondary ion emission induced by fission fragments.

This problem is close to the foregoing one and is not less important for the operating longevity of different nuclear devices. The experiments with non-separated fragment beams showed a very large number of sputtered atoms per fragment (up to 10^6 atoms/fragment). The investigation of this process on separated beams of fragments will make it possible to get a better understanding of its mechanism.

8. Study of the secondary electron emission induced by fission fragments.

This problem is not only of theoretical but also of practical interest for understanding the processes occuring in the thermoelectron nuclear-to-electric energy converters and for designing the fission fragment detectors. At present a method is being developed for investigation of this process on the mass separator using the channel electron multipliers.

9. Interaction of fission fragments with the semiconductors.

This interaction comprises the investigation of the amplitude defect.

HEAVY NUCLIDE FAST FISSION CROSS SECTIONS

V.I. SHPAKOV
V.G. Khlopin Radium Institute,
Leningrad, Union of Soviet Socialist Republics

Abstract

Methods of actinide neutron fission cross section measurements in different neutron energy ranges are described. The uncertainty analysis for each method is made. The ways for obtaining more accurate values of the ^{235}U fission cross section used as standard reference data in relative measurements are discussed.

Introduction

Continuous development and improvement of nuclear energetic plants arouses constant increase of requests for nuclear data concerning both their accuracy and nomenclature. It is reflected in the IAEA directive papers, resolutions of international conferences and specialist meetings, in the World Request List WRENDA.

Some of the most important nuclear data are fission cross sections which are required at various stages in reactors design and operation, identified as

i) conceptual design studies,
ii) Detailed design of the chosen concept,
iii) Selection of efficient operating strategies,
iv) Determining the characteristics of the operating reactors,
v) Fuel transport, reprocessing and waste disposal and the activity of irradiated materials.

The most accurate fission cross section data are required to calculate the effective multiplication K_{eff}, the breeding ratio,

the fuel enrichment, the reactivity variation with burn-up and power, thermal power distribution, control requirements as well as to predict the generation of higher actinide isotopes, such as ^{242}Cm and ^{244}Cm, which are a major source of neutrons in irradiated fuel, and reducing them by incineration.

The highest accuracy requirements are for the primary actinides ^{235}U, ^{238}U and ^{239}Pu (together with ^{233}U and ^{232}Th for the thorium fuel cycle) which arise primarily for the prediction of K_{eff} and breeding. Typical requirements for the fission cross section accuracy are: thermal energy region $\pm$ 1%, 100 eV to 10 MeV $\pm$ 2%. The requirements for higher plutonium isotopes ^{240}Pu and ^{241}Pu are less stringent than those for ^{239}Pu.

The cross sections for the secondary actinides $^{242,243}Pu$ and some isotopes of Am, Cm, Bk, Cf are required with an accuracy of $\pm$ 10% to $\pm$ 20%.

At the same time some actinide isotopes are used for the neutron field metrology. The required cross section accuracy in this case should be better than 2%.

The ^{235}U is to be distinguished especially as its fission cross section is the most important international standard widely used as a reference value in relative measurements either of fission cross sections or of nuclear reactions. On account of the standard responsibility for numerous nuclear data the requirements for its accuracy are extremely high. According to Usachev's request the required accuracy amounts to 1.1, 1.4 and 2% for the 0.1 to 0.8 MeV, 0.8 to 4.5 MeV and higher than 4.5 MeV neutron energy regions respectively.

Methods of the Fission Cross-Section Measurements

The majority of fission cross-section data have been obtained by measurements relative to the ^{235}U fission cross section standard. These measurements, being the most simple ones, include the standard uncertainty as a systematic error and are sensitive to neutron scattering effects because ^{235}U has a non threshold cross-section.

To measure the ^{235}U cross section itself and those for some important nuclides like ^{238}U, ^{237}Np, ^{239}Pu absolute and absolutelike techniques have been applied. In these measurements both the neutron flux and the fission event counts are determined separately. These measurements may be divided into two groups:

i) Absolute measurements

ii) So called "Shape measurements".

In the former ones the neutron flux and the fission cross sections are determined absolutely. In the latter ones the shape of cross section energy dependence curve is measured using the known energy dependence of neutron flux monitor efficiency, which is normalized then to an absolute cross section value at some neutron energy point. The measurements of both groups should be united in consideration as they are similar in principal features and are performed employing the same technique.

Both absolute and shape measurements were performed in most cases in a wide range of neutron energies using either monoenergetic or white spectrum neutron sources, the latter ones being more efficient due to a possibility to carry out the measurements simultaneously for the whole energy range. In these cases neutron flux monitors with smooth and flat energy dependence are to be applied.

Similar methods have been used in all measurements to detect fission events which were either the 2-π multiplate ionization or gas scintillation chambers (with the exception of measurements /1/, where the silicon surface-barrier detector has been used). Both methodical problems and uncertainty origins were common therefore for all measurements. They will be considered later.

On the contrary, a visible variety appears when one considers the neutron flux determination. The most usable methods of absolute and shape measurements which have been carried out during the last 10 years may be incorporated into two groups:

i) Measurements using "black neutron counters" as neutron flux monitors.

ii) Measurements relative to the (n,p)-scattering cross section.

Herewith the so called absolute measurements were not really absolute ones as the $^{1}H(n,n)^{1}H$-scattering cross-section standard was used to determine either the neutron flux or the neutron monitor efficiency.

Measurements Using Black Neutron Counters

The ^{235}U induced fission cross-section measurements have been carried out at the Argonne National Laboratory (ANL) /2,3/ and at the National Bureau of Standards (NBS) /4/, USA, employing the so-called black neutron counter (BNC) as a neutron flux monitor, proposed and designed by Poenitz /5/. This counter was a cylindrical plastic or liquid scintillator, containing hydrogen. There was an entrance hole in the base of the cylinder going nearly to the cylinder center. The counter could operate only with a well collimated neutton beam which should be completely situated within the entrance hole. In this case neutrons reflected after collisions from the bottom of the hole have practically always been captured by the walls of the hole. Neutrons were registered by recoil proton counting. As a consequence the neutron counting efficiency achieved the value of nearly 100% in some neutron energy range defined by the counter dimensions. But the enlargening of the counter dimensions led to an essential increase of the counter background which could be especially crucial for the high energy neutron counting. The black neutron counter is not therefore a universal device for a large neutron energy range and application of specific counters for different energy regions is desirable. However, the validity of BNC at neutron energy higher than 8 - 10 MeV is doubtful.

The BNC counting efficiency can be accurately calculated using the Monte-Carlo computer code /6/, proposed by Poenitz. The experimental checking of efficiency calculation based on associated particle technique has shown an agreement within 1.5%. The energy dependence of BNC counting efficiency for the 40 cm long counter with a diameter of 13 cm is shown in Fig. 1.

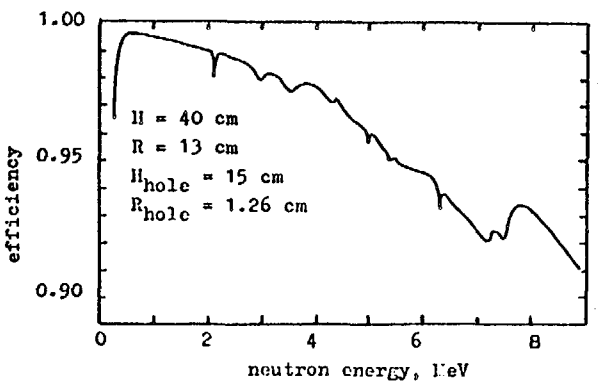

Fig. 1. Energy dependence of the black neutron counter efficiency.

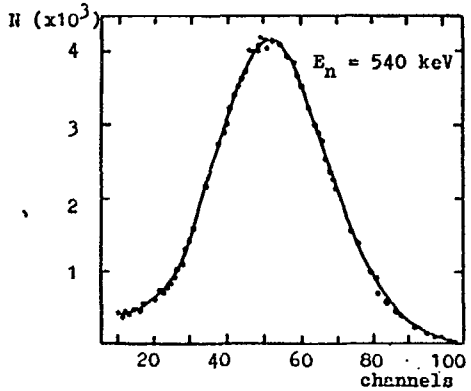

Fig. 2. Black neutron counter response.

The BNC pulse-height spectrum (Fig. 2) had a low energy tail, continued to zero energy. To calculate the total number of counts an extrapolation to zero energy is required. This procedure, being rather critical, was an origin of systematic uncertainty.

The measurements at the ANL were performed using the 3 MeV Van-de-Graaf accelerator for 85 keV to 3,5 MeV - neutrons (shape measurements) /2/ and for 200 keV to 8.2 MeV - neutrons (absolute measurements) /3/. The measurements at the NBS were performed also using Van-de-Graaf accelerator as a neutron source for 200 keV to 1.2 MeV - neutrons (absolute measurements) /4/.

The $^{2}D(d,n)^{3}He$ reaction has been used to produce neutrons with energy higher than 4.5 MeV and the $^{7}Li(p,n)^{7}Be$ reaction has been used for lower energy. To minimize the detector background pulse operation of the accelerators with the pulse duration of about several ns, as well as both pulse-height and time-of-flight selection have been used. The schematic drawings of the experimental setups are presented in Fig. 3.

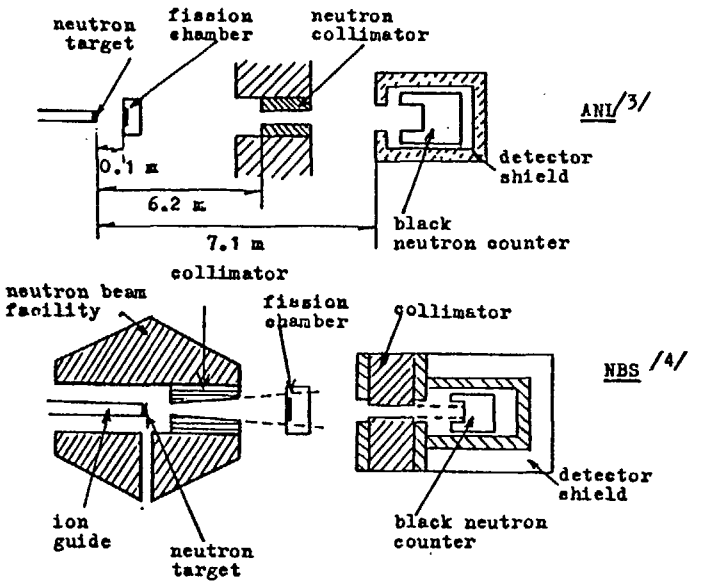

Fig. 3. Schematic drawings of the experimental setups at the measurements with black neutron counters.

The counting rate in the BNC for the same neutron flux was about 10^{6} times higher than that in the fission events detector. To achieve sufficient statistics both detectors had to be places at essentially different distances from the neutron source. Moreover, the fission chambers in measurements /2, 3/ were put in conditions of "open geometry" i. e. were exposed to the non-collimated neutron beam. These circumstances caused an increase of both neutron scattering effects and the neutron beam anisotropy and as a result an increase of the irradiation geometry uncertainty. A paraffin loaded with Li_2CO_3 facility was used at the NBS /4/ to form the neutron beam to a cone with a half-angle of 4.3° and with angular uniformity better than 1%.

The neutron flux monitors were located in all cases inside massive shields made of borated polyethilene and lead. Precise collimators were installed in front of detectors to fix the solid angle subtended by the detector and to insure that all the neutron flux was incident on the entrance hole of the detector.

The main effects affecting the measurement results were as follows:

i) Neutron detector background consisted of both constant, ambient background and that (mainly Gammas) connected with the neutron beam. The latter one has been determined by cutting down the collimator hole with a paraffin and lead plug.

ii) Fission chamber background produced mainly by scattered neutrons and by those of the second energy group with decreased energy arised when the $^{7}Li(p,n)^{7}Be$ was used to produce neutrons. These background components, being excluded in the neutron counter by the time-of-flight, could not be separated in the fission chamber due to a small flight base.

iii) Neutron flux distortion and attenuation occured due to neutron interaction with the entrance part of the collimator, neutron scattering from the inner surface of the collimator into the neutron counter, scattering and absorption of neutrons in the fission chamber, in air, and in the case of open geometry /2, 3/ due to scattering in structural materials in the vicinity of the fission chamber. Besides, back scattering effect from the shield into the counter for neutrons which passed primarily the counter without interaction was to be taken into account. Corrections for all effects mentioned have been calculated using cross-section data of the ENDF-B/IV library. Besides, the correction for neutron interaction with the collimator has been determined in /4/ experimentally by measuring with 4 collimators of different diameters.

iv) Total number of neutron counts was determined in work /4/ by Monte-Carlo fit of the pulse-height spectra to the Poisson distribution (Fig. 2). The way to determine either the low energy tail or the total number of counts in papers /2, 3/ has not been described.

v) Geometrical factors have been determined from the targed and collimator entrance diameter ratios. Nevertheless, it seems that some effects connected with the beam collimation, long distance between the detectors and open geometry could cause some additional errors and lead to a more complex dependence of the geometrical factor on the setup geometry.

vi) BNC counting efficiency was calculated using Monte-Carlo computer code /6/ based on the counter geometry, the H(n,n)H reaction differential cross section, scintillator light yield, taking into account neutron interaction with carbon nuclei and Poisson distribution of photo electron emission.

vii) Efficiency of the fission events counting was determined taking into account counting losses due to discrimination and fission fragment absorption in target deposits in a way which is similar to that used in all the fission cross section measurements.

The measurements employing the BNC, as it can be seen, contain a large number of both corrections and systematic uncertainty origins. It should be noted that the measurements /3/ are the repetition of those in work /2/ by the same authors using practically the same setup. However, the results of both measurements essentially disagree, the reasons of disagreement being not analyzed by the authors and unclear.

Typical values of both corrections and uncertainties of the measurements are given in Table 1.

Table 1

Typical values of corrections and systematic uncertainties at measurements using black neutron counter

Effect	Correction in %	Uncertainty in %
1. Neutron counter background	0.2 - 1.0	0.1
2. Fission chamber ambient background	0.1	0.1
3. Fission chamber background due to the 2-nd neutron group and the neutron peak tail	3 - 13	0.2 - 1.0
4. Neutron scattering in the entrance part of the collimator	1.5	0.2
5. Neutron scattering from the walls of the collimator into the counter	0.1 - 1.5	0.05 - 0.3
6. Neutron scattering in the fission chamber	1 - 2	0.2 - 0.5
7. Neutron absorption in the fission chamber	1 - 2.5	0.2 - 0.3
8. Neutron scattering in air	5 - 12	0.5 - 1.2
9. Neutron back scattering from the shield into the counter	0.1 - 1.5	0.2 - 0.5
10. Neutron scattering in the vicinity of the fission target		0.7
11. Total proton count determination		0.1
12. Dead time		0.2
13. Geometrical factor		0.5
14. Neutron counter efficiency	3.5 - 11.5	1 - 2
15. Fission event counting efficiency	0.1 - 0.5	0.1 - 0.2

Measurements Relative to the $^{1}H(n,n)^{1}H$-Scattering Cross Section

In these measurements the neutron flux was determined by counting of recoil protons produced by neutron interaction with a hydrogen containing thin radiator. The measurement method has some advantages which are simplicity, low sensitivity to a gamma background, high counting rates, efficiency in wide neutron energy range. This method is therefore the most applicable one for measurements using the white spectrum neutron sources.

The measurements employing such method have been performed at the Lawrence Livermore Laboratory (LLL) /8/, at the Los Alamos Scientific Laboratory (LASL) /1/, at the NBS /9, 10/, USA, and at the Nuclear Research Center, Karlsruhe (KFK) /11, 12/, FRG. The schematic drawings of the experimental setups are presented in Fig. 4.

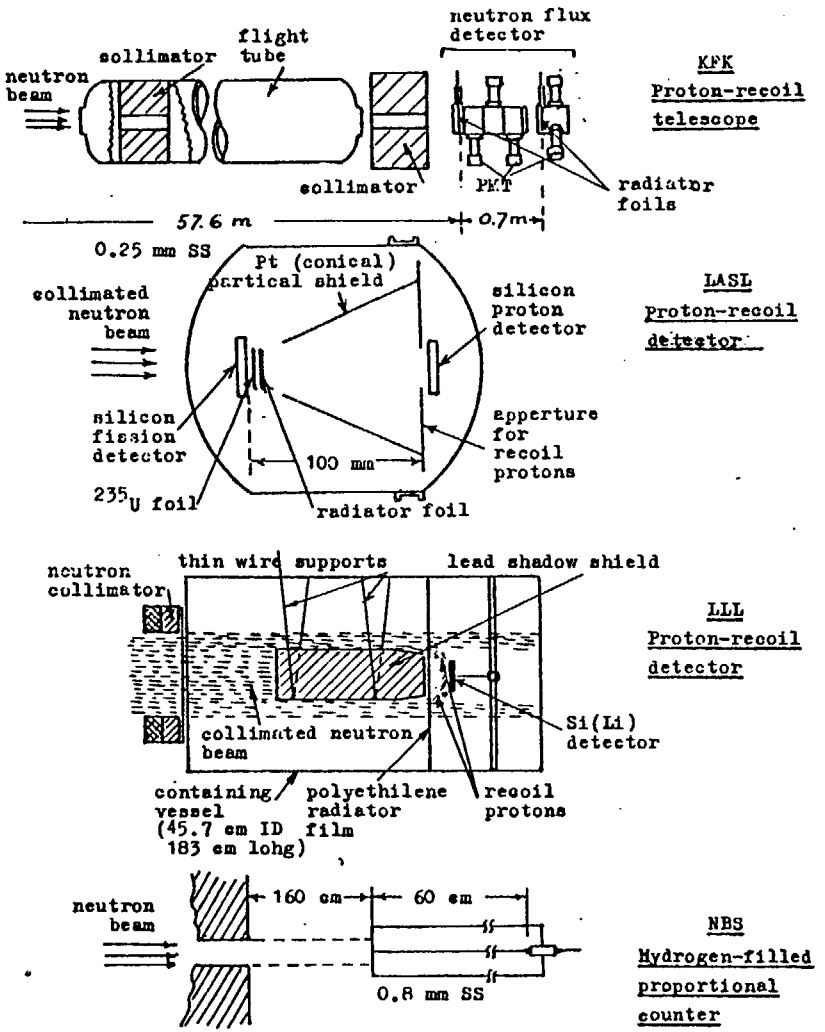

Fig. 4. Schematic drawings of the flux monitors at the measurements relative to the $^{1}H(n,n)^{1}H$ cross section.

The measurements /8, 9/ were performed using a linear accelerator of electrons with uranium and lead targets as a neutron source. Recoil protons were detected by silicon surface barrier detectors protected from the accelerator gamma flaches by massive lead cylinder. A proton synchrotron with uranium targets was used in the measurements /11, 12/. To detect recoil protons a telescope of gas scintillation counters was employed. In this case the detector shield was not installed due to decrease of both the gamma flash and the detector sensitivity to gammas which provided significantly lower neuton flux attenuation. In the measurements /1/ both the hydrogen radiator and the fission target were irradiated back to back. A silicon surface barries detector was used to detect recoil protons. In the measurements /9, 10/ performed at low neutron energy (up to 1200 keV) recoil protons were counted by a gas proportional counter. Hydrogen containing gas filled counter was used as a proton radiator.

In spite of the variety of other detector systems or experimental geometrical configurations the majority of systematic uncertainties are similar for all measurements mentioned. They are as follows:

i) Neutron monitor background consists of time independent background, background from the $^{12}C(n,\alpha)$-reaction on carbon and, in case of silicon detectors from reactions on silicon in which charged particles are produced. The total background value is less than that in the case of BNC.

ii) Fission chamber background at measurements with white neutron spectra is mainly connected with slowed down neutrons.

iii) Neutron flux attenuation is caused by scattering in fission targets and chamber windows as well as in the proton detector shield. It is less than that in case of the BNC, due to better beam collimation, long flight distances and near disposition of the detectors.

iv) In the measurements /1, 8, 9/ the recoil protons were collimated and their pulse-height spectra did not continue to zero energy. In the other worke /10, 11, 12/ the extrapolation of spectra to zero energy was desirable, the correction value being noticeable.

v) No geometrical factor was taken into account as it was possible to consider both detectors to be in the same neutron flux due to well collimated beams and long flight distances.

vi) Neutron monitor efficiency is calculated starting from the proton detection efficiency, the quantity of hydrogen in the radiator, the H(n,n)H scattering cross section and its angular dependence (which is known with the accuracy not better than 3% /13/).

vii) The time shift of neutron monitor discriminator depended on proton pulse height. This is an origin of the most significant uncertainty which led to the error in the energy scale.

viii) The energy calibration accuracy for both detectors defined not only the energy scale accuracy, but in case of the measurements with white neutron spectra could lead to the error of the cross-section value itself.

ix) The problems of determination of the fission events counting efficiency were the same as those in case of measurements with the BNC.

Typical values of both corrections and uncertainties are presented in Table 2.

Table 2

Typical values of corrections and systematic uncertainties at measurements relative to the $^{1}H(n,n)^{1}H$ cross section

Effect	Correction in %	Uncertainty in %
1. Neutron detector background	1 - 5	0.2 - 0.5
2. Fission chamber background	0.1	0.1
3. Neutron flux attenuation	1	0.1
4. Determination of total proton counts	0.5 - 5.0	0.2 - 1.0
5. Angular distribution of recoil protons	2.5	0.2
6. Neutron detector time shift		0.4
7. Energy scale of both the neutron and the fission detectors		0.5
8. Dead time	1.7	0.1
9. Fission events counting efficiency	0.1 - 0.5	0.1 - 0.2

Essential disagreement of data can be seen when one compares the measurement results obtained by this method even in case of measurements using the same setup /8, 9/.

The Time Correlated Associated Particle Method

An absolute method of fission cross section measurements has been developed at the V.G. Khlopin Radium Institute, USSR and independently at the Research Center Bruye-le-Chatel, France /14, 15/, which is called now the time correlated associated particle method (TCAPM). Later on this method has been employed in the joint measurement programme of the Khlopin Radium Institute (KRI) and of the Technical University of Dresden, GDR (TUD) /16/. Recently the TCAPM has been used at the NBS, USA /17/ and at the Institute of Nuclear Physics, China /18/.

The TCAPM allows to carry out fission cross-section measurements only at some fixed spot points of neutron energy but enables to exclude a significant part of the measurement uncertainty and hence to improve the measurement accuracy.

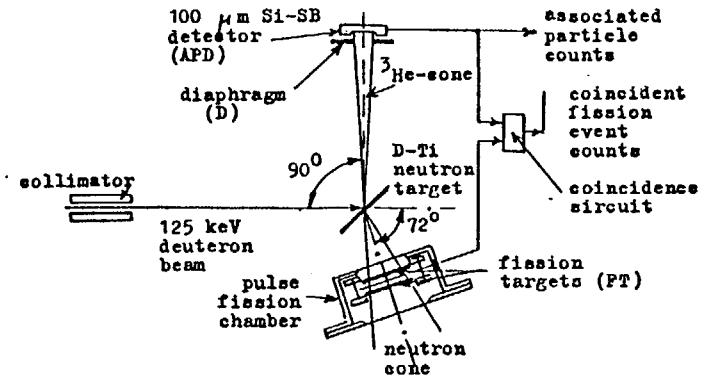

Fig. 5. Saheme of setup at measurements by the TCAPM with 2.6-MeV neutrons.

The basic idea of the TCAPM is illustrated in Fig. 5. The $^{2}D(d,n)^{3}He$ and $^{3}T(d,n)^{4}He$ reactions are used as a source of neutrons. The ^{3}He or ^{4}He particles associated with the neutrons are detected by the associated particle detector (APD) within the cone fixed by the entrance diaphragm (D). The neutron cone corresponding to the associated particle cone irradiates the fission target (FT). The fission events are registered in coincidence with the associated particles (AP). Provided the two main geometrical constrains are met:

i) the fission target is large enough to make the base of the neutron cone to lie completely inside the target,

ii) the fission target nonuniformity is negligible, the indu-

ced fission cross section can be determined from the formula:

$$\sigma_f = \frac{N_c}{N_{ap}\, n}$$

where N_c is the number of the coincidences, N_{ap} is the number of associated particles and n is the number of fissionable nuclei per cm^2.

The TCAPM has the following advantages:

- no geometrical factors are to be taken into account,
- determinations of either neutron flux or total associated particle counts are not necessary,
- fission events induced by background neutrons (scattered neutrons or neutrons from other reactions) are excluded,
- the AP-counting background can be essentially reduced by a proper choice of AP energy window near the peak.

Although this method seems to be a simple one its practical realization is often connected with considerable difficulties due to a high background of charged particles other than associated ones in the AP-channel which are both scattered deuterons and charged particles produced in (d,p), (d,α), (n,p), (n,α) accompanying reactions. Specific AP-channels are to be designed therefore for measurements at every neutron energy point. The AP-channels for 14 to 15 MeV, 8.5 MeV and 2.6 MeV-neutrons are described below.

a) Measurements with 14 to 15 MeV-neutrons

These measurements, being the most simple ones in methodical aspect, have been performed at all five laboratories mentioned above /16, 17, 18, 19/ Neutron generators and electrostatic accelerators with the 100 to 500 keV deuteron beam energy have been used as a neutron source employing the $^3T(d,n)^4He$ reaction. Fission targets were placed at the angles from 15 to 90° with respect to the deuteron beam. Associated alphas were counted at the corresponding angles in the rear hemisphere.

The energy of alphas was essentially higher than that of scattered deuterons due to high Q-value of the T(d,n)-reaction. Scattered deuterons then could be completely cut off with a protective filter across the alpha particle detector. The AP-channel background components were due to γ-rays, protons and tritons produced by the $^2D(d,p)^3T$ reaction occuring due to deuteron implantation into the tritium targets.

To reduce all the background components the 100μm thick scintillating plastic was applied as an AP-detector in the measurements /16, 19/ which was protected from both light and scattered deuterons by the 100 mg per cm^2 thick aluminium foil. Fig. 6 shows an

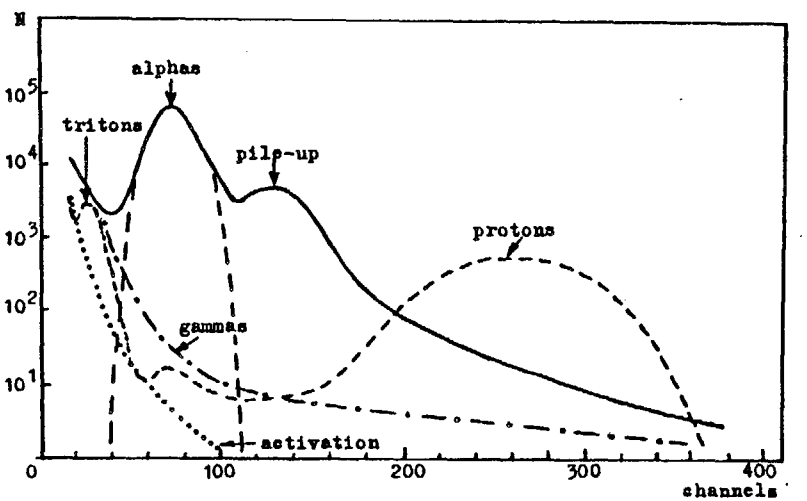

Fig. 6. Pulse-height spectrum in AP-channel at measurements by the TCAPM with 14.7-MeV neutrons.

example of the pulse-height spectrum in the AP-channel. It can be seen that the background under the α-particle peak does not exceed 0.1 - 0.2%.

Silicon surface-barrier detectors have been used to detect the AP in the measurements /17, 20/.

b) Measurements with 8.5 MeV-neutrons

These measurements have been performed within the joint measurement programme of the KRI, USSR and the TUD, GDR at the tandem-generator of the Central Institute of Nuclear Research, Rossendorf, GDR, with 9.5 MeV deuteron beam, the $^{2}D(d,n)^{3}He$ reaction being used.

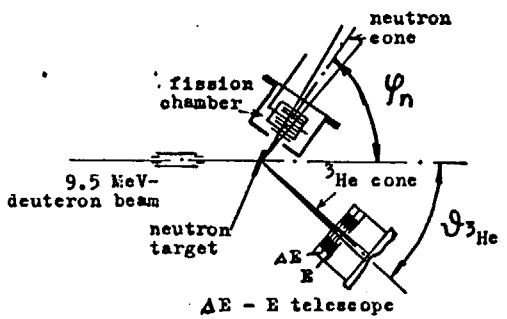

Fig. 7. Experimental setup at measurements by the TCAPM with 8.5-MeV neutrons.

In this case either neutrons or associated ^{3}He-particles were flying onward due to the big transfer velocity brought in by the deuteron momentum. Both the AP-detector and the fission targets were to be situated in the front hemisphere at the angless of 45 and 75° with respect to the deuteron beam and the 1 - 2 mg per cm^2 thick targets of deuterated polyethilene were used to produce neutrons. The AP-channel background components were due to both scattered deuterons with energy up to 9 MeV, and α-particles with energy of 3 to 5 MeV produced by the $^{12}C(d,\alpha)$ reaction on the target carbon.

Fig. 8 shows a typical charged particle pulse-height spectrum in the AP-channel measured with a thin silicon detector at deuteron energy of about 8 MeV. To separate associated ^{3}He particles from alphas a ΔE - E telescope consisting of two thin (12 μm and 40 μm) completely depleted silicon detectors was used. In this way α-particle background in ΔE - E_r energy window was decreased to 1.5.- 2% of total ^{3}He counts. In Fig. 8 a contour map of the two-dimensional ΔE - E_r spectrum is shown. A fast two-channel analyser /21/ was used as a particle identifier for the associated ^{3}He particles.

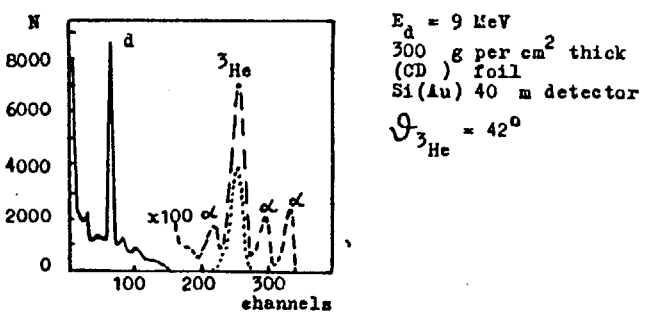

Fig. 8. Pulse-height spectrum in AP-channel in the case of 8.5-MeV neutrons.

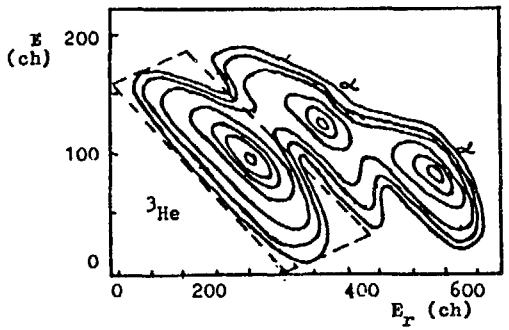

Fig. 9. AP-contour map at the measurements by the TCAPM with 8.5-MeV neutrons.

c) Measurements with 2.6 MeV-neutrons

These measurements have been also performed as a joint work programme of the KRI and TUD/16, 22, 23/ using a neutron generator with 120 keV deuteron beam and the $^2D(d,n)^3He$ reaction as a neutron source. Fission targets and AP-detector were installed at the angles of 72 and 90° with respect to the deuteron beam. The scheme of the experimental setup is shown in Fig. 5.

The surface-barrier detector with 100 μm-depth of depleted zone was used to detect ^{3}He-particles, being protected from scattered deuterons by 230 μg per cm^2 thick aluminium filter. Efficient separation of the ^{3}He-particles from scattered deuterons due to their low energy (about 800 keV) strongly depended on careful selection of the filter foils either by thickness ($\pm$ 5 μg per cm^2) or by quality and uniformity. When the foil characteristics required had been provided, the scattered deuterons contribution was negligible. The main components of the AP-channel background were due to protons and tritons produced in the $^2D(d,p)^3T$ side reaction,

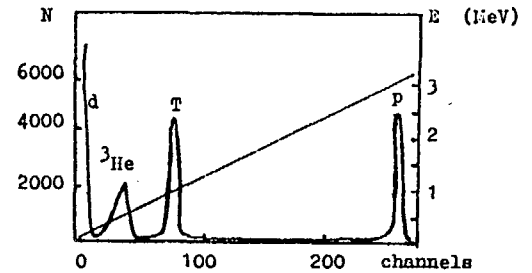

Fig. 10. AP-pulse-height spectrum at the measurements by the TCAPM with 2.6-MeV neutrons.

whose contributions were dependent on the detector spectrometric quality. The pulse-height spectrum of the AP-channel is shown in Fig. 10. The proton and triton background under the ^{3}He peak did not exceed the value of 2.5%.

Corrections and Uncertainty Origins of the TCAPM

The following corrections are to be introduced into the raw data obtained by the TCAPM:

- for background in the AP-channel
- for random coincidence background
- for neutron flux attenuation
- for fission events counting efficiency.

i) The background in the AP-amplitude window was determined by both measurements without neutron targets and cutting-off of the AP-cone with a thin foil. In the case of measurements with 2.6 MeV-neutrons the foil thickness was chosen to ensure complete ^{3}He-particle absorption and minimal energy losses for protons and tritons to determine proton and triton background. In the case of measurements with 8.5 MeV-neutrons the background was determined

by replacement of deuterated polyethilene target with a conventional polyethilene foil.

ii) Due to neutron beam collimation the number of coincidences was 20 - 30 times less than the total number of fission which resulted in a rather high level of random coincidences. To define accurately the correction for this effect an electronic setup was used which provided for the simultaneous registration of both total coincidences and random ones with the same circuit. Another way to determine this correction was to analyze AP - fission time distribution spectra.

iii) The neutron flux attenuation was calculated by a method based on the inverse problem of the radiation transfer theory /24/. The set of transfer equatios was solved by the Monte-Carlo method for real experimental conditions taking into account all the structural materials and gaseous mixture filling the chambers.

iv) Parallel plate pulse current ionization chambers were used in all the measurements for fission events detection. The detection efficiency was defined by two factors which are a fission fragment absorption in the fissile layers and counting losses due to discrimination in the counting channel. These problems are common for all the fission cross-section measurements as was mentioned above. The fission fragment absorption can be in principle sufficiently exactly calculated as a function of the fissile layer thickness, the neutron energy, the fission fragment range and of the fission product anisotropy (for example /25/). The counting losses due to discrimination usually are determined by extrapolation of the fragment pulse-height spectrum to zero energy. However, the fission fragment ranges which are now insufficiently known and depend on the deposit chemical composition (which is usually difficult to determine in turn) can be an origin of essential uncertainty of results. Besides, the extrapolation procedure also is not doubtless. The best way, therefore, to improve the accuracy of results is a direct experimental determination of fission counting efficiency, which is now in progress.

All the corrections considered are origins of the systematic uncertainties. Besides, another two circumstances are to be taken into account which are the target deposit uniformity and location of the neutron cone completely within the fission target. The target uniformity provided by careful target preparation, was checked for high α-activity samples by scanning with a detector with a small entrance diaphragm and for low α-activity samples by an ellipsometry or by an electron X-ray microprobe analysis.

The Coulomb multiple scattering of associated particles leads to broadening of the neutron cone due to a possibility to detect in the AP-cone scattered particles associated with neutrons flying outside the neutron cone. It may be especially crucial for the measurements with 2.6 MeV-neutrons where scattering probability increase due to lowenergy of the ^{3}He-particles. However, the systematic error, connected with this process will be negligible if the topography of the neutron cone is known and its long-time stability is ensured. In all the measurements the cone profile was mapped and its stability controlled for each AP-counting system by means of a 2 mm diameter plastic scintillator in coincidence with the AP-detector. Fig. 11 shows the neutron cone profile in case of measurements with 2.6 MeV-neutrons.

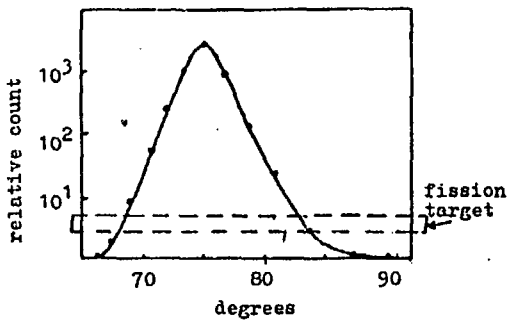

Fig. 11. Neutron cone profile at the measurements by the TCAPM with 2.6-MeV neutrons.

Typical values of both corrections and partial measurement uncertainties are presented in Table 3.

Table 3

Typical values of corrections and uncertainties of the TCAPM

Effect	Correction in %	Uncertainty in %
1. Coincidence statistics		0.7 - 1.0
2. Random coincidences	3 - 10	0.3 - 0.5
3. Background in AP-channel	0.1 - 3	0.01 - 0.3
4. Neutron flux attenuation	1.5 - 2.5	0.1 - 0.4
5. Fission counting efficiency		
a) Extrapolation to zero energy	0.5 - 2.5	0.1 - 0.5
b) Fission fragment absorption in target deposite	0.2 - 1.5	0 - 0.3

Analysis of Fission Cross-Section Measurement Results

It is impossible to consider fission cross section data for all nuclides within one paper. As an example the data for the ^{235}U will be analysed. This fission cross section is responsible for data accuracy of numerous relative measurements and is measured with the best accuracy.

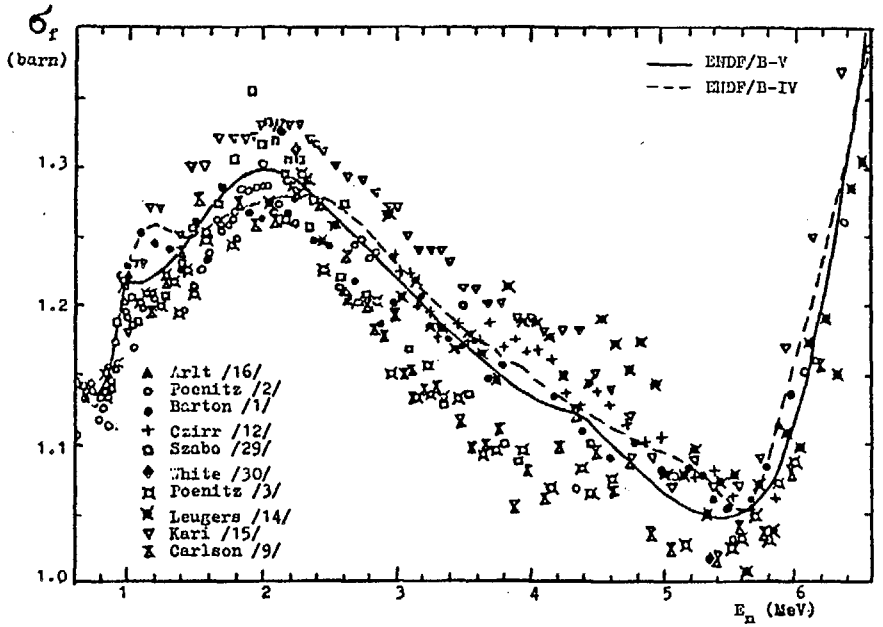

Fig. 12,a. Experimental data on the ^{235}U fast fission cross section.

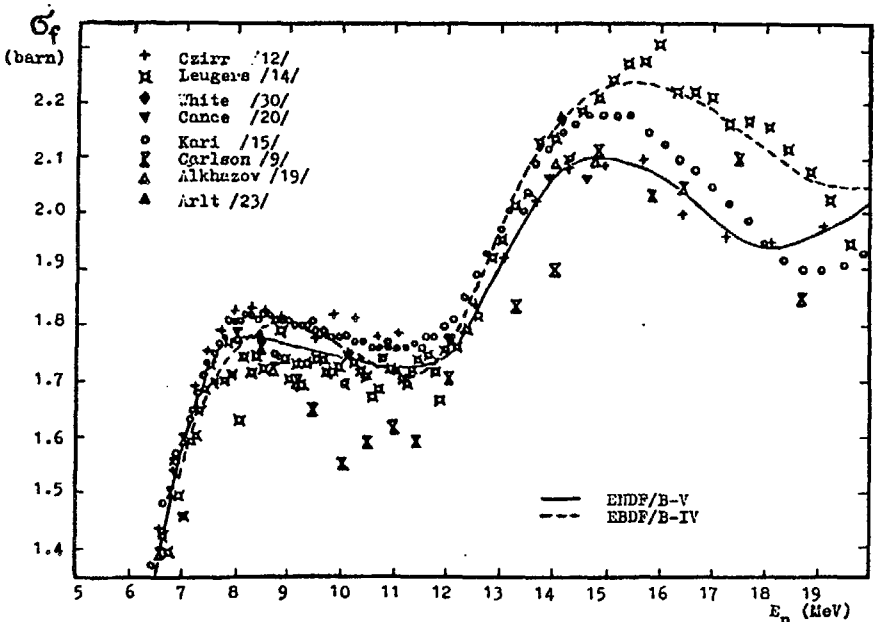

Fig. 12,b. Experimental data on the ^{235}U fast fission cross section.

Fig. 12 shows the results of the ^{235}U fission cross-section measurements performed during the last 7 years in comparison with the evaluation of the EHDF-B/IV and ENDF-B/V files. Essential discrepancies of experimental data either in magnitude or in shape can be seen. It is evident that these discrepancies can not be removed by renormalisation of shape measurements data. Fig. 13 shows the results of different evaluations performed during several last years.

The most significant disagreement of experimental results exists in the 13 to 20 MeV energy range where different data disagree by more than 10%. The new results obtained in recent absolute measurements for 14.1 - 14.7 MeV-neutrons by the TCAPM /16, 20/ which agree within the limits of the 1% accuracy (Fig. 14) allow to reduce the cross-section uncertainty in the 13 to 16 MeV energy region and to claim the required accuracy for 14 - 15 MeV neutrons to be achieved. Excellent agreement of the five independent measurements characterizes the TCAPM as the most accurate and reliable one.

The existing data at neutron energies higher than 16 MeV are so discrepant that it is difficult to expect an evaluation accuracy better than 6% in this energy range.

Discrepancies of data in the neutron energy region from 5 to 13 MeV reach 5 - 6%. The shape measurements /8, 9, 12/ show different shape of the energy dependence. Significant disagreement of different evaluations also can be seen. The result of absolute measurement by the TCAPM /22/ within the limits of 1.5% coincides with both Kon'shin evaluation /26/ and those of the ENDF-B/V and the JENDL-2 files. It is obvious that accessible accuracy of evaluations can not be better than 3 - 4%.

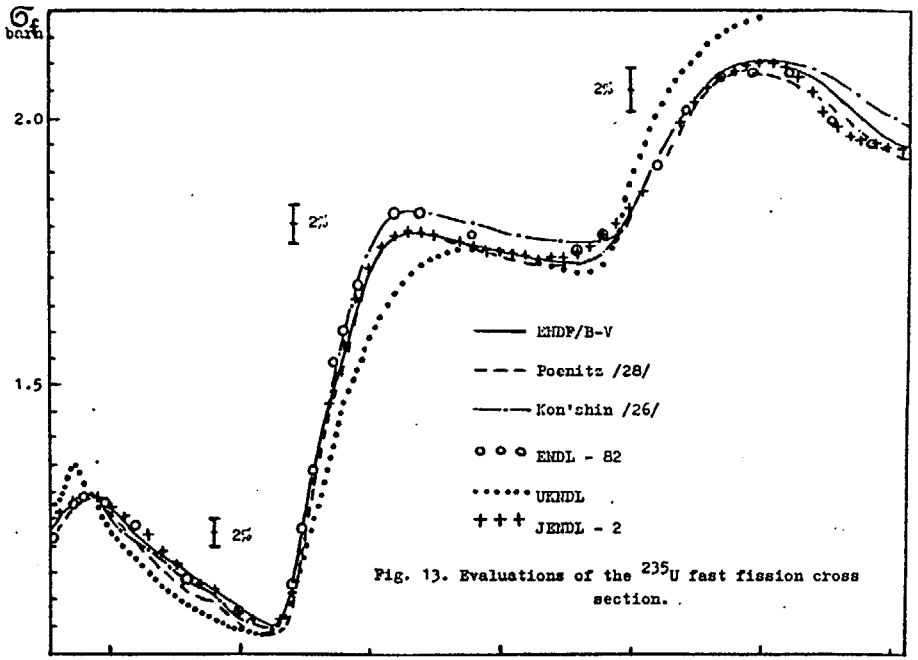

Fig. 13. Evaluations of the ^{235}U fast fission cross section.

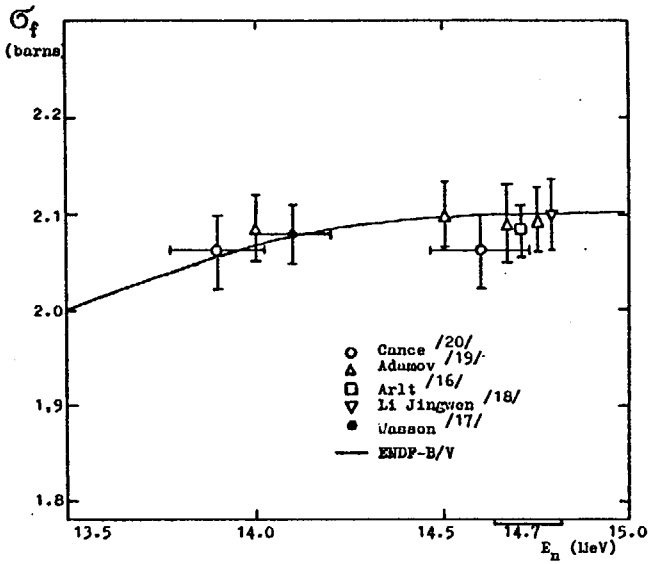

Fig. 14. Results of the ^{235}U fission cross-section measurements by the TCAPM with 14.0 - 14.7-MeV neutrons.

The data disagreement in the 1 to 5 MeV energy range exceeds 10% and difference in shape occurs as well. Although evaluations of different files agree rather well, the results of both measurements by the TCAPM /23/ and the recent shape measurements /3, 6, 10, 27/ which are in good agreement are 5% lower. It shows that existing evaluations may be doubtful. To elaborate more realistic evaluation the weights of some experimental results are to be revised. Concidering the available data it appears that it would be difficult for an evaluation to achieve an accuracy 1 - 2%.

Conclusion

It is obvious that the available experimental data for the ^{235}U do not yet reach the required accuracy except the 14 MeV point. What concerns other nuclides the data accurasies are much worse. Apparently the shape measurements techniques include some experimental discrepancies origins, which can not be identified now. There is essentially no value in producing more shape measurements using established technique, as additional ones will contribute little towards the reduction of the uncertainties.

According to recommendations of the IAEA consultant's meeting on the ^{235}U fast fission cross section held at Smolenice, CzSSR in March 1983, the only foreseeable way of improving the accuracy of the cross-sections is to perform:

i) accurate mono-energetic measurements using the TCAPM at as many energies as possible with the focus on discrepant regions,

ii) essentially improved shape measurements which can be used to determine the cross-sections between the spot point data.

References

1. Barton D.M. et al. - Nucl. Sci. and Eng., 60, 369 (1976).
2. Poenitz W.P. et al. - Nucl. Sci. and Eng., 53, 370 (1974).
3. Poenitz W.P. et al. - Nucl. Sci. and Eng., 64, 894 (1977).
4. Meier M.M., Wasson O.A., Duvall K.C. - Nucl. Cross Sect. for Technology; Knozwille, USA, 1979, (NBS Spec. Publ. 594, Washington, USA, 1980) p. 747.
5. Poenitz W.P. - Nucl. Instr. and Methods, 109, 413 (1973).
6. Poenitz W.P. ANL-7915, Argonne, USA, (1972).
7. Meier M.M. et al. "Nuclear Cross Sect. and Technology". Proc. of Internat. Conf., Washington D.C., USA, 1975. (NBS Spec. Publ. 425, Washington, USA, 1975) v. 1, p. 75.
8. Czirr J.B., Sidhu G.S. - Nucl. Sci. and Eng., 57, 18 (1975).
9. Carlson A.D., Patrick B.H., "Neutron Phys. and Nucl. Data for Reactors", Proc. of Internat. Conf., Harwell, UK, 1978, p. 881.
10. Wasson O.A., Proc. of NEANDC/NEACRP Spec. Meeting on Fast Neutr. Fission Cross Sect. of U-233, U-235, U-238 and Pu-239, Argonne, USA, 1976 (ANL-76-90, 1976) p. 237.
11. Lengers B., Cierjacks S., Brots P. et al., Ref. 10, p. 246.
12. Kari K., Cierjacks S., Ref. 9, p. 905.
13. Hopkins J.C., Breit G. - Nucl. Data Tables, A9, 137 (1971).
14. Cance M., Grenier G., Ref. 10, p. 257.
15. Alkhazov I.D. et al. "Neutron Physics", Proc. of 2-nd All-Union Conf., Kiev, USSR, 1973 (Obninsk, USSR, 1974) v. IV, p. 13.
16. Arlt R. et al. Ref. 4, p. 990.
17. Wasson O.A., Meier M.M., Duvall K.C., Nucl. Sci. and Eng., 80, 882 (1982).

18. Li Jiugwen et al. Proc. of Int. Conf. on Nucl. Data for Sciens and Technology, Antwerp, Belgium (1982)
19. Adamov V.M. et al. Ref. 4, p. 995.
20. Cance M., Grenier G. - Nucl. Sci. and Eng., 68, 197 (1978).
21. Arlt R. et al. Report ZfK-350, Dresden, GDR (1978), p. 209.
22. Alkhazov I.D. et al. Proc. of the X-th Internat. Symp. on Selected Topics of Interact. of Fast Neutr. with Nuclei, Gaussig, GDR, 1981 (ZfK-459, 1981), p. 40.
23. Arlt R. et al. Ref. 22, p. 44.
24. Dushin V.N. Proc. of the VIII-th Internat. Symp. on Interact. of Fast Neutr. with Nucl., Gaussig, GDR, 1978 (ZfK-382, 1979), p. 153.
25, Arlt E. et al. Preprint, Technical University of Dresden, GDR, 05-5-79, 1979.
26. Kon'shin V.A. et al. INDC (CCP)-148/L (1980).
27. Carlson A.D. IAEA Consultant's Meeting on ^{235}U Fast Neutron Fission Cross Section and ^{252}Cf Spontaneous Fission Neutron Spectrum, Smolenice, CzSSR, 1983.
28. Poenitz W.P., ANL/NDM-45 (1979).
29. Szabo I., Leroy J.L., Marquette J.P., Ref. 15, v. 3, p. 27.
30. White P.H. - Nucl. Energy, A/B, 325 (1965).

PULSED-BEAM ELECTROSTATIC ACCELERATORS AT THE I.V. KURCHATOV INSTITUTE OF ATOMIC ENERGY. INVESTIGATIONS OF FISSION ISOMERS PERFORMED AT THESE DEVICES

G.A. OTROSHCHENKO
I.V. Kurchatov Institute of Atomic Energy,
Moscow, Union of Soviet Socialist Republics

Abstract

Main principles to produce pulsed ion beams at the electrostatic accelerators in the I.V.Kurchatov Institute of Atomic Energy are briefly described. The parameters obtained for the ion current pulses are given. Some results of fission isomer investigations performed with pulsed beams of ions are shortly discussed.

At the moment the electrostatic accelerators are widely-applied devices. They are used in medicine, biology, metal science, in many branches of industry and last but not the least in their traditional field, i.e. the experimental nuclear physics.

High stability in the energy of the accelerated partciles (of the order of few hundredths of per cent), relatively high value of the current of the beam, up to hundred microamperes and more, the possibility to obtain the beam cross-over on the target of the order of tenth of millimeter, and even significantly less in special cases, the possibility to build accelerators (including the machines of the tandem type) to obtain the ions with energies in the range from hundreds of keV up to tens of MeV, along with comparatively simple construction of these machines, all these factors make them rather a cheap instrument of high qualitative value in numerous investigations in pure science or applications.

The high intensity of the accelerated particle beams makes it possible to perform the investigations with the use of secondary particles from nuclear reactions, induced by the primary beam in different targets. This fact widens considerably the possibilities of the

use of such accelerators. Thus, the use of tritium or lithium targets, bombarded with accelerated protons, or deuterium or tritium targets, bombarded with deutrons, gives us a possibility to perform the researches with neutrons in a wide region of neutron energies: from few tens of keV up to few MeV and more (17 MeV in the case of the T (d, n)^{3}He reaction). The neutron energy depends on the energy yield in the reaction, the primary beam energy, as well as on the angle between the primary beam direction and the detector position, as seen from the target. The neutron energy spread, or the energy resolution, depends on the energy spread in the primary beam, the solid angle of the neutron detector, the energy losses of the primary beam in the target, the energy yield and the kinematics of the reaction in use.

A considerable amount of experimental works in nuclear and neutron physics was done at the electrostatic accelerators with the use of primary and secondary beams of particles.

Since various methods were developed for these accelerators to obtain the pulsed beams, that is the beams the intensity of which changes with time according to a known law, the number of problems solved by using the electrostatic accelerators became significantly larger. These methods gave the possibility to investigate the time characteristics of the reactions and their products, which in some cases are more decisive (the half-lives of the reaction products, for example), the energy values, which characterize the reaction products (the energy and momentum measurements by the time-of-flight method), measurements of different time correlations in the processes under investigation.

The simplest way to obtain the beam with the time-modulated intensity is the use of electrostatic deflection of the accelerated beam. An electrostatic field, which is periodical in time, exists in the region of the deflecting system (Fig. 1). Thus, the transverse beam is periodically deflected from the straight trajectory in the absence of the field. The end of the beam moves over a diaphragm. When the beam passes through a hole in the diaphragm, the total current of particles from the accelerator hits the detector or the target. The rest of the time the beam is absent.

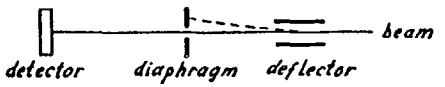

Fig. 1. The scheme of a simple deflecting system.

The use of a sine-shaped deflection field acting in a single plane permits the beam to go through the hole in the diaphragm twice for a period. The beam current hitting the detector or the target is shown schematically in Fig. 2, where Δt is the time when the beam moves through the hole in the diaphragm, and T is the period of the deflecting field.

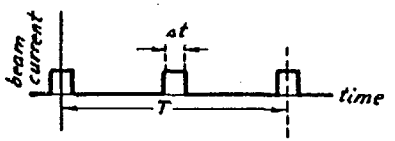

Fig. 2. The modulation of the beam intensity with time.

It is clear that the magnitude of Δt is one of the principal characteristics of the method: it is the time resolution of the experiment, i.e. the accuracy in the determination of a time moment. It dependes on the diameter of the hole and the velocity at which the end of the beam moves across the diaphragm. This velocity, in turn, depends on the amplitude and frequency of the deflecting field, as well as on the distance between the deflector and the diaphragm. Thus, the reducing of D, the hole diameter, the increasing of V, the amplitude, and ω, the frequency of the deflecting voltage feeding the deflector and the increasing of the distance L between the deflector and diaphragm lead to the reduction of Δt, i.e. the time resolution increases according to:

$$\Delta t = k\frac{D}{V\omega L} \qquad (1)$$

where k is a constant coefficient.

By changing the values in the right way, it is possible to make the value of Δt as small as it is needed. But there is another significant value which also chracterizes the system under consideration. It is the coefficient of use of the beam current. As soon as

the beam goes across the hole in the diaphragm twice per period, the total current I hits the detector (or the target) for the time $2\Delta t$, whereas the rest of the time the beam is absent. It results in the average value of the beam current hitting the detector according to:

$$\langle I \rangle = I \frac{2\Delta t}{T} \qquad (2)$$

that is the coefficient of use of the beam current equals to:

$$\eta = \frac{\langle I \rangle}{I} = 2 \frac{\Delta t}{T} = 4\pi\omega \, \Delta t \qquad (3)$$

or, if (1) is used for Δt,

$$\eta = 4\pi \, k \frac{D}{VL} \qquad (4)$$

It is seen from (4) that the changes in D, V and L, which improve the time resolution of an experiment, simultaneously decrease the coefficient of use of the beam current. This, naturally, decreases the counting rate of the investigated reactions. Thus, the need arises to increase the time of experiment to obtain a satisfactory statistical accuracy of the measurements. The increasing of the frequency T, of course, has no influence on the coefficient of use of the beam current. But such a change in the frequency reduces the value of T hence reducing the time between two successive pulses of current, i.e. the time during which it is possible to measure the time characteristics of the process under investigation.

For example, if the half-lives of reaction products are investigated, the high value of the repetition rate for the beam pulses could result in counting the events caused by many successive pulses of the beam, thus making the analysis of the data obtained more complicated or even completely impossible.

Of course, the situation can be improved, to some extent, if the deflector is fed by the voltage of a special shape, for example, by rectangular pulses, but the main features of the method are just the same. These shortcomings put certain limits for the use of such a simple method. Nevertheless, in a number of cases when the average counting rate of the reactions under investigation is high enough to obtain the sufficient accuracy at a required time resolution, the method is widely used.

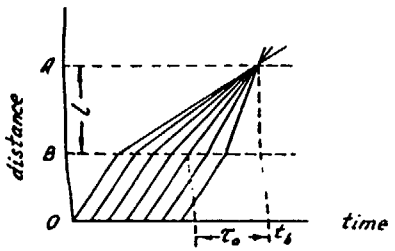

Fig. 3. The phase trajectories of the grouping ions.

Namely, such a method was used, for example, at the I.V.Kurchatov IAE in the USSR during the experiments with the fission isomer in the reaction $^{241}Am\ (n, \gamma)^{242mf}Am$ [1].

Wider experimental possibilities are given by another method, which is successfully used at present time. This method is known as a method of clystron-like grouping of particles in the beam. The main idea of the method is to change the velocity of ions leaving the ion source at different moments of time and having comparatively low energy (usually of the order of few tens of keV) so as to slow down the ions which left the source earlier and to speed up those which left it later. Then, at a definite distance from the place where the velocities were changed the ions will come together. This can be demonstrated by the diagram in Fig. 3. Here, the horizontal axis represents the time, the vertical one represents the distance. The point O is for the ion source, the point B, for the buncher, i.e. the device, which changes the energy (or the velocity) of ions. The straight lines indicate the path of an ion as a function of time. In the region between O and B all the lines are parallel, because the ions which left the source at different moments of time have the same energy and, hence, the same velocity. After B, i.e. after the buncher, the straight lines are changed for different ones. It corresponds to the fact that now the ions have different velocities. For the ions, which went through the buncher earlier, the inclination of the trajectory is larger than that before the buncher. It means that the velocity of such ions is less than that after leaving the source. The later the ion goes through the buncher, the less is the inclination of the trajectory. The latest ions have inclinations of trajectories

less than those before the buncher, i.e. their velocities have increased. After that the cycle of the velocity change is repeated. At the level A all the trajectories come together at a single point. All the ions will be at a distance l between B and A at the same time moment t_b and the grouping of the ions will take place. In this case the distance l is called a "grouping length". It is rather easy to obtain the value of an ion after the buncher. Let us consider the ion which has passed through the buncher at the moment t. At the moment t_b the ion must be at a distance l from the buncher, that is:

$$v(t) = l/(t_b - t) \tag{5}$$

How great is the energy change of the ion in the buncher? The ion energy before the buncher equals to:

$$qV_o = \frac{m}{2} v_o^2 \tag{6}$$

where m is the ion mass, q is the ion charge, v_o is the ion velocity before the buncher. After the buncher the ion energy must be equal to:

$$qV_1(t) = \frac{m}{2} v^2(t) = \frac{m}{2} \frac{l^2}{(t_b - t)^2} \tag{7}$$

Thus, the energy change of the ion must be:

$$q\,\Delta V(t) = qV_1(t) - qV_o = \frac{m}{2} \frac{l^2}{(t_b - t)^2} - \frac{m}{2} v_o^2 \tag{8}$$

or:

$$q\,\Delta V(t) = \frac{m}{2} v_o^2 \left[\frac{(l/v_o)^2}{(t_b - t)^2} - 1 \right] = qV_o \left[\frac{\tau_o^2}{(t_b - t)^2} - 1 \right] \tag{9}$$

where $\tau_o = l/v_o$ is the time during which the ion of the initial velocity moves over the grouping length distance.

Hence, to change the energy in the right way, the ion must meet an additional to that of the ion source potential in the buncher:

$$\Delta V(t) = V_o \left[\frac{\tau_o^2}{(t_b - t)^2} - 1 \right], \tag{10}$$

if V_o is the ion beam potential before the buncher. The ratio of the changing with time buncher potential to the constant in time ion source potential is:

$$\frac{\Delta V(t)}{V_o} = \frac{\tau_o^2}{(t_b - t)^2} - 1 \tag{11}$$

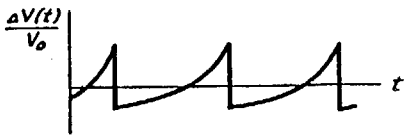

Fig. 4. The ideal time-modulated energy of the ions.

The graph of this function is represented in Fig. 4. The buncher usually consists of two coaxial cylinders with the potential $\Delta V(t)$ between them, the ion beam moving along the axis of the system.

Naturally, this is an idealized case.

To create the potential of the (11) shape one must overcome definite technical difficulties, because such a shape includes an infinite series of harmonics and each harmonic requires a noticeable amount of power due to inevitable energy losses. At the same time the capacity of the power supply, especially in case the power supply is mounted at the terminal of the accelerator, is always limited. That is why the grouping potential is, as a rule, of the sine-shaped form. In this case the grouping occurs only for the time intervals when the potential changes with time in accordance with ratio (11) (the solid part of the curve in Fig. 5). The deflecting system precludes the rest of the beam from going into the accelerator tube of

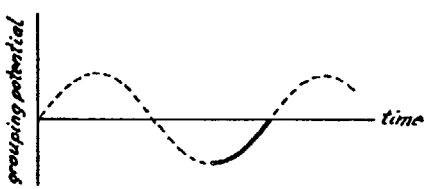

Fig. 5. The sine-shaped grouping potential.

the machine. It is clear that in this case the coefficient of the use of the beam current is also less than unity but it could be much greater than that of the first method.

Let us supply the grouping gap with the potential:

$$V(t) = V_m \sin \omega t \tag{12}$$

Then the total energy of the ion which has passed through the gap at the moment t_i will be:

$$qV(t_i) = qV_o + q\Delta V(t_i) = qV_o\left(1 + \frac{V_\sim}{V_o}\sin\omega t_i\right) \qquad (13)$$

Let us denote the ratio of the amplitude of the grouping potential to the beam potential as α :

$$\alpha = V_\sim / V_o$$

Then we have:

$$qV(t_i) = qV_o(1 + \alpha \sin\omega t_i) \qquad (14)$$

As soon as $qV(t_i) = \frac{m}{2} v^2(t_i)$, and $qV_o = \frac{m}{2} v_o^2$, expression (14) gives the velocity of the ion after the grouping gap as:

$$v(t_i) = v_o(1 + \alpha \sin\omega t_i)^{1/2} \qquad (15)$$

If the grouping length is equal to l, the corresponding time is equal to:

$$\tau_g = \frac{l}{v(t_i)} = \frac{l}{v_o}(1 + \alpha \sin\omega t_i)^{-1/2} \qquad (16)$$

and the moment of the ion arrival at the point of grouping:

$$t_g = t_i + \tau_g = t_i + \tau_o(1 + \alpha \sin\omega t_i)^{-1/2} \qquad (17)$$

The dependence of t_g on t_i for different values of the parameter α is shown in Fig. 6. The dependence for $\alpha = 0$ (the lack of the grouping potential) is shown by the straight line, which goes from the point t_o at the axis t_g at the angle of $\pi/4$. An ideal case (expr. (11)) is shown by the dotted line. If the current before the grouping gap equals I_i, the full charge which has passed through the gap for the time dt_i is equal to:

$$I_i |dt_i| \qquad (18)$$

At the grouping length the same ions give the current I_g during the time dt_g, i.e. the full charge in this case will be equal to:

$$I_g |dt_g| \qquad (19)$$

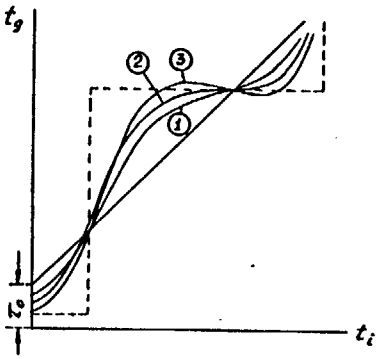

Fig. 6. The time of ion arrival at the grouping distance as a function of the moment the ion crosses the grouping gap.

Let us assume that the vacuum and the focusing of the beam are good enough for the charge not to be changed. Then

$$I_i |dt_i| = I_g |dt_g| \qquad (20)$$

and we have:

$$\frac{I_g}{I_i} = \left|\frac{dt_i}{dt_g}\right| = \frac{1}{|dt_g/dt_i|} \qquad (21)$$

From equation (17) we find:

$$\frac{dt_g}{dt_i} = 1 - \frac{\alpha\tau_o\omega}{2}\cos\omega t_i (1 + \alpha \sin\omega t_i)^{-3/2} \qquad (22)$$

and therefore:

$$\frac{I_g}{I_i} = \frac{1}{\left|1 - \frac{\alpha l \omega}{2v_o}\cos\omega t_i (1 + \alpha \sin\omega t_i)^{-3/2}\right|} \qquad (23)$$

Let us denote:

$$\gamma = \frac{l\omega}{2v_o} \qquad (24)$$

then

$$\frac{I_g}{I_i} = \frac{1}{\left|1 - \alpha\gamma \cos\omega t_i (1 + \alpha \sin\omega t_i)^{-3/2}\right|} \qquad (25)$$

At the given parameters α and γ the denominator in (25) has a minimal value if:

$$\sin(\omega t_i) = -\frac{\sqrt{1+3\alpha^2}-1}{\alpha} \text{ and } \cos(\omega t_i) = \frac{\sqrt{2(\sqrt{1+3\alpha^2}-1-\alpha^2)}}{\alpha} \quad (26)$$

that is

$$3/2\pi < (\omega t_i) < 2\pi \quad (27)$$

as it is seen in Fig. 5 (or curve 1 in Fig. 6). If the parameter α increases, the value of the denominator decreases, and with

$$\alpha = \sqrt{\frac{(1-\beta)(3-\beta)}{3}}, \text{ where } \beta = \frac{\gamma(\sqrt{6+\gamma^2}-\gamma)}{3} \quad (28)$$

the denominator in (25) turns to zero (curve 2 in Fig. 6).

If the parameter α increases still more, two points t_i appear, in which the denominator turns to zero. This situation is the overgrouping of the beam (curve 3 in Fig. 6). As soon as the initial beam has the definite ion energy spread, the parameter $\gamma = (1\omega)/(2v_0)$ has the spread, too. It means that it is not possible to choose the parameter α so as to satisfy equation (28) for all the ions. Usually, the value of the parameter α corresponds to an average energy of the ion in the beam. The ions with the energy exceeding the average value will be undergrouped, the ions with the energy lower than the average value, overgrouped (the full situation is shown in Fig. 6) and the beam pulse will be of finite width in time. There are some other reasons due to which the beam pulse turns to be of finite width. The ions in the beam move at different distances from the buncher axis, so the grouping potential differently affects different ions moving across the gap at the same time moment. The space-charge influence (the Coulomb repulsion) will also preclude the complete grouping.

In practice, the time width of the pulse of the order of one ns with the coefficient of the use of the beam current in the region of 20 - 25 per cent is usually obtained. Some special measures taken with decrease in the value of the coefficient of the use of the beam permit us to obtain the beam pulses with time width of tenths of ns. Among those are: an increase of the frequency of the grouping potential, the usual value of which is of the order of ten and more MHz, an increase of the initial (before the buncher) energy of ions, which in its turn requires the increased amplitude of the grouping potential with the usual value of few kV. Sometimes, to obtain the uniform conditions for the ions, travelling at different distances from the system axis, the grouping gap is provided with grids, which make the field between the electrodes more uniform. But the insertion of the grids results in additional losses of the current. The increase of the grouping frequency leads to decrease of the time interval between the successive pulses. To keep this time interval sufficiently large requires the use of a deflecting system to skip a few successive pulses. To be short, in each case one has to find a compromise solution of the problem in order to meet the experimental requirements best.

One more significant circumstance should be noted. As soon as the method of the clystron-type grouping is based on an artificial change of the ion energy, it leads to an increase of the energy spread for the ions constituting the beam pulse. The value of the energy spread by the order of magnitude coincides with that of the grouping potential amplitude and can reach the magnitude of one or two keV. This value is noticeably higher than that for the ions going from the ion source. In a large amount of experiments this value does not exceed the limits of the energy resolution required. Nevertheless, another problem arises. This problem is concerned with the beam focusing. The whole accelerating path long from the ion source to the outlet of the accelerating system comprises, in fact, a complicated multi-element optical system, which focusing properties are, in general, strongly dependant on the ion energy. The very grouping gap itself represents an electrostatic lens, the focal length of which changes with time. The energy of the ions coming into acceleration changes with time, too. Therefore, the installation of the system of the clystron-type grouping puts special requirements to the focusing properties of different elements of the ion-optical system of the accelerator. However, under the reasonable approach to the choice of the parameters and construction of the system the arising problems can be solved. It is enough to say that the method of the clystron-type grouping is more often used in practice. Such a method

was realized at one of the electrostatic accelerators in the I.V.Kurchatov IAE [2]. The main pulse features of this accelerator are as follows: the pulse duration equals 1.5 ns, the repetition rate of the pulses of the accelerator target is 2 MHz, the average current under these conditions is 8 microamperes. This accelerator was used in the following experiments: partial cross-section measurements for inelastic neutron scattering on ^{238}U [3], the fission isomer yield in the reaction ^{236}U (n, n')$^{236mf}U$ [4], the measurements of the cross-section ratio for the radiative capture and fission of ^{235}U [5], etc.

In the description of the two methods for obtaining the pulsed beams the works devoted to the fission isomers investigations and performed with pulsed beams have been mentioned. I would like to say a few words about the problem.

Fission isomers represent the nuclei of the heavy elements, which are staying in special excited states. The main feature of these states is that the life-time of such a state is unexpectedly large, i.e. from tenths of ns up to hundredths of s, along with a rather high excitation energy (somewhat 2.5 - 3.5 MeV over the ground state). Radiative transitions for these nuclei seem to be strongly forbidden, the neutron emission is precluded by the energy relations (the binding energy of the neutron is of the order of 5 MeV). Therefore, these nuclei exhibit the fission activity with the life-times in the said interval. The fission activity represents nearly unique feature of the fission isomer, due to which these isomers are recognized experimentally. At the moment the widely-accepted point of view is that the fission isomers are a sequence of the existence of the second stable state of the nucleus at a rather large deformation. Therefore, the fission isomers are often called shape isomers. This hypothesis permits us to explain (in many cases only qualitatively) many features of the phenomemon but such an explanation could not be regarded as an experimental verification of the hypothesis. In particular, it is one of the reasons why the attempts to obtain such an obvious experimental evidence as a large deformation in such states are made up to now. In some cases the experiments are aimed at checking some sequences of the accepted hypothesis.

The concept of the fission isomer of ^{242}Am as a shape isomer, along with the analysis of the experimental data on the prompt fission cross-section in the ^{241}Am (n, γ) reaction as a function of the neutron energy brings about a conclusion that the ratio between the cross-sections for the fission isomer production and for the prompt fission must be a weak function of the neutron energy. The single factor which is strongly dependent on the energy is the penetrability of the potential barrier between the two stable states: at the equilibrium deformation and at that corresponding to the shape of the fission isomer. But this factor influences both the channels under consideration.

The experimental data obtained partly at the Joint Institute for Nuclear Research in Dubna [6] and partly at the Institute of Atomic Energy in Moscow [1] are shown in Fig. 7. It is seen, the ratio of the yields for two channels regarded slowly changes with the energy in the region from one to five MeV. But as soon as the neutron energy goes below 1 MeV the situation changes rapidly and in the approximately 0.5-MeV energy interval the ratio changes by the order of

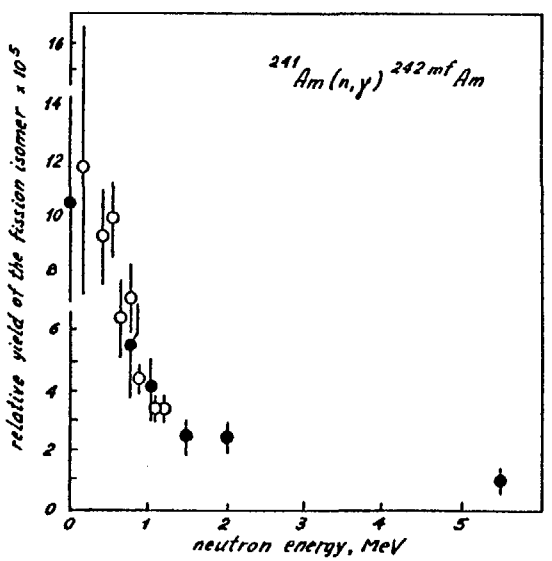

Fig. 7. The relative yield of the fission isomers in the ^{241}Am (n,γ) $^{242mf}Am$ reaction.

magnitude for the benefit of the isomer production. It is known from the analysis of the fission cross-section that the fission barrier (the barrier between both stable states in this case) lies in the region of 1 MeV of the neutron energy. Therefore, the experimental data shown in Fig. 7 give us a reason to suppose the isomer production channel does not go through the barrier, wheras the prompt fission does. In such a case the isomeric state is coupled with the equilibrium ground state deformation of the nucleus.

Ref. [7] reported the excitation function for the production of the ^{238}U fission isomer in the inelastic neutron scattering reaction. It was noted, the isomeric yield in this reaction is by the order of magnitude higher than the usual value in reactions with the radiative capture of neutron. Besides, it was noted the cross-section of the isomer production seems to have a local maximum near the reaction threshold.

The existence of such a maximum is hard to understand in the frame of the shape hypothesis. It is not clear either how to explain the amplification of the isomer yield in the (n, n') reaction.

To obtain additional experimental data the work [4] was done to investigate the yield of the fission isomer of the ^{236}U in the inelastic neutron scattering reaction as a function of the neutron energy. The data obtained are shown in Fig. 8. As it is seen, the cross-section for the ^{236}U isomer production in the (n, n') reaction again has a local maximum just near the reaction threshold. Besides, the

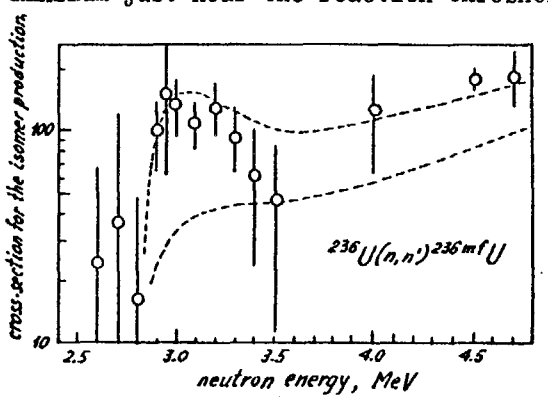

Fig. 8. The cross-section for the fission isomer production in the ^{236}U (n, n')$^{236mf}U$ reaction.

cross-section has the value near 200 microbarns, which is by the order of magnitude higher than usual values for the (n, γ) reaction (tens of microbarns).

If one supposes the fission isomers are coupled with the equilibrium deformation of the nucleus and the spin values play a significant role in the isomer production, rather simple evaluation shows that the local maximum and amplification of the cross-section value can easily be explained. The local maximum is due to the right without intermediate radiative transitions population of the isomeric state in the (n, n') reaction. The cross-section for this process decreases rapidly with the neutron energy. The cross-section for the population of the isomeric state through the intermediate radiative transitions increases more slowly. The sum of both means of isomeric state population gives the curve with the local maximum near the reaction threshold. The amplification of the isomer yield in the (n, n') reaction as compared with the case of the (n, γ) reaction is simply due to the fact that the inelastic scattering process can transfer to the residual nucleus the spin value higher than the radiative capture process does.

The smooth curves in Fig. 8 show the values of cross-sections of the isomer production for two spin values evaluated under a number of simplifying suppositions.

Of course, one should not regard the experimental data shown in Figs 7 and 8 as a final solution of the problem, but these data seem to be a serious alternative to the hypothesis of the shape isomerism.

REFERENCES

1. P.E.Vorotnikov, G.A.Otroshchenko, "Energetic dependence of the yield of the fission isomer in the reaction ^{241}Am + n". Neutron Physics, part 5, page 241, Moscow (1976).
2. P.E.Vorotnikov, V.A.Vukolov, M.L.Ganzeljuk, L.D.Kozlov, E.A.Koltypin, Yu.D.Molchanov, G.A.Otroshchenko, G.B.Yankov, "Neutron spectrometer based on the pulsing ESA". Neutron Physics, part 4, page 238, Moscow (1977).

3. P.E.Vorotnikov, V.A.Vukqlov, E.A.Koltypin, Yu.D.Molchanov, G.A.Otroshchenko, G.B.Yankov, "Fast neutron scattering on the U-238". Neutron Physics, part 2, page 119, Moscow (1977).
4. S.V.Dmitriev, G.A.Otroshchenko, "The production of the fission isomer of uranium-236". The Problems of the Atomic Science and Technology. Div. NC, is. 1 (40), 1981.
5. P.E.Vorotnikov, V.A.Vukolov, E.A.Koltypin, Yu.D.Molchanov, G.B. Yankov, "The measurements of the ratio between the capture cross-section and the fission cross-section for ^{235}U". Neutron Physics, part 1, page 314. Scientific Thought, Kiev (1972).
6. T.Nag, A.G.Belov, Yu.P.Gangrsky, B.N.Markov, I.V.Sizov, I.F.Kharosov, "Investigation of the reactions of the radiative capture of fast neutrons leading to spontaneously fissioning isomers of ^{242}Am and ^{244}Am". Preprint JINR, R7-5162, Dubna (1970).
7. K.L.Wolf, J.W.Meadows, Bull. Am. Phys. Soc. 19, 995 (1974).

THE NEUTRON ACTIVATION ANALYSIS USING NUCLEAR REACTORS

A.A. KIST
INP AS Uzbek SSR,
Tashkent, Union of Soviet Socialist Republics

Abstract

A review on the activation analysis techniques used for both fundamental and applied research at the Institute of Nuclear Physics of the UZSSR Academy of Sciences is presented.

The development of the present-day science and engineering in nearly all the directions is, to this or that degree, connected with the methods of studying matter composition and structure. This fact accounts for intensive development of modern analytical methods. In this regard, of special importance are nuclear-physical and radioanalytical methods. This extensive group includes various methods based on interaction of nuclear radiation with matter or those based on similarity of the stable elements behaviour and their radioactive nuclides. Similar instrumentation and closeness of theoretical bases permit so different methods as nuclear-activation, X-ray fluorescent, that of isotope dilution and many others to be integrated into a complex under the conditions of one laboratory.

The radio-activation analysis has been being developed for more than 40 years. As far back as 20 years ago it was possible to refer to it as to a "laboratory oddity" but at present it is a method which is used most extensively for various investigations. The appearance of accessible and powerful nuclear reactors started the development of neutron radio-activation analysis. In the 50es this method was basically used to analyze microimpurities in pure and semiconductor materials and rocks. Usually, the analytical methods involved employing deep radiochemical separation and purification in combination with primitive (from our point of view) counting equipment utilizing gas-filled counters. The development

of scintillation gamma-spectrometry increased the analysis efficiency considerably and the number of cases when this method was used in geological exploration grew larger. The appearance of high-resolution germanium-lithium, germanium and silicon-lithium detectors of gamma-radiation became another important step in the development of the method. At the same time the instrumental method sensitivity, its efficiency and multielement analyzing were raised significantly, the radiochemical procedures were simplified. It allowed us to increase the importance of the part played by this method in analyzing biological and natural samples (in natural sciences). At the present moment they amount to 30%. Now the radio-activation analysis is performed at large-scale nuclear centres employing nuclear reactors, as well as in specially-made analytical nuclear reactors. Use is made of cyclotrons, betatrons and other accelerators of charged particles, neutron generators, isotope sources of neutrons not only at the laboratories but immediately at industrial installations and plants. The activation analysis has become an indispensable component part in a number of engineering processes.

The basis of the nuclear activation methods is the measurement of induced radioactivity resulting from nuclear reactions in bombardment of a sample by charged particles, neutrons or γ-quanta. Since the induced activity value and, hence, that of sensitivity depend, apart from other reasons, on the cross-section of the nuclear reaction and sensitivity of the activating radiation, the neutron activation analysis by the (n, γ) reaction has been used most commonly for a number of problems. The reaction cross-section is very high for a lot of elements (in nuclear reactors with neutron fluxes up to 10^{15} n/cm^{-2}s^{-1}).

In this case the induced activity is described by the eq.:

$$A = \frac{N_f \sigma \theta \, m \, (1 - e^{-\lambda t})}{M} e^{-\lambda \tau}$$

where A is the number of decays per second; N is the Avogadro number; f is the neutron flux; σ is the activation cross-section; θ is the relative abundance of the activated nuclide; m is the mass of the element; λ is the decay constant of the analytical radionuclide; t is the activation time; τ is the "cooldown" time; M is the atomic weight of the element.

As seen from the equation, the activity depends on the activation cross-section of the neutron flux density, on the activation time and the "cooldown" time.

It should be noted that the above-mentioned expression descibes the activation process in the approximation sufficient for the experiment designing but not for the exact measurements or absolute (without a standard) method of analysis. To obtain a more exact expression, one should take into account the effect of secondary reactions (reactions on fast neutrons resulting in formation of one nuclide from different stable nuclides), reactions of the second order (those in which the nuclide formed undergoes a nuclear reaction once again and another nuclide is formed), the burn-out effect (when at high activation cross-sections and densities of a neutron flux the loss of the natural initial stable nuclide becomes appreciable), the self-shielding effect and other effects of the flux perturbation, the change of the activation cross-section with the neutron energy variation, the effects of neutron flux scintillations at short-time irradiation, etc.

Since in the exposure in a nuclear reactor dozens of radioactive nuclides may be produced, the main problem to be solved by an experimenter in developing analytical methods is the reliable measurement of the analytical nuclide activity against the background of a large number of impeding nuclides.

For this purpose various procedures are used. For example, varying the time conditions of the analysis (the exposure and "cooldown" time), one can obtain a reliable release of the activity of short-lived nuclides against the background of long-lived ones or vice versa. The fact that the activation cross-section changes with the neutron energy differently for different nuclides permits us varying the neutron flux spectrum within the known limits to change the relation of the activities of different nu-

clides. For example, applying a cadmium layer around a sample (other substances absorbing neutrons in a definite energy range are also used), one can succeed in reducing the activation degree of a number of nuclides (e.g., for ^{24}Na by a factor of 20 - 40) if the reaction proceeds mainly with thermal neutrons and, thus, in increasing the selectivity of determination of elements whose nuclides have resonance levels of activation in the range of epithermal neutron energies. On the contrary, the exposure in the thermal column of the reactor where thermal neutrons are predominant permits the influence of the epithermal-neutron reactions to be reduced and the part played by the fast-neutron ones to be practically reduced to zero.

The most commonly used method for increasing the analysis selectivity is the γ-ray spectrometry. The difference in the γ-ray energies makes it possible to determine from three to ten elements in a sample by means of the γ-spectrometric scintillation detectors and from 40 up to 45 elements in one sample using high-resolution γ-spectrometric ones.

Some more sophisticated instrument methods are also used, such as coincidence systems which reliably separate nuclides with the decay of a cascade nature, those of anticoincidences which, on the contrary, suppress the contribution of the cascade radiation, etc.

The methods of magnetic beta-spectrometry, those of detection of beta- and alpha-radiation, fission fragments, delayed neutrons, etc., are less widely used in the neutron activation analysis though in some cases they are extremely effective.

Though being extensively applied in various versions of the activation analysis, these and other methods constitute the basis of the instrumental version when decomposition of a sample does not take place.

Provided that the procedures of the neutron activation analysis are insufficient, the radiochemical version is used. In this case an element or a group of elements to be determined is separated by purification from impeding emitters or by isolation of the impeding nuclides themselves.

For this purpose use is made of practically all the methods of modern analytical and preparative chemistry: precipitation, extraction, ion exchange, distillation, different variants of extraction chromatography, isotope exchange, the recoil effect (the Scillard-Chalmers effect), electrochemical and many other methods. In this connection one should mention the little-used possibilities of thermochromatography (for example, in a chlorine flow) when a sample is stripped and its components are separated in one stage. This method is particularly convenient in a case of diffi-cultly soluble samples of, for example, rocks and minerals. In the radiochemical version use is often made of the so-called carriers or collectors which allow us to replace the manipulation of ultramicroquantities of chemical elements with that of their weight quantities and even to carry out nonquantitative isolation of elements if testing of the chemical yield has been provided for or use is made of substoichiometric methods of separation.

Sometimes, in order to increase the sensitivity and to remove the impeding elements, the element or a group of elements to be determined are preliminary concentrated.

This method may be considered to be an intermediate one between the instrumental and radiochemical versions, since the chemical procedures are carried out with inactive materials and can be realized at common laboratories, including those situated far from nuclear centres, while the measurements of activity have all the advantages of the instrumental analysis. In so doing, the initial sample may be considerably greater than the dimensions of the radiating channel or the radiation safety requirements allow. The preliminary concentration is particularly convenient for the analysis of liquid samples, when their storage and transportation is difficult due to their considerable volumes and when the danger of sample contamination or loss of individual elements as a result of interaction with the walls of containers becomes of greatest importance. The main disadvantage of this method is its dependence on purity of reagents and materials used and the analysis final sensitivity being higher than that of the instrumental analysis and lower than that of the radiochemical one, which is determined by the value of the "blank test" correction.

The concentration of an element can be determined by calculation from the activation equation but this method is practically not used because it requires the measurement of the absolute activity and because the parameters entering the equation may be known with insufficient accuracy. More frequently the relative method is used when the activity of a nuclide of a known amount of the initial element (a standard, a reference) is compared with that of a nuclide in the sample analyzed. In this case use is made either of the standards prepared by covering suitable substrates (a paper filter, quartz, etc.) with microvolumes of solutions of the elements to be determined, or of standard comparison samples made on the basis of a material similar to that being investigated, or of artificial mixtures of elements in concentrations close to the composition of the sample investigated (in this case the mixtures are fixed with an appropriate binder to give the standard a reproducible shape). It is possible to introduce the element to be determined into the matrix being investigated (the method of admixtures), to use some macrocomponent of the matrix as a standard (the inner standard) or to employ only one standard for one element with recalculation (conversion) to other elements using ratios established earlier (a monitor, a monostandard).

The main advantages of the activation analysis and of its versions are the following:

- the high sensitivity. In some cases the detection limit may reach 10^{-13} - 10^{-14} g. It is clear that the maximum sensitivity is realized in the radiochemical version;
- the use of samples of any weight. Under suitable conditions (in the absence of highly neutron-absorbing nuclei) the analysis can be made for samples weighing from decimal fractions of a milligram (e.g., in the analysis of almost inaccessible biostructures, in the local analysis and in the analysis of monomineral fractions) to several kilograms and even dozens of kilograms (this case is realized, for example, in the analysis of parts of bodies or bodies of experimental animals or human beings "in vivo");
- the analysis is practically independent of corrections for the blank test (except for the analysis with preliminary concentration) since all the contaminations introduced into the sample after its activation do not affect the analysis results since they are nonradioactive;
- the high capacity. In the instrumental version hundreds of samples can be analyzed daily. When the analysis is made for short-lived nuclides, a high proximity of the analysis is also attained;
- the analysis is independent of the valent state of the element and kind of the compound it is contained in;
- the analysis is a multielement one. In most of the cases several elements can be determined simultaneously and, if such a problem is offered, up to 40 - 50 elements can be determined in one sample;
- the possibility of using automatization: the instrumental analysis may be automated to some extent, which simplifies essentially the technique. In this case the sample is automatically transported for exposure and computers of various classes are used for measuring and processing the information obtained.

The activation analysis has some specific disadvantages. Among them are the possible production of one and the same nuclide in different reaction channels, radiation processes during irradiation, possible errors resulting from neutron absorption by some nuclei, etc., which should be particularly taken into account. However, all these disadvantages are compensated for enough by means of a number of special procedures.

Correctness of the activation analysis and its reproducibility, determined, in particular, by the value of recorded activity, are usually 10-20%, which is quite sufficient for the most of common problems, but can be increased up to values of the order of units (and in some cases even fractions) of relative percentage.

In general, the procedure of the activation analysis may be considered as a sequence of the following operations:

- design of the experiment including choice of the analyti-

cal nuclide and, hence, choice of the activation and "cooldown" time , choice of the neutron spectrum, sample weight, estimation of the probability of competing reactions or neutron absorption, choice of the sample and analysis method (instrumental, radiochemical, preliminary concentration) and choice of the detection system;

- selection of the sample, preparation of the sample to the experiment. In the simplest case the sample is packed into the polyethylene film, aluminium foil, quartz or polyethylene capsule. Possible impurities in the packing material should be taken into account. As all these materials are contaminated to some extent with various elements, the sample is often repacked, i.e. withdrawn out of the active packing and inserted in a non-active one;

- preparation of the standard. As has been mentioned above, most frequently a known amount of the element in the solution form is applied to and then dried on the suitable substrate or standard comparison samples are used;

- packing the samples and standards into separate bags or capsules and inserting them into a common block container or common capsule;

- irradiation of the samples and standards;

- hold out of the irradiated samples;

- repacking of the samples (in the case of the analysis of a high-purity substance, surface etching of the sample) conduction of radiochemical operations, if necessary;

- performance of the measurements;

- processing of the information and treatment of the result.

It should be taken into account that the neutron activation analysis is not only a method for determination of the total concentration of the element in the sample but can also be used for solving some problems of the behavior and distribution of the element in the substance.

For instance, it is possible to determine local concentrations of the element breaking the object under investigation into small fragments or scanning individual sections of the irradiated sample in the definite range of gamma-ray energies by means of the collimator. By scouring the material layers the concentration profiles of the element can be determined, which is very important for studying the diffusion and alloying of semiconductors.

The autoradiographic method can be used, under suitable conditions, for studies of the element distribution in flat samples. Detection of fission fragments or alpha-particles during irradiation by the solid-state detectors makes it possible to study distribution of boron and uranium with a high resolution.

Preliminary chemical treatment permits us to determine movable forms of elements in the plants, suitable for assimilation by the plants, to study the composition of subcellular strucutres, nucleic acids, proteins, etc. The fact that many pesticides contain such elements as chlorine, phosphorus, sulphur, zink, mercury, copper, bromine and other elements, makes it possible to detect the pesticides after their isolation. Use of special methods for catching aerosols and vapor-gaseous phase enables us to investigate air pollution by fractions and forms of the elements contained in the free air. By the combination of electrophoresis, ultrafiltration, electrodialysis and other methods dissolved, undissolved parts, colloid, complex, cation and anion forms of the elements can be separated from the waters. Other methods are also used to increase the information content of the activation analysis /1 - 5/.

Owing to many its advantages this method is being widely applied now in various fields of science and engineering /3-6/.

In geochemistry the high sensitivity of the method and possibility of detection of several elements simultaneously, when applying this method, are used, which permits many elements to be detected in the rocks. The possibility of analysing samples of small weights simplifies significantly selection and preparation of monomineral fractions. Of great importance for geochemistry are the local and autoradiographical methods for investigation of distribution of the elements in rock microsections.

The high capacity of the method made it possible to apply it successfully in the extractive and metallurgy industries. A number of automated machines for analysis of ores and technological products with the use of various versions of the activation analysis are known. Simultaneous detection of several elements permits as-

sociating elements to be detected, which enables more complex utilization of raw materials to be made.

The activation analysis is also important for technology of inorganic materials. In 50es a significant part of investigations on the activation analysis was devoted to the study of highly pure germanium and silicon. It is not an exaggeration to say that progress in semiconductor engineering is due, to a significant degree, to the high sensitivity of the radioactivation analysis. At present, the activation analysis is used in investigations of more complicated semiconductor materials, such as intermetallic compounds, etc., as well as in investigations of highly pure salts, studies of materials for reactor, laser and space engineering.

The high sensitivity and simultaneous determination of many elements are successfully used in ecological investigations of environmental pollution, particularly, in the problems of historical and background monitoring.

The same features as well as the possibility of analizing small weights of the samples are used in biological and medical investigations of variations in microelement concentration in the tissues of human beings and animals during various diseases. It is the activation analysis that attracted attention to possible part played by such elements as gold, rare-earth elements, scandium and others in the living beings, by iodine in the eye tissues, by manganese for diabetes, etc.

Very important are the efforts to use the activation analysis for the mass analysis for determining the risk degree for some diseases. The works on studying the element composition of the nuclei acids, subcellular structures, histons, etc.

In the agriculture the neutron activation analysis on the nuclear reactor may prove to be useful in studying the physiology of domestic animals and plants but, particularly, in abundance of microelements in the soil, including the forms (movable) suitable for assimilation by plants.

We can also mention such an exotic region as criminal law, where the neutron activation analysis with the use of the reactor is applied for determination of the contact of different objects with gold, for proving the poisoning with some elements, e.g. arsenic, for the establishment of the fact that the firearms have been used by the composition of the powder residue on the cheek and hand of a man who has used the arms, for identification of someone by the composition of someone's hair (note that such an identification is not unambiguous) and some other problems.

The above examples are far from exhausting the variety of possible applications of the neutron activation analysis with the use of the nuclear reactor.

The neutron activation analysis can be realized using some other sources. For example, in using the ^{252}Cf, Po-Be and other ampulla sources the activation analysis can be realized in the field and factory laboratories, in investigations of the sea ground, chinks, etc. The neutron generator permits us to extend the number of elements to be determined due to use of the fast neutron nuclear reactions. As has been mentioned, the neutron activation analysis can be realized on the cyclotrons, linear accelerators, betatrons, microtrons, subcritical fuel assemblies and breeders, etc. It is possible to determine the contents of the elements not only in the samples but also in the flow and in natural depositions.

In the presence of the neutron source the purely activation analysis can be supplemented by more particular methods, such as the neutron radiation analysis (with the recording of prompt gamma-rays), the delayed neutron method for determination of uranium, track autoradiographical method for the determination of uranium, boron, neutron absorption and scattering methods.

Finally, it should be pointed out that any laboratory possessing a neutron source (nuclear reactor and quite ordinary counting equipment: scintillation, proportional, gas-filled, semiconductor, etc. radiation detectors and recording instrumentation: scaling devices, discriminators, single- and multichannel analyzer, may use some other nuclear-physical and radioanalytical methods, in particular, X-fluorescent one with excitation of the characteristic radiation by

radionuclide sources, X-ray tubes and various accelerators as well as the isotope dilution method.

This complex of the methods permits most of the chemical elements of the periodic system to be determined in various matrices and in the widest range of concentrations, i.e. a varity of problems of the present day science and engineering to be solved.

The nuclear reactor can also be successfully used for production of isotope sources for small analytic laboratories. Among these sources of special importance, for some reasons, are antimony-beryllium sources. These sources represent one or several capsules containing ^{124}Sb surrounded by beryllium. Under the influence of ^{124}Sb gamma-radiation the (γ, n) reaction proceeds; the neutrons produced by this reaction can be used in the activation analysis, and ^{124}Sb sources can be produced, if necessary, in the research reactor.

For this purpose the aluminium block container of the standard size is filled with 200-250 g of melted metallic antimony. The block container is welded up by argon welding and checked for tightness. Then it is exposed to $5.10^{13} n/cm^{-2}s^{-1}$ flux for sixty days and left for "cooldown" for decay of the most short-lived isotope, ^{122}Sb. The sample obtained with an activity of about 4.10^{13}Bk is transported in a special container to the site, where the source is submerged into a special 2x2x3m tank filled with water. The 3-m thick water layer is a sufficient radiation shield. Under the water the source is inserted into the beryllium cylinder 180 mm in diameter and 80 mm high. As the source operates continuously under the water, the beryllium block is shielded with a 1-mm thick cover of sheet aluminium to avoid electrochemical corrosion. In this way the neutron source with a yield of about $10^{10} n/s^{-1}$ is formed. The beryllium block is shielded with an assembly containing 10-50 samples packed into the cylindric containers.

For a more complete use of neutrons the assembly can be surrounded with graphite. Such a source permits gold to be detected with a detection limit less than 10^{-4}%, indium, with that of 10^{-4}%. The main disadvantages of the source are a strong gamma-background of ^{124}Sb, which makes transport and transfer operations quite difficult, and the need for recharging the source with fresh block containers with irradiated antimony due to a relatively short half-life time of the nuclide.

The possibilities of the nuclear-activation analysis and its neutron version are far from being exhausted by the examples briefly enumerated above. The creation of special small-sized reactors (first of all the homogeneous ones), breeders and other sources could be of great importance for the development of this method. The use of the atomic station reactors might be of special importance for the neutron activation analysis purposes, which is quite possible and permissible from the point of view of the technological process. It is attested to by the experience of atomic nuclear power station operation gained in the USSR.

REFERENCES

1. G.Bouen, D.Giblons. Radioactivation analysis, Moscow, Atomizdat, 1968.
2. R.A.Kuznetsov. Activation analysis, Moscow, Atomizdat, 1965.
3. A.L.Yakubovich, E.I.Zaitsev, S.M.Przhiyalgovsky. Yadernofizicheskie metody analiza mineralnogo syrya, Moscow, Atomizdat, 1973.
4. A.A.Kist. Sovremennoe sostoyanie i perspectivy ispolzovaniya radioaktivatsionnogo analiza. Sb. Met. Analiza Prirod.Belkov. Problemy analiticheskoy himii, Moscow, Nauka, 1976.
5. A.A.Kist. Sovremennoe sostoyanie i perspectivy primeneniya yaderno-fizicheskikh metodov analiza v kontrole prirodnoy sredy. Sb. Yaderno-fizicheskie metody analiza v kontrole okruzhayushey sredy, Leningrad, Gidrometeoizdat, 1980, p. 4.
6. Sb. Aktivatsionny Analiz v nauke i tekhnike, Tashkent, FAN, 1980.
7. S.A.Bakiev, A.A.Kist, Zh.Rakhmanov, O.I.Askarov, G.G.Mingaliev. O vozmozhnosti sozdaniya polevykh i zavodskihk laboratoriy neytronno-aktivatsionnogo analiza na baze kalifornievogo i surmyano-berillievogo istochnikov neytronov, Tashkent, Preprint IYaF (INP) AN Uzbek SSR, P-3-95, 1982.

110 # ABSOLUTE MEASUREMENTS OF FISSION CROSS SECTIONS AVERAGED OVER THE FISSION NEUTRON SPECTRUM

L.V. DRAPCHINSKY
V.G. Khlopin Radium Institute,
Leningrad, Union of Soviet Socialist Republics

Abstract

The absolute fission cross sections averaged over the ^{252}Cf fission neutron spectrum are discussed. The calibrated ^{252}Cf neutron source technique, the time correlated and associated particle methods and related uncertainties are analyzed.

1. Introduction

1.1. Integral Measurements

Working in the field of nuclear data measurements experimenter may meet with measurements of two kinds: differential measurements and integral ones. In differential measurements the dependence on a single variable of some kind is investigated. In the case of fission cross section measurements the dependence of fission cross section on the neutron energy is a typical example. Strictly speaking all the measured values are averaged ones to some extent. Neutron sources, even nominally monoenergetic ones, produce neutrons over a range of energy. When neutron producing reactions are used the neutrons have some energy distribution due to various reasons including finite sizes of the source and detector. If the measurement is made at a certain angle with respect to the incident beam, the angular averaging takes place for the same reason. If the energy averaging is small, the measurement is called differential. When the energy averaging is significant compared to the energy range of the response function of the measured value the measurement is called an integral one. In integral measurements of fission cross sections the results are fission cross sections averaged over the neutron spectra

$$\bar{\sigma}_f = \int_0^\infty \sigma_f(E) \cdot \chi(E)\, dE \qquad (1)$$

where: $\chi(E)$ - neutron spectrum, normalized to unity

$$\int_0^\infty \chi(E)\, dE = 1$$

$\frac{\sigma_f(E) \cdot \chi(E)}{\bar{\sigma}_f}$ - the response function of the fission cross section.

The integral measurements of such a type can be called "simple" ones in contrast with more complex ones, which are influenced by a variety of cross section data. These integral measurements are difficult to interpret because there are a large number of nuclides and reactions as well as averaging over energy and angle, but the measurements can be very precise when compared to differential data measurements /1/. This assertion is especially true in the case of simple integral measurements.

The simple integral measurements are carried out mainly in benchmark neutron fields (BNF). BNF have been created in a few laboratories in various countries in the early seventies for the reactor dosimetry purposes. Classification and objectives of BNF are given in the documents of the IAEA

Consultants' Meeting on integral cross section measurements in standard neutron fields at Vienna in November 1976 /2/.

The ^{252}Cf fission neutron spectrum is the benchmark field of the highest category: the standard neutron field. It is of particular importance because it does not depend on any cross section data, and has a distribution of the natural source.

The simplicity of realization is an important quality of ^{252}Cf neutron spectrum when used as BNF. All you need is an intense small size ^{252}Cf source in a thin wall capsule, suspended in a medium with low scattering in a large room or outdoor. Such facilities are available for example at the National Bureau of Standards (USA) /3/, Physikalisch - Technische Bundesanstalt (FRG) /4/, Institute of Experimental Physics (Hungary) /5/.

1.2. Relative and Absolute Integral Measurements

The most part of fission spectrum averaged fission cross section measurements is carried out using the relative method. The measurements of this kind are called also the fission cross sections ratio measurements. The targets of both nuclides under study are irradiated in the same neutron flux. The result of fission rates measurements is the fission cross section ratio. When one of the nuclides used is a standard (mainly ^{235}U) the normalization of the results is possible.

The simplicity of such measurements is of great importance: there is no need in neutron flux determination. That is why the cross section ratio measurements are the dominant measurements in benchmark fields, where the absolute neutron flux determination is not a simple task. However, the fission cross section ratio measurements have inherent disadvantages. First of all the error of fission cross section includes the uncertainty of the standard used. Secondly, the systematic errors are possible due to the neutron scattering. These errors may be rather significant when measuring fission cross sections in a wide energy range of neutrons as it is in the case of fission neutron spectrum. The larger is a difference between fission cross section of measured nuclide and fission cross section of standard, the higher is the influence of the scattered neutrons.

The most informative are the absolute fission cross section measurements in the ^{252}Cf fission neutron spectrum. The data obtained in such measurements are of high accuracy and do not depend on any fission cross sections. Therefore these integral data are of use when solving a number of problems. Among them are:

- validation of energy - dependent cross section data and/or ^{252}Cf fission neutron spectrum data;
- normalization of fission cross section data obtained in the differential measurements;
- neutron flux calibration by absolute flux transfer technique.

The first of the abovementioned applications is connected with ^{252}Cf fission spectrum averaged fission cross sections calculations on the basis of evaluated differential cross section

data and various representations of ^{252}Cf fission neutron spectrum. If fission cross section $\sigma(E)$ weakly depends on the energy in the energy range of fission neutrons, the calculated integral cross section is insensitive to the shape of neutron spectrum. The comparison of calculated and measured fission cross sections makes it possible to carry out the validation of the differential data. The threshold cross sections are rather sensitive to the shape of neutron spectrum. In this case the validation of the fission neutron spectrum is possible provided the differential data on the cross section are reliable.

Normalization of data of the differential measurements using absolutely measured integral cross sections is the most rational for nuclides, which cross sections are almost energy independent in the energy range of fission neutrons, for example, ^{239}Pu, ^{235}U, ^{233}U.

When neutron field is used in the experiment the neutron flux calibration is required almost in all cases. A direct determination of neutron flux is difficult as a rule if possible at all. The flux transfer technique developed by the National Bureau of Standards (NBS) /6/ provides definite capabilities in these conditions.

Basically, the method makes it possible to transfer the neutron flux from a calibrated ^{252}Cf source to the neutron field under study. As an integral detector a ^{239}Pu fission chamber is used. The ^{239}Pu fission cross section is energy independent within $\pm$ 6 % between 10 keV and 5 MeV /6/. The fission rates ratio for the study field and the calibrated ^{252}Cf fission neutron field is

$$\frac{N_s}{N_c} = \frac{\bar{\sigma}_s (n\upsilon)_s}{\bar{\sigma}_c (n\upsilon)_c}$$

The neutron flux is obtained as

$$(n\upsilon)_s = \frac{N_s}{N_c} \cdot \frac{\bar{\sigma}_s}{\bar{\sigma}_c} \cdot (n\upsilon)_c \qquad (2)$$

The equation (2) involves only the ratio of spectrum averaged cross sections. For the ^{239}Pu detector this ratio is near to unity. In addition the errors of the ^{239}Pu fission cross section tend to cancel from the ratio. Hence, the total error of neutron flux calibration can be as small as 5 % /7/.

In general other then ^{252}Cf benchmark fields and integral detectors may be used in the flux transfer technique. It depends on the energy spectrum of the neutron field under study.

2. Absolute Measurements of Fission Cross Section Averaged over the ^{252}Cf Fission Spectrum

The absolute measurements of ^{252}Cf fission spectrum averaged fission cross sections are carried out in two ways: with Calibrated ^{252}Cf Neutron Source (or Field) Technique and with Time Correlated Associated Particle Method (TCAPM) /10/.

2.1. Calibrated ^{252}Cf Neutron Source Technique

Technical features of this method have been elaborated in detail by a group of authors at NBS, when measuring the ^{235}U fission cross section for ^{252}Cf fission neutrons /8/. The mea-

surements at the University of Michigan /9/ are strongly correlated with these of NBS and will not be considered here separately.

The idea of an experiment seems to be evident. Near-point ^{252}Cf source and a fissionable deposit are set on the definite separation distance. The fission cross section of study nuclide is derived from the fission rate, ^{252}Cf source strength and the source - fissionable deposit separation distance.

Nevertheless practical realization of such an experiment has a number of peculiarities. In the experimental arrangment two double fission chambers were mounted in a ligh frame on opposite sides of ^{252}Cf source, as shown in Fig. 1. This geometry enables to compensate the influence of the source position error: for a 10 cm deposit separation a source displacement of 1 mm changes the sum of the two chamber responses by less than 0.1 %. With such an experimental geometry the determination of the source-deposit separation distance is substituted by the determination of fissionable deposit separation distance. This can be done with much higher accuracy and without the source in place. All the distance determinations were performed very carefully with a theodolite and a depth micrometer fitted with an electrical contact. The reproducibility of the theodolite measurements is $\pm$ 75 μm. The position of each fissionable deposit was determined to an accuracy of $\pm$ 45 μm. All these position errors lead to an uncertainty in the ^{235}U fission cross section of $\pm$ 0.6 %.

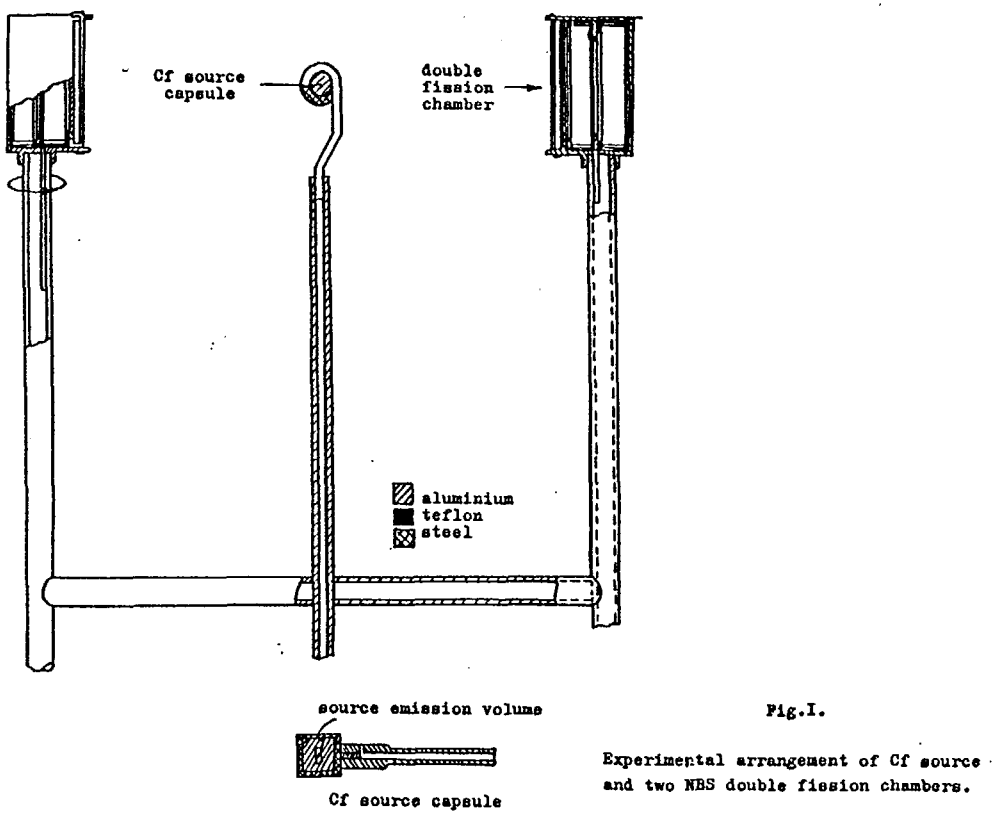

Fig.I.

Experimental arrangement of Cf source and two NBS double fission chambers.

Two corrections were applied to the fission rate data: (1) 0.75 % for the finite size of the fissionable deposit (12.7 mm - diameter oxides on polished platinum discs 19.1 mm - diameter and 0.13 mm thick); and (2) an average 0.1 % for combined effects of small displacement of the exact midpoint source position, and deposit mass difference.

To eliminate the influence of fission fragment momentum the measurements were performed at two orientations: one shown on the figure and the other with both chambers rotated by 180°.

The experiment was run with a single ^{235}U deposit in each fission chamber back-to-back with some other fissionable deposit. In such a way the fission cross section ratio measurement could be carried out simultaneously with the ^{235}U absolute fission cross section measurement /11/. The deposits were matched in pairs according to masses within several percent.

The corrections for the efficiency of fission detection must be applied in the absolute measurements. The losses in the fission events counting occur because of both the absorption of fragments in the deposit and the discrimination in the counting channel. The first correction was introduced using the simple expression $\frac{t}{2R}$, where t is the areal density of the deposit in mg/cm^2 and R is the average range of the fission fragment in the deposit. The correction for extrapolation to zero pulse height was determined using simultaneous pulse counting by two counting channels. Their discrimination levels were set at two different points in the valley region of the pulse height distribution. The valley region was assumed to be flat.

The mass assay of the fissionable deposits was based mainly on the comparison with the standard deposits available at NBS. The measured deposit and a standard one (back-to-back) were irradiated in the thermal beam at the NBS Research Reactor. The fission rate ratio was measured. The mass of the NBS reference deposit for ^{235}U has been determined to an accuracy of $\pm$ 1.2 %. The absolute α-counting was also used in combination with isotopic assay from mass spectrometry and α-decay constants from the literature.

The ^{252}Cf neutron source approaches an ideal point source with a source emission volume of about 1.4 mm^3. The $(CfO)_2SO_4$ pellets are encapsulated in a steel and aluminium capsule of $\sim$ 2 g and 0.34 cm^3. The source was calibrated in the NBS Manganous Sulfate Bath Facility against the internationally compared Ra-Be photoneutron standard source NBS-1.

Five corrections for neutron scattering

- support structures,
- source capsule,
- fission chamber,
- platinum deposit backings,
- total room return, must be determined.

The first four corrections were estimated by calculations. The platinum backings scattering was determined also by the measurements with a set of backings 0.13 to 0.41 mm thick.

Neutron scattering from the entire room was studied in two ways:

- with ^{252}Cf neutron source, moving it along the walls, floor, ceiling with the fission chambers in their normal position 188 cm above the floor;
- by measuring fission rates ratios for the ^{235}U deposit in its back-to-back position with the ^{238}U at 10 and 20 cm deposit separation.

The total room return background determined from these measurements was about 2 %. For all of the cross section measurements this room return background was greatly reduced by placing a cylinder of cadmium (90 cm long by 69 cm-diameter) around the source-detector assembly.

Table 1

Error Components for NBS Measurements of $\sigma_f(^{235}U, \chi_{Cf})$
("Old" - in 1975 /8/, "New" - revision, May 1982 /14/)

Error Components	Correction		Percent Error in Cross Section	
	Old	New	Old	New
Fissionable Deposit Mass	-	-	1.3	0.7.
Cf Source Strength	-	-	1.2	0.9
Fission in Other Isotopes	0.9987	same	0.1	same
Geometrical Measurements				
Fissionable Deposit Separation	-	-	0.6	same
Deposit Diameter	1.0075	same	0.1	same
Source Position	1.001	same	0.2	same
Undetected Fission Fragments				
Extrapolation to Zero Pulse Height	1.009	same	0.5	same
Absorption in Fissionable Deposit	1.0132	same	0.3	same
Neutron Scattering				
Room Return	0.9955	same	0.2	same
Source Capsule	0.9940*	0.9922	0.8*	0.4
Fission Chamber	0.9888	0.9873	0.4	0.2
Support Structures	0.9945	same	0.5	same
Deposit Backing (Pt)	0.987	0.990	0.8	0.2
T O T A L E R R O R			2.4	1.61

* Later this value was changed to the newly determined one 0.9922 (± 0.3 %) (also see text).

The corrections and error components for ^{235}U fission cross section measurement are listed in the Table 1. The correction sums for the three classes shown in the Table are (+0.85±0.64) % for geometrical measurement, (+2.23±0.42) % for undetected fission fragments and (-3.96±1.32) % for neutron scattering.

The ^{252}Cf fission spectrum averaged ^{235}U fission cross section was found to be (1.204±0.029) b.

Somewhat later, in 1976, the authors have performed the direct neutron source anisotropy measurement. This resulted in some change of correction for the source capsule scattering and the appreciable decrease of the related uncertainty. The total error of the ^{235}U fission cross section was reduced to ±2.25 % /13/.

By 1982 at the NBS several measures have been taken to decrease the uncertainty of a number of standards. In particular the error of the neutron source strength of NBS-1, the National Standard Photoneutron Source has been reduced from ±1.1 to ±0.8 % by comparison with the up-to-date $\bar{\nu}$ (^{252}Cf) values in a series of experiments. A sustained program to improve the mass scale of NBS fissionable isotope mass standards including the relative measurements and interlaboratory comparisons has led to an error assignment of ±0.5 % to the isotopic mass of the NBS ^{235}U deposit mass standard. In conclusion, high-precision Monte-Carlo calculations undertaken at the Los-Alamos Laboratory gave more accurate values of corrections for the neutron scattering by the fission chambers and the deposit backings. Also the uncertainties of these corrections were considerably reduced. All these steps resulted in the small change in the value of the ^{235}U fission cross section and the more remarkable decrease of the uncertainty

$$\bar{\sigma}_f\,(U\text{-}235,\ \chi_{Cf}) = (\,1.216 \pm 0.020)\ b$$

The new corrections and corresponding errors listed on the 17.05.82 shown in Table 1 /14/.

2.2. Time Correlated Associated Particle Method

Since 1972 the use is made of the Time Correlated Associated Particle Method at the V. G. Khlopin Radium Institute, Leningrad, USSR (RI), for the absolute measurements of fission cross sections averaged over the ^{252}Cf fission spectrum /10, 15, 16/.

The TCAPM use in the measurements of such a type has a number of peculiarities as compared to the usual TCAPM realization in a case of the neutron producing reactions, such as, for example, D (d, n)^{3}He, T(d, n)^{4}He. In average $\bar{\nu}_p(^{252}Cf)$ prompt neutrons are emitted in each ^{252}Cf fission event. One can say disturbing in a small extent the sequence of events that the fission fragment associates to the fission neutrons. Two peculiarities are evident here. First, not one neutron and one associated particle are time correlated, but ν neutrons and two fission fragments. Second, there is no strong angle correlation between the neutrons and the associated fission fragments. Nevertheless, these features do not cause significant difficulties. The $\bar{\nu}_p(^{252}Cf)$ value is the world wide standard and is known now to an accuracy of tenths of percent. That is quite suitable for the fission cross section measurement. It is of importance to note also, that ν neutrons may cause the only fission event in the target of the nuclide under study because the probability is too small for a single neutron to cause the fission event (less, than 10^{-6}) in the real experimental geometry. The second feature - the absence of a strong angle correlation - makes it impossible to restrict any definite neutron cone corresponding to the registered ^{252}Cf fission fragments. This compels to take into account a geometrical factor to describe the dimensions and the separation distance between the fissionable layer and the ^{252}Cf neutron source. Besides that the 2π-fission fragment detection is desirable to eliminate completely the influence of the fission neutron anisotropy on the results of the cross section measurements.

The main advantages of TCAPM as used for ^{252}Cf fission spectrum averaged fission cross section measurements are as follows:

- there is no need of either neutron flux determination or 100 % detection efficiency of ^{252}Cf fission fragments;
- the effects connected with scattered neutrons are reduced to minimum (if resolution time of coincidences is small enough).

For the purpose of calculation the most convenient experimental geometry would be the one, where a near-point ^{252}Cf source irradiates the target having a shape of some part of the spherical surface. The fissionable nuclide is deposited on the outer side of this surface, the ^{252}Cf source is at the center of the sphere. However, such a target is difficult both to manufacture and to calibrate. That is why the other geometry was chosen: a flat round target of a fissionable nuclide and a ^{252}Cf source of the smallest possible dimension, both deposited on thin backings fixed in the assembly by means of thin supports (Fig. 2, 3).

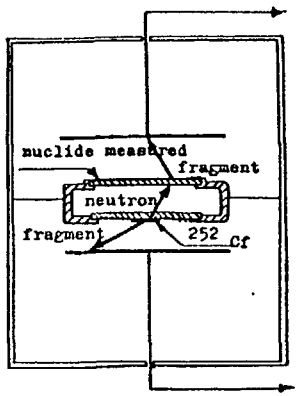

Fig.2. Experimental geometry in the cross-section measurements for ^{252}Cf fission-spectrum neutrons.

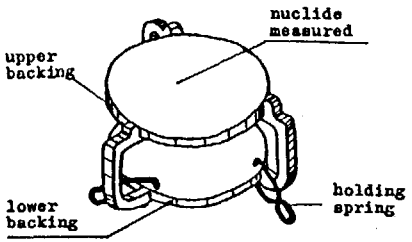

Fig.3. Assembly for holding the ^{252}Cf source and fissionable nuclide target.

The fission fragments of both ^{252}Cf source and a study nuclide were detected by ionization current pulse chamber. The ^{252}Cf source-target separation distance was chosen as a compromise in the following conditions. Small separation distance causes the increase of correction for neutron scattering by backings (stainless steel 24 mm-diameter 0.25-0.35 mm thick). The increase of the separation distance decreases the geometrical factor and hence a fission rate of the study nuclide. The ^{252}Cf neutron source strenght is limited by the time resolution of the registering channel ($5\text{-}7\cdot10^4$ s^{-1}). From these reasons the separation distance was chosen 3 to 4 mm. The assembly design (Fig. 3) ensured fixing of the source relative to the fissionable layer with an accuracy of $\pm$10 microns. This gave a correct determination of the geometrical factor. The mass of structural materials in the vicinity of both the target and the source was minimized and did not exceed 1.5 g. The effect of neutron scattering from more distant structural elements was suppressed to a large degree due to the high time resolution of coincidence circuit (20 ns).

The fission events of both the source and the target as well as coincidences between them were registered in the measurements. The cross-section values were calculated using the formula:

$$\bar{\sigma}_f = \frac{N_c}{N_f \bar{\nu} G n},$$

where: N_c - number of coincidences;
N_f - number of ^{252}Cf fission events;
$\bar{\nu}$ - ^{252}Cf prompt neutrons average number;
G - geometrical factor;
n - number of fissionable nuclei per 1 cm^2.

The geometrical factor G is defined by the solid angle subtended by the target, by the dependence of effective layer thickness on the neutron angular distribution, and by the neutron scattering. An exact calculation of the geometrical factor requires that

(a) the fissionable layer radius, the separation distance between ^{252}Cf layer and that of the fissionable nuclide, and the thicknesses of the backing material have to be accurately determined, the layers of ^{252}Cf and of the fissionable nuclide have to be strictly parallel;

(b) the layer of fissionable nuclide be uniform to better than 1 %;

(c) the backing be as thin as possible and their surfaces mirror-polished;

(d) the mass of structural materials be minimized in the vicinity of the ^{252}Cf source and target.

Inspite of the rather simple experimental geometry the analytical geometry factor computation used in the early works led to the expression containing the integrals (two of them multidimentional). Besides that a number of assumptions could not be avoided /15/. In particular, the effects of neutron multiple scattering and neutron spectrum attenuation were neglected. Later on a new method to calculate finite geometry effects was developed based on the inverse problem of the irradiation transfer theory. The set of transfer equations was solved by the Monte-Carlo method for real experimental conditions taking into account all the structural details (electrodes, chamber walls, supports), target backing and the gaseous mixture filling the chamber.

Two corrections were applied to the number of coincidences. The correction for the fission channel discrimination was determined from pulse-height spectrum analysis. The correction for fission fragments absorbed in the layer of fissionable nuclide was introduced in the same way as at NBS using the expression proposed by White /12/.

For the last years absolute measurements of the fission cross sections averaged over the ^{252}Cf fission spectrum have been carried out at RI for 10 nuclides from U to Am*. The nuclides of mass-separator purification were used in most cases. The admixtures of other fissionable nuclides in the targets did not exceed 0.1 %.

The use was made of two methods to prepare the targets:

(a) high frequency sputtering on rotating cooled backings;

(b) thermal evaporation on rotating backing with calculated rotation axes displacement in relation to the evaporated substance.

The nonuniformity of areal density had been checked by α-counting scanning. The mass assay was based on the α-counting with a low geometry surface-barrier detector.

The results of the absolute measurements of the fission cross sections averaged over the ^{252}Cf fission spectrum are given in Table 2. The error components of data, associated with determination of fission cross sections are listed in Table 3. The data given are to be considered as an illustration of possibilities of the TCAPM when measuring fission spectrum average fission cross sections. There are reasons for these possibilities to be considered far from being exhausted. In principle, TCAPM is suitable for the measurements to accuracies of about $\pm$ 1 %.

---

* Most part of the measurements was performed in the framework of the International Atomic Energy Agency Research Contract N 1718/RB and Research Agreement N 2791/CF

Table 2

Results of Absolute Measurements of Fission Cross Sections Averaged Over the ^{252}Cf Fission Neutron Spectrum, Carried out at RI

Nuclide	Fission Cross Section, barns
^{233}U	1.852 ± 0.026
^{234}U	1.204 ± 0.014
^{235}U	1.230 ± 0.017
^{236}U	0.612 ± 0.008
^{238}U	0.341 ± 0.006
^{237}Np	1.429 ± 0.023
^{239}Pu	1.814 ± 0.026
^{240}Pu	1.310 ± 0.037
^{242}Pu	1.082 ± 0.017
^{243}Am	1.145 ± 0.023

Table 3

Errors of Data Associated with Determination of Fission Cross Sections for ^{252}Cf Fission Spectrum Neutrons, % (RI Measurements)

Error Source		^{233}U	^{234}U	^{235}U	^{236}U	^{238}U [1]	^{237}Np	^{239}Pu	^{240}Pu	^{242}Pu	^{243}Am
$\sqrt{}$ (^{252}Cf)		0.20	0.20	0.20	0.20	0.20	0.20	0.20	0.20	0.20	0.20
Geometrical Factor		0.58	0.58	0.58	0.58	0.58	0.91	0.58	0.58	0.58	0.58
Mass Determination	Solide Angle	0.30	0.30	0.30	0.30	0.51 [2]	0.30	0.30	0.30	0.30	0.8
	Statistics	0.56	0.08	0.35	0.53	0.55	0.45	0.35	0.10	0.61	0.22
	Part of Measured Nuclide α-Activity	0.20	-	0.41	-	0.30 [4]	0.10	0.34	0.12	0.18	0.18
	Half-Life	0.28	0.41	0.20	0.17	0.30 [3]	0.47	0.12	0.15	0.41	0.54
Number of Fissions	Statistics	0.97	0.80	0.80	1.01	1.11	0.95	0.62	2.28	1.16	1.42
	Extrapolation to Zero Pulse Height	0.43	0.20	0.40	0.30	0.37	0.41	0.58	0.20	0.40	0.20
	Absorption in Layer	0.09	0.10	0.46	0.30	0.25	0.28	0.18	0.1	-	0.10
	Fission of Other Nuclides	0.05	-	-	-	0.14	-	0.71	1.48	-	0.87
Total Fission Cross Section Error		1.43	1.15	1.35	1.38	1.60	1.60	1.41	2.82	1.60	2.05

1) Layer mass was determined in 2π-geometry
2) Extrapolation to zero pulse-height
3) Correction for absorption in layer and α-scattering
4) ^{238}U Half-life error is taken into account in determination of a part of the measured nuclide α-activity

3. Calculations of Fission Cross Sections Averaged Over ^{252}Cf Fission Spectrum From Differential Data

The computation of fission cross sections averaged over the ^{252}Cf fission spectrum is carried out usually on the basis of evaluated fission cross section data from files, such sa ENDF/B, INDL/A or others. The ^{252}Cf fission neutron spectrum is represented mainly in the next two ways:

(1) Maxwell distribution

$\chi(E) \sim \sqrt{E} \exp(-E/T)$ using T = 1.42 MeV;

(2) Segment-adjusted evaluated spectrum, suggested by Grundl and Eisenhauer at NBS /17/.

$\chi(E) = \mu(E) \cdot M(E)$

where: M(E) - reference Maxwell distribution

$M(E) = 0.663\sqrt{E} \exp(-1.5\ E/2.13)$

$\mu(E)$ - analytic correction factor.

Its values and the energy ranges over which they are valid are given in Table 4 /17/.

Table 4

Energy Dependence of the $\mu(E)$ Correction Factor

Energy Interval (MeV)	$\mu(E)$
0.0 - 0.25	1 + 1.20E - 0.237
0.25 - 0.8	1 - 0.14E + 0.098
0.8 - 1.5	1 + 0.024E - 0.0332
1.5 - 6.0	1 - 0.0006E + 0.0037
6.0 - 20	1.0exp[-0.03(E - 6.0)/1.0]

Recently other ^{252}Cf fission neutron spectrum representations were used. For example Mannhart /18/ has tested various versions of the spectrum calculations made by Madland and Nix /19/ together with the results of the new spectrum measurements, which Böttger and Klein /20/ and Poenitz /21/ have performed recently.

In Table 5 the results are given of averaged fission cross sections calculations carried out at RI. The differential data on the fission cross sections are from ENDF/B-V and INDL/A files. The ^{252}Cf fission neutron spectrum used in two abovementioned representations: Maxwell distribution at T = 1.42 MeV, and the NBS segment-adjusted evalution. As it is seen in Table 5 the calculation based on the NBS segment-adjusted evaluation shows some lower cross section values (on 1-1.5 %) as compared to the use of Maxwell distribution. This difference is not significant taking into account that only the statistical computation accuracy amounts to ± 1 %.

Table 5

Fission Cross Sections for ^{252}Cf Fission Neutrons Calculated on the Basis of Different Representations of ^{252}Cf Neutron Spectrum and Differential Data Fission Cross Sections from Various Files

Neutron Spectrum Representation	Nuclear Data File	^{235}U	^{236}U	^{238}U	^{237}U	^{239}Pu	^{240}Pu	^{241}Pu	^{242}Pu	^{243}Am
Maxwell Distribution T=1.42 MeV	ENDF/B-V	1.238		0.311	1.348	1.783				1.205
	INDL/A Rev. 6				1.304	1.771	1.335	1.572	1.130	1.097
Grundl-Eisenhauer Segment-Adjusted Evaluation	ENDF/B-V		0.591	0.307	1.339	1.776			1.118	1.195
	INDL/A Rev. 6				1.297	1.767	1.327	1.570	1.123	1.090

4. ^{252}Cf Averaged Fission Cross Section Requirements

In Table 6 the major part of the ^{252}Cf fission spectrum averaged fission cross section data is given. These absolutely measured data obtained at different times at five scientific centers: Institut Voor Kernphysisch Onderzoek (Netherlands) /22/, NBS /8, 13, 14, 24, 25, 26/, RI /10, 16/, the University of Michigan /9/ and Institute of Experimental Physics (Hungary)/23/. The ^{235}U cross section data of one and the same author make it possible to see the process of making the cross section more accurate as time goes on. One may notice the last cross section values to be in the error bar limits of earlier results. It is seen also that there is a discrepancy of data of various authors for ^{238}U and ^{237}Np higher than the error limits assigned by authors.

Table 6

Fission Cross Section Averaged Over the ^{252}Cf Fission Neutron Spectrum (Absolute Measurements)

Nuclide	^{231}Pa	^{233}U	^{234}U	^{235}U	^{236}U	^{238}U
Cross Sections, barns	1.970±0.043 /23/	1.910±0.029/16/ 1.893±0.048/24/	1.204±0.014*)	1.207±0.052/25/ 1.204±0.029/8/ 1.215±0.022/9/ 1.205±0.027/13/ 1.266±0.019/10/ 1.241±0.018/16/ 1.216±0.020/14/	0.612±0.008*)	0.310±0.025/22/ 0.313±0.017/23/ 0.344±0.006/16/ 0.326±0.0065/24/

^{237}Np	^{239}Pu	^{240}Pu	^{241}Pu	^{242}Pu	^{243}Am
1.260±0.060/22/ 1.442±0.023/10/ 1.366±0.027/24/	1.800±0.060/22/ 1.831±0.027/16/ 1.824±0.035/24/	1.310±0.037*) 1.337±0.082/24/	1.616±0.030/24/	1.092±0.018/16/	1.145±0.023*)

*) RI Measurements

The appreciable discrepancy (to 12 %) for the ^{238}U fission cross section (Table 6) is observed when comparing with the calculated cross sections (Table 5). The discrepancy for the ^{235}U and ^{239}Pu fission cross sections seems to be less.

The agreement of the calculated and experimental values for the other nuclides is rather good. In this comparison one must take into account that inspite of the intensive work on the measurement and evaluation of the differential data on the fission cross sections these data are less accurate than the data obtained in integral cross section measurements.

The uncertainties of data even in the last ^{252}Cf fission spectrum measurements are far from required accuracy. Even the error of the evaluated data on the ^{252}Cf fission spectrum /17/ in the various energy ranges is $\pm$ 1.0 to 13 %. The uncertainties of the ^{252}Cf fission neutron spectrum propagate strongly in the calculated average fission cross sections when $\sigma_f(E)$ is a threshold cross section (^{238}U, ^{237}Np, ^{240}Pu nuclides). As an example the ^{238}U integral fission cross section sensitivity to the T-parameter of the Maxwell ditribution is shown in Table 7. Therefore the discrepances of calculated and experimental data in Table 6 may be attributed to the errors of the ^{252}Cf fission spectrum determination. However, the discrepancy for the ^{239}Pu indicates the underestimation of the differential data on the cross section in the corresponding files.

To increase the reliability of the ^{252}Cf fission cross section data the new absolute integral measurements seem to

Table 7

Dependence of ^{235}U and ^{238}U Fission Cross Sections on T-parameter of Maxwell Distribution

T, MeV	Fission Cross Sections, barns	
	^{235}U	^{238}U
1.35	1.238	0.300
1.42	1.239	0.314
1.49	1.240	0.328

be of use first and foremost for the most important nuclides: the ^{235}U, ^{238}U, ^{237}Np and ^{239}Pu. This conclusion agrees with the requests listed in the "World Request List for Nuclear Data 81/82" /27/. There are requests for the absolute integral cross section measurements there for the major nuclides including ^{236}U, ^{240}Pu. An accuracy requested is higher than $\pm$2 %.

A number of requests contains condition: a request should be considered fulfilled, when at least three measurements with different methods agree within the requested accuracy. Therefore it is worth-while to make use of both calibrated ^{252}Cf Neutron Source Technique and TCAPM for the measurements and also to make efforts for the future improvement of the experimental technique.

REFERENCES

1. Pearlstein S. - Evaluation and Processing of Nuclear Data. BNL-NCS-27892, 1980, p. 4.

2. Vlasov M. - IAEA Consultants' Meeting on integral cross section measurements in standard neutron fields. Vienna, 15-19 November 1976. Report INDC(NDS)-81/L+DOS (IAEA, Vienna, 1977).
3. Grundl J. A. et al. - Nucl. Techn., 1977, vol. 32, p. 315.
4. Alberts W. G. et al. - NBS Spec. Publ. 425, 1975, vol. 1, p. 273.
5. Buczko M. et al. - Int. Symp. on Californium-252 Utilization, Paris, April 26-28, 1976.
6. Crundl J. A. and Eisenhauer C. M. - Nuclear Cross Sections and Technology. - NBS Special Publication 425, 1975, vol. 1, p. 250 (Proceedings of a Conference, Washington, March 1975).
7. Kazu A. H. et al. - Neutron Standards and Applications. - NBS Special Publication 493, 1977, p. 335 (Proceedings of the International Specialists Symposium, Gaithersburg, March 1977).
8. Heaton II H. T., et al. - Ref. 6, vol. 1, p. 266.
9. Davis M. C. and Knoll G. F. - Ann. Nucl. Energy, 1978, vol. 5, p. 583.
10. Adamov V. M., Alexandrov B. M., Alkhasov I. D. et al. - Ref., 7, p. 313.
11. Gilliam D. M., Eisenhauer C. et al. - Ref. 6, p. 270.
12. White P. H. - Nucl. Instrum. Meth., 1970, vol. 79, N 1, p. 1.
13. Heaton II H. T. et al. - Proc. of NEANDC/NEAGRP Spec. Meeting on Past Neutron Cross Sections of U-233, U-235, U-238 and Pu-239, Argonna, USA, 1976 (ANL-76-90, 1976), p. 333.
14. Grundl J., Gilliam D., McGarry D. et al. - Memorandum for CSEWG Sub-Committee on Standards, 1982.
15. Adamov V. M., Drapchinsky L. V., Kudriavzev G. Yu. et al. - Preprint Radievogo Instituta, RI-52, Leningrad, 1976.
16. Adamov V. M., Alkhasov I. D., Gusev S. E., Drapchinsky L. V. et al. - Nuclear Cross Sections for Technology. - NBS Special Publication 594, 1980, p. 995 (Proceedings of the International Conference, Knoxville, Okt. 1979).
17. Grundl J. and Eisenhauer C. - Neutron Cross Sections for Reactor Dosimetry. - IAEA-208, 1978, vol. 1, p. 53 (Proceedings of a Consultant's Meeting, Vienna, Nov. 1976).
18. Mannhart W. - IAEA Consultant's Meeting on ^{235}U Past Neutron Fission Cross Section and ^{252}Cf Spontaneous Fission Neutron Spectrum, Smolenîca, CzSSR, 1983.
19. Madland D. G. and Nix J. R. - Preprint LA-UR-2645.
20. Böttger R., Klein H., Chalupka A., Strohmaier B. - Nuclear Data for Science and Technology, 1983 (Proceedings of a Conference, Antwerp, Sept. 1982).
21. Poenitz W. P., Tamura T. - Ref. 20, p. 331.
22. Pauw A. H., Aten W., Jr. - J. of Nucl. En., 1971, vol. 25, p. 457.
23. Dezcö Z. and Csikai J. - Neitronnaja Fizika (Proc. 4 th Nat. Conf. on Neutron Physics, Kiev, USSR, 1977) vol. 3, p. 32.
24. Grundl J. et al. - see Ref. 18.
25. Grundl J. et al. - Trans. Am. Nucl. Soc., 1972, vol. 15(2), p. 945.
26. Grundl J. and Eisenhauer G. - Ref. 7, p. 156.
27. WRENDA 81/82, INDC(SEC)-78/URSF, IAEA.

NEUTRON EMISSION AT SPONTANEOUS FISSION

M.V. BLINOV
V.G. Khlopin Radium Institute,
Leningrad, Union of Soviet Socialist Republics

Abstract

Integral and differential characteristics of the emission of spontaneous fission neutrons are considered. There is a discussion of the theoretical aspects and of the experimental investigation of the probability of neutron emission at different stages of the nuclear fission. Data are presented on the energy distribution of californium-252 spontaneous fission neutrons.

INTRODUCTION

Spontaneous fission neutrons are the source of information about many characteristics of the fission process - such as the total excitation energy at fission, the excitation energy of the fragments and their deformation energy at the moment of nucleus scission, viscosity of the nucleus moving to the point of scission, viscosity of the fragments at the establishing of the equilibrium form and a number of other important characteristics. Spontaneous fission neutron sources play an important role in many practical tasks. The average number and the energy spectrum of californium-252 spontaneous fission neutrons are international standards. I will dwell only upon some of the aspects of the emission of neutrons at spontaneous fission.

CHARACTERISTICS OF THE EMISSION OF SPONTANEOUS FISSION NEUTRONS

The average number of neutrons at spontaneous fission, that characterizes the total excitation energy rises with the increase of the mass of the nucleus undergoing the fission from $\bar{\nu} \simeq 1$ for uranium isotopes to $\bar{\nu} \simeq 4$ for fermium isotopes (fig. 1) /1/. It is worth mentioning that the sharp increase of $\bar{\nu}$ /M/ is slowed down in the region of Fm. It is shown in fig. 2 how the average energy of neutrons $\bar{E}$ changes with the average number of prompt neutrons $\bar{\nu}$ /2/. One can see that the energy of the neutrons $\bar{E}$ increases with the increase

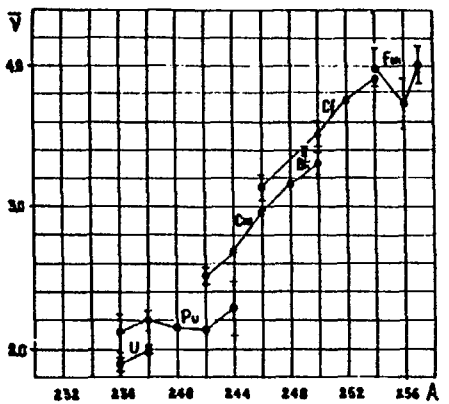

Fig. 1. Dependence of the average number of spontaneous fission neutron $\bar{\nu}$ on the mass of the fissile nucleus A

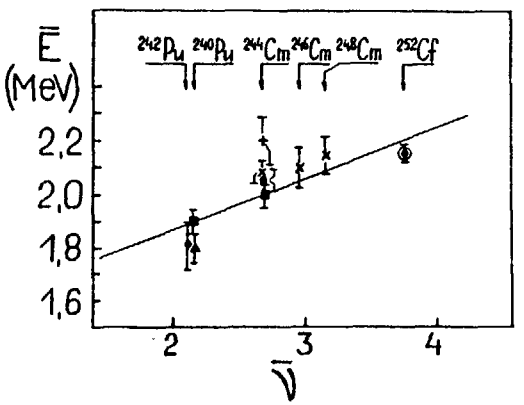

Fig. 2. Dependence of the average energy of neutrons $\bar{E}$ on the average number of prompt neutrons $\bar{\nu}$

of the average excitation energy. Terrell /3/ drew from the simplified evaporation model of Weisskopf the correlation $\overline{E} = 0.78 + 0.621\ (\overline{\nu} + 1)^{1/2}$. In fig. 3 there are presented the spectra of spontaneous fission neutrons of Pu-242, Cm-244 and Cf-252 /2/. These spectra are close enough to each other by their shape. The dependence of the number of neutrons on the angle in respect to the direction of fragments' motion (fig. 4) /4/ is also of interest among the other characteristics (for the sum of all the types of fission). This angular distribution is highly anisotropic and gives an evidence that the neutrons for the most part are emitted from the fragments. The dependence of $\overline{\nu}$ on the mass of the fragment A is one of the main differential dependences. Such a saw-toothed dependence /4/ is shown in fig. 5. Several interpretations of such a strange behaviour of $\overline{\nu}$ /A/ have been given and in the recent few years it has become clear that at the moment of the spontaneous fission of the nucleus the fragments are cold enough; their deformation energy then turns into the excitation energy, with the deformation of the fragments depending on their rigidity. Fragments with the filled shells (magic nuclei) are only slightly deformable and emit few neutrons, and fragments with the unfilled ones are strongly deformed and emit many neutrons. After a brief consideration of a number of some regularities concerning the emission of spontaneous fission neutrons it seems necessary to dwell upon the theoretical aspects of the probability of neutron emission at different stages of fission

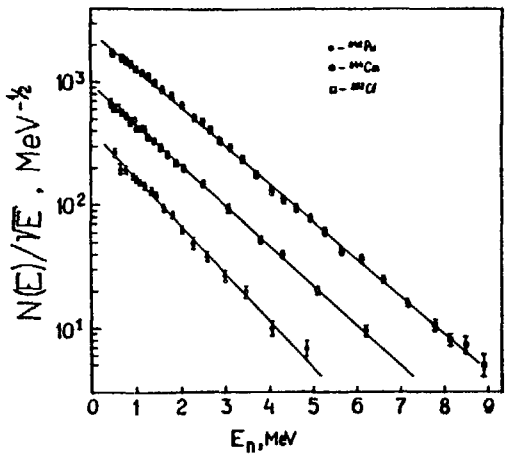

Fig. 3. Energy spectra of Pu-242, Cm-244 and Cf-252 spontaneous fission neutrons. Straight lines - Maxwellian distribution with the parameters T equal 1.21 MeV, 1.37 MeV and 1.42 MeV

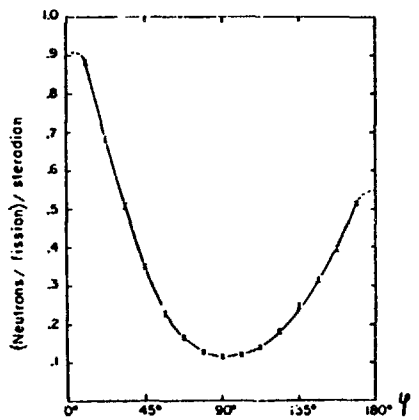

Fig. 4. Angular distribution of Cf-252 spontaneous fission neutrons

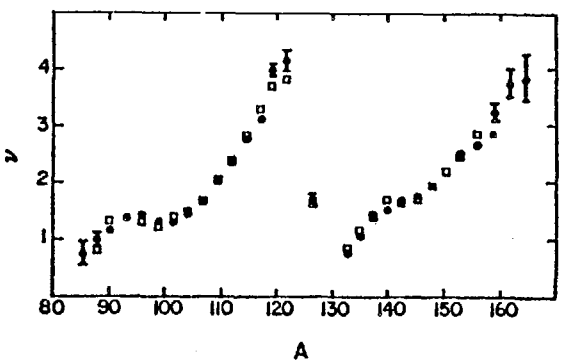

Fig. 5. Average number of the emitted neutrons in dependence on the mass of a Cf-252 fragment

and then procced to the experimental observations of the character of the emission process.

PROBABILITY OF NEUTRON EMISSION AT DIFFERENT STAGES OF THE PROCESS OF NUCLEAR FISSION

Let us consider different stages of nuclear fission and imagine the excitation energy of the nucleus and of fission fragments at these stages and the probability of neutron emission. The stage of the descent of the nucleus from the point of barrier penetrating to the point of scission is a highly important one as here the mass, charge distributions of fragments and the distributions of the kinetic energies are formed. Having passed the barrier, the nucleus continues to lengthen, its deformation increases and the total potential energy P falls down /$P = E_{coul.} + E_{surf.}$/. The difference ΔP turns into the excitation energy and the pre-scission kinetic energy /$P = E^* + E_{ps}$/. Then after the scission the Coulomb repulsion causes increase of the kinetic energy $E_k = E_{ps} + E_c$, and the excitation energy increases due to the deformation energy $E^* = E^*_{intern.} + E_{deform.}$. The correlation between $E^*_{intern.}$ and E_{ps} in determined by the dynamics of the descent. If the process is an adiabatic one, then $\Delta P = E_{ps}$ and $E^* = 0$, if it is a nonadiabatic one, but slow enough, then a statistical equilibrium is established between the collective and the one-particle degrees of freedom. Let's consider just this case. According to different estimations for fission of californium-252 the value $E_{excit.} \leq 10\text{-}20$ MeV. Let's take the time of descent from work /5/ to be equal 4×10^{-21} s. Then even for the energy 20 MeV, if we use a simplified formula for the life-time:

$$\tau = \frac{2A^{1/3}}{E_{excit.} - B_n} \exp \frac{B_n}{\left(\frac{E_{excit.} - B_n}{a}\right)^{1/2}} 10^{-21}\,\text{s}$$

where A - the mass of the nucleus, B_n - energy of neutron binding we obtain a very low probability of emission. But if the stage under consideration passes quickly enough/quick change of the form of nuclear potential/then the statistical equilibrium in the system is absent. Besides the probability of one-particle excitations will depend on the time of the stage, and in some cases one may expect transition of the particles into the state of continuous spectrum. In the work of Boneh and Frankel /6/ it has been obtained that on the stage of descent of the fissioning nucleus towards the point of scission emission of $0.3 \div 2.1$ neutrons per fission is possible if the transition time is $3 \div 1.5 \times 10^{-21}$ s respectively /including pair interactions somewhat decreases this probability/. The authors used in their calculations the data on the speed of nucleus surface change that are predicted by calculations of Nix /5/ on the liquid-drop model. Ledergerber et al. /7/ have considered the problem of dynamic excitation on the same stage of the fission process and noticed that excitations of this kind can have a marked probability. The most sharp changes of the nuclear potential are expected on the next stage - at the moment of the nucleus splitting, which increases the possibility of neutron ejection in this case. Fuller /8/, when considering a one-dimentional rectangular well in the center of which a hump is growing, has shown that with the time of the neck rupture being of the order of 1×10^{-22} s approximately 0.5 neutron per fission may be emitted at the moment of scission. At the moment of scission neutron emission can also take place due to the same mechanism as the emission of light charged particls but with a much higher probability.

After the scission of the nucleus because of a strong deformation of the fragments the forces arise that tend to return the fragments to an equilibrium form. If the transient time is of the order of 10^{-22} s or less, then as Rubchenya /9/ has estimated, noticeable probability of neutron emission (approximately 0.5 neutron perfission) appears at such a

quick change of the shape. The author predicts a dependence of this probability on the mass of the fragment. Thus, theoretical investigations show a possibility of fission neutrons emission at nonequilibrium processes.

Let's consider the question of the neutron emission probability during the period of fragments acceleration by the Coulomb field. The curve in fig. 6 shows the velocity increase of the fragment /10/. It is seen that if about half of the full velocity V_o is gained at $t \approx 10^{-21}$ s then 0.95 V_o is gained only at $t \approx 10^{-19}$ s. In the same figure the neutron emission time is shown calculated by the statistical model for different excitation energies. For $E^* = 20$ MeV the deficit in velocity of the fragment must be already taken into account and for $E^* = 40$ MeV V already equals 0.8 V_o.

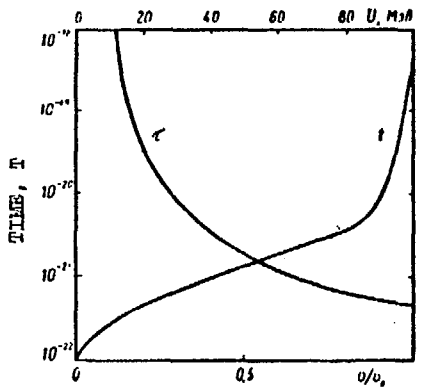

Fig. 6. Comparison of the fragment's velocity gaining time t and the neutron emission time τ by the fragment, excited to the energy U

If one could find a convincing proof of such a phenomenon it would be possible to measure very short times of neutron emission /less than 10^{-20} s/. Another interesting question concerning the stage after scission of the nucleus is the time necessary for establishing of the equilibrium shape of the fragments. Nix et al. /5/ have considered the influence of viscosity on this process /7/. For zero viscosity the fragments oscillate near their centers all the time, with all the excitation energy being concentrated in the form of collective vibrational energy. For finite values of viscosity the energy of collective motion dissipates after the scission and the excitation energy is present in the end in the form of internal energy. When viscosity is low the fragments oscillate yet but with an amplitude that decreases. With a higher than critical viscosity /0.1 $\tau_P = 6 \cdot 10^{-23}$ MeV$\cdot$s/fm^3/ the fragments don't oscillate any more but their lengthening decreases exponentially. This calculation is done for the fission of uranium-235 by thermal neutrons but the results seem to be very close also for the case of spontaneous fission.

The last stage is concerned with the emission of neutrons from heated equilibrium fragments moving at full velocities. Study of the characteristics of the neutrons

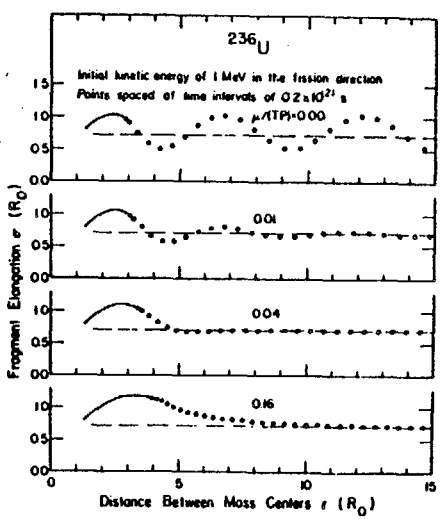

Fig. 7. Characteristics of the form of the fragment after scission of the nucleus for different values of viscosity μ in dependence on the distance between the centers of the fragments r

emitted at this stage has already given and in the future will present more interesting information about the thermodynamic properties of highly heated nuclei. The point is that in nuclear reactions at high energy of the incoming particles direct processes play a great role and it is hard to determine the excitation energy of the compound nucleus. In this case it is expected to receive a possibility to check the statistical theory of particles emission for certain excitation energies of the uniformly heated nucleus.

Thus neutron emission is possible at different stages of the fission process, yet the theoretical calculation of separate emission probabilities is a complicated task because the fission dynamics as a whole isn't clear, neither many other characteristics such as viscosity of the nucleus during descent period, viscosity of the fragments, emission time of neutrons at different excitation energies, etc.

The task of the experimental investigations is the search for neutron emission at different stages of fission, determination of probabilities and characteristics of these neutrons so that to obtain from this information the knowledge about different characteristics of the fission process and properties of the emission of neutrons from the excited fragments.

EXPERIMENTAL STUDY OF THE MECHANISM AND PROPERTIES OF SPONTANEOUS FISSION NEUTRONS EMISSION

Angular distributions of spontaneous fission neutrons give evidence that the emission is for the most part from moving fragments. To make the picture more precise in a number of works the energy spectra of neutrons have been measured for different emission angles with respect to the direction of motion of the fragments. A sharp anisotropy of the angular distribution of neutrons of different energies has been obtained in all the works, but it has been noted also that the distribution is somewhat more isotropic than it follows from the model of evaporation from fully accelerated fragments. Some authors connect this effect with emission in the process of fragments acceleration, others - with an isotropic emission in the moment of scission and even earlier - on the descent stage. The contribution of this component is evaluated in different works from 10 to 25 %. In one of the recent works /12/ the value of 5 % has been obtained which is much less than in the others /fig. 8/. Thus, the results of these works are very different yet and the conclusions are not the same. It seems that new investigations shall give an answer to this important and complicated question. In any case not less than 80-90 % (and maybe still more) of the emission

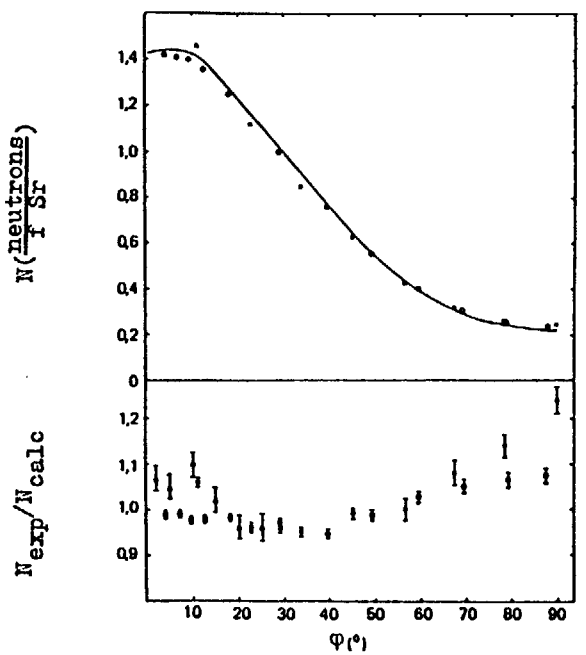

Fig. 8. Angular distributions of neutrons
a) experimental dependence of the number of neutrons on the emission angle in l. s.
b) dependence of the ratio of the experimental data to the calculated ones on the emission angle:
O - data of work /12/, X - data of work /4/

seems to take place on the final stage. But neutron emission even on the final stage gives information about the properties of the fissioning system at earlier stages.

Interesting results about the character of energy distribution in the scission point have been obtained from the variance of the excitation energy of one fragment /13/. It has been found that the excitation energy and the kinetic energy of separation of the californium-252 spontaneous fission fragments make up the sum less than 10 MeV. Thus the energy mainly is connected with potential energy - the energy of deformation and therefore the fragments are "cold" in the scission point. In this case the future excitation energy of the fragments is concentrated in the deformation energy. The dependence $\bar{\nu}$ (A) demonstrates a dependence of the deformation energy on the mass of the fragment. This dependence is "universal" for a number of nuclei at spontaneous and low-energy fission. In fig. 9 there are presented the curves for spontaneous fission of Cf-252, Fm-254 and Fm-256 /14/. It is seen that the general course of the dependence changes but little and thus the deformation energy of the fragments is determined mainly by the properties of the fragments and only slightly depends on the properties of the fissioning system. A special case can be expected for the system in which the fragments will have

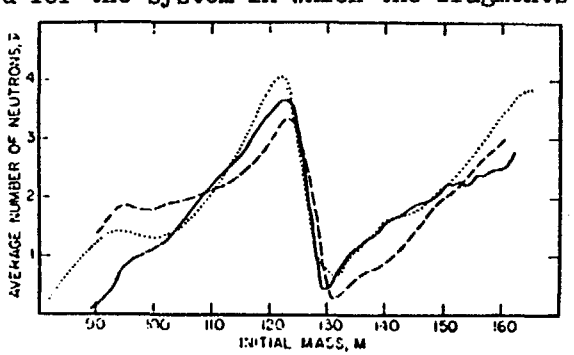

Fig. 9. Dependence $\bar{\nu}$ (A) for different isotopes of Cf and Fm (. . . - Cf-252, —— - Fm-254, - - - - Fm-256)

the filled neutron and proton shells /Z = 50, N = 82/. One can mark that the sawtoothed dependence $\bar{\nu}$ (A) is maintained in the spontaneous fission for a wide range of total kinetic energies and therefore excitation energies of the fragments /below 40 MeV/. That confirms the low excitation of the fragments in the scission point.

With the increase of the excitation energy of the fissile nucleus up to a few tens MeV, the character of $\bar{\nu}$ (A) changes from a saw-toothed to a monotonous one $\bar{\nu} \sim A$ which is predicted by the liquid-drop model. Therefore the shells in the fragments play a decisive part at spontaneous fission and then with their destruction the character of the dependence changes.

If we regard the dependence of the average energy of neutrons in the c. m. system on the mass of the fragment $\bar{\varepsilon}$(A) (fig. 10) /15, 16/ then, to explain such a dependence it is also necessary to suppose the presence of strong shell effects in the fragments.

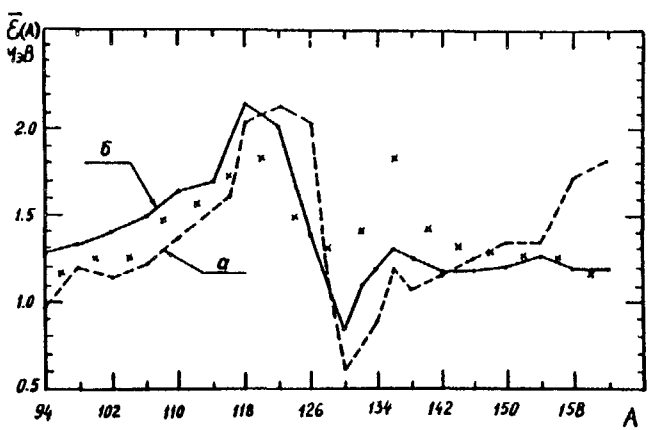

Fig. 10. Dependence of the average energy of neutrons on the mass of the fragment $\bar{\varepsilon}$ (A) /15/. Solid line-calculation /16/

Now the measurements of energy distributions and angular dependences for different masses and kinetic energies of californium-252 spontaneous fission fragments are under way at the Radium Institute /12/. In fig. 11

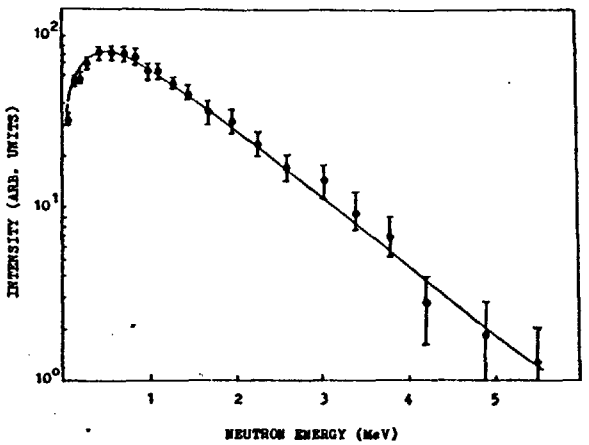

Fig. 11. Energy spectrum of neutrons for fragments with M = 108 ± 5 MU and excitation energy E = 20 ± 5 MeV. Solid line - calculation

there is a spectrum from this work of the neutrons (c. m. system), emitted from the fragments with the mass M = 108 MU and with the excitation energy 20 MeV /12, 16/. The calculated spectrum obtained in this work is presented in the same figure and is in good agreement with the experimental data. The calculation was done by the statistical model of Hauser-Feschbach taking into account the cascade evaporation of neutrons. At present the data analysis for different masses and excitation energies is under way. In the same work a search for forward neutron emission has been carried out (the "shock-wave" type effect). However even for the cases with a strong deformation of the fragments, where the effect could be expected tobe maximal, this phenomenon hasn't been observed /fig. 12/ /12/.

It is possible to point out that further investigations of the neutron emission mechanism at spontaneous fission of different nuclei is undoubtedly of great interest. Then I would like to dwell on the measurements of the integral distribution of californium-252 spontaneous fission neutrons because it is widely used as a standard for practical purposes.

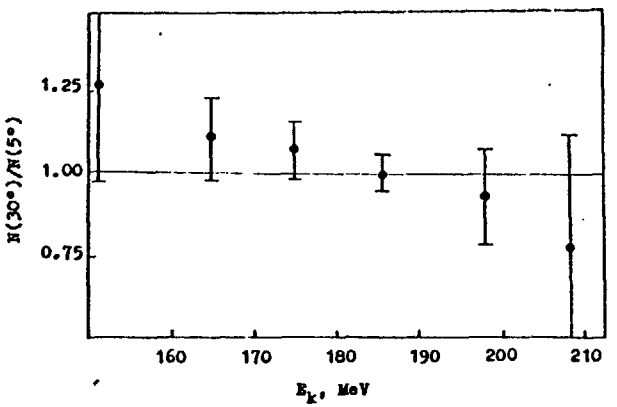

Fig. 12. Angular distribution of neutrons in lab. s. for M = 108 MU as a function of the total kinetic energy of the fragments

INTEGRAL SPECTRUM OF CALIFORNIUM-252 SPONTANEOUS FISSION NEUTRONS

The need in using the standard neutron energy spectrum is high enough both is science and in technology. The IAEA has recommended to use the spectrum of Cf-252 spontaneous fission prompt neutrons as such a standard because it is very convenient from many sides. Cf-252 has a large neutron yield /$10^9 \frac{1}{mgs}$/ with a low weight of the source, a good N_f/N_α ratio, simplicity in manufacturing and a comparatively long half-life /2.6 years/. The spectrum of Cf-252 fission neutrons ranges from zero to tens of MeV.

At present this standard spectrum is in wide use, though the precision with which it is known, doesn't yet satisfy many tasks. One of the main reguirements in specification of this standard is to settle a more precise form of the spectrum in the region of low energies /less than 1 MeV/ and of high energies /more than 7 MeV/.

In the work recently fulfilled at the Radium Institute measurements in a broad energy interval 0.01-10 MeV /17/ have been carried out. The measurements were done by the time of flight method using the $^{235}U(n, f)$ reaction for detection of neutrons. Application of this thresholdless reaction with rather a smooth and well known dependence of the fission cross-section on the energy of the neutrons enables in one experiment and with one detector to obtain information about a very broad energy range, including the low-energy part. Thus it is possible to avoid the "joining" of the data from detectors of different type - the organic scintillators /energy region more than 0.2 MeV/ and "lithium" detectors (region less than 1 MeV).

An ionization chamber with uranium-235 layers (assembly is 100 mm in diameter, 12 mm high) has been manufactured for registration of neutrons as a fast detector. The uranium, containing 99.9 % of U-235 was deposited on both sides of thin aluminium foils (0.05 mm thick), Preparation of the layers was done by the method of multiple deposition of uranium nitrate. The homogeneity of the layers was within the limits of ± 5 % and their average weights were within the limits of ± 1 % (with an average density 1 mg/cm^2). The total weight of the uranium was 0.8 g. The casing of the chamber was made of foil (0.2 mm thick). During the work methane at atmospheric pressure was blown through the chamber. The separation of the fragments pulses from alpha-particles was good enough (fig. 13).

A miniature fast ionization chamber (fig. 14) served as a detector of californium fission fragments. The amplitude spectrum of fragments from this chamber is

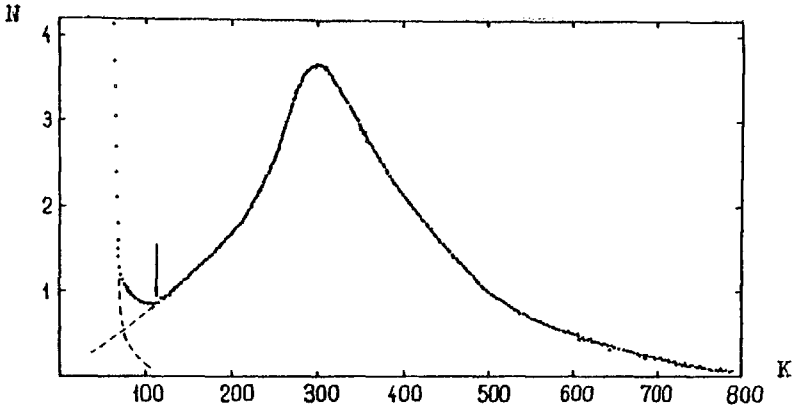

Fig. 13. Amplitude distribution of the pulses from fission fragments and alpha-particles of uranium-235

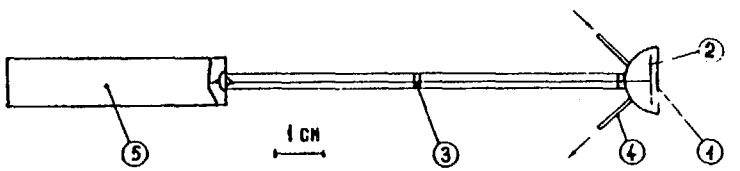

Fig. 14. Design of the ionization chamber: 1 - platinum backing with a californium layer, 2 - collecting electrode, 3 - insulator, 4 - capillary inlet, 5 - preamplifier

presented in fig. 15. The efficiency of fragments registration was more than 99 %. The total weight of the chamber was 1.5 g and the weight of the preamplifier - 5.1 g.

The full time resolution of the spectrometer with the two chambers was 1.5 ns. The time resolution of the californium chamber was 0.49 ns, and that of the uranium chamber - 1.2 ns.

The measurements were carried out on three flight distances (25, 50 and 100 cm) in a large experimental room in order to decrease the background of scattered neutrons.

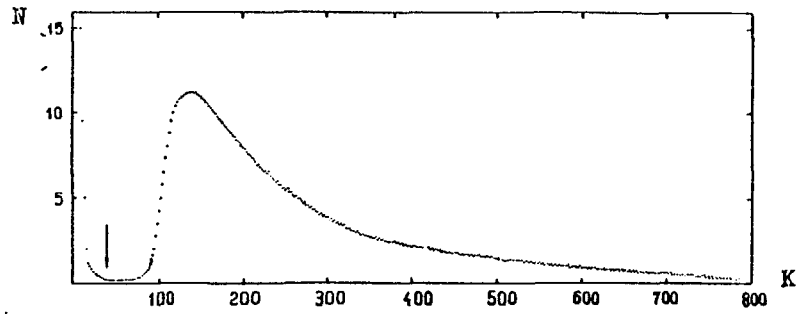

Fig. 15. Amplitude spectrum of the pulses of Cf-252 fission fragments

The background connected with true-random coincidences (noncorrelated fragments) decreased due to the pile-up inspector that analysed the time intervals between the pulses and excepted the cases when the intervals were less than 200 ns. Precision in determination of the time "zero" was 0.08 ns.

When processing the experimental results corrections were made for neutron scattering in the detectors and the environment. As the ionization chambers both of the source and of the neutron detector had been designed with small masses (the weights of the chambers were 1.5 g and 65 g respectively), the corrections for neutron scattering by the chambers were small. They were easily accountable by calculations using the single interaction approximation. The correction functions for neutron scattering by air medium were found by calculation and changed from 30 % for E_n = 10 keV to 0.5 % at E_n = 1 MeV.

The results of the measurements are presented in fig. 16. In the next fig. 17 the ratio of the experimental data to the Maxwellian distribution with T = 1.42 MeV is shown $N(E) \sim E^{1/2}(-E/T)$. In general the experimental data are close to the Maxwellian distribution in the region 0.01÷6 MeV, but further the data start to deviate from it.

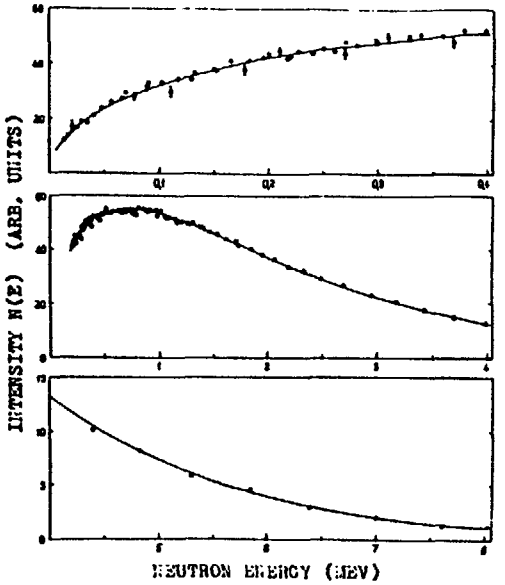

Fig. 16. Energy spectrum of Cf-252 spontaneous fission neutrons

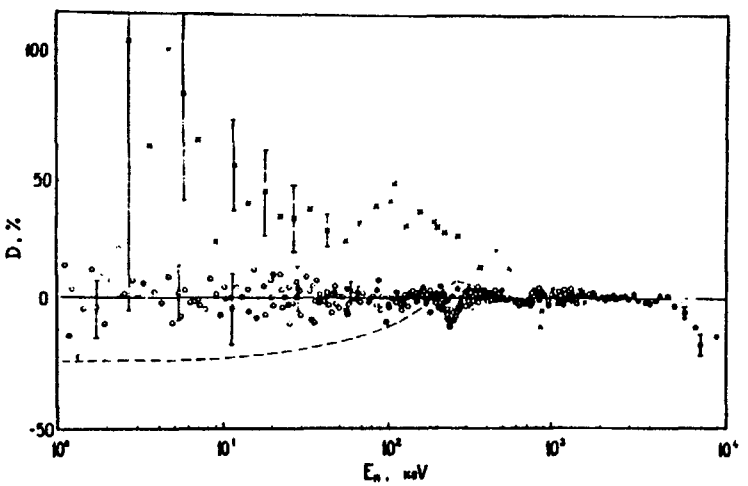

Fig. 17. Ratio of the experimental results obtained in work /17/ to the Maxwellian distribution (•) (T = 1.42 MeV). Dotted line - evaluation

It is necessary to note that the works carried out recently at different laboratories, demonstrate an increase of the measurement precision, improvement of experimental conditions, using of neutron detectors of different types. Still there exist great data discrepancies, especially in the energy region more than 7 MeV. Further measurements are needed in the whole energy region to determine the important standard with a high precision.

REFERENCES

1 DAKOVSKIY, M., LAZAREV, Yu. A., OGANESIAN, Yu. Ts. Preprint of JINR, Dubna, R15-7119 (197)(Rus.).
2 BLINOV, M. V. Proc. of the IAEA Consultants meeting on Neutron Source properties (Debrecen, 1980), INDC(NDS)-114 GT 1980.
3 TERRELL, J. Phys. Rev. 113 (1959) 527.
4 BOWMAN, H. R. et al. Phys. Rev. 126 (1962) 2120.
5 NIX, J. Nucl. Phys. A 130 (1969) 241.
6 BONEH, Y., FRANKEL, Z. Phys. Rev. C 10 (1974) 893.
7 LEDERGERBER, T., PALTIEL, Z. Phys. Lett. B 56, N 5 (1975) 417.
8 FULLER, R. Phys. Rev. 126 (1962) 684.
9 RUBCHENIA, V. A. Preprint of the Radium Institute RI-28 (1974) (Rus.).
10 EISMONT, V. P. Atomnaya Energiya, 19 (1965) 113 (Rus.).
11 DAVIES, K., SIERK, A., NIX, J., Phys. Rev. C 13 (1976) 2385.
12 BATENKOV, O. I., BLINOV, M. V., VITENKO, V. A. Phys. and Chem. of Fission 1979 (Proc. of Symp.), Vienna IAEA, 1980, p. 267.
13 NIFENECKER, H. et al. Phys. and Chem. of Fission 1973 (Proc. of Symp.) Vienna IAEA, 1974, p. 117.
14 GINDLER, J. et al. Phys. Rev. 16 (1977) 1483.
15 PIKSAJKIN, V. M. et al. Jadernaja Physika 25 (1977) 723 (Rus.).
16 GERASIMENKO, B. F., RUBCHENYA, Y. A., POZDNIAKOV, A. V. Neutron Physics (Proc. V. All Union Conf., Kiev, 1980) Moscow, CNIIAtominform, part 3, p. 114 (1980) (Rus.).
17 BLINOV, M. V., BOYKOV, G. S., VITENKO, V. A. Nuclear Data for Science and Technology (Proc. of an Intern. Conf. Antwerp, 1982) p. 479 (1983).

EXPERIMENTAL STUDIES OF FAST NEUTRON RADIATIVE CAPTURE CROSS-SECTIONS

V.N. KONONOV
Institute of Physics and Power Engineering (FEI),
SC AE USSR,
Obninsk, Union of Soviet Socialist Republics

Abstract

The lecture deals with the problems of experimental studies of fast neutron radiative capture cross-sections. The main attention is paid to the neutron energy range of 1 keV - 1 MeV, which is most essential for solving a number of problems of nuclear power engineering with fast neutron breeder reactors, as well as to the studies of highly-excited nuclei and investigations in nuclear astrophysics. Consideration is given to the experimental measurements of capture cross-sections at electrostatic accelerators and linear accelerators of electrons. The main experimental results and their theoretical analysis are summarized.

I. INTRODUCTION

The radiative capture or (n, γ) reaction is one of the main processes of interactions between neutrons and atomic nuclei with the energy up to ~ 1 MeV. There are also three main aspects determining the necessity of the detailed study of neutron radiative capture cross-sections.

First of all, the radiative capture cross-sections are important nuclear data employed for physical calculation of nuclear reactors. The advanced development of fast neutron breeder reactor concept for nuclear power engineering required a detailed study of all kinds of interactions between neutrons and nuclei in the energy range up to 1 MeV and more (fig. 1). Though the breeding ratio (BR) of nuclear fuel in a plutonium reactor can, basically, reach the meaning of 2.5 (as it was first shown by A.I.Leipunsky in 1949),

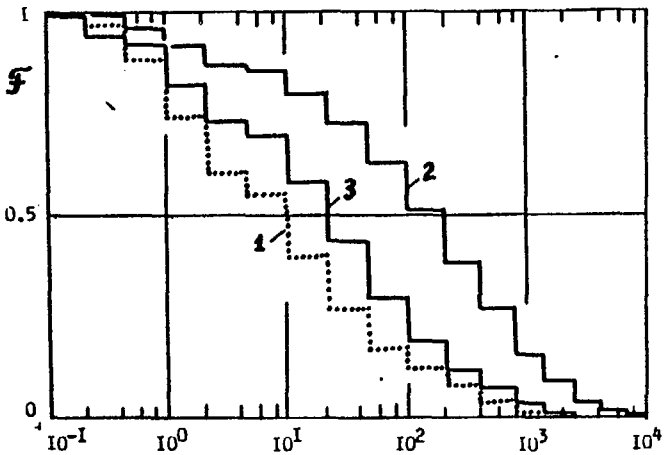

Fig. 1. The distribution function of neutron capture and fission reactions in ^{239}Pu and ^{238}U over the neutron spectrum of the high-power fast reactor active zone. 1 - capture in ^{239}Pu, 2 - fission in ^{239}Pu, 3 - capture in ^{238}U.

an attempt to obtain high thermodynamic and technological characteristics by means of utilizing a liquid-metal coolant (sodium), ceramic oxide fuel and stainless steel as the main structural materials resulted in a strong softening of neutron spectra. It caused a noticeable increase of neutron absorption at the expense of the (n, γ) reaction in the fuel itself, in the structural and technological reactor materials, as well as in the fission products accumulated in the reactor during its operation. In its turn, it resulted in a decrease of BR of large power reactors to the level of 1.2 - 1.3. The fact that we had to spend the largest portion of the BR excess (BR-1) on technological needs was a stimulus to the intense development of investigations of a complex of problems connected with the optimization of physical and technical-economical characteristics of fast reactors /1/. One of the starting-points in considering these problems is the nuclear data and, in particular, the data on neutron absorption cross-sections for nuclear fuel, structural materials and fission products. Note, that the neutron radiative capture cross-sections for fission products

are necessary not only from the point of view of physical calculations of reactors and their main technical parameters. They also play an important part in calculating the radiation situation in fuel processing , in evaluating the danger of environmental contamination. The main peculiarity of the problem of obtaining nuclear data on fission products is that the number of nuclides accumulated as a result of a commercial power reactor operation is great and most of them are unstable. That is why it is impossible to carry out in the near future a direct measurement of fast neutron radiative capture cross-sections for lots of fission products. In this connection the problem of obtaining the experimental data on the neutron capture cross-sections has appeared for a wide range of stable isotopes whose nuclear properties are close to the most important fission products, as well as of developing methods for calculation and capture cross-section evaluation on the basis of the theoretical presentations and systematics of the main parameters characterizing the interaction between neutrons and nuclei.

There is a second aspect closely related to this problem. It determines the urgency of the detailed study of the fast neutron capture cross-sections. That is the employment of these reactions for thorough nuclear-physical investigations: the study of the highly-excited state of atomic nuclei and the mechanism of nuclear reactions. The peculiarity of the neutron radiative capture reaction consists in the fact that due to the absence of a centrifugal barrier in the reaction exit channel the interaction of neutrons with a non-zero orbital momentum becomes essential at the energies as high as several keV. In this case one can single out the energy ranges of neutrons, in which interactions with this or that orbital momentum predominate. The second peculiarity of the neutron radiative capture, which is important from the point of view of studying the nucleus structure and nuclear reactions, is that the capture cross-sections are dependent on both the neutron and radiative strength functions. These two circumstances are the basis for the analysis of fast neutron average radiative capture cross-sections with the aim to obtain experimental information on neutron (S_l) and radiative (S_γ) strength functions for s-, p- and d-neutrons /2/.

The third way of employing the experimental data on the fast neutron radiative capture cross-sections is connected with nuclear astrophysics. Almost all the theories of the nuclide origin and abundance in the universe consider the neutron radiative capture to be the main process of heavy nuclei fusion in stars. On the basis of the experimental data on fast neutron radiative capture cross-sections and from the abundance of chemical elements and their isotopic composition one can estimate such key values as the univerge age and obtain information on its evolution at early stages of development /3/.

The urgency of the problems and wide range of pure and applied problems in these three seemingly far from each other fields arouse the interest of many investigators from various laboratories throughout the world in the research of fast neutron radiative capture cross-sections. This is the subject of discussions at lots of conferences on the problems of nuclear technology and pure research. At the same time there exist a lot of problems to be solved and the needs for new data on fast neutron capture cross-sections /4/ are far from being fully satisfied at the present time.

2. EXPERIMENTAL METHODS OF STUDYING FAST NEUTRON RADIATIVE CAPTURE CROSS-SECTIONS

2.1. The Brief Outline of the Methods

Any experiment on measuring neutron radiative capture cross-sections consists in detecting the number of capture events in the investigated sample, which is placed in the neutron flux. According to the way of capture event detection, the methods are divided into three main groups:

(a) the method based on neutron flux depression at the passage of neutrons through the sample;

(b) the method of detecting induced activity of a radioactive nuclide formed in the course of capture;

(c) the method of detecting prompt capture γ-rays [5].

Besides, one can, in principle, employ methods based on mass-spectrometry measurements.

The first method was mostly employed in the spherical geometry version. The absolute value of a neutron capture cross-section in this method can be obtained from the relative measurements.

The principle drawback of the method is the necessity of using thick samples and the corresponding difficulty in taking into account the resonance self-shielding effects. The method of transmission in the spherical geometry, for all its simplicity, is interesting rather from the historical point of view.

The activation method has a high sensitivity and is fairly simple. At the present time it is most often employed for γ -ray detection with a Ge-Li semiconductor spectrometer. Among the activation method disadvantages we point out the limitedness of its employment only in the cases when the (n, γ)-reaction products are radioactive nuclides with convenient life-times and decay scheme. The activation procedure suggests the use of a steady source of monoenergetic neutrons and, therefore, is rather low-productive. Though by the present time the use of this procedure has enabled us to obtain a great number of experimental data, the accuracy and reliability of many of them are low. This is due to the fact that in many experiments the impurity of slow (resonance and thermal) neutrons often distorted the measuring results. Besides, this method suggests a good knowledge of the decay scheme and its qualitative characteristics, i.e. the detected radiation yield per decay event of a radioactive nuclide. In spite of these essential disadvantages, the activation method was widely used in the research of fast neutron capture cross-sections and, in particular, for measuring isomer excitation cross-sections.

The method based on the capture prompt γ-rays detection is the most versatile and can be employed in a wide energy range of neutrons: from the resonance one to several MeV. An important advantage of the method is a possibility of its using together with the time-of-flight method. This combination makes the experiments on measuring neutron capture cross-sections fairly effective and allows us to obtain detailed information in a wide energy range of neutrons. At the present time the method based on detecting prompt γ -rays of capture is employed in many laboratories. Let us go into details of this method.

2.2. The Method of Detecting Prompt Capture γ -Rays

At the neutron radiative capture for the time less than 10^{-14}s only one or a few γ -quanta are emitted with a total energy almost equal to the sum of neutron binding energy in a compound nucleus and the neutron kinetic energy ($U = B_n + E_n$). The average number of emitted γ -quanta ("multiplicity") M varies from 1 to 4 or more and depends on concrete properties of the compound nuclei. For light nuclei and nuclei near by the closed shells $M = 1 - 2$ and the γ -ray spectra are hard ($E_\gamma \simeq 5 - 8$ MeV). For most medium and heavy nuclei the multiplicity is 3 - 4 and the average energy of capture γ-rays is 1.5 - 2 MeV. In a number of cases a change of spectra and multiplicity of prompt capture γ -rays in passing from one neutron resonance to another and also in varying the neutron energy in the unresolved resonance region is observed. In the latter case the γ -ray spectrum variation is due to the change of the contribution of neutrons with different orbital momenta. These circumstances make the main demand on the method of detecting events of neutron radiative capture by the prompt γ -rays. The detector must be insensitive to the spectrum and multiplicity of γ -rays.

There are two ways of solving this problem. The first one is the use of the total absorption detector, which detects all capture events regardless of the spectrum distribution of γ -quanta. A large liquid scintillation detector (LLSD), which is often called a scintillation tank, is one of such detectors. The second way consists in using detectors whose detection efficiency may be unambiguously related to the total energy of the emitted γ -quanta cascade. Among these are the Moxon-Ray detector (MRD) and "total energy" detectors (TED).

The scintillation tanks used for measuring fast neutron capture cross-sections have been developed in a number of laboratories. Their volume varies from some dozens of litres to 4000 l. The number of photomultipliers used for collecting light in large detectors can reach a hundred and in small detectors, about a dozen. In these detectors the 4π -geometry of γ -ray detection is realized. For this purpose provision is made for an open channel passing through the detector centre, in which the sample is located and the neutron beam travels. To decrease absorption of neutrons scattered in the sample, the channel walls are made of a material with poor absorption properties and up to 50% of trimethyl borate, which suppresses the absorption of moderated neutrons in the scintillator hydrogen,

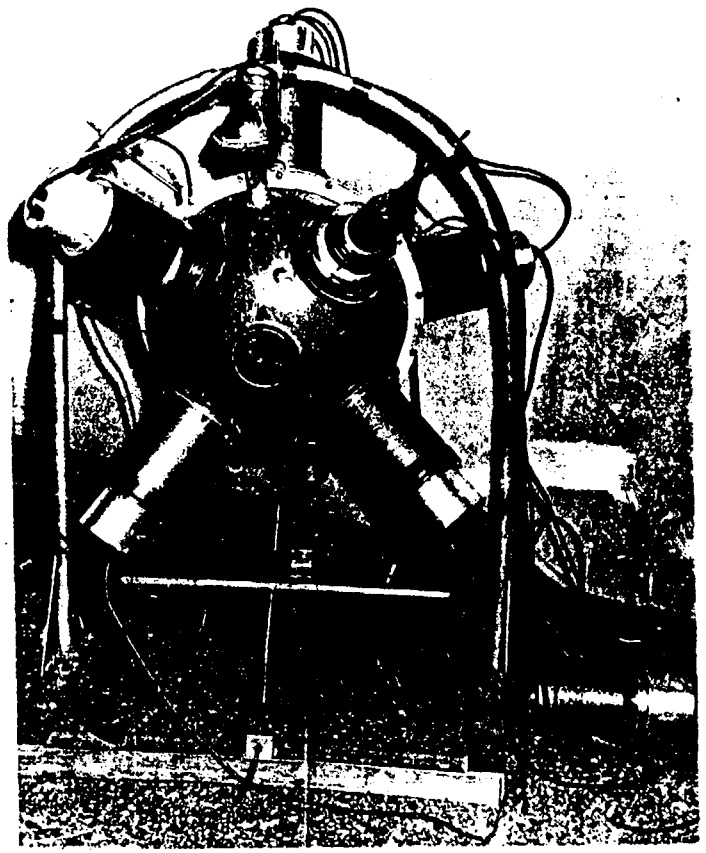

Fig. 2. A general view of the 17-l scintillation tank used for measuring neutron radiative capture cross-sections in Obninsk.

is added into the scintillator. In the detector with a small volume (17 l) it turned out that a heavy scintillator free of hydrogen on the basis of hexafluorine benzene can be used. In designing scintillation tanks one aims at obtaining 0.9 - 0.95 probability of interaction of at least one γ -quantum from the capture prompt γ -ray cascade. In this case the actual efficiency of capture event detection at the threshold of 1.5 - 2 MeV is $\sim$ 50%, the sensitivity to scattered neutrons at the energy of 100 keV is 10^{-4} - 10^{-2}.

The necessity of using a high threshold of detection results in the increase of detector sensitivity to γ -ray spectra variations. Making corrections to the zero threshold by means of extrapolating the amplitude spectrum, one can compensate for this increase but it significantly complicates the measuring procedure. The total error of measuring fast neutron capture cross-sections by a scintillator tank, which is related to the γ -ray sensitivity for nuclei with M = 2 - 5, is 5 - 7%. Fig. 2 shows a general view of the scintillation tank of the 17-l volume used for measuring neutron capture cross-sections in Obninsk. In this detector two types of scintillators are used:

- nonhydrogenous (C_6F_6) and
- hydrogenous with the addition of 60% of trimethyl borate

(the concentration ratio of hydrogen and boron atoms is 15:1). Fig. 3 presents amplitude spectra of this detector response in detecting single γ-quanta (E_γ = 4.43 MeV from the Pu-Be source) and multi-quantum events with $M \simeq 6$ (^{252}Cf, E_γ = 0.8 MeV). Since the scintillation tanks have a greater efficiency of detecting capture events, they are noticeably sensitive to the γ -ray spectrum and have a fairly high level of intrinsic background due to the cosmic radiation and natural radioactivity (1 - 100 puls./s).

An attempt to exclude the dependence of neutron capture event detection efficiency on multiplicity and γ -ray spectrum shape for small-sized detectors with insignificant intrinsic background resulted in using counters whose efficiency is proportional to the the single γ -quanta energy. A version of such a detector consisting of a thick (1 - 2 cm) graphitic (or bismuthic) radiator and a flat plastic scintillator 0.2 - 1 mm thick was named the Moxon-Ray detector. It is characterized by the response to γ-rays with the energy above 200 keV in the form of a peak $\sim$ 20% wide with the energy of $\sim$ 100 keV and linear dependence of single γ-quanta detection efficiency on their energies $\mathcal{E}(E_{\gamma i}) = c\Omega E_{\gamma i}$, defined by the character of γ -ray interaction and passage of Compton electrons through the radiator. That is why the number of counts of such a detector is proportional to the number of capture events, whatever their spectrum and multiplicity:

$$N_\gamma = \sum_i \nu(E_{\gamma i})\, \mathcal{E}(E_{\gamma i}) = c\Omega\nu$$

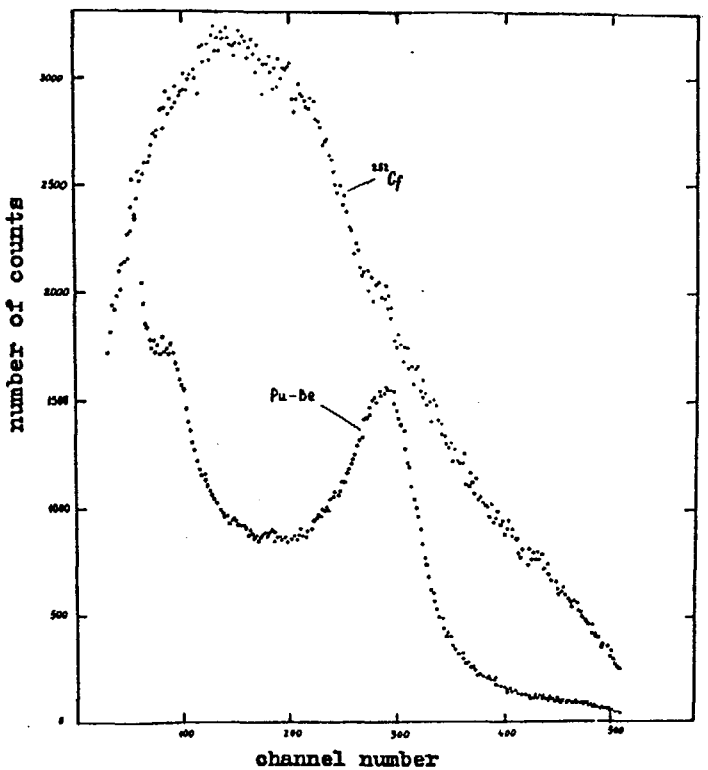

Fig. 3. Amplitude spectra obtained in detecting γ -rays with the energy of 4.43 MeV from the Pu-Be source and ^{252}Cf fission events with the help of the 17-l scintillation tank.

This relation is true under the condition that from the whole cascade only one γ -quantum is detected, i.e. $\varepsilon(E_{\gamma 1})$ must be insignificant. Since the efficiency of capture event detection is low (less than 5%), the MRD is small-sized and has minor intrinsic background and neutron sensitivity. It enables us to use this detector for the experiments at the electrostatic accelerator under the conditions of short path-lengths (up to 5 - 7 cm).

The next step in the development of the capture event detection technique was the total energy detector (TED) employing a method of a weight function suggested by Maier-Leibnitz (ref. 6) for obtaining the total energy of γ -rays from the A (V) amplitude spectra. The G (V) weight function may be found by solving the integral equation:

$$\int_0^\infty G(V)\, W(E_\gamma, V)\, dV = \frac{E_\gamma}{\varepsilon(E_\gamma)\Omega} ,$$

where $W(E_\gamma, V)$ is a function of response to single γ -quanta with the energy E_γ, $\varepsilon(E_\gamma)\Omega$ is the probability of γ -quanta detection. The weight function is usually a polinomial of the second or third order. The total energy of γ -rays passed through the detector in detecting the A (V) amplitude spectrum is:

$$Q = \int_0^\infty A(V)\, G(V)\, dV$$

This relation is also true for determining the total energy in the case of a γ -ray cascade and, consequently, for determining the the number of such events, if the total energy of γ -rays in the cascade is fixed and known, as in the case of capture event detection. At that, as in the case of the MRD, a restriction is placed on the TED efficiency value, so as to provide that not more than one γ -quantum from the cascade will be detected. However, this limiting condition may be removed by proper selection of the weight function. As it was shown by the recent investigations carried out in Obninsk, the γ -ray total energy may be regenerated with the accuracy of 2 - 3% from the amplitude spectra of the 17-l scintillation tank with the use of the weight function of the type:

$$G(V) = c \cdot U^{-0.39} \cdot V^{1.75}$$

Though the cascade γ -quanta energy summation takes place appreciably in the detector of this type, the introduction of dependence on the total energy U into the weight function provides for the preservation of capture event detection efficiency with an accuracy of 2 - 3% for a great variety of conditions, i.e. in changing multiplicity from 1 to 5 and total energy, from 4 to 10 MeV.

The improvement of the method of determining the total γ -ray energy results in the fact that recently the TED has become the main instrument for measuring neutron capture cross-sections by prompt γ -rays. Several laboratories started employing scintillators on the deuterobenzene (C_6D_6) basis in such detectors and, as a result, the sensitivity to scattered neutrons was decreased

to the value of 10^{-4} - 10^{-5}. Owing to these achievements, reliable measurements of fast neutron capture cross-sections proved to be possible for a number of structural materials.

2.3. Experimental Facility

Nowadays, the majority of fast neutron capture cross-section measurements have been carried out at the time-of-flight spectrometer on the basis of the linear electron accelerator (LINAC) and the Van de Graaf electrostatic generators (EG). The investigations of fast neutron capture cross-sections are also performed at neutron spectrometers on the basis of a pulsed fast reactor, synchrocyclotrons and, besides, at slowing-down time spectrometers in lead.

The spectrometers based on the LINAC (ORELA in the USA, GELINA in Belgium, Fakel in the USSR, etc.) are rather complex and expensive installations. The source of fast neutrons with a continuous spectrum of an average energy of ~ 1 MeV is a braking target of heavy elements (uranium, tantalum). For softening the neutron spectrum a polyethylene moderator 2 - 4 cm thick is used. The measurements of capture cross-sections at these installations are usually carried out at path lengths of 30 - 50 m and a burst duration of 4 - 5 ns. An important advantage of neutron spectrometers on the LINAC basis is a possibility to cover a great energy range from the thermal energies to several MeV. It enables us to make absolute measurements of fast neutron capture cross-sections employing the saturated resonance procedure. However, using these installations for the experiments on capture cross-sections we run into certain difficulties in determining the detector background value in the neutron energy range above 5 - 10 keV, which in this case is several times higher than the useful effect value and is in complex dependence on the neutron energy. The routine procedure of background measuring by using black resonant filters may cause an incorrect determination of the background value /7/ , which is one of the main reasons for systematic discrepancy in the results of measuring a number of fast neutron capture cross-sections.

A great amount of experimental data on fast neutron capture cross-sections was obtained at electrostatic accelerators operating in a pulse ns mode (Karlsruhe, Obninsk, etc.). Experimental procedures at these relatively simple and inexpensive plants are

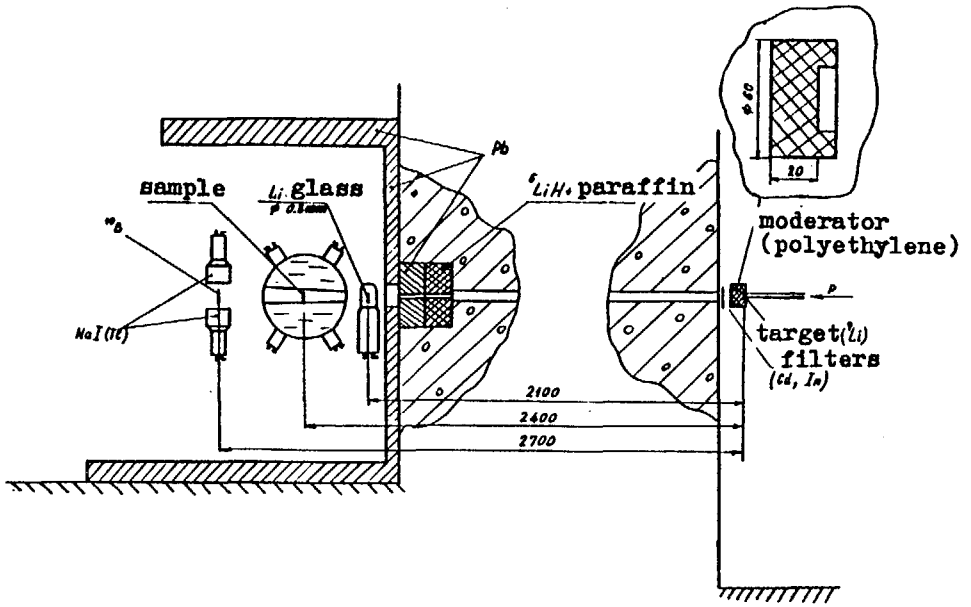

Fig. 4. A layout of the fast and resonance neutron spectrometer on the basis of the Van de Graaf pulsed accelerator of EG-1 in Obninsk.

in the process of constant updating. In particular, at the EG-1 accelerator in Obninsk a resonance neutron spectrometer mode has recently been put into effect, which enabled us to essentially expand the potentialities of the plant and to make absolute measurements employing the saturated resonance procedure /8/ . Fig. 4 shows the installation diagram. As a source of neutrons with the continuous spectrum both in the fast neutron region (3 - 1000 keV) and in the resonance one (2 - 100 eV) the reaction ^{7}Li (p, n)^{7}Be is used. At path lengths of 2 - 2.7 m and, in some experiments, of 0.4 - 0.7 m the capture event detector (scintillation tank of 17 l) and neutron spectrum measurement detectors (a thin glass scintillator with ^{6}Li and detector with a boron plate) were placed. The equipment spectra obtained in the fast neutron and resonance regions are shown in fig. 5. At fast neutron measurements the beam is always shuttered by a sodium filter 7 mm thick, which permits the energy scale to be monitored in each operating series and, together with the region close to the γ -peak, the background value

to be determined. For the measurements in the resonance region the cadmium and indium filters are used for the same purposes as well as for eliminating recycled neutrons. In the resonance region the first resonances in uranium, tantalum and gold are saturated. The experimentally measured counting rates of capture events N_c and neutron flux monitor N_m in the resonance and fast energy ranges (fig. 5) can be represented in the following form:

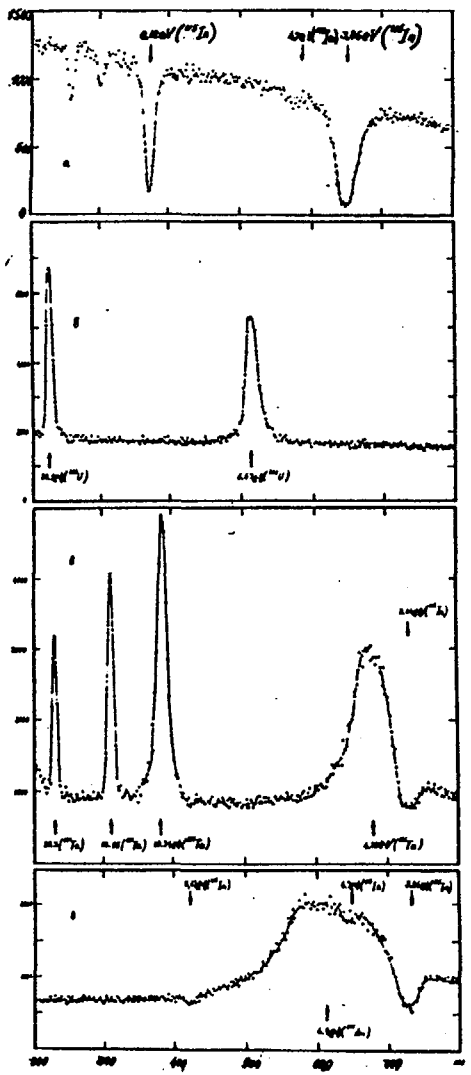

Fig.5 (1) channel number

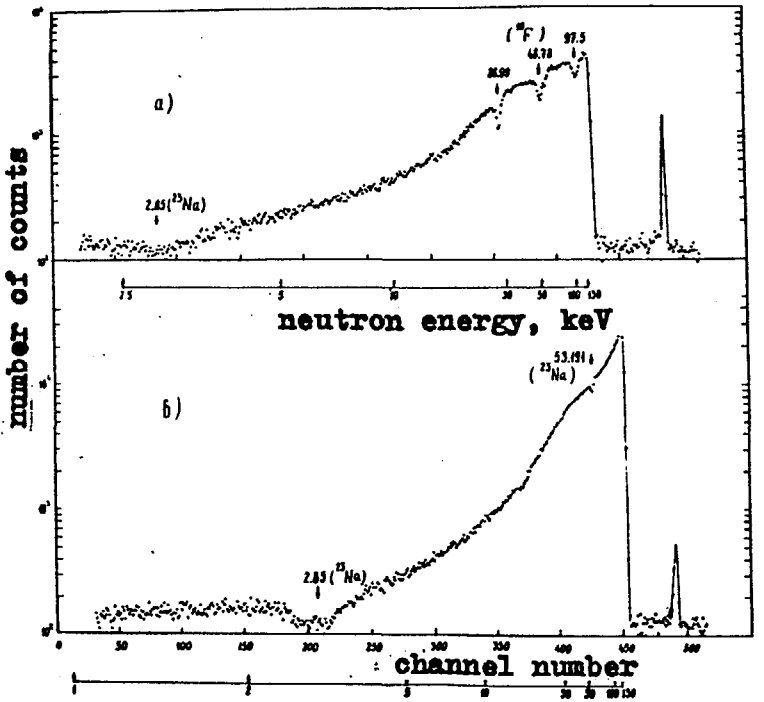

Fig. 5 (2)

Fig. 5. Instrumental time-of-flight spectra of the experiment on measuring capture cross-sections at the installation in Obninsk. 1 - time spectra in the resonance neutron region; the neutron beam is shuttered by filters of indium and cadmium; the channel scale value is 0.1 μs; (a) the neutron spectrum measured by a detector with the ^{6}Li glass; (b), (c), (d) capture event spectra measured by the scintillator tank with samples of ^{238}U, ^{181}Ta, ^{197}Au. 2 - time spectra in the fast neutron region; the channel scale value is 2.2 ns/channel; (a) the capture event spectrum in the ^{151}Eu sample measured by the scintillator tank; the neutron beam is shuttered by filters of ^{23}Na and Teflon; (b) the neutron spectrum measured by a detector with the ^{6}Li glass; the beam is shuttered by a ^{23}Na filter.

$$N_c^r = \phi^r \varepsilon_c \left[1 - \exp(-n\sigma_t)\right] \frac{\sigma_c}{\sigma_t} = \phi^r \varepsilon_c P_c$$

$$N_m^r = \phi^r \varepsilon_m \sigma_m^r$$

$$N_c^f = \phi^f \varepsilon_c n \sigma_c^f$$

$$N_m^f = \phi^f \varepsilon_m \sigma_m^f$$

The indices "r" and "f" refer to tests in the resonance and fast regions, ϕ is the flux of incident neutrons on the sample, ε_c is the efficiency of capture events detection, σ_m is the cross-section of the ^{6}Li (n,α) T reaction, ε_m is the inherent efficiency of the monitor's detection, n is the captive sample thickness. Combining these ratios, we can obtain the capture neutron cross-section in the fast region:

$$\sigma_c^f = \frac{(N_c/N_m)^f}{(N_c/N_m)^r} \frac{P_c}{n} \frac{\sigma_m^f}{\sigma_m^r}$$

In the saturated resonances $P_c \simeq 1$. That is why to obtain the absolute value of a capture cross-section in addition to experimentally measured values, we must know only one value, i.e. the relative travel of the ^{6}Li (n,α) T reaction cross-section, which follows the law $1/v$ in the wide neutron energy range.

Within this procedure with the use of the saturated resonance for the scintillator tank with the 17-l capacity the weight function method was also realized, which permitted the experiment errors due to the differences of γ-ray capture spectra for different nuclei and neutron energies to be minimized. At the installation systematic investigations of fast neutron capture cross-sections for a great number of nuclei are carried out with the use of separated isotope samples, basically.

It should be noted that the possibilities of improving the parameters of experimental installations on electrostatic accelerators are far from being exhausted. This is shown in fig. 6 representing the comparison of neutron flux density at the sample with a similar resolution at the ORELA spectrometer and at the electrostatic accelerator.

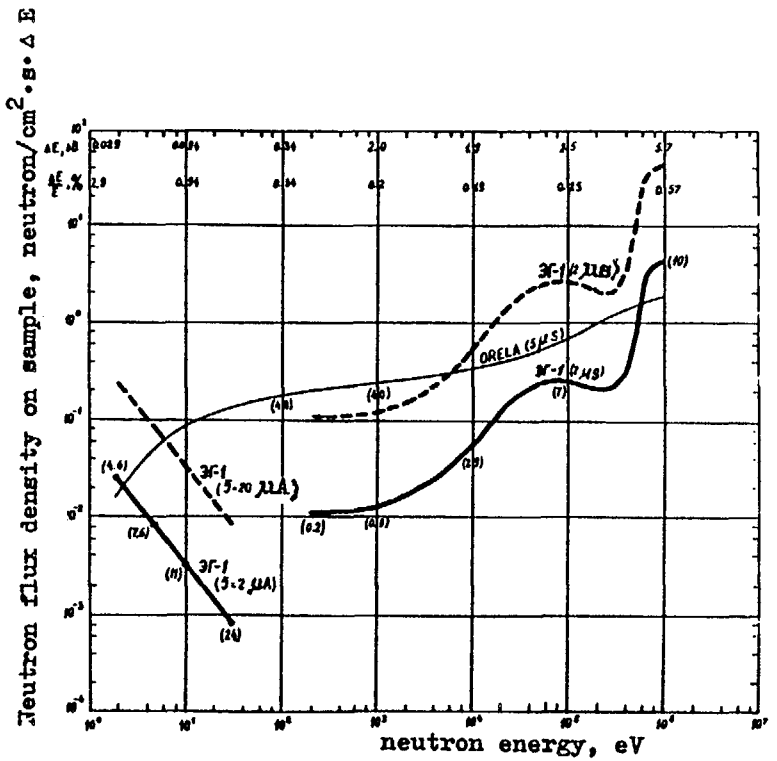

Fig. 6. Comparison of neutron flux density value at the sample in measuring capture cross-sections at the ORELA spectrometer and at that of fast and resonance neutrons on the basis of the Van de Graaf accelerator in Obninsk at the identical energy resolution shown at the top of the figure. Numbers in brackets stand for the path length value.

3. SOME RESULTS OF FAST NEUTRON CAPTURE CROSS-SECTION MEASUREMENTS

3.1. Nuclear Data for Fast Reactors

One of the key constants for calculating fast breeder reactors is the "alpha" ^{239}Pu value equal to the fission-to-capture ratio (σ_c/σ_f). The value α directly affects the most essential characteristics of a fast reactor. For example, the change of the α ^{239}Pu value, which is average over the spectrum, by 5% results

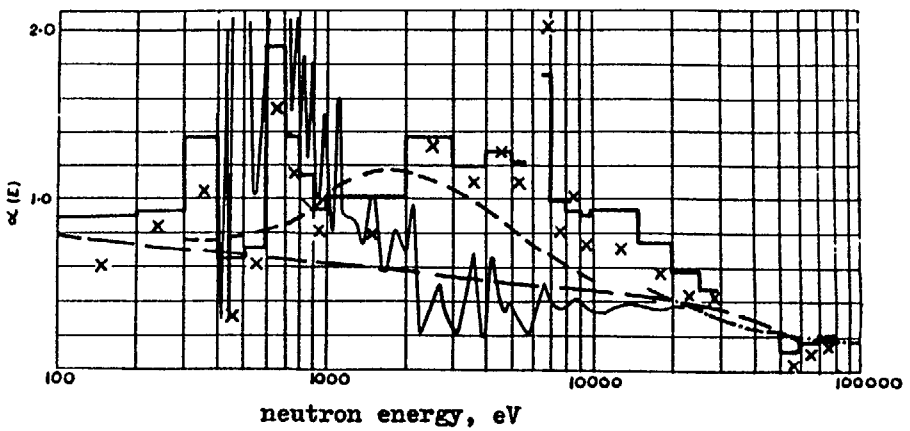

Fig. 7. The state of experimental data and estimates of the α-value of ^{239}Pu in the early 70es: ⩙ data obtained in Dubna; ⊓⊔ data obtained in Harwell; — — the Schmitt's estimate; - - the Ribon's estimate.

in the change of breeding ratio by 2%. Nevertheless, even in the early 70es there existed a great uncertainty in the α ^{239}Pu value (fig. 7), which caused a serious anxiety concerning the usefulness of developing nuclear engineering with fast neutron breeder reactors. In the period from 1970 to 1975 a great amount of measurements of the α value was made. These investigations are difficult due to a necessity of identifying capture events on the background of more likely processes of fission and scattering of neutrons in the presence of considerable radioactive background. As a result of these studies our knowledge of the α ^{239}Pu value has been substantially improved (fig. 8) and its error in the energy range pertaining to the fast reactors is as low as 5 - 7%, while the accuracy of knowing the average meaning of α over the fast reactor spectrum is 3 - 5% now /9/.

The second important reactor constant is the fast neutron capture cross-section in ^{238}U. That is the process determining the rate of reprocessing the new ^{239}Pu fuel. The peculiarity of the neutron capture cross-section in a ^{238}U even-even nucleus lies in the fact that the strong resonance structure in it manifests it-

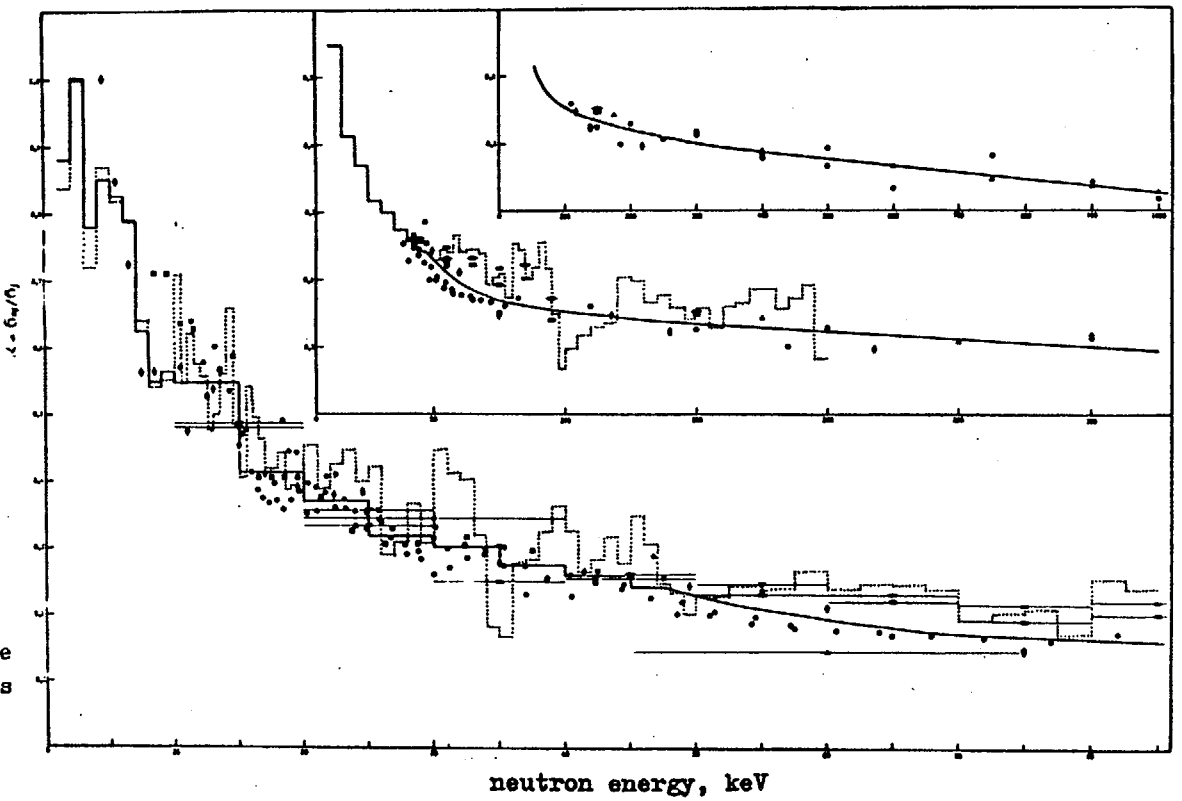

Fig. 8. The energy dependence of the α-value of ^{239}Pu in the region of 1 keV - 1 MeV: —— the Kononov's estimate; — the Poletaev's estimate [9]; • results of measurements obtained in Obninsk; ⋮⋮ the summary results of measurements in Oak Ridge.

self up to the neutron energies of several dozens of keV. Therefore, in the breeding blanket where the ^{238}U nuclei concentration is great a noticeable decrease of neutron absorption takes place as a result of the resonance self-shielding effect. The factor of the neutron capture cross-section resonance self-shielding in ^{238}U for a fast power reactor is $f_c \simeq 0.75$, which causes a reduction in the average operating capture cross-section in ^{238}U from ~ 0.4

to ~ 0.3 b and displaces the neutron balance not in favour of nuclear fuel breeding. The modern requirements to the accuracy of the fast neutron capture cross-section knowledge and that of the f_c value in ^{238}U are 2.5 - 3%. Yet, at the present time this accuracy level is far from being reached.

In the neutron energy range up to ~ 500 keV the main experimental results on the capture cross-section in ^{238}U were obtained at the resonance neutron spectrometers on the basis of LINAC. Despite the great attention paid to obtaining these data in the laboratories in Harwell, Oak Ridge and others, the disagreement between the results of different laboratories is substantial and reaches 20 - 30%. Probably, these disagreements are caused by the inadequacy of the background measuring procedure. Recently, the absolute measurements of neutron capture cross-sections and resonance self-shielding factors in ^{238}U have been carried out at the spectrometer of fast and resonance neutrons on the basis of the EG-1 electrostatic accelerator in Obninsk /10/. The measurement conditions in this experiment greatly differ from those at the LINAC. The expected accuracy of these measurements is 3 - 5% in the most part of the neutron energy range interesting from the point of view of fast reactors.

Together with the nuclear data for fuel-and-raw materials, those on capture cross-sections for structural materials (isotopes of iron, chromium, nickel, molybdenum, etc.) and fission products are of equal interest. In this direction a great amount of measurements have also been made. In particular, in Obninsk they have obtained a lot of experimental data on cross-sections of fast neutron capture by the rare-earth element isotpes, many of which are important fission products. However, in this field of researches the needs of nuclear engineering for nuclear data have not been fully satisfied /4/.

3.2. Nuclear-Physical Investigations

In the radiative capture reaction a noticeable contribution of neutrons with a nonzero orbital momentum manifests itself even at the neutron energy of some keV, which is due to the lack of centrifugal barrier in the reaction outlet channel. Besides, the radiative capture reaction cross-section is a result of competition with emitting elastically and inelastically scattered neutrons and the contribution of the partial l-wave may be written in the following simplified form:

$$\sigma_{\gamma l} \sim \frac{1}{k^2} \cdot \frac{S_{\gamma l} S_{nl} (kR)^{2l+1}}{\mathcal{E}_1 S_{\gamma l} + \mathcal{E}_2 S_{nl} (kR)^{2l+1}}$$

where $S_{\gamma l}$ and S_{nl} are the reduced radiative and neutron strength functions, $\mathcal{E}_1$ and $\mathcal{E}_2$ are the spin factors; in the neutron energy range under consideration $(kR) \ll 1$. For S-neutrons usually $\mathcal{E}_2 S_{nl} (kR)^{2l+1} \gg \mathcal{E}_1 S_{\gamma l}$ even at the neutron energy of some hundreds of eV and the partial capture cross-section in the keV region for them is $\sigma_{\gamma s} \sim 1/E$. For p- and d-neutrons there are regions in which the partial capture cross-section $\sigma_{\gamma l} \sim (kR)^{2l+1}$, i.e. they grow with the increase of neutron energy (if $\mathcal{E}_2 S_{nl} \cdot (kR)^{2l+1} < \mathcal{E}_1 S_{\gamma l}$) and the regions in which the contribution of waves with $l \neq 0$ is "saturated" and the partial cross-sections become decreasing:

$$\sigma_{\gamma l} \sim 1/E \text{ (where } \mathcal{E}_2 S_{nl} (kR)^{2l+1} > \mathcal{E}_1 S_{\gamma l})$$

This peculiarity of the energy dependence of s-, p- and d-neutron contribution to the total average neutron capture cross-section is the basis for its decomposition into partial contributions in the neutron energy range of 1 - 300 keV. In the neutron energy range of 100 - 300 keV the contribution of neutrons with $l \geq 3$ is insignificant as yet, but the primary levels of many nuclei lie in this region and under favourable conditions the inelastic scattering channel can open up. The even-even nuclei having a collective level with $J^{\pi} = 2^+$ in this energy range are of special interest. According to the law of momentum and parity conservation, the inelastic scattering of incident s-, p- and d-neutrons with the excitation of the 2^+ level of the even-even target nucleus results in neutron emission with the orbital momenta 2, 1 and 0, respectively. Since the permeability of the nuclear surface for outgoing inelastically scattered neutrons with the nonzero momentum is strongly suppressed by the presence of the centrifugal barrier, the competition of the inelastic scattering opening channel against the radiative capture results, first of all, in the suppression of partial contribution

due to the d-neutron capture. This peculiarity of the even-even nuclei capture cross-section behaviour close to the first 2^+ level enables us to evaluate the contribution to the d-wave capture cross-section and to determine neutron strength functions reliably enough.

Fig. 9 shows partial contributions of the s-, p- and d-neutrons to the radiative capture cross-section in the energy range of 5 - 300 keV for ^{115}In and ^{170}Er, which reflect the peculiarities of the behaviour of neutron contributions with different orbital momenta for the nuclei in the S_1 maximum region and even-even nuclei in the S_0 and S_2 maximum regions. In addition to the neutron strength functions the average radiative capture cross-sections depend also on the magnitude of the relation $\langle \Gamma_\gamma \rangle / \langle D \rangle$. Though separate data on the radiative width and density of levels cannot be obtained from the average cross-section analysis, their relation called by analogy the radiative strength function is also of a certain interest.

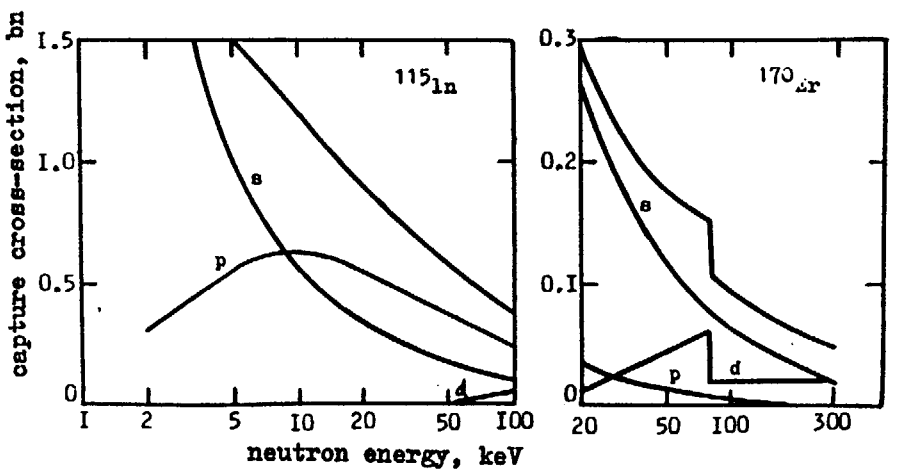

Fig. 9. Partial contributions of s-, p- and d-neutrons to neutron radiative capture cross-sections for ^{115}In and ^{170}Er.

When analysing average capture cross-sections, the one calculated within the statistical theory is fitted to the measured one. The fitting parameters are the neutron S_1 and S_2 and the radiative strength functions. As a rule, the average capture cross-sections are not highly sensitive to the S_0 value. Recently, the method of average capture cross-section analysis has been constantly improved both from the point of view of closer consideration of a number of factors in calculating capture cross-sections within the statistical theory (taking into account fluctuations of neutron widths, energy dependence of the total radiation width and nuclear level density, as well as inelastic scattering) and in terms of obtaining more reliable experimental data on neutron capture cross-sections in a wide range of neutron energy.

In the recent studies carried out in Obninsk the experimental data on average capture cross-sections for a large group of rare-earth nuclei have been obtained. The measurements were made at a nanosecond time-of-flight spectrometer on the basis of a pulsed Van de Graaf accelerator and covered the neutron energy range of 5 - - 350 keV. When analysing the capture cross-sections obtained within the statistical theory frame, it turned out that it is important to describe the experimental data error with the use of a covariance matrix, since the main components of the measured cross-section error are of a systematic character. It enables us to be more strict in determining the cross-section curve obtained in the experiment and, consequently, to derive the information contained on average resonance parameters to a better extent. Fig. 10 presents the results of measurements and analysis of capture cross-sections for isotopes of ^{166}, ^{168}, ^{170}Er. The results of these studies show that for the nuclei investigated in the rare-earth region (isotopes of Nd, Sm, Eu, Gd, Dy, etc.) within the accuracy limit of experimental data there are no essential deviations from the description of average neutron capture cross-sections within the statistical theory of nuclear reactions. The data obtained on neutron strength functions for the d-neutrons have an accuracy of 15 - 20% and confirm the presence of the maximum (3 d-resonance) in S_2 in this region of nuclei (fig. 11). Besides, on the basis of these results one can assume possible splitting of the 3 d-resonances.

Moreover, as a result of these investigations new data on the anomalous dependence of nuclear level density for a number of rare-earth isotopes were obtained, as well as an indication of a possible systematic difference between radiative strength functions for neutrons with different orbital momenta.

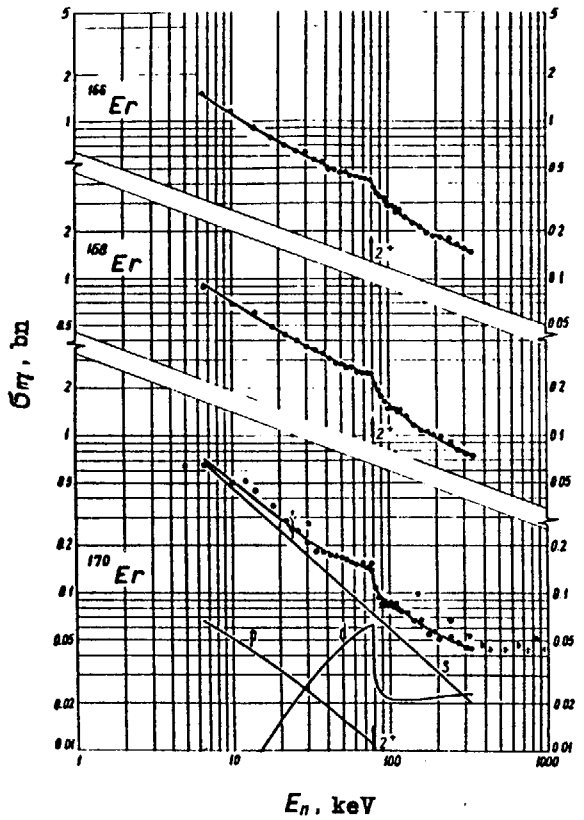

Fig.10. Neutron radiative capture cross-sections for erbium isotopes Dots stand for experimental data, lines, for calculation results according to the statistical theory.

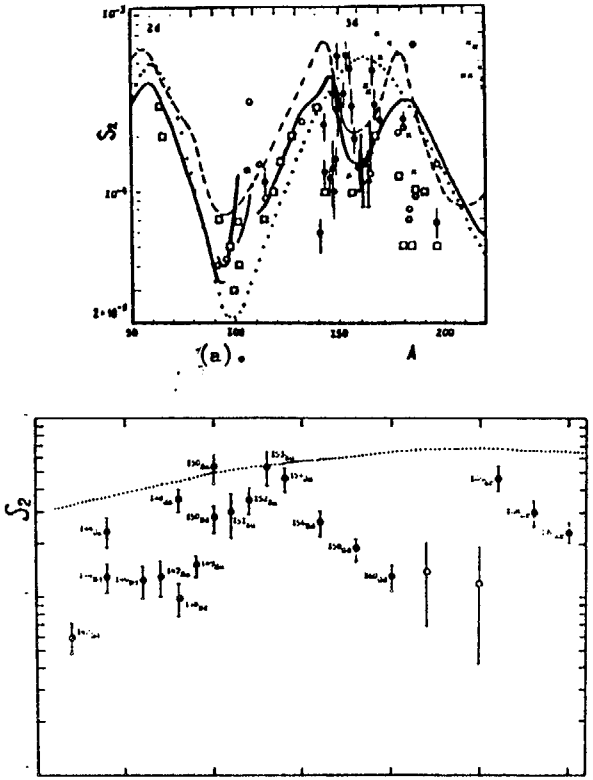

Fig.11. Neutron strength functions for d-neutrons. Experimental data: ▯ from the analysis of ion cross-sections; ∮ from the analysis of neutron capture cross-sections obtained in Obninsk. Calculation results: .... the spherical optical model; - - -, —— the channel strong coupling method.

These examples illustrate what can be derived from fast neutron radiative capture cross-sections for the study of highly-excited nuclei structure.

3.3. The Neutron Radiative Capture and Heavy Element Genesis

The first detailed experimental data on the fast neutron radiative capture cross-sections for a wide range of nuclei obtained (1946)by Hughes et al.enabled Alfer, Bethe and Gamow to establish correlation between the natural abundance of chemical elements and their nuclear properties. From this time on the neutron capture cross-section investigations are closely related to the theories of heavy element genesis in the universe, primarily, with the s-process model, according to which the heavy element genesis happened as a slow (as compared with the β-decay periods) successive capture of neutron by nuclides being in the β-stability band. The success of the s-process model was mostly due to the correlation ob-

served between the abundance of isotopes and neutron capture cross-sections for a chain of isotopes of strontium, zirconium, tin, tellurium, samarium, among which there were nuclides whose genesis was related to one s-process (shielded nuclei).

The problem of element fusion in the s-process can be considered as a successive slow (relative to the β-decay) neutron capture by the original nuclei A_0 of the iron group, which is described by a system of conventional differential equations:

$$\frac{d\Psi(A_0,\tau)}{d\tau} = -\sigma_c(A_0)\,\Psi(A_0,\tau)$$

. . . . . .

$$\frac{d\Psi(A_1\tau)}{d\tau} = \sigma_c(A)\,[\Psi(A-1,\tau) - \Psi(A_1\tau)]$$

where $\Psi(A_1\tau) = \sigma_c(A)\cdot N(A_1\tau)$, $\sigma_c(A)$ is the neutron capture cross-section for a nuclide A, $N(A_1\tau)$ is the number of accumulated nuclides A depending on the integral radiation dose $\tau = \int \phi_n dt$ by the neutron flux ϕ_n. For heavy nuclei with fairly large neutron capture cross-sections in the s-process the equilibrium between accumulation and burn-up of the given nuclide is established, which results in the observed constant product of the neutron capture cross-section by the abundance.

Though this system has an analytical solution, it is difficult to use it due to the uncertainty of the data available on capture cross-sections and the solution divergence. That is why Kleiton et al. developed the approximation method of obtaining the solution, as a result of which we could quantitatively analyse the data on natural abundance of elements within the s-process model.

Later, in Obninsk the solution of the system describing heavy element fusion in the s-process was made with the help of the analog computer (AC) "Baykal" /3/. The neutron radiative capture cross-sections necessary for the solution of the problem at the energy of 25 keV for all nuclei participating in the s-process were taken from the experiment and calculated within the statistical theory of nuclear reactions on the basis of the systematics of the parameters of nuclear level density and radiative widths. The cross-sections used, both experimental and estimated, are given in fig. 12. Some

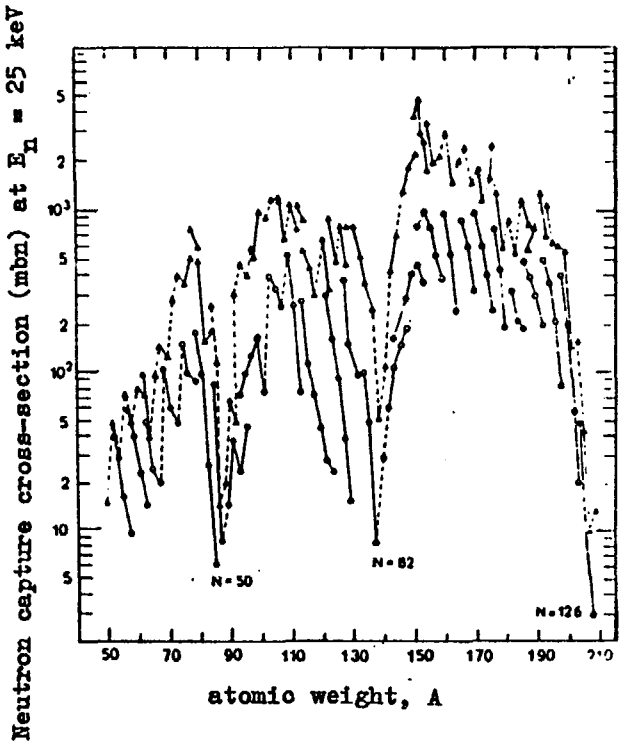

Fig.12. Neutron radiative capture cross-sections at the energy of 25 keV: •, o experimental and calculated data for even-even nuclei; ▲, Δ the data on odd nuclei. The isotopes of one and the same element are connected by lines.

of the results obtained for $\Psi(A_1\tau)$ are shown in fig. 13. The form of the solutions appeared to be similar to that obtained by Kleiton. Note that the system solutions obtained are not highly sensitive to the value σ_c, except for regions with an insignificant value of capture cross-sections (near-magic nuclei, those of the group of iron, cobalt, nickel). The comparison of dependences of the $\Psi(A_1\tau)$ solutions on A at the fixed values of τ with the values $(\sigma_c \cdot N)$ known from the experiment for nuclei formed basically in the s-process (given in fig. 13) confirmed the fact that we failed to explain the element abundance observed by the effect of only one fixed meaning of the integral neutron flux for the whole region of nuclei masses A = 60 - 210.

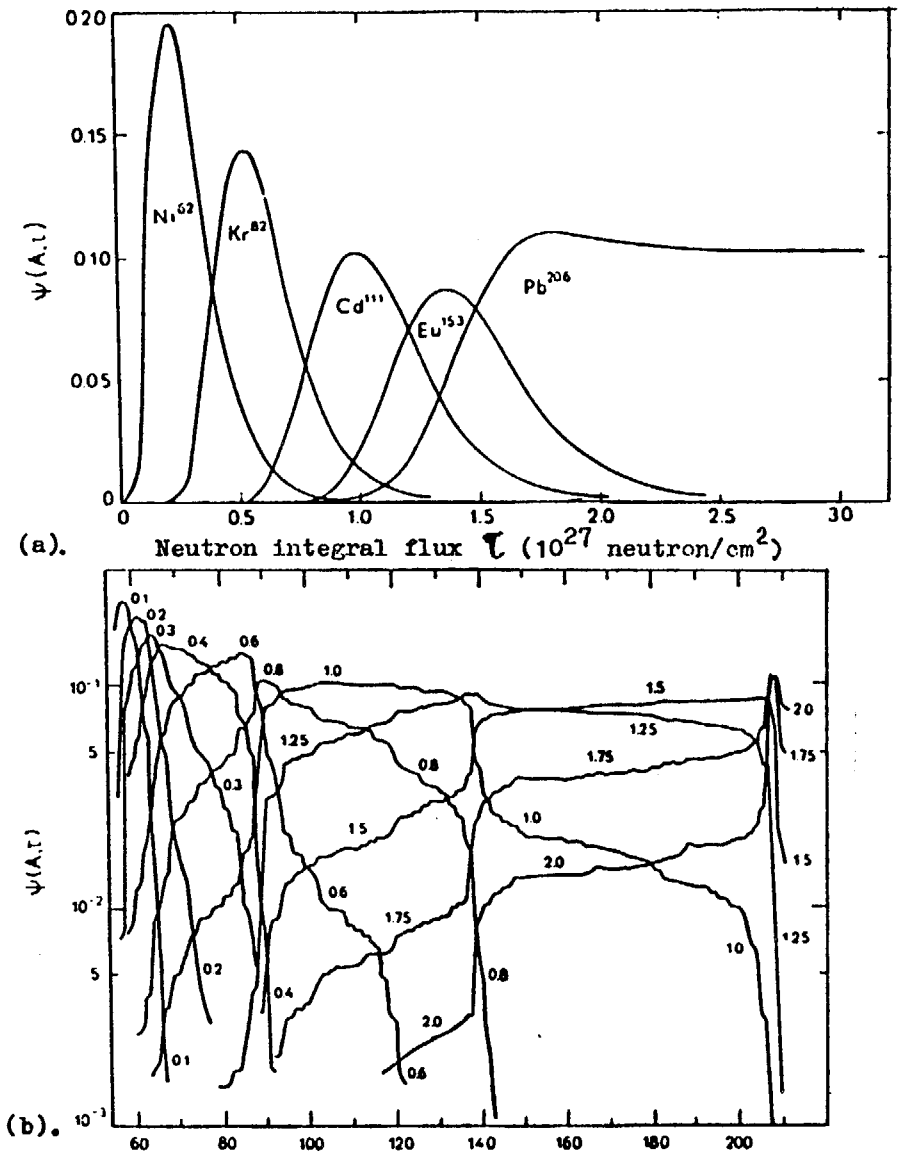

Fig.13. Solutions of $\psi(A,\tau)$ depending on the value of the integral neutron flux τ (in terms of 10^{27} neutr./cm^2) for certain nuclei (a) and depending on the atomic weight A at the fixed values of τ (b). The initial amount of nuclei is ^{56}Fe (56.0) = 1.

Fig. 14 shows the dependence of the product of a neutron capture cross-section at an average energy of 25 keV by abundance on the atomic weight taken from ref./3/. The dots stand for experimental or estimated data (capture cross-section calculation within

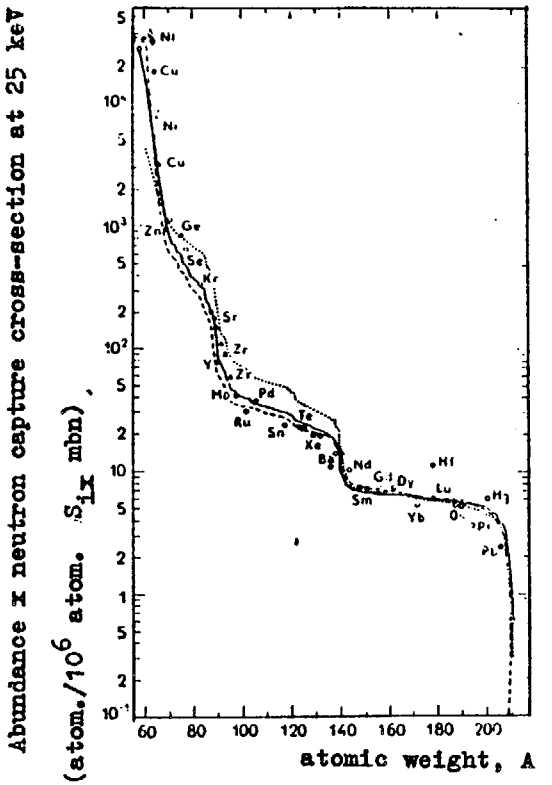

Fig.14. Correlation between the nuclei abundance in the solar system N_s and neutron radiative capture cross-sections at kT = = 25 keV. The theoretical curves $\psi(A) = N_s(A)\cdot\sigma_c(A)$ are calculated for three types of distribution function of the neutron exposures $\rho(\tau)$:

.... $\rho(\tau) = 1.14\cdot\exp(-\tau/0.17)$;

----$\begin{cases}\rho(\tau) = 24\cdot\tau^{-3.2} \text{ at } \tau < 1.35\\ \rho(\tau) = 0 \text{ at } \tau > 1,\ 3,\ 5;\end{cases}$

——$\rho(\tau) = 2.3\cdot10^3\exp(-\tau/0.22) + 1.6\cdot10^5\exp(-\tau/0.059)$

•, o nuclei formed in the s-process only, experimental and calculated neutron capture cross-sections; ▲ nuclei formed mostly in the s-process, experimental neutron capture cross-sections.

the statistical theory) basically for the nuclei formed in the s-process. The lines indicate the calculation results for various assumptions on the function of neutron integral flux distribution $\rho(\tau)$.

We succeeded in obtaining the best description of the experimental data on the dependence of the product of a capture cross-section by abundance when using the distribution function:

$$\rho(\tau) = G_1 \exp(-\tau/\tau_1) + G_2 \exp(-\tau/\tau_2)$$

where $G_1 = 2.3 \cdot 10^3$, $\tau_1 = 0.22\ \text{mbn}^{-1}$, $G_2 = 1.6 \cdot 10^5$, $\tau_2 = 0.059\ \text{mbn}^{-1}$. The calculation results with this distribution function are given in fig. 14 by a solid line. In using this distribution the experimental data in the region of lead have a better description, too. The distribution functions in the form of a sum of two exponents can be assigned a physical meaning on the assumption that two stages of element fusion are present in the s-process with two types of neutron sources.

Since our paper /3/ was published, there appeared new data both on the radiative capture cross-sections and natural abundance of elements, which, on the whole, confirmed the concepts of the s-process model of the heavy element formation under the conditions of integral neutron flux superposition. In Karlsruhe from the analysis of the s-process branching in the region of ^{176}Lu and using this meaning of τ_0 the age of the Universe was estimated at $6 \cdot 10^9$ years, which agreed with the estimate of $7 \cdot 10^9$ years obtained by using the ^{238}U - ^{232}Th clock. Thus, the use of the experimental data on the fast neutron radiative capture cross-sections enables us to reconstruct the genesis of a lot of heavy elements, as well as to establish the chronology of evolution of the Galaxy.

REFERENCES

1. Leypunsky A.I., Orlov V.V., Lytkin V.B., Troyanov M.F., Yurova L.N. Methods of effective utilization of fuel in nuclear energetics with fast reactors. - Atomnaya Energiya, 1976, v. 31, No. 4, pp 383 - 392.
2. Kononov V.N. Some results of experimental investigations of s-, p- and d-neutron interaction with atomic nuclei. - In: III International School of Neutron Physics (Alushta, 1978). D3-11787, Dubna, JINR publication, 1978, pp 415 - 436.
3. Shorin V.S., Gribunin V.M., Kononov V.N., Sidorova I.V. Fusion of elements in s-process. - Astrofizika, 1971, v. 7, No. 3, pp 489 - 500.
4. WRENDA 81/82. World Request List for Nuclear Data. Ed. by D.W. Muir, Vienna, IAEA, 1982.
5. Stavissky Yu.Ya., Abramov A.I., Vankov A.A., Kononov V.N. et al. Radiative capture of fast neutrons. - Atomizdat, Moscow, 1970.
6. Maier-Leibnitz H., Schmitt H.W., Armbruster P. Average Number and Energy of Gamma-Rays Emitted as a Function of Fragment Mass in ^{235}U Thermal-Neutron-Induced Fission. - In: Physics and Chemistry of Fission (Proc. of Symp., Salzbourg, 1965), v.2, Vienna, IAEA, 1965, pp 143 - 161.
7. Cornelis E., Vanpraet G.J., Bastian C. et al. Average Capture Cross Sections of the Fission Product Nuclei ^{104}, ^{105}, ^{106}, ^{108}, ^{110}Pd. In: Nuclear Data for Science and Technology (Proc. of the Int. Conf., Antwerp., 1982) pp 222 - 225.
8. Kononov V.N., Poletaev E.D., Kazakov L.E. et al. A spectrometer of fast and resonance neutrons on the basis of the EG-1 electrostatic accelerator in the FET. - In: Problems of Nuclear Science and Engineering. Ser.: Nuclear Constants, 1981, is. 1 (40), pp 67 - 71, CSRIAR; Employment of the weight function method in experiments on measuring neutron radiative capture cross-sections - In: Neutron Physics (Proc. of the 5th All-Union Conf. on Neutron Physics, Kiev, September 15 - 19, 1980), CSRIAR, 1980, part 4, pp 114 - 118.
9. Kononov V.N., Poletaev E.D. The status of experimental data on the alpha ^{239}Pu value. - Atomnaya Energiya, 1978, v. 45, No. 3, pp 187 - 192.
10. Kononov V.N., Poletaev E.D., Kazakov L.E. et al. The absolute method for measuring fast neutron radiative capture cross-section in Uranium-238. - In: Neutron Physics (Proc. of the 5th All-Union Conf. on Neutron Physics, Kiev, September 15 - 19, 1980) CSRIAR, 1980, part 2, pp 280 - 284; Measurement of factors of neutron capture cross-section resonance blocking for Uranium-238. - Same, pp 276 - 279.

INVESTIGATIONS OF WEAK INTERACTIONS WITH POLARIZED NEUTRONS

Yu.A. MOSTOVOY
I.V. Kurchatov Institute of Atomic Energy,
Moscow, Union of Soviet Socialist Republics

Abstract

The neutron-polarized experiments in beta-decay and nucleon-nucleon interactions, which have considerably contributed to formation and development of the weak-interaction theory, are discussed in the present lecture.

The modern theory of weak interaction is a consistent one, covering decay of various particles within a wide energy range and considering different properties of particles. Recently, new particles, vector bosons, predicted by this theory, have been discovered. The discovery of these particles is a new step towards unification of the theories of electromagnetic and weak interactions. Seeing such a great progress made in understanding of weak-interaction processes, it is difficult to imagine that as far back as at the beginning of this century the science did not know anything about weak interactions, that the first theory of nuclear β-decay was suggested by E.Fermi only fifty years ago and non-conservation of parity, the fundamental property of weak interaction, was discovered only twenty five years ago.

During this time the weak interaction theory has been worked up from the Fermi's β-decay theory to the universal four-fermion weak interaction theory (Gell-Mann, Feynmann, Marshak, Sudarshan) and further to the Weinberg-Salama theory eliminating the locality difficulties and succeeding in unification of the weak and electromagnetic interactions.

Progress in understanding the weak interaction is the result of a wide number of experiments both in the high and low energy regions.

The present lecture will be restricted to a minor part of these experiments, those associated with use of polarized neutrons.

Why are the polarized neutrons an important tool in the investigations of the weak interaction?

First, in the case of complex nuclei the strong interaction of nucleons affects manifestation of the weak interaction in β-decay. The free neutron decay occurs outside the nucleus. Therefore investigation of the neutron β-decay permits the information about the Hamiltonian of the weak interaction to be obtained without limitations imposed by inaccurate knowledge of the nuclear structure.

Second, the characteristic feature of weak interaction is that they do not converse parity. The non-conservation of parity manifests itself in distribution of the directions of particle emissions with respect to the spin of the decaying nucleus. For investigations of the weak interaction processes polarized neutron sources are needed. Therefore it is important that there are techniques for obtaining highly polarized neutron beams.

Third, information about the neutrino produced in β-decay can only be obtained by registration of recoil nuclei. When the neutron beam is used as the gaseous source of β-decay the registration of recoil protons is carried out simply enough.

Finally, for studying the weak interaction in nucleon-nucleon interactions it is important that neutrons have no electric charge.

Neutron decay is a process which could permit all the problems of β-decay investigation to be solved. However, this possibility is restricted by insufficient intensity of polarized neutron beams. Development of the technique of producing neutron beams of higher intensity makes it possible to obtain higher accuracies of investigations.

The modern theory of the weak interaction has been developed on the basis of the β-decay theory suggested by E.Fermi in 1934. The essence of the theory was that the electron and neutrino emitted in β-decay of the particle are born at the moment of β-decay. Fermi determined the β-interaction Hamiltonian as the operator of neutron transformation to proton and Dirac's wave functions of the four particles, neutron, proton, electron and neutrino, involved in the process. In the most general interaction invariant the Hamiltonian expression may have five variants of interaction: scalar S, tensor T, polar-vector V, axial-vector A and pseudoscalar P couplings. The names of the interactions are due to the form of conver-

sion of component combinations for possible Dirac functions. In the allowed β-transitions, and the neutron decay is one of them, the pseudoscalar variant cannot manifest itself. The rest may give different contributions to the weak interaction Hamiltonian. Since various variants predict essentially different properties of the weak interaction, the contributions of individual variants are to be determined by the experiment. In the general form, with allowance for possible difference in constants for different parity and under assumption of their complexity, these contributions may be characterized with sixteen constants. Sixteen independent experiments are to be conducted for their complete experimental determination. So far such a complete set of experiments has not been carried out. Using assumptions based on scarce experimental data, it is possible nevertheless to find out relations between the constants. In order to reduce the number of constants to four: C_S, C_V, C_A and C_T it is necessary to use assumptions on the time parity (constant reality) and on complete non-conservation of the space parity.

In the case of neutron β-decay the probability of decay at given directions of electron and neutrino-emission with respect to the neutron spin is determined by

$$W \sim 1 + \frac{v_e}{c} a(\vec{p}_e \vec{p}_\nu) + P\left[\frac{v_e}{c} A(\vec{p}_e \vec{\sigma}) + B(\vec{p}_\nu \vec{\sigma}) + \frac{v_e}{c} D \vec{\sigma}[\vec{p}_e \vec{p}_\nu]\right]$$

where $\vec{p}_e, \vec{p}_\nu$, are the unit vectors of the directions of electron and neutrino emissions, $\vec{\sigma}$ is the polarization direction, P is the degree of beam polarization, $\beta = \frac{v_e}{c}$ and a,A,B and D are the electron-neutrino, electron spin, neutrino spin and three-vector correlation coefficients.

The correlation coefficients are the functions of the weak interaction constants. Therefore three coefficients a,A and B together with $f\tau$, neutron life-time characteristic, permit four independent equations to be obtained for experimental determination of the contributions of four types of interaction.

The coefficient D is determined by imaginary parts of the weak interaction constants which may be nonzero in the case of violation of T-invariance.

Let us consider the experiments on investigation of β-decay of polarized neutrons, which have been carried out.

T-Invariance and Reality of Constants

In the decay of K mesons the decay to 2π meson have been observed in addition to common 3π meson decay. This process violates T-invariance. Is this violation generally typical of weak interaction? To answer this question experiments on search for effects violating T-invariance in the neutron decay were carried out.

The expression for decay probability contains term $D\vec{\sigma}[\vec{p}_e \vec{p}_\nu]$, where $\vec{\sigma}$ is the neutron spin, $\vec{p}_e$ and $\vec{p}_\nu$ are the unit vectors in the direction of electron and neutrino emission. This term changes its sign in transition from t to -t. Therefore, if T-invariance in β-decay is violated the decay probabilities for t and -t are different and the coefficient D characterizing the degree of the invariance violation will prove to be nonzero. To find $D \neq 0$ it is not necessary to change the time direction. It is easy to see that $\vec{\sigma}[\vec{p}_e \vec{p}_\nu]$ also changes the sign when $\vec{\sigma} \to -\vec{\sigma}$. For separation $\vec{\sigma}[\vec{p}_e \vec{p}_\nu]$ combination one must select the directions of $\vec{\sigma}, \vec{p}_e$ and $\vec{p}_\nu$ vectors, so that their averaged directions would be mutually orthogonal, and compare the decay probability for two directions of the neutron beam polarization vector.

The direction $\vec{p}_e$ is determined by the position of the decay electron detector relative to the beam. In the experiments carried out at the I.V.Kurchatov Institute of Atomic Energy the direction of neutrino emission was determined using the time-of-flight proton spectrometry method, when protons pass the field-free region in the direction normal to the common axis of the electron detectors. This method selects the decay events with neutrino emission of definite angle cone whose axis is normal to the common axis of the electron detectors to be selected.

The essence of the method is schematically shown in Fig.1. In the recording of protons with $p_k > p_{min} = p_\nu \cdot \cos\theta_{max}$ the decay events with neutrino emission within the solid angle limited with θ_{max} are selected. Fig.2 presents the setup of the experiment performed in 1968, which realizes this idea. For the proton spectrometry the time during which the protons passed the field-free gridded cylinder was measured. Then the protons which have passed the gridded cylinder were accelerated and focussed to the

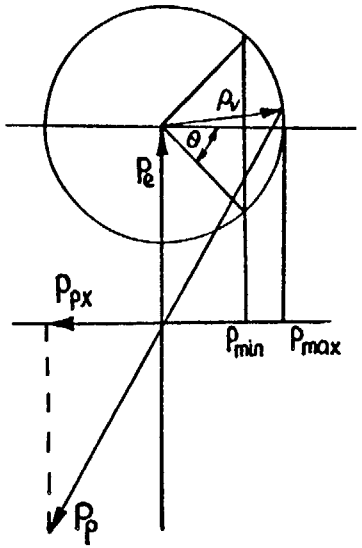

Fig. 1. Momentum diagram of neutron decay products.

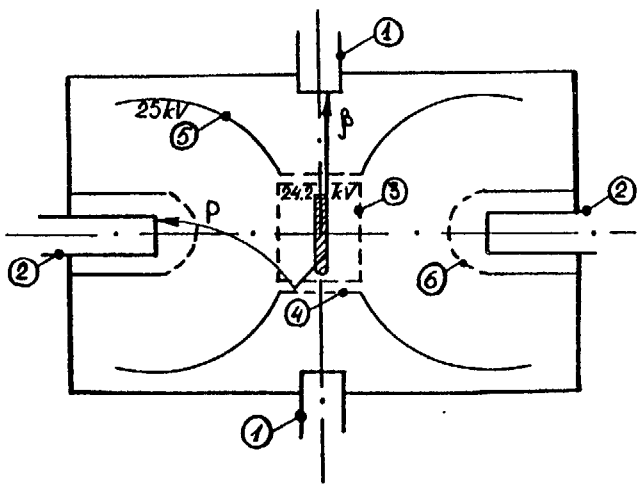

Fig. 2. Measurement of D correlation coefficient.
The scheme of the IAE experiment.

1. β -detectors
2. β -detectors
3. Inner gridded cylinder
4. Outer cylindric grid
5. Outer hemisphere
6. Gridded hemisphere

detector by means of the 25 kV spherical field. The free-field cylinder was surrounded by an additional coaxial gridded cylinder Potential $1\,kV$ applied between the cylinders created an electrostatic mirror to reflect protons back into the field-free region without altering their velocity components along the proton axis.

Very important is the symmetry of the setup. Two pairs of the proton and electron detectors placed above and below the beam in a symmetrical configuration were used. It enabled one to compensate for spurious effects which might arise because of inaccuracy in mutual orthogonality for average values of the directions $\vec{\sigma}$, p_e and p_ν. The measurement results showed that D is zero within the experimental error: $D=-0.01\pm0.01$. Since the coefficient D is expressed through the imaginary parts of the weak interaction constants, this result may be given as the angle θ between the complex values C_A and C_V : $\theta=(181.3\pm1.3)^\circ$. Thus, the experiment showed that the constants are real but have opposite signs. Later this experiment was repeated twice, in 1974 and 1978, using a more intense beam. Much attention was given to searching for the possibility of appearance of spurious asymmetries. The setup was improved. The system of the gridded cylinder and proton detector were periodically rotated around the common axis of the proton detectors. These rotations made it possible to detect and average spurious effects simulating non-conservation of the time parity which resulted from azimuthal nonuniformity of recoil recording proton losses.

A similar experiment was carried out in 1976 by the joint French-American group in Grenoble. They also used a symmetric configuration of the experiment setup (Fig 3), but had no proton-focusing system, which could result in azimuthal nonuniformities in proton recording at the detector ends. A high beam intensity permitted to obtain a good statistical accuracy of the result.

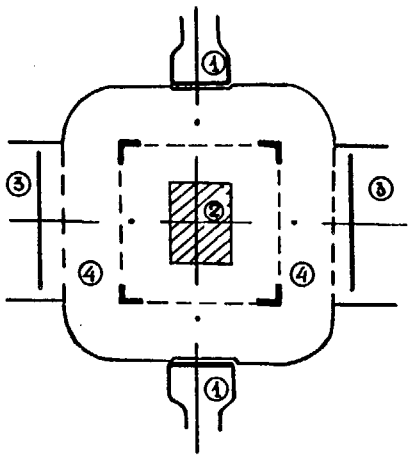

Fig. 3. Measurement of D correlation coefficient.
The scheme of the Grenoble experiment.
1. β -detectors
2. Beam cross section
3. ρ -detectors
4. Accelerating space

The results of the experiments on search for T-invariance violation are listed in the Table.

D	θ	Laboratory	Year
$+0.04 \pm 0.05$	$(175 \pm 6)^\circ$	ANL	1960 /1/
$-0,14 \pm 0.20$	$(198 \pm 27)^\circ$	Chalk -River	1960 /2/
$-0,01 \pm 0.01$	$(181.3 \pm 1.3)^\circ$	IAE	1968 /3/
$-0,0027 \pm 0.0033$	$(180.35 \pm 0.43)^\circ$	IAE	1974 /4/
-0.0011 ± 0.0017	$(180.14 \pm 0.22)^\circ$	JLL	1976 /5/
$+0.0022 \pm 0.0030$	$(179.71 \pm 0.39)^\circ$	IAE	1978 /6/

The absence of the strong interaction in the finite state in the neutron decay case allows one to expect an accuracy of the order of 10^{-4} to be obtained before the effects principally undistinguishable from non-conservation of time parity have arisen. Such an accuracy has not been attained yet and, as a result, new experiments are to be expected in the nearest future.

Angular Distribution of Lepton Emisstion Relative to the Neutron Spin

The relation between electron and neutrino-helicities for V and A interactions, on the one hand, and S and T interactions, on the other, have opposite signs. Therefore the question on the interaction form realized in the nature is very essential.

At present all experiments support the V and A variants though earlier erroneous experiments led to the S and T variants. Very important for choice of the V-A variant were studies of polarized neutron decay.

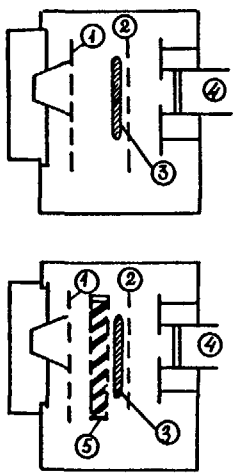

Fig. 4. Measurement of A and B correlation coefficients.
The scheme of the first ANL experiment.
1. e -detector
2. Grid
3. Beam cross section
4. ρ -detector
5. Collimator

The first experiment was carried out in the Argon National Laboratory (ANL). They measured the asymmetry of the emission of electrons and neutrinos relative to the direction of the decaying neutron spin. The experiment setup is shown in Fig.4. Coincidences of pulses from the electron and proton detectors were recorded in two directions of the beam polarization vectors. In the measurement of the coefficient A of the electron-spin correlation the

electron emission direction was determined by the detector's position and coincidences were used for selection of decay events. In the measurement of the coefficient B of the neutrino-spin correlation special collimating slits were used, limiting the proton emission so that protons associated predominantly with a definite direction of neutrino emission were recorded.

The Table shows the relation between A and B and various combinations of V,A,S and T values.

	S+T	S-T	V+A	V-A	Experiment
A	-1.0	-0.1	-1.0	-0.1	-0.114 ± 0.019
B	-0.1	-1.0	+0.1	+1.0	$+0.88\pm0.15$

The experimental results obviously support the V-A variant. However the experiment accuracy did not permit appreciable (up to 40%) contributions of the S and T variants. Therefore later these experiments were continued both in the USA(ANL) and in the USSR (I.V.Kurchatov IAE). The experimental setups are shown in Figs 2,5,6.

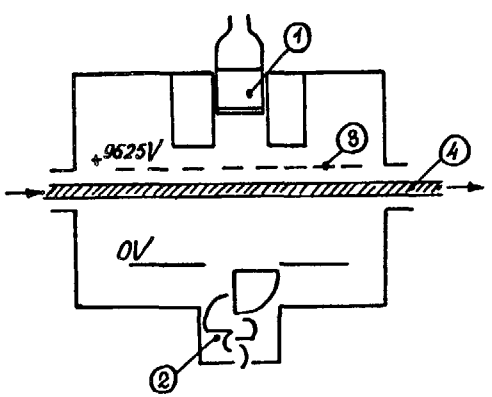

Fig. 5. Measurement of A and B correlation coefficients.
The scheme of the later ANL experiment.

1. β-detector
2. ρ-detector
3. Grid
4. Beam n

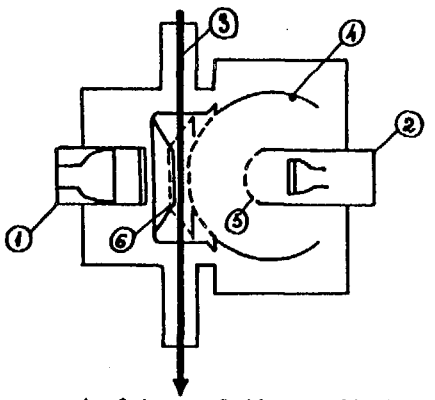

Fig. 6. Measurement of A correlation coefficient.
The scheme of the IAE experiment.

1. β-detector
2. ρ-detector
3. Beam n
4. Spherical electrode
5. Minor spherical grid
6. Diaphragm

For measurement of the neutrino spin correlation at IAE the setup described above was used. The direction of the polarization was changed so that it would coincide with the neutrino emission cone axis. From comparison of the number of decays with neutrino emission in the opposite spin directions (Fig.7) it was found that $B=0.995\pm0.035$.

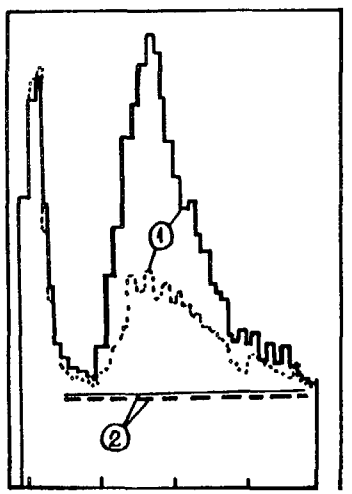

Fig. 7. The IAE experiment.

1. Time-of-flight proton spectra for two spin directions
2. Background level

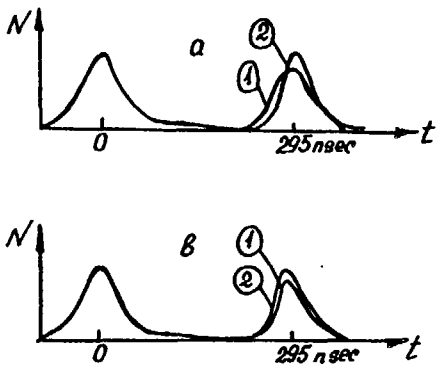

Fig. 8. The ANL experiment.

Time-of-flight proton spectra

a, b - opposite spin directions

1, 2 - polarized and depolarized beams

In ANL the experiment was set up in such a manner that the decay events were recorded for any direction of neutrino emission (Fig.5). The spectra of the proton detector decays relative to the electron one were taken at opposite directions of the spin (Fig.8). From the shift of the delay spectra it was found that $B=1.01\pm0.05$. In the same experiment the coefficient A of the electron-spin correlation was measured. The counts of decay events by the electron detector were compared for two spin directions. Coincidences with the protons were then necessary for suppressing the background. However, use of the coincidences led to contributing to the change in counting from the coefficient B because of incomplete collection of protons. This contribution was taken into account by computing the experiment model.

At IAE the A determination experiment was made so that there were no contribution of B. To this end (see Fig.6) a special diaphragm limited the beam region from which electrons were recorded while a proton collection system was designed so that it ensured complete recording of the protons produced in this region.

The results of A and B measurements (see the table) are in good agreement with the V-A variant of the theory. They permitted the limitation to possible contribution of S and T to be improved to 15-10%. Further improvement of the B determination accuracy is desirable. Under assumption of the absence of the S and T contributions the A measurement result permits us to obtain a fundamental value of the relation between the constants C_A and C_V in the weak interaction.

$$C_A/C_V = -1.261\pm0.012$$

Improvement of the technique for obtaining higher intensities of the polarized neutron beams opens ever new possibilities in the neutron decay experiments. At present several experiments are being prepared in the world, both on refinement of the value of the correlations described and on investigation of other, finer, processes induced by the weak interaction.

Correlation	Coeff.	Result	Laboratory	Year	
$(\vec{G}\vec{p}_e)$	A	-0,114±0,019	ANL	1960	/1/
		-0,115±0,008	ANL	1969	/7/
		-0,120±0,010	IAE	1971	/8/
		-0,113±0,006	ANL	1975	/9/
		-0,115±0,006	IAE	1976	/10/
		-0,114±0,005	IAE	1978	/11/
$(\vec{\sigma}\vec{p}_\nu)$	B	+0,88 ± 0,15	ANL	1960	/1/
		+0,96 ± 0,40	Chalk-River	1960	/2/
		+1,01 ± 0,05	ANL	1970	/12/
		+0,995±0,035	IAE	1970	/13/

Weak Nucleon-Nucleon Interaction

In the β-decay case four particles participate in the weak interaction, two of which are hadrons, and two-leptons: $n+\nu\to p+e$ It was found that there are also other processes induced by an interaction of the same power as the weak one. For the meson decay $\mu\to e+\nu_e+\tilde{\nu}_\mu$ (or in the symmetric form $\mu+\nu_\mu\to e+\nu_e$) no nucleons are involved. All four particles are leptons. The theory of universal four-fermion weak interaction suggested that the weak interaction exists in all the processes

involving four Fermi-particles. According to this theory the weak interaction should manifest itself for the nucleon-nucleon case, too. The difficulty in the experimental verification of this prediction is due to the fact that in the nucleon-nucleon case the weak interaction occurs simultaneously with the strong one.

The verification became possible due to non-conservation of parity in the weak interaction. The non-conservation of parity served as a tag which allowed the weak effects to be separated against the background of about the 10^7 times more intense strong ones. A weak nucleon-nucleon interaction may give a number of effects experimentally observable, such as asymmetry in divergence of γ-quanta in the (n,γ) reaction, induced by polarized neutrons (A_γ), circular polarization of γ-quanta emitted by unpolarized nuclei (P_γ), asymmetry in divergence of light and heavy fragments in fission caused by polarized neutrons (A_f), asymmetry in emission of secondary neutrons in this kind of fission, turn in the direction of the neutron beam polarization vector when the neutrons pass through the unpolarized matter, asymmetry in transmission of polarized neutrons by the matter for different polarization directions.

It was found that in some cases the expected value of the 10^{-7} effects may be enhanced significantly. The enhancement coefficient may reach 10^3–10^4 and is due to motion of nucleons in the nucleus which results in hindering processes induced by the strong interaction.

The first to obtain the experimental results $A_\gamma = (-6.1\pm1.5)10^{-4}$ on existence of the nucleon-nucleon weak interaction was the Yu.G. Abov's group at the Institute of Theoretical and Experimental Physics (ITEP) (Moscow, 1964). They studied the asymmetry in divergence of γ-quanta produced in the $^{113}Cd(n,\gamma)^{114}Cd$ reaction. The divergence asymmetry is caused by the admixture of the parity prohibited EI transition to the allowed MI transition. In the experiment it was important to separate γ-quanta with 9MeV energy corresponding to the given transition because at 8.5-MeV energy another transition was observed, having inverse asymmetry. The measurements were repeated many times both with Cd and with other elements.

Another effect predicted by the Soviet physicists Vladimirsky and Andreev was discovered by Danilyan et al. at ITEP, too. They found the effect of asymmetry in divergence of light and heavy fragments in fission of uranium by polarized neutrons $A_f = (3.6\pm1.0)10^{-4}$. Here enhancement mechanisms associated with the structural features of the compound nucleus manifested themselves as well, so that it proved to be of the order of 10^{-4}. A detailed review of experimental works on A_γ and A_f asymmetry measurements was made by Byrne /16/.

The weak nucleon-nucleon interaction is observed in neutron optics phenomena. In Grenoble Forte et al. /17/ investigated turn of the neutron beam polarization vector in cross polarization, with neutrons passing through the Sn sample. A pure nucleon-nucleon interaction predicts small turn of a spin. The structural features of the nuclei in this case may lead to significant enhancement of the effects as well. In the case of two Sn isotopes, for example, it was found that

$$\varphi(^{117}Sn) = (36{,}7 \pm 2{,}7)\cdot 10^{-6}\ rad/cm$$
$$\varphi(^{124}Sn) = (0{,}48 \pm 1{,}49)\cdot 10^{-6}\ rad/cm\ .$$

A high value of the effect, obtained using ^{117}Sn, made it possible to suggest existence of a new type of interaction which leads to violation of the space parity. Later, however, it was explained in terms of the weak nucleon-nucleon interaction. Great enhancement of the effect in ^{117}Sn results from the structure features of the compound nucleus having the p-level at 1.33 eV. The weak interaction permits mixing the p-and s-levels of different parity, which is the cause of appearance of the parity-violating effects. This effect observed in the thermal region should be stronger for neutrons having energies corresponding to p-level.

Such an energetic dependence was confirmed in the experiments with longitudinally polarized neutrons. In this case another effect, difference in transmission of the neutron beam for two polarization directions, was observed instead of that of polarization vector reversal. Lobashov et al /18/ from the Leningrad Institute of Nuclear Physics (LINP) carried out experiments with ^{117}Sn and found asymmetry in the transmission cross section, equal to $(5.6\pm0.8)\cdot10^{-6}$, which agrees with the effect observed at the Laue-Langeving Insti-

tute (ILL). The experiment was carried out with thermal neutrons. The same effect in the resonance energy region was performed at the Laboratory of Neutron Physics of the Joint Institute for Nuclear Research /19/. At a neutron energy of 1.33 eV the asymmetry in transition was found to be $(4.5\pm1.3)\ 10^{-3}$ as it had been predicted. In addition to Sn the same energy dependence was obtained using La and Br.

The set of the above experiments clearly shows that in the neutron optics the parity-violating effects are also due to the weak nucleon-nucleon interaction.

The strong dependence of the effect magnitude on the structure features of the compound nucleus permitted the measurements of this type to be used for investigation of the characteristics of the nuclear levels.

From the view point of investigation of the weak interaction properties it is of special interest to detect and measure the effects in the simplest system, neutron-proton interaction, where no nuclear structure enhancement exists.

In the investigations of the circular polarization of γ-quanta in the $n+p \to d+\gamma$ reaction an effect was observed, which proved to be stronger than that predicted by the theory. The same reaction was studied by Cavaignac et al /20/ at ILL in 1977 (see Fig.9). The target containing hydrogen in the state of parahydrogen was set in the beam of polarized neutrons. Parahydrogen has a small scattering cross section and, besides, it does not depolarize the neutron beam in scattering due to zero spin. On both sides of the target two liquid scintillation detectors were placed which recorded γ-quanta. The effect to be found was change in γ-quanta counting in the reversal of the polarization direction. The measurements with two detectors permitted to exclude the influence of fluctuations of the reactor power on the effect to be sought. In the absence of enhancement the effect expected should be very small. For measuring this effect the method developed earlier by V.M.Lobashov (LINP) was used. The common counting system did not permit to record such a high intensity of γ-quanta, which would allow the effect of about 10^{-7} to be measured. The current system was used. Against the background of great fluctuations of the mean current of the photomultiplier the variable

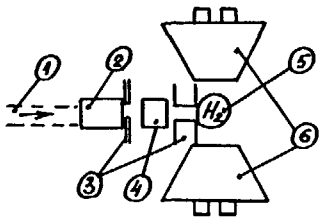

Fig. 9. Neutron-proton interaction.
The scheme of the ILL experiment.

1. Neutron guide	4. Spin-reversal system
2. Polarizer	5. H_2-target
3. Collimator	6. γ-detectors

component synchronous with the frequency of reversal of the polarization direction was observed. Though it took a prolonged time, experiment has not permitted a sufficient accuracy which is needed for detection of the weak nucleon-nucleon interaction without nuclear enhancement to be attained. The obtained value of the asymmetry, $A_\gamma = (0.6\pm2.1)\ 10^{-7}$, is in contradiction with the circular polarization measurements but agrees with the theory predictions. The interest in detection of the weak neutron-proton interaction is very great and new experimental data should be expected to appear in the nearest future.

CONCLUSION

In conclusion I would like to emphasize once more that the experiments with polarized neutrons were not only ones which supported development of the weak interaction theory. But nowadays, when the qualitative experiments have played their part and what is sought for is clarification of fine effects and reaching accurate quantitative verification of the theory, the experiments with polarized neutrons must become increasingly more important because the interpretation of their results is determinative and unambiguous. That is why so many efforts are being made to obtain ever more intense beams of polarized neutrons and new proposals of

conducting experiments on investigation of the problems of fundamental physics by means of polarized neutrons are being continuously made.

References

1. Burgy M.T., Krohn V., Novey T., Telegdi V. Phys.Rev., 1960, v.120, No.5, p.1829.
2. Clark M., Robson J. Can. J.Phys., 1960, v.38, p.693.
3. Erozolimsky B.G., Bondarenko L.N., Mostovoy Yu.A. et al. Ya.F., 1970, t.11, s.1049.
4. Erozolimsky B.G., Mostovoy Yu.A., Fedunin V.P. et al. Piz'ma v ZhETF, 1974, t.20, s.745.
5. Steinberg R.J., Liand P., Vignon B., Hughes V.W. Phys.Rev. Lett., 1974, v.33, p.41.
6. Erozolimsky B.G., Mostovoy Yu.A., Fedunin V.P. et al. Ya.F., 1978, t.28, vyp.1, s.98.
7. Christensen C., Krohn V., Ringo G. Phys.Rev., 1960, v.28B, p.44.
8. Erozolimsky B.G., Bondarenko L.M., Mostovoy Yu.A. et al. Pis'ma v ZhETF, 1971, t.13, s.356.
9. Krohn V., Ringo G. Phys.Lett., 1975, v.55B, p.175.
10. Erozolimsky B.G., Frank A.I., Mostovoy Yu.a., Arzumanov S.S. Pis'ma v ZhETF, 1976, t.23, s.730.
11. Erozolimsky B.G., Frank A.I., Mostovoy Yu.A. et al. Ya.F., 1979, t.30, vyp.3, s.692.
12. Christensen C., Krohn V.,Ringo G.Phys.Rev., 1970, v.C1, p.1693.
13. Erozolimsky B.G., Bondarenko L.N., Mostovoy Yu.A. et al. Ya.F., 1970, t.12, s.323.
14. Abov Yu., Krupchitsky P.A., Oratovsky Yu.A. Ya.F., 1965, t.1, vyp.3, s.479.
15. Danilyan G.V.,Vodennikov B.D.,Dronyaev V.P. et al. Pis'ma v Zh. ETF, 1977, t.26, s.197.
16. Byrne J.Rep.Prog.Phys., 1982, v.45, p.115.
17. Forte M.,Heckel B.R.,Ramsey N.F. et al.Phys.Rev.Lett., 1980, v.45, No.26, p.2088.
18. Lobashov V.M.,Preprint L.I.Ya.F., N 622, 1981.
19. Alfimenkov V.P., Borzakov S.B. Vo Van Thuan et al. Preprint OIYaI R 3-82.411, 1982.
20. Cavaignac J.F., Vignon B., Wilson Richard. Phys.Lett., 1977, B67, No.2, p.148.

NUCLEAR DATA MEASUREMENTS IN NEUTRON EXPERIMENTS AT STEADY STATE ATOMIC REACTORS

V.P. VERTEBNYI
Institute for Nuclear Research,
Academy of Sciences of Ukrainian SSR,
Kiev, Union of Soviet Socialist Republics

Abstract

A review of intense filtered neutron beam methods for nuclear data measurements is given. These data may be useful for many applications including the reactor physics.

Neutron physics and atomic reactor technology are closely related since the time of fission discovery. Atomic reactor conceptions, which were usually idealized, were stimulated by neutron physics researches (for example, the "fast breeder reactor"). Attempts to realize these concepts lead to deviations from the ideal conception. A new situation required more precise neutron data measurements, such as neutron data measurements of new materials and isotopes (a clear example is the ^{239}Pu alpha problem in the 70es /1/). Now, neutron cross sections, neutron resonance parameters are known for all the stable and transactinide isotopes /2/. However, we must not think that these data are complete. In spite of a lot of successes of the neutron reaction theory, the precision of neutron cross section parametrization is not high enough, since neutron strength functions (for the p-wave, especially) and radiative widths frequently have been measured with not sufficiently high precision. For radioactive isotopes with $A < 200$, including radioactive fission products, there are very few neutron resonance data. In recent times similar efforts in this direction have been undertaken in the USSR and FRG /3/.

It is well known that most neutron data were obtained in neutron physics experiments at pulse neutron sources (charge particle accelerators, Dubna pulse reactor IBR); the stationary thermal reactor being a most wide available intense neutron source can also be used successfully to obtain the neutron data for reactors and other applications. The experience of the USSR and other countries confirms this. Some examples one may find in reference /3/. It should be noted that thermal reactor is an intense source not only of thermal neutrons, but also of intermediate as well as fast neutrons. Vlasov M.F. et al. at the Kiev atomic reactor have fixed 20 Mev neutrons using thin radiator method, Popov A.B. and Samosvat G. have fixed even 30 Mev neutrons. A.V.Murzin, V.F.Bibik and author of this paper in neutron activation experiment on super-pure silicon have observed such reactions as $^{28}Si(n,p\ )^{24}Na$ with threshold more than 14 Mev neutron energy and with the theoretical cross section plateau near. The IRT thermal reactors were used in wide investigations of inelastic fast neutron scattering by nuclei. These classical investigations are tabulated in Moscow-Bagdad atlas /5/. Wide possibilities for neutron physics research with intermediate neutrons were demonstrated by using the neutrons filtered beams technique in the region of so-called unresolved resonances.

Neutron Resonances Investigations in Unresolved Region Using Filtered Beams

It is curious but after many years of neutron resonance investigations average neutron resonance parameters are not known very

well. The reason is connected with large fluctuations of these parameters. Consequently, to enlarge the accuracy it is necessary to average these parameters using quite a number of resonances, i.e. the energy interval as wide as possible. And this leads consequently to the energy region, where modern neutron spectroscopy methods do not allow us to resolve the resonances ("unresolved region") and even their very existence can not be proved by the direct measurements. The evaluations of average neutron resonance parameters in the unresolved region may be made to some extent with the neutron filtered beam technique. Recently, it has been much developed at the steady-state atomic reactors afterwards Simpson et al. pioneer experiments /6/.

Main Methods of Filtered Beams Technique

Some elements, presumably light and middle have the interference minima in the total cross section at certain neutron energies. The cross section may be equal to zero or to a very small value; for example, scandium has minimum at neutron energy 2 keV (Fig.1). The thick scandium rod in reactor shield channel, which usually is used for neutron beam collimation, will transmit only the neutrons in the region of 2 keV minimum, i.e. it will work as a filter.

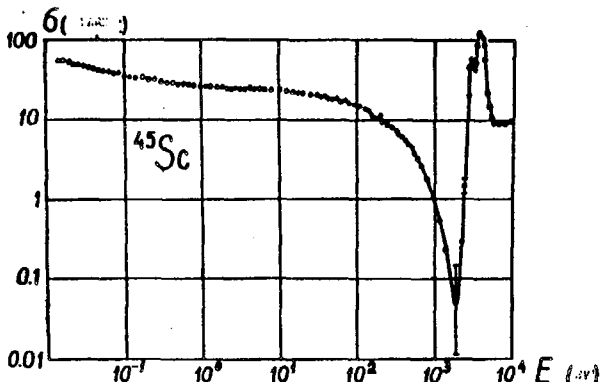

Fig.1. Total cross section of scandium upon neutron energy as measured by Wilson in 1966 (USA).

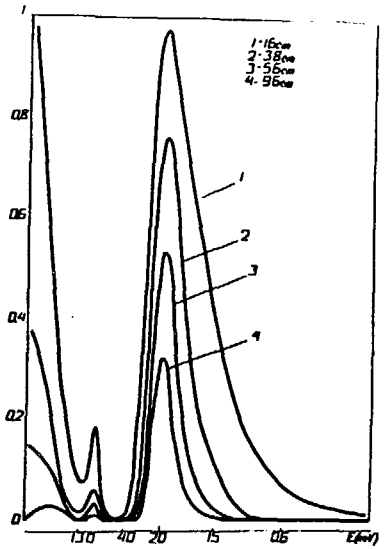

Fig.2. Transmission of different thickness scandium filters upon neutron energy as measured by Kirilyuk A.L., Vorona P.N. et al. (USSR).

In Fig.2 the Sc filters transmissions of different thicknesses are shown, as they were measured by Kiriljuk A.L. et al. With using nearly 1m-long Sc rod one can obtain rather good neutron beam with energy 2 keV. It is not so good as one may think because there are other minima in the energy region 8-80 keV, which are not so deep as 2 keV one. Background from them at some extent may be suppressed by other substances. In general, however, for Sc filter this background is relatively large, near 24% /6,12/.

To obtain the filtered neutron beam with energy 24.3 keV, iron is widely used, its minimum is well known by reactor shield constructors. To suppress other Fe minima, aluminium and other substances are usually added. For example, 23 cm of iron plus 36 cm of Al and plus of 6.5 cm sulphur transmit quasi-monochromatic beam with average neutron energy E=24.3 keV and peak half height width -

Δ E = 2 keV. Silicon filter is also widely used /6,9/. There are two "windows" in Si total cross section at the neutron energies 144 and 55 keV. Using 37 cm-silicon rod gives us these peaks; their widths at half maximum height are 24 keV and 2 keV, correspondingly. By adding S or Ti rods into the filter it is possible to choose any of these lines. At the Kiev atomic reactor we usually used monocrystallic silicon. There it was shown /10/ that, even without cooling, perfect Si monocrystals transmit thermal neutrons very well together with simultaneous suppression of fast neutrons and gamma-rays. Cadmium ratio for $1/v$ detector is about 1000 (A.V.Murzin's measurement). Monocrystallic Si filter is preferred as compared to polycrystallic one, as in many experiments it is easier to use thermal neutrons for comparison with standards /11,13/. Parameters of typical beam filters, which are used in the Soviet Union and other countries are given in Table 1.

It should be mentioned that filtered neutron beams have many useful qualities: they are usually well collimated (diameter of beam 4 - 40 mm); gamma-ray background is rather low; excluding scandium filter, faster neutron background is also very low (2 - 3.5); neutron filters have large enough intensity of intermediate neutrons in the region of fast reactor neutron spectrum.

Background measurement procedure, naturally, depends upon a type of the experiment. However, in all cases the background may be measured using suitable resonance scatterers (absorber). The background is generally measured using difference between count rates with and without the resonance scatterer /6,12/.

So, in case of Sc filter the background may be measured by inserting in Mn-slab (4-11 g/cm^2) beam; Mn resonance peak almost coincides with scandium "window"; for Fe-filter Ti is used and sulphur resonances are used when we use 144 keV Si beam; if we want to deal with 55 keV Si beam, it is suitable to use the resonance peak of sulphur. This method is to be used when neutron detector pulse does not strongly depend on neutron energy (nonspectrometric

Table 1

Examples of the Neutron Filters

Examples extracted out of references 3/8-17/;
USSR - Obninsk (1970); Dimitrovgrad (1970); Kiev (1973); USA (1978); Chechoslovakia; FRG, India.

Scandium. E_e = 2 keV; $\Delta E_n \sim 0.6$ keV

Idaho (MTR, USA); Sc 1067 mm; Ti 14 mm; $\varphi = 10^7$n/sec.
Kiev (WWR-M, USSR); Sc 850 mm; $\varphi = 1.2\ 10^8$n/sec.

Iron. E_n = 24.3 keV; $\Delta E_n \sim 2$ keV

BNL (HFBR, USA) ^{56}Fe - 30.5 cm; Al - 7.8 cm; $\varphi = 10^7$n/sec, Fe -22.8 cm; Al - 36.2 cm; S - 6.3 cm; Kiev (WWR-M, USSR) Fe - 25 cm; Al - 35 cm; $\varphi = 10^7$n/sec.

Silicon. E_n = 55 keV, $\Delta E_n \sim 2$ keV

Kiev (WWR-M, USSR). Si (crystal) - 87.5 cm
S = 20.5; ^{10}B. $\varphi = 2.6\ 10^7$n/sec.

Silicon . E_n = 144 keV, $\Delta E_n \sim 25$ keV

Kiev (WWR-M, USSR), Si (crystal) - 87.5 cm;
Ti - 17.5 cm; ^{10}B. $\varphi \sim 5.5\ 10^8$n/sec.

Silicon - thermal neutrons

Kiev (WWR-M, USSR); Si (crystal) - 87.5 mm;
$\varphi_{therm} \sim 10^8$n/cm sec (evaluation).

Oxygen. E_n = 2.35 MeV, ΔE_n = 0.11 MeV /15/

USA. O_2 - 183 cm, Bi - 8 cm; $\varphi = 5\ 10^5$n/sec.

^{3}He-counters etc.). When H_2 counters are used the background can be evaluated by measuring the proton recoil spectra. Neutron spectrum after iron filter, as measured by Murzin A.V. using the hydrogen counter CHM-38 (p=3 at), is shown in Fig.3 /13/ It is due to shortage of the Sc filter that, the Mn scatterer for the background measurements reduces not only 2 keV - neutrons, but the background neutrons in other scandium "windows". As a result a difficulty arises, that is the necessity to measure the coefficient of background suppression K /6,12/. It depends in general upon type of experiment.

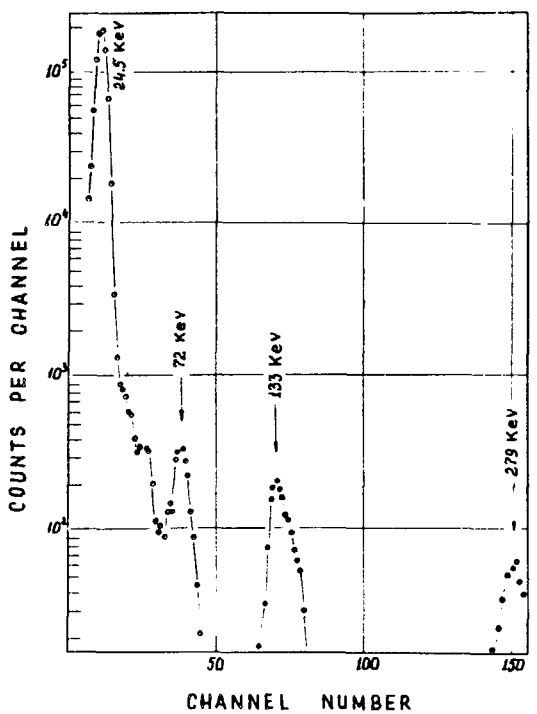

Fig.3. The neutron spectrum for the iron filter as measured by Murzin A.V. et al. with hydrogen proportional counter CHM-38.

For background lowering sometimes the method of twice selection was used /15,12/. In channel, which went throughout reactor, Mn scatterer was inserted; 2-keV neutrons were scattered with it and then went through Sc-filter. At the Kiev reactor Mn-scatterer was used after Sc-filter in 2π -detector (Fig.4) /12/.

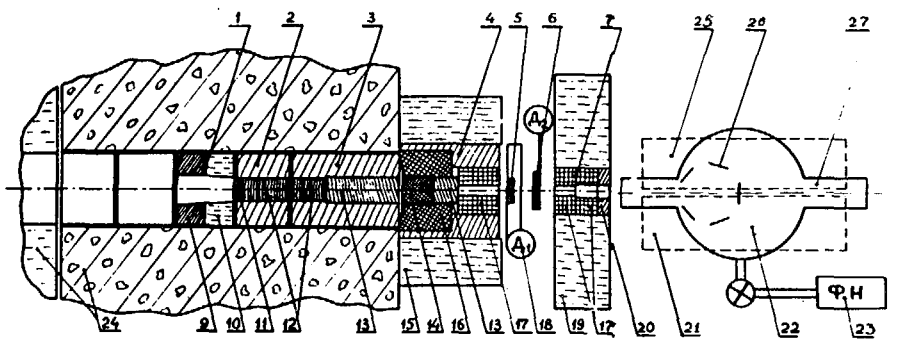

Fig.4. The experimental arrangement for the neutron resonance self-protection research with the self-indication method. 12-14-parts of the filter, 1-3-collimators; 25-^{3}He-counter detector; 22-vacuum chamber with scatterer samples; 5,26-variable samples of the same material; 6-the resonance scatterer for the background measurement. For the case of the scandium filter sample in position 26 is replaced by the Mn scatterer and a sample, for which the transmission is measured, is placed in position 5; consequently the twice selection of the neutron is obtained.

In order to plan an experiment, it is necessary to account for the neutron flux decrease by the filter itself which forms filter beam from "white" reactor spectrum. Interference minimum cross section, in reality, is not equal to zero: for Sc it equals 240 mb at 2 keV; for ^{56}Fe, 7.5 mb at 24.5 keV and for natural iron, 450 mb;

for silicon, 100 mb at 144 keV. It follows from these data that 96 cm-thick scandium three times reduces the neutron intensity; natural iron filter reduces it four times, but the pure ^{56}Fe isotope filter reduces it only by 2-3 per cent. Usually filter consists of many components which serve to suppress other "windows". To prevent neutron activation it is recommended to shield filter body from the site of neutron beam entrance with B^{10} or ^{6}Li slabs.

There were communications about possibilities of other filters; narrow band ^{238}U filter with E_n=186 eV and ΔE_n = 1.4 eV /15/; Mill and Harvey /15/ suggest using ^{170}Er, ^{184}W, ^{68}Zn, ^{86}Sv, ^{64}Zn, ^{60}Ni, ^{54}Fe, ^{58}Ni; ^{52}Cr and ^{54}Fe to create neutron filter beams with energy 0.060; 0.160; 0.400; 0.500; 2.2; 4.0; 4.5; 14; 47 and 48 keV, correspondingly. Probably sulphur will be rather a good filter for wide spectrum band from 1 eV to $2\cdot10^4$ eV, as at this range $\sigma_t < 1$ b, and out of it $\sigma_t \sim 3-5$ b.

Some experimentors in München, Obninsk and Dimitrovgrad /18-20/ used resonance maximums in order to get quasimonochromatic neutron beams with resonance scattering. Broder, Nesterov and Chamjanov have successfully used Na resonance scatterer (E = 2.7 keV ΔE = 0.52 keV). There are other possibilities (for example ^{152}Sm, E_o = 8 eV; $\sigma_o \sim 2\ 10^5$b). For better experimental condition the resonancer scatterer should be placed near core in throughout channel.

Some Experiments with the Filter Beams Evaluation of the Average Neutron Resonance Parameters

The average resonance parameters can be evaluated if resonance self-protection is studied. It is neutron resonance existence that makes the observed total cross section to be dependent upon sample thickness. In Fig.4 a scheme of the experiment is shown and in Fig.5 some results are shown. Here $\sigma_t^{obs} \equiv \ln T/n$, T - sample transmission, n - sample thickness; $T = 1/\Delta E \int \exp(-n\sigma_t(E))\, dE$; σ_s^{obs} - the observable scattering cross section at the self-indication neutron scattering experiment. For very thin samples in the case of S-neutrons $\sigma_t^{obs} = \overline{\sigma}_t = 2\pi^2 \lambda^2 S_o \sqrt{E} + 4\pi\langle R'^2\rangle$; where R' - the optical model scattering length, S_o - the S-wave neutron strength function. For thick samples resonance neutrons are "eaten out" of the beam and σ_t^{obs} will be equal to some value between

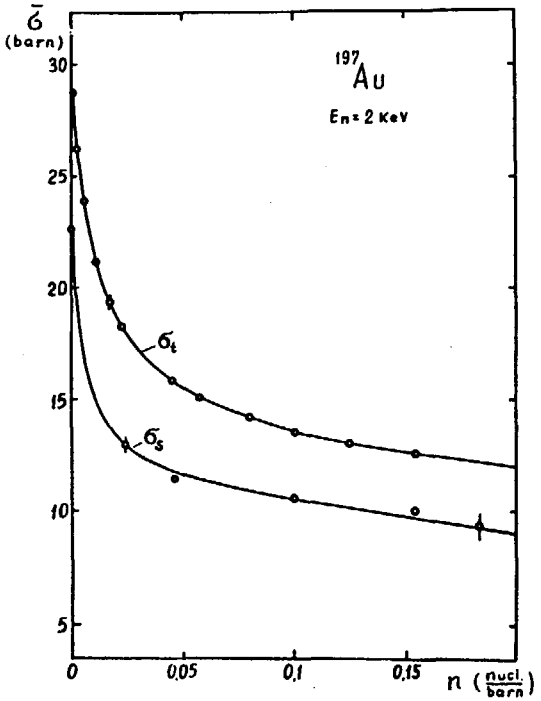

Fig.5. The observable total cross section (upper curve) and scattering (lower curve) cross section of ^{197}Au upon the sample thickness.

resonances, i.e. will be close to $4\pi R'^2$. So, it is possible to separate resonance and potential processes if we vary the sample thickness. Seth /21/ and Lynn /22/ suggested relatively simple formula for transmission experiment treating, but they did not account for resonance distance fluctuations. Novoselov /12/ described Monte-Carlo IBM Programm with the account both Porter-Tomas and Wigner distributions and Doppler-broadening. The resonance self-protection may also be measured with the self-indication in the scattering, capture and fission (Figs 5,6). These additional experiments increase the reliability if all of them are treated simultaneously. The case of thin samples deserves a special attention. In this case it is possible to get the analytical expressions /25, 26/. Zaretsky and Urin /26/ gave such formula, supposing zero Doppler-broadening: $\overline{\sigma_s} = \langle \sigma_s \rangle - 2\pi^2 \lambda\!\!\!^{-} n_1 (\overline{T_0} + \gamma \overline{T_{1+}} + \overline{T_{1-}})$ where $T_0 \sim S_0$, $T_{1+} \sim S_1^{3/2}$ and $T_{1-} \sim S_1^{1/2}$. Measurements of such values on different filters permit evaluation of S and p-neutron strength functions. Pavlenko E.A., Gnidak N.L. et al. have carried out such experiments with very thin tantalum samples (transmission, scattering and capture experiments) and have shown that it is possible to evaluate a full set of all the resonances parameters even in the energy region where the resonances cannot be directly observed at the time-of-flight experiments. In order to give some impression of filter beam possibilities, results for europium isotopes are given below:

^{151}Eu $10^4 S_0 = 4.1 \pm 0.11$ (stat) $\pm$ 0.13 (fl)

$R' = 7.58 \pm 0.08$ (stat) $\pm$ 0.05 (fl) f.

Europium 153 $10^4 S_0 = 1.95 \pm 0.10$ (stat) $\pm$ 0.11 (fluct)

$R' = 8.16 \pm 0.09$ (stat) $\pm$ 0.07 (fluct) f.

Relatively low errors are due to averaging on many neutron resonances.

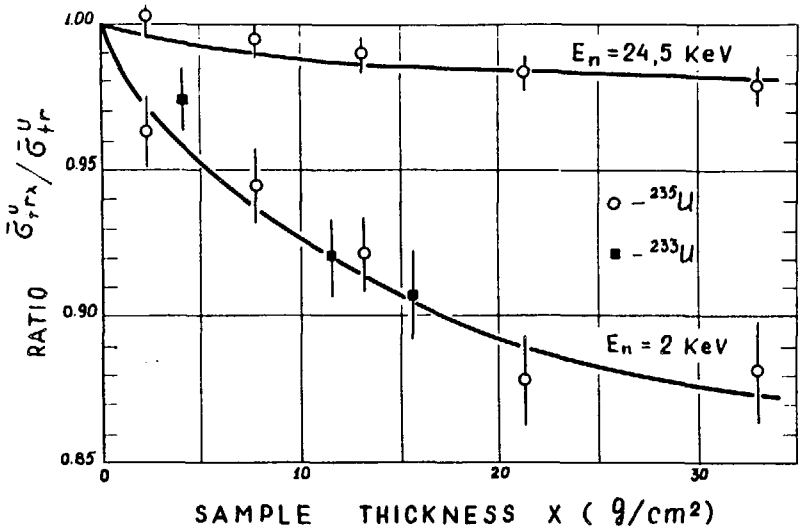

Fig.6. Ratio of the average fission cross section $\bar{\sigma}_{frx}$ with the uranium screen of thickness x to the average fission cross section without the screen for ^{233}U and ^{235}U isotopes upon the screen thickness x. Lower curve was obtained for 2 keV neutrons (Sc filter), upper one was obtained for 24.5 keV neutrons (Fe filter). At neutron energy 24.5 keV neutron resonance structure is yet manifested.

Gamma-ray spectra at Intermediate Neutron Capture

Long time neutron capture gamma-ray spectra were studied only with thermal neutrons. The most data were measured by Groshev, Demidov et al. and Bartholomeev et al. Thermal neutron capture is, as a rule, due to one of resonances (positive or negative) close to zero. Later experiments on some single resonances appeared. It was understood that reduced gamma-rays fluctuated in accordance to Porter-

Tomas distribution and thermal neutron data in some relation were not enough representable: needs appeared in spectra averaged by as much as possible resonances. Bollinger et al. /17/ used an incore ^{10}B filter, which selected neutrons with the average energy 1 keV and half-height width 0.5 keV. In this case S-wave capture is the most probable. Broder, Nesterov, Chamjanov used Sc (2 keV), Fe (24.5 keV) and Na (2.87 keV) filteres for titanium isotopes capture gamma-rays spectrum studying at higher neutron energies. Many isotopes were studied at BNL /29/. Additional information will be obtained if the neutron energy is increased including additional transitions which appear since p-wave excites opposite parity levels or weak transitions in thermal neutrons become intense; when spectra are studied at different neutron energies it is possible to evaluate p-neutron strength functions and ratios of E1 to M1 transitions. Useful information can be obtained about gamma-strength functions. One of the examples of such investigations are experiments of Murzin et al. /30/, who have measured ^{147}Sm capture spectra with the filter beams at the Kiev atomic reactor. In Fig.7 on the right side shown are the lowest levels of ^{148}Sm and possible transitions from compound states, which created by the s- and p-neutrons. On the left side shown are experimental Ge(Li)- spectra. Here one can see very well the shifts of E1 and M1 transitions on 4^+ and 3^- levels with neutron energy increasing and intensity increasing of the transitions, which are due to the p-neutrons. Murzin et al. /30/ using this have reliably evaluated p-strength functions, and ratio E1 and M1 transitions. In Fig.8 ^{147} Sm reduced gamma-rays widths are shown in arbitrary scale. So, gamma-ray spectra measurements with filters give very useful physical and constants information.

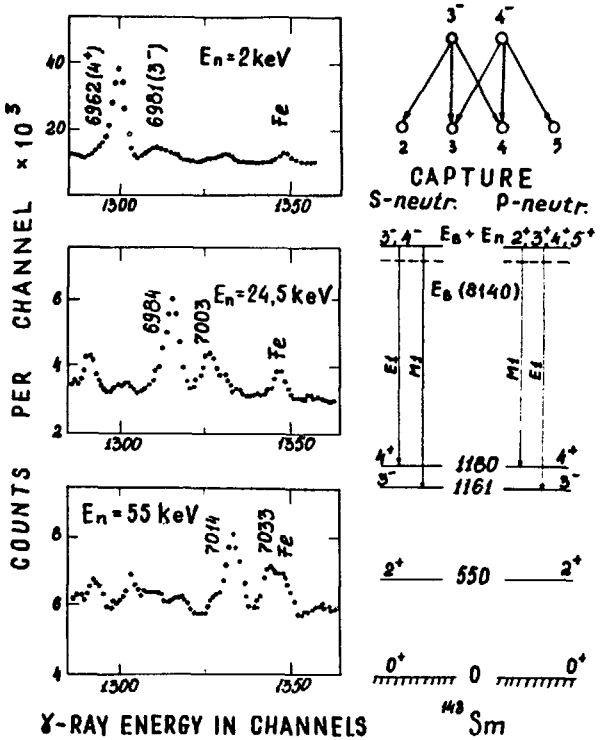

Fig.7. The same parts of gamma-ray spectrum in $^{147}Sm(n,\gamma)^{148}Sm$ reaction which were obtained at neutron energies 2 keV (Sc), 24.5 keV (Fe) and 55 keV (Si), are shown to the left; decay schemes are shown to the right. With the neutron energy increase the relative intensity of compound state decay to the level 1161 keV. (3^-) increases because the neutron p-wave part grows.

(n,α) Reaction Investigation with Filter Beams on Heavy Isotopes

These reactions have low probability for slow neutrons because of low transparency of a nucleous Coulomb barrier. Their cross sections are in 10^6 or more times less than capture cross sections. But these measurements are important because they allow to

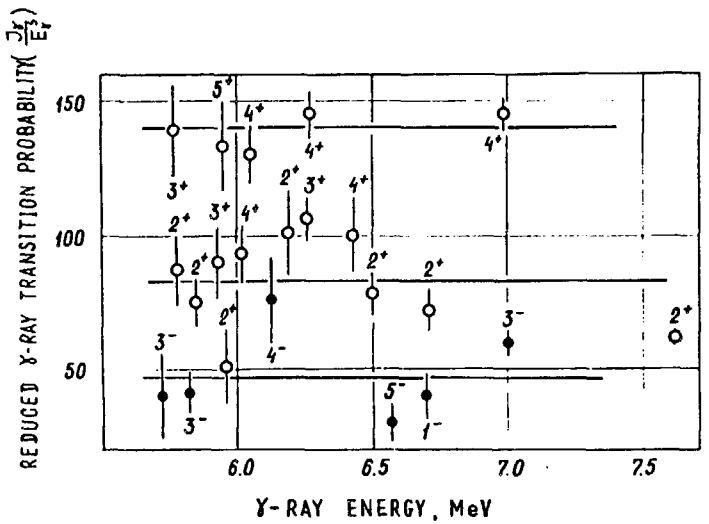

Fig.8. The reduced probabilities of the ^{148}Sm gamma-ray decay for different multipoles upon the gamma-ray energy.

get some data about compound state structure and reactor materials properties. Andreev and Popov's review /31/ about thermal neutron reactions, and Popov's review/52/ about resonance neutron reactions are well known. These authors made the largest contribution to the (n,α) investigations. Ju.P.Popov et al. in Dubna (JINR) have investigated α - resonances from ^{67}Zn to ^{159}Os. They have studied alpha-widths fluctuation laws, have evaluated its average values. However, high width fluctuations (Porter-Thomas distribution) caused relatively high uncertainties in the average values. In order to decrease these uncertainties averaging on many resonances is needed. For this reason Dubna and Kiev groups at the Kiev atomic reactor WWR-M have carried out (n,α) experiments with the filter beams on isotopes ^{147}Sm, ^{143}Nd and other isotopes at neutron energies 2, 24.5 and 144 keV /33/. Results for ^{147}Sm (n,α) ^{144}Nd are shown in Fig.9.

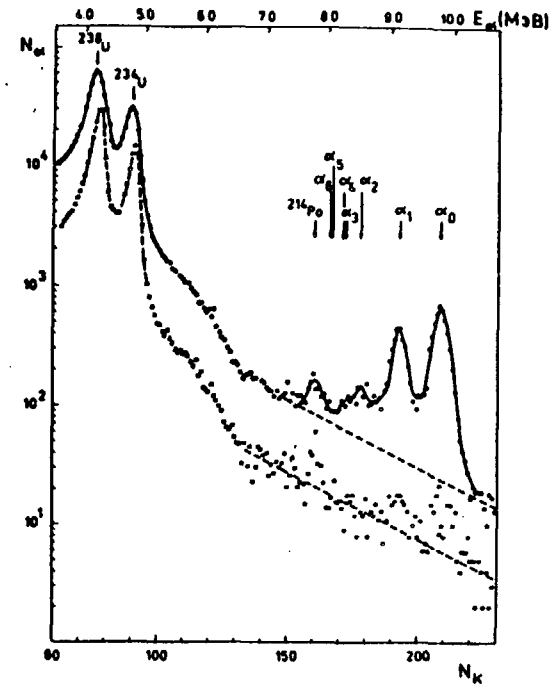

Fig.9. The experimental alpha-particle spectrum for ^{147}Sm (n,α) ^{144}Nd reaction as it was measured with Sc-filter (E_n =2 keV). An exposition time is 117 hours. The lower curve represents the background (for shorter measuring time); upper curve includes the effect itself plus background (with dotted line real background is shown). One can see the transitions not only at ground and first excited states, but at higher levels. The average total cross section of the (n,α) reaction is equal to (231$\pm$ 24) microbarn.

It was proved that alpha-width average values were in accordance with the statistical theory. Structure effects have not been observed yet.

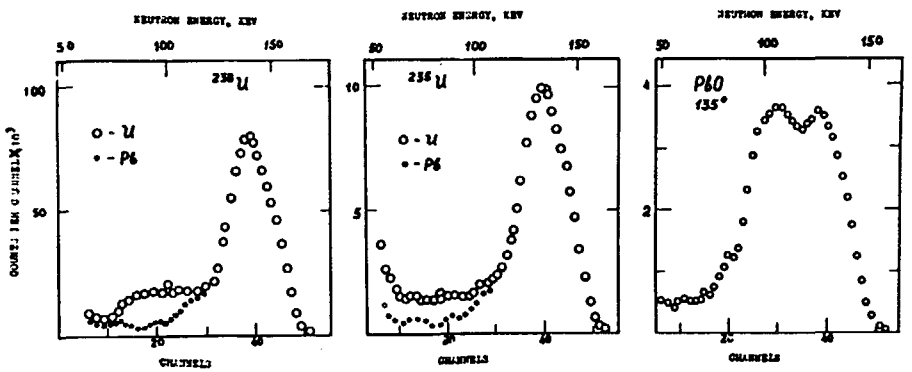

Fig.10. Experimental spectra of the neutrons, scattered on ^{238}U and ^{235}U and PbO, as they were measured by Murzin A.V. et al. with silicon filter (E_n = 144 keV) at the 135° angle. The exposition was 12 hours. Black points indicate results for pure lead; lead isotopes have low levels.

Other Investigations

Without detailed discussion I would like to mention the following items: 1. Inelasting scattering of neutrons near threshold. Murzin's results (Fig.10), which have been obtained at the Kiev atomic Reactor in 1979, demonstrate good possibilities of such research. Brugger and Tsang /35/ have studied angular distribution of neutron elastic and inelastic scattering with ^{238}U nuclei at the neutron energy 144 keV with Si-filter. 2. Capture cross sections by activation methods. 3. Doppler-effect. 4. Gamma-ray decay schemes. 5. Biological investigations /15/.

It is reasonable to suggest that filter beam technique owing to high intensity might be widely used in physical and applied research.

The author thanks Drs. Gnidak N.L., Kirilyuk A.L., Murzin A.V., Pavlenko E.A. and Pschenichnyi V.A. for discussion and critical notes, Professor Block R.C. for possibility to read his and Dr.Brugger's filter use review before publication.

REFERENCES

1. Kononov V.N. Yadernye konstanty, 5(32) (1978). Kon'shin V.A. et al; inbid 4(31), 1978.
2. Neutron Cross Sections BNL 325, 1973, 1977 and 1981 editions.
3. Vertebnyi V.P. IV International School on Neutron Physics, Dubna 1982 D 3,4-82-704, p.66-86.
4. Popov A.B., Samosvat G. Yadernaya Physica v. 15, 350 (1980).
5. Atlas of Gamma-Ray Spectra from the Inelastic Scattering of Reactor Fast Neutrons, Moscow, Atomizdat 1978, M.R.Ahmed et al. (Baghdad); A.M.Demidov et al. (Moscow).
6. Simpson O.D., Miller L.G. Nucl. Instr. Meth. 68, 245 (1968).
7. Dadakina A.F. Byulleten' Informatsionnogo Centra po Yadernym dannym. 1963, v.3, p.226; 1965; ibid 1967, v.4, p.20.
8. Zhuravlev K.D., Kroshkin N.I. Atomnaya Energia 42.56 (1977).
9. Kuzin E.N. et al. Atomnaya Energia 35, 66 (1973).
10. Vertebnyi V.P., Vlasov M.F., Koloty V.V., Ukr.Phys. Zhurnal 19, 510 (1974); R.M.Brugger, Nucl.Instr. 135,289 (1976).
11. Vertebnyi V.P., Gnidak N.L., Murzin A.V. et al., Neutronna a Physica (Proc.conf.), v.2, Moskva, 1977, p.223.
12. Vertebnyi V.P., Gnidak N.L., Kirilyuk A.L. et al., "Voprosy Atomnoy Nauki i Techniki,ser. "Yadernye Konstanty",1,32 (1980), Obninsk.

13. Murzin A.V. et al. in "Neytronnaya Physica", Proc.Kiev Conf., p.2,p.252, 1977.
14. Razbudey V.F. et. al. Nucl.Data for Technology, Proc.Conf., NBS Special Publ. 890 (1980); KirilYuk A.L. et al. "Yadernye Konstanty", 2, 13 (1981), Obninsk.
15. Block R.C., Brugger R.M. in Nucl. Physics and Nucl.Data in Science and Technology, v.2, Chapter V, Pergam.Press (private communication).
16. Kobajashi K. et al. Nucl.Sci.Eng. 65, 374 (1978).
17. Murzin A.V., Libman V.A., Rudyk A.F. in "Neutron Physics" 2, 244, 1980, Proc. Kiev Conference.
18. Dilg W., Vanach H., Forschung Bericht, K 69-37 (19).
19. Broder L.L., Nesterov B., Chamyanov L.P., Yadernaja Physica 13,3 (1971).
20. Dilg W., Vonach H., Proc.Int. Conf. on Statistical Physics of Nuclei, New York 1980.
21. Seth K. Ann. Phys. 40, 183 (1966) and references on his earlier papers.
22. Lynn L.E. Proc. Phys. Soc. 82, 903 (1963).
23. Neutron Cross Sections BNL-325, 19 .
24. Murzin A.V. et al. in "Neutron Physics" (Proc. Kiev Conf.) p.2, 252 (1980).
25. LukYanov A.A. "Slowing down and capture of resonance neutrons", Atomizdat, 1974; Supplement.
26. Zaretsky D.F., Urin M.G. "Neutron Physics" (Proc. Kiev Conf.) p.1 (1977).
27. Bollinger L.M. et al., Phys.Rev. C, p.1951 (1970).
28. Broder L.L. et al., "Yadernaya Physica", 13, 3 (1971).
29. Chrien R.S. in "Sec. Int. Symposium on Neutron Capture", Petten, Proc. Conf. p.99 (1974); NBS Sp. Publ. 425, Proc. Conf., v.11, 912 (1975).
30. Murzin A.V., Libman V.A., Lubchenko N.A., Rudyk A.F. in "Neutron Physics", Proc. Kiev Conf., p.2, Ts. NII Atominform, Moscow, 1980, p.262.
31. Andreev V.N., Popov Yu.P., Bulleten' Informatsionnogo Centra po Yadernym Dannym , 2, 5 (1963).
32. Popov Yu.P., EChAJa, 2, 925 (1972); Antonov A. et al.,YINR P3-10372 ,Dubna, 1971.
33. Vertebnyi V.P. et al., JINR, P3-11392, Anjeevski Yu. et al., JINR, P3-80-779; P3-13013, Dubna (1980).
34. Greenwood R.C., Chrien R.S., Nucl. Instr., 138, 125 (1976).
35. Tsang R.I., Brugger R.M., Nucl. Sci. Eng., 72, 52 (1979).
36. Groshev L.V., Demidov A.M., Proc. Int. Conf. on Peaceful Use of At. En., Geneva, v.2, p.39 (1955); Bartholomeev G.A., Kinsey V.V., Walker W.H., Phys. Rev., 77, 723 (1980).

MULTIPLICITY SPECTROMETRY

G.V. MURADYAN
I.V. Kurchatov Institute of Atomic Energy,
Moscow, Union of Soviet Socialist Republics

Abstract

The method of the gamma multiplicity spectrometry, its combination with neutron spectrometry, and measurements of neutron resonance cross sections, neutron resonance spins and half widths for the (n,gamma f) process are discussed.

I.INTRODUCTION

A new way of measuring neutron cross-sections and of investigating both interaction of neutrons with nuclei and decay channels of excited nuclei-multiplicity spectrometry of gamma-quanta and neutrons emitted by excited nuclei - has been developed in I.V.Kurchatov Institute of Atomic Energy /1/.

The principles of multiplicity spectrometry, its combination with neutron spectrometry and, on this basis, measurement of both the neutron cross-section of neutron resonance spins and the ($n,\gamma f$) process width are discussed in the present work.

2. MULTIPLICITY SPECTROMETRY

The tendency to study the nuclear processes more profoundly and to obtain the nuclear constants with a high accuracy necessitates the simultaneous measurement of as many quantities characteristic of the nuclear process under study as possible. Unlike a complex of experiments where these quantities are measured separately, their simultaneous measurement yields more complete data on the process as alongside the separate quantities it is possible to determine their correlations.

The particle energies, their angles of emission and momenta are usually considered as measured quantitites. Introduction of a new one i.e. multiplicity of particles and quanta both emitted by excited nuclei, and measurement of the corresponding spectrum, multiplicity spectrum (MS), make it possible to expand the range of problems being solved and to improve the accuracy of measurements of nuclear constants.

What do we mean by the MS? Let us imagine an experiment on counting the number of γ -quanta emitted in a nuclear event, e.g. in capture of a neutron by a nucleus. Repeating the experiment many times we could come to conclusion that the number of γ-quanta, or the so-called multiplicity of γ -quanta, changes, generally speaking, from one event to another. In other words, the multiplicity (ν) has some spectrum of values A(ν). It is the spectrum that we call a MS.

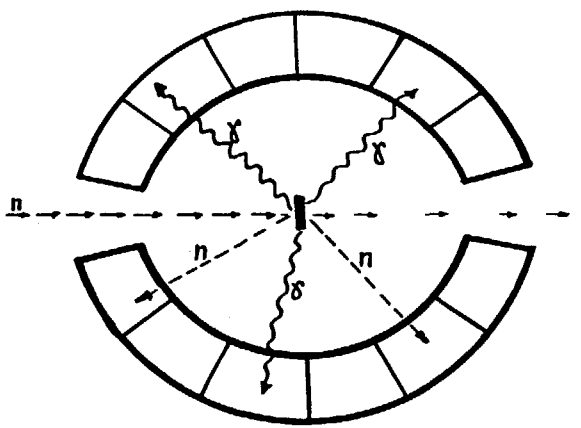

Fig.1. Scheme of the multisection 4π -detector for measurement of multiplicity spectrum.

The MS can be measured by a multisection 4π -detector (Fig.1). The sample with the nuclei of interest is placed in the centre of the detector. The number of the recorded event (N) versus coincidence multiplicity (K) of the different section signals resembles roughly the MS, i.e. $A(\nu) \approx N(K=\nu)$. In the general case

$$N(K) = \sum_{\nu} f(k,\nu) \cdot A(\nu) \qquad (1)$$

where f(k, ν) is the detector response functions for different values of the emitted-particle multiplicity (ν). The more the number of

the sections and the closer the efficiency of recording one particle to 100%, the closer $N(k)$ to $A(\nu)$.

The connection between the MS and the physical parameters of a nuclear process can be found by using some models of particle emission. Let us consider a case when this connection is so unambiguous that its details could be determined easily by the qualitative analysis. The question is the total multiplicity of neutrons and γ-quanta both emitted in the interaction of slow neutrons with nuclei. The MS of this process would consist of high-resolved maxima (Fig.2) corresponding to the scattering (s), radiative capture (γ) and fission (f) processes. Indeed, one neutron is emitted in scattering, therefore, in this case $A_s(\nu)$ is equal to zero everywhere except a point $\nu = 1$, i.e. the first maximum in $A(\nu)$ corresponds to scattering.

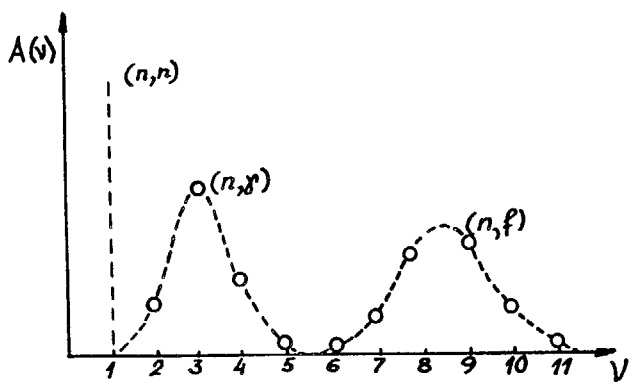

Fig.2. Multiplicity spectra for scattering, radiative capture and fission.

About 4 γ-quanta are produced in radiative capture; the capture MS, $A_\gamma(\nu)$, is concentrated in the region of $\nu \sim 4$, i.e. the capture process is responsible for the second maximum of $A(\nu)$. In the case of fission $\nu \sim 10$; the fission MS, $A_f(\nu)$, is at $\nu \sim 10$, i.e. the third maximum is caused by fission. Thus, the total MS

$$A(\nu) = \sum_j A_j(\nu) \qquad (2)$$

where $j = s, \gamma, f$, decomposes into three spectra in accordance with three known channels of the excited-nucleus decay. The experimental detection of extra peaks or singularities could point other, possibly still unknown, ways of deexcitation. The sensitivity of the MS to the decay channels of excited nuclei is not restricted to the considered case. We shall see below that the MS of γ-quanta is also sensitive to some smaller details of the excited nucleus decay. Detection of these details becomes possible in case of combining the multiplicity spectrometry of γ-quanta with the measurement of other quantities and, expecially, with the neutron and gamma spectrometries. The possibility of principle for the combination follows from the scheme of the MS measurement presented in Fig.1. As seen from the figure, the γ-quantum energy and the recording time can be measured in every section simultaneously with the MS and data on the angular distributions and correlations can be obtained from the section number. It should be noted that the neutron time-of-flight spectrometry can be realized by using the recording time. The following moment is of great importance: the application of the MS measurement together with the determination of the above quantities does not lead, in practice, to any loss of the event collection rate as far as the multiplicity spectrometry itself is realizable only at a highly efficient recording. Moreover, a multisection detector permits an increase in the total flow of recorded events.

Thus, the combination of the multiplicity spectrometry with other spectrometric measurements opens a real possibility to carry out the effective plural measurements, i.e. simultaneous determination of many parameters for every event. Such measurements include much more data than the determination of the same parameters by means of the individual measurements, which are not related to the same event.

Below we shall consider the multiplicity spectrometry of γ-quanta and neutrons produced in neutron reactions. The MS in neutron resonances seem to be of special interest. It is dictated by the following circumstances. First, separating the neutron resonance we identify rather purely the states with the certain quantum characteristics. Second, the partial widths of the different decay processes fluctuate strongly from one resonance to another, creating the prerequisites for separation and investigation of these processes. Third, the cross-sections in resonances are large (up to $\sim 10^5$ barn) which makes it possible to reach high event collection rates using relatively thin targets from which the nuclear radiation, first of all, γ-quanta and fast neutrons, emanates easily.

3. COMBINATION OF MULTIPLICITY AND NEUTRON SPECTROMETRIES

The first installation for studying the MS of γ-quanta and neutrons was built in I.V.Kurchatov Institute of Atomic Energy in 1974 /2/. The detector (Fig.3) consists of 12 NaI(Tl) crystals arranged like a camomile (hence, the detector's name is "Romashka", which means "Camomile" in English), the detector volume being 26 l. The detector is provided with a through channel where the sample investigated is placed and through which the collimated neutron beam passes. To detect neutrons emitted in deexcitation the channel is surrounded with a (n,γ), converter made of mixture of boron-10 and paraffin. The γ-quanta of boron-10 are detected in the same NaI(Tl) crystals.

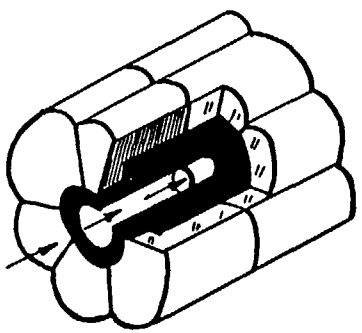

Fig.3. The first multisection detector "Romashka".

An uranium target of a 60-MeV pulsed linac serves as a neutron source. When the electrons arrive at the target, γ-bremsstrahlung appears and causes the production of neutrons in the same target as a result of the (γ,n) and (γ,f) reactions. The shape of the neutron spectrum is close to that of the evaporation spectrum with maximum at an energy of $\sim$2MeV. A hydrogeneous moderator is used to increase the intensity of resonance neutrons.

The neutrons are investigated by time-of-flight spectrometry, i.e. by measuring the time required for the neutron flight through a given distance, i.e. a flight path. "Romashka" is placed on the 26-m flight path in a separate room. The resolution of the neutron spectrometer at a neutron energy of 100eV is $\sim$0.3 eV, which is the value of the same order of magnitude as the resonance width.

For every event recorded by the detector the electronic circuit of the installation generates the codes of the time of flight, the coincidence multiplicity (K) and the energy release in the whole detector (E_γ). The codes arrive in an electronic computer where they are analyzed and classified. A set of time-of-flight spectra 32000 channels in length differing in the K and E values is a result of measurement. At the same time the electronic computer monitors the operation of all detector sections and other parts of the installation. Fig.4 gives the detector response to γ - quanta of a radioactive ^{60}Co source and to the spontaneous fission of ^{252}Cf. As is seen from Fig.4, the 12-section "Romashka" resolves the two types of decay rather well. Later on more perfect spectrometers were developed. One of the recent detectors also made on the basis of NaI(Tl) crystals has 48 sections and a total volume of 200 liter (Fig.5). It consists of separate rectangular scintillators. Such scintillators allow the detector geometry, the number of sections and other parameters to be changed operatively. The response of the 48-section detector to the spontaneous fission of ^{252}Cf is shown in Fig.6 together with the analogous response of the 12-section detector. It is clear that the 48-section detector makes it possible to reduce considerably the fraction of recording the fission events for small values of coincidence multiplicity where the appearance of the radiative capture MS could be expected. It should be noted that N(k) differs noticeably from A(ν) even for the 48-section detector. This difference must be the more appreciable, the higher is ν.

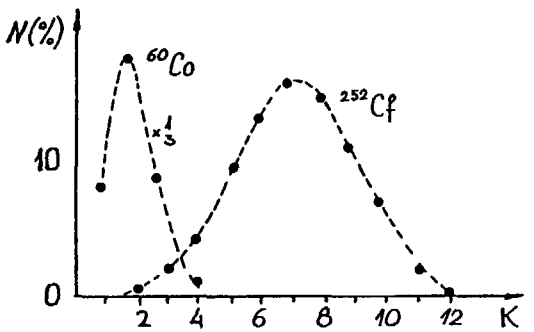

Fig.4. Response of "Romashka" to ^{60}Co and ^{252}Cf.

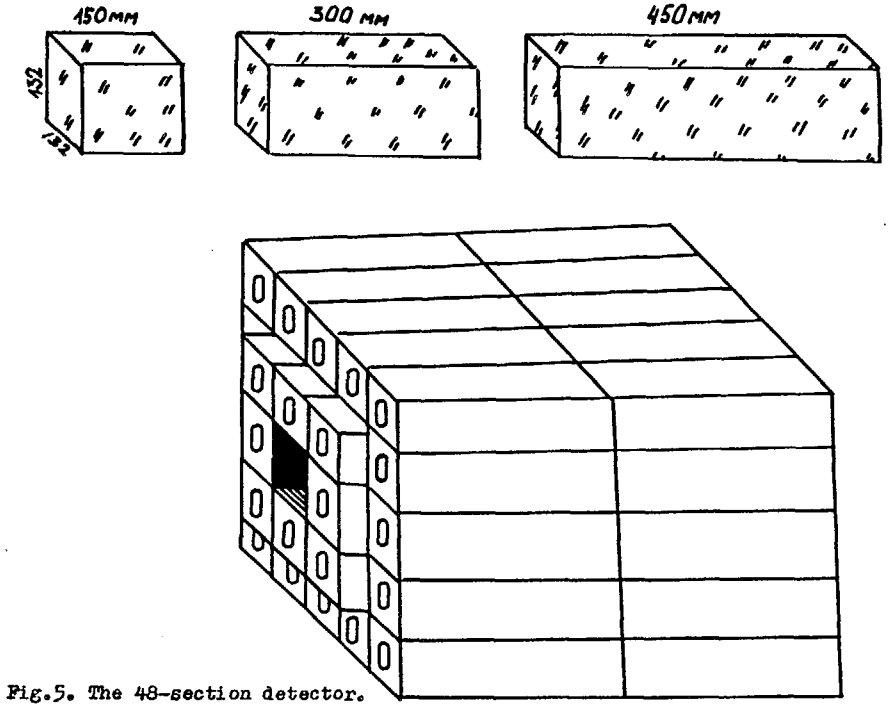

Fig.5. The 48-section detector.

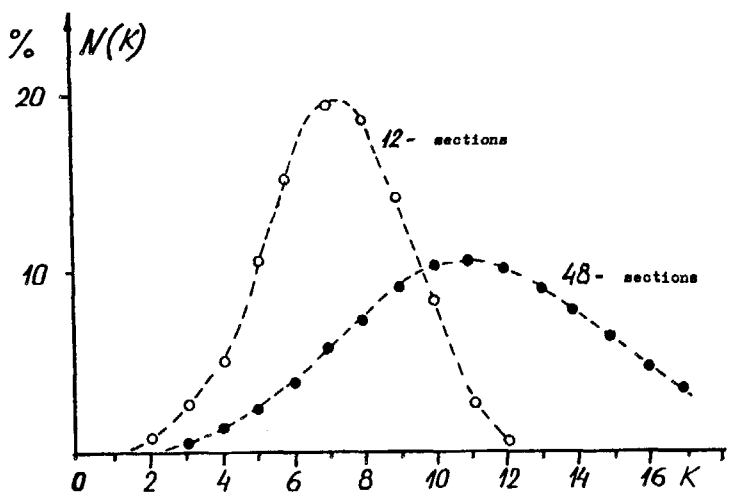

Fig.6. Responses of the 12-and 48-section detectors to spontaneous fission of ^{252}Cf.

Indeed, if the efficiency of γ -quantum recording is ε, $N(k) = \varepsilon$ for the $K=\nu$ -fold coincidences. For example, at $\varepsilon=0.95$, $\nu=2$ and 10 we have $\varepsilon^2 \approx 90\%$ and $\varepsilon^{10} \approx 60\%$. In spite of this, the spectrum N(k) is fairly well determined by the spectrum $A(\nu)$, i.e. the changes in $A(\nu)$ cause practically the same noticeable changes in $N(k)$. Such a conditionality makes it possible to carry out a wide range of investigations for which the knowledge of the coincidence multiplicity spectrum N(K) is quite enough. The concrete problems considered below pertain just to this range of problems.

4. MEASUREMENT OF NEUTRON CROSS-SECTIONS

Owing to its high efficiency the MS measured can be combined with spectrometry of neutrons incident on the sample under investigation. From the obtained data it is possible to determine the number of the capture and fission events versus neutron energies and then from these dependences to find the cross-sections for both capture (σ_γ) and fission (σ_f) as well as the alpha-value ($\alpha \equiv \sigma_\gamma/\sigma_f$). The energy dependence of the alpha-value is of interest from the angle of studying the decay singularities of a compound nucleus. Unlike the partial cross-sections (σ_γ and σ_f) $\alpha = \sigma_\gamma/\sigma_f = \Gamma_\gamma/\Gamma_f$ is not sensitive to the cross-section for compound nucleus production and depends only on outlet channel widths. In the given case it is known, that Γ_γ depends weakly on neutron energy and, therefore, the singularities in the energy dependence of alpha-value are to be attributed to the fission width singularities.

The knowledge of the alpha-value with a high accuracy is of great importance to the nuclear reactor optimization, when the better accuracy than 5% is required. It is this accuracy which can be achieved with multiplicity spectrometry. Fig.7 represents the fission-capture MS obtained in the uranium-235 measurements by the 48-section detector. It is clear that the two processes are highly resolved. Within the range of $K \sim 3$ where the capture events are mainly recorded the fraction of fission is less than $\sim 1\%$, the fission events only being recorded in the range of $K > 8$. The time-of-flight spectra of the 4 - and 10 - fold coincidences are given in Fig.8. The individual neutron resonances as well as their different behaviour in these spectra due to different alpha-values are seen distinctly. It should be noted that the same spectra were obtained for coincidence multiplicities K=1,2...30.

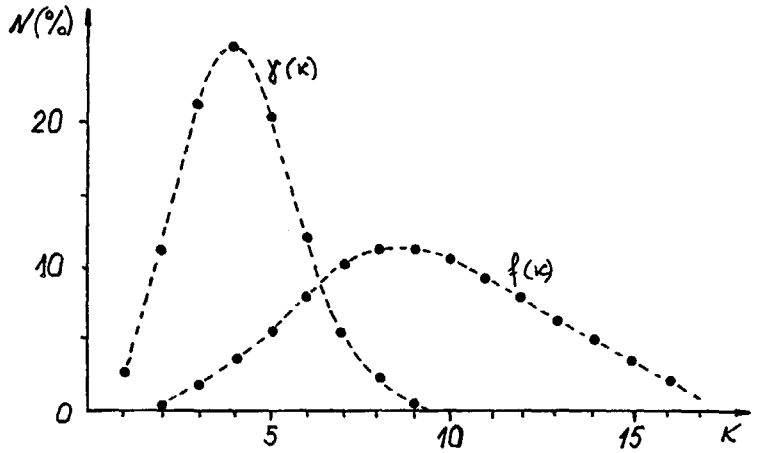

Fig.7. Capture and fission multiplicity spectra of uranium-235 obtained with the 48-section detector.

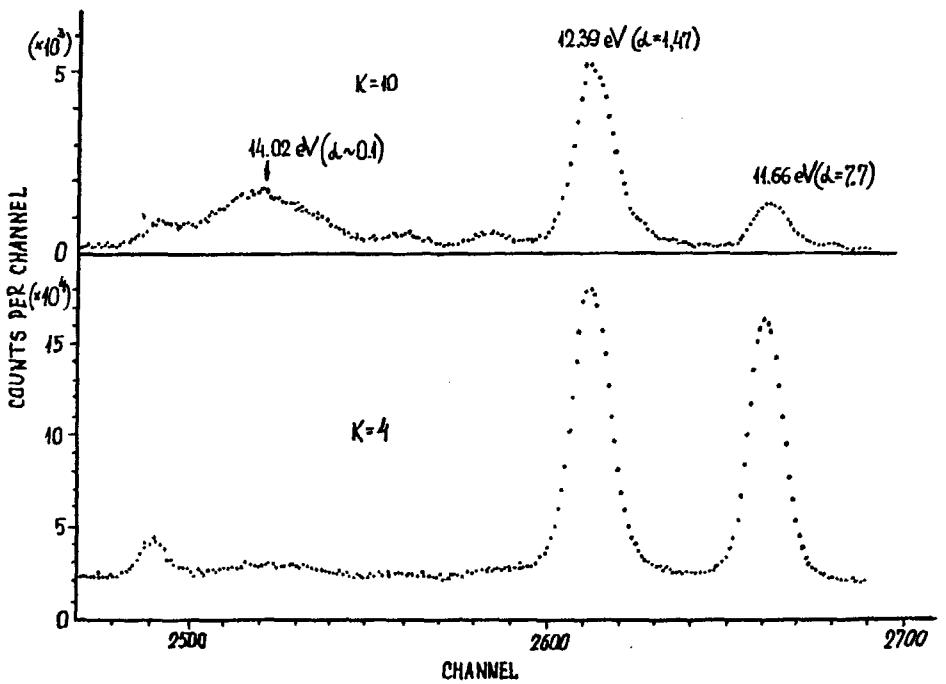

Fig.8. Time-to-flight spectra of uranium-235 for K=4 and K=10.

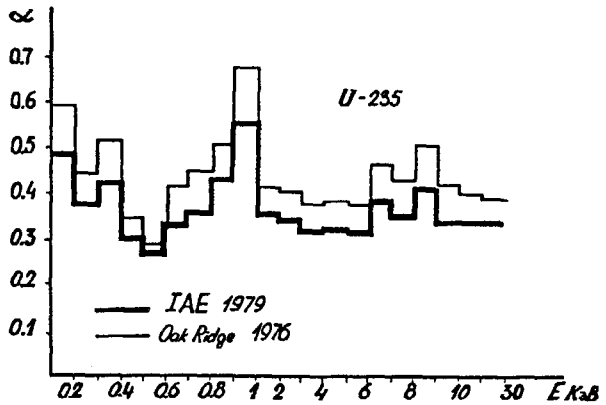

Fig.9. Alpha-value of uranium-235.

The results of the alpha-value measurements are presented in Fig.9 /4/. The singularities in the energy dependence of alpha-value are seen, which is explained at present by a two-humped fission barrier /5/. As is seen from the figure, our data fall lower than the Oak Ridge data /9/. This difference is rather significant for calculations of reactors. It should be noted that the accuracy of our data is ~5%, that of the Oak Ridge data being ~15%. Therefore, the observed difference of ~20% is permissible. The same picture is also observed in the difference of the resonance region /6/, wherein the accuracy of our data is sufficiently high, being 2%. It should be pointed out that unlike our absolute data, the Oak Ridge data are relative, as they are normalized to data on the capture and fission cross-sections in the thermal region. It may well be that the difference, to some extent, results from the inaccuracy of the calibration data.

The possibility of distinguishing the radiative channel of nuclear decay from the MS can be also used to investigate fissionable isomers. It is known /7/ that for most of such isomers the expected probability of radiative decay is by several order of magnitude lower than that of fission, in consequence of which difficulties arise in distinguishing the events of radiative transition against a great number of fissions. Introduction of the multiplicity spectrometry per-

mits the radiative transition to be additionally, about by a factor of 100, purified of fission. It follows from that only ~1% of fissions is detected in the region K<2 where the events of γ-cascading-down can mainly be concentrated. It should be noted, that distinguishing the radiative channel yields data on the isomer nature and, if the nature is known, information on the characteristics of the isomer state, for example, on the permeability of the internal barrier for the shape isomers.

5. GROUPING OF NEUTRON RESONANCES

1. In the above interaction of a neutron with a nucleus the MS $A(\nu)$ decomposes easily into the simple components $A_j(\nu)$, as the different $A_j(\nu)$ are concentrated in the different regions of the variable ν, i.e. highly resolved. The application of neutron spectrometry allows one to solve the problem of the MS decomposition into the separate components (not necessarily corresponding to the (n,n), (n,γ) and (n,f) processes) even in case of overlapping the MS components. These are the cases when the dependences of $A_j(\nu)$ on the incident neutron energy E_i are different. Let us suppose that at a given j the MS shape

$$a_j(\nu) \equiv \frac{A_{ij}(\nu)}{\sum_\nu A_{ij}(\nu)} \qquad (3)$$

does not depend on i. Then the MS, $A_i(\nu)$, representing the sum of $A_j(\nu)$ can be written in the form

$$A_i(\nu) = \sum_j C_{ij} \cdot a_j(\nu) \qquad (4)$$

where C_{ij} are the weights of the different channels. Eq.(4) is to be considered as a system of equations in C_{ij} and $a_j(\nu)$. Under concrete conditions the system can be solved with one or another unambiguity and the certain conclusions concerning the behaviour of the different MS components can be done.

2. Let us consider the MS of γ-quanta of radiative caputure in the neutron resonances (denoted below with subscript i). The variation of the MS shape from one resonance to another can be connected with a variety of their quantum characteristics. The isolated resonances have the sufficiently definite quantum numbers, therefore, for these resonances C_{ij} =1 or 0 at a given j and normalized $A_i(\nu)$. In particular, for the s-resonances the groups correspond to two spin states: $I \pm 1/2$. The measurement for the purpose of the spin grouping of the s-resonances were performed for ^{113}Cd /8/. The recorded spectrum normalized to unity, i.e. $n_i(k) = N_i(k) / \sum_k N_i(k)$, is directly used for grouping. By analogy with Eq.(4) the expected spectrum of coincidence multiplicity can be presented in the form

$$n_i^{(0)}(k) = C_{i1} \cdot a_1(k) + C_{i2} \cdot a_2(k) \qquad (5)$$

The values $a_1(k)$, $a_2(k)$, C_{i1} and C_{i2}, which corresponded to the minimum of the expression

$$\sum_{k,i} \eta_{ki}^2 \left| n_i^{(0)}(k) - n_i(k) \right|^2 \qquad (6)$$

(where η_{ki} are the weights allowing for errors and fluctuations) in case of $C_{i1} + C_{i2} = 1$, were chosen as a solution. The results of treatment are given in Fig.10 in the form of dependence of C_{i1} upon the resonance number i. The even grouping is obvious. The ratio of the numbers of resonances in the two groups observed is ~4, corresponding to expectation of the statistic model. At the same time it shows that the spin of the group with $C_{i1} = 1$ is $I + \frac{1}{2} = 1$. In the general case the question about the belonging of the group to the concrete quantum numbers can be solved either comparing $a_i(k)$ with the cascade-imitated calculations or comparing the results of grouping with the known data on identification of quantum numbers for several resonances.

It should be noted that the possibility of grouping is due to N(k) within the group changing much less than in passing from one group up to another. In the case under consideration the intragroup changes exist really and are connected with the Porter-Thomas fluctuations.

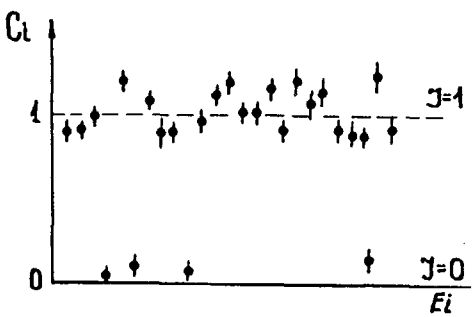

Fig.10. Grouping of the ^{113}Cd neutron resonances by means of multiplicity spectrum.

At $\nu = 1$ the fluctuations are maximum, as $\nu = 1$ corresponds to the only transition, the transition to the ground state. At $\nu > 1$ the number of transitions is very large and, therefore, the fluctuations are small. At the large number of neutron resonances the presence of groups can be observed also in the case when the intragroup fluctuation is comparable with the intergroup one. Increase in the number of the observed resonances is connected with increase in the flight path and, therefore, with loss of the event collection rate in resonances. But this increase is permissible because of the high efficiency of the MS measurement. Fig.11 represents the time-of-flight spectrum of uranium-238 measured by the 24-section detector on the 120-m flight path. The spectrum for the 26-m flight path is given in the same figure for comparison. The improvement of resolution is clearly seen in the case of the 120-m flight path.

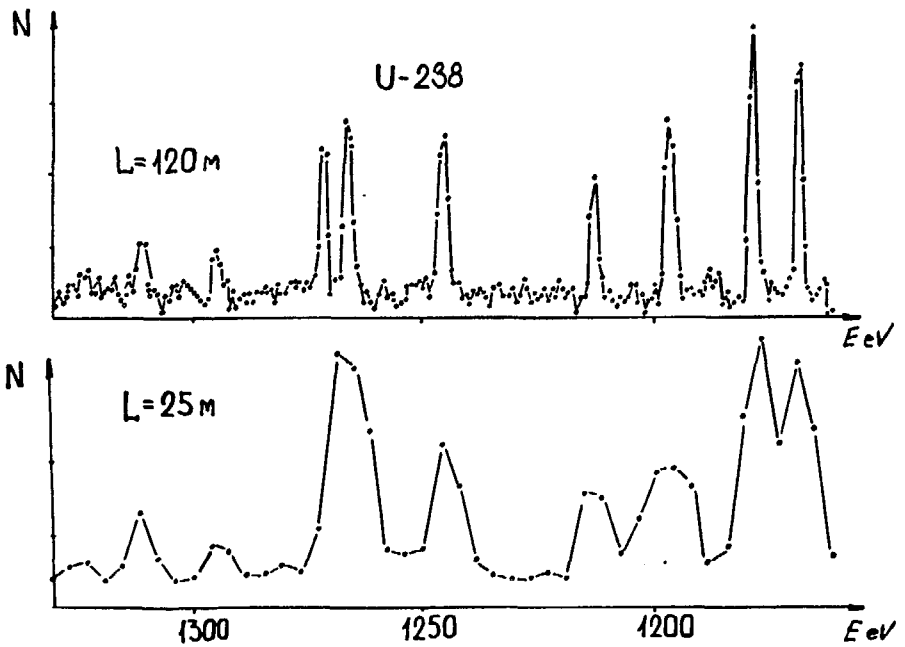

Fig.11.Time-of-flight spectra for the 26-m and 120-m flight paths.

6. ANALYSIS OF THE COMPLEX DECAY CHANNELS

We shall consider the case when the MS components are different for different j and practically independent of i, the relative probabilities C_{ij} changing with i in different ways. In this case the MS $A(\nu)$ can also be decomposed into the separate components. In so doing, in addition to establishing the basic components the stability of $a_j(\nu)$ for any given j makes it possible to recognize and study the hardly probable decay channels.

The MS of γ-quanta produced in an usual fission of a nucleus is a typical process when the MS is practically bound to be unchangable. So the detection of fluctuations in the MS of fission γ-quanta could indicate the presence of an unusual fission channel. The emission of one or several γ-quanta by a nucleus prior to fission, i.e. the $(n, \gamma f)$ process, can be such a channel. In this case, unlike the usual (n, f) fission, the MS is shifted in the direction of larger and Eq.(5) can be written as

$$n_i^{(o)}(k) \simeq C \cdot [\Gamma_{if} \cdot a_f(k) + \Gamma_{i\gamma f} \cdot a_{\gamma f}(k)] \qquad (7)$$

$$a_f(k + \Delta k) \approx a_{\gamma f}(k)$$

where Γ_{if} and $\Gamma_{i\gamma f}$ are the widths of the (n,f) and $(n,\gamma f)$ processes, respectively; $\Delta k = \Delta\nu$ is the mean multiplicity of the γ-quanta preliminarily emitted in the $(n,\gamma f)$ process; C is the proportionality factor. The width Γ_{if} is to the Porter-Thomas fluctuations with the number of degrees of freedom ~ 1. These fluctuations ensure a great variety in the system of equations (7), which, in turn, allows the values of Γ_{if}, $\Gamma_{i\gamma f}$ and Δk to be estimated by minimizing a sum similar to (6).

The investigations of the $(n,\gamma f)$ process were carried out for uranium-235 and plutonium-239 with the 46-section detector. $\bar{\Gamma}_{\gamma f} \approx (5 \pm 2)$ meV and $\bar{\Gamma}_{\gamma f} < 2$ meV were obtained for plutonium and uranium, respectively.

7. CONCLUSION

Thus, multiplicity spectrometry opens new possibilities of studying nuclei and determining the neutron cross-sections with the highest accuracy owing to the MS sensitivity to the decay channels of an excited nucleus, its high efficiency and equipment compatibility with other spectrometric measurements.

REFERENCES

1. G.V.Muradyan. Multiplicity spectrometry. - Atomnaya Energiya, 1981, v.50, N 6, pp.394-398 (in Russian).
2. G.V.Muradyan, Yu.V.Adamchuk, Yu.G.Shchepkin. - Problems of Atomic Science and Engineering (Voprosy Atomnoi Nauki i Tekhniki). Ser.Some Problems of Solid State Physics.Moscow,1974,p52(in Russian)
3. G.V.Muradyan, Yu.V.Adamchuk, Yu.G.Shchepkin, M.A.Voskanyan.- Multiplicity spectrometer for measurement of neutron cross-sections. Preprint IAE-3807/14,Moscow, 1983, (in Russian)
4. G.V.Muradyan, Yu.G.Shchepkin, Yu.V.Adamchuk, M.A.Voskanyan. A measurement of U-235 absolute alpha value in the neutron energy range from 0.1 to 30 keV. - In proc.: Nuclear Cross Sections for Technology (International Conf., USA, Knoxville, Oct.22-26, 1979) 1980, pp 488-490.
5. V.M.Strutinsky. Shell effects in nuclear masses and deformation energies. - Nucl.Phys.A, 1967, v.95, p.420.
6. Yu.V.Adamchuk, M.A.Voskanyan, G.V.Muradyan, P.Yu.Simonov, Yu.G.Shchepkin. Measurement of alpha value on uranium-235 resonances. - In proc.: Nuclear Data for Science and Technology (International Conf., Antwerp., 6-10 September, 1982), pp.730-732.
7. Wgigmann H., Theobald J.P. Evaluation of fission barrier parameters from near-barrier fission and isomeric half-life data.- Nucl.Phys.A, 1972, v.187, p.305.
8. Yu.V.Adamchuk, M.A.Voskanyan, V.I.Zhuk, D.A.Markov, G.V.Muradyan, G.I.Ustroev, A.D.Kharitonov, Yu.G.Shchepkin. Technique of measuring neutron cross-sections and quantum characteristics of nuclear levels. - In proc.: Neutron Physics (4th All-Union Conf., Kiev, April 18-22, 1977) Moscow, 1977, part 3, pp.113-118 (in Russian).
9. R.Gwin, E.A.Silver, R.W.Ingle and H.Weaver, Nucl.Scin.Eng., 59, 79 (1976).

NUCLEAR SPECTROSCOPY AND DECAY DATA FOR ACTINIDES

V.M. KULAKOV
I.V. Kurchatov Atomic Energy Institute,
Moscow, Union of Soviet Socialist Republics

Abstract

The methods of alpha, beta and gamma spectroscopy for obtaining transactinium nuclear data relevant to reactor applications are discussed.

The spectroscopy of nuclear radiations is the oldest branch of the nuclear physics. By means of it the abundant experimental material on properties of nuclei and their nuclear characteristics has been collected: nuclei level energies, life-times and others (state spins and parities, types of nucleus decays, multipolarities of electromagnetic transitions). Information obtained with the help of nuclear spectroscopy has made it possible to develop theoretical models of a nucleus structure, to predict new, earlier unknown nuclear properties. Moreover, the nuclear spectroscopy has given extensive reference material on radionuclides, without which the calculation of nuclear power systems and methods of nuclear fuel reprocessing would be impossible.

In the suggested lecture we shall dwell on methods of the nuclear spectroscopy and nuclear data obtained through it for actinide element isotopes, on demands for these data in various fields of nuclear technology and on the present-day situation of the nuclear data.

1. According to the types of heavy nucleus radiations, the precision methods of alpha-, beta- and gamma-spectroscopy, various coincidence techniques and methods determining nuclide half-lives are commonly developed.

(a) Alpha-spectroscopy

Since the great majority of isotopes of actinide elements decays with the alpha-particle emission, the alpha-spectroscopy is one of the main methods of investigation of heavy nuclei. The circumstance that alpha-particles possess quite a certain charge and energy permitted magnetic spectrographers with high resolution (~0.03%) to be used in carrying out these investigations. Semiconductor detectors began to be widely used in the recent years for these purposes. The information obtained by means of alpha-spectroscopy contains data on energies and relative intensities of alpha-groups, on energy characteristics and quantum properties (spins, parities) of daughter nucleus excited states.

(b) Beta-spectroscopy

The main method of precision beta-spectroscopy is magnetic and electrostatic spectrometers. At present, beta-spectrometers have been created with resolution of ~ 0.5 eV over the whole range of energies measured. Such a high resolving power has given rise to new methods of analysis of a substance, in particular, to the electron spectroscopy for chemical analysis (ES CA). The information from beta-spectroscopy includes: probabilities of beta-transitions, energy levels of daughter nuclei, their quantum characteristics, energies, intensities and electromagnetic transition multipolarity types.

(c) Gamma-spectroscopy

Gamma-spectroscopy methods have covered a path from first gas-filled counters through precision semiconductor spectrometers. Semiconductor detectors with resolution of ~ 2keV for gamma-ray energy about 1 MeV have been worked out by the present time.

(d) Half-lives

In a brief lecture it is impossible to consider in detail all developed methods for measurement of half-lives. Therefore, we shall enumerate only main methods with short comments.

1. The direct measurement of a decay curve. The method is suitable for the case of comparatively short half-lives (up to 10 years). The measurement accuracy can significantly be risen by applying differential procedures.

2. The specific activity method. It is employed at long half-lives and consists in determining the source activity (with the aid of an ionization chamber or calorimeter) and the number of radioactive nuclei.

3. Determination of a half-live by means of a daughter product growing accumulation for the known time interval.

The half-live of radioactive isotope is the most important constant defining its individual properties and behaviour in physical, chemical and technological processes. The accurate knowledge of half-lives is specifically significant in reactor calculations. Since the discovery of radioactivity an extensive material by measuring half-lives has been accumulated, whose critical analysis is far from a simple problem.

2. As mentioned above, the nuclear spectroscopy has accumulated the extensive experimental material on isotope half-lives energies, intensities (quantum yields) and quantum characteristics of radiations. As the nuclear power engineering progressed and technological processes of nuclear fuel reprocessing were improved, the need for accurate values of "decay" characteristics of isotopes, especially isotopes of actinide elements and fission products has immeasurably grown.

However, the data users have right away faced a problem. The point is that different research groups (various laboratories) give different values of the same data, not overlapping within the limits of measurement errors. In this connection rather important has been the problem of assessment of the data by sophisticated physicists and creation of an estimated data international file available for users in different countries. It is clear that the exchange of data (especially the estimated ones) is beneficial to the entire scientific community, since it saves every state's means.

This problem has been taken up by the IAEA (nuclear data section (NDS)). Under the aegis of IAEA two international meetings were held on the evaluation of actinide isotope nuclear data. The first meeting took place in Karlsruhe(FRG) in 1975, the second one, in Cadarache (France) in 1979. After the first meeting two groups were formed joined by the coordinated research program (CRP) and having the aim to take regular care of the nuclear data status. One of the groups is engaged in the neutron data status and possible comparison of evaluations of cross-sections in reactions with neutrons. The second one, the status of measurement and decay evaluation of nuclear data. The last meeting of these groups was held last year in Gule (Belgium). The recommended evaluated nuclear data values are elaborated and distributed both through reactions with neutrons and through decay of actinide element isotopes. As a result of work of the groups the problems of their presentation on magnetic types as well as their dissemination and exchange are also discussed at the meetings.

At the present time, the TsAYaD (Center on atomic and nuclear data) of the USSR State Committee for Utilisation of Atomic Energy is a member of the world network of centers on "decay" data. As for actinides, the TsAYaD, within the framework of international obligations, has performed for the recent years the evaluations of chains with mass numbers of 238, 240, 242 and 244.

3. In the table for a number of practically important isotopes examples are presented of reached and required accuracies in the values of half-lives and alpha- and gamma-emission intensities. It is indicated in the last column, calculations of what processes require the accuracy given in the table. The examples are taken from materials by an international group on the measurement and evaluation of nuclear data on the actinide element isotopes decay /1,2/ .

The complete tables of required and reached accuracies at the measurements and evaluations of $T_{1/2}$, $T_{1/2}$ (s.f.), $I_\alpha, I_\gamma, I_\beta$ are published in /1,2/

From the examples given it is seen that the accuracy needed for calculations was reached for far from all actually significant isotopes. Therefore, the problem of more precise determination of decay nuclear data and qualified evaluation of these data is not removed from the agenda.

4. In this section we shall dwell on some works by Soviet scientists carried out for the recent 2-3 years.

At I.V.Kurchatov Institute of Atomic Energy measured were the periods of spontaneous fission ($T_{s.f.}$) and first moments of distribution of the total number of prompt neutrons ($\bar{\nu}$ and σ_ν^2) per fission event for uranium isotopes /3/ . The measurements were made using a neutron detector on the basis of ^{3}He-counters in a hydrogen-containing moderator, the source studied being placed in the centre. The work was performed in an underground laboratory at the depth of 80 m with a drastically reduced external background

Nucleous	Type of nuclear data	Needed accuracy, %	Accuracy reached as of VIII.1982 %	Where data are needed
Pa-231	I_α	2	2-5	Non-destructive analysis of nuclear fuel(NDA)
U-233	I_γ	1	10	Thorium cycle research
U-234	I_α	1	4	Thorium cycle and NDA
	I_γ	2	10	
U-235	I_α	1	5-10	Determination of amount, and NDA
	I_γ	1	10	
U-238	I_α	1	5-20	Determination of amount, NDA
	I_γ	1	15	
Pu-239	I_γ	2	10	
Pu-240	$T_{1/2}$ for spontaneous fission, I_γ	2	4	Medicine
		1	2-5	
Pu-242	I_γ	5	10	Determination of amount, NDA
Am-241	I_γ	1	2-3	Calibration of γ-detectors, NDA
Cm-243	I_α	2	2-10	Analysis of fuel assemblies, NDA
	I_γ	1	5-10	
Cm-245	I_α	2	0,5-5	Analysis of fuel assemblies, NDA
	I_γ	2	unknown	
Cm-246	$T_{1/2}$	1	2	- " -
	I_α	2	1-5	
	I_γ	2	unknown	

and induced fission of sample nuclei. The detector was additionally protected with a borated polyethylene layer and anti-coincidence plates made of scintillation plastic, suppressing the meson background of installations (factor >100).

The detector's efficiency to neutrons of californium-252 spontaneous fission spectrum ($\bar{\nu}$ = 3.735) amounted to 0.49. When changing to spectra of a uranium correction of ~ 2% was made to change efficiency, obtained by the numerical modelling of processes of neutron propagation in the detector.

For the measurements use was made of high-enriched uranium isotopes with the weight from 20 to 50 g. The contribution of self-multiplication and induced fission by neutrons of the (α, n) - reaction to the counting speed for spontaneous fission events was experimentally estimated and measured. For the processing of the measured results the shape of multiplicity distribution of prompt neutrons was taken to be Gaussian.

The following results were obtained:

Isotope	$T_{s.f.}$	$\bar{\nu}$	σ_ν^2
U-238	$(8.3 \pm 0.4)\ 10^5$ years	1.97± 0.10	1.03± 0.08
U-236	$(2.7 \pm 0.4)\ 10^{16}$ years	1.79± 0.18	1.02± 0.12
U-235	$> 3.10^{18}$ years	-	-

The results for U-238 agree well with the values recommended in the literature. The spontaneous fission half-life and mean number of prompt neutrons per U-236 fission event confirm the only measurements made in works /4/ ($T_{s.f}=(2.42\pm0.17)\cdot10^{16}$ years) and /5/ ($\bar{\nu}=1.89\pm0.05$). The U-235 spontaneous fission half-life is consistent with recent measurements $T_{s.f}=(9.8\pm2.8)\cdot10^{18}$ years /6/.

The Pu-238 half-life was determined by a direct observation of the decay curve /7/ . The content of Pu-239 and Pu-240 isotopes was evaluated from the study of specimen alpha-radiation spectrum. The accidental error of measurement results in each series at the confidence level of 0.99 did not exceed 0.1%. The estimated value of the Pu-238 half-life came up to $T_{1/2}=86.96\pm0.55$ year with the confidence level P=0.99.

The Cm-245 half-life was determined by four various methods /8/: 1) through the ratio of molar concentrations of Cm=245/Cm-244 and alpha-activity of Cm-244/Cm-245; 2) according to the ratio of molar concentrations of Cm-245/Cm-244 and Pu-240/Pu-242; 2) according to alpha-activity of Cm-245; 3) through the growing of Pu-241 with the use of Pu-239 mass concentration values in a solution-marker.

In all four methods the half-life of curium-245 was determined regarding the Cu-244 half-life, which value was taken to be equal to 18.099±0.015 years. Finite results were calculated by the maximum likelihood method with allowance for non-eliminated systematic errors for the confidence level P=0.95. The average weighted half-life value calculated according to experimental results, amounted to 8445±200 years for the confidence level P=0.95.

The einsteinium-253 half-life was determined from alpha-spectrometric measurement data and according to results of the total alpha-activity measurements in $2\pi\alpha$ -geometry /9/. In the experiment use was made of einsteinium extracted from the mixture of californium isotopes irradiated in a high-neutron flux reactor CM-2. The measurements were conducted for $\sim 6.2 \cdot T_{1/2}$. The Es -253 half-life calculated as a mean-weighted value from measurements of 20 samples was 2o.31±0.16 days with the confidence level of 0.95.

The ratio of probabilities of BK-249 alpha and beta-decay obtained by the direct measurement of specific alpha-and beta-activities of a radio-chemically pure berkelium sample, turned out to be equal to $(1.48 \pm 0.12) \cdot 10^{-5}$ at the confidence level of 0.95 /10/. The Cf-249 half-life, calculated according to the speed of its accumulation in the BK-249 preparation with the use of the found value of probabilities ratio α/β and previously defined BK-249 half-life of 329±4 days, amounted to 360±13 days.

Absolute intensities of U-237 (E_γ -208 KeV) and Np-238 (E_γ -984 KeV) γ-rays were found by the γ-spectrometry method using a Ge(Li)-spectrometer /11/. The γ-spectrum of U-236 and Np-237 samples irradiated in a thermal neutron flux was measured. The Ge(Li) - detector absolute efficiency was determined using standard spectrometric γ-sources. The following values for an absolute intensity of γ-rays were obtained:

U-237, $I_{\gamma\,abs}$ - 21.5±1.4%

Np-238, $I_{\gamma\,abs}$ -22.7 ±0.7%

The data on half-lives of 46 transactinium element isotopes being most long-living (from Th-228 till Fm-257), published until July 1st, 1981 in the Soviet and foreign literature, are summarised in the paper /12/. The work presents the sum total of results of original investigations, compilations of accepted and recommended half-lives. From the given data the following conclusions have been drawn:

(1) the necessity of refinement of half-lives of many practically interesting isotopes is evident (U-232, Np-237, Pu-241, 244, Am-242 m, Cm-243, 245, 247, Bk-247, 249, et al);

(2) the stability of Th-232 half-lives is observed at the consecutive reduction in error;

(3) absolute values of half-lives of U-233, 234, Pu-239, Am-241, Cm-245, Cf-249 are decreased;

(4) half-lives of U-238, Np-236, Pu-244, Cm-244, 246, Bk-249, Fm-257 are increased;

(5) the decrease in errors of measurements of Th-232, Cm-244, 245, 246, 248, Bk-249, Cf-249, 250, 252 half-lives are observed.

In conclusion, let us note that at the present time there is a number of issues where collected are the evaluated and recommended decay data for actinides.

Users of these data can employ the editions:

1. Table of isotopes (Ed. by M.Lederer and V.S.Shirli), 7th ed., USA.

2. File listing of IAEA nuclear data section - INDC(NDS)-127/NE.

3. Regular issues of "Data Sheets" magaznine.

Besides, the users of nuclear data on decay can obtain evaluated and recommended data on magnetic tapes both at the international center of IAEA nuclear data section and national centers of a number of countries (the USSR, USA, Great Britain, Japan, France).

REFERENCES

1. Second IAEA Advisory Group Meeting on Transactinium Isotope Nuclear Data, INDC (NDS)-106/LN.

2. Actinide Newsletter, issue 6, March 1983, ORNL.

3. Fourth CRP Meeting on the Measurement and Evaluation of Transactinium Isotope Nuclear Data, INDC(NDS)-126/NE.

4. H.Conde and M.Holmberg, J.Nucl.Energy, 25, 331, 1971.

6. H.R. von Gunten et al., Phys.Rev. C23, 1110, 1981.

7. V.D.Sevastyanov, V.P.Yaryna. Voprosy atomnoy nauki i tekhniki. Ser.: Yadernyje konstanty (Nuclear constants), is. 5(44), Ts NII Atominform, M., 1981, p.21.

8. V.G.Polyukhov, G.A.Timofeev, V.V.Kalygin, P.A.Privalova. Radiokhimiya (Radiochemistry), v.24,No.4, 1982, p.490.

9. V.G.Polyukhov, G.A.Timofeev, A.A.Elesin.Radiokhimiya, v.24, No.4, 1982, p.494.

10. V.G.Polyukhov, G.A.Timofeev, B.I.Levakov. Radiokhimiya, v.25,No.1, 1983, p.92.

11. A.V.Bushuev, O.M.Matveeva, V.N.Ozerkov, V.V.Chachin. Voprosy atomnoy nauki i tekhniki. Ser.: Yadernyje konstanty, is. 2(46), 1982, p.30.

12. V.M.Surin, E.F.Fomushkin. Voprosy atomnoy nauki i tekhniki. Ser.Yadernyje konstanty, is. 2(48), 1982, p.3.

ON NEUTRON YIELD FOR THE O, F (α, n) REACTIONS

V.A. VUKOLOV
I.V. Kurchatov Institute of Atomic Energy,
Moscow, Union of Soviet Socialist Republics

Abstract

An evaluation of cross sections and neutron yields for the (alpha,n) reaction on oxygen, fluorine and some structural materials was made on the basis of the experimental data reported in the literature up to 1982.

INTRODUCTION

Recently a considerable interest has again been aroused by neutron production in interaction of α-particles with light nuclei. This interest has been dictated by a number of nuclear technology problems, such as development of analytical means of control and radiation protection of nuclear fuel, production of neutron and isotope energy sources on the basis of α-active materials. The latter are widely applied in medicine, geology, space industry and other fields of science and engineering. Development of these energy sources requires knowledge of neutron yields for light impurity elements for construction of biological shielding. Judging from the requests /1/, for the above problems to be solved, the (α, n) reaction cross sections and neutron yield must be known with an accuracy of about 10% in the α-particle energy range up to 10 MeV and for the elements from Be to Ca. In view of extending circle of users who often are no specialists in the field of nuclear physics , analysis, evaluation of experimental data and establishment of recommended values on their basis become particularly important.

In the present work an attempt is made to obtain evaluated cross-section data and yields of neutrons for the (α, n) reaction on oxygen, fluorine and some structural materials containing these elements by means of the analysis of the experimental data reported in literature up to 1982. Meeting requirements on these data is of highest priority according to the IAEA classification /2/.

1. EVALUATION METHOD

The evaluation procedure includes two main stages: compilation of the reaction cross section data and determination, on the basis of selected data, of recommended values and their uncertainties using statistical models of analysis.

At the first state the data are compiled and their uncertainties analyzed, analysis of the measurement methods is carried out and, when necessary, correction of the data is made for the best values of constants and calibration standards. At this stage obviously erroneous measurements are preliminary excluded from consideration. The criterion of such exclusion is deviation of the results by more than 3 standard errors, given by the authors, from the weighted average value determined on the set of other works or the authors themselves present new results instead of old ones.

At the second stage the selected experimental data are distributed over appropriate energy groups. Division of the entire energy region of measurement into groups is determined from the following conditions: the group must include, if possible, the data from all works considered and its size must not be lower than the maximum energy resolution used in the measurement. It is clear that under these conditions the division group size can vary within the whole measurement region under consideration. Then within each group the average value of the cross section with weights equal to $\omega_i = 1/(\Delta\sigma_i)^2$ (where $\Delta\sigma_i$ is the measurement error in the individual experiment) is calculated. From the average values of cross sections in each group a preliminary excitation function is determined. Its energy dependence is used for renormalization of all experimental data within the group to the average value of energy of the given group. Thus, for each group we obtain n values of cross sections σ_i with errors $\Delta\sigma_i$. From these values we calculate the weighted average value of the cross section: $\bar{\sigma} = \sum \omega_i \sigma_i / \sum \omega_i$ and their errors /3/: internal $\Delta\sigma = 1/\sqrt{\sum \omega_i}$ allowing only for uncertainties of σ_i, and external: $\Delta\sigma' = \sqrt{\frac{1}{n-1}\sum(\sigma_i - \bar{\sigma})^2 / \sum \omega_i}$ depending both on uncertainty of σ_i and on deviation from the weighted average value $\bar{\sigma}$. In accordance with Birge's criterion /4/: $\frac{|\Delta\sigma^2 - \Delta\sigma'^2|}{\Delta\sigma^2} \cdot \left(\sqrt{\frac{2}{n-1}}\right)^{-1} = K$, the value $k > 2$ indicates the presence of an unaccounted systematic error in the data series treated. After finding out the results of the works whose effect on K is decisive, they are subject to a more thorough analysis over the entire measurement region, checked for normality of distribution of their deviations from the weighted average value over the groups. If the deviations are not conditioned statistically, then the data found out in such a manner are eigher rejected or assigned with a great uncertainty. Then the value of K is again calculated.

If $K < 2$ then the larger value from the internal and external errors is assigned as the uncertainty of the weighted average value. If condition $K < 2$ cannot be obtained from the analysis, then the cross section values in individual groups are calculated as arithmetic mean over n values of σ_i with uncertainty $\Delta\sigma = t_p(n)\sqrt{\sum(\sigma_i - \bar{\sigma})^2/n(n-1)}$ where $t_p(n)$ is the Student's coefficient for (n-1) degrees of freedom and confidence coefficient P. The values in the groups, obtained in such a way, determine the evaluated values of the excitation function over the whole measurement region under consideration.

The calculation procedure described is realized when a sufficient amount of experimental data is available so that each group treated has results of at least two measurements. If this condition is not safisfied, two frequent cases should be considered.

In the first case a certain energy range of measurements is presented primarily by experimental data of one work and only partly is overlapped with the measurements of other authors. Then the evaluation procedure described above is carried out for the data lying in the overlapping region of measurements. The value of uncertainty for evaluated values of the excitation function is obtained by quadratic addition of the errors presented by the authors and error of the normalization coefficient.

In the second case in a certain energy range there are no experimental data at all. Then the evaluated data within this range are calculated by extrapolation of the evaluated experimental data from other regions or in terms of an appropriate theoretical model.

2. EXPERIMENTAL CROSS-SECTION DATA AND YIELD OF NEUTRONS FOR THE O,F (α,n) REACTIONS

In the review the works published in literature up to 1982 were included. Search for literature sources of interest was made using international libraries NSR and CPND /5/. About 20 experiments were found out and analyzed. Since no numerical data on measurement results had been found they were taken from the original works. The results of measurements of the (α,n) reaction cross sections on oxygen /6-9/ and fluorine /10/ are shown in Fig.1. Fig.2 shows the measured values of yields for these elements /9,11/. Tables 1,2 list the results of neutron yields using isotope sources of α -particles and data on cross-section measurement in individual resonances for fluorine /23, 24/, respectively.

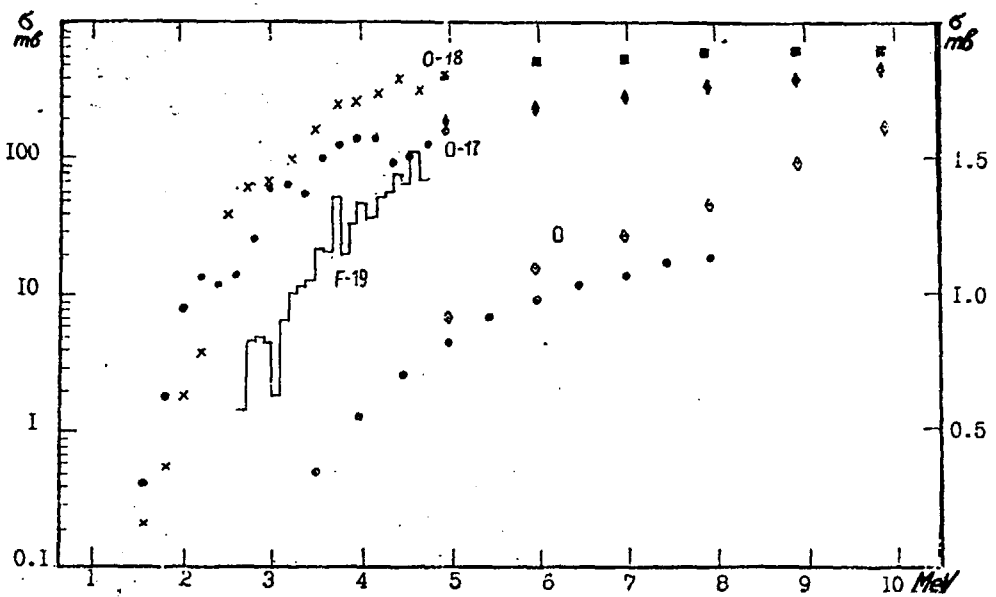

Fig.1. Cross section of the O and F(α,n) reactions. At the top, for O^{17},O^{18} and F^{19} (left scale): • - O^{17}/6/, x-O^{18}/7/, ◊ - O^{17}/8/, ▪ - O^{18}/8/, ⌐ - F^{19}/9/. At the bottom, for natural oxygen (right scale): • - /9/, ◊ - /8/.

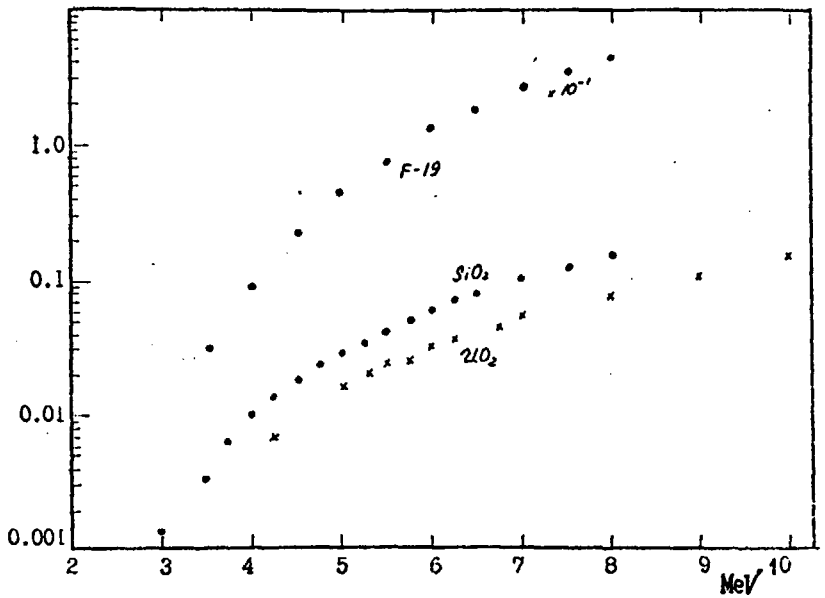

Fig.2. Yield of neutrons from the targets: F^{19} /9/- o , SiO_2-/9/- • , UO_2-/11/-x.

The analysis of the experimental results and measurement methods showed:

1. All the works can be classified by measurements with thin or thick targets using an accelerator or α -active isotopes as the source of α -particles.

2. All the measurements are very similar methodically: as detectors for registration the proportional (He^3, B^{10}) counters surrounded by hydrogen-carbon moderating medium with efficiency weakly dependent on the neutron energy are used; calibration of efficiency is made using source of known intensity and neutron energy spectrum.

3. The typical accuracy of the experiments on thin targets is higher than 10% and is mainly determined by the error in target thickness measurement (up to 10%), calibration error (up to 2 %), corrections for deviation of the detector efficiency on constancy depending on neutron energy and associated neutron escape from the detecting system (up to 5%).

4. The typical accuracy of experiments on targets with thicknesses exceeding α-particle path (thick), so that the accuracy of their measurement is of no importance, is less than 10%. Use of isotope α-particle sources allows a higher accuracy of the results to be obtained /12,13,15/.

5. Another source of errors seriously restricting the measurement accuracy may be presence of uncontrolled impurities of light elements in the targets investigated.

6. Existing spread of the data for the O (α,n) reaction cross section is 25% /8,9/, for yields of neutrons, 15% /16,18/; for fluorine only one measurement is available /10/ though comparison of the cross sections in different resonances shows a significant discrepancy (e.g. for resonances E_α=2.7305; 3.286 MeV /23,24/), for the yields the discrepancy is 70% /9,12/.

Table I.

N	Source	E MeV	Target	Neutron yield per 10^6 α-particle	Reference
1	2	3	4	5	6
1.	Po-210	5.305	oxygen	0.07	/12/
2.	Po-210	5.305	O^{18}	31	/13/
3.	Po-210	5.305	oxygen	0.068 ± 0.11	/14/
4.	Po-214	7.687	oxygen	0.56 ± 0.03	/15/
5.	Pu-238	5.50(72%) 5.46(28%)	PuO_2	$(2.0\pm0.2)\times10^{-2x}$	/16/
6.	- " -	- " -	- " -	$(2.204\pm0.033)\times10^{-2x}$	/17/
7.	- " -	- " -	- " -	$(2.31\pm0.14)\times10^{-2xx}$	/18/
8.	- " -	- " -	- " -	$(2.291\pm0.027)\times10^{-2x}$	/19/
9.	- " -	- " -	- " -	$(2.25\pm0.11)\times10^{-2x}$	/20/
10.	Am-241	5.5(85%) 5.44(15%)	AmO_2	$(2.2\pm0.3)\times10^{-2x}$	/21/
11.	Po-210	5.305	fluorine	10 12	/12/
12.	Po-210	5.305	fluorine	11.6 ± 0.2	/14/
13.	U-234	4.7	UF_6	$(2.50\pm0.18)^x$	/22/
	U-235	4.40	UF_6	$(1.53\pm0.11)^x$	
	U-236	4.48	UF_6	$(1.65\pm0.12)^x$	
	U-238	4.18	UF_6	$(1.18\pm0.11)^x$	

Notes: x) To obtain neutron yields in units "number of neutrons per 10^6 alpha particle" and take into account contribution of spontaneous fission neutrons, the data on decay constants from work /32/ were used: Pu-238-$T^{\alpha}_{1/2}=(87.74\pm0.09)$; $T^{SF}_{1/2}=(4.77\pm0.13)\ 10^{10}$; $\bar{\nu}=(2.21\pm0.08)$; Am-241-$T^{\alpha}_{1/2}=(432.8\pm0.6)$; U-234-$T^{\alpha}_{1/2}=(2.454\pm0.006)\ 10^{15}$; U-235-$T^{\alpha}_{1/2}=(7.037\pm0.011)\ 10^{8}$; U-236-$T^{\alpha}_{1/2}=(2.342\pm0.003)\ 10^{7}$; U-238-$T^{\alpha}_{1/2}=(4.468\pm0.05)\ 10^{9}$; $T^{SF}_{1/2}=(8.19\pm0.09)\ 10^{15}$; $\bar{\nu}=(1.98\pm0.07)$.

xx) The original work gives the value 25% higher than this one. The value presented in the Table was reported by the authors after corrections had been made for neutron multiplication on account of the fission reaction (15%) and for neutron yield on account of the (α,n) reaction for light impurity elements in the samples (10%) /19/.

Table II

E MeV	σ (mbarn) /23/	/24/	E MeV	σ (mbarn) /23/	/24/
1	2	3	4	5	6
2.498	3	-	3.12	3.5	-
2.609	6	-	3.153	25	13.6
2.730	14	19.6	3.246	20	32.9
2.84	16	-	3.286	25	6.3
2.87	2	-	3.35	25	27.1
2.90	2	-	3.468	17	16.5
2.94	10	-	3.526	-	16.3
3.01	3.5	-	3.574	-	42.6
3.07	7	-	3.752	-	110

Notes: x) In /23/ the measurement accuracy is 30%; target thickness is 20 keV.

xx) In /24/ the results of cross-section measurement in the resonances connected with excitation of the ground state of nucleus Na-22: measurement accuracy is 15%, target thickness is from 4 to 7 keV.

3. EVALUATION OF THE EXPERIMENTAL DATA O (α,n) REACTION

In interaction of α-particles with oxygen in the energy region up to 10 MeV the (α,n) reaction proceeds only on O^{17}, O^{18} isotopes; the reaction energies for these isotopes are 0.588 and 0.698 MeV, respectively. For O^{16} this reaction is endoergic with the reaction energy 12.135 MeV.

The cross section of the O^{17} and O^{18} (α,n) reaction was measured in /6,7/ for the energy region from 1 MeV to 5.2 MeV with accuracy $\pm$25% and in /8/ for E_α from 5 MeV to 12.5 MeV with accuracy $\pm$10%.

In work /9/ Bair and Willard /6,7/ made repeated measurements of the cross section for O^{18} at E_α =(4.62-4.8) MeV and found that the results of earlier measurements for O^{17} and O^{18} had been underestimated by a factor of 1.35. The reconsidered error became equal to $\pm$7%.

In the same work the authors, basing on the measurements of neutron yield from a thick SiO_2 target, calculated the cross section of the (α,n) reaction for natural oxygen in the energy region (3.5-8) MeV; the accuracy of its determination was $\leq$ 10%. Fig.1 shows the results from /6,7/ corrected in accordance with the recommendation of work /9/.

Thus, there are two sets of the data obtained by different authors, which agree in the overlapping measurement region (5-8)MeV in the limits of accuracy $\pm$10% reported by the authors. In obtaining the evaluated values the results of /6,7/ increased by a factor of 1.35 and normalizing factor (1.067$\pm$0.064) were taken as the basis. This factor is the ratio of the weighted average cross section for natural oxygen found from the results of /8,9/ to the average cross section /9/ in the (5-8)MeV energy region. For energies higher than 5 MeV the results of /8/ reduced by a factor of 1.067 were taken as evaluated values. The evaluated error in the values is $\pm$10% at energies up to 5MeV and $\pm$12% at energies higher than 5MeV and is determined by quadratic addition of the errors in the original measurements and normalizing factor ($\pm$6%).

The evaluated data for O^{17} and O^{18} are given in Table 3 (columns 2,3).

The neutron yield from the target where α-particles lose completely their energy is determined by:

$$Y(E_\alpha) = \kappa \int_0^{E_\alpha} [\sigma(E_\alpha)/(dE/dx)]\, dE, \qquad (1)$$

where κ is the number of the isotope nuclei per gram of the target material in which the (α,n) reaction proceeds; $\sigma(E_\alpha)$ is the reaction cross section; dE/dx is the stopping power of the target material. The main difficulty in the calculation of the neutron yield is associated with uncertainty of the stopping power values. Fig.3 shows the results of semiempirical calculations of the stopping power for oxygen and uranium reported in two recent works /25,26/. In the same figure the calculation results (dE/dx) for uranium dioxide and the experimental results /27/ are presented. The calculation was made in accordance with the Bragg's rule/28/

$$dE/dx = \frac{\sum a_j A_j (dE/dx)_j}{\sum a_j A_j}, \qquad (28)$$

where A_j is the isotope mass number j, a_j is the number of atoms of this isotope in the molecule of matter.

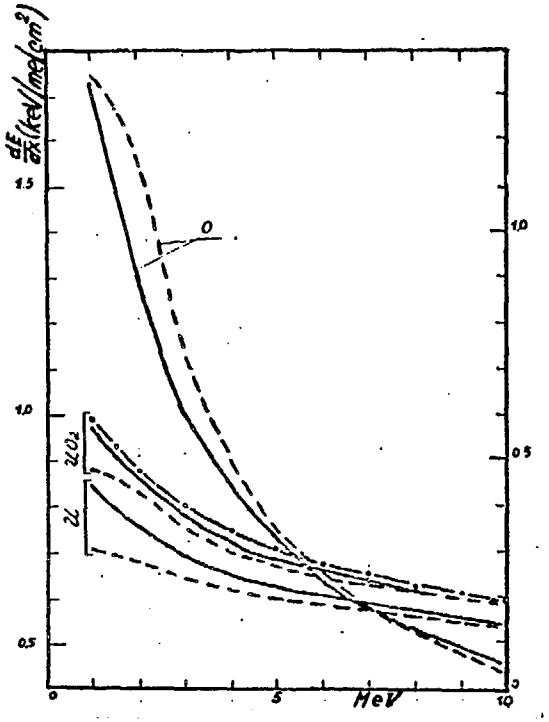

Fig.3. The stopping power values for oxygen (left scale), uranium, uranium dioxide (right scale): —/25/, ~ /26/, ·–·–/27/.

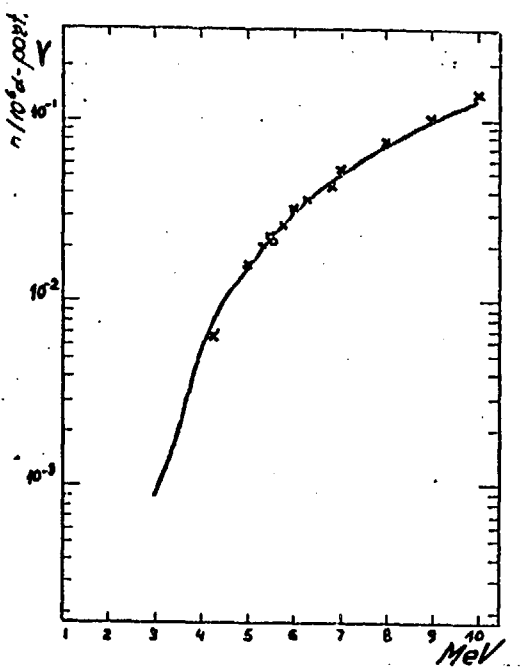

Fig.4. Comparison of the calculation results for neutron yields on uranium dioxide with the experimental data:/11/-x and /16-20/-o.

As is seen from the figure, the discrepancy between the two results is significant, particularly for α -particle energies lower than 5MeV. The accuracy 5% which is usually attributed to these data may be spoken about only for energies exceeding 5 MeV. For example, the discrepancies for oxygen are 5% at 5 MeV while at 2 MeV they uncrease up to 20%; for uranium the discrepancies are 10% at 5MeV and 30% at 2MeV. The stopping power values for uranium dioxide, calculated by formula (2), using the data of /25 and 26/, differ at 5 MeV by 7%. The experimental values of the stopping power, whose accuracy is ±2%, are systematically higher by 13% than those calculated from the results of /25/.

The choice of the best values (dE/dx) was made from the comparison of the results of the neutron yield calculation by (1) using various stopping power data with the experimental data.

Fig.4 shows the results of neutron yield calculations for uranium dioxide using the stopping power values from /26/ and the experimental data available. A good agreement of the calculation values with the results of /11/ can be seen. Though the data of /11/ are preliminary, the corrections unaccounted in these results are small (less than 4%), as has been pointed out in /29/, and cannot affect essentially the experimental values; the expected measurement accuracy is to be about 2%. For measurements on $^{238}PuO_2$ at E_α =5.50MeV Fig.2 shows the weighted average value taken from /16-20/; it is equal to $(0.227 \pm 0.003)\ 10^{-1}$ n/10^6 α - particles and agrees with the calculated value $(0.24 \pm 0.2)\ 10^{-1}$.

Thus, the results of the semiempirical calculations of the stopping power from /26/ agree reasonably with the experimental data /27/ and give a good description of the experimental neutron yields.

Table III.

EVALUATED CROSS-SECTION DATA AND YIELD OF NEUTRONS FOR REACTION O(α,n).

E	SIGMA(MBARN)		F	YIELD(n/10**6 α/PARTICLES		YIELD (%)
MEV	170	180	MEV	O	238Pu	170/O
-1.0	14.F-04	3.F-04	1.0	25.F-09	89.F-10	*
1.0-1.1	11.F-03	11.F-03	1.1	83.F-09	30.F-09	17.0
1.1-1.2	21.F-03	56.F-04	1.2	13.F-08	46.F-09	28.0
1.2-1.3	28.F-03	56.F-04	1.3	18.F-08	64.F-09	35.0
1.3-1.4	11.F-02	42.F-03	1.4	49.F-08	17.F-08	35.0
1.4-1.5	84.F-03	56.F-03	1.5	84.F-08	30.F-08	30.0
1.5-1.6	14.F-02	56.F-02	1.6	39.F-07	14.F-07	14.0
1.6-1.7	33.F-02	84.F-02	1.7	46.F-07	16.F-07	16.0
1.7-1.8	14.F-01	84.F-02	1.8	66.F-07	23.F-07	35.0
1.8-1.9	11.F-01	14.F-01	1.9	16.F-06	54.F-07	23.0
1.9-2.0	46.F-01	71.F-02	2.0	24.F-06	85.F-07	35.0
2.0-2.1	87.F-01	19.F-01	2.1	46.F-06	16.F-06	41.0
2.1-2.2	19.F 0	40.F-01	2.2	92.F-06	32.F-06	45.0
2.2-2.3	14.F 0	59.F-01	2.3	15.F-05	50.F-06	40.0
2.3-2.4	12.F 0	59.F-01	2.4	20.F-05	67.F-06	38.0
2.4-2.5	9.F 0	27.F 0	2.5	30.F-05	13.F-05	23.0
2.5-2.6	10.F 0	86.F 0	2.6	97.F-05	32.F-05	11.0
2.6-2.7	24.F 0	27.F 0	2.7	12.F-04	40.F-05	12.0
2.7-2.8	14.F 0	50.F 0	2.8	16.F-04	54.F-05	10.0
2.8-2.9	12.F 0	60.F 0	2.9	21.F-04	69.F-05	8.9
2.9-3.0	49.F 0	101.F 0	3.0	29.F-04	96.F-05	8.2
3.0-3.1	88.F 0	21.F 0	3.1	32.F-04	10.F-04	11.0
3.1-3.2	92.F 0	75.F 0	3.2	39.F-04	13.F-04	13.0
3.2-3.3	44.F 0	116.F 0	3.3	48.F-04	16.F-04	12.0
3.3-3.4	32.F 0	136.F 0	3.4	60.F-04	19.F-04	10.0
3.4-3.5	65.F 0	87.F 0	3.5	68.F-04	22.F-04	11.0
3.5-3.6	68.F 0	236.F 0	3.6	89.F-04	29.F-04	9.4
3.6-3.7	121.F 0	269.F 0	3.7	11.F-03	37.F-04	9.0
3.7-3.8	144.F 0	249.F 0	3.8	14.F-03	44.F-04	9.1
3.8-3.9	140.F 0	316.F 0	3.9	17.F-03	53.F-04	8.8
3.9-4.0	108.F 0	266.F 0	4.0	19.F-03	61.F-04	8.7
4.0-4.1	173.F 0	245.F 0	4.1	22.F-03	69.F-04	9.0
4.1-4.2	159.F 0	250.F 0	4.2	24.F-03	77.F-04	9.2
4.2-4.3	121.F 0	360.F 0	4.3	28.F-03	88.F-04	8.8
4.3-4.4	105.F 0	394.F 0	4.4	30.F-03	10.F-03	8.2
4.4-4.5	81.F 0	300.F 0	4.5	33.F-03	11.F-03	8.0
4.5-4.6	80.F 0	410.F 0	4.6	35.F-03	12.F-03	7.6
4.6-4.7	133.F 0	409.F 0	4.7	44.F-03	14.F-03	7.5
4.7-4.8	125.F 0	258.F 0	4.8	46.F-03	14.F-03	7.5
4.8-4.9	122.F 0	400.F 0	4.9	51.F-03	16.F-03	7.4
4.9-5.0	120.F 0	341.F 0	5.0	55.F-03	17.F-03	7.4
5.0-5.5	187.F 0	403.F 0	5.5	79.F-03	24.F-03	7.4
5.5-6.0	206.F 0	440.F 0	6.0	11.F-02	33.F-03	7.5
6.0-6.5	230.F 0	470.F 0	6.5	14.F-02	42.F-03	7.7
6.5-7.0	258.F 0	494.F 0	7.0	17.F-02	53.F-03	7.8
7.0-7.5	285.F 0	515.F 0	7.5	21.F-02	64.F-03	8.0
7.5-8.0	315.F 0	535.F 0	8.0	25.F-02	76.F-03	8.2
8.0-9.0	350.F 0	575.F 0	9.0	35.F-02	10.F-02	8.3
9.-10.0	403.E 0	610.F 0	10.0	46.E-02	14.F-02	8.6

This circumstance permits us to use them for obtaining the evaluated neutron yields. Table 3 lists neutron yields for natural oxygen (column 5), for Pu^{238} (column 6) and the contribution to the total yield of neutrons for 10^{17} (column 7) expressed as a percentage. The neutron yield for energies lower than 1MeV is obtained by extrapolation of the evaluated cross section values to the threshold energy. The total evaluated error of the yield values is about ±20% at energies lower than 1.5MeV and ±15% at other energies. The total uncertainty included the error ±7% resulted from the spread of the stopping power data.

The comparison of our evaluated data on neutron yields with those evaluated earlier in /30/ after multiplying them by 1.35 shows that the values from/30/ are lower by about 10% at energies up to 3.5MeV and by 25% at 7MeV. The discrepancy seems to be due to different ways of data matching over the cross sections of the O (α,n) reaction /6-8/ in the overlapping region of measurements and to use of other stopping power values /27/. All the known experimental results agree, within the accuracy reported by the authors, with the evaluated values, except for the data on the neutron yield on oxygen for 7.7MeV α - particles, which is twice as great as our value /5/.

F (α,n) reaction

The F-19 (α,n) reaction is endoergic with the reaction energy of 1.95MeV. In the literature only one measurement of the total cross section of the F(α,n) reaction in the (2.6-5.1)MeV α -particle region is known. Its accuracy is ±15%. In work /9/ the neutron yield from PbF_2 and ZnF_2 thick targets with energies from 3.5MeV to 8MeV is measured. The yield was converted to a fluorine target making use of the stopping power data from /25/; the evaluated error is ±7%. Some works are known where the neutron yield has been measured on the isotope α -particle sources: ^{Po} -210 /12,14/ with an accuracy up to 10% and that on uranium hexafluoride at various uranium isotope content /22/ with an accuracy of ±7.3%.

For comparison of the experimental data we calculated the neutron yield for fluorine using the results from /10/ and /22/; the stopping power data were taken from /26/. Fig.5 shows the calculated and experimental results /9,12,14/. One can see three curves with the systematically differing data. The lowest have been obtained using the cross section on thin targets, measured in /10/. The values higher by 20% are the experimental results taken from /9/. Finally, the highest results systematically higher by 60% than the values of /10/ were obtained in /12,14,22/, where the isotope α -particle sources were used. The discrepancies are essential taking into account that the experimental errors reported by the authors /9,22/ are about ±7%.

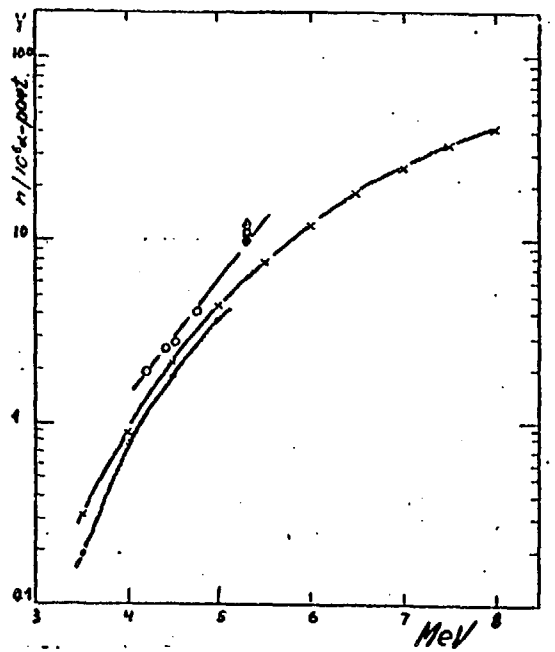

Fig.5. The calculation results of neutron yields on fluorine
×- /9/, ◊-/2/, □-/14/, ⊙ -the results have been obtained from calculation on the basis of the experimental yields for uranium hexafluoride /22/, ~ the results are calculated by means of the cross section measured.

It should be pointed out that in work /22/ uranium hexafluoride samples weighted up to 0.4 kg were used, corrections for neutron absorption and multiplication in the samples have been thoroughly considered; however nothing is said about the sample compositions though it is known /19,21/ that the presence of light impurity elements (Be,C,O) in the sample could be the cause of the higher yield of neutrons observed.

Table IV.

EVALUATED CROSS-SECTION DATA AND YIELD OF NEUTRONS FOR REACTION 19F(α,n).

E	SIGMA(MBARN)		E	YIELD(n/10**6 α-PARTICLES)			
				F-19		UF_6	
MEV	σ	Δσ	MEV	Y	ΔY	Y	ΔY
2.4-2.6	8.E-1	3.E-1	2.6	5.E-3	2.E-3	3.E-3	1.E-3
2.6-2.7	16.E-1	3.E-1	2.7	10.E-3	2.E-3	6.E-3	1.E-3
2.7-2.8	50.E-1	9.E-1	2.8	26.E-3	5.E-3	16.E-3	3.E-3
2.8-2.9	56.E-1	*10.E-1	2.9	45.E-3	8.E-3	27.E-3	5.E-3
2.9-3.0	52.E-1	9.E-1	3.0	62.E-3	11.E-3	38.E-3	7.E-3
3.0-3.1	20.E-1	4.E-1	3.1	69.E-3	12.E-3	42.E-3	8.E-3
3.1-3.2	77.E-1	*14.E-1	3.2	96.E-3	17.E-3	58.E-3	10.E-3
3.2-3.3	12.E 0	2.E 0	3.3	14.E-2	2.E-2	83.E-3	15.E-3
3.3-3.4	13.E 0	2.E 0	3.4	19.E-2	3.E-2	11.E-2	2.E-2
3.4-3.5	14.E 0	2.E 0	3.5	24.E-2	4.E-2	14.E-2	2.E-2
3.5-3.6	27.E 0	5.E 0	3.6	34.E-2	6.E-2	20.E-2	4.E-2
3.6-3.7	25.E 0	4.E 0	3.7	44.E-2	8.E-2	26.E-2	5.E-2
3.7-3.8	65.E 0	*12.E 0	3.8	69.E-2	10.E-2	41.E-2	7.E-2
3.8-3.9	23.E 0	4.E 0	3.9	78.E-2	14.E-2	47.E-2	8.E-2
3.9-4.0	41.E 0	7.E 0	4.0	95.E-2	17.E-2	57.E-2	10.E-2
4.0-4.1	54.E 0	*10.E 0	4.1	12.E-1	2.E-1	70.E-2	13.E-2
4.1-4.2	43.E 0	8.E 0	4.2	14.E-1	2.E-1	80.E-2	14.E-2
4.2-4.3	60.E 0	*11.E 0	4.3	16.E-1	3.E-1	96.E-2	14.E-2
4.3-4.4	66.E 0	*12.E 0	4.4	19.E-1	3.E-1	11.E-1	2.E-1
4.4-4.5	87.E 0	*16.E 0	4.5	23.E-1	4.E-1	14.E-1	2.E-1
4.5-4.6	76.E 0	*14.E 0	4.6	26.E-1	5.E-1	15.E-1	3.E-1
4.6-4.7	130.E 0	*23.E 0	4.7	32.E-1	6.E-1	19.E-1	3.E-1
4.7-4.8	80.E 0	*15.E 0	4.8	36.E-1	6.E-1	21.E-1	4.E-1
4.8-4.9	102.E 0	*18.E 0	4.9	41.E-1	7.E-1	24.E-1	4.E-1
4.9-5.0	95.E 0	*17.E 0	5.0	45.E-1	8.E-1	27.E-1	5.E-1
5.0-5.5	*135.E 0	*12.E 0	5.5	79.E-1	11.E-1	47.E-1	6.E-1
5.5-6.0	*170.E 0	*15.E 0	6.0	124.E-1	14.E-1	72.E-1	8.E-1
6.0-6.5	*200.E 0	*18.E 0	6.5	181.E-1	18.E-1	105.E-1	11.E-1
6.5-7.0	*235.E 0	*21.E 0	7.0	250.E-1	24.E-1	144.E-1	14.E-1
7.0-7.5	*260.E 0	*24.E 0	7.5	331.E-1	31.E-1	190.E-1	17.E-1
7.5-8.0	*280.E 0	*26.E 0	8.0	423.E-1	39.E-1	242.E-1	22.E-1

To obtain the evaluated data the experimental results were normalized to the weighted average value of the neutron yield for fluorine at 4.40, 4.48, 4.76MeV, determined from /9,10,22/. The results for 4.18MeV were not analyzed since they did not meet the Birge's criterion. In the statistical analysis the results of /10/ and /22/ were assigned with uncertainties 18% and 12.4%, respectively, obtained by adding 10% to the authors'uncertainty due to discrepancy in the fluorine stopping power values in /25,26/.

The evaluated values of the F(α,n), reaction cross section at energies up to 5MeV were based on the results of work /10/ multiplied by the normalization factor (1.21 ± 0.14); at energies higher than 5MeV the cross-section values were determined by the data of /9/. The evaluated error in the cross-section value is $\pm$20% up to E_α =5MeV, which is determined by the experiment and normalization errors, and $\pm$10% at energies higher than 5MeV (7% is the measurement error, 5% is the uncertainty in the stopping power values, 3% is given for possible sharp change in the cross section in the averaging range). The evaluated values of neutron yield on fluorine and uranium hexafluoride were calculated by formula (1) using the stopping power data from /26/. The evaluated error in the yield values is the same as for the cross section data since the uncertainty in the stopping power values was allowed for earlier. The evaluated cross section and yield values together with the errors are presented in Table 4.

The comparison with the known experimental results shows that the neutron yields on fluorine for E_α= 5.3MeV in /12,14/ exceeds the evaluated value by a factor of 1.5. The data of /31/ on neutron yield from the 241AmF source became known after the evaluation had been completed. The neutron yield reported there was (3.44 ± 0.13) being 35% lower than our results.

CONCLUSION

The analysis of the experimental results available shows that currently the recommended results can be found with an accuracy $\pm$10% for the O(α,n) reaction and $\pm$20% for fluorine. The uncertainty in the stopping power values decreases the accuracy of the recommended neutron yield data, particularly, at energies lower than 5MeV.

Therefore, to obtain more reliable results on neutron yields on materials of complicated compositions, it is necessary not only to continue the cross-section measurements on these targets but to carry out measurements of the stopping powers of various matters.

REFERENCES

1. Day-Day N., - INDC(SEC)-76/URSF, 1981.
2. Okamoto K., - Importance and priorities for compilation of selected CPND and Photonuclear Data, NDS Meetings, Vienna, 1982.
3. Grigoryan Y.I., Sokolovskij L.L., Chukreev F.E., The evaluation of Nuclear Data, INDC (CCP)-75/LN, 1976, January.
4. Birge R.T., Phys.Rev., 1932, 40, 207.
5. Ignatochkin A.E., Matick E.A. Osnovnye kontseptsii poiska po biblioteke NSR-Recent References Preprint IAE-3394/6,M.,1981.
6. Bair J.K., Willard H.B., Phys.Rev., 1962, 128, 299.
7. Bair J.K., Haas F.X., Phys.Rev., 1973, C7, 1356.
8. Hansen L.E., e.a., Nucl.Phys., 1967, A98, 25.
9. Bair J.K. Comes del Campo, Nucl.Sci.Eng., 1979, 71, 18.
10. Balakrishnan M., e.a., Pramana, 1978, v.10, N3, p.329.
11. West D., Sherwood A.C., - UKNDC(79)P94, 1979, p.57.
12. Anderson H.L.-Preliminary Reports N3, Nucl.Sci.Series Nat. Res.Counsil, 1948.
13. Serdjukova I.A., e.a.,Izv.Akad.Nauk SSSR, ser.Fizika, 1957, 21 , 1018.
14. Gorshkov G.V., e.a.,Atomnaya energiya, 1962, t.13, v.8, p.65.
15. Gorshkov G.V., e.a.Atomnaya energiya, 1962, t.13, v.5, p.475.
16. Rutherford W.M., e.a., - Nucl.Appl., 1967, v.3, p.366.
17. Herold T.R.,-Nucl.Appl., 1968, v.3, p.19.
18. Anderson M.E., Neef R.A., Nucl.Appl.Technol., 1969, v.7, p.62.
19. Arhipov V.A., e.a.Atomnaya energiya, 1972, m.32, v.4, p.310.
20. Bair J.K., Butler H.M.,-Nucl.Techn., 1973, v.19, p.202.
21. Lees E.W., Lindley D.,-Ann. of Nucl.Energy, 1978, v.5, p.133.
22. Sampson T.E., - Nucl.Sci.Eng., 1974, v.54, p.470.
23. Williamson R.W., Katman T., Burton B.S.,-Phys.Rev., 1960, 117, p.1325.
24. Van der Zwan L., Geiger K.W., -Nucl.Phys., 1977, A284, p.189.
25. Northcliffe L.C., Schilling R.F., Nucl.Data Tables, 1970, 7,233.
26. Anderson H.H., Ziegler J.F., Stopping and ranges of ions in matter, v.4, Pergamon Press, 1977.

27. Nitzki V., Matzke H., Phys.Rev., 1973, B8, 1894.
28. Bragg W.H., Kleeman R., On the α-particles of radium and their loss of range in passing through various atoms and molecules Phil.Mod., 1905, 10, 318.
29. West D., Sherwood A.C., UKNDC (81) P100,1981, p.45.
30. Liskien H., Paulsen A.,- Atomkernenergie, 30,1(1971), p.59.
31. Capgras A., Examples of Theoretical and Experimental determinations of neutron yield from (α,n) reactions in the light elements. Paper to Meeting on "Neutron Source Properties", 1980, Debrecen, Hungury.
32. Lorenz A.,-INDC(NDS)-127/NE,IAEA,1981.

APPLICATION OF THEORETICAL MODELS TO THE EVALUATION AND PREDICTION OF ACTINIDE NEUTRON CROSS-SECTIONS

V.A. KONSHIN
Institute of Nuclear Energetics of Byelorussian,
Academy of Sciences,
Minsk, Union of Soviet Socialist Republics

Abstract

A further development of the optical-statistical approach to the evaluation and prediction of neutron cross-sections, in particular, generalization of the coupled-channel method and systematics of the nuclear level density are discussed. The level density model is described; the parameters permitting the actinide level density to be calculated have been obtained.

INTRODUCTION

The formalism for calculation of neutron cross-sections on the basis of the statistical model was developed rather long ago /1-3/. One can consider that there are no difficulties in principle in using the optical-statistical model in the calculation of neutron cross-sections for the intermediate-weight nuclei other than the correlation effects which can increase the average reaction cross-sections by higher values than those due to contribution from the direct reactions /4,5/.

A number of difficulties arises in applying the optical-statistical model to the calculation of neutron cross-sections in case of fissionable nuclei, the evaluation of neutron cross-sections for such nuclei being rather complicated.

In case of the fissionable nuclei there are practically no experimental data, for example, on the cross-sections for inelastic scattering by levels because the experiments are difficult to carry out, the available data being very scanty and rather unreliable. There are unexplained systematic errors which do not always manifest themselves to a sufficient extent. Even for ^{238}U where the competi-

tion of the fission reaction is not strong the experimental data on $\sigma_{nn'}$, for the first level differ by a factor of 1.5 and, therefore, one often cannot give credence to the errors stated by the experimentors.

The fissionable nuclei are also difficult to study theoretically. The case is that the fission theory has not yet reached a stage when the nuclear data could be quantitatively predicted. Thus, the theoretical predictions of the fission barriers are made to an accuracy of 1-2 MeV /4/, whereas for the purpose of evaluation the accuracy must be 100 keV. The fission is the main competitive process and, therefore, it should be taken into account in the theoretical model calculations. This effect is very considerable. Thus, for the cross-section of neutron inelastic scattering by the first level of ^{239}Pu at 50 keV the competition effect of fission amounts to about 80%. The correct allowance for fission probability is a very complex problem as it involves the calculation of σ_f.

In addition, the heavy fissionalbe nuclei have a high density of excited states which, as a result of it, are resolved to comparatively low energies. The low excitation energies of the first levels cause necessity for taking into account the competition of the radiative capture when calculating the inelastic scattering cross-section.

The program developed by us makes it possible to perform the self-consistent calculation of neutron cross-sections of all types and to take into account the competition of the fission process with other ones. The discrete and continuous spectra of transition states of the fissionalbe nucleus are considered in this case and in calculating the fluctuation factors of fission widths the present-day ideas of a two-humped structure of the fission barrier were used, which is of special importance for the subbarier fission calculation. Moreover, in case of the fissionalbe nuclei, it is necessary to take into account the ($n, \gamma f$) process when the fission of the excited compound nucleus after emission of a primary gamma-ray is possible. The allowance for this process is especially important when calculating the radiative capture cross-section as it leads to the stronger spin and energy dependences of radiative widths. The coupled-channel method and the statistical model were joined in a computer program, the neutron transmission coefficients from the nonspherical optical model being used in the statistical model.

The correctness of calculation of neutron transmission coefficients is extremely important when evaluating the cross-sections for inelastic scattering which in contrast to radiative capture depends rather strongly on these coefficients. The allowance for the collective effects in the nuclear level density seemed to be very significant.

2. CALCULATION OF NEUTRON CROSS-SECTIONS FOR FISSIONABLE NUCLEI

The statistical model can be used for the self-consistent calculation of neutron cross-sections of the fissionable nuclei within the incident neutron energy range from 1 keV to 5 MeV. The Hauser-Feshbach model assumes that the compound nucleus formation and disintegration processes are independent of each other and, hence, this model ignores the effects of increase in cross-section in the elastic channel. These effects can be taken into account by the Teppel method /5/.

We shall dwell at some length on the calculation of the cross-section for inelastic scattering by the fissionable nuclei.

In order to obtain the excitation cross-section of the target nucleus level with an energy $E_{q'}$, the expression for probability of the compound nucleus disintegration must be integrated over all directions θ of an outgoing neutron, summed over all projections m, m_j, m_i and all values of momenta l, j, J, l', j' and averaged over possible directions of the target nucleus spin. As a result, the expression for the excitation cross-section of the level $E_{q'}$ with allowance for the competitions of fission and radiative capture is written as

$$\sigma_{nn'}(E,E_{q'}) = \frac{\pi}{k^2}\cdot\frac{1}{2(2i+1)}\sum_{lj} T_{lj}(E)\sum_{J}(2J+1)\frac{\sum_{l'j'} T_{l'j'}\left(E-\frac{A+1}{A}E_{q'}\right)S_{\alpha\alpha'}}{T_{comp}+\sum_{l''j'q''} T_{l''j''}\left(E-\frac{A+1}{A}E_{q''}\right)} \quad (1)$$

Here i is the spin of the target ground state; l and j are the orbital and total momenta of the incident neutron, respectively; l' and j' are the same of the outgoing neutron; J is the spin of the compound nucleus. The summation in the denominator is performed over all neutron channels of the compound nucleus disintegration which obeys the energy, purity and total momentum conservation laws.

The factor $\frac{A+1}{A}$ in the transmission coefficients of the exit and elastic channels takes into account that the neutron energy goes over partially to the recoil nucleus energy.

The quantity T_{comp} in (1) takes into account the competition of the neutron disintegration channels allowed by the conservation laws and includes the transmission coefficients for radiative capture and fission:

$$T_{comp} = T_{\gamma J\pi}\left(\frac{A}{A+1}E + S_n\right) + T_{fJ\pi}\left(\frac{A}{A+1}E + S_n\right) \qquad (2)$$

Here $\left(\frac{A}{A+1}E + S_n\right)$ is the excitation energy of the compound nucleus, $T_{\gamma J\pi}$ and $T_{fJ\pi}$ are the "effective" transmission coefficients for radiative capture and fission, respectively.

The "effective" transmission coefficient for fission, $T_{fJ\pi}$, in the range of fissionable nucleus transition states can be calculated analogously to the neutron transmission coefficient:

$$T_{fJ\pi} = 2\pi\frac{\Gamma_{fJ\pi}}{D_J}. \qquad (3)$$

The fission width $\Gamma_{fJ\pi}$ can be determined using the Bohr-Wheeler expression /6/:

$$\Gamma_{fJ\pi} = \frac{D_J}{2\pi}\sum_k P(E_{fk}, \hbar\omega_k) \qquad (4)$$

where $P(E_{fk}, \hbar\omega_k)$ is the transmission coefficient of the k-th fission barrier with a height E_{fk} and a curvature parameter $\hbar\omega_k$ /7/:

$$P(E_{fk}, \hbar\omega_k) = \frac{1}{1 + \exp\left[-\frac{2\pi}{\hbar\omega_k}(E - E_{fk})\right]} \qquad (5)$$

Here E_{fk} is the energy of the known transition states.

The summation in (4) is made over transition states with a spin J and a parity π. An approximate transition state diagram for even-mass nuclei was suggested by Lynn /8/. While developing this diagram a saddle-shaped mass asymmetry was taken into account. This led to the low-lying $K^\pi = 0^-$ band for barrier B and to lowering the $K^\pi = 2^+$ band for barrier A.

The diagram is known only up to an energy of 1.8 eV above the fission threshold. In view of the fission thresholds for ^{239}Pu, ^{241}Pu and ^{235} being equal to -1.6 and -0.6 MeV, respectively, such an approach can be used near the threshold for ^{239}Pu and ^{241}Pu and in the range of allowed levels in the case of ^{235}U.

In the framework of the phenomenological approach to the fission process the question about the nuclear level density in the fission point remains unsettled. It follows from the conception of the two-humped fission barrier that the single-particle state density for actinides at the Fermi energy in case of the fission deformation is considerably higher than in case of the equilibrium deformation, i.e. the level density in the saddle point must be higher at excitation energies within the discrete spectrum of transition states. The independent particle model assumes that at excitation energies above the boundary of the discrete spectrum of transition states the level density in the fission point must be lower. However, the loss of symmetry effects of the saddle-shaped configuration can cause such an increase in contribution of the rotational states being enough to compensate for or even to exceed the loss.

There are no direct experimental data on the level density in the fission point other than the fission cross-sections. Information on the level density that can be obtained from σ_f depends strongly on assumptions on the fission barrier height; vice versa, the fission barrier heights obtained from σ_f depend on assumptions on the level density. Therefore, in order to calculate $T_{fJ\pi}$ at high energies where the transition state diagram is unknown, we use, as Lynn did /9/, the simple formula for the transition state density analogous to the formula derived from the constant temperature model:

$$\rho_f(E, J, \pi) = \frac{2J+1}{2}\exp\left[-\frac{(J+1/2)^2}{2\sigma^2}\right]C_f \exp\left(\frac{E}{\Theta_f}\right), \qquad (6)$$

where σ, C_f, Θ_f are the parameters of the continuous density of the fissionable nucleus transition states obtained from the experimental data on σ_f for the nucleus under consideration. In this case the concept "constant temperature" can refer only to a narrow energy range, each energy area having its own value of Θ_f.

Thus, the "effective" transmission coefficient $T_{fJ\pi}$ for fission with allowance for the discrete and continuous spectra of

fissionable nucleus transition states can be written in the form:

$$T_{fJ\pi} = \sum_{K} P(E_{fK}, \hbar\omega_K) + \int_{E_{fo}}^{\infty} \rho_f(E, J, \pi) P(E_{fo} + E, \hbar\omega), \qquad (7)$$

where $P(E_{fK}, \hbar\omega_K)$ and $P(E_{fo} + E, \hbar\omega)$ are determined from (5) whereas $\rho_f(E, J, \pi)$ is determined by expression (6).

The agreement of the calculated cross-section for fission with the experimental data serves as a criterion that the given method allows for the competition of fission in a correct way.

Thus, using the approximate transition state diagram up to an energy of about 1.8 MeV above the fission threshold, the approximate heights of fission barriers from experiments on the (d, pf) and (t, pf) reactions /10/ and the constant-temperature model for the level density at higher energies we have determined the level density parameters and refined the transition state diagram and the barrier heights basing on the experimental data for σ_f of the nuclei under consideration. The change in E_f by 0.2MeV and in $\hbar\omega$ by 10% did not turn out to affect seriously the quality of the σ_f fitting on condition that the corresponding compensating changes were made also for the other parameters.

For actinides one peak of the fission barrier is, as a rule, higher than the other one (^{237}U for which both the peaks are identical is an exception), hence the lesser value from $T_{fJ\pi}^{(A,B)}$ can be taken as the "effective" transmission coefficient for fission, which proves to be adequate in accuracy for calculating neutron cross-sections /9/. In cases when both $T_f^{(A)}$ and $T_f^{(B)}$ are much less than 1 (subbarrier fission) the formula of type (1) becomes invalid for calculating σ_f and, therefore, another method should be used to calculate σ_f /11/.

Indeed, after the first gamma-ray emission there is a possibility of deexcitating the nucleus through neutron emission and by fission. The neutron emission is possible when the excitation energy after emission of the first gamma-ray is higher than the neutron separation energy. Therefore, when calculating the transmission coefficient for radiative capture by use of the cascade theory of gamma-ray emission /12/ it is necessary to consider the competition of the ($n, \gamma n'$) and ($n, \gamma f$) reactions with radiative capture /16/.

The consideration of the ($n, \gamma n'$) process when calculating the transmission coefficient for radiative capture turned out to be appreciable only at neutron energies higher than the average energy of the first-cascade gamma-rays ($\mathcal{E}_\gamma \sim$ 1MeV). Thus, the calculation has shown that for ^{242}Pu the consideration of this process at a neutron energy of 0.5 MeV reduces $\overline{\Gamma_\gamma}$ only by 0.5%.

The consideration of the $(n, \gamma f)$ process is more significant for the fissionable nuclei when the disintegration of the excited compound nucleus is energetically possible after emitting the primary gamma-rays.

The weak energy dependence of radiative capture width for both types of spectral factor at incident neutron energies up to 1 MeV where there is an experimental information on cross-section for radiative capture does not allow one to choose one of the types. But the type of spectral factor affects considerably the calculated values of widths $\langle \Gamma_{\gamma f} \rangle$.

The following values were obtained experimentally for ^{239}Pu: $|\Gamma_{\gamma f}^{0^+} - \Gamma_{\gamma f}^{1^+}| < 4$ MeV /17/, $\Gamma_{\gamma f}^{1^+} = 4.1$ 0.9 meV /18/ and $\Gamma_{\gamma f}^{1^+} =$ $= 6.1$ 2.9 meV /19/. Results of calculations by use of the different models of level density and the different types of spectral factor a are given in Table 1. The calculation using the spectral factor with

Table 1.

Theoretical and experimental values of $\Gamma_{\gamma f}$ widths for ^{239}Pu

Level density model and type of spectral factor	$\langle \Gamma_{\gamma f} \rangle^{0^+} - \langle \Gamma_{\gamma f} \rangle^{1^+}$, mV	$\langle \Gamma_{\gamma f} \rangle^{1^+}$, mV
Fermi-gas model; Lorentz factor	5.94	5.46
Fermi-gas model; Weisskopf factor	10.59	11.55
Fermi-gas model with collective modes included; Lorentz factor	3.62	3.11
Fermi-gas model with collective modes included; Weisskopf factor	7.25	7.28
Superfluid model with collective modes included; Lorentz factor	5.80	5.24
Superfluid model; Weisskopf factor	11.42	13.37
Experiment /17/	$<$4 meV	-
/18/	-	4.1 ± 0.9
/19/	-	6.1 ± 2.9

the Lorentz dependence generalized for deformed nuclei yields the values of $\Gamma_{\gamma f}$ which agree with the experimental values within their errors.

Thus, the stronger dependence of the calculated widths $\langle\Gamma_{\gamma f}\rangle^{J\pi}$ on type of the spectral factor in comparison with $\langle\Gamma_\gamma\rangle$ makes it possible to conclude that within accuracy of the available experimental data on $\Gamma_{\gamma f}$ the Weisskopf representation of the spectral factor leads to the worse agreement with the experimental data on $\Gamma_{\gamma f}$ widths than the Lorentz dependence does, the latter ensures the satisfactory agreement with the experimental values of $\Gamma_{\gamma f}$. It should be noted that this conclusion depends on values of the parameters ($B_n, \Delta, \langle D\rangle$ and especially T_f) used in the calculations. Therefore, in calculating the cross-sections it is of great importance to use the parameters optimized over the whole set of experimental data. That is why below in calculating the transmission coefficients for radiative capture for the purpose of nuclear data evaluation the spectral factor in the Lorentz form was used.

The consideration of the ($n, \gamma f$) and ($n, \gamma n'$) processes leads, as could be expected, to a change in energy dependence of radiative widths $\langle\Gamma_\gamma\rangle$ (Fig.1). This change becomes rather drastic at energies above 1 MeV (at 1 MeV the consideration of these processes leads to decrease of $\langle\Gamma_\gamma\rangle$ by a factor of 1.5). Naturally, such a change of $\langle\Gamma_\gamma\rangle$ affects also the cross-section for radiative capture.

The analysis made by us has shown that in case of nuclei with a negative fission threshold the allowance for the competition of fission and inelastic scattering with the gamma-deexcitation only after emitting the primary gamma-rays holds true only at low energies of incident neutrons ($E_n \leq 0.5$ MeV). It is due to the fact that at higher energies of incident neutrons there is also definite probability of nuclear fission after emitting two successive gamma-rays. So, in calculating the radiative capture width the competition of fission and inelastic scattering with gamma-deexcitation was considered for one more cascade. It allowed the radiative capture widths for the ($n, \gamma f$) and ($n, \gamma n'$) processes to be calculated with considerable accuracy. The majority of the second cascade gamma-rays is emitted at a nucleus excitation energy below $B_n + 0.5$ MeV, as at higher excitation energies the fission and inelastic scattering processes dominate. As the average gamma-ray energy $E_\gamma \geq 1$ MeV, the nucleus excitation energy becomes lower than the fission threshold after two next cascades of deexcitation and the processes other than gamma-deexcitation are impossible. The comparison of the radiative capture widths obtained for the nuclei ^{238}U and ^{239}Pu with the results of calculations including the competition of fission and inelastic scattering only after the first cascade of gamma-deexcitation shows that at low energies of incident neutrons the widths practically agree (see Fig.2).

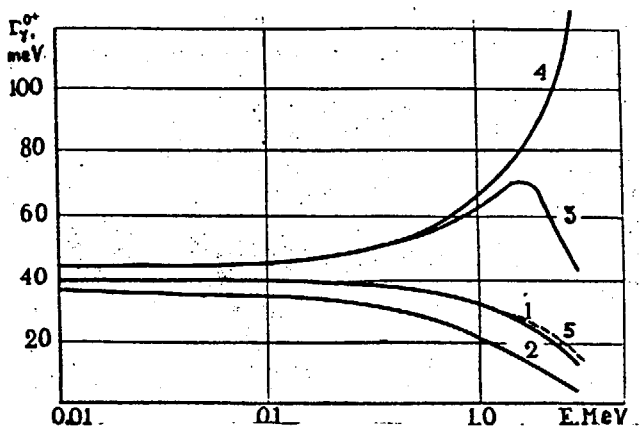

Fig.1. Calculated energy dependence of Γ_γ^{0+} for ^{239}Pu: 1 - with the ($n,\gamma f$) and ($n,\gamma n'$) processes included, Lorentz spectral factor; 2 - with the ($n,\gamma f$) and ($n,\gamma n'$) processes included, Weisskopf spectral factor; 3 - with the ($n,\gamma n'$) process alone included, Lorentz spectral factor; 4 - without including the ($n,\gamma f$) and ($n,\gamma n'$) processes, Lorentz spectral factor; 5 - the same conditions as for curve 1 and with the ($n,2\gamma f$) process additionally included.

At higher energies the behaviour of Γ_γ is different. For ^{238}U which has a positive fission threshold the allowance for the competition of the fission and inelastic scattering processes in the second cascade of gamma-deexcitation leads to a slight decrease in radiative capture width whereas in case of ^{239}Pu the reduction of Γ_γ is more essential (by about 5%).

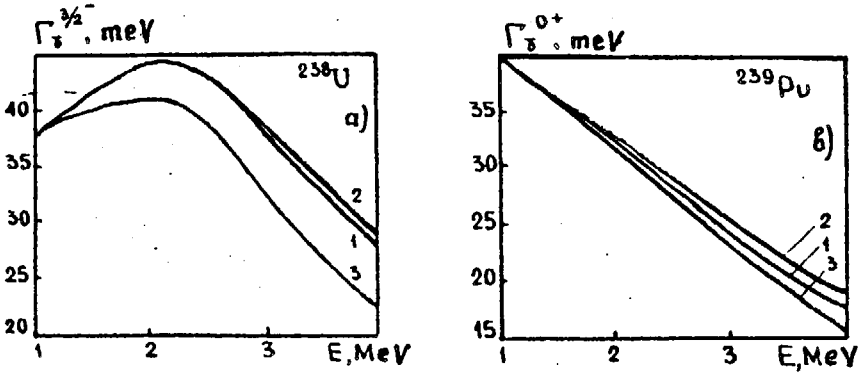

Fig.2. Comparison between various approaches to calculating the radiative capture widths: (a) $\Gamma_\gamma^{3/2^-}$ for the target nucleus ^{238}U; (b) $\Gamma_\gamma^{0^+}$ for the target nucleus ^{239}Pu; curve 1 - calculations with allowance for the competitions of fission and inelastic scattering after two cascades of gamma-rays; curve 2 - the same but only after the first cascade of gamma-rays; curve 3 - according to /20/.

The correct consideration of the competition of fission and inelastic scattering at nucleus excitation energies higher than B_n is also of importance. It can be seen in Fig.2 where the results of calculations made with and without allowance for the contribution from the second cascade gamma-rays emitted at nucleus excitation energies higher than B_n into Γ_γ are compared.

3. APPLICATION OF THE COUPLED-CHANNEL METHOD TO EVALUATION OF NEUTRON CROSS-SECTIONS FOR FISSIONABLE NUCLEI

The heavy fissionable nuclei are strongly deformed and so the neutron scattering cannot be adequately described by the convenient optical model which does not consider the direct connection between the orbital motion of an incident neutron and the nuclear rotation, which leads to a direct excitation of nuclear rotational levels in inelastic scattering.

For the heavy nuclei the coupling between the different channels is rather strong and the coupled-channel method is efficient.

The coupled-channel method /21/ considering this connection describes more correctly the neutron interaction with the deformed nuclei.

Born's distorted wave method /22/ is a success in cases when the nuclear deformation β is small ($\beta \leq 0.1$). At higher β the differential cross-sections of the elastically and inelastically scattered neutrons are described inadequately by the distorted wave method, as the low-lying collective states affect not only the inelastic scattering processes but also the elastic channel. Therefore, in this case it is more preferable to use the coupled channel method, i.e. to seek a precise solution of the quantum-mechanical problem on scattering by the deformed nonspherical potential with an intrinsic structure.

The spherical optical model does not take into account the intrinsic nuclear structure (i.e. the structure of a potential by which the scattering takes place). Therefore, the elastic scattering by the potential is a single direct process which can be calculated in this model. At the same time the experimental data on angular distribution of inelastically-scattered neutrons (their preferable emission along the direction of incident neutron motion is borne in mind) show that a substantial fraction of inelastic scattering results from the direct mechanism, pointing to a necessity of including an intrinsic structure in the optical model potential.

For the heavy well-deformed nuclei in the form of ellipsoid of revolution the lower levels are determined by the collective nuclear rotation and the intrinsic nuclear state can be connected with rotations and characterized by the $\mathcal{D}$-functions (by the top-functions). In this case the system of one-channel optical equations does not decompose into individual equations and it is necessary to solve the whole system, the connection between the equations being determined by deformation of the nucleus. At distances larger than nuclear radius this system decomposes into individual optical equations describing the inlet elastic channels and the outlet elastic and inelastic channels.

A change in the optical model leads to that in a form of the optical potential. This is due to the absorption cross-section being slightly overestimated in the spherical optical model as the direct inelastic scattering in this model is considered as taking place

through the compound nucleus. Therefore the imaginary part of the potential responsible for absorption in the coupled-channel model must be less than that in the spherical optical model.

The application of the coupled-channel method makes it necessary to develop complex computer programs and the application of these programs to the evaluation of neutron data asks for a knowledge of the optical potential parameters. Such programs have been developed abroad /21,23,24/ and in our country /25,26/. However, because of a long computer time required the nonspherical optical potential parameters were not determined automatically using the χ^2- criterion even for the program of /23/ which is most suitable for the purpose of the neutron data evaluation. The high-speed program involving the coupled-channel method and developed by us differs from the programs of /24-26/ in the following. Störmer's five-point method is used for the numerical integration of the system of coupled equations. It makes it possible to reduce considerably the computer time in comparison with the modified Numerov's method. Störmer's method allows one to obtain a solution at a point z if the solutions at n preceding equidistant points z-h, z-2h,...z-nh are known. The accuracy of approximation grows with n, the error being equal to $O(h^{n+1})$ for $n \geq 4$(our calculations were made at n=5).

The system of N coupled equations can be written in the form:

$$U''(z) = V(z)U(z), \tag{15}$$

where $U(z)$ is the N-dimensional column of solutions and $V(z)$ is the NxN matrix.

The partial solution $U(z)$ for n=5 is obtained in Störmer's method from the following relationship:

$$U(z) = 2U(z-h) - U(z-2h) + \frac{h^2}{240}[299\,V(z-h) - 176\,V(z-2h) + 194\,V(z-3h) - 96\,V(z-4h) + 19\,V(z-5h)], \tag{16}$$

where $V(z) = U''(z) = V(z)U(z)$

The Störmer's method offers the following advantages. To obtain $V(z_i)$ the method requires multiplying the matrix A into the vector U at every integration step. Thus, it is necessary to make N^2 multiplications at every step and it takes a major part of computer time. Nevertheless, this method is quicker than the Runge-Kutta method.

One would think it is necessary to make 5 multiplications in eq.(16) to obtain $V(z_i)$ and it looks as if the application of eq. (16) is slower by a factor of 5 than, for example, in case of the two-point method, where:

$$U(z) = 2U(z-h) - U(z-2h) + V(z-h) \tag{17}$$

However, it is not right as four multiplications have been made before we reach the point (z). In other words, with the vectors $V(z_i)$ obtained for r_i= r -2h, r-3h, r-4h and r-5h there is nothing to do in eq.(16) but to carry out 4N multiplications and 4N summutions in addition to N^2 multiplications. If N is sufficiently large, the use of eq.(16) does not strongly increase the computer time in comparison with the two-point scheme. And as eq.(16) allows the greater integration step h to be used, the calculations are really accelrated.

Some authors /27,28/ state that the modified Numerov's method is more suitable and quicker for the numerical integration of coupled equations, because it permits the greater step h to be used. We have investigated both the methods and found no advantages of the modified Numerov's method. This is the point that this method requires twice N^2 multiplications at every step in order to obtain the value of the function U(r) and even though makes it possible to increase the integration step (which has not found by us when comparing the Störmer's and Numerov's methods), this increase is not enough to compensate for time required for the additional N^2 multiplications.

In solving the Schrödinger equation its division into the angular and radial parts is usually made /25/. The solution of the system of equations for the radial part must obey the certain boundary conditions and the unknown matrix elements as well as dispersions containing all data on the neutron interaction with the nucleus are determined from the joining equation (i.e. from the condition of equality of two solutions in the nuclear interaction area and in the free motion area).

The method of joining the solutions is described, e.g., by Ignatyuk et al. /25/. To obtain the solution the following property is used: the linear combination $\sum_s a^{(s)} \tilde{R}^{(s)}$ of the partial solutions $\tilde{R}^{(s)}$ is also the solution of the system of coupled equations for the radial part. The coefficients $a^{(s)}$ are determined from the asymptotic boundary conditions.

Our program uses another method of joining which requires one matrix inversion and naturally reduces the computer time. One can write that the i-th partial solution of system (15) is the linear combination of the asymptotic solutions with coefficients α_k^i the incident wave being only in the inlet channel k. Then the joining equation can be written in the form:

$$U_j^i(R_{join}+x) = \sum_k \alpha_k^i \{F_j(R_{join}+x)\delta_{jk} + C_{jk}[G_j(R_{join}+x) + iF_j(R_{join}+x)]\},$$
$$U_j^i(R_{join}-x) = \sum_k \alpha_k^i \{F_j(R_{join}-x)\delta_{jk} + C_{jk}[G_j(R_{join}-x) + iF_j(R_{join}-x)]\} \quad (18)$$

These expressions represent the system of 2N equations with 2N unknowns α_k^i and C_{jk}. It is possible to avoid calculating the coefficients α_k^i in the following way. Multiplying the first equation by $G_j(R_{join}-x)$ and the second one by $G_j(R_{join}+x)$ and subtracting the second from the first one we shall obtain

$$U_j^i(R_1)G_j(R_2) - U_j^i(R_2)G_i(R_1) = \sum_k \alpha_k^i \{z\delta_{jk} + iC_{jk}z\}, \quad (19)$$

where $R_1 = R_{join}+x$, $R_2 = R_{join}-x$, $z = F_j(R_1)G_j(R_2) - F_j(R_2)G_i(R_1)$. Now multiplying the first and second equations (18) by $F_j(R_2)$ and $F_j(R_1)$, respectively, and subtracting the second from the first one we shall obtain:

$$U_j^i(R_1)F_j(R_2) - U_j^i(R_2)F_j(R_1) = \sum_k \alpha_k^i C_{jk} z \quad (20)$$

We shall determine the matrices A_j^i and B_j^i in the following way:

$$A_j^i = \frac{U_j^i(R_1)G_i(R_2) - U_j^i(R_2)G_j(R_1)}{z} \quad (21)$$

$$B_j^i = \frac{U_j^i(R_1)F_j(R_2) - U_j^i(R_2)F_j(R_1)}{z} \quad (22)$$

Now the joining equations (18) take the form

$$A_j^i = \sum_k \alpha_k^i (\delta_{jk} + iC_{jk}), \quad (23)$$
$$B_j^i = \sum_k \alpha_k^i C_{jk}, \quad (24)$$

and it is possible to get rid of the coefficients α_k^i and to obtain the final expression for the joining equation and determining the C-matrix elements:

$$B_j^i = -\sum_k (A_k^i + iB_k^i) C_{jk} \quad (25)$$

As seen from eq.(25), the C-matrix elements can be obtained either by division of two NxN matrices or by multiplication of the matrix B_j^i from the left side of eq.(25) by the matrix inverse to that in the right side. If this multiplication or division of the matrices is considered to be a solution of a set of linear equations whose right sides represent the B matrix column, we obtain the values for the fixed j. Moreover, if a single inlet state is considered, the coefficients C_{jk} are required only for the values of K corresponding to this state.

The above described method of the numerical integration of coupled equations for the radial wave functions and of the joining of the solutions with the asymptotic one at $z \to \infty$ requires choosing the certain values for the integration step h and the joining radius R_{join}. The choice of the h and R_{join} values seems to affect significantly both the accuracy and speed of computations: an increase in integration step (the joining radius) makes consistently shorter the time required for computations, but reduces the accuracy of the obtained results. So the choice of the h and R_{join} values was investigated in a number of works where both Numerov's /26/ and Störmer's /24/ methods were used for solving the Schrödinger equation and where $h \sim 0.1$-0.3 fm was recommended. From physical considerations we have decided to connect the value of integration step with length of potential diffuseness characterizing the rate of change in potential depth and accepted the integration step h equal to 1/3 a_R, where a_R is the diffuseness of the real part of potential. Such a choice of integration step permits three cal-

culations to be made along the diffuseness length, which is seemingly enough to describe the potential variations with considerable accuracy. The calculations show that decrease in the step does not lead to improving the accuracy of calculations, but takes longer computer time. The diffuseness for both the imaginary and the real parts of the potential in the coupled-channel calculations is about 0.5-0.8 fm, the value of integration step used by us agrees roughly with the values of h determined in /24,26/.

As a rule, the joining radius is chosen from the condition $R_{join} = R_R + (7\text{-}10)a_R$ /25/ or determined by the tentative numerical calculations /24/. But such a choice of joining radius results in its value being independent of incident neutron energy whereas it was empirically shown in /24/ that in order to reach the required accuracy of calculations in decreasing the neutron energy the joining radius must increase. Let us determine the relationships allowing one to choose the joining radius taking into account the foregoing.

We must choose such a value z for the joining radius that makes it possible to ingnore an influence of interaction potential U(r), that is

$$U(z) \ll E \tag{26}$$

The expression for the neutron wave number K is defined as $K \sim C\sqrt{E - U(z)}$. Then taking into account that condition (26) is satisfied at $z \geq R_{join}$ we obtain

$$\frac{\Delta K}{K} \sim \frac{-U(z)}{2E} \tag{27}$$

Upon integrating (27) between the limits from R_{joint} to ∞ we obtain the expression for the total relative error due to ignoring the remainder of the potential at $z > R_{join}$:

$$\int_{R_{joint}}^{\infty} \frac{dK}{K} = -\frac{1}{2E}\int_{R_{joint}}^{\infty} U(z)dz \tag{28}$$

From this expression it is possible to determine the value R_{join}. It is seen that the total relative error in determining K represents a half of ratio of integral of the interaction potential, ignored in the calculations, to energy. To determine R_{join} we shall write (for $z \geq R_{join}$):

$$U(z) \sim \frac{-V_R}{1+\exp\frac{z-R_R}{a_R}} \cong -V_R \exp\frac{R_R - z}{a_R}. \tag{29}$$

Let us substitute (29) in (28) and integrate

$$-\frac{1}{2E}\int_{R_{joint}}^{\infty} U(z)dz \cong \frac{V_R}{2E}\exp\frac{R_R}{a_R}\int_{R_{joint}}^{\infty}\exp\left(-\frac{z}{a_R}\right)dz = \frac{V_R}{2E}\exp\left(\frac{R_R}{a_R}\right)a_R\exp\left(-\frac{R_{joint}}{a_R}\right).$$

We shall suggest that the total relative error in determining R_{join} should not exceed 10^{-4}. Then

$$\frac{V_R}{2E}a_R \exp\frac{R_R}{a_R}\exp\left(-\frac{R_{joint}}{a_R}\right) = 10^{-4} \tag{30}$$

Upon taking logarithm of (30) we shall obtain the relationship for determining the joining radius:

$$\frac{R_R}{a_R} + \ln\frac{V_R}{E} + \ln a_R - \ln 2 + 4\ln 10 = \frac{R_{joint}}{a_R} \tag{31}$$

or

$$R_{joint} = R_R + a_R\left(\ln\frac{V_R}{E} + \ln a_R - \ln 2 + 4\ln 10\right).$$

Finally we have

$$R_{joint} \cong R_R + \left(\ln\frac{V_R}{E} + 8{,}5\right)a_R \tag{32}$$

It is seen from (32) that to reach the required accuracy the value of joining radius should grow with decreasing the energy. It must be remembered that when deriving (32) we took into account only the real part of the interaction potential V_R, and that allowance for its imaginary part slightly increases the value of R_{join}. So to calculate R_{join} we used the expression

$$R_{join} = R_R + \left(\ln\frac{V_R}{E} + 10\right)a_R \tag{33}$$

The values of R_{join} for incident neutron energies of 0.1, 1.0 and 15 MeV (at $V_R \sim 45$ MeV, $R_R \sim 7.5$ fm, $a_R \sim 0.6$ fm) are equal to 17.2, 15.8 and 14.2 fermi, respectively.

As in solving the system of coupled equations by Störmer's method the first derivative of the function being calculated is not used, we, as noted above, make the joinings at two points: R_{join}-x and R_{join}+x. The choice of interval 2x between the joining points also affects both the accuracy of solving the system of equations and the calculation rate: decrease in x leads to degeneracy of the system of equations (25) and reduces the accuracy of solution, increase in x takes up more computer time. The calculations have shown that the choice of interval between the joining points

equal to $x=2h=2/3\,a_R$ together with expression (33) for R_{join} allows the C-matrix elements to be calculated with an accuracy of about 10^{-4}.

The generalized optical model calculations require the multiple determination of the Klebsch-Gordan and Rack coefficients taking long computer time. So a special algorithm for calculating the vector addition coefficients was developed permitting one to speed up their calculations and to reach a required accuracy. The feature of this algorithm consists in the following. If we take the logarithms of the formulas for the Klebsch-Gordan and Rack coefficients, we shall neglect the products and divisions of factorials in these formulas and shall have only the sums and differences of their logarithms. As a computer operates on integral numbers with a higher speed and accuracy, we shall eliminate half-integral magnitudes using the doubled values of momenta and their projections. Accepting the values of $n!$ with a high accuracy (e.g. for n=0-200) as the initial data we determine the values of vector addition coefficient logarithms as the sum and difference of values of $\ln(n!)$, where n are the required values of momenta and their projections. As the addition and subtraction operations are carried out with a higher speed than multiplication and division, the rate of calculations grows. Moreover, $\ln(n!) \ll n!$ and, hence, it is not necessary to operate on large numbers and the accuracy becomes considerably better.

The contribution from the great angular momentum which could be ignored in the spherical optical model should be taken into account in the coupled-channel method. This can be explained in the following way /24/. If there is no coupling between the levels, a neutron which enters a nucleus with a great angular momentum (value of ℓ) should leave the nucleus with the same angular momentum. The scattering matrix elements are small in this case, as the centrifugal force decreases them either for the inlet channel and for the outlet one. In case of the coupled channels the neutron can escape with a lower value of ℓ leaving the reminder of angular momentum in the target nucleus. Hence, the effect of centrifugal force is weaker in this case and the contribution from the higher angular momenta cannot be ignored.

When there is no coupling between the channels, a single value of ℓ corresponds to one value of J^π. So it is possible to assume that $J_{max} = \ell_{max} + 1/2$. In case of the coupling with an excited level of the target nucleus there are the contributions from high orbital momenta ℓ in the coupled equations for small J, the contributions from small ℓ existing in the equations for large J. It follows that there cannot be any simple relationship between ℓ_{max} and J_{max}. As a rule, either ℓ_{max} or J_{max} is assigned in advance for calculations. If a maximum value of the system total momentum J_{max} is given, the contribution from all possible values of orbital angular momentum ℓ is taken into account in the coupled equations at any $J \leq J_{max}$. If a maximum value of the orbital angular momentum ℓ_{max} is given, the coupling of levels with $\ell > \ell_{max}$ is not considered in the coupled equations and, hence, the coupled equations are solved incorrectly even at small J. To obtain the same results, as in case of assigning J_{max}, it is necessary to increase the value of ℓ_{max} /24/. This, in turn, leads to necessity to solve the coupled equations for very large J which can be neglected and, consequently, requires a long computer time.

But to assign a value of J_{max} in advance is not quite satisfactory. It is more preferable to use procedures where the values of J_{max} are chosen automatically to satisfy a predetermined accuracy. We use such a procedure. We begin the calculations from $J_o = I + 1/2$, where I is the spin of the target nucleus, and solve the coupled equations for positive $J = J_o \pm n$ (where n=1,2,3...) until the contribution from the C-matrix coefficients at a given J in the value of cross-section for direct inelastic scattering becomes less than 10^{-3}.

In this case the contribution from all possible values of ℓ is taken into account at any J. Such a procedure allows one to avoid necessity of assigning in advance the value of J_{max} which depends on both the incident neutron energy and the number of target levels considered in the coupling scheme.

When carrying out the numerical calculations we used the results of investigations /24,26/ on the influence of different physical approximations upon values of cross-sections being calculated.

In case of expanding the potential in the Legendre polynomials the difference in the C-matrix coefficients is about 10^{-2} for λ=2(P2) and λ=2 and 4(P4), being less than 10^{-3} between λ=2 and 4(P4) and λ=2.4 and 6(P6). The difference in cross-sections and strength functions is a few percent between P2 and P4, being less than 1% between P4 and P6. Expansion P2, consequently, should not be used in calculations as it leads to considerable errors, expansion P4 being satisfactory.

The use of deformation of the spin-orbital term in the potential causes a change of the order of 10^{-3} in the C-matrix coefficients and a change in cross-sections and strength functions by less than 1% in comparison with the spherical spin-orbit potential. The difference in values of polarization obtained in case of using the deformed and the spherical spin-orbit term is equal to 2-7%. In the calculations we used the spherical spin-orbit term, as the influence of this approximation on results of the neutron cross-section calculation is negligible. The level coupling is an important factor in the coupled-channel method. At incident neutron energies below 1 MeV the use of the three-level coupling (the first and second excited levels with the ground one) leads to errors $\lesssim$ 2% in σ_n and σ_γ, $\lesssim$ 5% in S_0, and about 20% in $\sigma_{nn'}$, the four-level coupling causing errors $\lesssim$ 0.5% in σ_n and σ_γ, and $\lesssim$ 1% in S_0. With increasing the neutron energy from a few keV to a few MeV the sensitivity of the calculated values to the chosen coupling scheme decreases, but the coupling scheme must be invariable within the whole energy range. The use of the two-level coupling is enough to calculate the reaction cross-section, the integral cross-section for elastic scattering, and the strength function. In this case the error in the calculations is less than 10% for the cross-sections and the strength function S_0, being less than 20% for the p-wave strength function S_1.

The three-level coupling should be used in calculating the differential cross-section for elastic scattering and the p-wave strength function S_1. The errors in the integral cross-sections and in the strength functions are less than 3% in using this coupling.

When calculating the cross-section for inelastic scattering by the n-th level it is necessary to consider the coupling with the (n + 1)-th level. The use of four- and five-level couplings keeps the C-matrix coefficients invariable with an accuracy of 10^{-3}. Therefore, we have carried out the main calculations taking into account the three - and four - level couplings for even-even target nuclei and the five-level coupling for odd nuclei. The errors due to the 8% uncertainty in the deformation parameter β_2 are equal to $2 \cdot 10^{-2}$ in the C-matrix coefficients (absolute error), less than 2% in σ_γ and σ_n, less than 5% in the strength functions and about 20-30% in $\sigma_{nn'}$ (Eq.). The 8% uncertainty in the deformation parameter β_2 leads to errors in σ_n, σ_γ, S_0 and $\sigma_{nn'}$ which have the same order of magnitude as the uncertainty in cross-sections due to using the three-level coupling. The neglect of the deformation parameter β_4 can lead to considerable errors. The error in β_4 equal to $\pm$ 0.05 causes errors of $5 \cdot 10^{-2}$ in the C-matrix coefficients and errors equal to a few percent in the cross-sections.

The C-matrix coefficients and the neutron cross-sections $\sigma_t, \sigma_n, \sigma_{nn'}^{2+}, \sigma_{nn'}^{4+}$ calculated with this program were compared for ^{238}U with the JUPITER computations suggested by Kikuchi /24/ as a test. For comparison we used the same potential as Kikuchi. The comparison has showed that the C-matrix coefficients differ by less than 10^{-4}, the neutron cross-sections differing by less than 0.1%.

Such an agreement with the results of /24/ is achieved taking into account that Kikuchi used the earlier value for the constant of transformation of energy into wave number: $K = 0.2178 \frac{M}{M+1} \sqrt{E_{lab}}$

where E_{lab} is in MeV and K in Am^{-1}. A refined constant equal to 0.219677 is used in our calculations.

The reduction of the numerical calculation time made it possible to join the coupled-channel method with the optimization problem of searching the potential parameters by use of χ^2-criterion. The calculation of the neutron cross-sections and angular distributions for ^{238}U with the BESM-6 computer takes 3 min at 0.1 MeV and 20 min at 10 MeV. The optimization of the potential parameters was carried out using the searching program which uses the conjugate-gradient method, the parameters being fitted by the experimental data simultaneously over the whole energy area ranging from 1 keV to 15 MeV rather than in individual points. The automatic search

of the nonspherical potential parameters was made for eight parameters: $V_R, W_D, r_R, r_D, a_R, a_D, \beta_2$ and β_4 /29/.

To determine the potential parameters it is possible to use in a direct way the experimental data only on the neutron strength functions S_0, S_1, the total cross-section for interaction σ_t and the cross-section for potential scattering $\sigma_p = 4\pi R'^2$. The experimental data on angular distributions of elastically and inelastically-scattered neutrons at energies below 3 MeV cannot be used for obtaining the optimal potential parameters, as these data contain the isotropic part due to the compound contribution which is appreciable at large angles. At higher energies it is possible to use only the experimental data in which the contributions from level groups are precisely divided. In other cases only the comparison between the theoretical data on the angular distributions of elastically-scattered neutrons and the experimental one has to be made.

The procedure of searching a potential common for the actinide group consisted in the following. At the first stage an optimal set of potential parameters was determined for the nucleus ^{238}U the experimental information for which is most extensive. Moreover, the zero spin of the ^{238}U ground state makes the search less time-consuming. The estimated values for S_0, S_1 and σ_p within the energy range of a few keV /32/ and for σ_t at energies ranging from 1 keV to 15 MeV were used as experimental data which were a basis for obtaining the potential parameters. The most reliable experimental data on angular distributions of elastically- and inelastically-scattered neutrons at 2.5 and 3.4 MeV /30,33/ where the contribution from the lower levels was distinguished and where it was possible to neglect the contribution from the compound mechanism were also used in addition to the above data.

In the calculations the coupling of the first three 0^+, 2^+ and 4^+ levels of the ^{238}U ground rotational band was taken into account. The allowance for the additional level coupling changes the calculated values of cross-sections by lower values than the errors of the available experimental data, but requires much longer computer time.

In searching the parameters it was assumed that the optical potential has the following form:

$$U(r) = -V_R f(r, a_R, R_R) + 4iW_D a_D \frac{d}{dr} f(r, a_D, R_D) + \left(\frac{\hbar}{m_\pi c}\right)^2 V_{so} \vec{l}\vec{\sigma} \frac{1}{r}\frac{d}{dr} f(r, a_R, R_R), \quad (34)$$

where

$$f(r, a, R) = \left[1 + \exp\left(\frac{r-R}{a}\right)\right]^{-1}. \quad (35)$$

For the deformed terms V_R and W_D the radius was taken as:

$$R_{R,D} = r_{R,D} A^{1/3} [1 + \beta_2 Y_{20}(\theta) + \beta_4 Y_{40}(\theta)]. \quad (36)$$

The spin-orbit potential V_{so} was not deformed, its radius being

$$R_R = r_R A^{1/3}$$

The use of the spin-orbit term deformation in the potential leads to changes of the order of 10^{-3} in the C-matrix coefficients and to changes less than 1% in the cross-sections and strength functions in comparison with the spherical spin-orbit potential.

It was assumed when fitting that the parameters V_R, W_D, a_R and a_D depend linearly on the energy, but there happend to be no necessity to introduce the energy dependence of the diffuseness of the potential real part to describe the experimental data. However, the introduction of the energy dependence for the diffuseness of the potential imaginary part a_D markedly improves the description.

As a result of the careful optimization over the above experimental data, the following values of the nonspherical optical potential parameters for ^{238}U have been obtained:

$$V_R = (45.87 - 0.3\,E)\ \text{MeV}, \quad r_R = 1.256\ \text{fm}, \quad r_D = 1.260\ \text{fm},$$
$$W_D = \begin{cases} (2.95 \pm 0.4E)\ \text{MeV} & (E \le 10\text{MeV}), \\ 6.95\text{MeV} & (E > 10\ \text{MeV}) \end{cases} \quad a_R = 0.626\ \text{fm}, \quad a_D = (0.555 + 0.0045E)\ \text{fm}$$
$$V_{so} = 7.5\ \text{MeV}, \quad \beta_2 = 0.216, \quad \beta_4 = 0.080 \quad (37)$$

The calculations by use of these parameters make it possible to describe the available experimental data for ^{238}U at energies ranging from 1 to 15 MeV practically within the experimental errors. The comparison between the calculated and experimental data on $\sigma_t(^{238}U)$ in the range of 0.1-15 MeV is given in Fig.3.

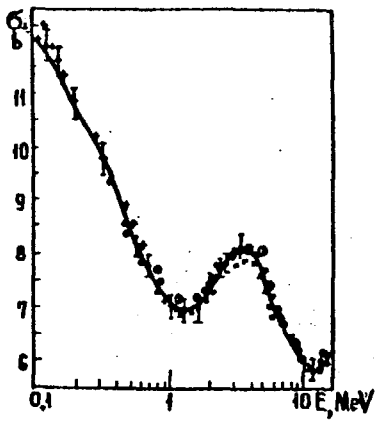

Fig.3. Comparison between experimental and calculated data on σ_t for ^{238}U at energies of 0.1-15 MeV.

Figs 4-6 show the differential cross-sections for elastic and inelastic scattering of neutrons at 3.4, 8.56 and 15.2 MeV. The calculated values of the strength functions S_0, S_1 and the potential scattering radius R' are compared in Table 2 with their values estimated on the experimental data.

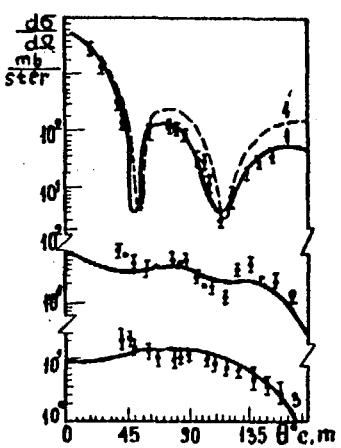

Fig.4. Derivative cross-sections for 3.4 - MeV neutron scattering by ^{238}U nuclear levels: 1 - ground 0^+ state; 1 - the first excited level (2^+, 44 keV); 3 - the second excited level (4^+, 148 keV); 4 - elastic scattering by spherical potential with parameters taken from /35/.

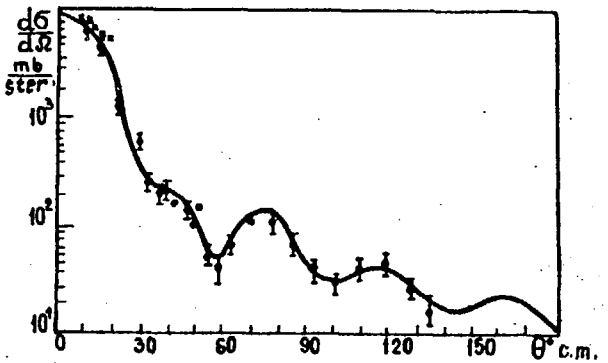

Fig.5. Derivative cross-sections for 8.56 - MeV neutron scattering by the nucleus ^{238}U (sum of the 0^+, 2^+ and 4^+ levels).

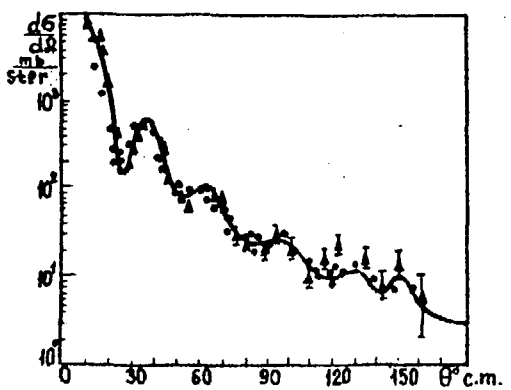

Fig.6. Derivative cross-sections for 15.2 - MeV neutron scattering by the nucleus ^{238}U (sum of the 0^+, 2^+ and 4^+ levels).

Calculated and evaluated values S_0, S_1, R' — Table 2.

Nucleus	Quantity	$S_0 \cdot 10^4$, $eV^{-1/2}$		$S_1 \cdot 10^4$, $eV^{-1/2}$		R', fm	
		calculation	evaluation	calculation	evaluation	calculation	evaluation
^{238}U		1.16	1.168±0.5	1.95	1.93±0.50	9.48	9.44±0.25
^{235}U		1.05	1.07±0.07	2.40	2.0±0.5	9.14	9.15±0.25
^{239}Pu		1.15	1.10±0.17	2.2	2.3±0.4	9.05	9.10±0.25
^{240}Pu		0.96	1.10±0.16	2.0	2.8±0.8	9.0	8.56±0.60

The value of the deformation parameter β_2 for ^{238}U obtained by Lagrange /23/ is 0.198, differing by about 8% from the value of β_2 obtained in this work. This difference results from somewhat different experimental values of S_0, S_1 and σ_p used to determine the potential parameters in both the works and characterizes essentially the error in determining the parameter β_2 due to uncertainties in the starting experimental data. The error in determining the real and imaginary parts of the potential does not exceed 0.2 MeV.

At the second stage of obtaining the common potential for heavy nuclei an attempt was made to describe the available experimental data for the nuclei ^{235}U, ^{239}Pu and ^{240}Pu with the geometric parameters obtained for ^{238}U. The following data were used: our estimated values of σ_t (at energies to 15 MeV), S_0, S_1, R' and the experimental data on angular distributions in case of ^{239}Pu and ^{235}U, only the estimated values of S_0, S_1, R' and σ_t (at energies to 3.5 MeV) in case of ^{240}Pu. The calculations were made under the assumption of the following level coupling scheme:

^{235}U $\frac{7^-}{2}$, $\frac{9^-}{2}$, $\frac{11^-}{2}$, $\frac{13^-}{2}$, $\frac{15^-}{2}$;

^{239}Pu $\frac{1^+}{2}$, $\frac{3^+}{2}$, $\frac{5^+}{2}$, $\frac{7^+}{2}$, $\frac{9^+}{2}$;

^{240}Pu 0^+, 2^+, 4^+.

To describe these experimental data it turned out to be quite enough to include in the potential the isotopic dependence obtained in case of ^{238}U for depths of the potential real and imaginargy parts and to fit the deformation parameters β_2 and β_4. It happened to be possible to write the depths of the potential real and imaginary parts taking into account the isotopic dependence obtained in the couse of preparing in the following way:

$$V_R = 49.72 \mp 17\,\frac{N-Z}{A} - 0.3\,E; \qquad W_D = 5.22 - 10\,\frac{N-Z}{A} + 0.4\,E \quad (38)$$

The deformation parameters for the potential with the above values of V_R and W_R are

$\beta_2 = 0.201$, $\beta_2 = 0.217$, $\beta_2 = 0.191$ and 0.195
$\beta_4 = 0.072$, 0.082, 0.094 and 0.078

for the nuclei ^{235}U, ^{239}Pu, ^{240}Pu and ^{232}Th, respectively. The obtained values of the deformation parameters agree well with the values theoretically predicted /34/ from the microscopic model by use of the Yukawa single-particle potential and the modified liquid-drop model ($\beta_2 = 0.216$, $\beta_4 = 0.084$).

The set of the above parameters permits the available experimental information for the above nuclei to be described practically within the experimental errors. The example of the experimental data description for ^{239}Pu is given in Figs 7 and 8. In case of ^{240}Pu there are no experimental data on angular distributions of the elastically-scattered neutrons; the angular distributions of the 5 MeV neutrons scattered by the nucleus ^{240}Pu as theoretically predicted by use of the coupled-channel method are presented in Fig.9.

Thus, the neutron data for the actinides for which there is no experimental information can be obtained by the coupled-channel method with the parameters V_R and W_D in the form (38) and with the geometric parameters in the form (37). To do this, it is necessary only to fit the values of the deformation parameters β_2 and β_4 for every nucleus basing on the experimentally estimated values of S_0, S_1 and R', which does not need long computer time. If there are no experimental data on S_0, S_1 and R', the parameters β_2 and β_4 could be taken from the microscopic calculations /34/.

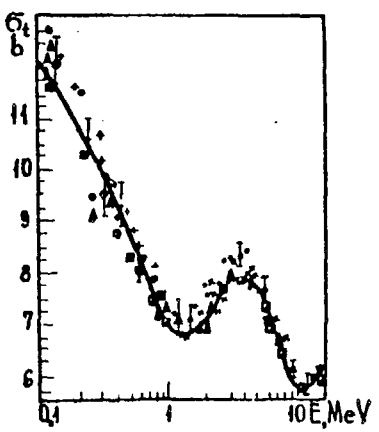

Fig.7. Comparison between experimental and calculated data on σ_t for ^{239}Pu at energies of 0.1-15 MeV.

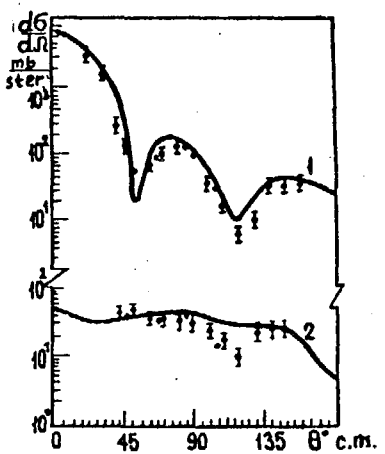

Fig.8. Derivative cross-sections for 3.4 - MeV neutron scattering by the nucleus ^{239}Pu: 1 - sum of the $1/2^+$ and 8 keV $3/2^+$ levels; 2 - sum of the 57 keV $5/2^+$ and 76 keV $7/2^+$ levels.

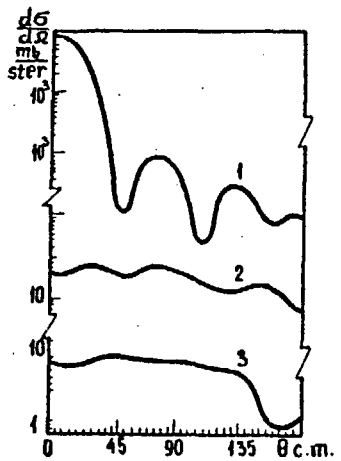

Fig.9. Derivative cross-sections for 5-MeV neutron scattering by the nucleus ^{240}Pu: 1 - ground 0^+ state; 2 - 43 keV 2^+; 3 - 142 keV 4^+ level.

The potential obtained by us differes consistently from other ones by the inclusion of the energy dependence of the geometric parameter a_D, which permits the competition between the surface and volume absorption to be taken into account in an "efficient" way (it is of special importance at energies above 10 MeV).

The use of the volume absorption at high energies would lead to necessity of fitting, at a minimum, three more potential parameters (depth, radius and diffuseness of the imaginary part describing the volume absorption), whereas the use of the surface absorption diffuseness increasing with energy, $a_D = a_0 + a_1 E$ makes it possible to take into account the volume absorption and to describe the experimental data at high energies by one parameter.

The coupled-channel method as considered here makes it possible in case of fissionable nuclei to describe the experimental data on angular distributions of the elastically-scattered neutrons, to calculate the cross-sections for the direct excitation of levels and to picture the shape of the inelastically-scattered neutron angular distribution on the 4 level within the experimental errors. The detailed structure of the inelastically-scattered neutron angular distribution on the 2 level is reproduced somewhat worse, the structure obtained in the calculations being less noticeable than that from the experiment. The same difficulties arise when describing the behaviour of the angular distribution for the $5/2^+$ and $7/2^+$ levels of ^{239}Pu. It should be noted, however, that the measurement reliability for the first excited level is low (it must be taken into account that the energy of the recoil nucleus is comparable with the first level energy).

For the heavy deformed nuclei the most correct approach to the calculation and evaluation of the neutron cross-sections is the generalized optical model. But this method is too complex and involves considerable expenditures of computer time, so the spherical optical model is still widely used to calculate and to estimate the neutron cross-sections of nuclei including the deformed ones. As the model contains a good many parameters, to attain a good agreement with experiment within some limited energy ranges is comparatively simple. However, the potential parameters obtained in such a way turns out to be different for the neighbouring nuclei. Moreover, these parameters presented by different authors are rather unlike.

One of the most important advantages of using the coupled-channel method for the purpose of estimation is a possibility of obtaining and using the common, for a group of nuclei, parameters of the optical potential, which appears to be impossible for the spherical optical model.

The spherical optical model calculations cannot reproduce the general tendency in the strength function variation for the heavy nuclei. However the calculations by using the generalized optical model with a common set of potential parameters reproduce well this tendency in the change of S_0 and S_1.

The comparison between the cross-sections for the total interaction σ_t in the case of ^{239}Pu which we have calculated by use of the spherical and generalized optical models show that the calculated cross-sections are not different at low energies. While the use of the deformed potential allows one to describe σ_t for ^{239}Pu with an accuracy better than 2% over the whole energy range, in using the spherical potential the difference between the calculated and experimental values of σ_t amounts to about 8% in some energy ranges.

The comparison of the elastic-scattering cross-sections calculated by using the spherical and deformed potentials with the experimental data shows that the spherical optical model describes worse the cross-section for elastic scattering especially at large angles.

The cross-section for the compound nucleus formation σ_c is most sensitive to the choice of the model (spherical or nonspherical). In the spherical optical model calculations $\sigma_c^{sp} = \sigma_t - \sigma_n^{dir}$, whereas in the coupled-channel method $\sigma_c^{nonsp} = \sigma_t - \sigma_n^{dir} - \sigma_{nn'}^{dir}$. As $\sigma_{nn'}^{dir}$ depends strongly on energy, the calculation of σ_c by using the spherical optical model through fitting the model parameters to σ_t proves to be rather doubtful. It can be seen from Fig.10 where σ_c for ^{238}U calculated by the coupled-channel method with the potential parameters obtained by us and by use of the spherical optical model with the parameters from /35/ are compared. The difference between σ_c^{sp} and σ_c^{nonsp} is rather significant and depends upon energy, which does not permit one to renormalize the results of the calculations with the spherical potential to the

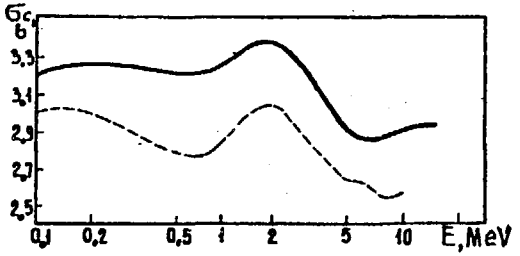

Fig.10. Comparison between cross-sections for compound nucleus formation σ_c (^{238}U) calculated by use of the spherical optical model (solid line) and by the coupled-channel method (dashed line).

results of the calculations obtained by using the generalized optical model. The difference between the neutron transmission coefficients calculated on the basis of the spherical and nonspherical models turns out to be of the same order of magnitude as the difference between the values of σ_c.

The influence of the deformation effects on the calculated cross-sections cannot be substituted by the equivalent set of the spherical optical potential parameters. As observed in /23/, the effect of the parameters of both the quadrupole, β_2, and hexadecapole, β_4, deformations is significant. This effect is illustrated in Fig.11 where the comparison is given for the values of σ_t in case of ^{239}Pu calculated with allowance for the parameter β_2 alone and the parameters β_2 and β_4. It is seen from Fig.11 that the difference between the values of σ_t amounts to $\pm$10%; and the conclusion can be drawn that for the accurate evaluation of the actinide cross-sections the deformation parameters β_2 and β_4 should be taken into account.

It is clear from the above-cited results that the generalized optical model should be used as a way to evaluate reliably the neutron cross-sections of the heavy deformed nuclei. The use of the spherical optical model is permissible only in the cases when the required accuracy in the calculations of cross-sections is low (less than 20-30%).

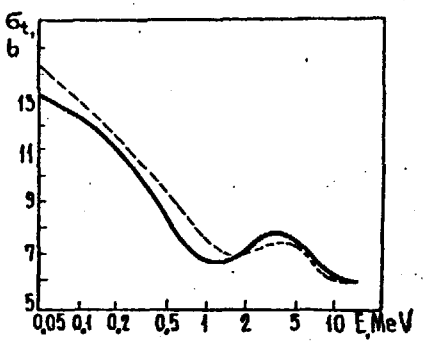

Fig.11. Comparison between $\sigma_t(^{239}Pu)$ calculated with allowance for the quadrupole deformation β_2 alone (dashed line) and for both the quadrupole and hexadecapole β_4 deformations (solid line).

The coupled-channel method described above is developed for the nuclei with rotational or vibrational bands of levels. There is still no mathematical program which would allow the coupling of these bands to be taken into account.

A theory of nonaxial even-even deformed nucleus was developed by Davydov and Chaban in /36/. In the framework of this approach the Hamiltonian of intrinsic motion takes into account both rotation and vibration of the nucleus. This theoretical approach makes it possible to describe the lower band levels with a high accuracy. This theory, in principle, can be extended to dynamics of neutron interaction with a nucleus, i.e. can be used to calculate the neutron scattering by nuclei. The task consolidates essentially the solving of two problems (1) determination of the intrinsic Hamiltonian parameters (deformation parameter, softness parameter and parameter of nuclear nonaxiality, then the three parameters are fixed), (2) calculation of the neutron scattering process with determination of the corresponding parameters of nuclear potential.

This program is being developed in our laboratory. The interaction cross-sections and other characteristics of the excited nucleus has happened to depend strongly on degree of its twisting. The elements of channel coupling have been calculated for this model. The allowance for nuclear vibrations has been shown to lead to increase in these coefficients, i.e. to increase in the calculated contributions from direct reactions.

4. INFLUENCE OF VARIOUS NUCLEAR LEVEL DENSITY CONCEPTS ON THE CALCULATION OF ACTINIDE NEUTRON CROSS-SECTIONS

The level density from the Fermi-gas model is widely used at present in the calculations based on the statistical theory. The model relationships are founded on the idea of the total agitation of collective degrees of freedom in the excited nucleus, and so they do not take into account the collective effects. A semimicroscopic method of level density calculation developed recently by Soloviev et al. /37-39/ makes it possible to take into account the contribution from vibrational and rotational motions. When calculating the level density, the methods of statistical averaging /40-42/ are also widely used, although a number of problems concerning difference between the collective motions of the nuclei at different excitation energies, agitation of collective modes with single-particle ones, etc. remains unsolved in the framework of the adiabatic assessment of collective effects.

These problems can be solved on the basis of the microscopic methods for direct modelling of the structure of highly-excited nuclear states /43/. But these methods of calculating the level density prove to be rather time-consuming especially at high energies, limiting the possibility of their application to nuclear data evaluation.

That is why to learn the influence of the collective effects in the level density upon the calculation of average neutron cross-sections of heavy nuclei we have employed the statistical method of describing the averaged characteristics of the excited nuclei as developed by Ignatyuk et al. /40, 41, 44/. This method takes into account the existance of shell heterogeneities in the single-particle level spectrum, the correlation effects of the superconducting type and the coherent effects of collective nature. We have prepared a special computer program allowing one to calculate the level density and to extract the parameter a for the following models: the conventional Fermi-gas model, the Fermi-gas model with back shift in pairing energy, the Fermi-gas model with an energy dependence $a(E)$ for taking into account the shell effects /45/, the

Fermi-gas model with collective modes (both rotational and vibrational) of motion included, the superfluid nucleus model which makes it possible to include the residual interactions of correlation type and the simple version of which has been suggested in /41/, the same model but with collective modes included.

The allowance for shell effects in the Fermi-gas model is made by including both the dependence of the parameter a upon excitation energy and the shell correction δW. The energy dependence of the parameter a is most essential for the nuclei with the nearly completed shell. For the nuclei investigated in our work the values of shell corrections are comparatively small and this effect can be neglected.

When including the collective effects the equation for level density takes the form

$$\rho(U,T) = K_{rot}\, K_{vib}\, \rho_{p\text{-}s}(U,T) \qquad (39)$$

The coefficients of level density increase K_{rot} and K_{vib} stipulated by the rotational and vibrational modes, respectively, and the factor σ^2 in accordance with the adiabatic assessment are determined by the expressions /44,46/:

$$K_{rot} = F_\perp t \qquad (40)$$

$$K_{vib} = \exp(0{,}25\, a^{2/3} t^{4/3}) \qquad (41)$$

$$\sigma^2 = F_\perp^{2/3} F_\parallel^{1/3} t, \qquad (42)$$

where $F_\perp$ and $F_\parallel$ are the perpendicular and parallel moments of inertia, respectively, and t is the excited nucleus temperature.

The question about validity of the adiabatic assessment of K_{rot} and K_{vib} at excitation energies above 10 MeV remains undoubtedly unsettled in the framework of the above approach.

The relationships of level density from the superfluid nucleus model were taken from /44/. Unlike /44/ we have used K_{vib} in the form (41) and have not considered the energy dependence of the parameter a which can be neglected at small δW. The formulas of the superfluid model are valid not only for the even-even nuclei, but also, as shown in /44/, for the odd and odd-odd nuclei if we define the excitation energy as:

$$U = U_{\text{even-even}} + \begin{cases} \Delta \text{ for odd nuclei} \\ 2\Delta \text{ for odd-odd nuclei.} \end{cases}$$

The considered models of level density lead to different dependences of level density upon energy, which affects the values of cross-sections calculated by using the statistical model.

The allowance for collective effects drastically decreases the value of a and when calculating by means of the Fermi-gas and the superfluid nucleus models the values of a become comparable to each other and to the quasiclassical assessment ($\bar{a}$ =0.075A and for ^{243}Pu: $\bar{a}$ =18.22MeV^{-1}).

The above models of level density do not allow the growing sum of levels in the discrete spectral range to be described adequately. The requirement to describe the discrete spectrum of levels would evidently be too rigid for any model of level density the main parameter of which is determined from the density of neutron resonances. So the use of the constant temperature model at low energies whose parameters are determined from the condition of describing the discrete spectrum and which ensures the joining with the model accepted at energies close to the neutron binding energy looks natural.

The constant temperature model is usually subjected to criticism from the angle of its physical substantiations. Its success becomes clear from the calculations basing on the superfluid nucleus model which gives a weaker drop of $\rho(U)$ to the zero excitation energy than the Fermi-gas model. At low energies $\rho(U)$ in accordance with the superfluid nucleus model gives practically a straight line in the semilogarithmic scale.

The joining of the level density models (the constant temperature model and the superfluid nucleus model) was determined from the conditions of description of growing sum of the discrete spectrum levels and of equality of level densities calculated with both the models and their logarithmic derivatives at the joining point.

In the framework of the constant temperature model the parameters of spin dependence of $\sigma_\perp^2$ for 41 nuclei with sufficiently studied discrete spectra have been determined by means of the maximum likelihood method. It proved that $\sigma_\perp^2$ for even-even and odd

nuclei do not differ and on an average can be described by a linear dependence on mass number A

$$\sigma_I^2 = 0.15624A - 26.76 \qquad (43)$$

The use of these values of σ_I^2 makes it possible to describe adequately in terms of the constant temperature law the growing sums of levels $N(U,J)$ for the nuclei ^{234}U, ^{235}U, ^{239}Pu, ^{240}Pu, ^{245}Cm, ^{246}Cm for which a relatively great number of levels with a given J are identified. This shows a possibility of substituting if necessary the discrete spectrum by the continuous one employing the constant temperature model and the law:

$$f(U,J) = \frac{(2J+1)\exp\left[-\frac{J(J+1)}{2\sigma_I^2}\right]}{2\sigma_I^2} . \qquad (44)$$

with the parameter σ_I^2 given by (43)

The equation (43) should be used up to an energy where the discrete spectrum can be considered to be identified quite reliably (we shall denote this boundary as E_{boun}). From E_{bound} to E_x (the point of joining the superfluid nucleus model and the constant temperature model) σ_I^2 would be determined by linear interpolation between σ_I^2 given by (43) and $\sigma_I^2(E_x)$ calculated by the superfluid nucleus model. At higher energies the calculation by the superfluid nucleus model is to be used.

For nuclei whose discrete spectra are identified poorly it is possible to use dependence (43) and the following values:

E_{bound} = 1.2 MeV for even-even nuclei,

E_{bound} = 0.6 MeV for odd nuclei,

E_{bound} = 0.3 MeV for odd-odd nuclei.

The results of determination of the parameter T in the constant temperature model show that the temperature T for even-even nuclei has very small fluctuations about the mean value $\overline{T}$=0.385 MeV. For odd nuclei the fluctuations of T are markedly higher and moreover the value of T on an average is somewhat lower than for even-even nuclei, which is a consequence of missing the levels in the spectra of odd nuclei. For odd nuclei having the most studied discrete spectra (for example ^{235}U) the temperature T is close to the mean value for the even-even nuclei.

The values of the parameter E_o in the constant temperature model for even-even nuclei are grouped very compactly in the vicinity of zero; for odd nuclei $E_o = -\Delta_o$ and for odd-odd nuclei $E_o = -2\Delta_o$ where Δ_o is the correlation function in the ground state (E_o = -0.0397 MeV for ^{235}U; E_o =-0.1665 MeV for ^{239}Pu). The use of the superfluid nucleus model taking into account the contribution from collective modes in the level density ensures the joining of the models at sufficiently low temperatures and at the points of joining E_x equal to 4, 3.2 and 2.4 MeV for even-even, odd and odd-odd nuclei, respectively (E_x =3.2, 4.1 and 2.6 MeV for ^{235}U, ^{238}U and ^{239}Pu, respectively).

The calculation of the average density of neutron resonances $\langle D\rangle_{theor.}$ with the above parameters shows that a great bulk of experimental data for actinides agrees with the theoretical predictions within ±50%.

The data on neutron resonance density were used to obtain the asymptotic value for the main parameter of level density a in the range A=225-254. This relationship turned out to look as

$$\frac{a(S_n)}{A} = 1.487\ 10^{-3}A + 0.4529 \qquad (45)$$

which differs from the systematics of [44] by a faster decrease in $\frac{a(S_n)}{A}$ with increasing A. This decrease can be caused by closing the shell as in case of double magic nuclei.

As the calculated cross-sections for fission at energies above 1 MeV are usually fitted to experimental data, the cross-section for radiative capture $\sigma_{n\gamma}$ in the calculations by use of the statistical theory proves to be most sensitive to the choice of the level density model. The question about the choice of the level density model can be unambiguously settled only for the nuclei for which there are the experimental data on $\sigma_{n\gamma}$ in a wide energy range. The nucleus ^{238}U whose cross-section for radiative capture was measured in a number of works is most suitable from this point of view. Let us investigate taking this nucleus as an example the influence of different level density concepts on the energy dependence of $\sigma_{n\gamma}$, analyze also the influence of uncertainties in $\langle D\rangle_{obs}$ and $\langle\Gamma_\gamma\rangle$ on calculation of $\sigma_{n\gamma}$ and consider the question about choice of the spectral factor.

The neutron transmission coefficients required for the statistical calculations were calculated by using the coupled-channel method with the non-spherical optical potential parameters which have been obtained by us and carefully optimized over the experimental data.

The conclusion was drawn in a number of works (see, e.g. /47/) that the Weisskopf factor makes it possible in many cases to attain the adequate description of $\sigma_{n\gamma}$, but it does not ensure an agreement as to the energy dependence of radiative strength functions /48/. The use of the Lorentz dependence is physically more substantiated, but in this case the description of the energy dependence of $\sigma_{n\gamma}$ becomes worse and the calculated values of $\sigma_{n\gamma}$ happen to be essentially higher than the experimental ones.

As the transmission coefficient for radiative capture depends on the level density of the compound nucleus, the above discrepancy with experiment can be assumed to result from incorrectness of the used level density model (the Fermi-gas model). Such a conclusion was drawn in /49/, but in this work the calculation for ^{238}U was conducted only to an energy of 1 MeV ignoring the competition of fission and above all without the use of the neutron transmission coefficients calculated by the nonspherical optical model.

The calculation of neutron cross-sections of ^{238}U was made on the basis of the formalism above described, the Teppel formalism etc. being used in the calculations at energies above 1.3 MeV. The level diagram of the nucleus ^{238}U was taken from /50/.

The calculated cross-sections for excitation of discrete levels of the target nucleus at incident neutron energies lower than 1.5MeV where the cross-sections practically do not depend on the choice of the level density model agree well with the experimental data.

Thus, the chosen parameters of the statistical model describe all the neutron cross-sections except $\sigma_{n\gamma}$. The calculated cross-sections for radiative capture depend strongly on the level density model in use, making it possible on the basis of comparison between the calculated and experimental values to chose a level density model permitting one to attain the best agreement with experiment in a wide energy range.

The cross-sections for radiative capture of neutrons by the nucleus ^{238}U calculated by using the spectral factors of both types and the level densities from different models are compared in Fig.12

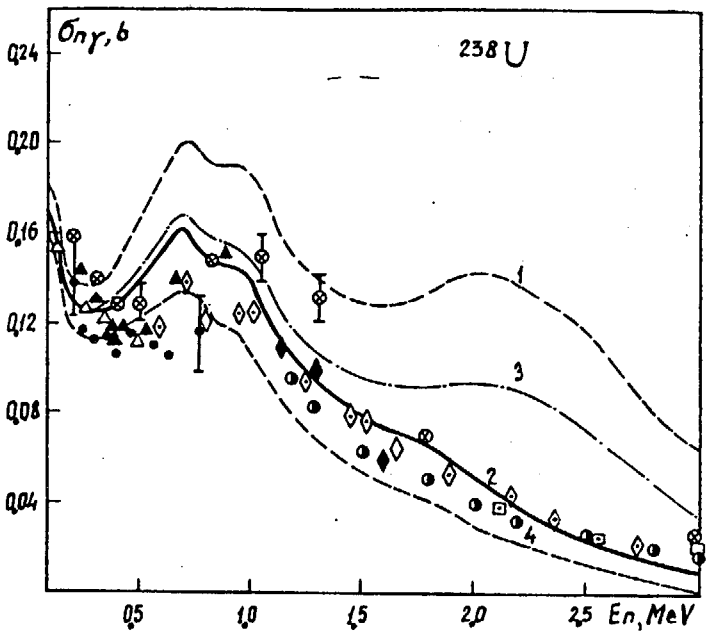

Fig.12. Comparison between experimental data on $\sigma_{n\gamma}(^{238}U)$ and theoretical data obtained by use of different level density models: 1 - Fermi-gas model, Lorentz spectral factor; 2 - Fermi-gas model with collective effects included, Lorentz spectral factor; 3 - superfluid nucleus model with collective effects included, Lorentz spectral factor; 4 - Fermi-gas model with collective effects included, Weisskopf spectral factor $\langle D\rangle_{obs}$=24.8 eV /55/, $\langle\Gamma_\gamma\rangle_{obs}$= 23.5 MeV, T_n determined by the coupled channel method).

with the experimental data on $\sigma_{n\gamma}$ in the energy range from 0.1 to 3.0 MeV (where noncompound mechanisms of radiative capture can be neglected). The comparison shows that the best fit to the experiment over the whole range is obtained by use of the level density from the Fermi-gas model with collective modes included. The use of the level density from the superfluid nucleus model leads to the discrepancy with the experiment in the energy range from 1.2 to 3.0 MeV, whereas at energies up to 1.2 MeV the agreement is the same as when using the level density from the Fermi-gas model with collective modes included.

The greatest discrepancy between calculation and experiment occurs for the level density from the conventional Fermi-gas model. The introduction of the energy dependence of the parameter a in the Fermi-gas model for level density results in no essential change of the calculated values of $\sigma_{n\gamma}$. Thus, at 3 MeV this effect attains less than 4%. It is attributed to comparatively small values of the shell corrections δW for ^{238}U and ^{239}U, allowing the dependence $a(U)$ in the level density from the superfluid nucleus model to be neglected.

The use of the Weisskopf spectral factor in the calculations does not yield the better fit to the experimental data on $\sigma_{n\gamma}$ than the fit obtained with the Lorentz spectral factor and the level density from the Fermi-gas model with collective modes included (curve 4 in Fig.12). Therefore, taking into account the better physical validity of the Lorentz factor, as evidenced by the results of describing the radiative strength functions /48/ and the experimental data on the $(n, \gamma f)$ process widths, we consider it reasonable to use just this spectral factor in the calculations by the statistical theory.

It should be noted that uncertainties in such quantities as $\langle D \rangle_{obs}$ and $\langle \Gamma_\gamma \rangle_{obs}$ and the used values of neutrons transmission coefficients can considerably affect the choice of the best model of level density for the description of $\sigma_{n\gamma}$ (Fig.13).

The width of radiative capture of ^{238}U was normalized to the estimated value $\langle \Gamma_\gamma \rangle_{obs}$=23.5 meV /52/ that agrees with the value 23.55 meV estimated by Rahn and Havens /53/ and with the value 23.43 meV $\pm$0.11 meV $_{stat}$ $\pm$0.70 meV $_{syst}$ obtained by Poortmans et al. /54/. The 4% error in $\langle \Gamma_\gamma \rangle$ leads to the same error in the calculated $\sigma_{n\gamma}$.

In case of $\langle D \rangle_{obs}$ there are far greater uncertainties due to difficulties in identifying S - and p-levels. Thus, according to the recent assessment of De Saussure et al./32/ $\langle D \rangle_{obs}$=24.78$\pm$2.0 eV, being consistently higher than $\langle D \rangle_{obs}$=20.8 $\pm$ 0.3 eV /55/. This discrepacy is due to the fact that weak levels considered in /55/ as S-levels are actually, as determined by Corvi et al./56/, the p-levels. The difference in $\sigma_{n\gamma}$ due to the use of the two extreme values of $\langle D \rangle_{obs}$ is about 15%. It should be noted that the results of the present calculations for ^{238}U show evidence for a high value of $\langle D \rangle_{obs}$=24.8 eV /32/.

The existing uncertainties in $\langle \Gamma_\gamma \rangle$ and $\langle D \rangle$ do not allow one to explain such a considerable discrepancy between experiment and calculation based on the conventional Fermi-gas model for level density.

It is seen in Fig.13 that the neutron transmission coefficients obtained by using the spherical and nonspherical optical models affect the calculation of $\sigma_{n\gamma}$. The difference between the values of $\sigma_{n\gamma}$ for these two cases depends on energy and ranges from 5 to 20%.

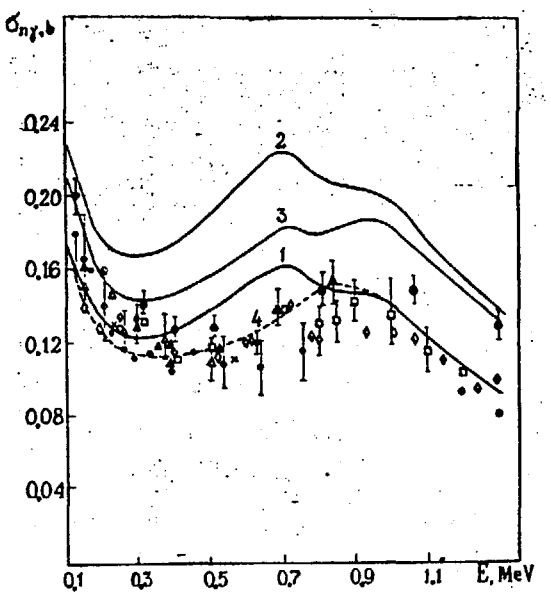

Fig.13. Comparison between experimental and calculated data on $\sigma_{n\gamma}$ (^{238}U) The calculation was made for the Fermi-gas model with collective effects included, with the Lorentz spectral factor and $\langle \Gamma_\gamma \rangle_{obs}$= 23.5 meV. Curve 1 - $\langle D \rangle_{obs}$= 24.8 eV /55/. T_n were determined by the coupled-channel method for a ground nuclear state alone; curve 2 - $\langle D \rangle_{obs}$= 17.7 eV /51/, nonspherical potential; curve 3 - $\langle D \rangle_{obs}$= 17.7 eV, spherical potential; curve 4 - $\langle D \rangle_{obs}$= 24.8 eV, T_n were determined by the coupled-channel method for both ground and excited nuclear states.

The neutron transmission coefficients applied when calculating the processes of the compound nucleus disintegration by the statistical model, strictly speaking, should represent the transmission coefficients for the excited states of the nuclei as they characterize the probability of capture in the inverse reaction of the particle emitted by the excited nucleus. It is required by the detailed balancing principle. When using the spherical optical model the dependence of the neutron transmission coefficients on excitation energy is neglected, as pointed in /57/. In practice, these coefficients are identified with the neutron transmission coefficients for the ground states of nuclei. The coupled-channel method can be used to calculate the neutron transmission coefficients for the excited states. We have studied the effect of using such coefficients for the two first excited states of the ground rotational band of ^{238}U. The influence of these states is determinative when taking into account the competition of inelastic scattering.

Table 3 lists the values of the neutron strength functions S_0 and S_1 for the ground state and the excited ones which were calculated by use of the coupled-channel method. As is seen from the table, the values of strength functions and, hence, the transmission coefficients for different states differ essentially, especially at low energies of incident neutrons. These differences decrease with increasing the energy. The difference between the transmission coefficients manifests itself more strongly in the reaction of radiative capture of neutrons. The performed calculations of $\sigma_{n\gamma}$ (^{238}U) show (Fig.13) that the use of the neutron transmission coefficients for the excited nuclear states obtained by the coupled-channel method permits the experimental data at energies up to 1 MeV to be described significantly better. So to obtain more reliable data, it is necessary to use the transmission coefficients for excited nuclear states although it leads to complication of calculations.

Table 3.

Strength functions of S - and ρ -neutrons for the ground state and excited ones of ^{238}U nucleus

Neutron energy, MeV	$S_0 \cdot 10^4$, $eV^{-1/2}$			$S_1 \cdot 10^4$, $eV^{-1/2}$		
	ground state	2^+ state	4^+ state	ground state	2^+ state	4^+ state
$0.5\ 10^{-3}$	1.163	1.032	0.790	1.947	1.893	3.745
0.005	I.I33	I.0I6	0.780	I.94I	I.7I7	2.997
0.0I	I.I2I	I.006	0.774	I.944	I.72I	3.003
0.03	I.09I	0.98I	0.757	I.952	I.73I	3.0I0
0.I	I.034	I.003	0.736	I.9I6	I.73I	3.407
0.2	0.990	0.920	0.7I7	2.I09	I.828	3.068
0.4	0.945	0.9I2	0.7I2	I.80I	I.462	2.463
I.0	0.820	0.790	0.695	I.428	I.I5I	I.I83

The performed analysis shows that the use of the conventional Fermi-gas model for level density leads to an appreciable discrepancy between the experimental data and $\sigma_{n\gamma}$ for even-even nuclei calculated with both the types of spectral factor. This discrepancy cannot be explained by uncertainties in the used parameters.

The calculated curve of $\sigma_{n\gamma}$ at energies up to 1.2 MeV in case of the level density from the superfluid nucleus model with collective modes included and with the Lorentz spectral factor agrees with experiment as well as in using the level density from the Fermi-gas model with collective modes included. However, some uncertainty in the parameters of the used version of the superfluid model, in particular, in the phase transition energy, does not allow one to affirm that the same relation between the two calculated curves will occur also for other nuclei. The calculations of $\sigma_{n\gamma}$ (^{242}Pu) show (Fig.14), that the value of $\sigma_{n\gamma}$ calculated by use of the level density from the superfluid model with collective effects included seems to be greater than the value obtained for the level density from the Fermi-gas model with collective modes included. It should be noted that in case of using the level density from the superfluid nucleus model the calculation of $\sigma_{n\gamma}$ with the Weisskopf spectral factor at energies up to 1 MeV yields higher values than with the Lorentz spectral factor. For the Fermi-gas model the contrary is the case. The pointed uncertainty needs its subsequent investigation.

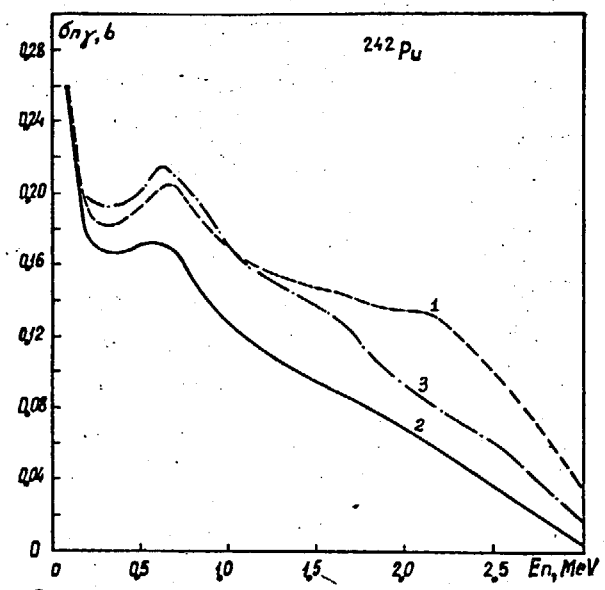

Fig.14. Calculated data on $\sigma_{n\gamma}$ (^{242}Pu) obtained by use of different level density models and the Lorentz spectral factor: 1 - conventional Fermi-gas model; 2 - Fermi-gas model with collective modes included; 3 - superfluid model with collective mode included $\langle D\rangle_{obs}$ = 14.233eV; $\langle\Gamma_\gamma\rangle_{obs}$ = 22.60 meV.

So when estimating $\sigma_{n\gamma}$ for ^{240}Pu and ^{242}Pu we have employed the results of the calculations the level density by using the Fermi-gas model including collective modes and the Lorentz spectral factor. It should be noted that at energies ranging from the boundary between the discrete and continuous spectra of the target nuclear levels (1.15 MeV) to 2 MeV the calculation yields somewhat overestimated values of $\sigma_{n\gamma}$ due to underestimating the level density of the residual nucleus at these energies. It is particularly noted in case of the conventional Fermi-gas model.

The comparison between the experimental data for $\sigma_{n\gamma}$(^{239}Pu) and the theoretical ones obtained by use of the different level density models is given in Fig.15.

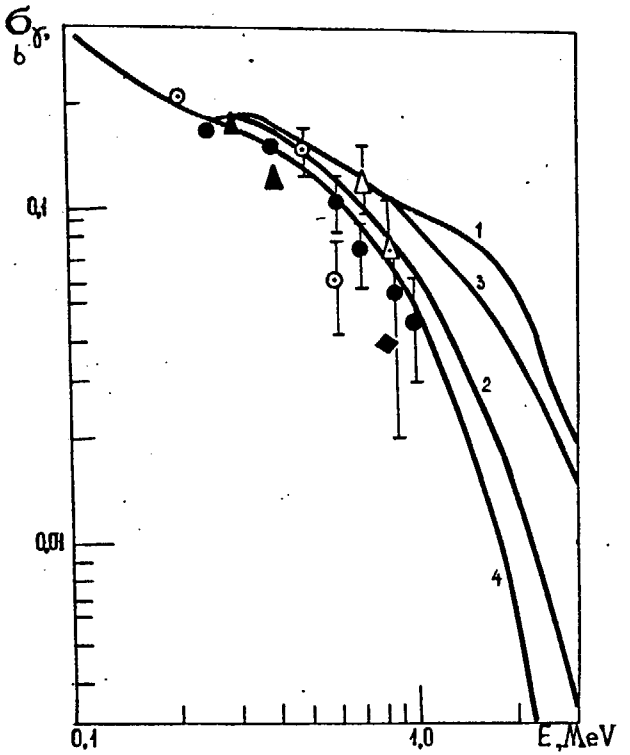

Fig.15. Comparison between experimental data on $\sigma_{n\gamma}$(^{239}Pu) and theoretical data obtained by use of different level density models: 1 - Fermi-gas model, Lorentz spectral factor; 2 - Fermi-gas model with collective modes included, Lorentz spectral factor; 3 - superfluid model with collective modes included, Lorentz spectral factor; 4 - Fermi-gas model with collective modes included, Weisskopf spectral factor. $\langle D\rangle_{obs}$ = 2.38 eV; $\langle\Gamma_\gamma\rangle_{obs}$ = 43.3meV.

The use of the neutron transmission coefficients from the generalized optical model and the allowance for the direct excitation of the lower levels make it possible to provide the satisfactory fit of the experimental and theoretical cross-sections for excitation of the lower levels, as well as of the levels whose cross-sections are completely determined by compound nucleus disintegration.

The choice of the level density model does not practically affect the value of the total cross-section for inelastic scattering. The discrepancies between the level densities of the target nucleus taken from different models cause changes in the relation between the cross-sections for scattering by the discrete and continuous spectra of levels as well as in the cross-sections for discrete level excitation.

As is seen in Figs 16 and 17, the best fit between the calculated and experimental cross-sections data for excitation of the ^{239}Pu levels is provided by use of the level density from the Fermi-gas model with collective modes included and with the neutron transmission coefficients calculated by the coupled-channel method.

Using the nonspherical optical potential, the Lorentz spectral factor and the level density from the Fermi-gas model with collective modes included it is possible to attain the self-consistent description of cross-sections of all the types, including $\sigma_{n\gamma}$, for the even-even target nuclei of the ^{238}U type in a wide energy range. For the odd target nuclei the main thing is the correct allowance for the competition of fission and, therefore, the choice of different models for the level density affects to a less extent the values of the calculated cross-sections in the energy range under consideration ($\sigma_{nn'}$, σ_f and σ_t, up to 5 MeV; $\sigma_{n\gamma}$, up to 0.8 MeV).

The theory of fission has not yet reached a stage when it is possible to predict σ_f quantitatively. When estimating the cross-sections we carried out the parametrization of σ_f, determined the fission transmission coefficients in order to take into account the competition of fission with other processes. The fission process is a complicated, insufficiently studied phenomenon. One of the substantial uncertainties in the calculation of σ_f lies in the transition state diagram of the fissionable nucleus and in the form of level density in the continuous energy range. This uncertainty is especially great for the even target nuclei, as for these nuclei it is necessary to take into account the high centrifugal barrier.

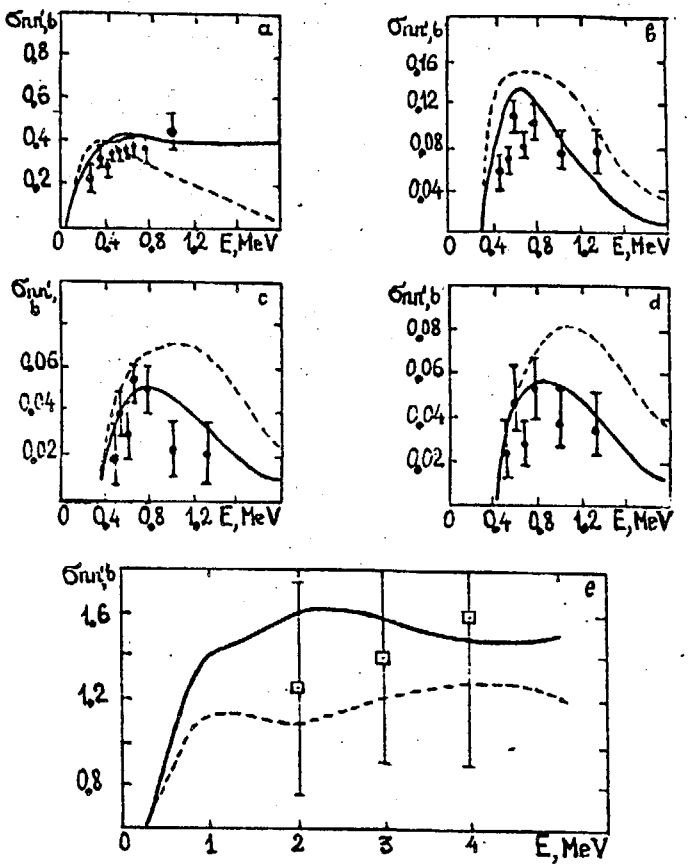

Fig.16. Comparison between experimental and calculated data on cross-sections for ^{239}Pu nuclear level excitation. The calculations were made with transmission coefficients from the coupled-channel method (solid line) and from the spherical optical model (dashed line): a - sum of 57 - keV and 76 - keV levels; b - 285 keV level; c - 330 - keV level; d - 387 keV and 392 - keV levels; 1-total cross-section for inelastic scattering.

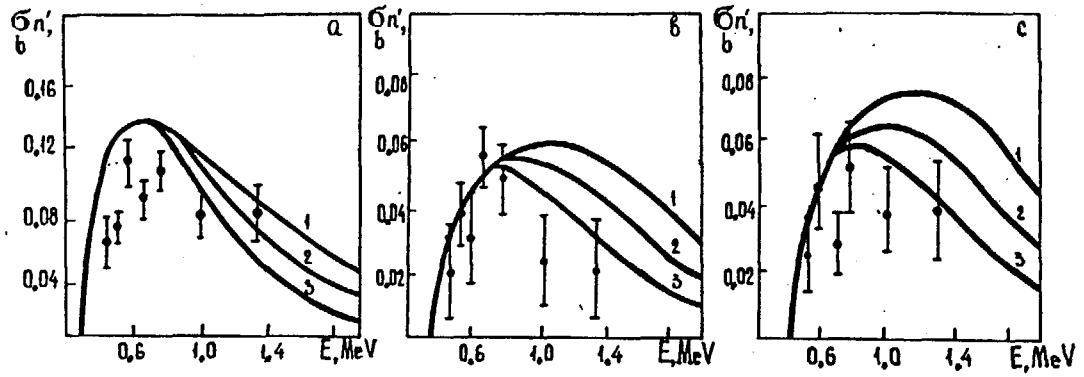

Fig.17. Cross-sections for ^{239}Pu nuclear level excitation for different level density models: 1 - Fermi-gas model; 2 - superfluid model; 3 - Fermi-gas model with collective modes included.

In an attempt at describing the cross-section for fission it is necessary to consider a number of features such as:(1) the asymmetry of the first hump of fission barrier /58/, as there is a strong dependence of nuclear level density upon nuclear symmetry and the level density for the assymetric nucleus increases in comparison with the axially-symmetrical longitudinal deformation due to the growing number of independent rotational excitations which become possible;(2) the level density in the continuous energy range;(3) the temperature dependence of fission barriers at energies higher than 10 MeV; 4) the possible existence of two parallel second humps 0.3-0.5 MeV apart in the energy range above the threshold.

Hence, with an unified set of parameters in the framework of the statistical approach using the neutron transmission coefficients obtained from the optical model it is possible to calculate simultaneously the cross-sections for the reactions of fissionable nuclei going through the compound nucleus formation with an accuracy of ~5% in σ_t and σ_{nx} , ~15% in $\sigma_{n\gamma}$, 20-30% in $\sigma_{nn'}$ and to parametrize σ_f with an accuracy of about 10%. In the lack of experimental data on $\sigma_{n\gamma}$ and $\sigma_{nn'}$ for fissionable nuclei it is possible to calculate them using the developed method with the above accuracies. The experimental data on σ_f , average parameters $\langle\Gamma_\gamma\rangle$ and $\langle D\rangle$, and on nuclear level diagram are minimum information necessary to calculate $\sigma_{nn'}$ and $\sigma_{n\gamma}$.

REFERENCES

1. Hauser W., Feshbach H. The Inelastic Scattering of Neutrons.- "Phys.Rev.", 1952, v.87, p.366-373.
2. Feshbach H., Porter C.E., Weisskopf V. Model for Nuclear Reactions with Neutrons. -"Phys.Rev.", 1954, v.96, p.448-456.
3. Lynn J.E. Fission Barrier Theory and its Application to the Calculation of Actinide Neutron Cross-Sections. - Proc. of the Course on Nuclear Theory for Applications, Trieste, 1978. IAEA, Vienna, 1980, p.353-415.
4. Lynn J.E. Fission Theory and its Application to the Computation of Nuclear Data. - Proc. of a Consultants Meeting on the Use of Nuclear Theory in Neutron Nuclear Data Evaluation, Trieste, 1975, IAEA, Vienna, 1976, v.1, p.325-390.
5. Teppel J.W., Hoffman H.M., Weidenmuller H.A. Hauser Feshbach Formulas for Medium and Strong Absorption. - "Phys.Letters", 1974, v.B49, p.1-4.
6. Lynn J.E. Interpretation of Neutron-Induced Fission Cross-Sections and Related Data. - Proc. of the Conference on Nuclear Data for Reactors, Paris, 1966, IAEA, Vienna, 1967, p.89-114.
7. Hill D.L., Wheeler J.A. Nuclear Constitution and the Interpretation of Fission Phenomena.- "Phys.Rev.", 1953, v.89, p.1102-1145.
8. Lynn J.E. The Theory of Neutron Resonance Reactions. - Clarendon Press, Oxford, 1968.
9. Lynn J.E. Systematics for Neutron Reactions of the Actinide Nuclei. - AERE-R7468, Harwell, 1974.
10. Fission of Doubly Even Actinide Nuclei Induced by Direct Reactions. -"Phys.Rev.", 1974, v.9, p.1924-1947, Auth.: Back B.B., Hansen O., Britt H.C. and Garrett J.D.

11. Gai E.V., Ignatyuk A.V., Rabotnov N.S., Smirenkin G.N. Two-humped barrier in quasi-classical approximation. - Proc. of a Symposium on Physics and Chemistry of Fission, Vienna, 1969. IAEA, Vienna, 1969, pp.337-346.
12. Blatt J.M., Weisskopf V.F. Theoretical Nuclear Physics., New-York-London, 1952.
13. A Study of the Photofission and Photoneutron Processes in the Giant Dipole Resonance of ^{232}Th, ^{238}U and ^{237}Np.- "Nucl.Phys.", 1973, v.A199, p.45-64. Auth.: Veyssiere A., Beil H., Bergere R., Carlos P., Lepretre A.
14. Blokhin A.I., Ignatyuk A.V. Dependence of excited state density on parity. - In book: "Neutron Physics" (Proc. of the 3-rd All-Union Conference on Neutron Physics, Kiev, 1976). Ed.TsNII Atominform, Moscow, 1976, part 3, pp.3-7 (in Russian).
15. Soloviev V.G., Stoyanov Ch., Vdovin A.I. Semi-Mircoscopic Calculation of the Level Density in Spherical Nuclei.- "Nucl.Phys.", v.A224, p.411-428.
16. Zenevich V.A., Klepatskii A.B., Konshin V.A., Sukhovitskii E.Sh. On possibility of predicting cross-sections for neutron radiative capture by fissionable nuclei.-In book: "Neutron Physics" (Proc. of the 5th All-Union Conference on Neutron Physics, Kiev, 1980). Ed.TsNIIAtominform, Moscow, 1980, part 3, pp.245-249 (in Russian).
17. Zen Chan Bom, Panteleev Ts., Tyan San Khak. Attempt of experimental discovery of the $(n,\gamma f)$ process in ^{239}Pu fission by resonance neutrons. - Izv.Akad.Nauk SSSR, ser.fiz., 1973, v.37, pp.82-85 (in Russian).
18. Gamma-Ray Multiplicity in ^{239}Pu Fission Induced by Resonance Neutrons. Experimental Evidence for the $(n,\gamma f)$ - Reaction.- "Nucl.Phys.", 1973, v.A216, p.395-406. Auth: Ryabov Yu., Trochon J., Shackleton D., Frehaut J.
19. Borukhovich G.Z., Zvezdkina T.K., Ivanov K.N. et al. Measurement of gamma-ray multiplicity in ^{239}Pu fission by resonance neutrons. - Preprint LINP (Leningrad Institute of Nuclear Physics) N 452. Leningrad, 1978 (in Russian).
20. Sukhovitskii E.Sh., Klepatskii A.B., Konshin V.A., Antsipov G.V. Allowance for $(n,\gamma f)$ process in calculating radiative capture widths and average cross-sections of fissionable nuclei.- In book:"Neutron Physics" (Proc. of the 4th All-Union Conference on Neutron Physics, Kiev 1977) Ed.TsNIIAtominform, Moscow, 1977, part 4, pp.68-74 (in Russian).
21. Tamura T. Analysis of the Scattering of Nuclear Particles by Collective Nuclei in Terms of the Coupled-Channel Calculation. - "Rev. of Modern Physics", 1965, v.37, p.679-708.
22. Chase D.M., Wilets L. and Edmonds A.R. Rotational - Optical Model for Scattering of Neutrons. - "Phys.Rev"., 1958, v.1080-1092.
23. Lagrange Ch. Evaluation of Neutron-Nucleus Cross Sections in Heavy Nuclei with a Coupled-Channel Model in the Range of Energy from 10 keV to 20 MeV. - Proc. of the EANDC Topical Discussion on "Critique of Nuclear Models and Their Validity in the Evaluation of Nuclear Data", Tokyo, 1974, Ed.by T.Fuketa, JAERI, 1975, p.58-67.
24. Kikuchi Y. Research of the Best Running Conditions of Nuclear Codes for Coupled-Channel Calculation of Neutron Interaction with Heavy Deformed Nuclei. - Proc. of a Panel on Neutron Nuclear Data Evaluation, Vienna, 1971. IAEA, Vienna, 1973, IAEA-153, p.305-366.
25. Ignatyuk A.V., Lunev V.P., Shorin V.S. Coupled-channel calculations of cross-sections for neutron scattering by collective nuclear states. - Voprosy Atomnoi Nauki i Tekhniki (Problems of Atomic Science and Engineering), ser.Yadernye Konstanty (Nuclear Constants). Ed.TsNIIAtominform, Moscow, 1974, issue 13, pp.59-114 (in Russian).
26. Dzyuba B.M., Marshalkin B.E., Povyshev V.M., Tyapin A.S. Permissible calculation simplifications in the coupled-channel method. - Voprosy Atomnoi Nauki i Tekhniki (Problems of Atomic Science and Engineering), ser.Yadernye Konstanty (Nuclear Constants). Ed.Atomizdat. Moscow, 1976, issue 23, pp.147-157 (in Russian).

27. Raynal J. Optical Model and Coupled-Channel Calculations in Nuclear Physics.Lectures given at the Seminar on Computing as a Language of Physics, Triest, 1971, IAEA, Vienna, 1972, p.281-322.
28. Delaroche J.P., Lagrange Ch., Salvy J. The Optical Model with Particular Consideration of the Coupled-Channel Optical Model. - Proc. of the IAEA Consultants Meeting on the Use of Nuclear Theory in Neutron Nuclear Data Evaluation, Trieste, 1975, IAEA, Vienna, 1976, v.1, p.251-312.
29. Klepatskii A.B., Konshin V.A., Sukhovitskii E.S. Optical Potential for Heavy Nuclei. - INDC (CCP)-161/L, IAEA, Vienna, 1981, p.9-18.
30. Differential Cross-Section Measurements of Fast Neutron Scattering for ^{208}Pb, ^{232}Th and ^{238}U at 2,5 MeV.- NEANDC(E) 180"L", Commisariat a l'Energie Atomique, France, 1977, Auth.:Haouat G., Sigand J., Lachkar J., Lagrange Ch., Duchemin B., Patin Y.
31. Woods R.D., Saxon D.S. Diffuse Surface Optical Model for Nucleon-Nuclei Scattering. - "Phys.Rev.", 1954, v.95, p.577-578.
32. Evaluation of the ^{238}U Neutron Cross-Sections for Incident Neutron Energies up to 4 keV.-"Progress in Nuclear Energy", 1979, v.3, p.87-124. Auth.: De Sanssure G., Olsen D.K., Perez R.B., Difilippo F.C.
33. Differential Cross Section Measurements for 3.4 MeV Neutron Scattering from ^{208}Pb, ^{232}Th, ^{235}U, ^{238}U and ^{239}Pu.- NEANDC(E)-196 "L", Commissariat a l'Energie Atomique, France, 1978. Auth.: Haonat G., Lachkar J., Lagrange Ch., Patin Y., Sigand J., Shamu R.E.
34. Moller P., Nilsson S.G., Nix J.R. - Calculated Ground State Properties of Heavy Nuclei. - "Nucl.Phys.", 1974, v.A 229, p.292-319.
35. Lambropoulos P. Fast Neutron Total and Scattering Cross-Sections of ^{238}U. - "Nucl.Sci.Eng.", 1971, v.46, p.356-365.
36. Davidov A.S., Chaban A.A. Excited States of Nuclei "Nucl. Phys.", 1960, v.20, 499-508.

37. Soloviev V.G., Stoyanov Ch., Vdovin A.I. Semi-Microscopic Calculation of the Level Density in Spherical Nuclei. - "Nucl.Phys.", 1974, v.A224, p.411-428.
38. Soloviev V.G., Malov I.A. A Model for Describing the Structure of Highly Excited States in Deformed Nuclei. - "Nucl.Phys.", 1972, v.A196, p.433-451.
39. Voronov V.V., Komov A.L., Malov L.A., Soloviev, V.G., Nuclear level density for $230 \leq A \leq 254$. - Yadernaya Fizika, 1976, v.24, pp.504-507 (in Russian).
40. Ignatyuk A.V. Statistical Characteristics of Excited Nuclei. Proc. of the Meeting on the Use of Nuclear Theory in Neutron Data Evaluation, Triest, 1975, IAEA, Vienna, 1976, v.1, p-211-249.
41. Ignayuk A.V., Shubin Yu.N.A simple model for description of pair correlations in excited nuclei. - Izv. Akad. Nauk SSSR, ser.fiz., 1973, v.37, pp.1947-1952, (in Russian).
42. Dossing T., Jensen A.S. Nuclear Level Densities with Collective Rotations Included. - "Nucl.Phys.", 1974, v.A222, p.493-511.
43. Malov L.A., Soloviev V.G. and Voronov V.V. Semi-Microscopic Description of the Density of Excited States in Deformed Nuclei. - "Nucl.Phys.", 1974, v.A224, p.396-410.
44. Ignatyuk A.V., Istekov K.K., Smirenkin G.N. A role of collective effects in systematics of nuclear level density. - Yadernaya Fizika, 1979, v.29, pp.875-883, (in Russina).
45. Ignayuk A.V., Smirenkin G.N., Tishin A.S. A phenomenological descritpion of energy dependence of level density parameter. - Yadernaya Fizika, 1975, v.21, pp.485-490 (in Russina).
46. Ignatyuk A.V., Istekov K.K., Smirenkin G.N. Systematics of level density parameters. - In book: "Neutron Physics" (Proc. of the 4th All-Union Conference on Neutron Physics, Kiev, 1977). Ed.TsNIIAtominform, Moscow, 1977, part 1, pp.60-65 (in Russian).
47. Calculations of Cross-Sections for the Radiative Capture of Fast Neutrons. - Proc. of the Intern.Conference on Nuclear Data for Reactors, Helsinki, 1970. IAEA, Vienna, 1970, v.2, p.281-292. Auth.: Tricke M.P., Lopez M.M., Friesenhahn S.J. et al.

48. Bartholomcev G.A. Radiation Strength Functions. - "Advanced Nuclear Physics", 1974, v.7, p.232-264.
49. Blokhin A.I., Ignatyuk A.V., Platonov V.P., Tolstikov V.A. Influence of collective effects in level density on energy dependence of cross-sections for radiative capture of fast neutrons. - Voprosy Atomnoy Nauki i Tekhniki (Problems of Atomic Science and Engineering), ser. Yadernye Konstanty (Nuclear Constants). Ed. Atomizdat, Moscow, 1976 issue 21, pp-3-14 (in Russian).
50. Lambropoulos P. Fast Neutron Total and Scattering Cross Sections of ^{238}U. - "Nucl.Sci.Eng.", 1971, v.46, p.356-365.
51. Mughabhab S.F. and Garber D.I. Neutron Cross-Sections - BNL-325, 3d Edition, v.1, 1973.
52. Abagyan L.P., Korchagina Zh.A., Nikolaev M.N., Nesterova K.I. Evaluation of average resonance parameters of ^{238}U. - Yadernye Konstanty (Nuclear Constants). Ed. TsNIIAtominform. Moscow, 1972, issue 8, part 1, pp.121-153.(in Russian).
53. Rahn F., Havens W.S., Jr. A Review of the Total Radiation Width of the Neutron Resonances of ^{238}U. - EANDC(US)-179/U, Columbia University, 1977.
54. Cross Sections and Neutron Resonance Parameters for ^{238}U below 4 keV. - Proc. of the Intern.Conference on the Interaction of Neutrons and Nuclei, Lowell, 1976, USERDA Publication, 1976, p.1246-1252. Auth.:Poortmans F., Cornelis E., Mewissen L. et al.
55. Neutron Resonance Spectroscopy. ^{232}Th and ^{238}U. - "Phys.Rev.", 1972, v.6, p.1854-1869. Auth.:Rahn F., Camarada H.S., Hacken G. et al.
56. Corvi F., Rohr G., Weigman H. P-Wave Assignment of ^{238}U Neutron Resonances. - Proc. of the Conference on Nuclear Cross Sections and Technology, Washington, 1975. NBS Spec.Publ. 1975, v.2, p.733-737.
57. Ignatyuk A.V., Lunev V.P. On differences of neutron strength functions for ground and excited nuclear states. - In book: " Neutron Physics" (Proc. of the 5th All-Union Conference on Neutron Physics, Kiev, 1980). Ed.TsNIIAtominform, Moscow, 1980, part 1, pp.77-81 (in Russian)
58. Bjornholm S., Bohr A., Mottelson B.R. Role of Symmetry of the Nuclear Shape in Rotational Contributions to Nuclear Level Densities. - Proc. of the Symposium on Physics and Chemistry of Fission, Rochester, 1973. IAEA, Vienna, 1974, v.1, p.367-373.

SYSTEMATICS OF FISSION PROBABILITY CHARACTERISTICS FOR HEAVY NUCLEI

B.I. FURSOV, G.N. SMIRENKIN
Institute of Physics and Power Engineering (FEI),
Obninsk, Union of Soviet Socialist Republics

Abstract

This paper suggests a new approach to a phenomenological description of the dependence of the fission probability on Z and N. It is based on a statistical description of the decay widths of excited nuclear levels and a modern model of the fission barrier. The intention to develop this systematics for a more precise prediction of neutron fission cross-sections for a wide set of transuranium nuclei near the valley of stability has required not only a fairly advanced description of the fission barriers E_f, but also a critical analysis of the reference experimental data and the correct estimation of the neutron compound nucleus formation cross-section.

INTRODUCTION

The heavy nucleus fission probability characteristics are of great interest in connection with important practical and scientific aspects of using the data to be expected. In a wide range of excitation energy values the nuclear fission and neutron emission processes are dominating modes of compound nucleus decay. The probability of these competitive reactions is determined by the ratio of appropriate mean widths: the fission one, Γ_f, and the neutron one, Γ_n. In case of low excitation energies (the "cold" nuclei) the probability of above-barrier fission can be characterized to a reasonable accuracy for many purposes by a constant value of Γ_n/Γ_f. This property simlifies significantly a systematization of experimental data that always attracts our attention.

In spite of the fact that recently a bulk of experimental data on the fission cross sections and nuclear fissionability has considerably been increased due to a progress in theoretical descriptions and deep rebuilding in knowledge of the fission probability, the scientific and practical needs are frequently beyond the scope of it. In this connection one can emphasize, for example, such problems as the neutron-rich nuclear fusion in multiple neutron capture reactions occuring, for example, in astrophysical media and practically accomplished in nuclear explosions or, vice versa, the formation of neutron-deficient nuclei occuring in multiple neutron emission by excited nuclei, particularly, in reactions with heavy ions. The urgency of constructing the systematics suited for extrapolating into the Z and N regions up to now inaccessible for experimental investigation is defined by the following conditions.

Firstly, the nuclides which fissionability has been studied in the (n, f) and direct reactions are concentrated near the valley of stability and the possibilities of extending this region have been exhausted to a large extent.

Secondly, a theory for the present is not able to predict the fission process characteristics of interest with required accuracy, therefore, a phenomenological approach dominates in describing these ones as before.

At last, in the third place, the fission cross-sections and Γ_n/Γ_f systematics used up to now are purely empiric and, as will be shown, this places very severe restrictions on their applicability.

This lecture suggests some approach to a phenomenological description of the Γ_n/Γ_f dependence on Z and N freed from the mentioned defect of previous systematics. It is based on a statistic approach in describing the widths of excited nucleus decay and the modern model of a fission barrier. The intention to develop this systematics up to more precise prediction of neutron fission cross-sections for a wide set of the transuranium nuclei near by a valley of

stability has required not only a fairly advanced description of the fission barriers E_f but also a critical analysis of the reference experimental data and the correct estimate of the neutron compound nucleus formation cross-section.

In conclusion of this paper on the basis of a wide set of experimental data concerning the Γ_n/Γ_f ratio we shall discuss the problem of the influence of shell reconstruction in heavy nuclei when excitation energy is increased ("heated" nuclei) on observed characteristics of a neutron fission and emission processes probability. This question is practically important in connection with the problem of super-heavy nuclear fusion at the boundary of a periodic system.

1. TRADITIONAL FISSION PROBABILITY SYSTEMATICS

Any attempts has been made to systematize directly these fission cross-section values in some early works. In the work of Smith et al. /1/given is the empiric relation for the fission cross-sections of heavy nuclei in the region of first "plateau" (E_n= 2-5 MeV)

$$\sigma_f = -39{,}031 + 17{,}321 \cdot Z^2/A^{3/2} \quad \text{(barn)} \qquad (1)$$

satisfactorily describing experimental data in the Th-Pu region. The analogous systematics has been proposed still earlier by Barshall and Henkel /2/ which differed from /1/ only by the $Z^{4/3}/A$ parameter. Apparently, both these concepts are equivalent since in the narrow region Z and A are appreciably only the ratio of exponents in the Z^m/A^n parameter which is similar in /1,2/, m/n = 1.33. The defect of these systematics is in indefinite growth of σ_f with increase of Z^m/A^n, while σ_f should have the neutron compound nucleus formation cross-section σ_{CN} as its limit. Defects of this empiric description suited only for the narrow nuclear region of $Z \lesssim 94$ are apparent.

The approach proposed by Vandenbosch and Huizenga /3/ is more promising. These authors have considered the ratio of mean neutron and fission widths Γ_n/Γ_f connected with the fission cross-section by the following relation:

$$\sigma_f/\sigma_{CN} \simeq \left(1 + \Gamma_n/\Gamma_f\right)^{-1} \qquad (2)$$

Having considered a set of the Γ_n/Γ_f values involving as well the more numerous data obtained from the (α,xn) and (d,xn) multiple neutron emission reaction cross-sections for x = 2-4

$$\sigma_{xn}/\sigma_{CN} \cdot P_x = \prod_i^x \left(\frac{\Gamma_n}{\Gamma_n+\Gamma_f}\right)_{A-i,E_i} = \left\langle \frac{\Gamma_n}{\Gamma_n+\Gamma_f} \right\rangle^x_{\bar{A},\bar{E}} \qquad (3)$$

has been described by a family of the linear relations:

$$\lg\left(\Gamma_n/\Gamma_f\right) \simeq C_1 + C_2 \cdot A \qquad (4)$$

where C_1 is strongly dependent on Z and C_2 is slightly dependent ($C_2 > 0$). Moreover, P_x is the x neutron emission probability in (3), E_i is the excitation energy of residual nucleus after emitting i-neutrons,

$$\bar{E} \simeq \left[(x+1)/2\right] \cdot 8\,\text{MeV}\,, \quad \bar{A} = A - (x-1)/2\,.$$

Developing this approach Sikkeland et al. /4/, on the basis of the numerous data, mainly in the $Z \geqslant 98$ region obtained in the reactions with heavy ions (HI,xn) for x = 3-8 has proposed the empiric relation for transuranium nuclei:

$$\lg\left(\Gamma_n/\Gamma_f\right) = C_1 Z + C_2 N + C_3 + \delta$$

$$\text{where } C_1 = -0.276, \quad C_2 = \begin{cases} 0.140, \\ 0.050 \end{cases} \quad C_3 = \begin{cases} 5.46 & N \leqslant 153 \\ 19.23 & N \geqslant 153 \end{cases} \qquad (5)$$

and δ = 0 for even - Z nuclides, and δ = 0.12 for odd - Z nuclides. According to (5) the $\lg\left(\Gamma_n/\Gamma_f\right)$ data make up a set of equidistant broken lines of equal slope slightly displaced depending on a parity of Z and having a salient point at N = 153. The Z = const and N = const lines in the Γ_n/Γ_f dependence (4) and (5) on the A

total nucleon number form a regular net. According to the Behrens's systematics /5/ the similar property is revealed in the neutron fission cross-section ratios for the first "plateau" energies of (E_n = 3-5 MeV).

We shall state a problem to analyze primarily the Γ_n / Γ_f dependence on a nuclear nucleon composition and under the traditional systematics we shall consider the basic concepts of Vandenbosch and Huizenga /3/ and the concrete definition of these in the work of Sikkeland et al. /4/.

2. EXPERIMENTAL INFORMATION ON THE Γ_n/Γ_f VALUES

Consider the information on fairly "cold" nucleus fission probability obtained by formula (2) from the σ_f fission cross-sections and the σ_f / σ_{CN} fissionability in the first "plateau" region. The main sources of experimental data are the fast neutron fission cross-sections /6-24/ and the excitation functions for fission processes after the direct (t,pf), (^{3}He,df), (^{3}He,tf), etc. reactions /28-32/. In these two excitation processes fissionabilities fairly well agree with each other.

The Γ_n / Γ_f data obtained from multiple neutron emission reactions conform to the more high excitations $\overline{E}$ averaged over mass and energy distributions of the residual nucleus within a decay chain. We shall not consider these in contrast to traditional systematics /3, 4/ that combine the data related to different excitation energies. Classification and discrimination of the data over energy, as will be seen further, are of principal significance when analyzing the dependence on the nucleon composition of a nucleus and using the systematics mentioned above to its description.

The term "plateau" applied above has actually expressed the main property of fission cross-section or fissionability involving the fairly faint energy dependence which permits in some cases to talk about the independence of these characteristics on excitation energy. This "rule" is approximate and suitable within the limited energy region depended mainly on the relation of the fission E_f and the neutron emission B_n thresholds.

As an example in fig.1 presented are the ^{242}Pu (1), ^{240}Pu (2), Cf^{249}(3) neutron fission cross-sections measured by the authors, the Γ_n / Γ_f values extracted from these for the same nuclei and the used σ_{CN} values calculated according to the optic model with the optimized potential parameters.

Pay attention to the fact that the concept of "plateau" does not coincide in the Γ_n / Γ_f ratio and the fission cross-section, as can be seen from the fig.1. It is seen, for example, that the growing Γ_n / Γ_f relation of about 8% per MeV conforms to the "plateau" in the ^{242}Pu fission cross-section and the $\Gamma_n / \Gamma_f (E_n)$ values for two other nuclei are more stable. In general, if one takes into account the strong Γ_n / Γ_f changes in a wider energy range including the low-energy part (where it is needed to take into account the Γ_γ radiation width contribution, as well) and the region near the (n,n'f)-reaction threshold one should consider the Γ_n / Γ_f constancy to be not trivial in the "plateau" region.

Data used in the further analysis, which will be given in the figures and tables, have been obtained by averaging in the 2-to 4-MeV neutron energy range or the appropriate excitation energies for direct reactions. When selecting the Γ_n / Γ_f values a preference has been given in the first place to the data obtained from the (n,f) reaction

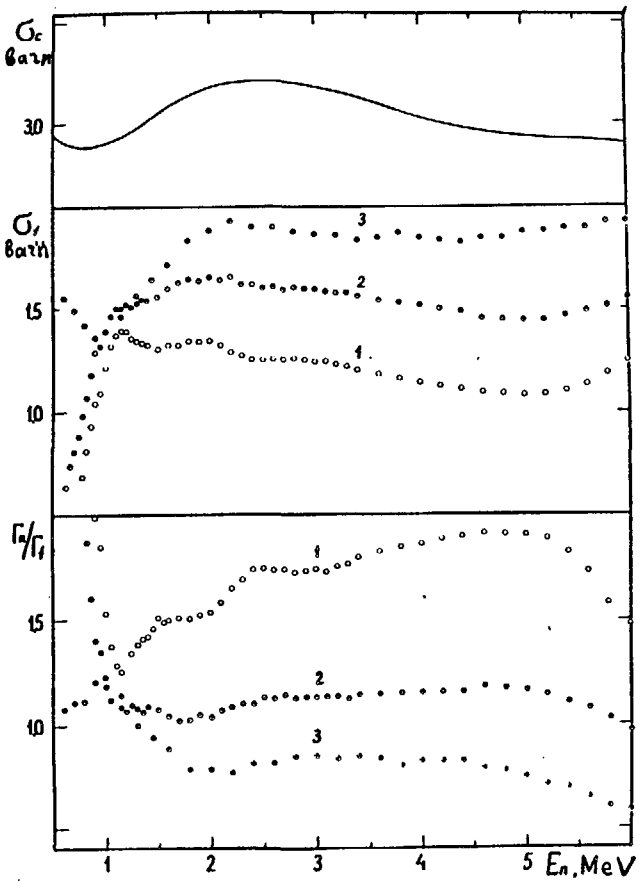

Fig.1. At the top: the neutron compound nucleus formation cross-section for (^{238}U + n).
In the middle: the fission cross-sections for Pu-242 (1), Pu-240 (2), Cf-249 (3).
At the bottom: the Γ_n/Γ_f values for the same nuclei.

and in the second one, to the results extracted from direct reactions proceeding under the action of ^{3}He ions.

The accuracy of the main neutron data in the $\Gamma_n/\Gamma_f \geqslant 1$ region is about 5 to 10% and the direct reaction data is about 10 to 15%.

This error increase for certain nuclei has been connected with disagreement of the results by different authors or with the uniqueness of the information source as well due to the fact that in the 1 region the error rises as fissionability

$P_f = \sigma_f/\sigma_{CN}$ approaches to unity as

$$\Delta \ln (\Gamma_n/\Gamma_f) \simeq - \frac{\Delta \ln P_f}{1 - P_f} \qquad (6)$$

attaining about 40% for most light isotopes /33,34/.

It is seen from fig.2 that the Γ_n/Γ_f dependence on nucleon composition is much more complicated than it has been imagined by the authors of the traditional systematics /3,4/. The Sikkeland's et al.

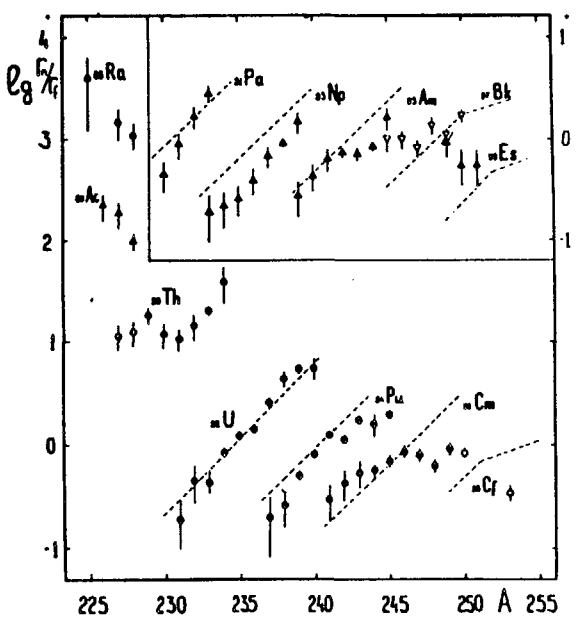

Fig.2. The dependence of Γ_n/Γ_f on the nucleon composition of a nucleus (circles are even Z; triangles are odd Z, light signs are only B_k and C_f). The dashed line is the Sikkeland's systematics.

relationship (5) is shown in fig.1 by the dashed line. The strongest effect to be considered is a disturbance of the $\ell g\,(\Gamma_n/\Gamma_f)$ linear dependence on A or N. In further considering some deviations from the systematics of (4) and (5) it is suitable to combine the nuclei studied into the following three groups:

1. The Pa - Np nuclides (their Γ_n/Γ_f run follows traditional concepts).

2. The Pu - Es nuclides (their $\ell g\,(\Gamma_n/\Gamma_f)$ slope is decreased when A rises, while , as for Cf and Es, there is a region where the $d\,\ell g\,(\Gamma_n/\Gamma_f)/dA$ derivative changes its sign).

3. The Ra - Th nuclides, there observed is the pattern of deviations being mirror opposite to those of the second group.

Then, consider briefly some aspects of the theoretical description.

3. MAIN THEORETICAL RELATIONSHIPS

In the excitation region of interest the statistical approach is adopted for describing the C.N. decay average widths according to which

$$\Gamma_n^J/\Gamma_f^J = \frac{2A^{2/3}}{\mathcal{E}}\cdot\frac{\int_0^{E-B_n}\rho_n(U,J)\cdot(E-B_n-U)\,dU}{\int_0^{E-E_f}\rho_f(U,J)\,dJ} \qquad (7)$$

where ρ_f and ρ_n are the level densities for the given excitation energy U and the angular momentum J in the transient state of the A fissioning nucleus and the A-1 residual nucleus after neutron emission, respectively. B_n is the neutron binding energy, $\mathcal{E} = \frac{\hbar^2}{2mr_0^2} \simeq$ 10 MeV. The universal C.N. decay characteristic which does not depend on the reaction inlet channel properties is the Γ_n^0/Γ_f^0 ratio for the zero angular momentum. Later, this will be considered omitting the $J = 0$ index.

The level densities depend exponentially on the S(U) nucleus entropy as well as depend exponentially on the excitation energy and as a result of this the integrals in expression (7) are approximately the functions of the upper limits only, i.e. it can be written with the accuracy up to of preexponential factors

$$\frac{\Gamma_n(E)}{\Gamma_f(E)} \sim \frac{\rho_n(E-B_n)}{\rho_f(E-E_f)} \sim \frac{K^n_{rot}(E-B_n)}{K^f_{rot}(E-E_f)}\cdot\exp\left[S_n(E-B_n)-S_f(E-E_f)\right] \qquad (8)$$

In the relation (8) noted are the important factors determining an energy dependence of the Γ_n/Γ_f ratio including K^n_{rot} and K^f_{rot}, that is the rotational enhacement of level density factors, the relation of which can differ strongly from unity if the nucleus has different symmetry in the ground and transient states /32-34/.

A successive description of intrinsic excitation level densities with regard to the single-particle spectrum shell structure at Fermi boundary is accomplished according to a superfluid nucleus model using numerical calculations complicated enough.

Because this model is cumbersome, it does not suit for solving our problem and we shall adopt the simplified models which at the expense of some uncertainties in description give a possibility to investigate the regularities of interest in a convenient analytical form.

Here we use simple relations of the two models /35/; the model with a constant temperature

$$\rho_T(U) = C\cdot\exp(U'/T) \qquad S_T(U) = U'/T \qquad (9)$$

$$\Gamma_n/\Gamma_f = \frac{2TA^{2/3}}{\mathcal{E}}\cdot\frac{C_n}{C_f}\cdot\exp\left(\frac{E_f'-B_n'}{T}\right) \qquad (10)$$

when constructing the Γ_n/Γ_f systematics for "cold" nuclei and

the Fermi-gas model as well

$$\rho_{FG}(U) = c \cdot \exp\left(2\sqrt{aU'}\right) \qquad S_{FG}(U) = 2\sqrt{aU'} \tag{11}$$

$$\Gamma_n/\Gamma_f = \frac{2A^{2/3}}{\alpha} \cdot \frac{t_n^2}{t_f} \cdot \frac{C_n}{C_f} \cdot \exp\left[2\sqrt{a_n(E-B_n')} - 2\sqrt{a_f(E-E_f')}\right] \tag{12}$$

in the strongly heated nucleus fission probability analysis. In relations (9-12) $U' = U + \delta$ is the effective excitation energy with inclusion of this the even-odd discrepancies have been taken into account in level densities due to the pairing effects of nucleons; $E_f' = E_f + \delta_f$ and $B_n' = B_n + \delta_n$ are the effective values for the fission barrier height and the neutron binding energy, in this case

$$\delta_i = n\Delta_i \;, \qquad n = \begin{cases} 0 \text{ for odd-odd nuclei} \\ 1 \text{ for A-odd nuclei} \\ 2 \text{ for even-even nuclei} \end{cases} \tag{13}$$

Δ is the parameter determined from the even-odd nucleus mass differences taken for simplicity to be equal for the neutron and proton components; a_n and a_f, $t_n = \left(\frac{E-B_n'}{a_n}\right)$ and $t_f = \left(\frac{E-E_f}{a_f}\right)$ is the level density parameter and the nuclear temperature in the neutron and fissioning decay channels; t_i depends on energy as opposed to the $T = T_n = T_f = \text{const}$, i.e. a parameter in relations (9) and (10). The relations (10) and (12) differ from the appropriate results of the work (35) only by inclusion of the C_n/C_f ratio which can take into consideration a difference of the level density collective increase coefficients in the neutron and fissioning channels (see the relation (8)).

The level density model with constant temperature while not possessing a definite physical meaning has well been used for describing experimental data and in the small ($U < 5$ MeV) excitation region has been considered as an alternative of the noninteracting particle model (a Fermi gas model). The reason of the simplified parametrization success (9) can be understood from the calculations carried out according to the superfluid nucleus model which takes into account the pairing correlations between nucleons. As is seen from fig.3 in the region below critical energy the ($U_{cr} \simeq 6$-8 MeV) phase transition from the ($U < U_{cr}$) superfluid state into the ($U > U_{cr}$) normal one, taking into consideration a residual interaction, "straightens" the rapidly falling convex curve of the "Fermi-gas" model. While the energy dependence in a superfluid nucleus model is not strongly line-

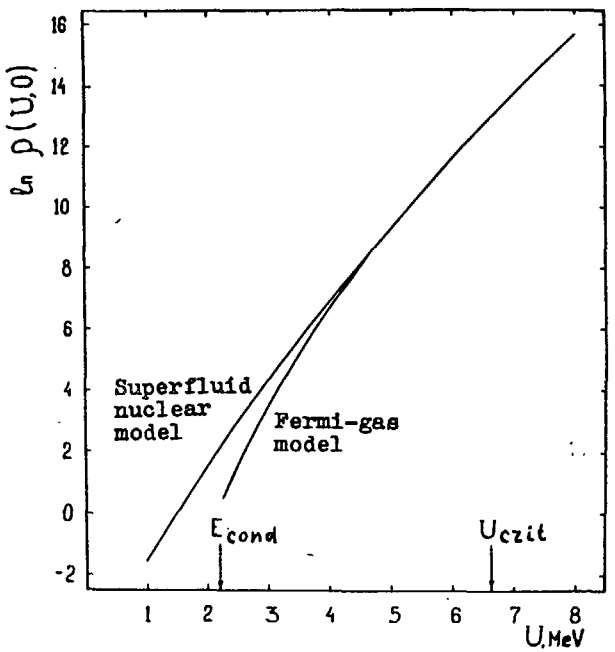

Fig.3. The nuclear level density in a superfluid nuclear model and in a Fermi-gas one ($\delta = E_{cond}$) for the even-odd system. The arrows show the critical energy values of U_{crit} and the condensation energy of $E_{cond} = U_{crit}$/3.11.

ar, at the small $U_1 - U_2$ difference the $\rho(U_1)/\rho(U_2) = exp\left(\frac{U_1-U_2}{T}\right)$ relation will serve as the fair approximation of the level density ratio in the relation (8). Exactly this situation is typical of describing the Γ_n/Γ_f ratio in the heavy nucleus region where the E_f and B_n parameters are close. In the $U > U_{cr}$ region the relations (11) and (12) of the Fermi-gas model are the good approximations to the accurate superfluid nucleus model results.

The lack of the prominent even-odd differences in Γ_n/Γ_f, as is shown by experimental data in fig.2, is not apparantly following from the relation (10) since the exponent index besides the unequal δ_f and δ_n parameters involves the B_n binding energy which changes by leaps when N is changed by unity, and if N is even, then /36/

$$B_n(Z,N) - B_n(Z,N-1) = B_n(Z,N) - B_n(Z,N+1) = 2\Delta \qquad (14)$$

Note in the $E_f' - B_n'$ difference the part varying discretely with the nucleon number and having designated B_n° as the binding energy in the N-even nucleus and, since in accord with (13) and (14),

$$B_n = B_n^\circ - 2m\Delta$$
$$\delta_f - \delta_n = (1-2m)\Delta \qquad m = \begin{cases} 0 & \text{N-even} \\ 1 & \text{N-odd} \end{cases} \qquad (15)$$

obtain the result independent of the N parity

$$E_f' - B_n' = E_f - B_n + \delta_f - \delta_n = E_f - B_n^\circ + \Delta \qquad (16)$$

Thus, we have showed that in the exponential factor in the relation (10) the corrections for pairing to thresholds and level densities compensate for each other. Note, that the qualitative interpretation of this property has still been proposed from common considerations in the work /35/. The $(B_n^\circ - \Delta)$ difference entering (16) and equal, in accord with (14), to the neutron binding energy averaged over the neighbouring nuclides

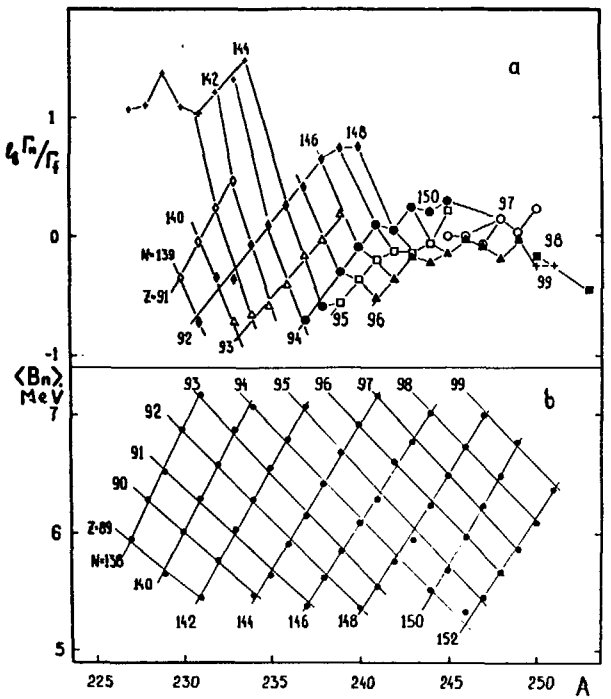

Fig.4. The correlation of the dependences of $\lg(\Gamma_n/\Gamma_f)$ and $\langle B_n \rangle$ on the mass number of A. The lines connect points with the fixed values of Z and N.

$$B_n^\circ - \Delta = \frac{1}{4}\left[B_n(Z,N-1) + 2B_n(Z,N) + B_n(Z,N+1)\right] \equiv \langle B_n \rangle \qquad (17)$$

does not possess even-odd discrepancies and represents the smooth Z and N function (see fig.4). It is proposed that the Δ parameter determining even-odd discrepancies of level densities in the fissioning and residual nucleus transient state after the emission of neutron is the same, $\Delta_f = \Delta_g$, then from (16) it follows

$$E_f' - B_n' = E_f - \langle B_n \rangle \qquad (18)$$

Abandonment of simplified assumption leads to the $(\Delta_f - \Delta_g)$ appearance in relation (18), i.e.,

$$E_f' - B_n' = E\,(A\ odd) - \langle B_n \rangle + \Delta_f - \Delta_g \quad . \tag{19}$$

and, consequently, to even-odd discrepancies in fission barrier heights

$$E_f = E_f\,(A\ odd) - \frac{(-1)^N + (-1)^Z}{2} \tag{20}$$

and, respectively, the $\exp\left(\frac{\Delta_f - \Delta_g}{T}\right)$ factor involved in (10). In this case the main result is not changed which consists in the fact that factors discretely changing in the effective E_f' fission thresholds and the B_n' neutron emission are mutually compensated for and, as a result, the Γ_n / Γ_f relation, in accord with experiment, is smoothly depended on Z and N. From (18) the relation in (10) is transformed into the form

$$\Gamma_n / \Gamma_f = G \cdot \exp\left(\frac{E_f - \langle B_n \rangle}{T}\right), \quad G = \frac{2T\,A^{2/3}}{\hbar^2} \cdot \frac{C_n}{C_f} \exp\left(\frac{\Delta_f - \Delta_g}{T}\right) \tag{21}$$

This is readily generalized in the case of a two-humped fission barrier where it is needed to take into account the two transient state systems connected with the A inner and B outer humps /37/

$$\Gamma_n / \Gamma_f = \Gamma_n / \Gamma_f^A + \Gamma_n / \Gamma_f^B \quad . \tag{22}$$

For describing each of the summands in (22) the common relation (7) is used as well as anyone of its modifications for a specified level density model (10) or (12). In the frames of the constant temperature model and assuming $T_A = T_B = T$ relation (21) is transformed into the form

$$\Gamma_n / \Gamma_f = G \cdot \exp\left(\frac{E_f^M - \langle B_n \rangle}{T}\right); \tag{23}$$

$$G = \frac{2T\,A^{2/3}}{\hbar^2}\left[C_n/C_f^A \cdot \exp\left(\frac{E_f^A - E_f^M}{T}\right) + C_n/C_f^B \cdot \exp\left(\frac{E_f^B - E_f^M}{T}\right)\right]$$

where $E_f^M = \max\left\{E_f^A, E_f^B\right\}$ is the highest of the humps that has been observed in the fission cross section according to a typical break due to a sharp fall of the barrier penetrability.

4. Region of traditional systematics applicability and fission barrier effect on Γ_n / Γ_f ratio

The values of $\langle B_n \rangle$ are shown in the low part of fig.4 being calculated in accord with (17) from the nucleus mass tables /36/. The family $\langle B_n \rangle$ as a function of Z and N form a regular structure, i.e. grid of approximately equal slope straight lines that can be approximately described by the relation

$$\langle B_n \rangle \simeq C_1 Z - C_2 N + C_3 \tag{24}$$

According to the Sikkeland's systematics (5) the value of $lg\,(\Gamma_n / \Gamma_f)$ should follow a similar relationship. It is apparent that existence of similar dependence for a fission barrier produces the condition for traditional systematic applicability. However, it is seen from fig.4 that if the Z = const, N = const lines for $\langle B_n \rangle$ form the regular grid within the total nuclear region considered, then $lg\,(\Gamma_n / \Gamma_f)$ has this property only within a comparatively narrow interval involving the first group nuclei as well as the Th heavy isotopes and the Pu light ones. The traditional systematics is expected to have a region of validity which is limited for "cold" nucleus fission to this range. With increase of a number of neutrons in the second group nuclei and decrease in the third group ones, the Z = const lines are distorted and then change a nature of the Γ_n / Γ_f dependence on N so that the regularity produced for $\langle B_n \rangle$ is not seen at all.

Since the $\langle B_n \rangle$ dependence on Z and N ensures the regularity described by these systematics (4) and (5) the conclusion is naturally suggested that the nature of experiment deviations is connec-

ted with a fission barrier structure and the $E_f(Z,N)$ dependence due to it. This has not been put in question by the authors of traditional systematics (4) and (5) since, on the one hand, there are no appropriate data and, on the other hand, the concepts of a fission barrier available at that time have entirely been based on a liquid drop model that does not give rise to doubt in the weak E_f dependence on N. Now we discuss in more detail the influence of fission barrier structure on the Γ_n/Γ_f dependence on nucleon composition, primarily, on the N neutron number.

Correlation between the $\ell g\,(\Gamma_n/\Gamma_f)$ and E_f^M relationships on a nucleon composition can be seen from fig.5. The curves are plotted "by eye" through the experimental Γ_n/Γ_f and E_f^M data /38-39, 6, 28,30, 32/ for some nuclei with even Z but these are in mutual agreement. In the upper part of fig.5 shown is one of the lines of the Sikkeland's systematics (5) for Z = 92 being in the best agreement with experiment. The associated straight line within the limits of point scattering fairly describes the E_f^M behaviour for uranium but does not conform to the character of all the family depicted by the dotted lines. Of course, as far as the other (Th,Pu) nuclei are concerned, one can isolate linear parts of the $E_f^M(N)$ dependence with about the same slope. The applicability of traditional systematics (4) and (5) for the Γ_n/Γ_f description for cold nuclei is limited by this region $90 \lesssim Z \lesssim 95$, $140 \lesssim N \lesssim 146$, that is well seen from fig.4.

Thus,in a general case, the $E_f^M(N)$ dependence is fairly complex, therefore, the phenomenology in the way of simple relations (4) and (5) can be justified only in connection with remarkable scattering of the Γ_n/Γ_f data and even then in limits of the narrow Z and N interval. Once more it should be emphasized that the weak and close

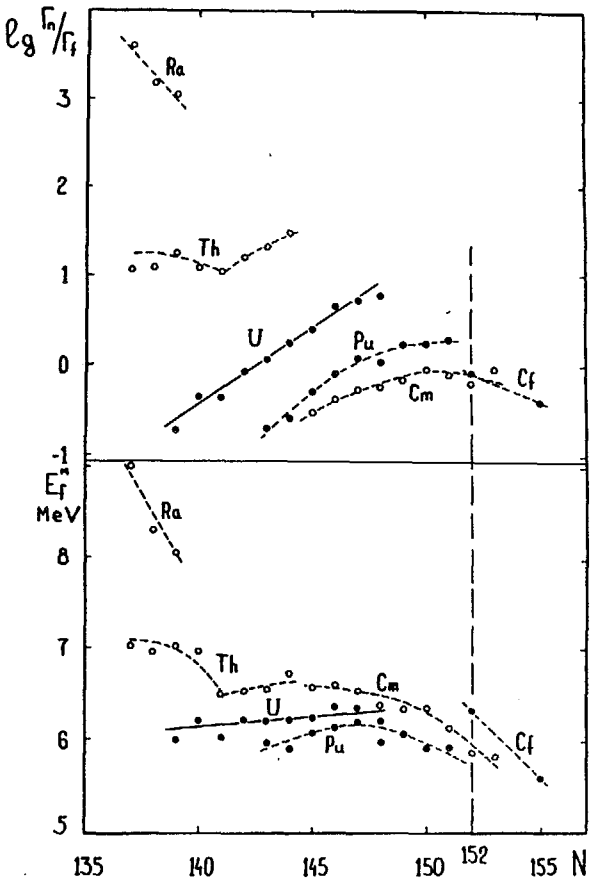

Fig.5. The correlation of the dependences of $\ell g\,(\Gamma_n/\Gamma_f)$ and E_f^M on the number of neutrons in a fissionable nucleus.

to linear $E_f \equiv \widetilde{E}_f$ dependence on N in a liquid-drop model, on the contrary, satisfies these relations. It means that nucleon shells in a fissioning nucleus are responsible for these deviations.

The Γ_n/Γ_f relation is influenced not only by E_f^M but the height of the smallest of humps as well in accord with the G relation in (23). Therefore, the building construction of a new Γ_n/Γ_f

systematics, which we are proceeding to, requires developing a rather simple but at the same time correct description of the E_f^A and E_f^B barrier heights.

5. Simple description of transuranium fission barrier dependence on nucleon composition

The potential deformation energy, $V(\alpha)$ can be represented as a sum of the two components: the liquid-drop energy $\tilde{V}(\alpha)$ and a shell correction $\delta W(\alpha)$; in accordance with this the E_f^A and E_f^B hump heights can be expressed as follows

$$E_f^i = \tilde{V}(\alpha) - \delta W_g + \delta W_f^i \qquad (25)$$

where δW_g is the shell correction for the ground state of nuclear equilibrium deformation counted from the $\tilde{V}(0) = 0$ ground liquid-drop model state, δW_f^i is the shell correction for the i-th maximum $V(\alpha)$ counted from the potential liquid-drop model energy at the appropriate deformation $\tilde{V}(\alpha_i)$ (see fig.6).

The liquid-drop barrier component $\tilde{V}(\alpha)$

In a nuclear fission model in terms of liquid drop widely distributed is the description of a nuclear shape as the expansion by Legendre polynomial. In this parametrization the potential nuclear energy is found to be a hypersurface in the $\alpha_2 \ldots, \alpha_n$ deformation space. However, for the analysis and description of many properties of fairly heavy nuclei including the barrier shell structure it can be restricted by "one dimensional" liquid-drop model which considers only one parameter of the $\alpha_2 = \alpha$ quadrupole deformation, i.e, the $\alpha_n = 0 (n > 2)$ hypersurface cross section.

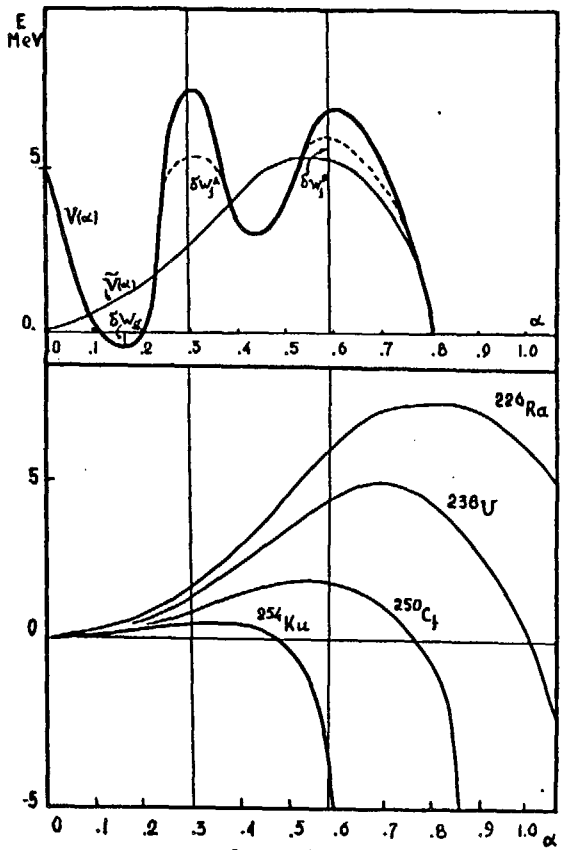

Fig.6. The schematic representation of the double-humped fission barrier structure in the relation of (25).

In this case a nuclear potential energy can be represented as a power series relative to the α variable in which we shall hold the first two terms

$$V(\alpha) = E_{S0}\left[\frac{2}{5}(1-x)\alpha^2 - \frac{4}{105}(1+2x)\alpha^3 + \cdots\right] \qquad (26)$$

$$x = \frac{E_{C0}}{2E_{S0}} = \frac{c_3}{2a_2}\cdot\frac{Z^2}{A}(1-KI^2) \qquad (27)$$

$$E_{s0} = a_2 \cdot A^{2/3}(1-KI^2) \quad , \quad E_{c0} = C_3 \frac{Z^2}{A^{1/3}} \quad , \quad I=(N-Z)/A \qquad (28)$$

where a_2 , C_3 , K are the parameters in the Myers's and Swiatecki's mass formula /41/.

The liquid-drop model barrier calculations

$$\tilde{V} = E_{s0} \xi(x) \qquad (29)$$

in which α_n with the even indices have been held (symmetric forms) up to $n = 18$ are carried out by Cohen and Swiatecki (CS) /42/. The nondimensional function dependence $\xi_{CS}(x)$ tabulated in /42/ in the $(1-x) \ll 1$ up to $x \simeq 0.6$ region, we are interested in, is fairly approximated by

$$\xi_{CS}(x) \simeq (1-x)^3 \cdot [0.7259 - 0.3302(1-x) + 0.6387(1-x)^2 + 7.8727(1-x)^3 - 12.006(1-x)^4] , \qquad (30)$$

which values markedly differ from analogous ones that correspond to the relation resulting from /26/

$$\xi(x) = \frac{98}{15} \frac{(1-x)^3}{(1+2x)^2} \qquad (31)$$

Moreover, the extreme deformations (the s.p. saddle points of the liquid-drop model) differ, too,

$$\tilde{\alpha}_{CS}^{S.P.}(x) \simeq 1.3239(1-x) + 5.5608(1-x)^2 \ldots \qquad (32)$$

$$\tilde{\alpha}_2^{S.P.}(x) = 7 \cdot \frac{1-x}{1+2x} \qquad (33)$$

where the first relation represents an approximation of the calculation results carried out by Cohen and Swiatecki for $1-x \ll 1$ and the second one is an analytical result following from the approach /26/ for $\tilde{\alpha} = f(x)$.

A fit of the α_2 , C_3 , K liquid-drop model parameters to the nuclear masses experimental data that gives the mutually agreed $V(\alpha)$ and δW_g values has been carried out by Myers and Swiatecki /43/ . Later the same authors /41/ having refined the δW_g definition gave a new set of the parameters

$$a_2 = 17.9439 \text{ MeV}; \quad C_3 = 0.7053 \text{ MeV}, \quad K = 1.7826 \qquad (34)$$

which is widely used in calculations.

The approximated relation (26) appreciably overestimates $\tilde{V}(\alpha)$ and in order to reach agreement with experiment the authors of works: Metag et al., Wigman, Theobald /44/ (their simple method for the double-humped barrier structure description is used by us with some improvements) have been forced to select arbitrarily the liquid-drop model parameters at normalizing the δW_g (Z,N) dependence.

We have tried to eliminate the defects these works /44/ by preserving the suitable parametrization (26)

$$\tilde{V}(\alpha) \simeq E_{s0} [C_1(x)\alpha^2 - C_2(x)\alpha^3] \qquad (35)$$

and the realistic parameters (34) but have defined again in (35) the $C_1(x)$ and $C_2(x)$ coefficients, so that with the help of the typical expressions (31),(32), namely,

$$\xi(x) = \frac{4}{27} \frac{C_1^3(x)}{C_2^2(x)} \quad , \quad \tilde{\alpha}^{S.P.}(x) = \frac{2}{3} \frac{C_1(x)}{C_2(x)}$$

one can reproduce the description of the accurate $\xi_{CS}(x)$ and $\tilde{\alpha}_{CS}^{S.P.}(x)$ values.

As a result, the relation (35) is transformed into

$$\tilde{V}(\alpha) = E_{s0} \xi_{CS}(x) \left[\frac{\alpha}{\alpha_{2\,CS}^{S.P.}(x)}\right]^2 \cdot \left[3 - 2\frac{\alpha}{\alpha_{2\,CS}^{S.P.}(x)}\right] \qquad (36)$$

Shell corrections

In a liquid-drop model the barrier is stable relative to the axial symmetry and inversion symmetry disturbances. In case of a real nucleus it is not so. Theoretical calculations performed by the shell correction method show that peaked heights considerably decrease: the A barrier with regard to the γ deformation disturbing nuclear axial symmetry /45/ and the B barrier when involving the

α_n deformation with odd indices, in particular, the α_3 octupole deformation /45,46/. In the $\alpha \sim \alpha_A$ region the nucleus is stable relative to the α_3, α_5 plane-asymmetric deformations. The influence of assumptions about nuclear symmetry nature during fission is shown in fig.6. The solid curve corresponds to the nuclear symmetric configurations ($\gamma = 0$, $\alpha_{2\nu+1} = 0$) and the dashed one corresponds to the real situation. Of course, both these should be understood as the $\min V(\alpha_n, \gamma)$ projections on the $\alpha = \alpha_2$ plane.

The δW_g (Z,N) shell corrections have been calculated according to Myers-Swiatecki /41/ as difference between the M_{exp} experimental mass and the mass calculated from a liquid-drop model formula (taking into consideration even-odd discrepancies)

$$M_{ldm} - \Delta_g \cdot \frac{(-1)^N + (-1)^Z}{2}$$

assuming the A-dependence of the $\Delta_g \simeq 11/A^{1/2}$ parameter averaged over a wide nuclear region. However, the unique $\delta W_{g\,MS}$ values reveal an even-odd structure resulting from the fact that the adopted phenomenologic Δ_g description does not reflect any more complex dependence of this parameter. The "toothed" Γ_n / Γ_f dependence occured does not correspond to experimental data. We have eliminated this effect in such a manner that by analogy with $\langle B_n \rangle$ have introduced a value

$$\langle \delta W_g \rangle = \frac{1}{4} \left[\delta W_g (N-1) + 2\,\delta W_g (N) + \delta W_g (N+1) \right] \qquad (37)$$

averaging even-odd differencies of "experimental" shell corrections of the ground state in the M-S work /41/.

For building the fission barrier systematics, as it follows from the relation (25), it is necessary to set up empirically the law of changing of two δW_f^A and δW_f^B shell corrections with a number of nucleons (fig.6). For this purpose we shall take advantage of the weak α_A and α_B extreme deformation dependence on nucleon composition in the Z and N regions of interest resulting from the curves in fig.7 and other theoretical calculations /45,47/. We have ignored it at all, having taken the constant $\alpha_A = 0.30$ and $\alpha_B = 0.58$ values as is shown in figs 6,7 by thin solid lines (in calculations we usually use the other parameter of the $\epsilon \simeq 3/2\,\alpha$ quadrupole deformation; it varies in the $\epsilon_A \simeq 0.4$-0.5, $\epsilon_B \simeq 0.8$-0.9 limits for the most nuclei of interest).

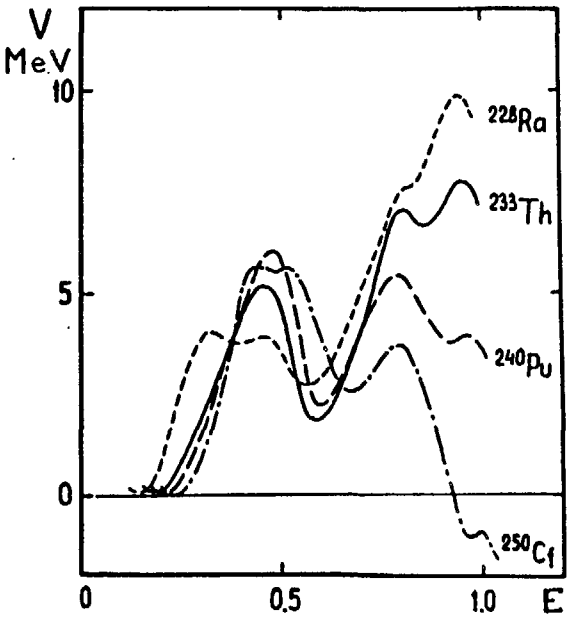

Fig.7. The fission barrier structures for different nuclei (the calculated ones). It is seen the wean dependence of extreme deformations of $\epsilon = 3/2\,\chi$ on the nucleon composition of a nucleus.

Knowing the $\tilde{V}(\alpha_1)$ and $\langle \delta W_g \rangle$ values from the relation (25) and the E_f^i experimental data /30,32,38,39,48,49/ one can determine the δW_f^i shell corrections. At the first stage we have assumed

these to be constant but then for refining this description we have introduced the weak dependence on Z and N

$$\delta W_f^A(Z)\,[\mathrm{MeV}] = \begin{cases} 2{,}6 & Z \le 97 \\ 2{,}6-0{,}1(Z-97) & Z > 97 \end{cases}$$

$$\delta W_f^B(Z)\,[\mathrm{MeV}] = \begin{cases} 0{,}6+0{,}1(Z-97) & Z \le 97 \\ 0{,}6 & Z > 97 \end{cases} \qquad (38)$$

$$\delta W_f^B(Z,N)[\mathrm{MeV}] = \delta W_f^B(Z,N_0) + 0{,}04(N-N_0)\,, \quad N_0=143$$

which markedly improved the description of both the E_f^i barrier heights and the Γ_n/Γ_f ratio in the $Z>92$ region.

Notice, that at $\Delta_f \neq \Delta_g$ the relation (25) in accordance with (19) should be applied for describing the A-odd fissionable nuclei, but, in general, it should be supplemented with a discrete summand in accord with the formula (20). The given systematics assumes

$$\Delta_f^A = \Delta_f^B = \Delta_g + 0{,}2\ [\mathrm{MeV}] \qquad (39)$$

Discussion

The E_f^A and E_f^B calculation results according to the formulas (25), (36)-(39) with the parameters mentioned above are given in table 1 (columns 4,5) where these are compared with the E_f^i experimental values (columns 6,7) taken from the compilation /38/ and for the Bk - Fm region from the works /39,40/. The similar results are shown in figs 8,9 for nuclei in the vicinity of $\Delta N = \pm 10$ of what might be called the valley of stability /43/.

$$N - Z = 0{,}4\ A^2/(A+200) \qquad (40)$$

These ones are given in fig. 8 in a compact and more suitable for discussion form, in terms of the E_f^i dependence on nucleon composition. In fig. 9 the calculation results are compared with experimental ones obtained from the analysis of the various Ra-Es heavy nuclei fission probability characteristics.

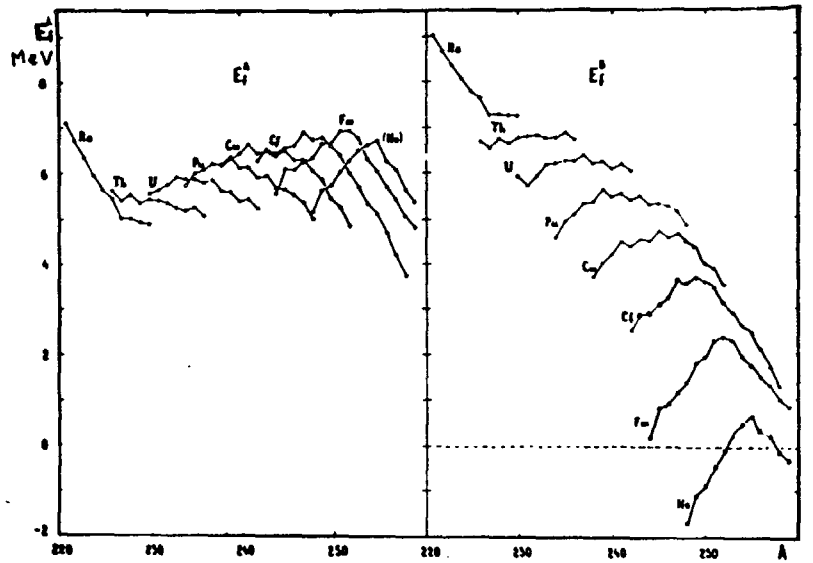

Fig.8. The dependence of fission barriers on the mass number of A in the region of stability valley.

The E_f^B outer hump height is very sharply dependent on the nucleon composition of nuclei, particularly, on Z. On the contrary, the E_f^A inner hump height changes with Z and N more weakly. The heavy nucleus region is divided by uranium into two groups characterized by different hump height ratios:

$$E_f^A < E_f^B \qquad Z \le 92$$
$$E_f^A > E_f^B \qquad Z > 92 \qquad (41)$$

The E_f^i properties mentioned above directly result from dependence of $\tilde{V}(\alpha_A)$ liquid-drop model barrier component on the X fissionability parameter (27) as is shown in fig.6. If the $\tilde{V}(\alpha_A)$ decrease from Ra to Fm is accounted for ~ 1.5 MeV and compensated for with an excess by δW_g shell correction increase, then in this case $\tilde{V}(\alpha_B)$ decreases by a factor of 5. In the E_f^A and E_f^B value behaviour markedly re-

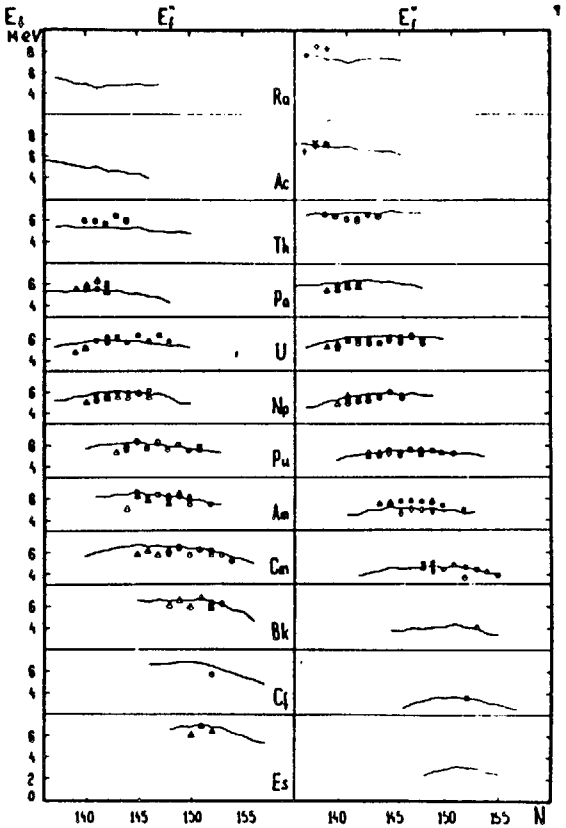

Fig.9. The dependence of fission barriers of E_f^i on the number of neutrons of N. Experimental points: ▲ - /32/ ■ - /38/, ● - /48/, ◆ - /39/, × - /30/, + - /49/.

vealed is the δW_g (Z,N) ground state shell structure. The E_f^i maximum in the $Z > 98$ region is connected with the $N = 152$ sub-shell filling-up; when approaching the $N = 126$ sub-shell we can see a sharp rise of E_f^i near Ra.

The agreement between the E_f^i calculated values and the experimental ones over a set of the $Z \geqslant 92$ nuclei is characterized by the root-mean-square $\Delta E_f^A = \Delta E_f^B = 0.26$ MeV deviations that are comparable with the 0.3 - 0.5 MeV scatter calculated similarly by different authors and the given 0.2 - 0.3 MeV uncertainty in the barrier determination.

There are a few methods for the determination of heavy nucleus barrier hump height. Thus, the near-threshold fission cross section region contains the most direct information on the greatest $E_f^M = \max\left\{E_f^A, E_f^B\right\}$ hump height. Often according to a characteristic break resulting from the sharp exponential barrier penetrability drop at $E \lesssim E_f^M$ one can evaluate the E_f^M value with accuracy up to some hundreds of keV without recourse to the δ_f (E) behaviour analysis. The more effective methods for the E_f^B outer hump height determination has proved to be the spontaneously fissioning isomer excitation functions. Therefore, in the region of distributing the latter ($Z > 92$) where $E_f^A > E_f^B$ the data on both hump heights are more reliable. Note, that in the E_f^i theoretical calculations /45,46/ in the $Z \geqslant 92$ region a fair description is attained of the available experimental data.

The $E_f^A \lesssim E_f^B$ inverse relation realized in the $Z \lesssim 92$ region is far less favourable, particularly, when the hump height difference is not great. Here, there are no reliable methods for the determination of the smaller humps and at selecting considered parameters one should be governed by the more indirect information: the vibrational resonances position /32/. In this connection it is appropriate to remember about the "thorium anomaly" where the theoretical calculations /45,46/ predict the E_f^A values for Th being considerably less than the experimental ones extracted from the analysis.

Table 1.

Experimental data and calculation results accoding to the systematics, barrier heights E_f^i, Γ_n/Γ_f values and fission cross sections σ_f.

Z	A compound nucleus	$\langle B_n \rangle$, MeV	calculation E_f^A, MeV	calculation E_f^B, MeV	experiment E_f^A, MeV	experiment E_f^B, MeV	calculation Γ_n/Γ_f	calculation σ_f, barn	experiment(n,f)-reaction Γ_n/Γ_f	experiment(n,f)-reaction σ_f, barn	N° reference	experiment, direct react. Γ_n/Γ_f	experiment, direct react. σ_f, barn	N° reference
1	2	3	4	5	6	7	8	9	10	11	12	13	14	15
	229	6.89	5.20	4.97			0.03	2.91						
	230	6.83	5.15	4.97			0.06	2.86						
	231	6.68	5.48	5.25			0.09	2.78				0.19	2.55±0.43	32
U	232	6.54	5.40	5.34	5.2	5.1	0.19	2.55				0.43	2.12±0.23	32
	233	6.40	5.71	5.74			0.36	2.24	0.38	2.20±0.30	11			
	234	6.18	5.53	5.65	5.6	5.5	0.66	1.84	0.67	1.83±0.07	12.13			
	235	6.00	5.70	5.92	5.9	5.6	1.06	1.49	1.06	1.49±0.06	14	1.32	1.32±0.20	31
	236	5.88	5.47	5.80	5.6	5.5	1.51	1.22	1.52	1.22±0.04		1.62	1.17±0.18	31
	237	5.73	5.62	6.08	6.1	5.9	2.29	0.94	2.46	0.89±0.03	14	2.93	0.78±0.12	31
	238	5.55	5.30	5.90	5.7	5.7	3.32	0.72				4.26	0.59±0.09	31
	239	5.42	5.38	6.13	6.3	6.1	4.48	0.56	4.74	0.54±0.02	12.14			
	240	5.32	5.08	5.98	5.7	5.5	5.89	0.45				5.32	0.49±0.08	31
	241	5.22	5.20	6.27			8.54	0.33						
	242	5.09	4.90	6.15			12.9	0.22						
	243	5.00	5.02	6.48			19.8	0.15						
	231	7.10	5.28	4.32			0.01	2.99						
	232	6.96	5.69	4.86			0.03	2.95						
	233	6.77	5.63	4.93			0.06	2.87				0.24	2.46±0.32	32
Np	234	6.64	5.97	5.39	5.5	5.1	0.12	2.73				0.21	2.52±0.28	32
	235	6.46	5.87	5.41	5.5	5.2	0.24	2.48				0.34	2.29±0.27	32
	236	6.25	6.08	5.73	5.8	5.6	0.42	2.17				0.36	2.26±0.27	32
	237	6.10	5.87	5.63	5.7	5.4	0.62	1.90				0.65	1.87±0.24	32
	238	5.95	6.03	5.91	6.1	6.0	0.91	1.62	0.94	1.59±0.05	12.15	0.84	1.68±0.25	32
	239	5.77	5.74	5.73	5.9	5.4	1.26	1.37				1.33	1.33±0.13	32
	240	5.63	5.83	5.92			1.56	1.22						
	241	5.46	5.46	5.66			1.88	1.08						
	242	5.25	5.40	5.70			2.00	1.04						
	243	5.15	4.97	5.37			1.80	1.12						
	235	6.90	5.79	4.63		5.1	0.05	2.92						
	236	6.71	5.73	4.69		4.5	0.10	2.78						
	237	6.52	6.01	5.10			0.19	2.58				0.16	2.65±0.42	32
Pu	238	6.38	5.87	5.08	5.5	5.0	0.31	2.36				0.31	2.36±0.31	32
	239	6.21	6.09	5.42	6.2	5.5	0.50	2.07	0.36	2.28±0.13	16.17			
	240	5.99	5.82	5.26	5.6	5.1	0.74	1.79	0.67	1.86±0.06	12.18			
	241	5.83	5.91	5.47	6.1	5.4	0.92	1.62	0.87	1.67±0.06	12.18	1.31	1.35±0.20	31
	242	5.72	5.61	5.28	5.6	5.1	1.06	1.51	0.99	1.57±0.05	12.18	1.41	1.30±0.20	31
	243	5.60	5.70	5.48	5.9	5.2	1.25	1.40	1.27	1.38±0.05	12.18			
	244	5.45	5.37	5.25	5.4	5.0	1.48	1.27				1.64	1.19±0.18	31
	245	5.35	5.45	5.44	5.6	5.0	1.66	1.18	1.65	1.19±0.05	18			
	246	5.24	5.15	5.23			1.93	1.08						
	247	5.03	5.14	5.32			2.26	0.97						
	237	6.99	6.08	4.44			0.07	2.89						
	238	6.77	6.41	4.90			0.14	2.72						
	239	6.58	6.28	4.89	6.2		0.24	2.51				0.31	2.36±0.33	32
	240	6.39	6.48	5.22	6.5	5.2	0.36	2.28				0.34	2.32±0.28	32
Am	241	6.21	6.23	5.09	6.0	5.1	0.49	2.09				0.62	1.92±0.21	32
	242	6.04	6.33	5.31	6.5	5.4	0.60	1.95	0.64	1.91±0.07	12.15	0.56	2.00±0.26	32
	243	5.91	6.02	5.12	5.9	5.4	0.67	1.88	0.73	1.81±0.18	19.20	0.70	1.84±0.20	32
	244	5.79	6.11	5.32	6.3	5.4	0.74	1.81	0.68	1.87±0.07	15	1.55	1.23±0.17	32
	245	5.63	5.76	5.08	5.9	5.2	0.82	1.73				1.66	1.18±0.13	32
	246	5.46	5.76	5.19			0.84	1.72						
	247	5.26	5.28	4.82	5.5		0.80	1.76						
	248	5.04	5.10	4.74			0.64	1.93						

Table 1. (cont.)

I	2	3	4	5	6	7	8	9	I0	II	I2	I3	I4	I5
	239	7.00	6.I4	4.00			0.07	2.90						
	240	6.86	6.09	4.08			0.I2	2.76						
	24I	6.66	6.36	4.48	6.3	4.3	0.22	2.56				0.32	2.37± 0.3I	32
Cm	242	6.43	6.I2	4.37	5.8	4.0	0.32	2.36				0.42	2.20± 0.24	32
	243	6.29	6.28	4.65	6.4		0.40	2.24				0.7I	I.83± 0.26	32
	244	6.20	6.07	4.57	5.8	4.3	0.48	2.I2	0.37	2.30± 0.30	2I	0.58	I.99± 0.22	32
	245	6.07	6.25	4.87	6.2		0.62	I.95	0.72	I.83± 0.I3	22.23			
	246	5.89	5.97	4.7I	5.7	4.2	0.78	I.77	0.47	2.I5± 0.26	2I			
	247	5.74	6.06	4.9I	6.0		0.89	I.68	0.96	I.62± 0.I0	22.23			
	248	5.57	5.70	4.67	5.7		0.96	I.62	0.I4	2.80± 0.70	2I			
	249	5.35	5.64	4.7I	5.6		0.93	I.65	0.99	I.60 ± 0.I4	33.34			
	250	5.I9	5.I3	4.3I	5.3		0.74	I.83						
	25I	5.08	5.02	4.3I			0.54	2.08						
	243	6.70	6.28	3.89			0.I6	2.69						
	244	6.54	6.48	4.23			0.22	2.58						
	245	6.5I	6.38	4.25	6.4		0.29	2.44				I.I2	I.48± 0.2I	32
Bk	246	6.38	6.68	4.67	6.5		0.47	2.I5				0.99	I.59± 0.I8	32
	247	6.I5	6.46	4.58	6.5		0.73	I.83				0.8I	I.75± 0.23	32
	248	5.98	6.59	4.83	6.3		0.92	I.66				I.23	I.42± 0.23	32
	249	5.72	6.I8	4.53	6.I		I.03	I.57				I.05	I.55± 0.22	32
	250	5.44	6.0I	4.48	6.I	4.I	0.87	I.7I	I.02	I.58 ± 0.II	24			
	25I	5.27	5.38	3.96			0.54	2.08						
	252	5.I2	5.I2	3.82			0.30	2.48						
	253	5.00	4.46	3.26			0.I6	2.79						
	254	4.90	4.2I	3.I2			0.08	2.98						
	246	6.74	6.I8	3.40			0.I8	2.67						
Cf	247	6.6I	6.5I	3.86			0.3I	2.42						
	248	6.38	6.32	3.80			0.50	2.II						
	249	6.I8	6.46	4.06			0.66	I.9I						
	250	5.98	6.I2	3.85	5.5		0.74	I.83	0.70	I.88 ± 0.I2	25.26			
	25I	5.75	6.07	3.92	6.2		0.72	I.86						
	252	5.56	5.54	3.5I	5.3		0.56	2.06						
	253	5.43	5.4I	3.49	5.3		0.37	2.34	0.29	2.50 ± 0.30	27			
	254	5.34	4.90	3.09			0.24	2.60						
	255	5.23	4.79	3.09			0.I7	2.77						
	256	5.04	4.20	2.6I			0.II	2.9I						
	257	4.85	3.93	2.45			0.07	3.05						
	245	7.23	5.87	2.I2			0.02	3.08						
	246	7.06	6.20	2.59			0.04	3.02						
	247	6.97	6.I6	2.69			0.07	2.95						
	248	6.86	6.53	3.2I	6.8		0.I3	2.8I						
Es	249	6.76	6.54	3.35	6.7		0.24	2.57				0.84	I.96± 0.3I	32
	250	6.56	6.86	3.80			0.45	2.20				0.54	2.33± 0.33	32
	25I	6.I8	6.52	3.59	6.6		0.74	I.84				0.62	2.2I± 0.29	32
	252	5.89	6.4I	3.6I			0.7I	I.88						
	253	5.7I	5.84	3.I6			0.49	2.I6						
	254	5.56	5.63	3.08			0.29	2.50						
	255	5.46	5.04	2.60	5.4		0.I6	2.78						
	256	5.30	4.82	2.49	4.8		0.I0	2.96						
	25I	6.76	6.38	2.63			0.I7	2.73						
	252	6.54	6.2I	2.59			0.29	2.49						
	253	6.20	6.22	2.74			0.39	2.32						
Fm	254	5.94	5.69	2.33			0.34	2.4I						
	255	5.8I	5.55	2.32	5.7		0.22	2.65						
	256	5.72	5.04	I.94			0.I4	2.84						
	257	5.6I	4.93	I.95			0.I0	2.97						
	258	5.50	4.42	I.56			0.06	3.06						

The considerable difficulties arise in the light actinide region and at the determination of the B barrier height. At present there is an opinion based on both the theoretical estimations and the experimental data analysis that in the $Z \lesssim 92$ region a significant change of a barrier structure takes place, which is merely far from being reduced to the sign change in inequality of (41). The theoretical calculations /45,50/ show that an oscillating nature of the shell correction in case of the light ($Z < 92$) nuclei results in somewhat like the B outer hump splitting and the three-peaked barrier structure appearance. This barrier structure with the two intermediate minima and three maxima calls in question not only the sub-barrier fission cross section resonances analysis (since it is not known with what states of barrier minima these ones are connected) but the estimations of the greatest hump height too.

The new and imperfectly investigated properties of light actinides convince us that the region of the given E_f^A and E_f^B systematics application should be limited at the bottom by the $Z \geqslant 92$ region. Moreover, the introduction of uranium into this systematics gave rise to certain difficulties, since, due to the approximate equality of two maxima over height and the possible B barrier structure for U-isitopes, one failed to describe the $\delta W_f^B(Z,N)$ value in the frame of universal dependence (38). Correlation of the calculated values in systematics with the U-isotopes experimental data has required adding of a term being square dependent on N into the last relation (38)

$$\delta W_f^B(Z,N) = \delta W_f^B(Z,N_0) + 0{,}04\,(N-N_0) + 0{,}007\,(N-N_0)^2,\quad N_0 = 143$$

It should be expected that in the "pure" double-humped barrier structure region the phenomenologic $E_f^i(Z,N)$ description obtained by us will lose accuracy when removed from the valley of stability where the group of experimentally investigated isotopes is concentrated. Among the factors which result in this inevitable for semiempiric systematics effect aside from the apparent ones being connected with simplifying a real pattern it is necessary to note the inaccuracy of used parameters and the model itself employed to describe the uniform $\tilde{V}_f(\alpha,x)$ component. We believe that using this systematics one should not go from the valley of stability over N by more than 10 units.

6. The Γ_n/Γ_f ratio systematics and (n,f)-reaction cross section description

Rewrite (23) in the more modified form:

$$\Gamma_n/\Gamma_f = G_A \cdot \exp\left[\frac{E_f^A - \langle B_n\rangle}{T}\right] + G_B \cdot \exp\left[\frac{E_f^B - \langle B_n\rangle}{T}\right] \qquad (42)$$

$$G_i = \frac{2T\,A^{2/3}}{\partial\varepsilon} \cdot \exp\left[\frac{\Delta_f^i - \Delta_g}{T}\right]$$

For creating the Γ_n/Γ_f systematics it is necessary to determine the G_A and G_B coefficients in (42) from the E_f^i and B_n values calculated in the previous section by fitting (42) to the Γ_n/Γ_f experimental values.

For this purpose the Γ_n/Γ_f ratios obtained from the neutron fission cross section have been used alone since these are measured with high accuracy and, except for individual values, the Γ_n/Γ_f extracted from σ_f are mutually well agreed within the investigated nucleus region. The attempt to use for this fitting the Γ_n/Γ_f values obtained from measurement of fissionability in the direct reactions because of the poor data precision results in large scattering of these data and the fit found to be less definite.

The experimental data are presented in table 1 of column 11 either as the reference work results or the results averaged from the two works (the references are presented in table 1 of column 12) characterized by the highest precision. Whenever possible, these results are averaged over the E_n = 2 - 4 MeV region. If the reference works presents the fission cross section ratios, then, as a standard, the σ_f (^{235}U) value being equal to 1.22 barn obtained by averaging the ENDF/B-V evaluation for ^{235}U over the energy region of E_n= 2-4 MeV has been used.

The σ_f uncertainties presented in table 1 assume the standard error to be equal to 3%.

As for extracting the Γ_n / Γ_f value from σ_f as consistent with (2), the data are needed about the neutron compound nucleus formation cross section. The estimation of the σ_{CN} value can be carried out according to the unified optic model calculation /51/

$$\sigma_{CN} = \sigma_t - \sigma_{sel} - \sigma_{2^+} - \sigma_{4^+} \qquad (43)$$

where σ_t is the total cross section, σ_{sel} is the shape elastic cross section (elastic scattering across the compound nucleus is negligible and ignored), σ_{2^+} and σ_{4^+} are the direct inelastic scattering cross sections at the lower-lying vibration levels of the even-even target-nucleus. Another possibility of estimating σ_{CN} is by identifying it with the total inelastic cross section

$$\sigma_{CN} \simeq \sigma_{nn'} + \sigma_f + \sigma_{n\gamma} \qquad (44)$$

where $\sigma_{nn'}$ is the neutron inelastic scattering cross section minus the direct inelastic scattering at the 2^+ and 4^+ levels, $\sigma_{n\gamma}$ is the radiative capture cross section. The partial cross sections in (44) are known well enough from evaluating the nuclide constants of importance for nuclear power engineering, in particular, ^{238}U /52,53/.

Table 2.

(^{238}U + n) compound nucleus formation cross section in the E_n = 2 - 4 MeV region

Data of works	/10/	/11/	/12/	Adopted value
σ_{comp}, barn	3.22	3.06	3.10	3.10

The appropriate data for the E_n = 2 - 4 MeV energy range listed in table 2 allows us to adopt for the A mass number target-nucleus

$$\sigma_{CN}(A) = \sigma_{CN}(^{238}U) \cdot \left(\frac{A}{238}\right)^{2/3}$$
$$\sigma_{CN}(^{238}U) = 3,1 \cdot barns \qquad (45)$$

The Γ_n / Γ_f values extracted from the σ_f experimental values with due regard to (45) are presented in table 1 (column 10).

The procedure of fitting relation (42) to the Γ_n / Γ_f experimental values is shown in fig.10. At $E_f^{max} \equiv E_f^A > E_f^B = E_f^{min}$ to be carried out for the $Z \geqslant 93$ nuclei when the argument $\exp\left(\frac{E_f^{min} - E_f^{max}}{T}\right)$ values are equal to 0 or 1 (abscissae), the ordinate takes the G_A and $G_A + G_B$ values, respectively (the extreme values at the lower-lying straight line are plotted by the least squares method through

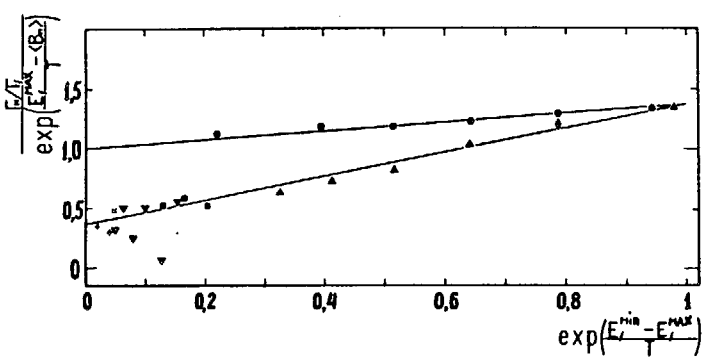

Fig.10. The determination of the G_A and G_B values according to the relation of (42) from the experimental values of Γ_n/Γ_f (see the text).

the experimental Np - Cf nucleus values). For the U nuclides the barrier ratio is inversed to $E_f^{min} = E_f^A < E_f^B = E_f^{max}$. In accord with this at the argument values to be of 0 or 1 the ordinate takes the G_B and $G_B + G_A$ values (the extreme values at the upper straight line are plotted through the experimental U-nuclide values). In consequence of fitting, the values

$$G_A = 0.37 \text{ and } G_B = 1.00$$

are obtained that correspond to the $C_n/C_f^A = 0.064$ and $C_n/C_f^B = 0.174$ values.

The Γ_n/Γ_f and σ_f values calculated using the G_A and G_B constants are presented in table 1 (columns 8,9, respectively).

As is seen from fig.11 the systematics (the calculated σ_f values for different nuclei are connected by solid line) are compared with the experimental σ_f data, the neutron fission cross sections "derived" from measurements of fissionability in the direct reactions /31, 32/ using the values in accordance with (45) as well as the systematics by Behrens /5/ (the dashed line).

In table 3 for the three investigated nuclear region spaces the value is given

$$\chi^2 = \sum_{i=1}^{n} \left[\frac{\sigma_{fi}^{exp.} - \sigma_{fi}^{syst.}}{\sigma_{fi}^{syst.}} \right] \qquad (46)$$

to serve as the agreement criterion between the systematics and the experimental data: at fair description $\chi^2/n \sim 1$ where n is the number of the points considered. It follows from table 3 and fig.11 that the given systematics describes favourably, on the whole, the neutron fission cross sections throughout the nuclear region.

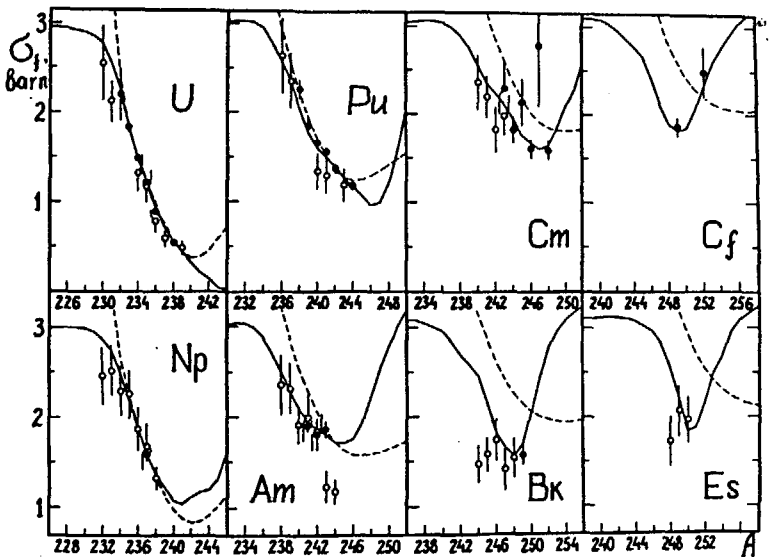

Fig.11. The comparison of the neutron fission cross-sections values calculated according to the present systematics for E_n=2-4MeV with the experimental ones. The black points are the data measured in the (n,f) reaction: the light points are the results "simulated" from the fissionability measurements in the direct reactions. The solid line is the present systematics (a calculation), the dashed line is the systematics by Behrens /5/ (a calculation).

Comparison with the direct reaction data

The direct reactions are widely used for investigating low-energy fission allowing us to measure P_f fissionability value weakly dependent on the inlet channel properties throughout a distribution of the angular momenta transmitted to the nucleus. This condition allows us to use the data for evaluating and predicting σ_f for a wide nuclear region unaccessible for direct measurements in (n,f) reaction.

Table 3.

Fission cross section systematics χ^2/n criterion fit to experimental data

Z		(n,f)-reaction data		direct reaction data		Sum of data	
		present work	/15/	present work	/15/	present work	/15/
92-94	n	13	13	19	19	32	32
	χ^2/n	0.8	1.4	0.8	8.5	0.8	5.6
95,96	n	9	9	11	11	20	20
	χ^2/n	0.9	7.9	3.1	6.4	2.1	7.1
97-99	n	3	3	8	8	11	11
	χ^2/n	0.6	21.2	4.7	28.2	3.6	26.3
92-99	n	25	25	38	38	63	63
	χ^2/n	0.8	6.1	2.3	12.0	1.7	9.7

Such the attempts are undertaken in the works by Britt et al.(in /32/ from the experimental P_f data for (^{3}He, xf) reactions x = d or t , in /31/, for (t,pf) reaction). However, it is impossible to take these ones without supplementary analysis due to conflicting assumptions about the fast neutron compound nucleus formation cross section value needed for fitting direct reaction results to neutron data: σ_{CN} =3.1 barns for all the nuclei in case of (^{3}He,xf) reaction /32/ and considerably higher in (t,pf) reaction, σ_{CN} =3.7 barns /31/. This discrepancy can not be connected with some difference in the values being equivalent in neutron energy excitation: 2-4 MeV in /32/ and 2-2.25 MeV in /31/, the σ_{CN} = 3.1 barns in /32/ is adopted for E_n = 1-5 MeV region. For the most part, the discrepancy in

Table 4.

The mean square angular momenta $\overline{J(J+1)}$ values at the exitation energies being equivalent to E_n= 2-4 MeV and fission probability correction ranges.

Reaction	$\overline{J(J+1)}$	Fission probability correction
n,f	10.8	-
^{3}He,df	15.8	0.2 - 2.5%
t,pf	28.6	6.5 - 13%

the σ_{CN} value in these two cases is explained by the J-dependence of Γ_n/Γ_f not taken into consideration and its effect on fissionability.

In table 4 listed are the mean square $\overline{J(J+1)}$ angular momenta values transmitted to the nucleus in the (n,f), (^{3}He,df) and (t,pf) reactions according to /54/ at the excitation energies being equivalent to E_n = 2÷4 MeV as well as the fissionability correction ranges due to difference in the angular momenta transmitted in (t,pf) and (^{3}He,df) reactions, on the one side, and (n,f)-reaction, on the other side. From the table it follows that for (n,f) and (^{3}He,df) reactions the $\overline{J(J+1)}$ values slightly differ and this leads to the negligible correction which decreases with the Z nucleus growth (at the same time increases with the N growth for fixed Z). In the (t,pf)-reaction the mean square angular momentum is considerably greater and this leads to the prominent P_f decrease (i.e., the increase in correction) in comparison with the similar nucleus fissionability in previous cases, explaining to a greater extent why for agreement with the neutron data in /31/ one has to take the unreasonably large C.N. formation cross section.

In fig.11 and table 1 (column 13) given are the fission cross section data "simulated" from fissionability measurements in the (^{3}He,xf) and (t,pf) reactions with regard to difference in the angular momenta transmitted to the fissioning nucleus. The σ_{CN} values in accord with (45) have been used for calculating. The errors presented in table 1 (column 14) involve the experimental errors and the uncertainty in the σ_{CN} value evaluated to be 10%. As it follows from table 3 the inclusion of these data into consideration in accord with (46) does not make considerably worse the agreement criterion between the systematics and the experiment.

Notes on empirical systematics by Behrens /5/

In fig.11 the σ_f systematics is compared with the empiric systematics by Behrens /5/. Here we do not consider the absolute fission cross sections but the ratio of these ones to σ_f (^{235}U), which have been presented as combinations of the third order polynomials, the eight coefficients of which are found by fitting to the neutron data set. The dashed curve representing in fig.11 the systematics /5/ is obtained by renormalization to the σ_f = 1.22 barn value for ^{235}U in the energy range of E_n = 2-4 MeV (in /5/ the averaging has been carried out through the energy 3-5 MeV region for which σ_f (^{235}U) = 1.16 barns). Thus, the present systematics and the Behren's results /5/ have been reduced to the uniform standard.

Both systematics give the close, consistent with experiment values for the U-Pu nuclei in the vicinity of the valley of the most stability where the most precise neutron data are concentrated. When going away from it, in particular, into the neutron-deficient region, as well as with the Z growth, the agreement is disturbed and in this case the systematics /5/ considerably differs from experimental data. At the sufficiently great deficiency of neutrons the Behrens's systematics from the physical point of view gives a meaningless result of $\sigma_f > \sigma_{CN}$. This is not fundamental disadvantage, since it is readily eliminated following the σ_f determination through the Γ_n/Γ_f ratio according to (2). As is seen from table 3 the discrepancy is more appreciable between the systematics /5/ and experimental data for the nuclei heavier than curium, here this one can be discarded as inconsistent with the experiment. The description proposed in this work corresponds to the experimental data throughout the nuclear range studied. The relative mean square error in this systematics

$$\varepsilon = \left[\frac{1}{n} \sum_{i=1}^{n} \left(\frac{\sigma_{fi}^{exp} - \sigma_{fi}^{syst.}}{\sigma_{fi}^{syst.}} \right)^2 \right]^{1/2} \qquad (47)$$

for the experimental n = 63 points in the U-Es region has accounted for 15%, this satisfies requirements for the "exotic" nuclide fission cross section accuracy. The developed description can be used for estimating or predicting the σ_f, E_f^i and Γ_n/Γ_f values in case the experimental data are not available or discrepant.

7. On the heated heavy nucleus fission probability

Let us return to the problem of traditional systematics which, as we have noted, in the region of heavy actinides is completely based on the multiple neutron emission probability experimental data for which the excitation energy averaged over evaporation chain is considerably higher than that considered in previous sections (the first fissionability plateau). At the top of fig.12 these data defined by the Γ_n/Γ_f value and averaged over a cascade in accord with (3) are compared with the direct experimental Γ_n/Γ_f data and its description obtained for the "cold" nuclei. The experimental information presented at

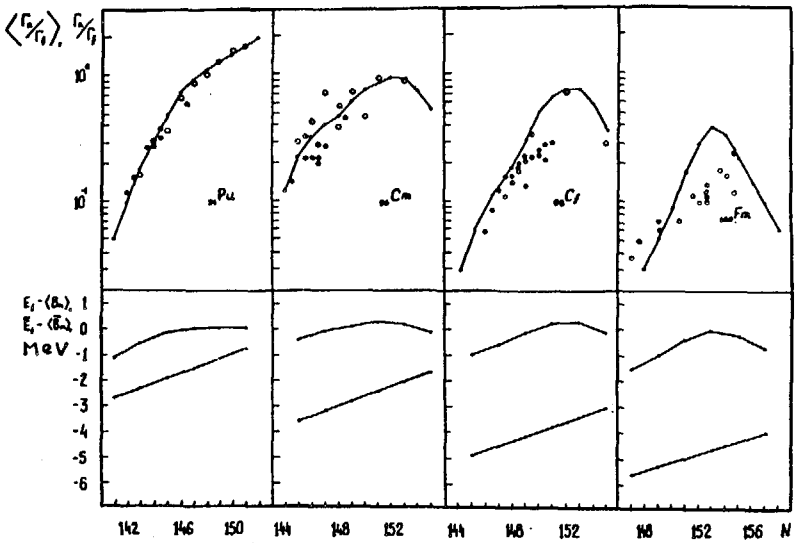

Fig.12. At the top is the ratio of $(\Gamma_n/\Gamma_f)_{cold}$: o is the experiment, the values are obtained from the fissionability of P_f; curves are the present systematics; the ratio of the Γ_n/Γ_f : ● are the experimental data of the (HI,xn) reaction, ◑ are the data of (α,xn). At the bottom are the $E_f - \langle B_n \rangle$ and $\widetilde{E}_f - \langle \widetilde{B}_n \rangle$ threshold differencies. On the abscissa axis is the number of neutrons N in the nucleus, for $\langle \Gamma_n/\Gamma_f \rangle - \overline{N}$.

the top of fig.12 is:

(a) the $(\Gamma_n/\Gamma_f)_{cold}$ values obtained from P_f (see, table1) (light signs);

(b) the $\langle \Gamma_n/\Gamma_f \rangle$ values obtained from σ_{xn} for the $A \leq 4$ light charged particles reactions /3/ (half-shaded signs);

(c) the $\langle \Gamma_n/\Gamma_f \rangle$ values obtained from /3,55-57/ for the (HI,xn) heavy ion reactions being lighter than neon (shaded signs);

(d)(the curves) the $(\Gamma_n/\Gamma_f)_{cold}$ systematics according to table 1.

Of the experimental information presented in fig.12 typical is a great variety of the C.N. excitation methods and a wide spectrum of the $\overline{l}$ transmitted angular momenta. However, because we have been restricted to the (HI,xn) reactions with not heavy ions the factor mentioned above does not play any valid part. The same fig.12 is a confirmation for the mentioned above from which it follows that the difference in the $\langle \Gamma_n/\Gamma_f \rangle$ values obtained in the (α,xn) and (HI,xn) reactions strongly differing by the $\overline{l}$ value is comparable with the similar experimental points scattering.

The consideration of experimental data presented in fig.12 shows that the discrepancy between the cold and heated nuclei with the Z growth is increased as the shell contribution into E_f rises, attaining the greatest value in the Γ_n/Γ_f peak for Fm corresponding to the $\delta W_g < 0$ shell correction minimum and the $N = 152$, $Z \simeq 100$ closed deformed shell. The $lg\langle \Gamma_n/\Gamma_f \rangle$ value does not reveal the $lg(\Gamma_n/\Gamma_f)_{cold}$ structure monotonously increasing in the scatter limits approximately according to the linear law as is prescribed by traditional systematics /4/.

From the mentioned above it is clear that the nature of considered discrepancies is connected with shell effects and the changing of this influence on the E_f, B_n parameters and, as a result, on the Γ_n/Γ_f ratio. Consider this problem in some detail since we are not interested in it only in connection with interpretation of experimental data and the Γ_n/Γ_f systematicses but also in a wider scope, i.e. from the viewpoint of investigating shell reconstructions with excitation energy increase.

The influence of shell effects on the Γ_n/Γ_f value as well as on other excited nucleus decay characteristics is decreased as the excitation energy increases. From the theoretical considerations of the heated nucleus shell reconstruction phenomenon carried out by Strutinsky and Kolomiyez /58/, as well as by Bohr and Mottelson /59/, it follows that at the $U \simeq 50$ MeV excitation energy the shell nonuniformities have practically disappeared and the nucleus has become the good object for describing in terms of the liquid-drop nuclear model. In particular, the Γ_n/Γ_f ratio at such the energies should behave as if fission is blocked by the barrier of the nuclear liquid-drop model considerably differing according to shape and height from the cold nucleus fission barrier. This theoretical prediction has been examined on light nuclei in the $N = 126$ spherical shell region in /60,61/. Heavy actinides in the vicinity of the $N = 152$ deformed shell have been investigated from the view point mentioned above in /62/ but with very limited experimental material.

As for the question considered in this work, the decisive significance belongs to the bond, investigated in /58,59,63/, of the $S(U)$ nucleus entropy energy dependences and the $a(U)$ level density parameter in a Fermi-gas model with the δW shell correction value for the $\tilde{V}$ nuclear potential energy in the liquid-drop model.

Energy dependence of the a parameter is introduced by the relation

$$a(U) = \tilde{a}\left[1 + \delta W \frac{f(U)}{U}\right], \quad f(U) = 1 - e^{-\lambda U}, \quad \tilde{a} = cA \tag{48}$$

where the $\lambda = 0.06$ MeV^{-1} and $C = 0.093$ MeV constants are obtained in /63,64/ by fitting the superfluid nuclear model to the observed neutron resonance density.

The expression for square entropy

$$S^2(U) = 4a(U)\cdot U = 4\tilde{a}\left[U + \delta W\left(1 - e^{-\lambda U}\right)\right] \tag{49}$$

at $U > 3\lambda^{-1} \simeq 50$ MeV corresponding to $1 - f(U) = e^{-\lambda U} < 0.05$ is close to its asymptotic limit

$$\tilde{S}^2(U) = 4\tilde{a}\left(U + \delta W\right) = 4\tilde{a}\,\tilde{U}\,, \tag{50}$$

that is described by the liquid-drop model.

For investigating the shell reconstruction effects in the Γ_n/Γ_f energy dependence consider the simplified one-humped barrier model in which the $V(\alpha)$ and $\tilde{V}(\alpha)$ minima and maxima positions coincide. In this case the $\tilde{E}_f$ threshold and $\tilde{B}_n$ neutron emission binding with the similar $\tilde{E}_f$ and $\tilde{B}_n$ values in the liquid-drop model are established by relations:

$$E_f = \tilde{E}_f + \delta W_f - \delta W_g^N$$
$$B_n = \tilde{B}_n + \delta W_g^{N-1} - \delta W_g^N \tag{51}$$

therewith, both the shell corrections for the δW_g^N original nucleus and the δW_g^{N-1} residual one in a ground state and the δW_f fissioning nucleus in a transient state correspond to the definition

$$V(Z,A,\alpha) = \tilde{V}(Z,A,\alpha) + \delta W(Z,A,\alpha) \tag{52}$$

where $V(Z,A,\alpha)$ is the A_Z real nucleus potential energy with the α deformations.

Consider the $S_n - S_f$ difference defining the main Γ_n/Γ_f ratio part exponentially dependent on $U_f = E - E_f'$ and $U_n = E - B_n'$. For this purpose express $S_n - S_f$ using relations (49,50) and having taken the trifle of terms

$$\frac{4\tilde{a}\,\delta W\left[1 - f(U)\right]}{\tilde{S}^2} = \frac{\delta W\cdot e^{-\lambda U}}{\tilde{U}} \ll 1 \tag{53}$$

at the $U \geq 10 - 15$ MeV energies transform $S_n - S_f$ into the form

$$S_n - S_f \simeq \tilde{S}_n - \tilde{S}_f - \frac{\delta W_g^{N-1} \cdot e^{-\lambda U_n}}{\tilde{t}_n} + \frac{\delta W_f \cdot e^{-\lambda U_f}}{\tilde{t}_f} \qquad (54)$$

where the $\tilde{S}_i$ entropy and the $\tilde{t}_i = \frac{\tilde{S}_i}{2\tilde{a}_i}$ temperature asymptotic behaviour in the neutron and fission channels are determined by the expression obtained with the use of relations (49,50,51)

$$\frac{\tilde{S}_n^2}{4\tilde{a}_n} = E - B_n' + \delta W_g^{N-1} = E - \tilde{B}_n' - \delta W_g^N = \tilde{E} - \tilde{B}_n' \qquad (55)$$
$$\frac{\tilde{S}_f^2}{4\tilde{a}_f} = E - E_f' + \delta W_f = E - \tilde{E}_f' + \delta W_g^N = \tilde{E} - \tilde{E}_f'$$

Similarly, one can express the preexponential in the relation (12) and, as a result, obtain:

$$\Gamma_n/\Gamma_f = \exp\left[-\frac{\delta W_g^{N-1}}{\tilde{t}_n} \cdot e^{-\lambda U_n} + \frac{\delta W_f}{\tilde{t}_f} \cdot e^{-\lambda U_f}\right] \cdot \tilde{\Gamma}_n/\tilde{\Gamma}_f \qquad (56)$$

where the first cofactor reflects shell contributions in the neutron and fission channels into the Γ_n/Γ_f ratio exponentially damping with the U energy and the second cofactor

$$\tilde{\Gamma}_n/\tilde{\Gamma}_f = \tilde{G} \cdot \exp(\tilde{S}_n - \tilde{S}_f) = \tilde{G} \cdot \exp\left[2\sqrt{\tilde{a}_n(\tilde{E} - \tilde{B}_n')} - 2\sqrt{\tilde{a}_f(\tilde{E} - \tilde{E}_f')}\right] \qquad (57)$$

is a classical limit determining the Γ_n/Γ_f asymptotic behaviour at $U > U_S$ and it coincides with the relation (12) if all the parameters are replaced by the analogous ones from the drop nuclear model. Figure 13 shows the consequences obtained. There given are the Γ_n/Γ_f calculation results from the formula (12) with the $a(U)$ dependence in accord with (48) for the A = 250 hypothetical nucleus close to Fm with the $\tilde{a}_f = \tilde{a}_n = A/10$, $\delta W_f = -\delta W_g^{N-1} = -\delta W_g^N = 2$ MeV parameters, i.e., $\tilde{E}_f = 2$ MeV, $\Delta_i = 0$, $E_f = B_n = \tilde{B}_n = 6$ MeV for the four $\delta W = 0,1,2,3$ MeV values that correspond to $\tilde{E}_f = 6,4,2,0$MeV. The dashed line shows the analogous $\tilde{\Gamma}_n/\tilde{\Gamma}_f$ dependence calculated from the formula (57) with the same $\tilde{E}_f$, $\tilde{B}_n$, $\tilde{a}$ parameters. It is seen from fig.13 that the Γ_n/Γ_f asymptotic behaviour follows

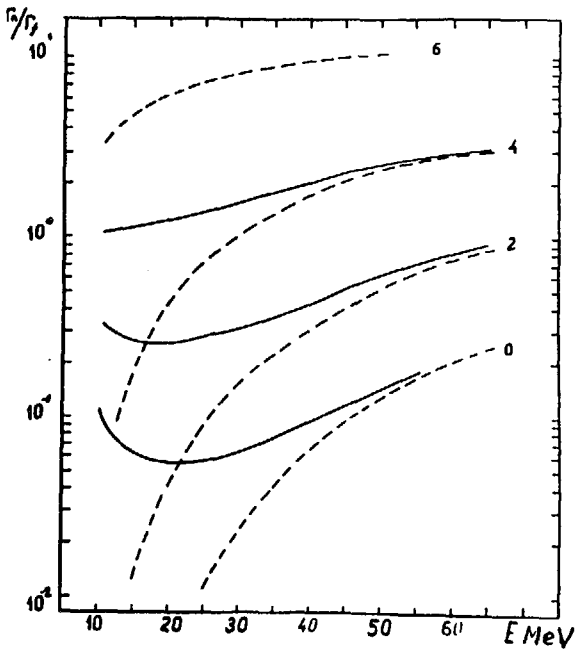

Fig.13. The shell effects in the dependence of Γ_n/Γ_f on the compound nucleus excitation energy E. The solid curves are the calculation of Γ_n/Γ_f for the "true" thresholds of E_f and B_n. The dashed curves are for the "fictitious" ones of E_f and B_n corresponding to a ligued-drop nuclear model. The figures near curves are the values of $\tilde{E}_f$ [MeV].

$\tilde{\Gamma}_n/\tilde{\Gamma}_f$ at $U \geq 50$ MeV in accord with the evaluations mentioned above.

Thus, the Γ_n/Γ_f asymptotic run corresponds to the liquid-drop model and explains the differencies in the cold and heated nucleus experimental data of the systematics mentioned above: the transition from E_f to $\tilde{E}_f$ occuring with the excitation energy growth decreases Γ_n/Γ_f, i.e. $\langle\Gamma_n/\Gamma_f\rangle$ in comparison with $(\Gamma_n/\Gamma_f)_{cold}$,

and flattens and in the limit eliminates a shell structure peculiar to $(\Gamma_n/\Gamma_f)_{cold}$.

Consider the correlation of the experimental data and the calculated curves in the upper and lower parts of fig.12. For this purpose take the $E \gg |E_f' - B_n'|$ approximation in (57) equivalent to the $\tilde{t}_f = \tilde{t}_n = t$ approximation and obtain Γ_n/Γ_f in the form

$$\tilde{\Gamma}_n/\tilde{\Gamma}_f = \frac{2A^{2/3}\tilde{t}}{\alpha} \cdot \frac{c_n}{c_f} \cdot \exp\left[\frac{\tilde{E}_f - \langle \tilde{B}_n \rangle}{\tilde{t}}\right] \qquad (58)$$

that differs from the analogous constant temperature model relation used in the $(\Gamma_n/\Gamma_f)_{cold}$ systematics by the fact that in the first case the $\tilde{t} = \sqrt{\tilde{U}/\tilde{a}}$ temperature has a physical meaning and all the other values correspond to the liquid-drop model. It can be expected, in particular, that $\tilde{c}_n/\tilde{c}_f$ will be close to 1, since the K_{rot} rotational enhancement of level density factor at the large excitations vanishes due to mixing the collective and nucleon excitation modes. The distinct correlation between the considered characteristics namely, the $(\Gamma_n/\Gamma_f)_{cold}$ and $\langle\Gamma_n/\Gamma_f\rangle$ dependences, on the one hand and $E_f - B_n$ and $E_f - B_n$, on the other hand, on Z and N obviously demonstrates the shell reconstruction effect in the Γ_n/Γ_f ratio for heavy nuclei.

In fig.14 the experimental data for the reactions emitting four neutrons are compared with the calculation, in which the Γ_n/Γ_f ratio for the first three nuclei in decay chain has been estimated from the formula (56) and for the latter one is carried out in accordance with the $(\Gamma_n/\Gamma_f)_{cold}$ systematics, the c_n/c_f coefficient is taken to be a free parameter. The calculation results fairly reproduce the $\langle\Gamma_n/\Gamma_f\rangle$ deviations from linear dependence, for the description of which in the Sikkeland's systematics (5) the broken line was used.

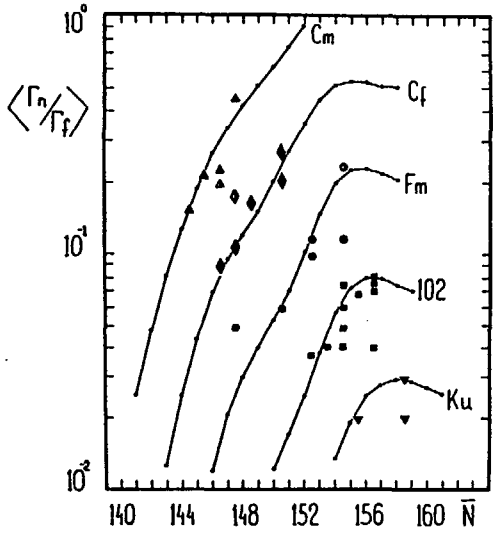

Fig.14. The $\langle\Gamma_n/\Gamma_f\rangle$ values as a function of the number of neutrons $\bar{N}$ for x = 4; ▲Δ, ●○, ■□, ▼▽, are the even values of Z from 96 to 104: the black signs are (HI,4n), the half-dashed signs are (α,4n).
The curves are the calculation according to the formulas of (56)-(58).

The $\langle\Gamma_n/\Gamma_f\rangle$ value according to (3) is the $(\Gamma_n/\Gamma_f)_i$ geometric average cofactors which are related to different excitations. The $(\Gamma_n/\Gamma_f)_i$ initial value and a number of successive ones correspond to the asymptotic strongly heated nucleus case and at the end of evaporation cascade will necessarily correspond to the cold nucleus case. Therefore, at any initial excitation energy the Γ_n/Γ_f shell effects will remain, the question is only of their scale (contribution). From this point of view the $\langle\Gamma_n/\Gamma_f\rangle$ value is not convenient for investigating the Γ_n/Γ_f energy dependence. For the same reason the c_n/c_f =0.32 coefficient value obtained from the analysis has not reached the

unity, though considerably increased as compared to the $(\Gamma_n/\Gamma_f)_{cold}$ systematics case $C_n/C_f \simeq 0.064$. The difference noted in the C_n/C_f values is not fortuitous and its appearance is worthy to consider. Both the $(\Gamma_n/\Gamma_f)_{cold}$ systematics and the more detailed analysis of low-energy fission probability /32,38/ reveal the considerable neutron and fission channel level density difference. This effect is connected with the disturbance of the fissionable nucleus axial symmetry when passing through inner barrier that has been predicted by the theoretical calculations /45/. The consequence of this property is the strong inequality of the rotational enhancement of level density factor for the cold nuclei /33/, in our description $C_n/C_f \ll 1$ corresponds to this. According to [34] it can be expected that the influence of a given factor will decrease when excitation energy is increased, i.e., $C_n/C_f \to 1$. In this case the shell reconstruction will play not the least part. The more definite opinion on this interesting problem can be obtained with the improvement of the Γ_n/Γ_f description and the information on decay of strongly excited nuclei itself.

For the study of a shell reconstruction phenomenon with energy from the two related $\langle\Gamma_n/\Gamma_f\rangle$ and Γ_n/Γ_f characteristics the experimental data on the energy dependence of the latter are of great value since the $\langle\Gamma_n/\Gamma_f\rangle$ values extracted from the analysis of the (HI,xn) processes by the geometric average method conform to the very small $\bar{A} = A - \frac{x-1}{2}$ and $E \simeq \frac{x+1}{2} \cdot 8$ MeV values at considerable scattering of these ones, particularly, in the E excitation energy. A more definite information on the Γ_n/Γ_f energy dependence can be obtained from "the pairing method" /57,65/ and its modifications /66,67/ that consists in correlation between the σ^{A}_{xn} and σ^{A-1}_{xn} cross sections. Since the residual nucleus after emitting one neutron in the 1-st reaction and formed one in the 2-nd reaction coincide over nucleon composition and energy, the relation

$$\prod_{i=0}^{x}\left(\frac{\Gamma_n}{\Gamma_f}\right)_{A-i} \Big/ \prod_{i=0}^{x}\left(\frac{\Gamma_n}{\Gamma_f}\right)_{A-1-i} \qquad (59)$$

according to (3) is equal to $(\Gamma_n/\Gamma_f)_A$ for the A-compound nucleus with the E initial excitation.

Similarly in the work /62/we have recovered the data on Γ_n/Γ_f for the Cf and No nuclei in the 40-70 MeV region which are presented in fig.15 along with the analogous Γ_n/Γ_f data for the more light subactinide nuclei as a function of the $E_f' - B_n'$ value being equal to $E_f - \langle B_n\rangle$ in accord with (18). It is seen from fig.15 that this dependence with a sharp break in the vicinity of the

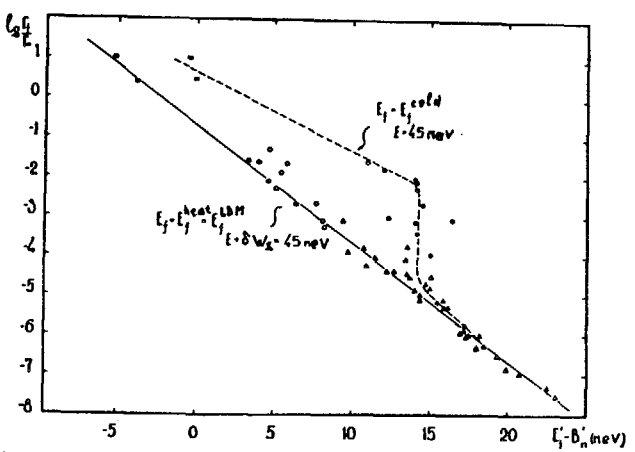

Fig.15. The dependence of $lg(\Gamma_n/\Gamma_f)$ on the $E_f' - B_n'$ difference for various assumptions of the value E_f: $E_f = E_f^{cold}$ is the black signs; $E_f = E_f^{heat} = \tilde{E}_f$ is the light signs. The different signs are provided for separating the values of Γ_n/Γ_f in the typical nuclear regions: Z = 98-102 - ■, □ ; Z = 80-85 - ●, ○ ; Z < 80 - ▲, △ .

double-magic Pb-208 where δW_g attains the above 10 MeV value at transition to the $\widetilde{E}_f - \langle \widetilde{B}_n \rangle$ liquid-drop model threshold difference value and the $\widetilde{E} = E + \delta W_g$ compound nucleus excitation energy is flattened in accordance with the expected relationship (58).

This example covering a wide set of the nuclei in the Z = 70-102, A≃ 180-260 energy range shows clearly not only the reconstruction of shells in nuclei but also the significance of the Γ_n / Γ_f experimental data for determination of the E_f uniform barrier component and solving the actual problem on choosing some parameters of a liquid-drop model. However, the existing experimental data are very poor and not accurate for this reason /62/. Everywhere we have used the M-S liquid-drop model parameters /41/ and as could be seen these have provided a fair description for a wide set of the E_f^i, $(\Gamma_n / \Gamma_f)_{cold}$, $\langle \Gamma_n / \Gamma_f \rangle$ experimental data. For the more comprehensive conclusions one should make the successive quantitative analysis of experimental data and further develop more accurate measurements of the data.

Conclusions

Conclusions from the analysis /68/ which results are given in this lecture can be stated as follows:

1. It has established the clear-cut correlation between structural peculiarities in dependence of the fission thresholds, neutron binding energy and Γ_n / Γ_f ratio for cold nuclei on Z and N and the smooth dependences of the same values for strongly heated nuclei. It has shown a decisive part of the nuclear shell structure and its reconstructing with energy in the formation of the observed fission probability properties. The extreme case of strongly heated nuclei corresponds to the liquid-drop nuclear model, therewith, the Γ_n / Γ_f experimental data for the 50 MeV excitation region can serve as a direct source of the liquid-drop fission barrier component $E_f(Z,N)$ information.

2. The concepts on the nucleon shell reconstruction with energy discard an advisability of systematics that integrate the Γ_n / Γ_f experimental data for nuclei with different excitation. It is shown that the ideas adopted as the basis of traditional systematics correspond to the asymptotic case described by a liquid-drop model.

3. The simple phenomenologic models have been suggested for describing the fission barrier and the Γ_n / Γ_f ratio that allow us to advance in the systematization of different fission probability characteristics experimental data both in the cold and heated states. In the first case we attain the evaluation accuracy for the neutron fission cross section data being absent or not reliably established that meets modern requirements for the nuclear data on nuclides being not available for investigation.

REFERENCES

1. H.L.Smith, R.K.Smith, R.L.Henkel. Phys.Rev., 1962,v.125,p.1329.
2. H.H.Barshall, R.L.Henkel, as reported in R.B.Leachmann. Proc. of the Second United Nations Intern. Conf. on the Peaceful Uses of Atomic Energy, P/2467 (United Nations, Geneva, 1958).
3. R.Vandenbosch, J.R.Huizenga. See /2/ P/688.
4. T.Sikkeland, A.Giorso, M.J.Nurmia. Phys.Rev.,1968,v.172,p.1232.
5. J.W.Behrens. Phys.Rev.Lett., 1977, v.39, p.68; J.W.Behrens and R.J.Howerton. Nucl.Sci.Eng., 1978, v.65,p.464.
6. I.M.Kuks, Yu.A.Selitsky , V.B.Funshtein et al., Proc. of Conf. on Neutron Physics, Kiev, 1977, v.3, p.161; E.A.Zhagrov et al., Proc. of Conf. on Neutron Physics, Kiev 1973, v.3, p.256.

7. P.E.Vorotnikov et al. Yadernaya Fizika, 1970, v.16, p.916.
8. B.M.Gohberg, G.A.Otroschenko, V.A.Shigin. Academy of Science USSR, Doklady, Physics, 1959, v.128, p.1157.
9. R.W.Lamphere. Proc. Simpos. on Phys. and Chem. of Fission, 1965, Salzburg, v.1, p.63, IAEA, Vienna, 1965.
10. D.W.Muir, L.R.Veeser. Proc.Third Conf. Neutron Cross Sect.Technology, v.1, Knoxvill, Tennessee, March 15-17, 1971, p.292.
11. P.E.Vorotnikov et al. Yad. Fiz., 1970, v.12, p.474.
12. B.I.Fursov, V.M.Kupriyanov and G.N.Smirenkin. Atomnaya Energiya, 1977, v.43, p.261; 1977, v.43, p.181; 1978 v.44, p.236; 1978 v.45, p.440; 1979, v.46, p.35.
13. J.W.Behrens, G.W.Carlson and R.W.Bauer. Proc. Conf. Nuclear Cross Sect. Technology, Washington, D.C.March 3-7, 1975, Special Publication 425, 1975, v.11, p.591.
14. J.W.Behrens and G.W.Carlson. Nucl. Sci. Eng., 1977, v.63, p.250.
15. J.W.Behrens, Lawrence Livermore Laboratory Reports, UCID-17370 (1977); UCID-17324(1976); UCID-17504(1976).
16. S.B.Ermagambetov and G.N.Smirenkin. Atomnaya Energiya, 1968, v.25, p.527; v.29, p.422.
17. D.M.Barton and P.G.Koontz. Phys.Rev., 1967, v.162, p.1070.
18. J.W.Behrens and G.W.Carlson. Proc. NEANDC/NEACRP Specialists Meeting Fast Neutron Fission Cross Sections, Argonne National Laboratory, June 28-30, 1976, ANL-76-90, p.47.
19. E.F.Fomushkin, G.F.Novoselov et al. Yadernaya Fizika, 1981, v.33, p.620.
20. C.D.Bowman, G.F.Auchampaugh, S.C.Fultz and R.W.Hoff. Phys.Rev., 1968, v.166, p.1219.
21. M.G.Silbert. Report LA-6239-MS, Los-Alamos Sci.Lab., 1976.
22. E.F.Fomushkin, G.F.Novoselov et al. Yadernaya Fizika, 1980,v.31, p.39; 1982, v.36, p.582.
23. M.S.Moore and G.A.Keyworth. Phys.Rev., 1971, C3, p.1656.
24. M.G.Silbert. Nucl. Sci. Eng., 1977, v.63, p.198.
25. V.M.Kupriyanov, G.N.Smirenkin, B.I.Fursov. Atomnaya Energiya, 1983, v.55 p. 31 .
26. M.G.Silbert. Nucl. Sci. Eng., 1973, v.51, p.376.
27. M.S.Moore, J.H.Mc.Nally and R.D.Baybartz. Phys.Rev., 1971, C4, p.273.
28. E.Konecny, H.J.Specht, J.Weber. Proc.Simpos. on Phys. and Chem. Fission, v.II, Rochester, 1974, IAEA, Vienna, 1974, p.3.
29. J.Weber, H.C.Britt, A.Gavron, E.Konecny, J.B.Wilhelmy. Phys.Rev., 1976, C13, p.2413.
30. H.J.Specht. Physica Scripta, 1974,v.10A, p.21.
31. J.D.Cramer, H.C.Britt. Nucl. Sci. Eng., 1970, v.41, p.77.
32. A.Gavron, H.C.Britt et al. Phys.Rev.,1976, C13, p.2374; 1977, C15, p.2238.
H.C.Britt,J.B.Wilhelmy. Preprint LA-UR79-614, 1981.
33. S.Bjørnholm, A.Bohr, B.R.Mottelson. Physics and Chem. of Fission (Proc. Simp., Rochester, 1973), Vienna, IAEA 1974, v.1, p.367.
34. A.V.Ignatiuk, K.K.Istekov, G.N.Smirenkin. Yadernaya Fizika,1979, v.30, p.1205.
35. J.R.Huizenga, R.Vandenbosh. Nuclear Reactions, vol.II, p.51. North-Holland Publ. Comp.,1962.
36. V.A.Kravtsov. Atomic Masses and Nuclear Binding Energy, Moscov, Atomizdat, 1974.
V.E.Viola, J.A.Swant and Graber. Atomic Data and Nuclear Data Tables, 1974, v.13, p.35.

37. V.M.Strutinsky, S.Bjørnholm. Nucl.Str. Dubna, Simp, 1968, IAEA, Vienna, 1968, p.431; Nucl. Phys.,1968, v.A122, p.1.
38. S.Bjørnholm, J.E.Lynn. Reviev of Modern Physics, 1980, v.52, No 4, p.725.
39. H.C.Britt. Phys. and Chem. of Fission, 1979, (Proc. Simp, Jülich, 14-18 May, 1979) IAEA, Vienna, 1980, p.3-28.
40. H.C.Britt, E.Cheifetz, D.C.Hoffman and J.B.Wilhelmy et al. Phys.Rev.,1981, C21, No 2, p.761.
41. W.D.Myers, W.J.Swiatecki. Ark. Phys., 1967, v.36, p.343.
42. S.Cohen, W.J.Swiatecki. Ann. Phys., 1963, v.22, p.406.
43. W.D.Myers, W.J.Swiatecki. Nucl.Phys., 1966, v.81, p.1.
44. V.Metag, R.Repnov, P.Von Brentano. Nucl.Phys., 1971, v.A165, p.289; H.Wigman, J.R.Theobald. Nucl.Phys.,1972, v.A187, p.305.
45. S.E.Larsson, G.Leander. Proc. Simp. Phys. and Chem of Fission, Rochester, IAEA, Vienna, 1974, v.I, p.177.
46. P.Möller. Nucl.Phys.,1972, A192, p.529.
47. S.G.Nilsson et al. Nucl.Phys., 1969, v.A131, p.1.
48. B.B.Back et al. Proc. Simp. Phys. and Chem. of Fission, Rochester, IAEA, Vienna, 1974, v.1, pp 3-25.
49. Yu.A.Selitsky. Physics of Elementary Particles and Atomic Nuclei, 1979, v.10, p.314.
50. P.Möller. See L.I.Lindner, A.Alm, A.Saudell. Nucl. Phys., 1978, v.A298, p.43.
51. G.Haouat, J.Lachkar, Ch.Lagrange, J.Jary, J.Sigand and Y.Patin. Nucl.Sci.Eng., 1982, v.81, No 4, p.491.
52. M.N.Nikolaev et al. Neutron Data for Uranium-238. Part II. The Analitical Review. A-34, 1979. Obninsk, Institute of Physics and Power Engineering.
53. G.V.Antsipov, V.A.Konshin et al. Nuclear Data Isotopes of Plutonium. 1982, Science and Technology, Minsk.
54. B.B.Back, Ole Hanzen, H.C.Britt and J.D.Garrett. Phys. Rev.,1974, C9, p.1924.
55. A.C.Ilinov, E.A.Cherepanov. Report II-0090. Institute of Nuclear Investigations of Academy of Sciences of the USSA, Moscow,1978.
56. T.Sikkeland, J.Maly, D.Lebeck. Phys.Rev.,1968, v.169, p.1000.
57. N.I.Tarantin. JETP, 1960, v.38, p.250.
58. V.M.Strutinski, V.M.Kolomiets. Materials of the 8-th Winter School of Leningrad Institute of Nuclear Physics of Academy of Science of the USSR, Leningrad, 1972, v.2, p.483.
59. A.Bohr, B.R.Mottelson. Nuclear Structure W.A.Benjamin, INC. New-York, Amsterdam, v.2, 1974.
60. A.V.Ignatiyuk et al. Yadernaya Fizika, 1975, v.21, p.1186.
61. A.V.Ignatiyuk, K.K.Istekov, G.N.Smirenkin. Yadernaya Fizika, 1983, v.37, p.831.
62. K.K.Istekov, V.M.Kuprianov, B.I.Fursov, G.N.Smirenkin. JETP Pisma, 1978, v.27, p.135.
63. A.V.Ignatiyuk, G.N.Smirenkin, A.S.Tishin. Yadernaya Fizika, 1975, v.21, p.485.
64. A.V.Ignatiyuk, K.K.Istekov, G.N.Smirenkin. Yadernaya Fizika, 1979, v.29, p.875.
65. V.V.Volkov, L.I.Guseva et al. JETP, 1972, v.36, p.1959.
66. P.D.Goldstone, H.C.Britt, R.Shoenmackers and J.B.Wilhelmy. Phys. Rev.Lett., 1977, v.38, No22, p.1262.
67. H.Delagrange, S.Y.Lin, A.Fleury, J.Alexander. Phys.Rev.Lett., 1977, v.39, No 14, p.867.
68. K.K.Istekov, V.M.Kuprianov, B.I.Fursov, G.N.Smirenkin. Yadernaya Fizika, 1979, v.29, p.1156; 1980, v.32, p.355.

DATA BASE AND SOFTWARE FOR NEUTRON SPECTRA UNFOLDING ON RESEARCH REACTORS

H.J. BONDARS
Peter Stuchka Latvian State University,
Riga, Union of Soviet Socialist Republics

Abstract

Methodology and software for the neutron spectrum unfolding using measurements of reaction rates of activation detectors are discussed. The recommended activation detector cross sections are presented.

Introduction

At present research reactors are widely used for measurements of reaction rates A_i by means of activation reactors to determine neutron spectra $\varphi(E)$ (neutron/(cm^2 · sec · MeV)). High accurasy of measurements (2% - 5%) can be obtained in the measured reaction rates. This is of great importance when measuring under complicated conditions. Measurements can be performed in a wide energy range (from 10^{-10} MeV to 18 MeV). Measurements of reaction rates are often the only relevant method to determine neutron spectra. The reaction rates are linked with a neutron spectrum by the equation of activation [1]

$$A_i = \int_{E_l}^{E_u} \varphi(E)\sigma_i(E)dE \quad , \; i=1,\ldots,N \; ,$$

where N is a number of isotops used in measurements, $\sigma_i(E)$ is neutron cross section, E_l and E_u are lower and upper energy bounds.

This equation falls in the category of incorrectly formulated mathematical problems [2]. To solve such equations a priori information is needed. When solving these equations additional research on existence, stability and uniqueness of the solution has to be carried out. Besides, equations of activation have some physical peculiarities. They are the following: 1) the number of isotopes used as detectors is limited ; 2)in some measurements the maximum number of detectors used is up to 40 but, as a rule, it does not exceed 20 - 25; 3) in measurements the resonance, fission, and threshold detectors are used; 4) knowledge of a spectrum in a wide energy range is often essential; 5) in different energy ranges, a different number of detectors operate but some energy regions lack detectors able to work there ; 6) the value i is discrete; 7) reaction rates and cross sections are known with errors; 8) $\sigma_i(E) \geq 0$; 9) $\varphi(E) \geq 0$; 10) the spectra to be unfolded have different smoothness in different intervals; 11) a priori information is usually given as a table.

Physical and mathematical peculiarities must be taken into account when solving equations of activation. To unfold neutron spectra a user (physicist), in the first place, has to develop or adapt the unfolding program, the neutron cross section library and the neutron spectrum library, and secondly, he has to solve an equation of activation taking into account its peculiarities.

1. Neutron Spectra Unfolding Programs

Presently several different unfolding programs are well-known and widely utilized [3] . These programs differ in the mathematical methods used, in program realization, in formats and in the content of the input and output set of data. On the computer ES 1022 the following programs have been adapted: SAND II [4,5] , LMP [6] , WINDOWS [7] , CRYSTAL BALL [8] , RESP JUL [9] , SPECTRA [10] , RFSP [11] , GIN [12] . The analysis of the mathematical methods used in these programs shows that all programs can be divided into four groups, mathematical methods of which differ substantially. The most developed program can be singled out in each of these groups and be recommended for the use on the Soviet computers ES and IBM 360 or 370 as well, so to say, on the computers where software is compatible with the previously used. The recommended programs are : SAND II, WINDOWS, RFSP JUL and PM. A test calculation was done to determine the necessary computing resources.

A variant with 11 detectors was used. Table 1 sums up the results obtained.

Table I. Computing Resources Necessary for Unfolding Programs.

Program	Real time (in min.)	Commercial time (in relative units)	Oper. memory (kilobites)
I. SAND II	2.5	6.5	II2
2. PL	I.7	4.5	I36
3. RFSP JUL	I2.7	2I.0	234
4. WINDOWS	2.0	5.0	248

In this table real time is the time of calculation in a single- program operation. The commercial time is the "count" of the computer resources used by the calculation programs: processor employment time, volume of operational memory, intensity of use of external devices and so on. As it follows from Table 1 the resources used are negligible and cannot be considered as a criterion for determining quality of the unfolding program.

2. Neutron Dosimetry Cross Section Libraries

International information centres on nuclear data provide users with several dosimetry libraries, out of which we have adapted the following : ENDF/B-4 [I3] , ENDF/B -5 [I4] , IRDF -82 [I5] , DOSCROS - 77 [I6] , BOSPOR - 80 [I7] , ZACRSS [I8] , DETAN - 74 [I9], ENDL - 78 [20] , BGS - I [2I] , JENDL - I [22] .

These cross section libraries differ both in their content and cross section evaluation. All the above-mentioned libraries have been adapted and analysed for the purposes in question. In this analysis those reacton rate measurements were used that were obtained by several laboratories in the following benchmark fields [I6] : BIG - TEN , Σ - Σ , CFRM, in fission spectra of U^{235} and Cf^{252} . As a result of this analysis the recommended cross section library RNDL - 82 was developed [23] . Table 2 presents cross sections from RBDL - 82, the libraries containing the most qualitative evaluations, half - life periods - $T_{I/2}$, E_γ - characteristics of γ-ray energy, $E_{\beta\ max}$ - maximum β-ray energy, $\eta - \gamma$ and β-ray emission probability and cross section category (see Ref.24). All cross sections having integrated measurements at least in four benchmark fields, with the difference between the measured and calculated reactions not exceeding 5%, are related to the first category. The cross sections having integrated measurements in three benchmark fields with error difference not exceeding 10% are related to the second category, the others, to the third category.

Details of calculations and the utilized values of measurements in the benchmark fields and so on can be found in Ref.[23]. RNDL-82 includes only these cross sections the reactions of which are most frequently used in reaction rate measurements and for which measurements in the benchmark fields have been made.

3. Calculation Strategies of Neutron Spectra Unfolding

Some general features can be singled out in all methods of unfolding. At first the solution sought is presented in an analytical form. Further on an iteration procedure is built to determine the solution, i.e., an initial approximation is set up, then the solution found is used as an initial approximation and so on, but in PM, instead of the increase in the number of iterations there is the increase in the polynom degree. Iterations are stopped by different integral criteria. Physicists employing unfolding methods usually do not consider and discuss the problems connected with additional studies of neutron spectra unfolding. Instead, the problem of selecting the best unfolding program from existing ones is sometimes posed. Such goals are set by interlaboratory comparison of unfolding programs. Sometimes an attempt is made to reduce the error of neutron spectrum unfolding to the error arising from the statistical error. Moreover, the error is determined without taking into account unstability of the solution obtained. The role of the a priori information cannot be underestimated both in setting the initial approximation and in determining the number of iterations. Sometimes separate test examples

Table 2. The Recommended Cross Sections of Activation Detectors.

No.	Detector	Library	$T_{1/2}$	E_γ, KeV	η %	Quality group
1	2	3	4	5	6	7
1.	$^{19}F(n,2n)^{18}F$	IRDF - 82	109.8 m	511.0034 (14)	193.4	3
2.	$^{24}Mg(n,p)^{24}Na$	IRDF - 82	15.00 (4)h	1368.53 (5)	100.0	2
				2754.09 (5)	99.863 (5)	
3.	$^{27}Al(n,\alpha)^{24}Na$	IRDF - 82	15.00 (4)h	1368.53 (5)	100.0	1
				2754.09 (5)	99.863 (5)	
4.	$^{27}Al(n,p)^{27}Mg$	DETAN - 74	9.462(11)m	843.76 (3)	71.8 (4)	2
				1014.44 (4)	28.0 (4)	
5.	$^{32}S(n,p)^{32}P$	ENDL - 78	14.29 (3)d	Epmax=1710,4(6)	100.0	2
6.	$^{46}Ti(n,p)^{46}Sc$	ENDF/B-5	83.83 (2)d	889.25 (3)	99.9840 (10)	2
7.	$^{47}Ti(n,p)^{47}Sc$	DETAN - 74	3.351(2)d	159.381(15)	68.0 (20)	2
8.	$^{48}Ti(n,p)^{48}Sc$	ENDF/B - 5	43.7 (1)h	983.5010 (20)	100.0 (5)	1
				1037.5	97.5 (5)	
				1312.007 (3)	100.0 (5)	
9.	$^{54}Fe(n,p)^{54}Mn$	IRDF -82	312.5 (5)d	834.827 (27)	99.9760 (20)	I
10.	$^{55}Mn(n,2n)^{54}Mn$	БОСПОР - 80	312.5 (5)d	834.827 (21)	99.9760 (20)	3
11.	$^{56}Fe(n,p)^{56}Mn$	ENDF/B-5	2.5785(6)h	846.754 (20)	98.9 (3)	I
				1810.72 (4)	27.2 (8)	
12.	$^{58}Ni(n,2n)^{57}Co$	ENDL - 78	36.08(9)h	1377.59 (4)	77.9 (23)	3
13.	$^{58}Ni(n,p)\ ^{58}Co$	БОСПОР - 80	70.80 (8)d	810.757 (18)	99.4 (3)	I
14.	$^{59}Co(n,\alpha)\ ^{56}Mn$	IRDF - 82	2.5785 (6)h	846.754 (20)	98.9 (3)	2
				1810.72 (4)	27.2 (8)	
15.	$^{63}Cu(n,\alpha)^{60}Co$	DETAN - 74	5.271(1)y	1173.210 (10)	99.900(20)	2
				1332.470 (10)	99.9824 (5)	
16.	$^{63}Cu(n,2n)^{62}Cu$	БОСПОР - 80	9.74 (2)m	511.0034 (14)	196.2	3
17.	$^{64}Zn(n,p)^{64}Cu$	IRDF - 82	12.701 (2)h	511.0034 (14)	35.74	3
				1345.9 (3)	0.49 (4)	
18.	$^{103}Rh(n,n)^{103}Rh$	ZACRSS	56.12 (1)m	20.07370 (2)	2.19 (12)	1
				20.21610 (2)	4.17 (21)	
19.	$^{115}IN(n,n)^{115}In$	ZACRSS	4.486 (4)h	336.241 (25)	46.7 (6)	I
20.	$^{127}J(n,2n)^{126}J$	БОСПОР - 80	13.02 (7)d	388.633 (11)	34 (3)	3
				666.331 (12)	33.1 (25)	
21.	$^{232}Th(n,f)$	IRDF - 82	-	-	-	2
22.	$^{235}U(n,f)$	IRDF - 82	-	-	-	I
23.	$^{237}Np(n,f)$	DETAN - 74	-	-	-	I
24.	$^{238}U(n,f)$	IRDF - 82	-	-	-	I
25.	$^{239}Pu(n,f)$	ENDF/B-4	-	-	-	I

are used to prove validity of unfolding programs. These and some other reasons are cause of sceptical attitude to neutron spectra unfolding. The unfolding aim is to determine a function out of the integral set. Besides, possibilities and incorrectness of the problem to be solved are not considered. Therefore, it is necessary to determine the goal of unfiolding. It consists in enlarging our knowledge of an initial approximation of the spectra sought. A set of measured reaction rates is used for this purpose. This problem is worth solving provided that the initial approximation characterizes the spectrum sought worse than it is determined by measured reaction rates. To determine the quality of the initial approximation it is necessary to compare the measured reaction rates and the calculated ones employing the initial approximation (taking into consideration errors of the measurements and calculated values).

Calculation strategies depend on the unfolding variant used, and they may vary. Though in the majority of cases the following points may be singled out :

(1) Determination of the initial description of the neutron spectrum in the point studied. Its source may be calculations, independent measurements, and general physical considerations.

(2) Setting up expediency of neutron spectra unfolding, on the basis of reaction rate comparison.

(3) Application of one or several unfolding methods with essentially different calculation strategies. It should be noted that all the mathematical methods make use of some approximation of the solution sought. Therefore, it is necessary to consider a priori information to determine the number of iterations.

(4) It is also necessary to study stability of solutions dependent on such factors as errors of measured reaction rates and the number of iterations.

(5) Measurements planning and unfolding.

4. Software and Neutron Spectrum Unfolding

Neutron spectrum unfolding is a very voluminous and time-consuming work carried out in many laboratories. To automate this work a computerized information system SAIPS has been developed. One of the advantages of this system is that there is no need for a physicist to have skills in programming. Moreover, the user has an easy access to the most updated and qualitative information. These and other advantages are attained by three-level operation of SAIPS. Let us consider these levels.

1st level. This level is concerned, in the first place, with designing of the system, its maintenance and development and with providing users with the distributional variant of the system; and secondly, with adaptation and/or development and approbation of the unfolding methods, neutron spectra libraries and cross section libraries; and third, with working out recommendations for program and cross section utilization.

On the first level programmers skilled in system programming are employed. As a rule, they are assisted by physicists. This work is carried out in a centralized way and in cooperation with the organizations concerned. Users (physicists) are supplied only with a distributive variant of the system. To set up and further develop SAIPS we have established connections, have regular exchange of information, are familiar with the activities of the International Centres on Nuclear Data, such as CJAD at FEI at Obnyinsk, IAEA in Vienna, Oak Ridge in USA and some other laboratories working at the same problem.

2nd level. This level is concerned with the adaptation and utilization of the distributive variant of SAIPS. SAIPS is developed with software supplied by the operating system OS ES. The distributive variant is generated according to the possibilities of each computing centre and according to the demands of users. A computerized information system is supplied in 9-track tapes with recording density 800 BPI. The user can be supplied with distributive variants, in which the system is given in a symbolic or load presentation.

3rd level. This is the level on which a physicist (user) carries out his calculations. He can do this without special skills in programming. When calculating it is enough to know the language of the user and be acquainted with the rules of writing some sentences of job control language of OS ES. The language of the user is created using terminology of the given physical supplement.

Using the default values facilitates writing the input data. The language of the user allows:

(1) to create in a unified form the input data for several unfolding programs;

(2) it permits us to simultaneously create the input data for several calculation variants copying some input data of the previous variants;

(3) it allows us to change cross section libraries, to utilize cross sections from different libraries, to utilize the recommended cross section library;

(4) it permits us to give the initial approximation to the input data; to calculate according to the given formula; to select from the indicated library the spectrum that makes least square difference between the measured and calculated reaction rates.

Thus, it is possible by means of the job control language:

1. To determine the spectrum library from which the initial approximation is selected.

2. To use the unfolding programs.

3. To print the calculated neutron spectrum or to record it on the magnetic tape.

REFERENCES

1. Berkurts K., Virts . Neutron Physics, Moscow, Atomizdat, 1968.
2. Tikhonov A.N., Arsenin V.Ya. Methods of calculation of incorrect problems, Moscow, Nauka, 1974 (in Russian).
3. Bondars H.J., Lapenas A.A. Methods of calculation of neutron spectra by the measured reaction rates in SAIPS. Part 1. Review of mathematical methods. - Publ. of AS Latv. SSR, Ser. Phys. and Techn. Scienc., 1980, No. 2, pp 3 - 15 (in Russian). Translation of Selected Reports on Neutron Spectrum Unfolding by Kh.Ya.Bondars, et al. IAEA, Vienna, INDC (CCP)-163/GR 1981 and 1982. Addendum.
4. McElroy W.N., Berg S., Crockett T., Hawkins R.G. SAND-II. A Computer-Automated Iterative Method for Neutron Flux Determination by Foil Activation, AFWL-TR-67-41, 1976, v. I - IV.
5. Berg S. Modification of SAND-II.BNWL-855, 1968.
6. Kramer-Ageev E.A., Troshin V.S., Tikhonov E.G. Activation methods of neutron spectrometry, Moscow, Atomizdat, 1976.
7. Stallmann F.W., Eastham J.F., Kam F.B.K. WINDOWS. A program for the analysis of spectral data foil activation measurement. ORNL/TM-6650, 1979.
8. Kam F.B.K. and Stallmann F.W. CRYSTAL BALL. A Computer Program for Determining Neutron Spectra from Activation Measurements. ORNL-TM-4601, 1974.
9. Fisher A. RESP-JUL. A Programme for Unfolding Neutron Spectra from Activation Data. JUL-1475, 1977, pp 1 - 83 (ORNL/RSIC-PSR-126).
10. Greer C.R. and Walker J. A Procedure for the Computation of Neutron Flux from Foil Activation Data, SPECTRA Code, Radiation Measurements in Nuclear Power, 1966.
11. Fisher A., Tury L. RESP. A Programme for Determination of Neutron Spectrum from Activation Data. KFKI-71-22. AS HPR, Budapest, 1971 (in Hungarian).
12. Zolotaryev K.I., Korolyeva V.P., Koleganov Yu.F., Chernov L.A. Measurement of Neutron Spectra on a Critical Assembly by the Activation Method. Atomnaya Energiya, 1979, v. 46, is. 2, pp 96 - - 100 (in Russian).
13. Magurno B.A., editor "ENDF/B-IV Dosimetry File". Report BNL-NCS-50446 (ENDF-216), NEACRP-L-145, NEANDC (US)-193/L, INDC (US)-70 (L), 1975.
14. Magurno B.A. ENDF/B Dosimetry File Version V. - Neutron cross sections for reactor dosimetry, v. 1. Vienna, IAEA-208, 1978.
15. Cullen D.E., Kocherov N., McLaughlin P.M. The International Reactor Dosimetry File (IRDF-82). IAEA-NDS-42/R, 1982.
16. Zijp W.L., Nolthenius H.J., Van der Borg N.J.C.M. Cross Section Library DOSCROS-77. ECN-25, 1977.
17. Bychkov V.M., Zolotaryev K.I., Pashchenko A.B., Plyaskin V.I. Organization of Computer Library of Evaluated Cross Sections of Threshold Reactions (BOSPOR-80) and its Testing by Integral Experiments. Nuclear Constants, 1981, is. 42, pp 60 - 67 (in Rus.)
18. Berzonis M.A., Bondars H.J., Lapenas A.A. Library of Neutron Cross Sections for the SAND-2 Program and its Maintenance Program. - Voprosy Atomnoy Nauki i Tekhniki. Ser. Yadernye Konstanty, 1978, is. 1 (28), pp 49 - 52 (in Russian).

19. Rieffe H.Ch., Nolthenius H.J. Cross Section Library DETAN-74. RCN-75-139, 1975.
20. Schwerer O. ENDL-78, LLL Evaluated Nuclear Data Library, 1978. IAEA-NDS-11 (Rev. 1), 1980.
21. Borisov G.A., Vasilyev P.D., Grigoryev E.I., Yaryna V.P., Lapenas A.A. Library of Group Cross Sections of Threshold Reactions (BGS-1). In: Metrologiya neytronnykh izmereniy na yadernofizicheskikh ustanovkakh. T.I.M. TsNII Atominform, 1976, pp 194 - - 217 (in Russian).
22. Day Day N. JENDL-1. Japanese Evaluated Nuclear Data Library. Version 1. IAEA-NDS-18 (Rev. 0). 1979.
23. Bondars H.J., Lapenas A.A. Recommended Cross Sections of Activation Detectors (RNDL-82). Part 1. Cross Sections of the (n, p) Reactions, LAFI-054. Part 2. Cross Sections of (n, n), (n,α), and (n,2n) Reactions, LAFI-057. Part 3. Cross Sections of the (n, f) Reactions, LAFI-059, Salaspils, 1983 (in Russian).
24. Zijp W.L., Baard J.H. Nuclear Data Guide for Reactor Neutron Metrology-EUR-7164 EN, 1981.

NUCLEAR DATA REQUIREMENTS FOR FAST NEUTRON REACTORS

V.N. MANOKHIN
Institute of Physics and Power Engineering (FEI),
Obninsk, Union of Soviet Socialist Republics

Abstract

The procedures for the quantitative formulation of nuclear data accuracy requirements for fast neutron reactor physics are described. The role of the International Nuclear Data Committee, national and regional committees and nuclear data centres in such development is discussed.

1. INTRODUCTION.

1.1. Nuclear data are needed for numerous branches of science and technology and first of all for nuclear power. To meet these needs the system of national, regional and international organizations (committees and centres) has been created to join efforts in compilation and evaluation of nuclear data as well as to specify and substantiate requirements in nuclear data.

During more than 15 years in the framework of IAEA and under the International Nuclear Data Committee the system of nuclear data centres successfully works.

Each of these centres makes compilation of all the numerical information on nuclear physics within the area of their responsibility and exchanges this information with other centres.

The world computer neutron data library, now containing experimental neutron data on cross-sections and other nuclear reaction parameters for $\sim$ 400 isotopes and elements (about 3 million values), was created as a result of the nuclear data centre activity. This library is the base for development of evaluated

data libraries which (directly or in group represention) are used in calculation of nuclear reactor parameters.

At the present time there are a lot of national (general and specialized purpose) evaluated data libraries.

The work on data evaluation, development of existing libraries and creation of new libraries is under way in many countries as well as in the framework of IAEA on the base of international cooperation.

One should note that the further development of experimental and theoretical investigations on nuclear structure and nuclear reactions plays important part in supporting the work on nuclear data evaluation.

The essential part of the activity of the International Nuclear Data Committee, national and regional committees and nuclear data centres is specifying and substantiating nuclear data requirements. The result of this work is the world request list WRENDA, which includes data requests for reactors, thermonuclear problem and safeguard.

1.2. As for the problem of fast neutron reactors the nuclear data are needed for undestanding physical process, underlying the work of nuclear power stations, for calculation of the optimal parameters of reactors and nuclear power station as a whole, for the out-of-pile fuel cycle, for the choice of the alternative ways of nuclear power development. The nuclear data are needed with required accuracy, because uncertainties in nuclear data lead to uncertainties in the prediction of reactor parameters. Large uncertainties in turn lead to the large and expensive margins in design. This requires the further refinement of nuclear data. But on the other hand the excessive refinement of nuclear data also requires excessively large investments in the development of experimental technique. The estimation of cost of experiment is usually done by the law of inverse dependence of the square of error, i.e., if we require half as much uncertainty, it is necessary to spend four times as much money to meet these requirements. That is why the task of subtantiating required nuclear data accuracy arised. In other words there is a task of choice of the optimal set of experiments (microscopic and integral), which are characterized by admissible accuracy for determination of each value and ensuring the required accuracies of reactor parameter calculation at minimum expenses.

1.3. Problem on uncertainties in nuclear data and requirements to them was examined by a lot of authors [1 - 14]. There are a number of reviews in which this problem is discussed thoroughly enough [9, 11]. The status of determination and satisfaction of nuclear data requirements has been discussed at many conferences and meetings, where the methods of determination of requirements, the target accuracies of reactor parameters and properties are discussed, the discrepencies in measurements and in evaluation are analyzed, the requirements for reactors and for other applications in science and technology are formulated. In this connection one should mention the conferences on nuclear data for reactors in Paris (1966, 1973), Helsinki (1970), on neutron cross sections and technology in Washington (1968, 1975) and in Knoxville (1971,1979), on neutron physics and nuclear data in Harwell (1978), on neutron physics in Kiev (1971, 1973, 1975, 1977, 1980), meetings on nuclear data for fission products in Petten (1977), on nuclear data for transactinide in Karlsrue (1975) and Kadarache (1979), on neutron

data for fast neutron reactor structural materials in Geel (1977, 1979), on nuclear data for reactor dosimetry in Vienna (1978), on nuclear data for radiation damage assessment in Vienna (198) et al. In the framework of IEAE there are also the working and advi - sory meetings on various aspects of nuclear data activities. The nuclear data accuracy requirements, developped in different countries and approved by national and regional nuclear data committees are included in the World request list on nuclear data WRENDA(IAEA) Every 2 years the IAEA carries out reexamination and publica - tion of this list. The WRENDA 81/82 issue includes about 1700 re - quests from 15 coutries and international organizations. The request list gives a fair picture of the requirements for evaluated nuclear data and it can be the guidance for planning evaluation and measurements of nuclear data. The fast neutron reactor requests are divided by priorities (priorities 1,2 and 3). The highest priority (priority 1) is assigned to requests for measurement and evaluation of nuclear data for reactors to be built in the near future, if:

(a) these data are still necessary to predict the different reactor properties after all information from integral experiments and operating reactors has been used; or

(b) information on an important reactor parameter is, in prin - ciple, attainable through mathematical calculation from nuclear data only; or

(c) these data are needed for materials required in reactor physics measurements.

Priority 2 is for the data to be needed during the next few years in the applied nuclear energy programme.

Nuclear data of more general interest has priority 3.

1.4. Comparing requirements in nuclear data accuracies developed by different specialists one can note differencies in magnitudes (ofen by factor 2), which are explained by differencies in the approaches in requirement determination. Different authors make different assumptions about the values of target accuracies, the importance of integral experiments, the correlative properties of nuclear data uncertainties et al.

The first step in the determination of nuclear data accuracy requirements is the formulation of target accuracies on the base of technical - economic considerations, i.e. the accuracy requirements in the prediction of facility parameters for whose calculation the nuclear data are needed. For target accuracy determination the consideration of technology and economy are used which enable us with confidence, to determine the target accuracy magnitudes.

The next step in procedure of the determination of nuclear data accuracy requirements is the calculation of sensetivity of these parameters to changes in nuclear data [18] . This gives possibility to determine which nuclear data are needed with better accuracy. The requirements to the evaluated nuclear data accuracy ensuring the given accuracy of reactor property calculation are for - mulated (by reactor specialists) at this stage. The required uncertainty must be considered as the evaluated nuclear data uncertainty correlated over given energy ranges. Problem of uncertainty definition is discussed in detail in work [15] . As regards the require - ments in new measurements, they are specified in process of nuclear data evaluation and must be formulated by evaluators.

For development of requirements to evaluated nuclear data one should have information about the target accuracies and the present evaluated nuclear data accuracies. Since the number of values for which accuracy requirements are needed is more than the number

of reactor properties which accuracies must be ensured, the task at first sight seems ambiguous. However, requirements of cost minimum on the totality of measurements and evaluations with adop - tion, similteneously, of dependence of each value determination cost on error (e.g., $1/\varepsilon^2$) makes this task simple.

One should also accept a certain model of correlative properties of uncertainties. The importance of taking into account the correlations between cross-sections at determination of required accuracies has been emphasized by various authors lately. In works [7, 17, 18] the review of history of problem is given and the formalism of development of requirements which ensure the accuracy of calculating several reactor parameters taking into account both microscopic and integral experiments at certain assumptions about correlative properties of uncertainty.

It is convinient to adopt that uncertainty is correlated fully within chosen intervals and the uncertainties in different in - tervals are independent. The use of common standards at relative measurements results in correlation of uncertainties for different isotopes.

The magnitudes of the evaluated nuclear data requirements depend essentially on assumptions about correlation intervals.

To undestand the transformation from the evaluated nuclear data accuracy for which requirements are formulated, to the requirement to new measurements, one should note the following.
To meet requirements, one should both improve the accuracy of separate experiments analyzing to the most extent and exluding uncertainties and develop new experimental technique. The fact is that the systematic uncertainties are revealed only in comparison of the results obtained by different methods. They are the systematic uncertainties that are usually connected not with single experimental point but with the energy region. We do formulate the requirements to this kind of uncertainty.

The account of already performed integral experiments for the determination of the microscopic data accuracy requirements to meet needs in the target accuracies in K_{eff} and BR relaxes these requirements (see [7]).

This fact has been taken into account in the soviet requests in WRENDA 75/76. These requests have priority 1 there. Further in connection with the great progress in integral measurements of critical assemblies the requirements to the first priority microscopic data have been decreased to achieved accuracies. That is why in WRENDA - 77/78 the second priority requests, i.e. the requests to the accuracy of only microscopic data has been left.

In some cases the use of integral experiments is necessary, because the required microscopic data accuracies can exceed the attainable accuracy in nuclear data measurement and further refine - ment will result in essential cost for measurements. Importance of integral experiments has been discussed in many works (full enough list of referencies is given in [9]).

The further content of this lecture will be devoted to discussion of the reactor parameter target accuracies, values of the achieved evaluated nuclear data accuracies, procedure of the development of accuracy requirement with or without taking into account integral experiments.

2. TARGET ACCURACIES

2.1. EFFECTIVE MULTIPLICATION COEFFICIENT (K_{eff}). The fuel characteristics are chosen so that the reactor is critical at the end of an irradiation period with the operational control rods in the

withdrawn position. The calculational uncertainty of K_{eff} because of uncertainty in nuclear data must be ± 1%. This requirement is substantiated by possibility to cover relevent uncertainties without reactor reconstruction. Further decreasing of uncertainty at the expense uncertainty in nuclear data will not result in essential decreasing of the full uncertainty because of uncertainty in fuel element production, which gives approximately the same uncertainty in K_{eff} that the uncertainty because of nuclear data in accuracy. The uncertainty in K_{eff} is mainly due to the uncertainties in the nuclear data of the principal fertile and fissile isotopes and structural materials. The requirement to accuracy of K_{eff} of 1% leads to the high accuracy requirement for the principal fissile and fertile isotopes.

2.2. BREEDING RATIO. The amount of uranium production and enreachment, the scope of fuel reprocessing needed for providing the developing nuclear power based on fast breeders is due to the planned rate of nuclear power development and the doubling time of breeder reactors. The doubling time is inversely proportional to the value (BR-1). The doubling time should be known with accuracy ± 10%. The required uncertainty for BR is ± 2% (on the assumption of 10% in doubling time and 1% in K_{eff}).

2.3. THE VARIATION OF REACTIVITY IN AN IRRADIATION PERIOD. The va - riation of reactivity with burn - out of fuel and build - up actinides and fission products in an irradiation period determines the operational control requirements and also the fuel reactivity at the end of the irradiation period. The target accuracy is ± 5%. Fission product bulk reactivity effect must be known to an accuracy of ± 10% to meet this requirement. The uncertainty on the reactivity variation is due to the uncertainties on the fission product capture cross sections and to the heavy atom balance associated to the burn - up.

2.4. CONTROL ROD REACTIVITY. The target accuracy in control rod reactivity is ± 5%. Present uncertainty is ± 10%.

2.5. HEAT GENERATION. The thermophysics calculation of the maximum reactor power requires knowledge of the peak to average power distribution. This factor influences directly the maximum power output, since this maximum power is limited by the temperature of the hottest reactor subassemby. The accuracy requirement of ± 1% results from economic considerations, the present uncertainty is ± 2%. Gamma - radiation of fuel elements contributes significantly to the heating of control elements and breeding elements. This leads to the requirements for data on γ -spectra and γ - interaction cross section.

2.6. RADIATION DAMAGE EFFECTS. Radiation damage influences economy, design and safety of nuclear reactors. The maximum irradia - tion can depend on radiation endurance of structural materials. Radiation damage leads to swelling and creeping of materials and changes in their properties. Radiation damage dose and dose gradients for the estimation of swelling and distortion of elements must be predicted. One should predict atomic displacement rates, helium production rates and material temperatures. There is a need to determine the flux and flux spectrum so that the observed changes in material properties can be correlated with the irradiation process. This leads to the dosimetry requirements. The accuracy requirements for the prediction of fluency and radiation damage dose are ± 5%, and for the prediction of dose and temperature gradients are ± 10%.

2.7. COEFFICIENTS OF REACTIVITY. A number of reactivity coefficients determine reactor kinetics. The most important parameter related to

fast neutron reactor safety is the Doppler reactivity effect. This arises mainly from the broadening of ^{238}U resonances in the energy range 0.5 - 10 KeV. There is also contribution of fissile isoto - pes and structural materials. The prediction of Doppler effect re - quires a knowledge of the resonance parameters and the scattering and absorbtion cross sections which determine the magnitude of the flux in the resonsnce energy region. The requirement for the pre - diction of Doppler effect is 10-15%. The present accuracy is close to required one.

Another safety parameter in sodium cooled fast reactors is the sodium voiding reactivity effect. The neutron scattering in sodium moderates neutrons and reduces the leakage probalility. The reacti- vity effect of the loss of sodium dependes on the type of fuel and the fuel enrichment. From point of view of neutron data the effect depends on the energy shape of the fission and capture cross sec- tions as well as on the sodium cross sections. The requirements for the prediction of the maximum positive sodium void effect is 10-15%.

The required accuracy should be reached mainly by improving cal- culational methods and to a less extent by improving the sodium scat- tering cross-sections. The present accuracy in the sodium void effect prediction is $\pm$ 20%.

2.8. HEAT GENERATION AND ACTIVATY OF IRRADIATED MATERIALS. A know - ledge of the decay heat of fuel elements is needed for the design of shut - down and emergency cooling system. The required accuracies are 2-5 %, a knowledge of the activity of irradiated fuel, coolant and structural materials is important for the determination of con- ditions of reactor equipment accessibility and fuel element handling, for the design of the shielding of fuel transportation and regenera- tion.

One needs to know neutron activity of irradiated fuel which is due to spontaneous fission of the curium isotopes and (α,n) - reac- tion on light isotopes (C, O). This requires a knoledge of the acti- nide fission and capture cross sections determining their balance in reactor, and the (α,n) cross section. For the determination of ac- cessibility of technological equipment one should know the activati- on of sodium after shut - down. Which is due to (n,2n) - process, and the activation of steel components because of the processes (n,p), (n,α), (n,2n) et al. Technology of fuel element production from regenerated fuel is determined by the accumulated activity of the ^{236}Pu and ^{238}Pu - isotopes. Their production cross sections should be known. The requirements to the prediction accuracy of the total activity is 20 - 30%.

3. THE METHOD OF DETERMINATION OF MICROSCOPIC NUCLEAR DATA ACCURACY

The method has been proposed for the determination of the requi- rements in nuclear data ensuring the prediction of the reactor para - meters with a given accuracy taking into account correlative proper - ties of uncertainties on the base of simple and realistic model [7]. This method helps us to determine qualitatively the required accuracies.

Relative variation of reactor parameter $\delta c/c$ is simply expres- sed by means of relative variations $(\delta\sigma/\sigma)_{\alpha ij}$ of the group va - lues of type α for isotope i in group j with proportionality coefficients or sensitivity coefficients $S_{\alpha ij}$

$$\delta c/c = \sum_{\alpha ij} S_{\alpha ij} (\delta\sigma/\sigma)_{\alpha ij} \qquad (1)$$

The coefficients $S_{\alpha ij}$ are calculated using the perturbation theo- ry [16, 18].

For determination of reactor parameter uncertainty one should make assumption on contributions of various ucertainties of for-

mula (1). Assuming that these contributions are random values uncorrelated between each other, the reactor parameter despersion is expressed through despersions of group microscopic values $d^2_{\alpha ij}$ as follows

$$D^2 = \sum_{\alpha ij} S^2_{\alpha ij} d^2_{\alpha ij} \qquad (2)$$

However, almost each nuclear constant may correlatate in 2-3 intervals on the whole energy range, that is why it is important to take into account uncertainty correlations. It was also proposed to divide uncertainty by components which differ by correlative properties. More often these are three components:(1) statistical - uncorrelated;

(2) uncertainty component which went over to the measured value from the error of the standard used. This component is present in uncertainties of all the values measured by means of this standard;

(3) possible uncertainty in the curve normalization which is constant within a given correlative interval and resulting from pos - sible systematic error. The expression for $\delta\sigma/\sigma$ as sum of three components is inserted into equation (1) and the terms with similar components describing correlating errors are combined so that the new sensitivity coefficient Z_β for a given correlative component of uncertainty appears as sums of $S_{\alpha ij}$ over the correla - tive regions. Now $\delta c/c = \sum Z_\beta (\delta\sigma/\sigma)^\beta$. Here the uncertainty components $(\delta\sigma/\sigma)^\beta$ are considered to be uncorrelated between each other and on that ground the transformation to formula (4) is made on the analogy with transformation from formula (1) to formu - la (2)

$$D^2 = \sum_\beta Z^2_\beta d^2_\beta \qquad (4)$$

Having given the left part, reactor parameter uncertainty, one should determine the set of uncertainties of separate values d^2_β .

Obviously, in such a form this problem is ambiguous. One may distribute differently contributions of uncertainties of different values into reactor parameter uncertainty. However, it is enough to put the condition of minimum cost for the set of experiments assuming si - multaneously relative cost values for measurement of different valu- es with uncertainties achieved up to now and extrapolating experi - ment cost in dependence of uncertainty ε , for example by the law $1/\varepsilon^2$, and the problem becomes simple.

We write the expression of experiment cost as follows

$$\sum_{\beta=1}^{N} \lambda_\beta / d^2_\beta$$

Here λ_β is constant, characterising the cost of experiments of determination of value, specified by index β . An example of considerations on the determination of λ_β is given in [7] . Namely, on assumption of equal ability of experimenters to get money, one may consider that the equal expenses were made for ob- taining the achieved accuracies d_{β_0} of different values and, as a result,

$$\lambda_\beta / d^2_\beta = \text{const}, \quad \beta = 1, \ldots, N$$

Having in mind that uncertainty must be limited above by achie - ved accuracies, the task of planning of optimal set of mic - roexperiments and evaluations ensuring the required accuracy of the calculation of K reactor parameters reduces to solution of the following extremum problem:

$$\sum_{\beta=1}^{N} \lambda_\beta / d^2_\beta \to \min \qquad (5a)$$

$$\sum_{\beta=1}^{N} Z^2_{\beta\ell} d^2_\beta \le D^2_\ell , \quad \ell = 1, \ldots, L \qquad (5b)$$

$$0 < d^2_\beta \le d^2_{\beta_0} \qquad (5c)$$

At one limitation on despersion of one reactor parameter only, the system is solved analytically [7] . In the work [17] the al-

gorithm of the task of planning optimal microexperiments and evaluations ensuring required acouracies of the arbitrary number of reactor parameters is developed. The accuracy requirements obtained as a result served the base for the soviet nuclear data requirement list presented in WRENDA-75 and in the successive issues with priority 2 (without taking into account integral experiments). In the same work the algorithm is expanded on the problem with taking into account integral experiments. In the case of simultaneous use of information on the integral and microscopic measurements the calculation accuracy D_e of reactor parameter C_e with sensetivity coefficients Z_e may be written as follows:

$$D_e^2 = \vec{Z}_e \, D(N+K) \cdot \vec{Z}_e^T \qquad (6)$$

where $D(N+K) = \left(I - D(N) F^T \left(V + F D(N) F^T\right)^{-1} F\right) D(N)$ (7)

here D(N) is covariance matrix of only microscopic experiments; F, matrix of size (N + K), sensetivity coefficients of integral experiments used; v, the matrix of integral experiment errors. The matrix D(N) may be transformed to diagonal form so that the diagonal elements of this matrix are the squares of microscopic data accuracies. Hence, the task of planning of set of microscopic experiments together with K integral experiments may be reduced to such extremum problem:

$$\sum \lambda_\beta / d_\beta^2 \to \min \qquad (8a)$$

$$\vec{Z}_\ell \, D(N+K) \, \vec{Z}_\ell^T \le D_\ell^2, \quad \ell = 1, \ldots, L \qquad (8b)$$

$$0 < d_\beta^2 \le d_{\beta_0}^2 \qquad (8c)$$

The accuracies d_β^2 are in eq. 8b as elements of the diagonal matrix D(N).

For solution of this problem the effective numerical methods have been developped. The required uncertainty obtained as a result is included into WRENDA-75 as the request from the USSR with priority 1 (requirements with taking into account integral experiments).

4. REQUIRED AND ACHIEVED ACCURACIES IN NUCLEAR DATA

The required in WRENDA nuclear data accuracies are specified by one standard deviation. However, the meaning of uncertainty is specified only in the USSR requests. So it is supposed in Usachev's requests that the uncertainty of a given point is supposed to be the sum of components with different correlative properties. The requirements in accuracy are specified for the most important uncertainty components, correlated over energy range, pointed out in the request. This uncertainty component determines the accuracy of the integral under the curve over this energy range. In requests for measurements the use of standards — $\bar{\nu}$ of ^{252}Cf, the ^{10}B (n, α) cross section (below 100 kev) and the ^{235}U (n, f) cross section is assumed. In all requests except those for standards, the accuracy is specified relative to standards, and the accuracy required of the standards is specified separately. The required and achieved accuracies for microscopic nuclear data are given below. The part of them are taken from Rowlands' review [9]. The data accuracies for the actinide isotopes and fission products are taken from the works by L.N.Usachev et al. [12-14], which served as a base of soviet request list in WRENDA-75 for the mentioned isotopes.

4.1. MAIN FISSILE AND FERTILE ISOTOPES [9]

There are high accuracy requirements for the fission and capture cross sections, $\bar{\nu}$ - value of ^{235}U, ^{238}U, ^{239}Pu, for the inelastic scattering cross section of ^{238}U. This accuracy is due,

first of all, to the requirements in prediction of K_{eff}(1%) and BR(2%). The following accuracies are needed for the thermal neutron energy region: ν - ± 0,3%, $\sigma_f, \sigma_c, \sigma_t, \sigma_s$ - ± 1%. For fast reactor spectrum region there are the following requirements:

Parameter	Fissile isotopes, %	Fertile isotopes, %
ν_f	0.3	1
σ_f	2	2
σ_c	4	3
σ_t, σ_s	2	5
σ_{in}	10	5
$\sigma_{n,2n}$	10	10

For the thorium fuel cycle reactors the same requirements are needed for ^{232}Th and ^{233}U as for ^{238}U and ^{235}U.

4.2. STRUCTURAL MATERIALS. The nuclear data of the coolant and structural materials are required for the determination of reactivity effects, reactor neutron spectrum, the reactor neutron balance, radiation damage, material activity and heating. There is need to know the sodium scattering and capture cross sections. The data are required for the capture and inelastic scattering cross sections of Fe, Cr, Ni (first of all), Ti, V, Mn, Co, Zr, Nb, Mo. The required accuracies for capture cross sections are 5-10%, for inelastic scattering cross sections, 5%. Data are required on the resonance structure of the cross sections because resonance shielding effects and Doppler effects are significant. This is one of the reasion why measurements for individual isotopes are required. For radiation damage problem partly, for neutron economy the data and, on (n,p) and (n,α) - reactions are needed.

4.3. A B S O R B E R S. In fast reactors both natural and enriched boron is used, tantalum is tested and Eu is being investigated. There are the following requirements in nuclear data for absorbers B, Cd, Eu, Gd, Er, Hf, Ta:

- capture cross sections are ± 5%,
- scattering cross sections, ± 10%.

The data on the individual isotopes are needed to predict the variation of reactivity with burnup and the activity and heating of the absorber.

4.4. ACTIVITION REACTIONS. Data for activation reactions are required for the calculation of radiactive contamination (activiation of coolant and mass tranfer of steel) of the primary circuit, the pumps and heet exchangers, for the calculation of the activation reactor elements which must be handled, tranported, stored and reprocessed. The major activation reactions are given below:

$^{54}Fe(n,p)^{54}Mn$ $^{58}Co(n,\gamma)^{59}Co$
$^{58}Ni(n,p)^{58}Co$ $^{62}Ni(n,\gamma)^{63}Ni$
$^{59}Co(n,\gamma)^{60}Co$ $^{58}Ni(n,\gamma)^{59}Ni$
$^{58}Fe(n,\gamma)^{59}Fe$ $^{54}Fe(n,\gamma)^{55}Fe$
$^{50}Cr(n,\gamma)^{51}Cr$ $^{22}Na(n,\gamma)^{23}Na$
$^{54}Fe(n,\alpha)^{51}Cr$ $^{40}Ar(n,\gamma)^{41}Ar$

The data averaged on reactor spectrum are needed. The required accuracy is 10 - 15%.

4.5. REACTOR DOSIMETRY. Dosimetry reactions are used for the measurement of flux and neutron spectra in reactors. Knowledge of the irradiation conditions is required for interpreting the

results of experimental irradiations for predicting material activation and for correlating the proporties of irradiated materials with the irradiation conditions.

Two main factors affect the physics of structural materials: the displacement of atoms and the generation of helium by (n,α) reactions. The prediction of atomic displacement rates and helium formation rates requires a knowledge of the total flux, the flux spectrum and the cross sections of the above-mentioned processes. A number of reactions are given below:

$^{27}Al(n,\alpha)^{24}Na$, ^{237}Np (n, f) F.P.
$^{56}Fe(n,p)^{56}Na$, ^{58}Ni (n,2n) ^{57}Ni
$^{63}Cu(n,2n)^{62}Cu$, ^{197}Au (n,γ)^{198}Au
^{238}U (n, f) F.P., ^{239}Pu (n, f) F.P.

In the framework of the IAEA the activity on the evaluation of dosimetry reactions is organized and the international data file is created.

4.6. TRANSACTINIDES. The nuclear data on transactinides are required for determination of build-up and burn-out of actinides and for the prediction of neutron activity of the fuel. We need to know the capture, fission and (n,2n) cross sections.

Some transactinides are built-up in power nuclear reactors in considerable amount. The neutrons cross sections of these isotopes are needed with high accuracy compared with that required for the main fissile and fertile isotopes. In reactors the isotopes are produced which, due to short half time and decay properties (emission of hard γ -rays or neutrons) lead to main difficulties in fuel management at its transportation and reprocessing. These are the isotopes ^{232}U, ^{238}Pu, ^{242}Cm, ^{244}Cm.

The neutron cross sections which are essential for the production of these isotopes:
$^{233}U(n,2n)$ and $^{237}Np(n,2n)$ for ^{232}U production,
$^{237}Np(n,\gamma)$, $^{241}Am(n,\gamma)$, $^{243}Am(n,\gamma)$ for the production of ^{238}Pu, ^{242}Cm, ^{244}Cm.

The question of the required acuracies for actinide nuclear data for build-up calculation was investigated in the works [10, 13, 14]. The main results are given below.

The accuracy of the prediction of same parameters calculated with the use of achieved nuclear data accuracies is given (for build-up calculation) in the table:

Isotopes	Capture		Fission		n, 2n	
	ach.	req.	ach.	req.		
^{238}U	8	8	5	4	20	15
^{239}Pu	10	3	4	4	50	50
^{240}Pu	20	4	10	10	50	50
^{241}Pu	20	7	8	5	50	50
^{242}Pu	50	15	30	30	50	50
^{243}Pu	50	50	50	50	50	50
^{242m}Am	30	20	30	20	50	50
^{241}Am	15	15	15	15	-	-
^{242}Am	30	30	30	30	-	-
^{243}Am	50	20	50	50	-	-
^{242}Cm	50	50	50	50	-	-
^{237}Np	50	15	10	10	50	25

The following table from the work [10] also shows the achieved and required accuracies for the build-up calculation:

Isotopes	Required	Achieved
^{236}Pu	30	55
^{238}Pu	20	60
^{240}Pu	5	12
^{241}Pu	4	24
^{242}Pu	10	31
^{241}Am	5	24
^{242}Am	20	28
^{243}Am	20	59
^{242}Cm	20	28
^{244}Cm	30	71

It is seen from the table that the achieved transactinide nuclear data accuracies do not ensure the required accuracy of the build-up calculation accuracy for fast reactors. More stringent requirements are formulated for capture cross sections of ^{240}Pu, ^{241}Pu, ^{242}Pu, ^{243}Am. The requirements to (n,2n) - reaction for ^{238}U, ^{237}Np, ^{238}Pu are essential. The achieved accuracy for the fission cross section is almost sufficent.

The required accuracies in the transactinide nuclear dara are determined having in mind the needed accuracy of calculating isotope production, neutron sources and reactor heating. In the work [14] the target accuracies of 5% for α-decay energy and 10% for neutron production are taken into account in addition to the tar - get accuracies for build-up of some nuclides. As a result more stringent requirements to the accuracies of some nuclear data are obtained: capture cross sections of ^{243}Am, ^{241}Am, ^{242}Pu and branching ratio of ^{242}Cm. The most stringent requirements are to capture cross sections of ^{237}Np, ^{242}Pu, ^{243}Am, ^{241}Am and (n,2n) - reaction cross sections of ^{237}Np and ^{238}U.

The highest priority of the required accuracies is for the following quantities:

Quantity	Functional
$^{237}Np(n,2n)$, ^{238}U (n,2n)	Production of ^{236}Pu
^{238}U (n,2n), $^{237}Np(n,\gamma)$	Production of ^{238}Pu
$^{242}Pu(n,\gamma)$, $^{243}Am(n,\gamma)$	Production of ^{244}Cm
$^{242}Pu(n,\gamma)$	Production of ^{243}Am
$^{243}Am(n,\gamma)$, $^{242}Pu(n,\gamma)$ $^{242}Cm_{BRSf}$	Total neutron production

Numerical magnitudes of the required accuracies mentioned above depend essentially on the target accuracies for the calculation of the quantities of interest.

Analized in [13] are requirements in nuclear data for the ^{232}U production calculation in reactors. The most important nuclear data for the ^{232}U build-up calculation in breeders are (n,3n) - reaction of ^{234}U, (n, γ) - reaction on ^{235}U and (n,2n) - reaction on ^{238}U and ^{237}Np.

4.7. FISSION PRODUCT. For determination of the reactivity effect of the bulk fission product (5-10%) the capture cross sections with accuracy of $\pm$ 10% and the scattering cross sections with accuracy of $\pm$ 30% should be known. The detailed neutron cross section dependence and reactor spectrum averaged values are needed.

In the works [12,13] it is shown that if the errors of all the cross sections are equal to 30%, and the fission product yield errors are equal to 3% (in fact the present accuracy is worse), one should obtain the estimation of the required uncertainty of averaged cross section of ± 7%. Assuming systematic uncertainty of 10% in all capture cross sections of individual fission products, one should estimate the averaged capture cross sections of fission product equalling ± 12%. The differencies among various evaluations of this value are approximately of same order of magnitude.

The nuclear data requirements obtained on the base of consideration of reactor core physics leed to 10% in the required uncertainty of averaged cross section of fission products. Assuming absense of correlation between the uncertainties of different cross sections, one may consider this accuracy to be achieved. Assuming systematic error, the admissible uncertainty is 7%.

Here we have the example of importance of the exact definition of the uncertainty meaning.

In dependence of the assumption on the uncertainty correlative properties two opposite conclusions may be made. Assuming statistical independence of the cross section uncertainties of different nuclides, one may conclude that there are no need to improve fission product cross sections, since one may consider the 30% uncertainty in capture cross sections of each fission product to be already achieved and that leeds to 10% - requirements for bulk fission product. However, if the uncertainty is correlated, then for achieving the same aim one must ensure the 7% - uncertainty in cross section of each nuclide for which purpose much work is needed both in measurements and evaluations. The second assumption seems to be more truthful.

The list of isotopes for which the improvement of capture cross sections is important for the calculation of the bulk fission product cross section in fast reactors is given below. (The isotopes are arranged in correspondence to their contributions to averaged cross sections, total contribution is 80%). The contribution of each isotopes of the first group to averaged cross section (^{133}Cs, ^{101}Ru, ^{99}Tc, ^{143}Nd) is not less 5%, of the second group (^{103}Rh, ^{145}Nd, ^{97}Mo, ^{149}Sm, ^{102}Ru, ^{131}Xe, ^{98}Mo, ^{151}Sm, ^{135}Cs, ^{93}Zr) is 5-2%, of the third group (^{105}Pd, ^{141}Pr, ^{100}Mo, ^{153}Eu, ^{103}Ru, ^{104}Ru) is 2-1%, of the others, less than 1%.

C O N C L U S I O N

Summing the results one should emphasize once more that ensuring of the required accuracy for some reactor parameters, which are important for reactor operation and choice of alternative ways, for out-of-pile fuel technology (including fuel transportation), for the processing of irradiated fuel and production of new fuel elements, for endurance investigations of fuel elements in dependence of neutron flux in reactor, leads to accuracy requirements of evaluated microscopic neutron data, which are yet not satisfied in spite of progress in experiments and evaluation.

It should also be emphasized that for effective achievement of admissible accuracies of reactor parameters it is necessary to exactly and clearly specify correlative properties of admissble uncertainties. Unfortunately it has not been made in WRENDA.

R E F E R E N C E S

1. Moorhead T.P. The effects of errors in cross section data on calculations for a large dilute fast reactor. Seminar on Physics of Fast and Intermediate Reactors, vol. II, Vienna, 1962.

2. Greebler P., Hutchins B.A. User Requirements for Cross Sections in the Energy Range from 100 eV to 100 keV. Proc. Conf. on Neutron Cross Section and Technology, Washington, 1966.
3. Smith R.D. Nuclear Data Requirements for Fast Reactor Design and Operation Proc. Conf. on Nuclear Data for Reactors, Paris, 1966.
4. Greebler P., Hutchins B.A., Cowan C.L. et al. Implication of nuclear data uncertainties to reactor design. Proc. Conf. on Nuclear Data for Reactors, Helsinki, 1970.
5. Zaritsky S.M., Troyanov M.F. About requirements to the accuracy of constants for reactor calculation, In: "Physics of nuclear reactors", issue 2, Moscow, Atomizdat, 1970.
6. Zaritsky S.M., Nikolaev M.N., Troyanov M.F. The requirements in nuclear data for fast reactor calculation. In: "Neutron physics", vol. 1, Kiev, 1973.
7. Usachev L.N., Bobkov Yu.G. Planning of an optimum set of microscopic experiment and evaluation, INDC(CCP)-19/U, Vienna,1972.
8. Usachev L.N., Manokhin V.N., Bobkov Yu.G. Nuclear data accuracy and its influence on fast reactor development. Approach to determination of requirements to nuclear data accuracy. Proc. Conf. on Nuclear Data in Science and Technology, Vienna, 1973.
9. Rowlands J.L. Nuclear Data for reactor design, operation and safety. Proc. Conf. on Neutron Physics and Nuclear Data, Harwell, 1978.
10. Usachev L.N., Bobkov Yu.G., Kolesov V.E., Krivtsov A.S. Determination of Transactinide Nuclear Data Required Accuracy for Burn-up Calculation in Fast Reactors. Proc. Conf. on Neutron Physics and Nuclear Data, Harwell, 1978.
11. Hammer Ph. Nuclear Data Needs. Plutonium Breeders. Proc. Conf, on Nuclear Cross Sections for Technology, Knoxville, 1979.
12. Bobkov Yu.G., Krivtsov A.S., Usachev L.N. The perturbation theory and sensitivity analysis is an effective approach to study of fission product kinetics in reactors. In: Voprosy atom - noj nauki i techniki. "Yadernye konstanty", Moscow, issue 3(38), 1980.
13. Bobkov Yu.G., Krivtsov A.S., Usachev L.N. The requirements in nuclear data of fission products and transactinide isotopes for fast reactors. In: Neutron physics, vol. 1, Moscow, 1980 (Proc. of Conf. on Neutron Physics, Kiev).
14. Usachev L.N., Kravchenko I.V., Krivtsov A.S. The required accuracies of transactinides isotopes for fast reactors from the point of view of out-of-pile fuel problem. IV Meeting on in - tercomparison of transactinide nuclear data evaluations, Vienna, 1981.
15. Usachev L.N. Unique definition of nuclear data accuracy. In: Yadernye constanty, issue 16, Moscow, Atomizdat, 1975. INDC(CCP)-45/L, Vienna, 1974.
16. Usachev L.N. The perturbation theory for breeding ratio and other ratios of values for varions processes in reactor. Atomnaya energia, 15, 472 (1963).
17. Bobkov Yu.G., Pyatnitskaya L.T., Usachev L.N. Planning of Neutron Data Experiments and Evaluations for Reactors, INDC(CCP)-46/L, Vienna, 1974.
18. Usachev L.N., Bobkov Yu.G. The perturbation theory and experiment planning in problem of nuclear data for reactors, Moscow, Atomizdat, 1980.

2. Greebler P., Hutchins B.A. User Requirements for Cross Sections in the Energy Range from 100 eV to 100 keV. Proc. Conf. on Neutron Cross Section and Technology, Washington, 1966.
3. Smith R.D. Nuclear Data Requirements for Fast Reactor Design and Operation Proc. Conf. on Nuclear Data for Reactors, Paris, 1966.
4. Greebler P., Hutchins B.A., Cowan C.L. et al. Implication of nuclear data uncertainties to reactor design. Proc. Conf. on Nuclear Data for Reactors, Helsinki, 1970.
5. Zaritsky S.M., Troyanov M.F. About requirements to the accuracy of constants for reactor calculation, In: "Physics of nuclear reactors", issue 2, Moscow, Atomizdat, 1970.
6. Zaritsky S.M., Nikolaev M.N., Troyanov M.F. The requirements in nuclear data for fast reactor calculation. In: "Neutron physics", vol. 1, Kiev, 1973.
7. Usachev L.N., Bobkov Yu.G. Planning of an optimum set of microscopic experiment and evaluation, INDC(CCP)-19/U, Vienna,1972.
8. Usachev L.N., Manokhin V.N., Bobkov Yu.G. Nuclear data accuracy and its influence on fast reactor development. Approach to determination of requirements to nuclear data accuracy. Proc. Conf. on Nuclear Data in Science and Technology, Vienna, 1973.
9. Rowlands J.L. Nuclear Data for reactor design, operation and safety. Proc. Conf. on Neutron Physics and Nuclear Data, Harwell, 1978.
10. Usachev L.N., Bobkov Yu.G., Kolesov V.E., Krivtsov A.S. Determination of Transactinide Nuclear Data Required Accuracy for Burn-up Calculation in Fast Reactors. Proc. Conf. on Neutron Physics and Nuclear Data, Harwell, 1978.
11. Hammer Ph. Nuclear Data Needs. Plutonium Breeders. Proc. Conf, on Nuclear Cross Sections for Technology, Knoxville, 1979.
12. Bobkov Yu.G., Krivtsov A.S., Usachev L.N. The perturbation theory and sensitivity analysis is an effective approach to study of fission product kinetics in reactors. In: Voprosy atom - noj nauki i techniki. "Yadernye konstanty", Moscow, issue 3(38), 1980.
13. Bobkov Yu.G., Krivtsov A.S., Usachev L.N. The requirements in nuclear data of fission products and transactinide isotopes for fast reactors. In: Neutron physics, vol. 1, Moscow, 1980 (Proc. of Conf. on Neutron Physics, Kiev).
14. Usachev L.N., Kravchenko I.V., Krivtsov A.S. The required accuracies of transactinides isotopes for fast reactors from the point of view of out-of-pile fuel problem. IV Meeting on in - tercomparison of transactinide nuclear data evaluations, Vienna, 1981.
15. Usachev L.N. Unique definition of nuclear data accuracy. In: Yadernye constanty, issue 16, Moscow, Atomizdat, 1975. INDC(CCP)-45/L, Vienna, 1974.
16. Usachev L.N. The perturbation theory for breeding ratio and other ratios of values for varions processes in reactor. Atomnaya energia, 15, 472 (1963).
17. Bobkov Yu.G., Pyatnitskaya L.T., Usachev L.N. Planning of Neutron Data Experiments and Evaluations for Reactors, INDC(CCP)-46/L, Vienna, 1974.
18. Usachev L.N., Bobkov Yu.G. The perturbation theory and experiment planning in problem of nuclear data for reactors, Moscow, Atomizdat, 1980.